Transition metal complexes of icosahedral monocarborane anions: Synthesis to catalysis

Patmore, Nathan

Award date:
2002

Awarding institution:
University of Bath

TRANSITION METAL COMPLEXES OF ICOSAHEDRAL MONOCARBORANE ANIONS: SYNTHESIS TO CATALYSIS

Submitted by Nathan Patmore

for the degree of PhD

of the University of Bath

2002

ProQuest LLC
789 East Eisenhower Parkway
P.O. Box 1346
Ann Arbor, MI 48106-1346

DEDICATION

This thesis is dedicated to Mum and Dad, for their love and support throughout my PhD

CONTENTS

ACKNOWLEDGEMENTS

Dr. Mary Mahon is thanked for her help in the collection and refinement of the majority of crystal structures in this thesis, as well as for doing her best to teach me some of the basics in crystallography. Dr Jonathon Steed is thanked for the collection and refinement of compound **II**. Catherine Hague and Dr. Chris Frost are thanked for their help in the assessing the performance of the silver(I) phosphine catalysts in the hetero-Diels-Alder reaction, and Dr. Gus Ruggerio is thanked for DFT calculations on the mechanism of this reaction. Dr. Mark Fox is thanked for the *ab initio*/GIAO/NMR calculations for $\{Ag_2(CB_{11}H_{12})_4\}^{2-}$. The University of Bath is thanked for funding. Adem, Jamie and Mike are thanked for amusing discussions both inside and outside the laboratory that has made my research a lot of fun.

I would like to thank my supervisor, Dr. Andrew Weller, for his considerable help, encouragement and support throughout my PhD. This, combined with his large enthusiasm for chemistry, has made my three years of research very enjoyable.

ABBREVIATIONS

CpH	Cyclopentadiene
Cp^*H	Pentamethylcyclopentadiene
NMR	Nuclear Magnetic Resonance
Hz	Hertz
Å	Angstrom (1×10^{-10} metres)
R	Alkyl group
δ	Chemical shift
ppm	Parts per million
$[BAr_F]^-$	$[B(C_6F_5)_4]^-$
$[TFPB]^-$ or $[BAr'_4]^-$	$[B\{3,5\text{-}C_6H_3(CF)_3\}_4]^-$
COD	Cyclooctadiene
Me	CH_3
Et	CH_2CH_3
Ph	C_6H_5
3D	3-dimensional
HOMO	Highest occupied molecular orbital
LUMO	Lowest unoccupied molecular orbital
TPP	Tetraphenylporphyrinate
CPMAS	Cross polarisation magic angle spinning
M	Metal
Mes	2,4,6-trimethylphenyl
IMes	1,3-demesitylimidazol-2-ylidene
Δ	Difference
Danishefsky's diene	1-Methoxy-3-(trimethylsilyloxy)-1,3-butadiene
L	Ligand
Bn	Benzyl
Pz	Pyrazolyl
ATI	Troponiminate

ABSTRACT

The treatment of $[MoCp(CO)_3X]$ (X = Cl, I) with one equivalent of $Ag(CB_{11}H_{12})$ in CH_2Cl_2 ultimately yields $[MoCp(CO)_3(x\text{-}\mu\text{-}H\text{-}CB_{11}H_{12})]$ (x = 7or 12), but the reaction proceeds via an intermediate species $[MoCp(CO)_3X{\cdot}Ag(CB_{11}H_{12})]_2$ (X = Cl, I). Both the final silver salt metathesis product, and intermediate species (X = I), have been isolated and fully characterised by elemental analysis, IR and NMR spectroscopy, and X-ray diffraction techniques. When the silver(I) salts of the more weakly nucleophilic $[closo\text{-}CB_{11}H_{11}Br]^-$ and $[closo\text{-}CB_{11}H_6Br_6]^-$ carborane anions are used instead metathesis is slowed or halted, and only the corresponding intermediate species can be isolated. An alternative technique of hydride abstraction from molybdenum, using $[CPh_3][CB_{11}H_{11}Br]$ and $[CPh_3][CB_{11}H_6Br_6]$, was used to generate $[MoCp(CO)_3(CB_{11}H_{11}Br)]$ and $[MoCp(CO)_3(CB_{11}H_6Br_6)]$ respectively, although the latter compound could only be characterised by NMR spectroscopy because it is unstable and very sensitive to nucleophilic attack. The synthesis of $\{MoCp(CO)_3\}^+$ ligated to a range of carborane anions allowed a ranking of the coordinating abilities of these anions to be made based upon the chemical shift of the Cp resonance.

A range of silver(I) phosphine compounds with the general formula $[Ag(PPh_3)_x(Y)]$ [x = 1 or 2; Y = $(closo\text{-}CB_{11}H_{12})^-$, $(closo\text{-}CB_{11}H_{11}Br)^-$, $(closo\text{-}CB_{11}H_6Br_6)^-$, $(closo\text{-}CB_{11}H_6Cl_6)^-$] were synthesised and fully characterised using elemental analysis, NMR spectroscopy, and X-ray diffraction techniques. The performance of some of these compounds in a hetero-Diels-Alder reaction was assessed to elucidate anion / activity and structure / activity relationships, as well as to allow comparisons between the thermodynamic and kinetic coordinating abilities of these carborane anions.

1 INTRODUCTION

1.1 Carboranes

Carboranes are molecules containing the basic arrangement of carbon and boron atoms in a polyhedral structure. The majority of known carboranes contain two carbon atoms. This is due to the ease with which they can be formed by reaction of precursor boranes, such as *nido*-$B_{10}H_{14}$, with an appropriate alkyne.[1] However, carboranes that contain one, three or even four carbons are also well documented.[2, 3]

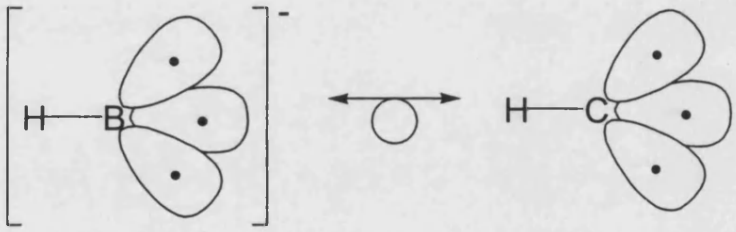

Figure 1.1: Frontier molecular orbitals of {B-H}$^-$ and {C-H}

Carborane analogues of boron clusters can be isolated because a {B-H}$^-$ fragment is isoelectronic and isolobal with a {C-H} fragment (Figure 1.1).[4] This means the fragments have the same frontier orbitals and number of bonding electrons, and the molecular orbitals (MO's) have similar symmetry and approximately the same energy meaning that, in theory, they can be interchangeable (Figure 1.2).

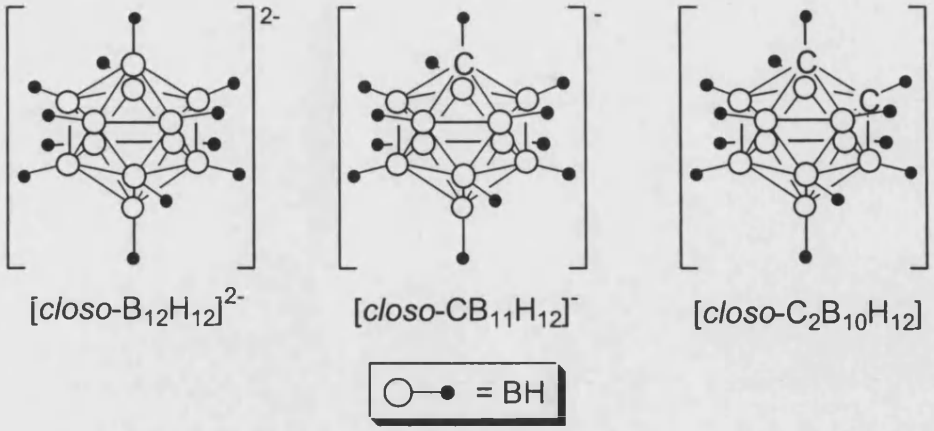

Figure 1.2: Interchange of $\{B\text{-}H\}^-$ fragment for a {C-H} fragment

The shape of a borane or carborane cluster can be predicted by the application of Wade's rules.[5] Counting the number of electron pairs donated to cluster bonding orbitals and relating this to the number of vertices gives the relevant polyhedral shape on which the cluster is based. This polyhedron might be complete, or missing up to 2 vertices (3 or more missing vertices is uncommon). A *closo*-cluster has $n + 1$ electron pairs, where n is the number of cluster vertices. This cluster has the shape of a complete polyhedron (or deltahedron) containing n vertices. A *nido*-cluster has one missing vertex and $n + 2$ electron pairs donated to cluster bonding. It is based upon a parent deltahedron having $n + 1$ vertices, with the vertex of highest connectivity removed. An *arachno*-cluster ($n + 3$ electron pairs) has two missing vertices and is based upon a deltahedron containing $n + 2$ vertices (Figure 1.3).

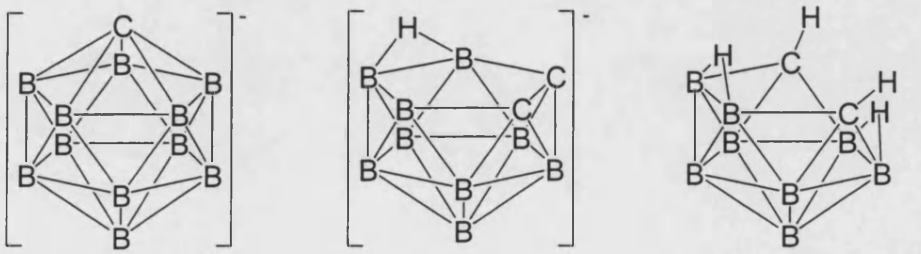

Figure 1.3: *Closo*, *nido* and *arachno* clusters based on an icosahedral polyhedron

In general *nido-* and *arachno-* clusters are less thermally and chemically stable than their *closo-* counterparts. This is due to the presence of relatively more reactive bridging hydrogens and the more open structure in *nido-* and *arachno-* clusters.

The properties and stability of anionic *closo*-monocarboranes, of general formula [*closo*-$CB_{n-1}H_n]^-$, have been studied extensively. Theoretical calculations performed on the [*closo*-$CB_{n-1}H_n]^-$ (n = 5-12) anions to determine their relative stabilities, show [*closo*-$CB_{11}H_{12}]^-$ to be the most stable in this family of carboranes.[6-8] All the [*closo*-$CB_{n-1}H_n]^-$ (n = 5-12) compounds have been isolated and structurally characterised,[9-15] but only the chemistry of [*closo*-$CB_{11}H_{12}]^-$ and [*closo*-$CB_9H_{10}]^-$ and their derivatives has been studied extensively. The chemistry of [*closo*-$CB_9H_{10}]^-$ is very similar to that of [*closo*-$CB_{11}H_{12}]^-$,[16-18] but is less developed than for [*closo*-$CB_{11}H_{12}]^-$ which is the anion under study in this thesis, and so will not be discussed in any detail.

1.2 The [*closo*-$CB_{11}H_{12}]^-$ Anion

1.2.1 Synthesis

The original synthetic strategy, proposed by Knoth in 1967,[9] is still one of the most effective routes for [*closo*-$CB_{11}H_{12}]^-$ synthesis. It starts with the addition of sodium cyanide to decaborane (equations 1.1 and 1.2).[19]

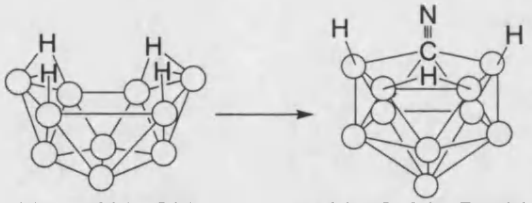

nido-$B_{10}H_{14}$ + 2NaCN ⟶ Na_2[*nido*-$B_{10}H_{13}CN$] + HCN (1.1)

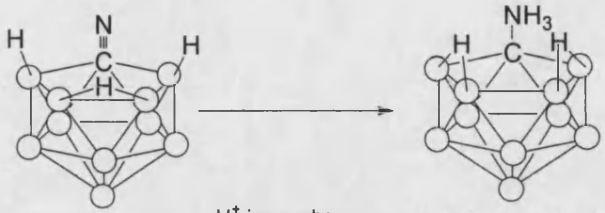

Na_2[*nido*-$B_{10}H_{13}CN$] $\xrightarrow{H^+ \text{ ion exchange}}$ *nido*-$B_{10}H_{12}CNH_3$ (1.2)

The coordinated amine is then converted into trimethylamine by reaction with dimethyl sulfate (equation 1.3).[20]

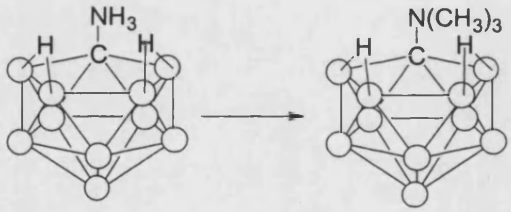

2 *nido*-$B_{10}H_{12}CNH_3$ + 3$(CH_3)_2SO_4$ + 6NaOH ⟶

2 *nido*-$B_{10}H_{12}CN(CH_3)_3$ + 3Na_2SO_4 + 6H_2O (1.3)

Removal of trimethylamine by reductive elimination using sodium yields a tri-sodium salt of this carborane, which is converted into the caesium salt of a *nido* carborane (equations 1.4-1.6).[21]

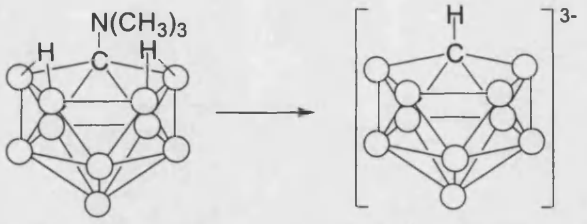

nido-$B_{10}H_{12}CN(CH_3)_3 + 3Na \longrightarrow Na_3[nido\text{-}B_{10}H_{10}CH] + Me_3N + \frac{1}{2}H_2$ (1.4)

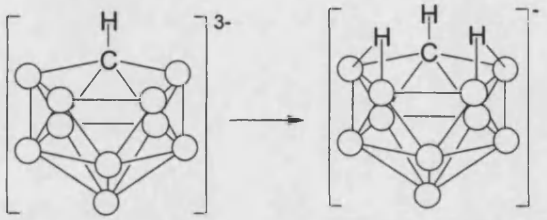

$Na_3[nido\text{-}B_{10}H_{10}CH] + 2H_2O \longrightarrow 2NaOH + Na[nido\text{-}B_{10}H_{12}CH]$ (1.5)

$Na[nido\text{-}B_{10}H_{12}CH] + CsCl \longrightarrow Cs[nido\text{-}B_{10}H_{12}CH] + NaCl$ (1.6)

The final step is to add the extra B-H fragment to the cage, necessary to make the compound *closo* (equation 1.7).[22]

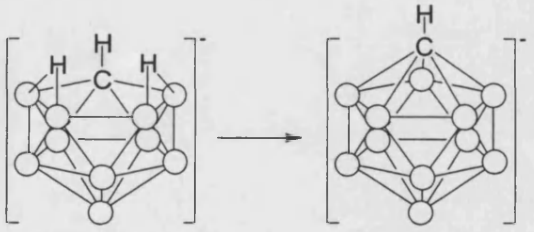

$Cs[nido\text{-}B_{10}H_{12}CH] + H_3B.N(C_2H_5)_3 \longrightarrow Cs[closo\text{-}CB_{11}H_{12}]$ (1.7)

This method is quite laboured, and the number of synthetic steps required from the relatively expensive decaborane starting material means that the $[closo\text{-}CB_{11}H_{12}]^-$ anion is considered expensive to produce. However, in our laboratories we routinely produce multigram quantities of $[closo\text{-}CB_{11}H_{12}]^-$ at a cost of £20 a gram.

Driven by a desire to reduce the expense and increase the availability of [*closo*-$CB_{11}H_{12}]^-$, the Michl group has recently published a novel synthetic strategy.[23] The first step is the synthesis of [*nido*-$B_{11}H_{14}]^-$ (50% yield) from inexpensive $NaBH_4$ and $BF_3{\cdot}Et_2O$ (equation 1.8).[24]

$$17[BH_4]^- + 20F_3B{\cdot}O(C_2H_5)_2 \longrightarrow 2[\textit{nido}\text{-}B_{11}H_{14}] + 15[BF_4]^- + 20\ O(C_2H_5)_2 + 20H_2 \quad (1.8)$$

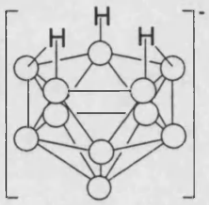

Treatment of this cage with a base, followed by carbon insertion with a carbene developed *in situ* generates [*closo*-$CB_{11}H_{12}]^-$ (42% overall yield) as the main product (equation 1.9). However, although this synthesis is attractive it can only be run on a 1g scale limiting its utility.

$$[\textit{nido}\text{-}B_{11}H_{14}]^- \xrightarrow{CHCl_3\ /\ Base} [\textit{closo}\text{-}CB_{11}H_{12}]^- \quad (1.9)$$

1.2.2 Reactivity

The [*closo*-$CB_{11}H_{12}]^-$ core is extremely rugged, however the periphery of the cage can be functionalised via electrophilic substitution of the B-H bonds. The difference in electronegativity between boron and carbon results in the slight polarisation of the cage with the most basic B-H bond in the 12 position, followed by B-H bonds on the lower, and then upper pentagonal belts (Figure 1.4).

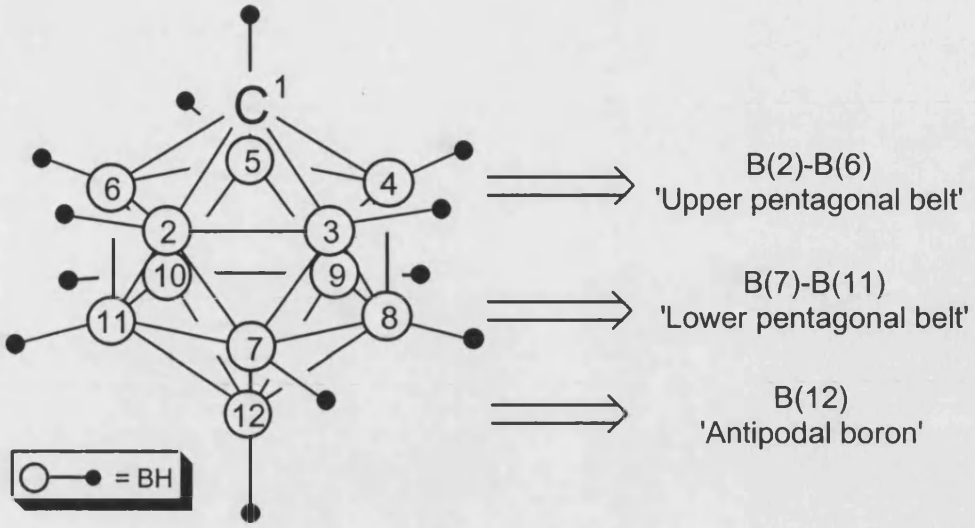

Figure 1.4: [*closo*-$CB_{11}H_{12}$]$^-$ with boron labelling scheme

The cage can therefore be selectively functionalised at each unique position because of the relative differences in the basicity of the B-H bonds. Furthermore, the hydrogen on carbon is acidic and can be substituted for a range of alkyl groups using nucleophilic substitution reactions. Functionalisation of the [*closo*-$CB_{11}H_{12}$]$^-$ cage can greatly effect the stability, solubility and nucleophilicity of the anion, as discussed in the next section.

1.3 Halocarboranes

1.3.1 Synthesis

The substitution of a B-H for a B-X (X = F, Cl, Br, I) bond in [*closo*-$CB_{11}H_{12}$]$^-$ requires increasingly harsh reaction conditions depending on the level of substitution desired. This is displayed well in the bromination reactions of [*closo*-$CB_{11}H_{12}$]$^-$ (Figure 1.5). Reaction of one equivalent of N-bromosuccinimide and $Cs[CB_{11}H_{12}]$

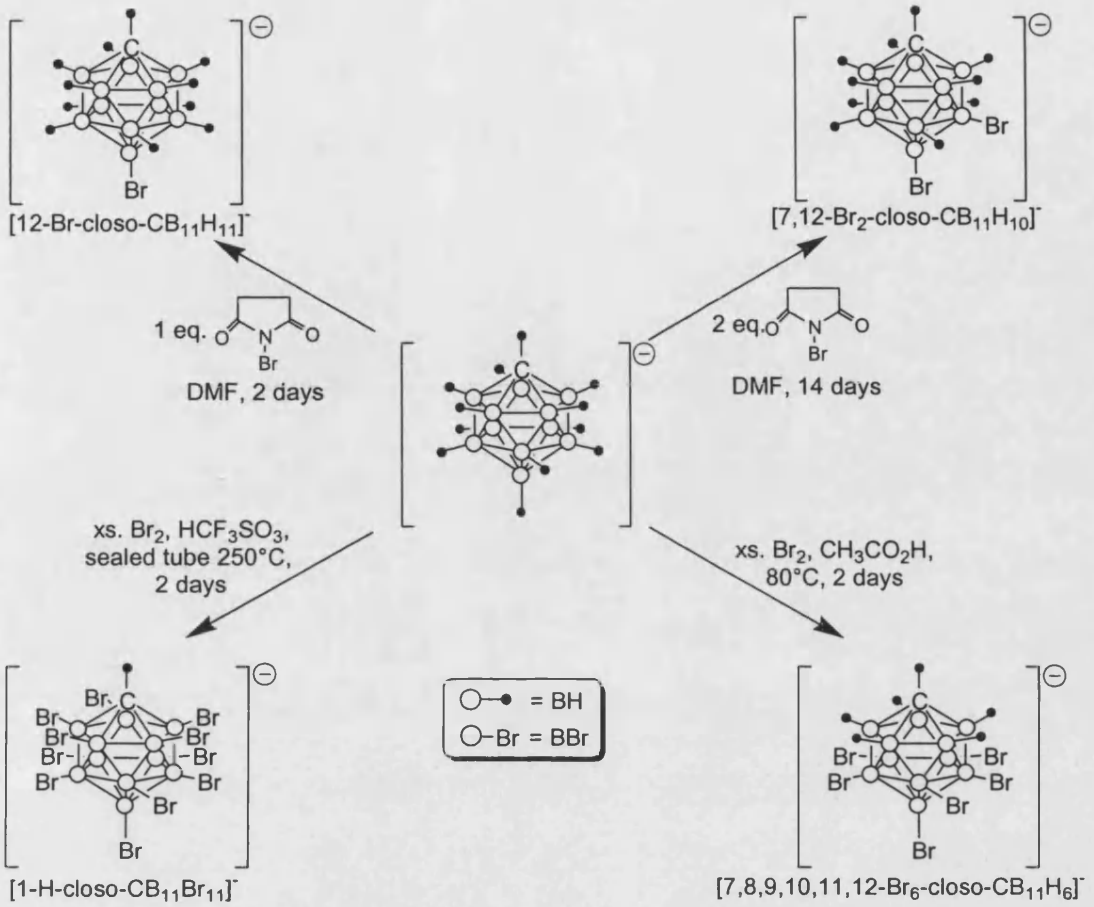

Figure 1.5: Bromination of the [*closo*-$CB_{11}H_{12}$]$^-$ anion

in dimethylformamide for 48 hours yields Cs[12-Br-*closo*-$CB_{11}H_{11}$].[25] If instead, two equivalents of N-bromosuccinimide are used, and the reaction mixture is left to stir 14 days, a second bromine is added to the cage in the next most reactive position, B(7), to give Cs[7,12-Br_2-*closo*-$CB_{11}H_{10}$]. In order to successfully hexahalogenate the cage, harsher reaction conditions are needed, and H(*closo*-$CB_{11}H_6Br_6$) is formed by the direct reaction of excess bromine with H(*closo*-$CB_{11}H_{12}$) in refluxing acetic acid for two days.[26] Despite the presence of excess bromine in this reaction, the conditions are still not sufficiently severe to induce electrophilic substitution on any of the upper pentagonal belt B-H bonds. In order to brominate every B-H bond on [*closo*-$CB_{11}H_{12}$]$^-$, triflic acid and bromine need to be combined in a sealed tube and heated at

250°C for two days to yield the [1-H-*closo*-$CB_{11}Br_{11}$]$^-$ anion, a method recently reported by Xie.[27]

The chloride derivatives [12-Cl-*closo*-$CB_{11}H_{11}$]$^-$,[25] [7,12-Cl_2-*closo*-$CB_{11}H_{10}$]$^-$,[25] [7,8,9,10,11,12-Cl_6-1-*closo*-$CB_{11}H_6$]$^-$[26] and [1-H-*closo*-$CB_{11}Cl_{11}$]$^-$[27, 28] can be prepared in a matter analogous to that of the bromide derivatives. The direct reaction of iodine with [*closo*-$CB_{11}H_{12}$]$^-$ under mild conditions yields [12-I-*closo*-$CB_{11}H_{11}$]$^-$.[26] However, unlike with bromine and chlorine, exhaustive iodination of [*closo*-$CB_{11}H_{12}$]$^-$ in refluxing glacial acetic acid yields only [7,12-I_2-*closo*-$CB_{11}H_{10}$]$^-$. If the electrophilicity of iodine is enhanced by using the mixed halogen ICl, the polyiodonated compounds [7,8,9,10,11,12-I_6-1-*closo*-$CB_{11}H_6$]$^-$[29] and [1-H-*closo*-$CB_{11}I_{11}$]$^-$ can be isolated.[27] The first fluorinated [*closo*-CB_{11}]$^-$ derivative reported was [2-F-*closo*-$CB_{11}H_{11}$]$^-$.[30] The method of preparation employed for its synthesis cannot be used for further, more selective, derivitisation of [*closo*-$CB_{11}H_{12}$]$^-$ as it is generated from the insertion of $BF_3{\cdot}OEt_2$ into [*nido*-7-$CB_{10}H_{13}$]$^-$. However, Strauss *et al.* have reported that the reaction of [*closo*-$CB_{11}H_{12}$]$^-$ with liquid anhydrous HF at 23°C results in the exclusive formation of [12-F-*closo*-$CB_{11}H_{11}$] (equation 1.10).[31]

$$[Cs][CB_{11}H_{12}] + HF \xrightarrow[23°C,\ 22h]{\text{anhydrous HF}} [Cs][12\text{-}F\text{-}CB_{11}H_{11}] + H_2 \qquad (1.10)$$

By elevating the temperature of reaction to 140°C the difluoro [7,12-F_2-*closo*-$CB_{11}H_{10}$]$^-$ anion can be isolated. Further attempts to increase the degree of fluorination by increasing the reaction temperature results in mixtures of [*closo*-$CB_{11}H_7F_5$]$^-$, [*closo*-$CB_{11}H_6F_6$]$^-$ and [*closo*-$CB_{11}H_5F_7$]$^-$ that are difficult to separate.[32]

If, instead, a mixture of HF and F_2 is used the [1-H-*closo*-$CB_{11}F_{11}$]$^-$ anion can be isolated in good yield (equation 1.11).

$$[Cs][CB_{11}H_{12}] + 11F_2 \xrightarrow[25°C,\ 48h]{HF(l)} [Cs][1\text{-}H\text{-}CB_{11}F_{11}] + 11HF \qquad (1.11)$$

It is also possible to synthesise carborane anions containing a mixture of halogen atoms. Taking carborane, [6,7,8,9,10,11,12-X_6-*closo*-$CB_{11}H_6$] (X = Cl, Br, I), and using the relevant reagents (triflic acid and I_2, Br_2, or ICl), in the sealed tube reactions developed by Xie *et al.*, the mixed halocarboranes [1-H-2,3,4,5,6-Y_5-7,8,9,10,11,12-X_6-*closo*-CB_{11}]$^-$ (X, Y = Cl, Br, I) can be isolated in good yield.[33]

1.3.2 Properties

Halogenation leads to significant changes in stability, solubility and perhaps most importantly, the nucleophilicity of the [*closo*-CB_{11}]$^-$ anion. The magnitude of change in these physical properties is related to the type of halogen used, as well as the degree to which the cage has been substituted.

The effect on stability from halogenation can be observed by comparing the silver(I) salts of [*closo*-$CB_{11}H_{12}$]$^-$ and [*closo*-$CB_{11}H_6Br_6$]$^-$. Unlike $Ag[CB_{11}H_6Br_6]$, $Ag[CB_{11}H_{12}]$ is light sensitive and will decompose upon heating or standing in an aqueous solution.[22] This is due to the susceptibility of H(7)-H(11) and in particular H(12) to electrophilic attack. This can also be seen in attempts to isolate trityl salts of [*closo*-$CB_{11}H_{12}$]$^-$ and [*closo*-$CB_{11}H_6Br_6$]$^-$. $Ag[CB_{11}H_6Br_6]$ reacts smoothly with trityl bromide to form $CPh_3[CB_{11}H_6Br_6]$, but the same reaction with $Ag[CB_{11}H_{12}]$ gives rise

to a number of products, the major product being one in which two cages are oxidatively coupled together via a B(12)-B(12) bond (equation 1.12).[34]

$$2[Ag(CB_{11}H_{12})] + 2CPh_3Br \longrightarrow 2AgBr + 2HCPh_3 + C_2B_{22}H_{22} \qquad (1.12)$$

Computational studies have been performed on conjugate Brønsted acids of [*closo*-$CB_{11}H_{12}]^-$ and its fluorinated derivatives to calculate their relative acidities and structures.[35] The results predict the calculated acidity order to be $H[CB_{11}F_{12}]$ > $H[CB_{11}H_6F_6]$ > $H[12\text{-}F\text{-}CB_{11}H_{11}]$ > $H[CB_{11}H_{12}]$ and found that $H[CB_{11}F_{12}]$ could be considered the strongest neutral Brønsted superacid known to date. The site of protonation in the most stable protonated form of each of these acids varies between the anions (Figure 1.6).

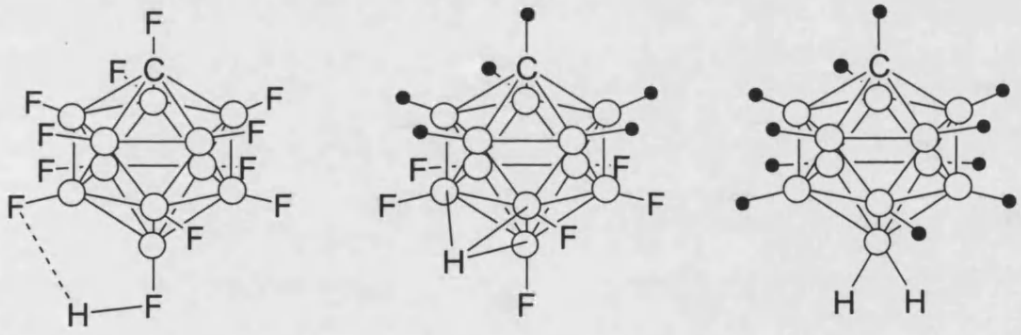

Figure 1.6: Calculated most stable protonation sites of some carborane anions

At the highest level of calculation (DFT B3LYP calculations at 6-311+G** level), $H[CB_{11}F_{12}]$ is protonated on F(12) but the proton is also hydrogen bonded to F(7). $H[CB_{11}H_6F_6]$ and $H[12\text{-}F\text{-}CB_{11}H_{11}]$ are protonated in the centre of a triangular face on

the surface of the cage, and $H[CB_{11}H_{12}]$ is protonated on B(12) to give two symmetrically arranged terminal hydrogens.

The high stability of the hexahalogenated carboranes, combined with very weak nucleophilicity (see section 1.4), allows the isolation of novel and interesting compounds.[36] Perhaps the most remarkable example of this comes from the use of halocarboranes as superacids (those stronger than 100% sulphuric acid). This has led to the isolation of the hydronium ion $[(H_9O_4)^+]$,[37] protonated fullerene $[(HC_{60})^+]$,[38] and protonated benzene $[(HC_6H_6)^+]$,[38, 39] as weighable solids that are stable at room temperature. The protonated fullerene and benzene are synthesised by condensing HCl onto solid $[R_3Si(CB_{11}H_6Cl_6)]$ at low temperature followed by removal of the volatiles at room temperature to yield $H[CB_{11}H_6Cl_6]$ in essentially quantitive yield (equation 1.14), which can then be reacted with C_6H_6 or C_{60} to yield their respective protonated forms.

$$(C_2H_5)_3Si(CB_{11}H_6Cl_6)_{(s)} + HCl_{(g)} \longrightarrow H[CB_{11}H_6Cl_6] + (C_2H_5)_3SiCl_{(g)} \qquad (1.14)$$

Previous attempts to isolate stable, protonated species of these compounds failed because the anions of the superacids used [e.g. $(SbF_6)^-$, $(HSO_4)^-$, $(CF_3SO_3)^-$] are too nucleophilic,[40] or promote cation decomposition.[41]

1.4 Weakly Coordinating Anions

Weakly coordinating anions are used to generate highly Lewis acidic metal centres. They should ideally have a low overall charge and high degree of charge delocalisation so that no atom, or group of atoms, has a high charge density. This implies that larger anions would be better, with the increased steric bulk further reducing the capability of the anion to interact with the metal by removing the centre of negative charge further from the centre of positive charge.

1.4.1 Weakly Coordinating Anions in Catalysis

Weakly coordinating anions play a major role in catalysis mediated by Lewis acidic cationic centres. In a typical catalytic cycle a ligand (X) is displaced to leave a cationic metal centre and a vacant coordination site (Figure 1.7). Reactant (A) can then co-ordinate to the metal and is activated towards reaction with (B) to give product (A-B). In this generalised scheme, the more weakly coordinating the anion the greater the availability of the vacant coordination site, and hence the better the catalyst.

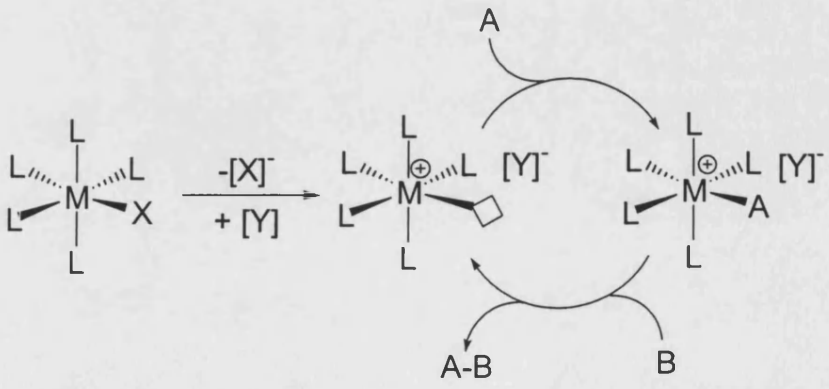

Figure 1.7: Generalised catalytic cycle for a Lewis acid catalyst

When describing a gap in a metal's coordination sphere the term *virtual coordination site* is perhaps a better description than *vacant coordination site*.[42] This is because there are four main ways that vacant sites in metal complexes can be filled (Figure 1.8).

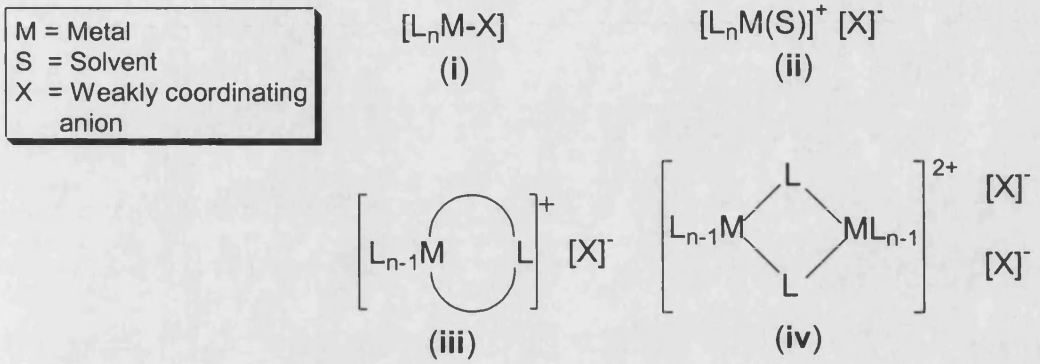

Figure 1.8: Four possible ways vacant coordination sites can be occupied

In **(i)** the vacant coordination site is occupied by the weakly coordinating anion, while in **(ii)** the solvent occupies this site instead. Scenario **(iii)** shows one of the ligands becoming bidentate in order to fill the metal's coordination sphere, an example being the formation of a C-H agostic intramolecular interaction with the metal.[43] The final option **(iv)** is that one of the ligands bridges two metal centres to form a binuclear complex, such as that commonly seen when using halide ligands. Options **(iii)** and **(iv)** mean that even when using the most weakly coordinating anion or solvent, generation of a truly vacant coordination site may be impossible. Instead weak or labile metal-ligand bonds may be formed instead.

There are a number of weakly coordinating anions that have been used to successfully partner metal cations, including $[ClO_4]^-$, $[CF_3SO_3]^-$, $[BF_4]^-$, and $[PF_6]^-$.[44-47] The tetraphenylborate anion $[(BPh_4)^-]$, and its derivatives, have received the most attention

in recent years as candidates for use as weakly coordinating anions. However, the $[BPh_4]^-$ anion can bind to metal centres through π interactions from one of its phenyl rings.[48] In order to reduce the π-bonding ability of the anion, and hence reduce its coordinating ability, fluorine or trifluoromethyl substituents have been added to form $[B(C_6F_5)_4]^-$ $(BAr_F)^-$,[49] and $[B(3,5\text{-}C_6H_3(CF_3)_2)_4]^-$ $(TFPB)^-$ [50] (Figure 1.9) which do not generally π-bond to metals and display greater stability and than $[BPh_4]^-$. Despite the reduced π bonding ability of $[TFPB]^-$, a few structurally characterised examples of it coordinated to a metal have been isolated, including $[Rh(\eta^6\text{-}TFPB)(COD)]$.[51]

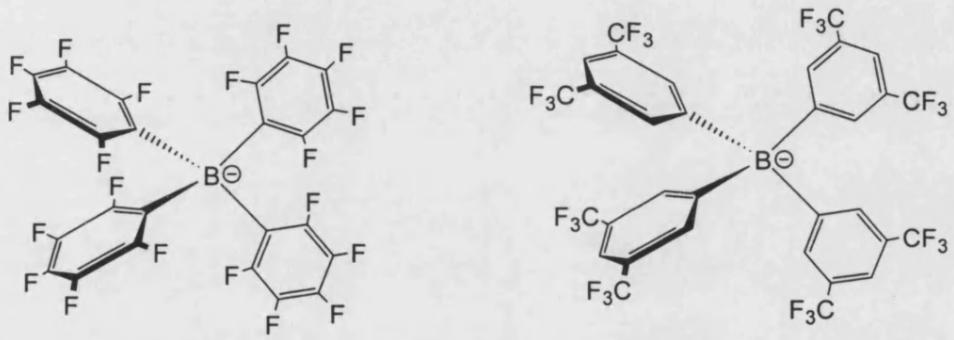

$[BAr_F]^-$ $[TFPB]^-$

Figure 1.9: $[B(C_6F_5)_4]^-$ and $[B(3,5\text{-}C_6H_3(CF_3)_2)_4]^-$

The incorporation of electron withdrawing groups on the phenyl rings also reduces the tendency for B-Ar bond cleavage by decreasing the amount of negative charge on the ipso carbon atoms. For example, the electrophilic cation $[FeCp(CO)_2(THF)]^+$ is phenylated in the presence of $[BPh_4]^-$, but is not arylated in the presence of $[TFPB]^-$.[52] However, whilst cleavage of the B-C bond in $[TFPB]^-$ is rare, it can occur. For example refluxing *trans*-$[Pt(PPh_3)_2(Me)(OEt_2)][TFPB]$ in toluene results in the formation of $[Pt(PPh_3)_2(3,5\text{-}CF_3\text{-}C_6H_3)_2]$.[53]

The fluorinated derivatives of the tetraphenylborate anion have been used to generate active catalysts for carbon monoxide and olefin copolymerisation,[54] or the production of adipic acid by methyl acrylate dimerisations.[55] Their most important application is in the stabilisation of olefin polymerisation catalysts, in particular the highly active group 4 metallocene complexes of the general type $[M(Cp)_2(R)]^+$ (M = Ti, Zr, Hf, Th). There is an extensive amount of literature on the role of tetraphenylborate anions in olefin metathesis, which is outside the scope of this report, and there are a number of excellent reviews on this topic.[56-58]

1.4.2 The Weakly Coordinating Nature of [*closo*-$CB_{11}H_{12}]^-$

The charge on [*closo*-$CB_{11}H_{12}]^-$ is delocalised relatively evenly about the anion via a σ bonded framework, and it can be thought of as a 3D analogue of benzene.[8] This efficient delocalisation of a single charge over a relatively large cluster and the absence of any basic site on the cage periphery makes it very weakly nucleophilic. The extremely large HOMO-LUMO gap in [*closo*-$CB_{11}H_{12}]^-$, similar to other *closo* boranes, can explain the unusually large degree of thermal and chemical stability the cluster possesses.

Reed's group was the first to efficiently demonstrate the weakly coordinating nature of the [*closo*-$CB_{11}H_{12}]^-$ anion.[59] By pairing $[Fe(TPP)]^+$ (TPP = tetraphenylporphyrinate) (Figure 1.10) with weakly coordinating anions and measuring the out of plane deformation of the central metal atom in the solid-state, an indication of the degree of nucleophilicity the anion has can be drawn. The more weakly coordinating the anion,

the greater the charge on the iron atom and hence the closer it will be to planarity with the nitrogen atoms of TPP. The [Fe(TPP)($CB_{11}H_{12}$)] complex was shown to be the closest to planarity with the shortest Fe-N bond length known, smaller than those of [Fe(TPP)($FSbF_5$)]$^-$, and [*closo*-$CB_{11}H_{12}$]$^-$ was considered the most weakly coordinating anion known at the time.

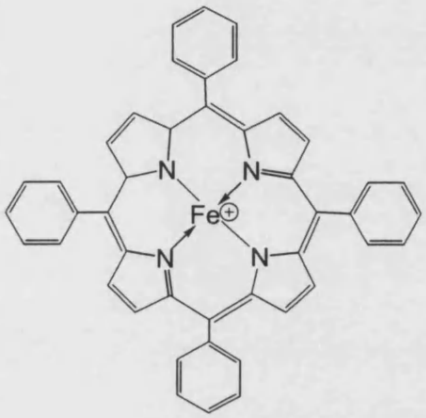

Figure 1.10: [Fe(TPP)]$^+$ cation

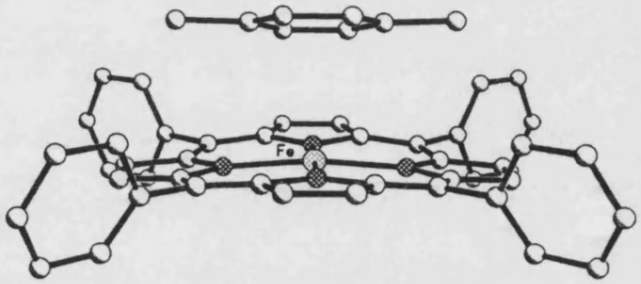

Figure 1.11: Crystal structure of [Fe(TPP)(*p*-xylene)]$^+$ [60]

A number of different methods have been developed to rank the relative coordinating ability of anions. The out of plane deformation of the iron atom in the [Fe(TPP)(anion)] complex[59] was one of the first, however, as more weakly coordinating anions, such as [*closo*-$CB_{11}H_6Br_6$]$^-$, were developed solvent molecules became competitive with the anion reducing the applicability of this technique (Figure 1.11).[60]

Another transition metal based ranking of anion nucleophilicity that was developed by Reed, compares the carbonyl stretching frequencies of [$FeCp(CO)_2X$] (X = weakly coordinating anion) compounds (Figure 1.12).[34]

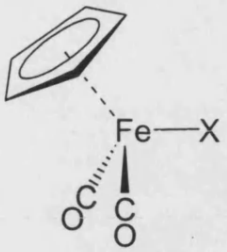

Figure 1.12: $[Fe(Cp)(CO)_2X]$ (X = weakly coordinating anion)

X	Average νCO in toluene (cm^{-1})
I-	2016
ClO_4^-	2049
$CB_{11}H_{12}^-$	2049
$SbF6^-$	2050
$CB_9H_5Br_5^-$	2096
$CB_{11}Me_{12}$-	2098
$CB_{11}H_6Br_6^-$	2108

Table 1.1: Average carbonyl stretching frequencies for $[Fe(Cp)(CO)_2X]$

An increase in the carbonyl stretching frequency correlates to diminished π back-bonding from the metal centre, reflecting increasing cationic character in the $[FeCp(CO)_2]^+$ moiety. Hence the weakest coordinating anion will have the highest carbonyl stretching frequencies (Table 1.1).[61] However, the results of this ranking scheme should be interpreted with care as the majority of $[FeCp(CO)_2X]$ compounds were generated *in situ* and could not be isolated or fully characterised, leaving doubt as to the actual species being monitored.

Perhaps the best method of ranking the nucleophilicity of weakly coordinating anions developed to date is based around the $[(^iPr)_3Si(X)]$ (X = weakly coordinating anion) species (Figure 1.13), which has two indicators as to the coordinating ability of X.[62] The first is in the solid state and is the degree deviation of the C-Si-C bond angle from the expected 120° of an ionic sp^2-hybridised $\{SiR_3\}^+$ fragment. The second is based on the downfield ^{29}Si NMR chemical shifts, some of which are measured in the solid state using CPMAS techniques to remove any ambiguity about the coordination of the anion. The ambiguity comes from fact that the anion can be partially displaced by solvent molecules according to the equilibrium shown in equation 1.13.[63] The more

positive ^{29}Si chemical shift indicates a more deshielded nucleus and thus the most cationic character.

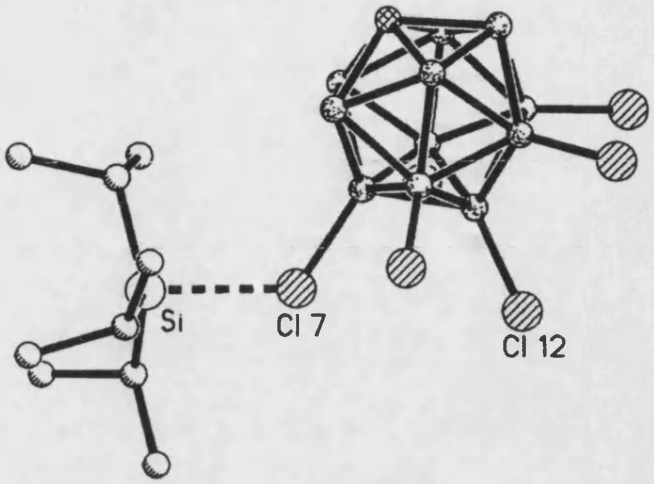

Figure 1.13: X-ray crystal structure of $^{i}Pr_3Si(CB_{11}H_6Cl_6)$[29]

$$^{i}Pr_3Si(anion) + toluene \rightleftharpoons [^{i}Pr_3Si(toluene)]^{+} + [anion]^{-} \quad (1.13)$$

The ^{29}Si NMR chemical shifts for compounds of the general formula $[(^{i}Pr)_3Si(anion)]$ are summarised in Table 1.2. The table shows that the coordinating ability of halocarborane anions decreases in the order I > Br > Cl > F. It can also be seen that the greater the degree of halogen substitution the more weakly coordinating the anion.

The $[Fe(TPP)]^{+}$ moiety has recently found use as a reporter of the ligand field strength of weakly coordinating anions, an electronic property that is not necessarily correlated with coordinating strength.[64, 65] In this series, carboranes are ranked as the weakest field ligands presently known.

Compound	Solvent	$\delta(^{29}Si)$/ppm	Ref.
$^{i}Pr_3SiH$	toluene	12.1	[16]
$^{i}Pr_3Si(OSO_2CF_3)$	toluene	40	[61]
$[^{i}Pr_3Si(toluene)][B(C_6F_5)_4]$	toluene	94	[16]
$^{i}Pr_3Si[B(C_6F_5)_4]$	none	107.6	[66]
$^{i}Pr_3Si(1\text{-}H\text{-}CB_{11}H_5I_6)$	none	97	[29]
$^{i}Pr_3Si(1\text{-}H\text{-}CB_{11}Br_5I_6)$	toluene	104.5	[33]
$^{i}Pr_3Si(1\text{-}H\text{-}CB_{11}H_5Br_6)$	toluene	105	[63]
$^{i}Pr_3Si(1\text{-}H\text{-}CB_{11}H_5Br_6)$	none	110	[29]
$^{i}Pr_3Si(1\text{-}H\text{-}CB_{11}I_5Br_6)$	toluene	108.8	[33]
$^{i}Pr_3Si(1\text{-}H\text{-}CB_{11}Cl_5Br_6)$	toluene	111.1	[33]
$^{i}Pr_3Si(1\text{-}H\text{-}CB_{11}Cl_{11})$	toluene	114.4	[33]
$^{i}Pr_3Si(1\text{-}H\text{-}CB_{11}H_5Cl_6)$	none	115	[29]
$^{i}Pr_3Si(1\text{-}H\text{-}CB_{11}Br_5Cl_6)$	toluene	115.8	[33]
$^{i}Pr_3Si(1\text{-}H\text{-}CB_{11}F_{11})$	toluene	120	[67]

Table 1.2: Downfield ^{29}Si Chemical Shifts for $^{i}Pr_3SiX$

1.5 Alkylated carboranes

A number of alkyl derivatives of [closo-$CB_{11}H_{12}$]$^-$ have been synthesised by conversion of B-H or B-I vertices to B-C. The B-I vertices of iodocarboranes can be converted to B-C vertices via palladium catalysed alkylation with Grignard reagents.[68] This technique, developed by Hawthorne *et. al*,[69] was first used to peralkylate the [*closo*-$B_{12}H_{12}$]$^{2-}$ anion.[70] Attempts to use similar conditions for peralkylation of [*closo*-$CB_{11}H_{12}$]$^-$ where unsuccessful, yielding uncharacterised products.[71] The first peralkylated carborane anion, [*closo*-$CB_{11}Me_{12}$]$^-$ (Figure 1.14) was synthesised by electrophilic substitution of B-H vertices using the strong methylating reagent, methyl triflate, and a hindered base (equation 1.14).[71]

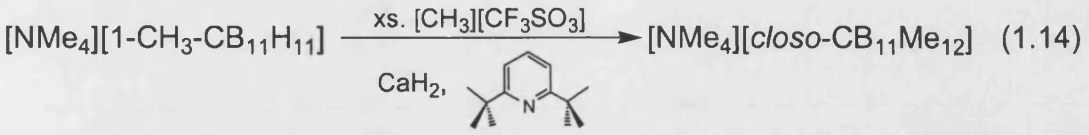

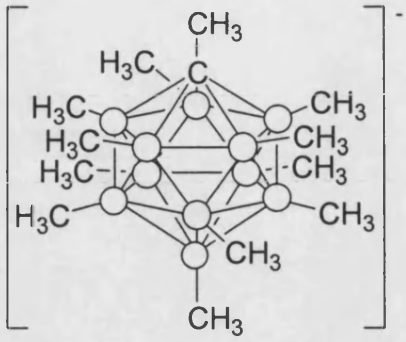

Figure 1.14: [*closo*-$CB_{11}Me_{12}$]$^-$

An apparently more convenient approach has been reported recently by Xie et al. involving the reaction of [*closo*-$CB_{11}H_{12}$]$^-$ with excess RBr (R = CH_3, CH_2CH_3) in a sealed pyrex tube at 200°C.[72]

Peralkylated carborane anions such as [*closo*-$CB_{11}Me_{12}$]$^-$ are stable to air, strong bases and weak acids but are destroyed in concentrated acids. Unlike other [*closo*-$CB_{11}H_{12}$]$^-$ derivatives, which have poor solubility, the [*closo*-$CB_{11}Me_{12}$]$^-$ anion is soluble in polar organic solvents (e.g. Et_2O and CH_2Cl_2) and even has a detectable solubility in hexane depending on the cation.[73]

The solid state structures of the thallium(I) and alkali (Li^+, Na^+, K^+, Rb^+, Cs^+) salts of [*closo*-$CB_{11}Me_{12}$]$^-$ adopt a number of interesting coordination motifs when crystallised from arene solvents (Figure 1.15).[74]

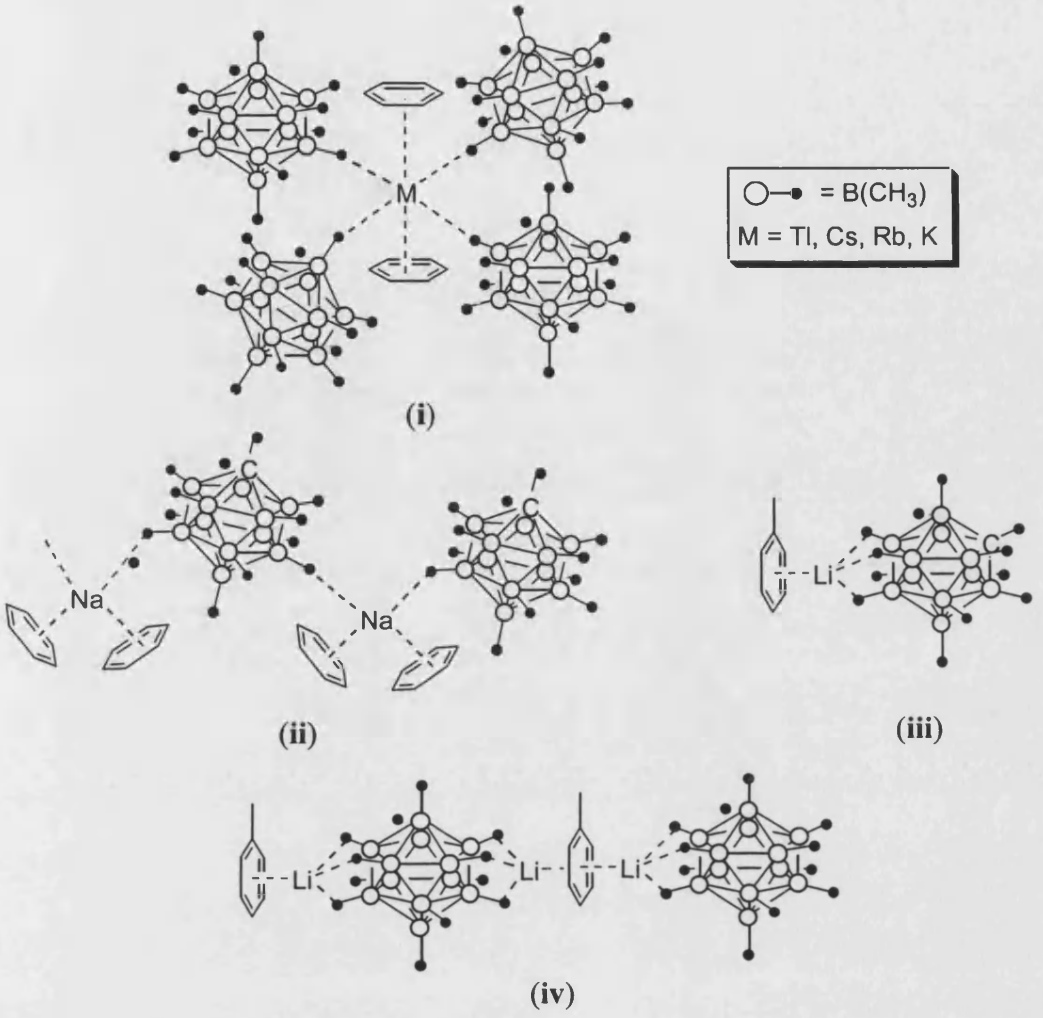

Figure 1.15: Structural bonding motifs of some [*closo*-$CB_{11}Me_{12}$]$^-$ salts [carbon vertice not located in (**i**) and (**iv**) due to cage disorder]

In the solid state, the larger Tl^+, Cs^+, Rb^+ and K^+ cations are sandwiched between two benzene molecules, with four [*closo*-$CB_{11}Me_{12}$]$^-$ anions equatorially arranged in a nearly square arrangement (**i**). Smaller Na^+ cations crystallise with *pseudo* tetrahedral coordination geometry in polymeric chains, bonded to two benzene molecules and two anions (**ii**). Li^+ possesses two crystalline motifs, one is a simple sandwich of a toluene molecule and [*closo*-$CB_{11}Me_{12}$]$^-$ (**iii**), the other a chain resulting from the sandwich of Li^+ with [*closo*-$CB_{11}Me_{12}$]$^-$ and a half occupied benzene (**iv**).

It is thought that peralkylated carborane anions could be even better candidates for use as weakly coordinating anions than halocarboranes, as the halogen lone pairs have been removed, and the only metal-anion interactions can be via C-H bonds. However, the carbonyl stretching frequencies of $[FeCp(CO)_2(CB_{11}Me_{12})]$[75] ($2125^{-1}$ and $2070cm^{-1}$) are similar to those of the $[closo\text{-}CB_{11}H_6Br_6]^-$ analogue ($2128cm^{-1}$ and $2088cm^{-1}$),[34] suggesting that both anions donate comparably to the metal centre or alternatively, ligation of $[FeCp(CO)_2]^+$ with the solvent (toluene) rather than the anion occurs in both cases. As none of these compounds have been characterised by techniques other than IR spectroscopy, caution should therefore be used in their assignment. The ranking of the nucleophilicity of $[closo\text{-}CB_{11}Me_{12}]^-$ using its $[R_3Si]^+$ salt has not yet been performed, perhaps because it decomposes in the presence of such a strong electrophile as is the case for $[B\{C_6H_4(CF_3)_2\}_4]^-$.[76]

The neutral $[closo\text{-}CB_{11}Me_{12}]^\bullet$ free radical has been isolated from the oxidation of $Cs[CB_{11}Me_{12}]$ with PbO_2/CF_3COOH as a stable crystalline solid[75] and has been elegantly used to isolate a $[R_3Sn]^+$ salt by oxidative cleavage of hexaalkyldistannyl. The extremely electrophilic group 14 $[R_3E]^+$ ions are normally very difficult to isolate as they have low solubility in sufficiently inert solvents, the only examples being adducts of $[R_3Si]^+$ to toluene[77] or halocarboranes.[29] $[n\text{-}Bu_3Sn][CB_{11}Me_{12}]$ was prepared as in equation 1.15, and its crystal structure determined that it displayed a nearly sp^2 hybridised Sn atom (Figure 1.16), suggesting only weak interactions between $\{B\text{-}CH_3\}$ and $[SnR_3]^+$.[78]

$$[closo\text{-}CB_{11}Me_{12}]^\bullet \xrightarrow[\text{Pentane}]{1/2\ {}^nBu_3Sn\text{-}Sn{}^nBu_3} [{}^nBu_3Sn][CB_{11}Me_{12}] \qquad (1.15)$$

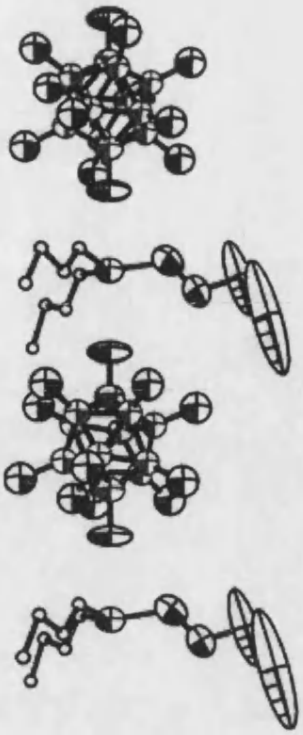

Figure 1.16: Crystal structure of [*n*-Bu_3Sn][$CB_{11}Me_{12}$] (Hydrogen atoms and one component of the disordered butyl groups are omitted for clarity) [78]

The Cs salt of [*closo*-$CB_{11}Me_{12}$]$^-$ has been converted to [*closo*-$CB_{11}(CF_3)_{12}$]$^-$ via partial fluorination, using anhydrous HF, followed by perfluorination with Bartlett's reagent (K_2NiF_6) (Figure 1.17).[79]

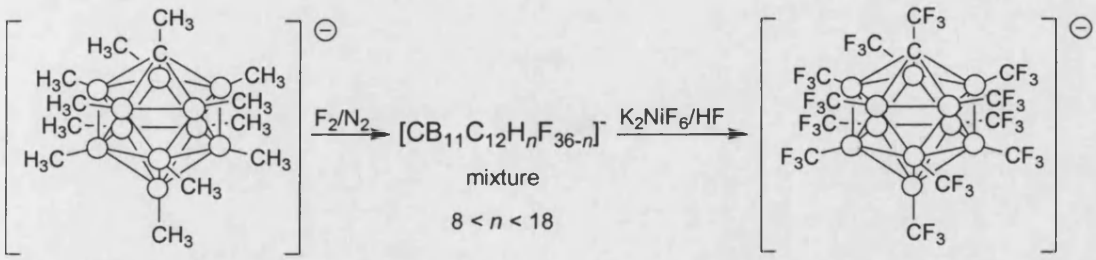

Figure 1.17: Synthesis of [*closo*-$CB_{11}(CF_3)_{12}$]$^-$

The large size (~8Å diameter), absence of strongly basic sites, oxidation resistance, and sterically protected delocalised charge makes [$CB_{11}(CF_3)_{12}$]$^-$ one of the closest approaches yet to the 'ideal' weakly coordinating anion. It is chemically resistant to

strong bases (20% KOH/EtOH) and strong acids (conc. H_2SO_4, anhydrous CF_3SO_3H and BF_3 /anhydrous HF). It is destroyed by heating to 250°C and by Na in anhydrous NH_3. Unfortunately, the applications of this anion are limited as it is explosive! Scratching of solid samples in a Pyrex flask result in an explosion and its caesium salt burns vigorously when ignited. This instability is due to the greater strength of the B-F bond (154 kcal/mol in BF_3) compared with the C-F bond (116 kcal/mol) coupled with the steric crowding of the substituents, calculated to be 144 kcal/mol, which is comparable to cubane (157 kcal/mol).[80]

1.6 Derivatisation of the C-H Vertex

Whilst the B-H bonds of [*closo*-$CB_{11}H_{12}$]$^-$ are hydridic and amenable to electrophilic substitution, the C-H bond is acidic and can therefore be lithiated with butyllithium.[11] Treatment of this lithio species with alkyl halides yields [1-R-*closo*-$CB_{11}H_{11}$]$^-$ derivatives.[25] This procedure can be done either before or after further derivitisation of the cage (Figure 1.18).[81]

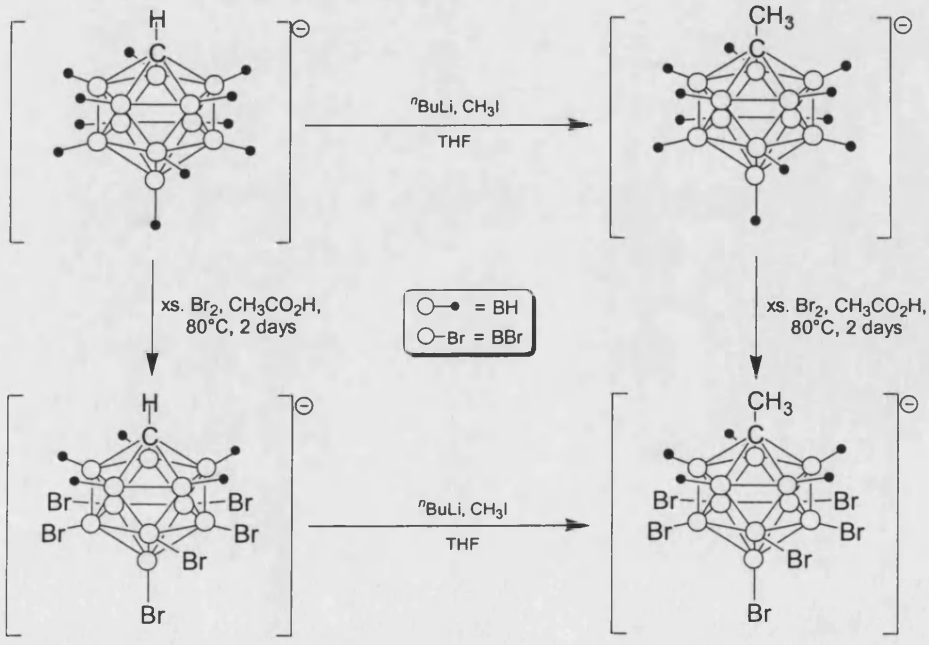

Figure 1.18: C-alkylation before and after bromination

The addition of an electron donating group such as CH_3 onto the cage can promote electrophilic substitution reactions of B-H bonds. For example, the direct chlorination of [*closo*-$CB_{11}H_{12}]^-$ in refluxing glacial acetic acid for one month affords a mixture of products with the general formula [*closo*-$CB_{11}H_{12-x}Cl_x]^-$ (x = 9 - 11). The halogenation is not driven to completion as the electron withdrawing nature of the halogen atoms on the cage inhibit the electrophilic substitution reactions of any remaining B-H bonds. This effect is reduced with [1-CH_3-*closo*-$CB_{11}H_{11}]^-$, which can be fully chlorinated under the same reaction conditions resulting in the isolation of [1-CH_3-*closo*-$CB_{11}Cl_{11}]^-$ as the sole product.[27] C-arylation of [*closo*-$CB_{11}H_{12}]^-$ is more complex than C-alkylation, and is a multistep synthesis (equation 1.16) evolving from the reaction of benzaldehyde and decaborane to yield [6-Ph-*nido*-6-$CB_9H_{11}]^-$. This is then converted to [1-Ph-*closo*-$CB_{11}H_{12}]^-$ by treatment with $BH_3(SMe_2)$ or $BH_3(NEt_3)$.[82] Subsequent derivitisation of this compound yields [1,12-Ph_2-*closo*-$CB_{11}H_{10}]^-$ in 38% yield.[83]

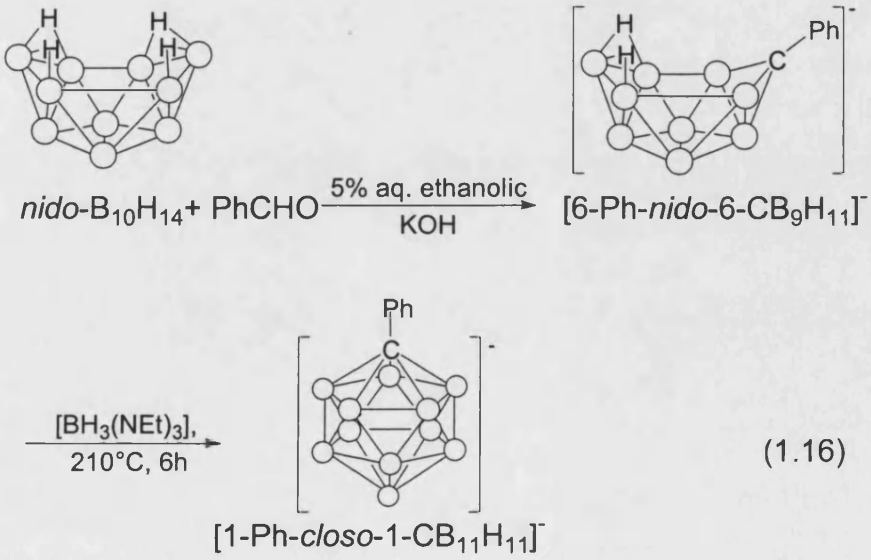

(1.16)

The compound $[1\text{-}NH_3\text{-}closo\text{-}CB_{11}H_{11}]^-$ has been synthesised[84, 85] and had further substitutions performed on it.[86] It is also possible to metallate the carbon atom of the cage (equation 1.17). The synthesis of $[N(n\text{-}Bu)_4]_2[CuCl(CB_{11}F_{11})]$ (Figure 1.19) demonstrates that there is still a wealth of coordination chemistry for *closo*-monocarboranes to be uncovered.[67]

$$[Cu(mesityl)]_n + N(^nBu)_4Cl + [N(^nBu)_4][1\text{-}H\text{-}CB_{11}F_{11}] \longrightarrow [N(^nBu)_4]_2[Cu(Cl)(CB_{11}F_{11})] \quad (1.17)$$

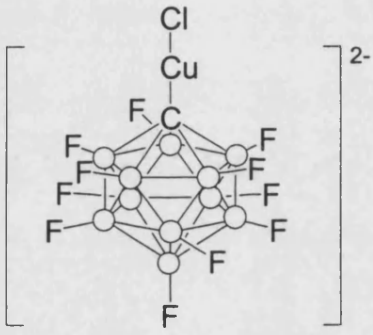

Figure 1.19: $[Cu(Cl)(CB_{11}F_{11})]^{2-}$

1.7 Mixed Halo-Alkyl Derivatives

One of the newest concepts in the design of new $[closo\text{-}CB_{11}H_{12}]^-$ derivatives is to combine the solubilising powers of alkylation with the inertness of halogenation. This has led to the formation of $[1\text{-}H\text{-}closo\text{-}CB_{11}Me_5X_6]^-$ (X = Cl, Br I) anions (Figure 1.20).[87]

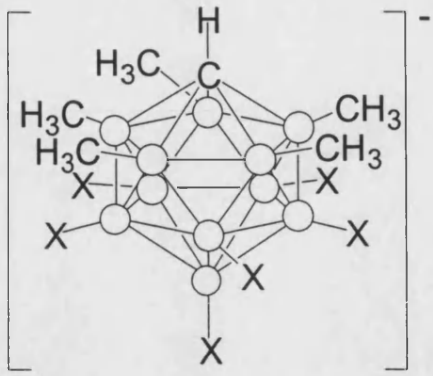

Figure 1.20: [1-H-*closo*-$CB_{11}Me_5X_6$]$^-$ (X = Cl, Br I)

These compounds have the stability in strong acids and bases associated with their hexahalogeno counterparts. The free acids are superacids, demonstrated by the ready protonation of benzene to form $[C_6H_7][HCB_{11}Me_5Br_6]$ that, remarkably, is stable to 150°C. The solubility of $[^iPr_3Si][HCB_{11}Me_5X_6]$ in organic solvents is of an order of magnitude higher than that of the unmethylated analogues, whilst the ^{29}Si NMR spectra display shifts similar to that of the hexahalogeno carboranes. The compound $[CH_3][HCB_{11}Me_5Br_6]$ can also be readily prepared, and is a stronger methylating reagent than methyl triflate.[87]

Very recently, the [*closo*-$HCB_{11}Me_5Br_6$]$^-$ anion has been used to generate the compound $[Si(mes)_3][HCB_{11}Me_5Br_6]$ (mes = 2,4,6-trimethylphenyl) which was characterised by X-ray crystallography and ^{29}Si NMR spectroscopy.[88] Amazingly, the silyl cation is sp^2 hybridised and totally free of any intermolecular interactions from the anion or intramolecular interactions from the 2,4,6-trimethylphenyl ligand.

1.8 Salts of [*closo*-$CB_{11}H_{12}$]$^-$ and its Derivatives

One of the most important attributes of a weakly coordinating anion, besides its nucleophilicity, is that a wide range of salts can be prepared to facilitate metal coordination or generation of a 'vacant' coordination site on the metal centre. The general procedures for the interconverision between the different salts of [*closo*-$CB_{11}H_{12}$]$^-$ and its derivatives are well documented and can be applied in a general manner regardless of the degree or type of substitution (Figure 1.21). Some of the more useful cations include silver(I),[89] thallium(I),[90] $[R_3Si]^+$,[29, 40] ferrocinium,[91] trityl,[34] and $[H(OEt_2)]^+$ or H^+.[26, 37, 38]

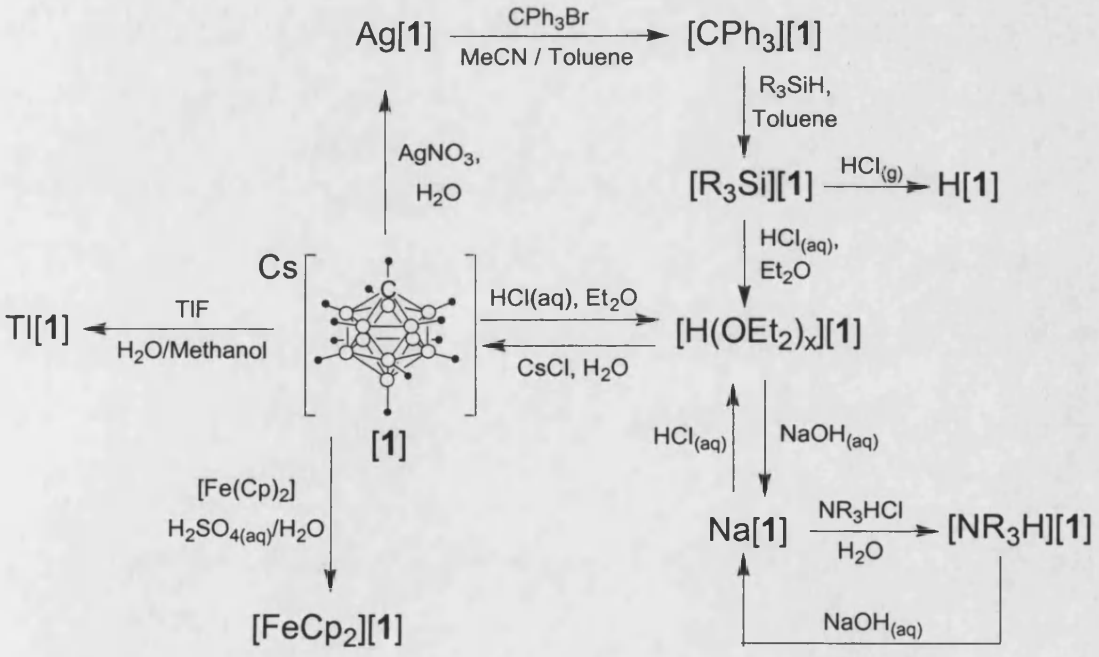

Figure 1.21: Interconversion of [*closo*-$CB_{11}H_{12}$]$^-$ salts

The facile interconversion between the various salts of [*closo*-$CB_{11}H_{12}$]$^-$ and its derivatives is a useful tool in generating metal complexes of the carborane anions, examples of which are shown in the next section.

1.9 Transition Metal Complexes of [*closo*-$CB_{11}H_{12}$]$^-$ and its Derivatives

The first significant report of the use of the weakly coordinating ability of *closo*-borate anions to generate novel metal complexes was reported by Zakharova, who used them to prepare the novel Pd(II) complexes $[(\eta^3\text{-}C_3H_5)Pd(RCN)_2]_2[B_{10}Br_{10}]$ (R = (CH_3, C_6H_5).[92] However, Reed was the first to champion the weakly coordinating properties of [*closo*-$CB_{11}H_{12}$]$^-$ and its derivatives, over 15 years ago.[59] Surprisingly there have been relatively few transition metal complexes characterised containing the [*closo*-$CB_{11}H_{12}$]$^-$ anion. This may be due to the perceived cost of the parent [*closo*-$CB_{11}H_{12}$]$^-$ anion, although the new synthesis recently reported by Michl *et al.* (section 1.2.1) should decrease the price significantly making it more accessible to general chemists.[23]

1.9.1 Transition Metal Complexes Without Metal-Anion Coordination

The [*closo*-$CB_{11}H_{12}$]$^-$ anion has been used to partner a number of platinum cations of the general type $[Pt(L\text{-}L)(C_2H_5)]^+$ (L-L = $R_2P(R')PR_2$).[93, 94] The ethyl group in these species adopts either an ethene/hydride or agostic alky coordination mode (Figure 1.22), depending on the nature of the diphosphine. The [*closo*-$CB_{11}H_{12}$]$^-$ anion shows no evidence of any strong intermolecular interaction with the cationic platinum species, either in the NMR spectra or solid-state structures of these complexes.

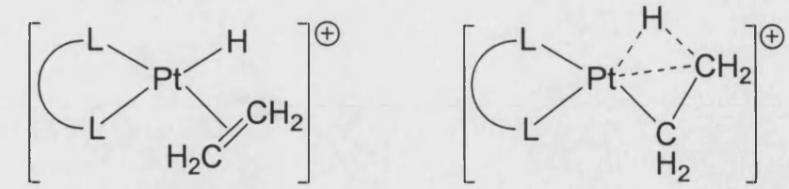

Ethene / hydride coordination Agostic ethyl coordination

Figure 1.22: The two coordination modes of (C_2H_5)

The isolation of copper(I) carbonyls was originally thought to need a superacid medium,[95] but it is the absence of counterion basicity that is actually required, as demonstrated with the use of the weakly coordinating $[AsF_6]^-$ anion.[96] The [1-Bn-$CB_{11}F_{11}]^-$ and [1-Et-$CB_{11}F_{11}]^-$ anions have also been used to isolate copper carbonyls. The presence of the benzyl group in [1-Bn-$CB_{11}F_{11}]^-$ negates the very weakly coordinating nature of the fluorinated cage, and hence reaction of the silver salt with CuCl in CH_2Cl_2 under a CO atmosphere yields [$Cu(CO)_2$(1-Bn-$CB_{11}F_{11}$)][97] with the benzyl group coordinated to the copper. This compound is only the second copper(I)

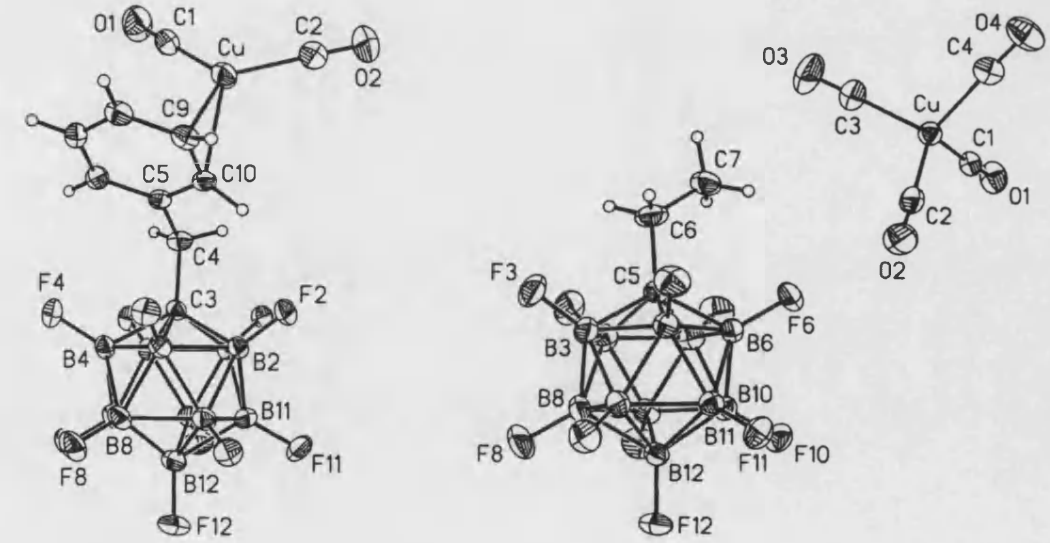

[$Cu(CO)_2$(1-Bn-$CB_{11}F_{11}$)] [$Cu(CO)_4$][1-Et-$CB_{11}F_{11}$]

(Ellipsoids drawn at the 50% propability level)

Figure 1.23: Crystal structures of Cu(I) carbony complexes [97]

dicarbonyl to be structurally characterised. The same reaction with Ag[1-Et-$CB_{11}F_{11}$] results in the formation of [$Cu(CO)_4$][1-Et-$CB_{11}F_{11}$], the first isolated copper(I) tetracarbonyl, with no anion-cation interactions in the solid state (Figure 1.23).[97] This is a nice demonstration of how arene groups should be avoided in systems designed for weakly coordinating anions.

In a similar manner, the [1-Et-$CB_{11}F_{11}$]$^-$ anion can also be used to isolate a nonclassical rhodium(I) carbonyl, [$Rh(CO)_4$][1-Et-$CB_{11}F_{11}$].[98] Nonclassical metal carbonyls are defined as those exhibiting $\nu(CO)_{average} > 2143cm^{-1}$. It is formed from the reaction of the characterised [(η^6-C_6H_6)$Rh(CO)_2$][1-Et-$CB_{11}F_{11}$] salt with CO, either in the solid state or in solution. The crystal structure displays weak F···Rh contacts [3.220(9) – 3.588(9)Å] and a weak C-H···Rh interaction [(C)H···Rh, 3.21Å] from the anion's ethyl group.

Reed has used monocarboranes to isolate a number of compounds containing the [Fe(TPP)]$^+$ moiety. This cation has been partnered with [*closo*-$CB_{11}H_{12}$]$^-$ to investigate the magnetic properties of a number of intermediate-spin iron(III) porphyrins.[99-101] These studies led to the use of [Fe(TPP)]$^+$ to deduce a ranking of ligand field strengths for a number of anions.[64, 65] The Brønsted acid of [*closo*-$CB_{11}H_6Cl_6$]$^-$ has been used to protonate [(TPP)Fe-O-Fe(TPP)] and yield a diiron hydroxy bridged cation species, which is a proposed step in the pathway of a number of biological pathways.[102] Attempts to isolate [Fe(TPP)($CB_{11}H_6Br_6$)] from the reaction of [Fe(TPP)(Br)] and one equivalent of Ag[$CB_{11}H_6Br_6$] resulted in the unexpected formation of [Fe(TPP)][$Ag(CB_{11}H_6Br_6)_2$] which contains the novel anion [$Ag(CB_{11}H_6Br_6)_2$]$^-$.[60]

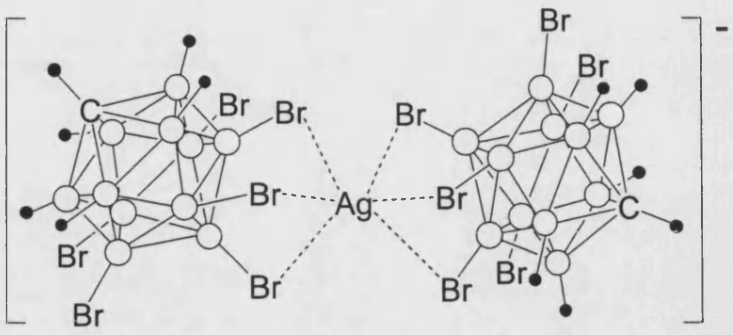

Figure 1.24: $[Ag(closo\text{-}CB_{11}H_6Br_6)_2]^-$

The carboranes on the $[Ag(CB_{11}H_6Br_6)_2]^-$ anion (Figure 1.24) have half their normal overall charge, introducing a new concept for reducing the nucleophilicity of an anion.

1.9.2 Transition Metal Complexes Containing Metal-Anion Interactions

There have been a number of silver salts of $[closo\text{-}CB_{11}H_{12}]^-$ and its derivatives isolated, the majority of which contain a variety of silver-arene interactions in the solid state.[22, 25, 31, 103] Other than these simple silver salts, the first transition metal complex isolated and structurally characterised containing ligated $[closo\text{-}CB_{11}H_{12}]^-$ was $[Fe(TPP)(CB_{11}H_{12})]$.[59] The solid state structure of this compound displays the cage bound to the iron centre via a B-H-Fe bond from the B(12) vertex. The lengthening of the B-H distance in this bond by *ca.* 0.2Å is indicative of an agostic type interaction.[43]

The compound $[Fe(Cp)(CO)_2(CB_{11}H_{12})]$ is the final product of the metathesis reaction between $Ag(CB_{11}H_{12})$ and $Fe(Cp)(CO)_2I$.[89] This reaction proceeds via an intermediate, postulated to be a halide bridged species (Figure 1.25).

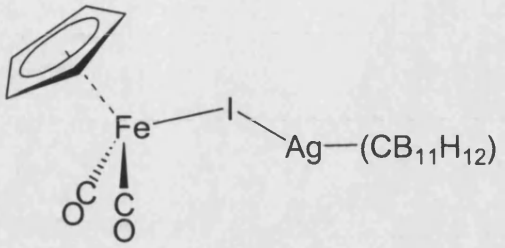

Figure 1.25: Postulated halide bridged intermediate

The $[closo\text{-}CB_{11}H_{12}]^-$ anion in the final product is coordinated via an agostic B-H-Fe interaction, again from the most basic B(12) vertex. The ^1H NMR spectra of $[Fe(Cp)(CO)_2(closo\text{-}CB_{11}H_{12})]$, and the closely related $[Fe(Cp)(CO)_2(closo\text{-}CB_9H_{10})]$, show that agostic binding of the anion to the metal persists in solution.[17] The ^1H NMR spectrum of $[Fe(Cp)(CO)_2(closo\text{-}CB_{11}H_{12})]$ also shows the presence of two different isomers, due to binding of the cage via the antipodal boron or the chemically equivalent lower pentagonal belt borons (Figure 1.26).

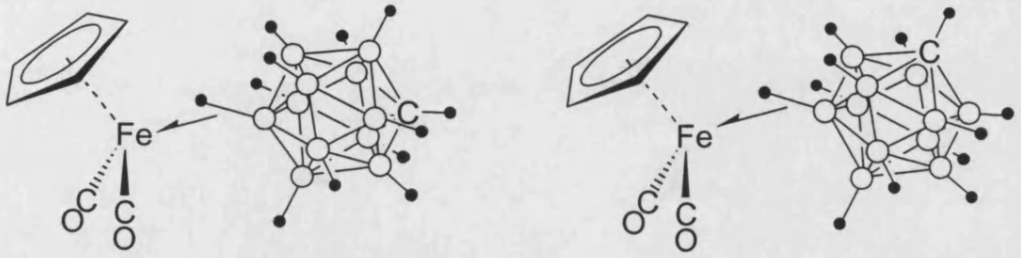

$[Fe(Cp)(CO)_3(\mathbf{12\text{-}\mu\text{-}H}\text{-}CB_{11}H_{11})]$ $[Fe(Cp)(CO)_3(\mathbf{7\text{-}\mu\text{-}H}\text{-}CB_{11}H_{11})]$

Figure 1.26: The two structural isomers of $[Fe(Cp)(CO)_2(x\text{-}\mu\text{-}H\text{-}CB_{11}H_{11})]$ (x = 7, 12)

Treatment of Vaska's complex, $[IrCl(CO)(PPh_3)_2]$, with $[Ag(CB_{11}H_{12})]$ or $[Ag(CB_{11}H_6Br_6)]$ does not result in the halide abstraction of chlorine.[34, 104] Instead a

metal-metal adduct is formed (Figure 1.27), which is a consequence of the anion's low nucleophilicity hindering the displacement of $[Cl]^-$.

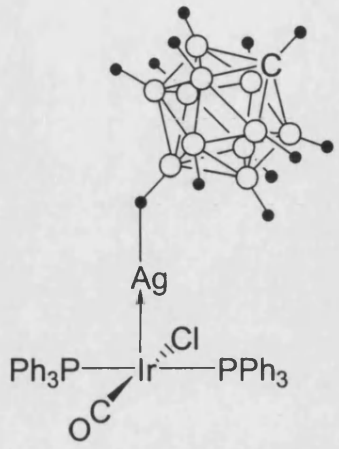

Figure 1.27: Adduct of $[Ag(CB_{11}H_{12})]$ and $[IrCl(CO)(PPh_3)_2]$

All of the previous examples show a metal interaction with one B-H vertex. However, the $[closo\text{-}CB_{11}H_{12}]^-$ anion can also bind to a metal *via* two or three B-H vertices. Because of the large size of the anion the number of metal-cage bonds is heavily dependant on the steric environment around the metal, elegantly displayed by Jordan *et. al* using some zirconium (IV) compounds. The oxidative cleavage of zirconium alkyls using $[Ag(CB_{11}H_{12})]$ as a one electron oxidant resulted in the formation of a range of compounds (equations 1.18 and 1.19), displayed in Figure 1.28.[91]

$$[(C_5H_4R')_2ZrR_2] + Ag[CB_{11}H_{12}] \longrightarrow [(C_5H_4R')_2Zr(R)(CB_{11}H_{12})] + {}^1/_2R\text{-}R + Ag^0 \quad (1.18)$$

1: $R = \eta^2\text{-}CH_2Ph$; $R' = H$

2: $R = CH_3$; $R' = CH_3$

$$[Cp^*Zr(CH_3)_3] + Ag[CB_{11}H_{12}] \longrightarrow [Cp^*Zr(CH_3)_2(CB_{11}H_{12})] + {}^1/_2CH_3CH_3 + Ag^0 \quad (1.19)$$

3

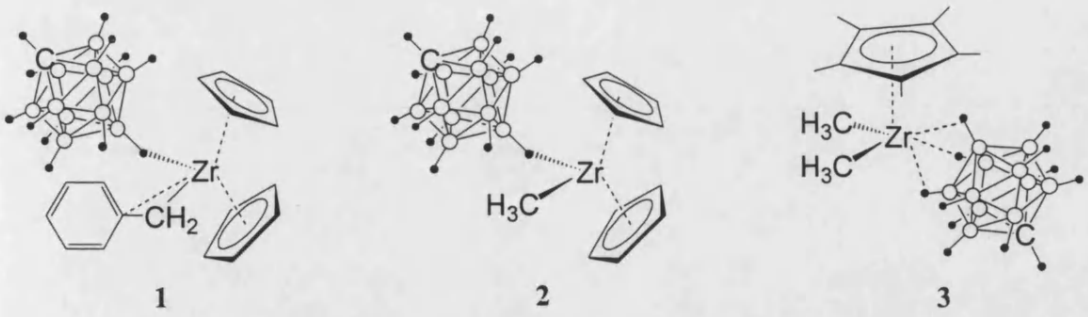

1 2 3

Figure 1.28: Structure of complexes **1**, **2** and **3**

The (η^2-CH_2Ph) group in **1** is bound to the metal through the methylene carbon and phenyl π system.[105] Compounds **1** and **2** have sufficient steric bulk around the metal to force the carborane to bond to the metal in an η^1 fashion, with a more linear B-H-Zr bond angle for **1** (*ca.* 159°) compared to **2** (*ca.* 123°), reflecting more steric crowding of the metal centre in **1**. The carborane in **3** coordinates in a tridentate manner because of insufficient steric shielding around the zirconium atom to dictate the way in which the cage can bind.

There have been a few examples isolated of [*closo*-$CB_{11}H_{12}]^-$ binding in an η^2 fashion, using square planar platinum and rhodium metals. A series of platinum compounds, with the general formula [Pt(L-L)($CB_{11}H_{12}$)] (L-L = chelating diphosphine) have been synthesised.[106] The compound [Rh(COD)($CB_{11}H_{12}$)] (COD = cyclooctadiene) (Figure 1.29) was prepared by treatment of $[Rh(Cl)(COD)]_2$ with 2 equivalents of [Ag($CB_{11}H_{12}$)].[107] Both of these systems show a distorted square planer coordination sphere around the metal, with the carborane bonded via two B-H-Metal bonds that display all the typical features of agostic B-H interactions in the solid state and solution (eg. close B-H-M interactions in the solid state and upfield shift of coordinated hydrides in the ^{1}H NMR spectrum).

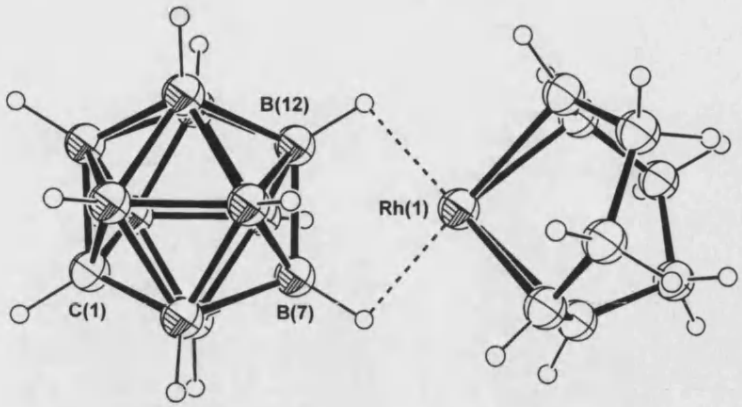

Figure 1.29: Crystal strucure of $Rh(COD)(CB_{11}H_{12})$[107]

(Ellipsoids are drawn at the 30% probability level)

The only structurally characterised example of a *substituted* [*closo*-$CB_{11}H_{12}$]$^-$ anion directly bound to a transition metal centre is [Fe(TPP)(*closo*-$CB_{11}H_6Br_6$)], prepared from the reaction of [Fe^{II}(TPP)] with one equivalent of the radical salt [$(BrC_6H_4)_3N^{\bullet}$][$CB_{11}H_6Br_6$].[65] The crystal structure shows the carborane anion bound to iron via Br(7) as opposed to Br(12) (Figure 1.30), because the antipodal bromine is too sterically hindered by the surrounding bromines. This is in contrast to [*closo*-$CB_{11}H_{12}$]$^-$ for which the antipodal B-H vertex interacts in [Fe(TPP)($CB_{11}H_{12}$)]

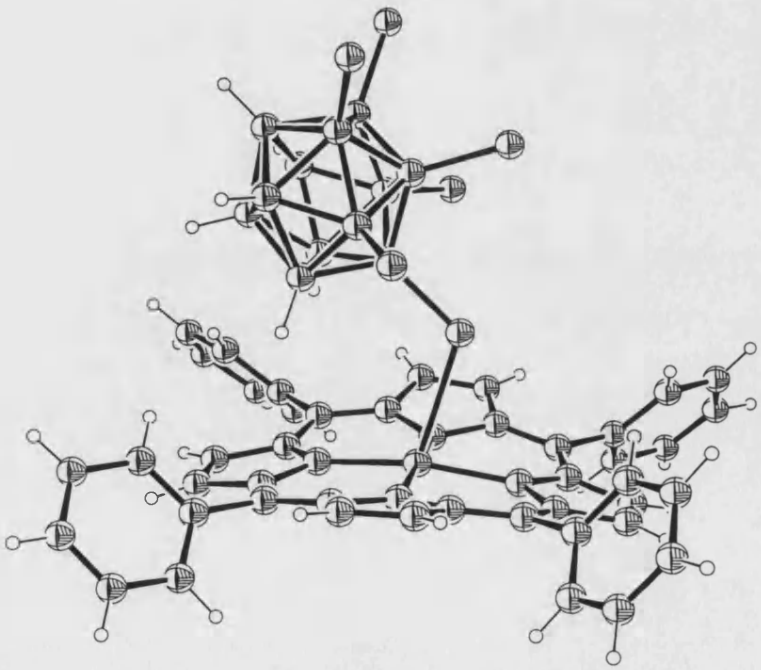

Figure 1.30: Crystal structure of [Fe(TPP)($CB_{11}H_6Br_6$)] [65]

(Thermal ellipsoids drawn at 30% probability level)

1.10 Catalytic Species Containing [*closo*-$CB_{11}H_{12}$]$^-$ and its Derivatives

The evaluation of the performance of catalysts containing [*closo*-$CB_{11}H_{12}$]$^-$ in alkene polymerisation reactions has been studied using compounds **1**, **2**, **3** (equations 1.18 and 1.19).[91] The most reactive of these species, **1** (Figure 1.28), polymerises ethylene in toluene solutions. As discussed previously, the less sterically bulky compound **2** contains a stronger metal-cage interaction and is less reactive in polymerisation than compound **1**, but can still oligomerise propene. Complex **3** does not polymerise or oligomerise alkenes at an appreciable rate, suggesting that η^3 coordination of a carborane cage makes it a lot less labile than when bound in an η^1 fashion, as is the case for **1** and **2**, blocking vacant sites needed for alkene coordination. Attempts have been made to use the related [$(Cp)_2Zr(\eta^2$-C,N-C{=N^{t}Bu}$CH_3)(CB_{11}H_{12})$] complex for the regioselective acetylation of alkynes and alkenes.[108] Initial reactions showed good reactivity but it is thermally sensitive, air sensitive and reacts with chlorinated solvents so a more robust complex containing the [$(CH_3)B(C_6F_5)_3$]$^-$ anion was used instead.

Until the work presented in this thesis, only two examples of comparative studies on the catalytic performance of [*closo*-$CB_{11}H_{12}$]$^-$ against other weakly coordinating anions had been reported. Rhodium complexes with nitrogen containing ligands (Figure 1.29) can catalyse aryl transfer to aldehydes (equation 1.20).[109] For this reaction, the counterions were ranked in the order [*closo*-$CB_{11}H_{12}$]$^-$ > $[PF_6]^-$ > $[BF_4]^-$ > $[OTf]^-$ in terms of their catalytic activity. [*closo*-$CB_{11}H_6Br_6$]$^-$ was not included in this study.

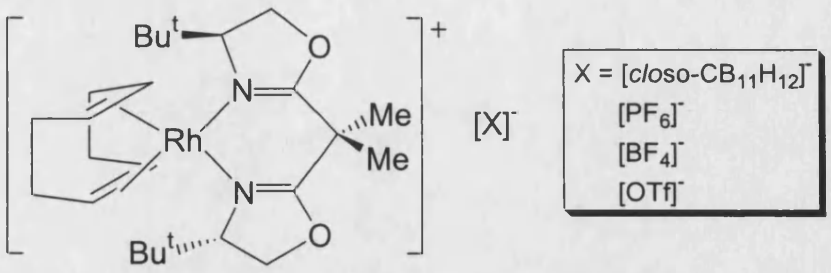

Figure 1.29: Rhodium catalysts used in aryl transfer to aldehydes

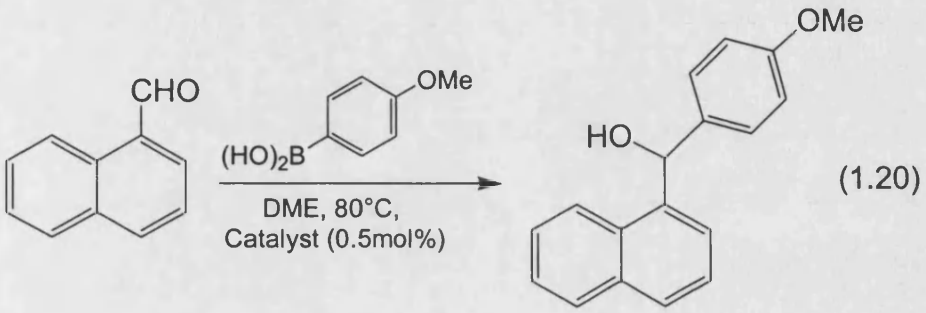

Another study has been performed on the rate of photoacid generation from diaryl iodonium salts containing weakly coordinating anions.[110] These iodonium salts are used as initiators for cationic polymerisation reactions. Figure 1.30 displays the structures of the initiators used in the reaction and equations 1.21 and 1.22 shows the reaction to form HX.

$$[Ar\text{-}I\text{-}Ar']^+[X]^- \xrightarrow{h\nu} [Ar\text{-}I]^{+\cdot}[X]^- + [Ar']^{\cdot} \quad (1.21)$$

$$[Ar\text{-}I]^{+\cdot}[X]^- + RH \longrightarrow Ar\text{-}I + [R]^{\cdot} + HX \quad (1.22)$$

The borate anions included in this study (compounds **4**, **5** and **7**) are thought to be some of the most weakly coordinating known because of the delocalisation of the charge over such a large molecule, similar to carboranes. The results showed the initiator activities decrease in the order **8** > **7** > **4** > **6** > **9** > **5** > **10**.

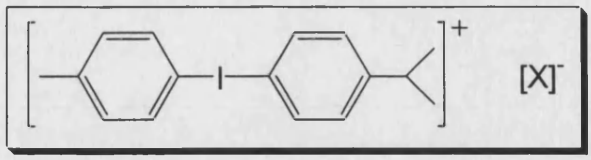

[X]$^-$

Imidazolide **4**: $[(C_6F_5)_3B{-}N\bigcirc N{-}B(C_6F_5)_3]^-$

Dianion **5**: 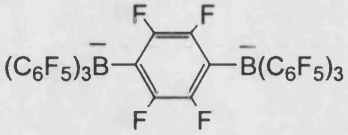

Carborane **6**: [*closo*-$CB_{11}H_6Br_6$]$^-$

Borate **7**: $[B(C_6F_5)_4]^-$

Gallate **8**: $[Ga(C_6F_5)_4]^-$

Antimonate **9**: $[SbF_6]^-$

Chloride **10**: $[Cl]^-$

Figure 1.30: Structure of initiators

The compound [$Li(CB_{11}Me_{12})$] has been used to generate a Li^+ cation stabilised only by solvent interactions making it a potent electrophile. Lithium cations are used for a number of organic transformations and this species has been used as a catalyst for pericyclic rearrangement reactions and displays very high rates of rearrangment (Figure 1.31).[111]

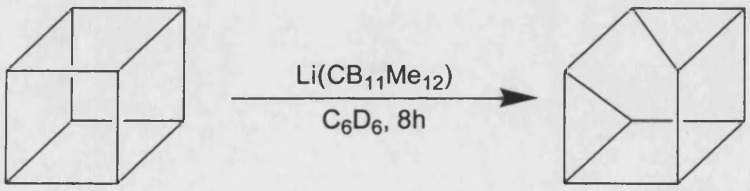

Figure 1.31: Rearrangement of cubane to cuneane

1.11 Summary

The chemical stability and weak nucleophilicity of a wide range of carborane monoanions has been presented. There are only a few examples of well characterised transition metal complexes of [*closo*-$CB_{11}H_{12}]^-$, and little work has been published on the transition metal chemistry of these monocarborane anions. The formidable array of [*closo*-$CB_{11}H_{12}$] derivatives developed recently, including the peralkyl- and perfluoro- carborane anions, show great promise as candidates for the title of most weakly coordinating anion. Once reliable synthetic strategies have been developed for metal complexation of these anions, there is a wealth of transition metal chemistry to be discovered. Applications range from improvements in rates for Lewis acid mediated catalytic reactions to generation of complexes that cannot be isolated with the more nucleophilic, less stable anions available at present. This thesis will detail synthetic strategies for the isolation of some well defined novel transition metal compounds containing [*closo*-$CB_{11}H_{12}]^-$ and its derivatives, and for the first time compare their reactivity with analogous complexes containing more traditional weakly coordinating anions.

1.12 References

1 W. L. Jolly, *Inorg. Synth.* **1968**, *11*, 19.
2 R. Wilczynski, L. G. Sneddon, *J. Am. Chem. Soc.* **1980**, *102*, 2857.
3 B. Stibr, T. Jelinek, Z. Janousek, S. Hermanek, E. Drdakova, Z. Plzak, J. Plesek, *Chem. Commun.* **1987**, 1106.
4 R. Hoffmann, *Angew. Chem. Int. Ed.* **1982**, *21*, 711.
5 K. Wade, *Adv. Inorg. Chem. Radiochem.* **1976**, *18*, 1.
6 M. J. S. Dewar, M. L. McKee, *Inorg. Chem.* **1980**, *19*, 2662.
7 M. L. McKee, *J. Am. Chem. Soc.* **1997**, *119*, 4220.
8 P. von R. Schleyer, K. Najafian, *Inorg. Chem.* **1998**, *37*, 3454.
9 W. H. Knoth, Jr., *J. Am. Chem. Soc.* **1967**, *89*, 1274.
10 D. E. Hyatt, F. R. Scholer, L. J. Todd, J. L. Warner, *Inorg. Chem.* **1967**, *6*, 2229.
11 W. H. Knoth, Jr., *Inorg. Chem.* **1971**, *10*, 598.
12 J. Plesek, T. Jelinek, B. Stibr, S. Hermanek, *Chem. Commun.* **1988**, 348.
13 T. Jelinek, B. Stibr, J. Holub, M. Bakardjiev, D. Hnyk, D. L. Ormsby, C. A. Kilner, M. Thornton-Pett, *Chem. Commun.* **2001**, 1756.
14 B. Stibr, O. L. Tok, W. Milius, M. Bakardjiev, J. Holub, D. Hnyk, B. Wrackmeyer, *Angew. Chem. Int. Ed.* **2002**, *41*, 2126.
15 S. R. Prince, R. Schaeffer, *Chem. Commun.* **1968**, 451.
16 Z. Xie, D. J. Liston, T. Jelinek, V. Mitro, R. Bau, C. A. Reed, *Chem. Commun.* **1993**, 384.
17 S. V. Ivanov, J. J. Rockwell, S. M. Miller, O. P. Anderson, K. A. Solntsev, S. H. Strauss, *Inorg. Chem.* **1996**, *35*, 7882.
18 T. Jelinek, B. Stibr, J. Plesek, M. Thornton-Pett, J. D. Kennedy, *J. Chem. Soc., Dalton Trans.* **1997**, 4231.
19 W. L. Jolly, *Inorg. Synth.* **1968**, *11*, 33.
20 W. L. Jolly, *Inorg. Synth.* **1968**, *11*, 35.
21 W. L. Jolly, *Inorg. Synth.* **1968**, *11*, 39.
22 K. Shelly, D. C. Finster, Y. J. Lee, W. R. Scheidt, C. A. Reed, *J. Am. Chem. Soc.* **1985**, *107*, 5955.
23 A. Franken, B. T. King, J. Rudolph, P. Rao, B. C. Noll, J. Michl, *Collect. Czech. Chem. Commun.* **2001**, *66*, 1238.
24 G. B. Dunks, K. P. Ordonez, *Inorg. Chem.* **1978**, *17*, 1514.
25 T. Jelinek, P. Baldwin, W. R. Scheidt, C. A. Reed, *Inorg. Chem.* **1993**, *32*, 1982.
26 T. Jelinek, J. Plesek, S. Hermanek, B. Stibr, *Collect. Czech. Chem. Commun.* **1986**, *51*, 819.
27 Z. Xie, C.-W. Tsang, E. T.-P. Sze, Q. Yang, D. T. W. Chan, T. C. W. Mak, *Inorg. Chem.* **1998**, *37*, 6444.
28 Z. Xie, C.-W. Tsang, F. Xue, T. C. W. Mak, *Inorg. Chem.* **1997**, *36*, 2246.
29 Z. Xie, J. Manning, R. W. Reed, R. Mathur, P. D. W. Boyd, A. Benesi, C. A. Reed, *J. Am. Chem. Soc.* **1996**, *118*, 2922.
30 F. S. Mair, J. H. Morris, D. F. Gaines, D. Powell, *J. Chem. Soc., Dalton Trans.* **1993**, 135.

31 S. V. Ivanov, A. J. Lupinetti, S. M. Miller, O. P. Anderson, K. A. Solntsev, S. H. Strauss, *Inorg. Chem.* **1995**, *34*, 6419.
32 S. V. Ivanov, A. J. Lupinetti, K. A. Solntsev, S. H. Strauss, *J. Fluorine Chem.* **1998**, *89*, 65.
33 C.-W. Tsang, Q. Yang, E. T.-P. Sze, T. C. W. Mak, D. T. W. Chan, Z. Xie, *Inorg. Chem.* **2000**, *39*, 5851.
34 Z. Xie, T. Jelinek, R. Bau, C. A. Reed, *J. Am. Chem. Soc.* **1994**, *116*, 1907.
35 I. A. Koppel, P. Burk, I. Koppel, I. Leito, T. Sonoda, M. Mishima, *J. Am. Chem. Soc.* **2000**, *122*, 5114.
36 Z. Xie, R. Bau, C. A. Reed, *Chem. Commun.* **1994**, 2519.
37 Z. Xie, R. Bau, C. A. Reed, *Inorg. Chem.* **1995**, *34*, 5403.
38 C. A. Reed, K.-C. Kim, R. D. Bolskar, L. J. Mueller, *Science* **2000**, *289*, 101.
39 C. A. Reed, N. L. P. Fackler, K.-C. Kim, D. Stasko, D. R. Evans, P. D. W. Boyd, C. E. F. Rickard, *J. Am. Chem. Soc.* **1999**, *121*, 6314.
40 C. A. Reed, *Acc. Chem. Res.* **1998**, *31*, 325.
41 J. W. Bausch, G. K. S. Prakash, G. A. Olah, D. S. Tse, D. C. Lorents, Y. K. Bae, R. Malhotra, *J. Am. Chem. Soc.* **1991**, *113*, 3205.
42 S. H. Strauss, *Chem. Rev.* **1993**, *93*, 927.
43 M. Brookhart, M. L. H. Green, *J. Organomet. Chem.* **1983**, *250*, 395.
44 M. R. Rhodes, K. R. Mann, *Inorg. Chem.* **1984**, *23*, 2053.
45 G. A. Lawrance, *Chem. Rev.* **1993**, *93*, 17.
46 W. H. Hersh, *Inorg. Chem.* **1990**, *29*, 713.
47 R. V. Honeychuck, W. H. Hersh, *Inorg. Chem.* **1989**, *28*, 2869.
48 L. C. Ananias de Caralho, M. Dartiguenave, Y. Dartiguenave, A. L. Beauchamp, *J. Am. Chem. Soc.* **1984**, *106*, 6848.
49 X. Yang, C. L. Stern, T. J. Marks, *Organomet.* **1991**, *10*, 840.
50 M. Brookhart, B. Grant, A. F. Volpe, *Organomet.* **1992**, *11*, 3920.
51 J. Powell, A. Lough, T. Saeed, *J. Chem. Soc., Dalton Trans.* **1997**, 4137.
52 P. V. Bonnesen, C. L. Puckett, R. V. Honeychuck, W. H. Hersh, *J. Am. Chem. Soc.* **1989**, *111*, 6070.
53 W. V. Konze, B. L. Scott, G. J. Kubas, *Chem. Commun.* **1999**, 1807.
54 M. Brookhart, F. C. Rix, J. M. DeSimone, J. C. Barborak, *J. Am. Chem. Soc.* **1992**, *114*, 5895.
55 M. Brookhart, S. J. Sabo-Etienne, *J. Am. Chem. Soc.* **1991**, *113*, 2777.
56 L. Jia, X. Yang, C. L. Stern, T. J. Marks, *Organomet.* **1997**, *16*, 842.
57 W. E. Piers, T. Chivers, *Chem. Soc. Rev.* **1997**, *26*, 345.
58 C. E. Y.-X., T. J. Marks, *Chem. Rev.* **2000**, *100*, 1391.
59 K. Shelly, C. A. Reed, Y. J. Lee, W. R. Scheidt, *J. Am. Chem. Soc.* **1986**, *108*, 3117.
60 Z. Xie, R. Bau, C. A. Reed, *Angew. Chem. Int. Ed.* **1994**, *33*, 2433.
61 C. A. Reed, *Acc. Chem. Res.* **1998**, *31*, 133.
62 Z. Xie, R. Bau, A. Benesi, C. A. Reed, *Organomet.* **1995**, *14*, 3933.
63 C. A. Reed, Z. Xie, R. Bau, A. Benesi, *Science* **1993**, *262*, 402.
64 C. A. Reed, F. Guiset, *J. Am. Chem. Soc.* **1996**, *118*, 3281.
65 D. R. Evans, C. A. Reed, *J. Am. Chem. Soc.* **2000**, *122*, 4660.
66 J. B. Lambert, S. J. Zhang, *Chem. Commun.* **1993**, 383.
67 S. V. Ivanov, J. J. Rockwell, O. G. Polyakov, C. M. Gaudinski, O. P. Anderson, K. A. Solntsev, S. H. Strauss, *J. Am. Chem. Soc.* **1998**, *120*, 4224.
68 B. Gruener, Z. Janousek, B. T. King, J. N. Woodford, C. H. Wang, V. Vsetecka, J. Michl, *J. Am. Chem. Soc.* **1999**, *121*, 3122.

69 W. Jiang, C. B. Knobler, C. B. Curtis, C. E. Curtis, M. D. Mortimer, M. F. Hawthorne, *Inorg. Chem.* **1995**, *34*, 3491.
70 T. Peymann, C. B. Knobler, M. F. Hawthorne, *Inorg. Chem.* **1998**, *37*, 1544.
71 B. T. King, Z. Janousek, B. Gruener, M. Trammell, B. C. Noll, J. Michl, *J. Am. Chem. Soc.* **1996**, *118*, 3313.
72 C.-W. Tsang, Z. Xie, *Chem. Commun.* **2000**, 1839.
73 B. King, I. Zharov, J. Michl, *Chemical Innovations* **2001**, *December 2001*, 23.
74 B. T. King, B. C. Noll, J. Michl, *Collect. Czech. Chem. Commun.* **1999**, *64*, 1001.
75 B. T. King, B. C. Noll, A. J. McKinley, J. Michl, *J. Am. Chem. Soc.* **1996**, *118*, 10902.
76 M. Kira, T. Hino, H. J. Sakurai, *J. Am. Chem. Soc.* **1992**, *114*, 6697.
77 J. B. Lambert, S. Zhang, S. M. Ciro, *Organomet.* **1994**, *13*, 2430.
78 I. Zharov, B. T. King, Z. Havlas, A. Pardi, J. Michl, *J. Am. Chem. Soc.* **2000**, *122*, 10253.
79 B. T. King, J. Michl, *J. Am. Chem. Soc.* **2000**, *122*, 10255.
80 B. D. Kybett, S. Carroll, P. Natalis, B. W. Bonnell, J. L. Margrave, J. L. Franklin, *J. Am. Chem. Soc.* **1966**, *88*, 626.
81 Z. Xie, C.-W. Tsang, F. Xue, T. C. W. Mak, *J. Organomet. Chem.* **1999**, *577*, 197.
82 T. Jelinek, C. A. Kilner, M. Thornton-Pett, J. D. Kennedy, *Chem. Commun.* **2001**, 1790.
83 A. Franken, C. A. Kilner, M. Thornton-Pett, J. D. Kennedy, *J. Organomet. Chem.* **2002**, *657*, 176.
84 J. Plesek, T. Jelinek, B. Stibr, *Polyhedron* **1984**, *3*, 1351.
85 K. Maly, V. Subrtova, V. Petricek, *Acta Cryst.* **1987**, *C43*, 593.
86 J. H. Morris, K. W. Henderson, V. A. Ol'shevskaya, *J. Chem. Soc., Dalton Trans.* **1998**, 1951.
87 D. Stasko, C. A. Reed, *J. Am. Chem. Soc.* **2002**, *124*, 1148.
88 K. Maeda, H. Janchenova, A. Lhotsky, I. Stibor, J. Budka, V. Marecek, *J. Electroanal. Chem.* **2001**, *516*, 103.
89 D. J. Liston, Y. J. Lee, W. R. Scheidt, C. A. Reed, *J. Am. Chem. Soc.* **1989**, *111*, 6643.
90 R. S. Mathur, T. Drovetskaya, C. A. Reed, *Acta Cryst.* **1997**, *C53*, 881.
91 D. J. Crowther, S. L. Borkowsky, D. Swenson, T. Y. Meyer, R. F. Jordan, *Organomet.* **1993**, *12*, 2897.
92 I. A. Zakharova, *Coord. Chem. Rev.* **1982**, *43*, 313.
93 L. Mole, J. L. Spencer, N. Carr, A. G. Orpen, *Organomet.* **1991**, *10*, 49.
94 N. Carr, L. Mole, A. G. Orpen, J. L. Spencer, *J. Chem. Soc., Dalton Trans.* **1992**, 2653.
95 Y. Souma, J. Iyoda, H. Sano, *Inorg. Chem.* **1976**, *35*, 968.
96 J. J. Rack, J. Webb, S. H. Strauss, *Inorg. Chem.* **1996**, *35*, 277.
97 S. M. Ivanova, S. V. Ivanov, S. M. Miller, O. P. Anderson, K. A. Solntsev, S. H. Strauss, *Inorg. Chem.* **1999**, *38*, 3756.
98 A. J. Lupinetti, M. D. Havighurst, S. M. Miller, O. P. Anderson, S. H. Strauss, *J. Am. Chem. Soc.* **1999**, *121*, 11920.
99 G. P. Gupta, G. Lang, Y. J. Lee, W. R. Scheidt, K. Shelly, C. A. Reed, *Inorg. Chem.* **1987**, *26*, 3022.
100 C. A. Koch, C. A. Reed, G. A. Brewer, N. P. Rath, W. R. Scheidt, G. Gupta, G. Lang, *J. Am. Chem. Soc.* **1989**, *111*, 7645.

101 G. P. Gupta, G. Lang, C. A. Koch, B. Wang, W. R. Scheidt, C. A. Reed, *Inorg. Chem.* **1990**, *29*, 4234.
102 D. R. Evans, R. S. Mathur, K. Heerwegh, C. A. Reed, Z. Xie, *Angew. Chem. Int. Ed.* **1997**, *36*, 1335.
103 Z. Xie, B.-M. Wu, T. C. W. Mak, J. Manning, C. A. Reed, *J. Chem. Soc., Dalton Trans.* **1997**, 1213.
104 D. J. Liston, C. A. Reed, C. W. Eigenbrot, W. R. Scheidt, *Inorg. Chem.* **1987**, *26*, 2739.
105 R. F. Jordan, R. E. LaPointe, C. S. Bajgur, S. F. Echols, R. D. Willett, *J. Am. Chem. Soc.* **1987**, *109*, 4111.
106 G. S. Mhinzi, S. A. Litster, A. D. Redhouse, J. L. Spencer, *J. Chem. Soc., Dalton Trans.* **1991**, 2769.
107 A. S. Weller, M. F. Mahon, J. W. Steed, *J. Organomet. Chem.* **2000**, *614-615*, 113.
108 A. S. Guram, R. F. Jordan, *J. Org. Chem.* **1993**, *58*, 5595.
109 C. Moreau, C. Hague, A. S. Weller, C. G. Frost, *Tet. Lett.* **2001**, *42*, 6957.
110 K. Ren, J. H. Malpert, H. Li, H. Gu, D. C. Neckers, *Macromolecules* **2002**, *35*, 1632.
111 S. Moss, B. T. King, A. de Meijere, S. I. Kozhushkov, P. E. Eaton, J. Michl, *Organic Letters* **2001**, *3*, 2375.

2 SILVER SALT METATHESIS REACTIONS

2.1 Introduction

Silver(I) salt metathesis is one of the most widely used methods for introducing an anion into a metal's coordination sphere.[1, 2] It requires a labile metal halide and a silver derivative of the anion. The precipitation of silver halide provides a large thermodynamic driving force towards the products of reaction (Equation 2.1), producing a metal complex with the anion bound to the metal. If the anion is a

$$L_nMX + AgY \longrightarrow L_nMY + AgX_{(s)} \quad (2.1)$$

Y = Weakly coordinating anion
X = Halide

weakly coordinating one (such as $[BF_4]^-$, $[PF_6]^-$, $[ClO_4]^-$ or $[BPh_4]^-$) it can then in turn be displaced by another anion, or a two electron donor ligand such as PR_3, alkene, alkyne, THF or CO making it a very powerful tool in the synthesis of cationic or neutral complexes. Examples of complexes synthesised via this route include $[FeCp(CO)_2L]^+$ (L = alkene,[3] alkyne,[4] and THF[5]), $[Rh(PPh_3)(CO)_3]^+$,[6] and the $[Mn(CO)_3(CH_3CN)_3]^+$ cation, generated from the reaction of $[Ag(PF_6)]$ and $[Mn(CO)_5Br]$, that has been shown to be a useful precursor for cationic manganese carbonyl compounds such as $[fac\text{-}Mn(CO)_3(PMe_2Ph)_2(CH_3CN)]^+$ and $[fac\text{-}Mn(CO)_3\{P(OMe)_3\}(CH_3CN)_2]^+$.[7]

The silver induced halide abstraction of alkyl halides was studied in detail during the 1960s and 1970s, from which a number of complex rate laws were determined.[8] In

contrast, the silver salt metathesis of transition metal halides has received very little mechanistic attention over the years. This is perhaps surprising given the ubiquitous use of this technique in producing a wide and varied range of transition metal complexes. The earliest foray into the elucidation of the mechanism of silver salt metathesis was by Graham in 1981.[9] The reaction between $[FeCp(CO)_2I]$ and $Ag(BF_4)$ in CH_2Cl_2 ultimately yields $[FeCp(CO)_2(BF_4)]$, but the normally very quick silver salt metathesis process is slowed so that complete reaction takes about two hours. It was therefore possible to monitor the reaction using ^1H NMR spectroscopy, which detected the presence of a number of reaction intermediates. These intermediates are postulated to be $[FeCp(CO)_2IAg][BF_4]$ and $[\{FeCp(CO)_2\}_2I][BF_4]$, and monitoring their relative concentrations allowed elucidation of a reaction mechanism. The first part of the mechanism is the rapid formation of $[FeCp(CO)_2IAg][BF_4]$ which decomposes to form $[FeCp(CO)_2(BF_4)]$ and AgI (Equations 2.2 and 2.3). The $[FeCp(CO)_2(BF_4)]$ generated then reacts with another equivalent of $[FeCp(CO)_2I]$, which is in excess in solution due to the poor solubility of $Ag(BF_4)$ in CH_2Cl_2, to yield $[\{FeCp(CO)_2\}_2I][BF_4]$ (Equation 2.4).

$Fp = \{FeCp(CO)_2\}^+$

$$FpI + Ag(BF_4) \xrightarrow{\text{Fast}} [FpIAg][BF_4] \qquad (2.2)$$

$$[FpIAg][BF_4] \xrightarrow{\text{Slow}} [Fp][BF_4] + AgI \qquad (2.3)$$

$$[Fp][BF_4] + FpI \longrightarrow [Fp_2I][BF_4] \qquad (2.4)$$

The second part of the mechanism starts once all of the $[FeCp(CO)_2I]$ has been converted to $[\{FeCp(CO)_2\}_2I]^+$ (Equation 2.5).

$$[Fp_2I][BF_4] \rightleftharpoons FpI + [Fp][BF_4] \qquad (2.5)$$

The $[FeCp(CO)_2I]$ generated from equation 2.5 reacts immediately with the second equivalent of $[Ag(BF_4)]$, but the concentration of $[FeCp(CO)_2(BF_4)]$ can now increase as the concentration of $[FeCp(CO)_2I]$ has decreased because of the formation of $[\{FeCp(CO)_2\}_2I]^+$ and $[FeCp(CO)_2IAg]^+$.

A similar study on the same $[FeCp(CO)_2I]$ system using the weakly nucleophilic [*closo*-$CB_{11}H_{12}]^-$ anion instead of $[BF_4]^-$ was performed by Reed.[10] The reaction takes two weeks to reach completion, but this time only one intermediate is observed in the reaction mixture. It was characterised by IR and NMR spectroscopy as $[FeCp(CO)_2I{\cdot}Ag(CB_{11}H_{12})]$, written as the neutral adduct instead of the ionic $[FeCp(CO)_2I\text{-}Ag][CB_{11}H_{12}]$ because in the IR spectrum the ν(B-H) stretches of [*closo*-$CB_{11}H_{12}]^-$ is split, suggestive of anion coordination. At no time in the reaction was the presence of the intermediate $[\{FeCp(CO)_2\}_2I]^+$ detected, as seen when using $[BF_4]^-$. Attempts to induce its formation by reaction of $[FeCp(CO)_2I]$ and $[FeCp(CO)_3(CB_{11}H_{12})]$ do not work, implying that the carborane anion is actually strongly bound with respect to $[BF_4]^-$.

Incomplete silver halide metathesis is observed in the reaction of $[Ag(CB_{11}H_6Br_6)]$ with HCl in diethyl ether.[2] The reaction reaches only 25% completion due to the formation of $[H(OEt_2)_2][Ag_3(CB_{11}H_6Br_6)_4]$, that precipitates out of solution. This

compound has a polymeric chain structure in the solid state and is therefore not very soluble resulting in the cessation of the reaction. Concurrent to this observation of incomplete metathesis by Reed, is the presence of a thermodynamic barrier to metathesis when using silyl halides. The treatment of a silyl halide with silver perchlorate results in the instantaneous formation of the metathesis product (Equation 2.6). The same reaction with silver hexabromocarborane does not proceed (Equation 2.7), but can be reversed (Equation 2.8) once the metathesis product has been synthesised by an alternative route showing that thermodynamically the metathesis reaction is disfavoured.[11]

$$^{i}PrSiI + Ag(ClO_4) \xrightarrow{\text{toluene}} {}^{i}PrSi(OClO_3) + AgI_{(s)} \quad (2.6)$$

$$^{i}PrSiI + Ag(CB_{11}H_6Br_6) \xrightarrow{\text{toluene}} \text{no reaction} \quad (2.7)$$

$$^{i}PrSi(CB_{11}H_6Br_6) + AgI_{(s)} \xrightarrow{\text{toluene}} {}^{i}PrSiI + Ag(CB_{11}H_6Br_6) \quad (2.8)$$

The mechanism of chloride abstraction has also been studied using metal nitrosyl complexes of general formula $[Mo(NO)_2L_2Cl_2]$ (L = PPh_3, CH_3CN, pyridine, PhCN, CH_2=CHCN). Reaction of these compounds with the silver(I) salts of $[BF_4]^-$, $[ClO_4]^-$ and $[PF_6]^-$ were monitored using conductimetry, potentiometry, IR, NMR and UV/Vis spectroscopy. The titration of successive amounts of the silver salts to a solution of $[Mo(NO)_2L_2Cl_2]$ leads to quantitative and successive formation of mono- and di-cationic complexes in which the chloride has been replaced by solvent molecules (Figure 2.1). No intermediates in the formation of the cationic species were observed. The complexes are in equilibrium and addition of stochiometric amounts of chloride ions to solutions of the di-cationic complexes reforms the neutral bis-chloride

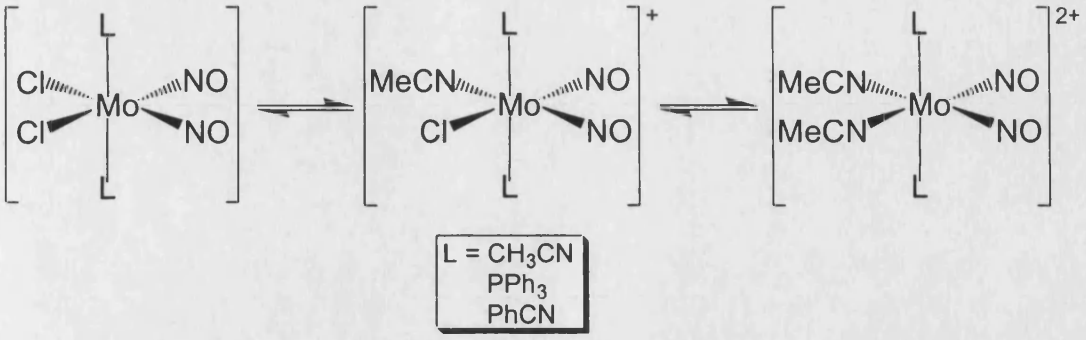

Figure 2.1: Formation of mono- and di-cationic complexes

complexes. Because of this equilibrium, it is not possible to isolate $[MoCl(NO)_2(PPh_3)_2(CH_3CN)]^+$ in a pure form as it disproportionates in solution to yield the dichloro and dicationic complexes.

A study on the kinetics of a silver salt metathesis reaction between a square planar platinum complex and $Ag(BF_4)$ (Equation 2.9) has recently been reported.[12]

$$[PtCl(Me)(N\text{-}N)] + Ag[BF_4] \xrightarrow{CH_3CN} [Pt(Me)(CH_3CN)(N\text{-}N)][BF_4] \qquad (2.9)$$

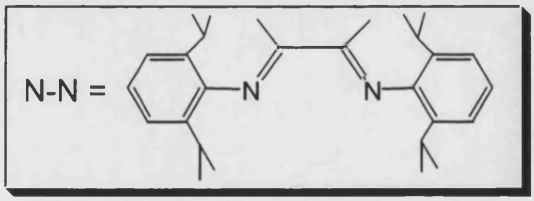

The reaction is slow, taking 24 hours to reach completion, and a reaction intermediate, $[\{Pt(Me)(N\text{-}N)Cl\}_2Ag]^+$, was isolated and structurally characterised. The kinetic study showed that, in solution, the initial reaction is the rapid formation of *two* intermediate complexes, both of which decompose slowly to yield the final metathesis product (Figure 2.2). However, the equilibria between the intermediate species and starting material are very fast, resulting in time averaged NMR signals even at low temperatures, precluding the observation of the solvent stabilised complex.

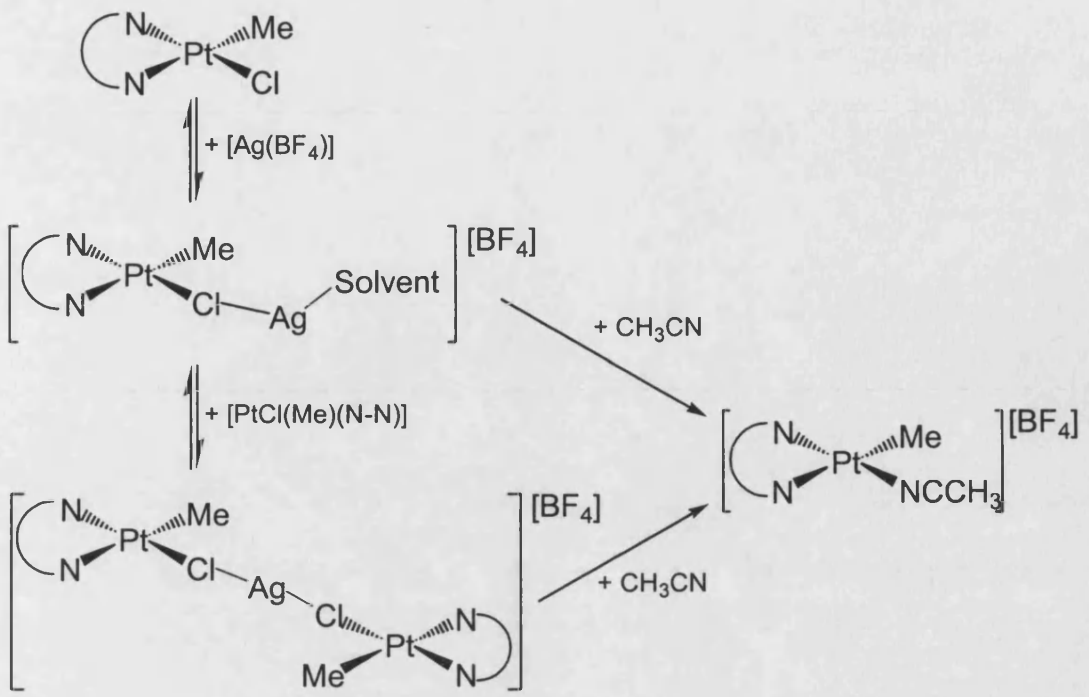

Figure 2.2: Proposed mechanism for the silver salt metathesis of [PtCl(Me)(N-N)]

Silver salt metathesis reactions proceed very smoothly in the majority of metal-ligand systems in which they are employed. However, there are several examples where metathesis reactions do not proceed smoothly. This can be for a number of reasons, including the formation of a stable silver-metal adduct species, only partial metathesis occurring, or there simply is an insufficient thermodynamic driving force for reaction. These situations tend to arise when using the silver(I) salts of weakly nucleophilic anions. The complex *trans*-$[PtCl_2(C_6F_5)_2][NBu_4]_2$ reacts with $Ag(NO_3)$ or $Ag(ClO_4)$ without any AgCl precipitation to give $[Pt_2Ag_2Cl_4(C_6F_5)_4][NBu_4]_2$.[13] The anionic portion of this complex is a dimer bridged by two silver atoms with Pt-Ag and Ag-Ag interactions.

An example of silver-metal adduct formation instead of metathesis is the generation of $[IrCl(CO)(PPh_3)_2 \cdot Ag(CB_{11}H_{12})]$ from the treatment of Vaska's complex,

$[IrCl(CO)(PPh_3)_2]$, with $Ag[CB_{11}H_{12}]$.[14] The stable Lewis acid-base adduct formed contains iridium bound to the silver through the lone pair in its d_{z^2} orbital (Figure 1.27, section 1.9.2).

Adduct formation as opposed to metathesis has also been observed when using the main group metals, tin and germanium. Treatment of $[\{(^nPr)_2ATl\}MCl]$ (M = Ge or Sn) with $[HB\{3,5\text{-}(CF_3)_2Pz\}_3][Ag(\eta^2\text{-toluene})]$ results in the formation of the 1:1 adduct $[HB\{3,5\text{-}(CF_3)_2Pz\}_3Ag\leftarrow M(Cl)\{(^nPr)_2ATl\}]$ (Figure 2.3).[15, 16] In comparison, if the same reaction is done with $[Ag(SO_3CF_3)]$ rapid metathesis occurs to generate $[\{(^nPr)_2ATl\}M][SO_3CF_3]$.

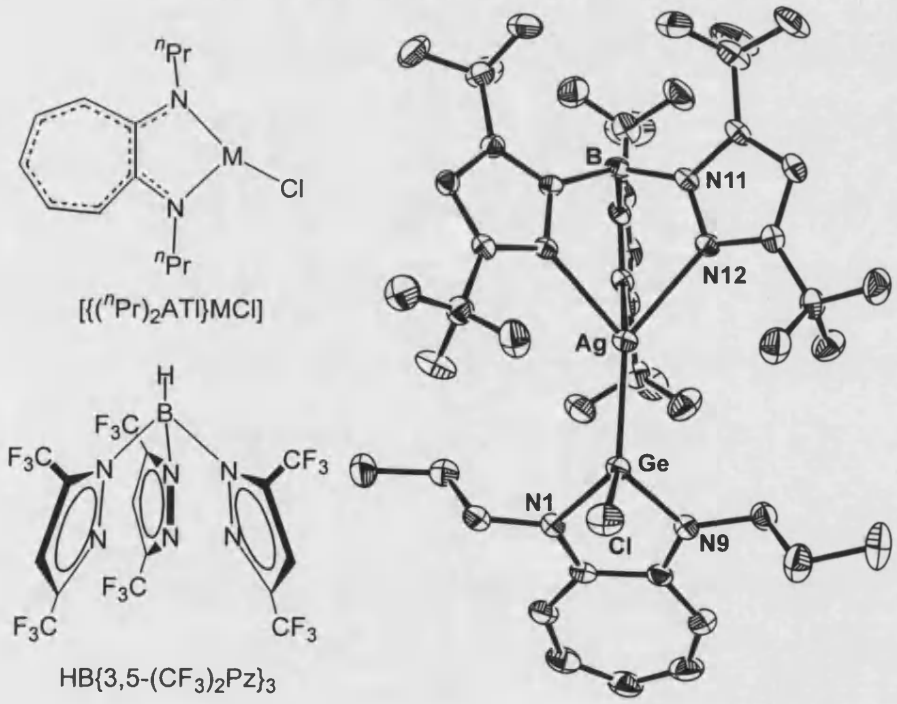

Figure 2.3: Crystal structure of $[HB\{3,5\text{-}(CF_3)_2Pz\}_3Ag\leftarrow Ge(Cl)\{(^nPr)_2ATl\}]$

This chapter will discuss the synthesis of a number of compounds using silver salt metathesis reactions with $[closo\text{-}CB_{11}H_{12}]^-$ and its derivatives. This work was started in 1999, when the only published work on the intermediates of reaction was on the

$\{FeCp(CO)_2\}^+$ system by Reed and Graham. However, none of these intermediates had been structurally characterised. Our goals were to try and isolate an intermediate in a silver salt metathesis reaction as well as to synthesise some novel transition metal complexes containing [*closo*-$CB_{11}H_6X_6]^-$ (X = H, Br). Examples of these anions coordinated to a transition metal centre are rare and it is important to find the best techniques for their synthesis, as well as determining how the anion binds and what properties the resulting species have. This chapter details the isolation and characterisation of the products and intermediates found in the reaction of $[MoCp(CO)_3X]$ (X = Cl, I) with $[Ag(CB_{11}H_6Y_6)]$ (Y = H, Br).

2.2 Results and Discussion

2.2.1 $[MoCp(CO)_3(x\text{-}\mu\text{-}H\text{-}CB_{11}H_{11})]$ (x = 7, 12)

Reaction of $[Mo(Cp)(CO)_3Cl]$ with one equivalent of $Ag(CB_{11}H_{12})$ in CH_2Cl_2 was monitored by IR spectroscopy. After 30 minutes, the two carbonyl stretching frequencies associated with the starting material (2056 and 1977cm^{-1}) were replaced by two stretching frequencies at higher frequency (2064 and 1980cm^{-1}). Continued stirring for a further 2 days results in the gradual precipitation of AgCl, and replacement of the these peaks in the carbonyl region of the IR spectrum by two CO stretches at an even higher wavenumber (2071 and 2001cm^{-1}). The AgCl precipitate was removed by careful filtration of the red solution formed through Celite, and red crystals grown in good yield by layering the reaction mixture with hexanes. The final product $[MoCp(CO)_3(x\text{-}\mu\text{-}H\text{-}CB_{11}H_{11})]$ (x = 7, 12), complex **I**, was fully characterised by X-ray crystallography, elemental analysis, IR and NMR spectroscopy.

The solid state structure of the zwitterionic complex **I** is show in Figure 2.4, with relevant bond lengths and angles in Table 2.1. The molybdenum adopts a four legged piano stool geometry with the carborane bound to the metal centre via a single B-H-Mo 3-centre-2-electron interaction. The X-ray diffraction data was of sufficient quality to be able to locate and freely refine the position of the bridging cage hydrogen (H12) in the electron difference map, while the carbon atom of the cage was located unambiguously by comparison of bond lengths and thermal parameters within the cage. The bond lengths and angles associated with the boron and carbon atoms of the carborane cage are unremarkable. The cage bonds, as expected, via the most basic, antipodal, B(12)-H(12) linkage [Mo(1)···B(12) 3.003(3) Å; Mo(1)-H(12) 1.92(3)Å]. The agostic nature of this bond to Mo(1) is demonstrated in solution by inspection of the NMR data discussed later, but evidence can be seen in the solid state by the movement of the B-H vector off the C(1)-B(12) axis by 18(1)°. This allows more efficient overlap of the bonding B(12)-H(12) σ electron pair with a suitable vacant orbital on the molybdenum centre, in addition to minimising the steric interaction between the cage and metal ligand set. The B(12)-H(12) bond length is the same as that seen in $[FeCp(CO)_3(CB_{11}H_{12})]$[10] [1.18(2)Å], but slightly shorter than other complexes where the cage is agostically bound and the hydrogen atom has also been freely refined which in both cases was 1.25Å.[14, 17] The B(12)-H(12)-Mo(1) bond angle of 153(2)° is similar to other M-H-B linkages where [*closo*-$CB_{11}H_{12}$]$^-$ is bound in an η^1 fashion and the hydrogen has been freely refined, eg. $[Fe(Cp)(CO)_2(CB_{11}H_{12})]$ 141(2)° and $[Fe(TPP)(CB_{11}H_{12})]$ 151(2)°. Both of these complexes also have the hydrogen 'tipped' off the C(1)-B(12) axis by 10° and 6° respectively (standard deviations unavailable).[10, 17]

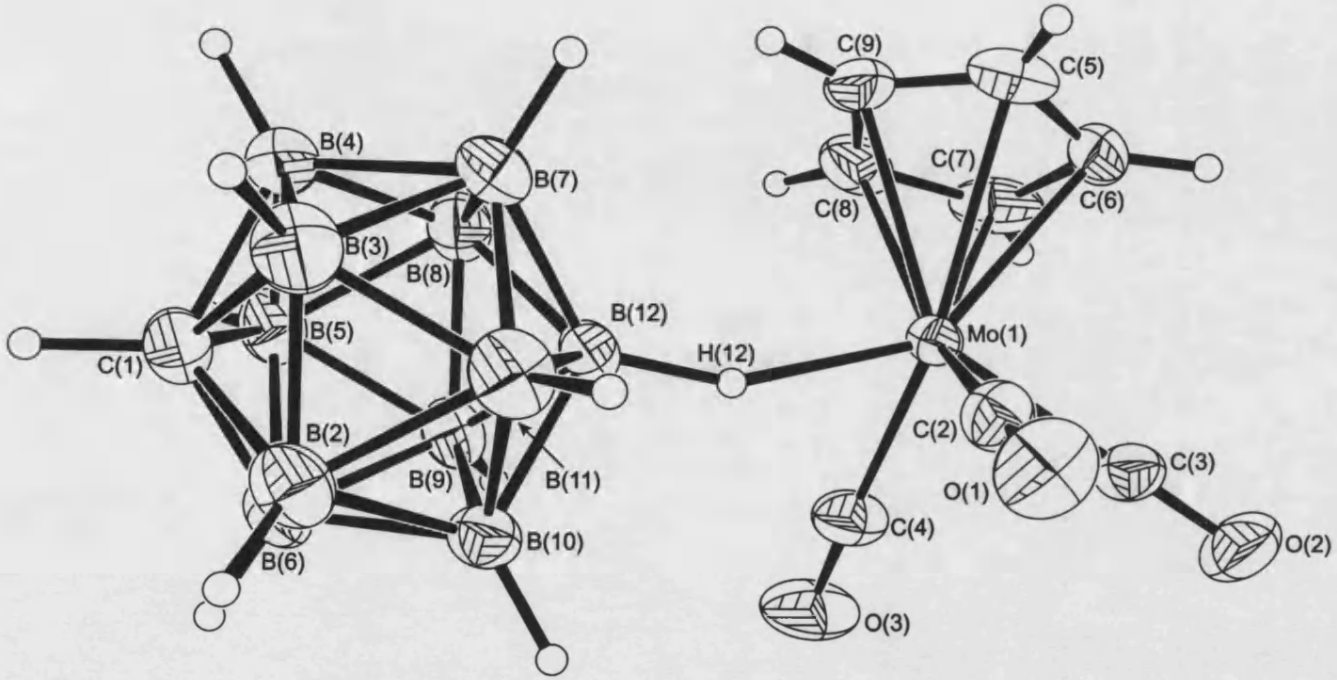

B(12)···Mo(1)	3.000(3) Å
B(12)-H(12)	1.18(3) Å
H(12)-Mo(1)	1.92(3) Å
B(12)-H(12)-Mo(1)	150(2)°
Mo(1)-B(12)-C(1)	176.4(1)°
C(1)-B(12)-H(12)	166(1)°

Table 2.1: Selected bond lengths and angles for complex **I**

Figure 2.4: Crystal structure of $[MoCp(CO)_3(CB_{11}H_{12})]$, **I** (ellipsoids drawn at 30% probability level)

The IR spectrum of **I** reveals the two expected CO stretching bands at 2071cm^{-1} and 2001cm^{-1}. These are shifted to a higher wavenumber than the starting material [$MoCp(CO)_3Cl$] (2056 and 1977cm^{-1}) reflecting weaker metal-ligand back bonding, indicative of reduced electron density and increased positive charge on the molybdenum centre. The bridging Mo(1)-H(12)-B(12) bond is observed as a very broad stretch around 2240cm^{-1}. The CO stretching frequencies of **I** can be compared to other complexes of the general formula [$MoCp(CO)_3X$] (X = weakly coordinating anion) (Table 2.2), as done by Reed for [$FeCp(CO)_2(X)$] (section 1.4.2). Using this table as a guide to rank the nucleophilicity of an anion, [*closo*-$CB_{11}H_{12}$]$^-$ fits in between $[SbF_6]^-$ and $[BF_4]^-$ in terms of coordinating ability.

X	Average νCO in CH_2Cl_2 (cm^{-1})	Reference
Cl^-	2017	[18]
BF_4^-	2021	[18]
closo-$CB_{11}H_{12}^-$	2036	This work
SbF_6^-	2040	[19]

Table 2.2: Average carbonyl stretching frequencies for [$MoCp(CO)_3X$]

The $^1H\{^{11}B\}$ NMR spectrum of **I** (recrystallised sample) at room temperature shows two Cp resonances at δ 5.86 and δ 5.79 in an approximate ratio of 1 : 2.5. The signals for cage {B-H} vertices are seen at δ 1.79 and δ 1.66, and a signal corresponding to the cage C-H is observed as a broad peak at δ 2.53. The peak for the bridging B-H-Mo proton is observed at δ -15.11 and appears as a partially collapsed quartet in the room temperature ^1H NMR spectrum, and as a broad singlet in the room temperature $^1H\{^{11}B\}$ NMR spectrum. The large upfield shift seen for this proton has been observed in related systems characterised by Stone which also contain B-H-Mo

bonds, such as [MoRuO{η^5-9-CH(C_6H_4Me-4)-7,8-$C_2B_9H_{10}$}(CO)$_2$(η^5-C_5H_5)].[20-22] The coupling constant for this bridging hydrogen [J(BH) = 87Hz] shows a decrease when compared with that of [N(Bu)$_4$][$CB_{11}H_{12}$] [J(BH) = 143Hz], and is indicative of a weakening of the B-H bond. The reduced coupling constant compared to that of a two-centre two-electron B-H bond mirrors the reduction in ^{13}C-^{1}H coupling found for C-H−M agostic linkages *versus* C-H bonds,[23] and is consistent with the agostic interaction observed in the solid state for **I** persisting in solution.

On cooling the sample to -90°C the ratio of the two peaks in the Cp region of the ^{1}H{^{11}B} NMR spectrum does not change significantly. Inspection of the highfield region of the spectrum at this temperature now shows two singlet peaks (Figure 2.5), due to thermal decoupling at the lower temperatures, at δ -15.46 and δ -15.55 in approximately the same ratio as the Cp resonances. This again suggests the presence of two isomeric forms in solution.

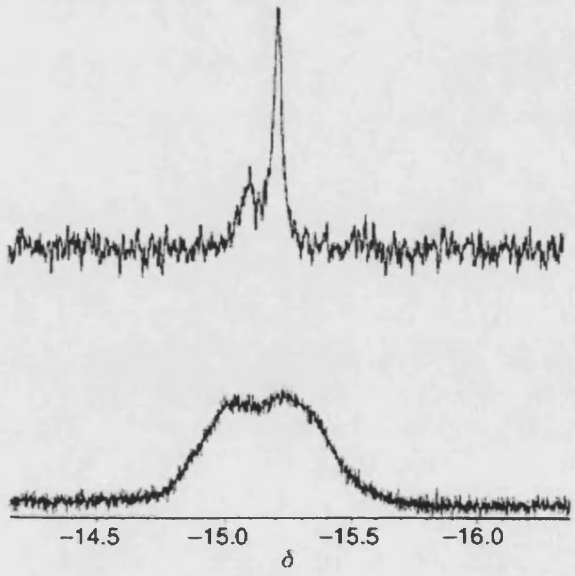

Figure 2.5: Highfield region in the ^{1}H{^{11}B} NMR spectrum at -90°C (top) and room temperature ^{1}H NMR spectrum (bottom) of complex **I**

The major isomer in solution is assigned as [$MoCp(CO)_3(12\text{-}\mu\text{-}H\text{-}CB_{11}H_{11})$] and the minor isomer as [$MoCp(CO)_3(7\text{-}\mu\text{-}H\text{-}CB_{11}H_{11})$] (Figure 2.6). This form of isomerisation has been observed in the related [$FeCp(CO)_2(CB_9H_{10})$] and [$FeCp(CO)_2(CB_{11}H_{12})$] compounds[24] as mentioned in section 1.8.2.

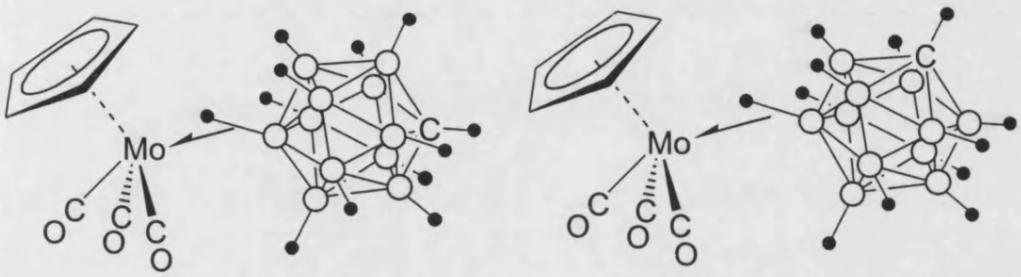

[$MoCp(CO)_3(12\text{-}\mu\text{-}H\text{-}CB_{11}H_{11})$] [$MoCp(CO)_3(7\text{-}\mu\text{-}H\text{-}CB_{11}H_{11})$]

Figure 2.6: Isomeric forms of compound **I** in solution

Further evidence of the two isomers in solution can be obtained from inspection of the $^{11}B\{^1H\}$ NMR spectrum. The major peaks observed at δ -13.7 (1B), δ -15.0 (5B) and δ -17.2 (5B) are indicative of a C_{5v} symmetric carborane and are assigned to the 12-isomer of **I**, assuming free rotation around the Mo(1)-H(12)-B(12) bond. The $^{11}B\{^1H\}$ NMR spectrum of the 7-isomer would be expected to display 7 peaks in the ratio 1:1:2:2:2:2:1 (Figure 2.7), but only two other unique resonances are observed in the ^{11}B NMR spectrum at δ -8.0 [J(BH) = 116Hz] and δ -21.9 [J(BH) = 68Hz]. These two peaks of the 7-isomer are tentatively assigned as the antipodal boron at δ -8.0, shifted 0.4 ppm downfield from B(12) in $Ag(CB_{11}H_{12})$ (d_6-acetone), and the peak at δ -21.9 as B(7) because of its upfield shift and low coupling constant which is diagnostic of coordination. The other peaks of the 7-isomer are presumably coincident with the peaks of the major isomer and cannot be observed.

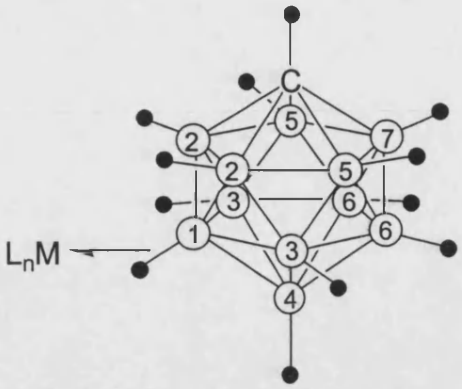

Figure 2.7: The seven unique boron positions of [7-μ-H-*closo*-$CB_{11}H_{11}$]$^-$ ligated to a metal

In the ^{11}B NMR spectrum of the 12-isomer, the ^{11}B-^1H coupling constant of the antipodal boron is *ca.* 90Hz, although care should be taken with this value as the doublet appears as a shoulder to a peak from a larger high field resonance. As expected, it is similar to that found in the ^1H NMR spectrum [J(BH) = 87Hz]. The coupling constants of the remaining two peaks corresponding to the lower [J(BH) = 151Hz] and upper [J(BH) = 151Hz] pentagonal belt borons of the 12-isomer, are similar to the values seen for [NBu_4][$CB_{11}H_{12}$] [CD_2Cl_2; B(7-11), J(BH) = 140Hz; B(2-6), J(BH) = 153Hz] indicating that they are not interacting with the metal in the 12-isomer.

A variable temperature NMR experiment between 20°C and 100°C was performed to probe whether or not the 7- and 12- isomers of **I** exchange in solution. Warming a solution of **I** in d_8-toluene resulted in the coalescence of the two Cp resonances at 100°C, perhaps indicating chemical exchange of the two isomers. There is a slight ambiguity in this experiment though, because as the temperature increases the signals of the already close in chemical shift Cp resonances broaden. In order to conclusively show exchange of the isomers, a ^1H EXSY (EXchange SpectroscopY) experiment was performed on **I** at 50°C. This is a 2-dimensional NMR experiment that can

indicate chemical exchange in slow (on the NMR timescale) exchange systems. The EXSY spectrum for **I** displays clear cross peaks between the two Cp resonances showing the two isomers to be related by an exchange process in solution.

This exchange process is likely to be an intramolecular rearrangement of the cage rather than an intermolecular exchange process given the relatively high strength of the Mo-H-B bond as evidenced by the highfield shifts and small coupling constants for the bridging hydrogen. The fluxionality of a metal about the surface of a boron cage has been observed for a large number of compounds, and is normally a very facile process that cannot be slowed at low temperature.[25, 26]

These results demonstrate that the solution and solid state properties of compounds containing [*closo*-$CB_{11}H_{12}$]$^-$ need to be compared carefully as the crystal structure of **I** shows only the presence of one of the two isomers seen in solution. This is most likely to be because of disorder within the crystal lattice of **I** that cannot be detected easily by X-ray crystallography due to the one electron difference between carbon and boron.

It was initially surprising to note that compound **I** is stable at room temperature in solution, and also in the solid state, for at least a week in air. The analogous compounds [$MoCp(CO)_3(BF_4)$] and [$MoCp(CO)_3(SbF_6)$], synthesised by Beck *et. al*, have to be prepared and handled at temperatures below 0°C, are extremely air sensitive, and will react with trace amounts of any weak nucleophile present. However, the similarity of carbonyl stretching frequencies in the $[BF_4]^-$, $[SbF_6]^-$ and [*closo*-$CB_{11}H_{12}$]$^-$ complexes (Table 2.2) suggests that all these anions have similar

coordinating ability in the scheme originally suggested by Reed.[27] The relative stability of **I** means that [*closo*-$CB_{11}H_{12}$]$^-$ is affording the metal some degree of stability either by steric shielding of the reactive metal centre, or by forming a stronger bond than $[BF_4]^-$ and $[SbF_6]^-$. In support of the strong Mo-H-B bond, **I** is stable in CD_2Cl_2 solutions containing 1 equivalent of acetone or water for at least 30 min. (as determined by ^1H NMR spectroscopy), and only strong nucleophiles such as $[Cl]^-$ displaces the anion in complex **I**. In contrast, the analogous $[MoCp(CO)_3(BF_4)]$ complex is extremely sensitive to the presence of water.[28] What is clear is that whilst some spectroscopic guides (i.e. IR spectroscopy) suggest that [*closo*-$CB_{11}H_{12}$]$^-$ is acting as a weakly coordinating anion in **I**, comparable with $[SbF_6]^-$, this cannot necessarily be directly related to the reactivity or stability of such complexes.

2.2.2 Isolation of the Reaction Intermediate; $[MoCp(CO)_3I{\cdot}Ag(CB_{11}H_{12})]_2$

Having isolated and characterised the final product of the reaction (**I**), attention turned to the isolation of the intermediate species seen in the IR spectrum of the reaction. Monitoring the reaction between $[MoCp(CO)_3Cl]$ and $[Ag(CB_{11}H_{12})]$ by IR spectroscopy showed that the intermediate species could not be isolated as the sole component of the reaction mixture at any stage of the reaction. If $[MoCp(CO)_3I]$ is used instead of $[MoCp(CO)_3Cl]$, complete reaction to the final metathesis product now takes seven days instead of just two. The longer reaction time is presumably due to the higher lattice energy of AgCl (calculated total lattice potential energy, U_{POT} = 864kJmol^{-1}) compared to that of AgI (U_{POT} = 808kJmol^{-1}).[29] The reaction of

$[MoCp(CO)_3I]$ and $[Ag(CB_{11}H_{12})]$ in CH_2Cl_2 was carefully monitored by IR spectroscopy, which after 3 hours showed the complete conversion of the starting material CO stretching bands to two new frequencies at 2054 and 1973cm^{-1}, corresponding to an intermediate species. Continued stirring results in the gradual formation of AgI as a dark precipitate and the complete conversion of intermediate to the final metathesis product, as determined by IR spectroscopy (Figure 2.8).

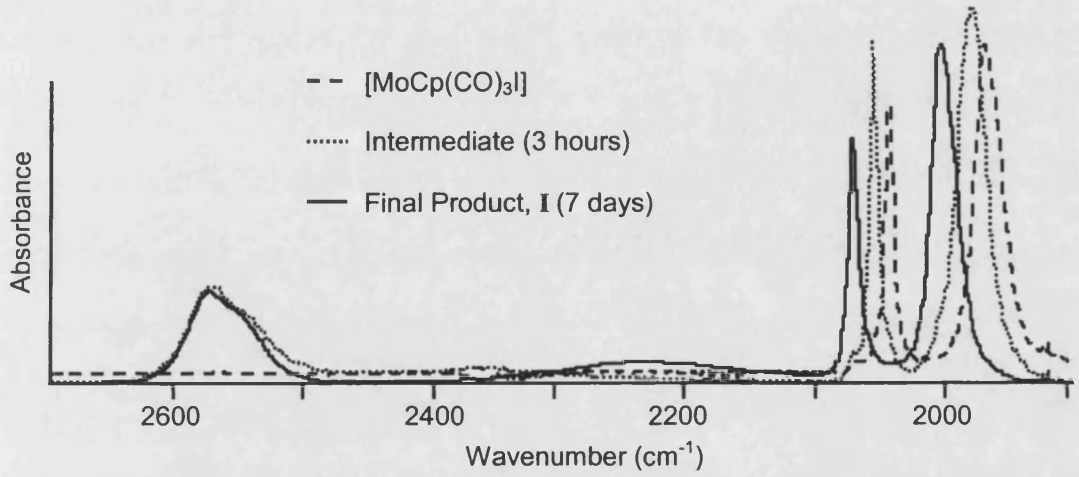

Figure 2.8: Selected IR spectra from the reaction of $[MoCp(CO)_3I]$ and $[Ag(CB_{11}H_{12})]$

The NMR spectra of the final metathesis product from this reaction are identical to those of compound **I**. As can be seen from Figure 2.8, after three hours of reaction the intermediate is the only species present, and can be isolated by removal of the solvent *in vacuo* to yield a red solid. Recrystallisation (CH_2Cl_2/hexane) at -30°C yielded small red crystals of the intermediate species in reasonable yield. The crystals were fully characterised by X-ray crystallography, micro-analysis, IR and multinuclear NMR spectroscopy and were shown to be $[MoCp(CO)_3I{\cdot}Ag(CB_{11}H_{12})]_2$, complex **II**.

The solid state structure of **II** is shown in Figure 2.9 with pertinent bond lengths and angles in Table 2.3. The molecule adopts a crystallographically imposed C_2 dimeric structure containing two silver atoms bridging two {$MoCp(CO)_3I$} fragments. The two Ag-I bond lengths are significantly different, Ag(1)-I(1) 2.9748(10)Å and Ag(1)-I(1A) 2.7599(9)Å. These Ag-I bond lengths are similar to that seen for other {Ag_2I_2} cores, which also display different bond lengths for the two Ag-X (X = halogen atom) interactions.[30, 31] To the best of my knowledge, no other examples of this {Ag_2X_2} type core exist that contains two transition metal halides bridged by two silver atoms. However, there have been recently reported examples of a similar type core where just one silver atom bridges two metal halides in a {X-Ag-X} fashion, [{$TpRe(NC_6H_4Me$-*p*)(Ph)I}$_2$Ag][PF_6][32] [Tp = tris-(pyrazolyl)borate]. The complex [{$Pt(Me)(N$-$N)Cl$}$_2$Ag][BF_4] [N-N = (1,5-Me_2-C_6H_4)$NC(CH_3)C(CH_3)N$(1,5-Me_2-C_6H_4)] has been reported very recently (2002),[12] and is one of the intermediates in the silver metathesis reaction between [$PtCl(Me)(N$-$N)$] and [$Ag(BF_4)$]. However, the crystal structure of this complex shows that, as well as bridging two halide atoms, the silver also bonds to one of the platinum metal centres so cannot be considered to have a true {X-Ag-X} type core. The Ag(1)-Ag(1A) bond length in **II**, 3.3426(11)Å, is too long to be considered a metal-metal interaction. The Mo-I bond length, 2.865(2)Å, is similar to that found in the related compounds [$Cp_2Mo_2(CO)_4(\mu$-$I)_2$][33] [Mo-I 2.853(1)Å] and [$MoCp(CO)_2(P(OEt)_3)I$][34] [Mo-I 2.8628(6)Å]. The puckered nature of the {Ag_2I_2} core and syn orientation of the two {$MoCp(CO)_3$} fragments, with respect to the Ag-I-Ag-I butterfly, leaves an apparent vacant coordination site on each silver centre. Inspection of the packing diagram reveals that a B(12) vertex from a carborane in an adjacent asymmetric unit is interacting with the silver, resulting in the

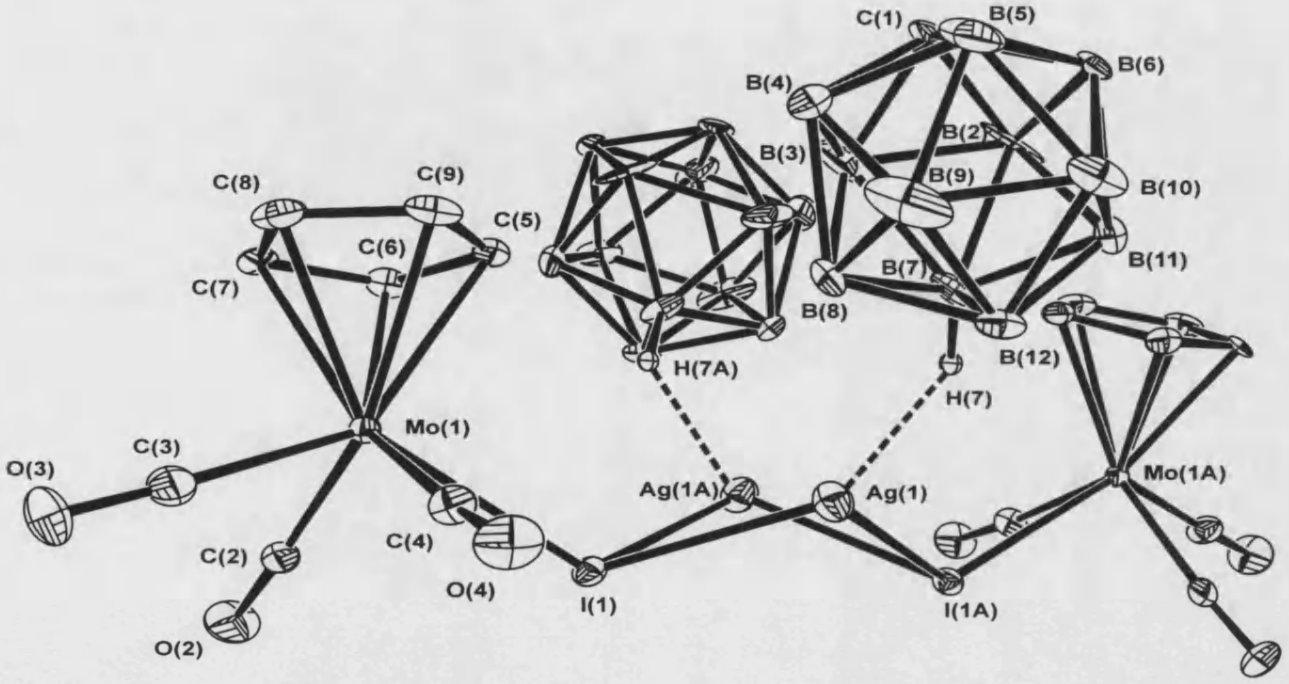

Figure 2.9: Crystal structure of $[MoCp(CO)_3I{\cdot}Ag(CB_{11}H_{12})]_2$, **II** (ellipsoids drawn at 30% probability level)

Mo(1)-I(1)	2.8599(8)Å
Ag(1)-I(1)	2.9748(10)Å
Ag(1)-I(1A)	2.7599(9)Å
Ag(1)-Ag(1A)	3.3426(11)Å
Ag(1)···B(7)	2.659(11)Å
Ag(1)-H(7)	1.96Å
Mo(1)-I(1)-Ag(1)	126.03(3)°
Mo(1)-I(1)-Ag(1A)	113.04(3)°
I(1)-Ag(1)-I(1A)	97.10(3)°
Ag(1)-I(1)-Ag(1A)	71.20(3)°
B(7)-H(7)-Ag(1)	116.3(6)°

Table 2.3: Selected bond lengths and angles for complex **II**

propagation of a polymeric structure containing alternating {$MoCp(CO)_3$} fragments in the solid state (Figure 2.10). Each carborane anion is therefore bridging two silver atoms via interactions from B(7)-H(7) [B(7)···Ag(1) 2.66(1)Å; H(7)-Ag(1) 1.97Å] and B(12)-H(12) [B(12)···Ag(1) 3.00(1)Å; H(12)-Ag(1) 1.97Å].

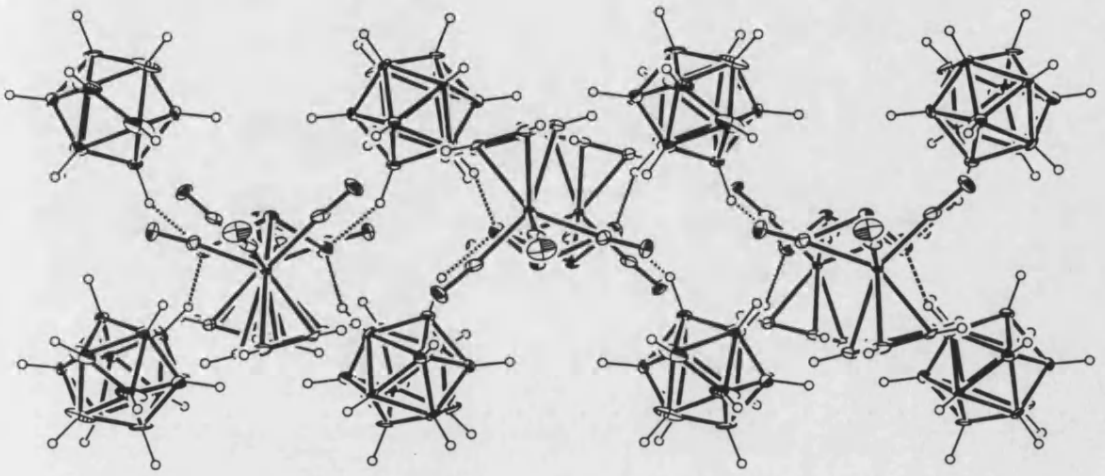

Figure 2.10: Extended solid state structure of **II**

Whilst it is unlikely this polymeric structure persists upon dissolution in CH_2Cl_2, evidence for the structure of **II** in solution comes from the inspection of the NMR data. The $^1H\{^{11}B\}$ NMR spectrum shows a single peak for the Cp resonance at δ 5.75, shifted downfield from $[MoCp(CO)_3I]$ (δ 5.63) but at a higher field than for **I** (δ 5.79, 12-isomer). This is consistent with the relative shift in CO stretches seen in the IR spectrum, that indicate an decrease in electron density on the metal as the reaction proceeds from $[MoCp(CO)_3I]$ → **II** → **I**. Evidence for the interaction of [*closo*-$CB_{11}H_{12}]^-$ and silver in solution comes from the ^{11}B NMR spectra. The $^{11}B\{^1H\}$ spectrum shows 2 peaks at δ -12.4 and δ -16.0 in the ratio of 1:10 (the latter peak is a coincidence of the upper and lower pentagonal belt resonances) indicating C_{5v} symmetry of the cage in solution. There are significant shifts in the ^{11}B NMR

spectrum of **II** compared to $[N(Bu)_4][CB_{11}H_{12}]$ (CD_2Cl_2), in which no metal-cage interactions are present, for both the antipodal ($\Delta = \delta$ -4.4) and lower pentagonal belt ($\Delta = \delta$ -1.9) boron resonances. In contrast, only the bonding B(12) resonance is shifted significantly in complex **I** (for 12-isomer: $\Delta = \delta$ -5.7), compared to $[N(Bu)_4][CB_{11}H_{12}]$. The upfield shift of a boron resonance is diagnostic of B-H metal interactions (for further discussion see section 4.2.5), indicating that both the antipodal and lower pentagonal belt borons are interacting with the silver in **II**. The relative shifts of each compound are best displayed in diagrammatic form (Figure 2.11).

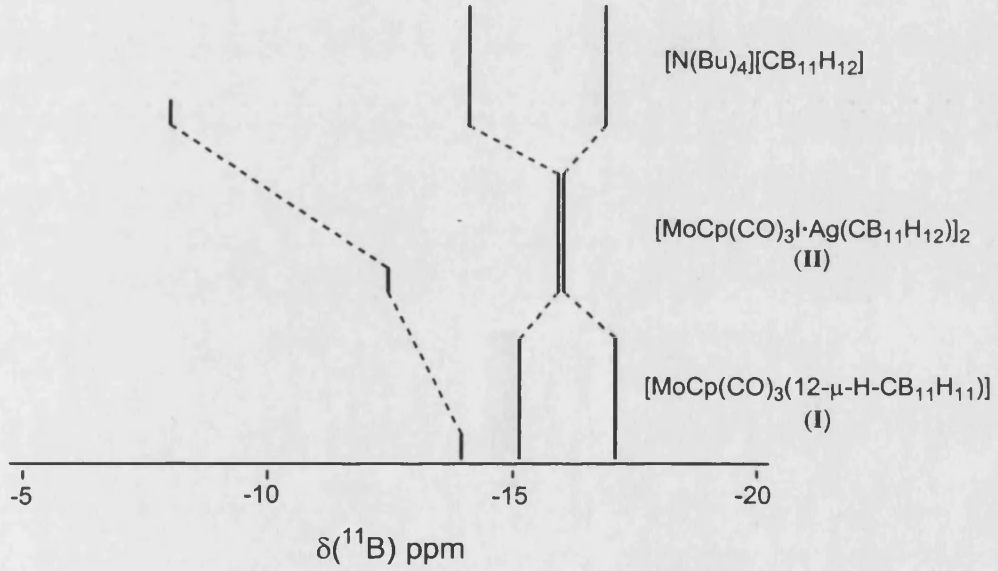

Figure 2.11: Comparitive $^{11}B\{^1H\}$ NMR shifts

Assuming that the polymeric motif is not retained in solution, the $[CB_{11}H_{12}]^-$ anion could be interacting with the silver in a η^2-fashion such as that seen for $[Rh(COD)(CB_{11}H_{12})]$,[26] or in an η^3-fashion like that of $[ZrCp(CH_3)_2(CB_{11}H_{12})]$.[25] Attempts to 'freeze' the fast fluxional process that is giving the cage C_{5v} symmetry in solution by recording an NMR spectrum at -90° still showed rapid exchange, preventing the distinction of an η^2 or η^3 bound cage experimentally. Even at low

temperature no ^{107}Ag-^{1}H or ^{109}Ag-^{1}H coupling was observed in the NMR spectra, although this phenomenon is not uncommon and has never been observed for any silver complexes of *closo*-monocarborane anions. The ^{109}Ag NMR spectrum of **II** displays a singlet at δ1335, which is shifted well downfield from the normal range expected for a Ag(I) centre (*ca.* δ500). This unusual shift indicates that the novel central core of this molecule may still be intact in solution.

In order to demonstrate conclusively that **II** is indeed an intermediate on the pathway to **I**, the reaction was monitored by ^{1}H NMR spectroscopy. The time dependant concentration profile of the reaction is displayed in Figure 2.12, showing the formation of **II** in a matter of hours, followed by its decomposition to **I** over several days. An important observation is that the mass balance of the system remains approximately constant throughout the reaction, meaning that the transformation of $[MoCp(CO)_3I] \rightarrow$ **II** $\rightarrow$ **I** is essentially quantitative.

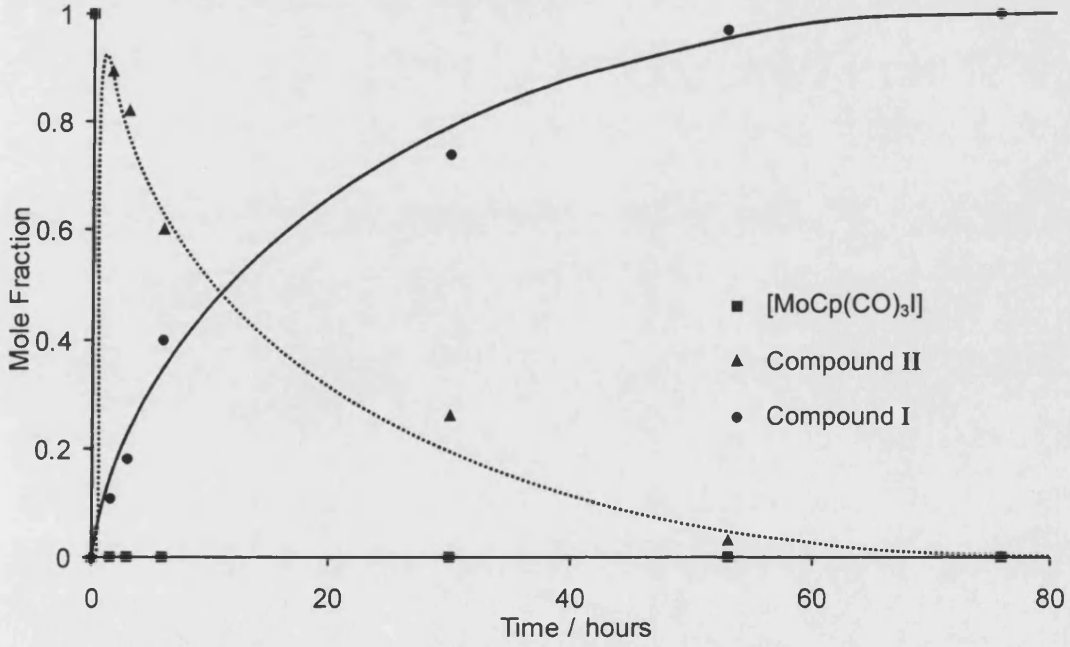

Figure 2.12: Graph of the relative concentration of reaction species *versus* time

The halide bridged complex $[\{FeCp(CO)_2\}_2I][BF_4]$ has been postulated as one of the intermediates in the reaction of $[FeCp(CO)_2I]$ and $[Ag(BF_4)]$.[9] The analogous $[\{MoCp(CO)_3\}_2I][CB_{11}H_{12}]$ species would be expected to have a Cp resonance similar to that of $[\{MoCp(CO)_3\}_2I][BF_4]$ (δ6.20),[35] shifted significantly downfield and distinguishable from **I**, but is not observed at any point in this reaction. This again highlights the relative strength of the B-H-Mo bond compared to B-F-Mo.

An attempt to make the more sterically hindered Cp^* analogue of compound **I** via silver salt metathesis was unsuccessful, with the ^1H NMR spectrum displaying more than 5 product species after 9 days of reaction. We suggest that this is due to unfavourable steric interactions between the bulky Cp^* ligand and the carborane anion in the intermediate compound. An alternative preparation of $[MoCp^*(CO)_3(CB_{11}H_{12})]$ via protonolysis using $[H(CB_{11}H_{12})]$ is discussed in the next chapter.

Having prepared complex **I** via silver salt metathesis with $[Ag(CB_{11}H_{12})]$, it was hoped to be able to use the same reaction to produce complexes with the even more weakly coordinating [12-Br-*closo*-$CB_{11}H_{11}]^-$ and [*closo*-$CB_{11}H_6Br_6]^-$ anions, which is discussed next.

2.2.3 $[MoCp(CO)_3I{\cdot}Ag(CB_{11}H_{11}Br)]_2$

The reaction of $[Ag(CB_{11}H_{11}Br)]$ with $[MoCp(CO)_3I]$ in CH_2Cl_2 was monitored by IR spectroscopy. After 1 hour no precipitate had appeared in the reaction mixture, but the IR of the clear red solution showed the replacement of the CO stretches for $[MoCp(CO)_3I]$ at 2044 and 1966cm^{-1} by two new peaks at 2053 and 1972cm^{-1}. The new species was isolated by the removal of the solvent *in vacuo* to yield a red powder, which was recrystallised at -30°C from a CH_2Cl_2 solution layered with hexane. The red crystals formed were characterised by X-ray crystallography, elemental analysis, IR and NMR spectroscopy and identified as $[MoCp(CO)_3I{\cdot}Ag(CB_{11}H_{11}Br)]_2$, complex **III**.

The asymmetric unit in the crystal structure of **III** contains two solvent molecules (CH_2Cl_2) and two crystallographically independent dimers, **IIIA** (Figure 2.13, bond lengths and angles Table 2.4) and **IIIB** (Figure 2.14, bond lengths and angles Table 5). Both are centrosymmetric dimers, with one half of each dimer symmetry generated from the other. Both configurations display a $\{Ag_2I_2\}$ central core appended by two $\{MoCp(CO)_3\}$ fragments, arranged mutually *trans* to one another. The Mo-I bond lengths are very similar in both independent molecules of **III** [**IIIA** 2.8792(2)Å; **IIIB** 2.8735(3)Å] but are slightly longer than found in **II** [2.8599(8)Å]. The carborane anion interacts in a bidentate fashion with silver via Ag-Br [Ag(1)-Br(1), 2.6457(4)Å; Ag(2)-Br(2), 2.7148(4)Å] and Ag-H interactions [Ag(1)-H(7), 2.43(2)Å; Ag(1)···B(7), 3.159(3)Å; Ag(2)-H(27), 2.13(2)Å; Ag(2)···B(27) 2.861(3)Å]. The Ag(1)-H(7) bond length in **IIIA** is longer than the average Ag-H bond length (2.24Å) in the related compound $[Ag(CB_{11}H_{11}Br).C_6H_6]$,[36] but has a similar Ag-Br distance (2.642Å). The

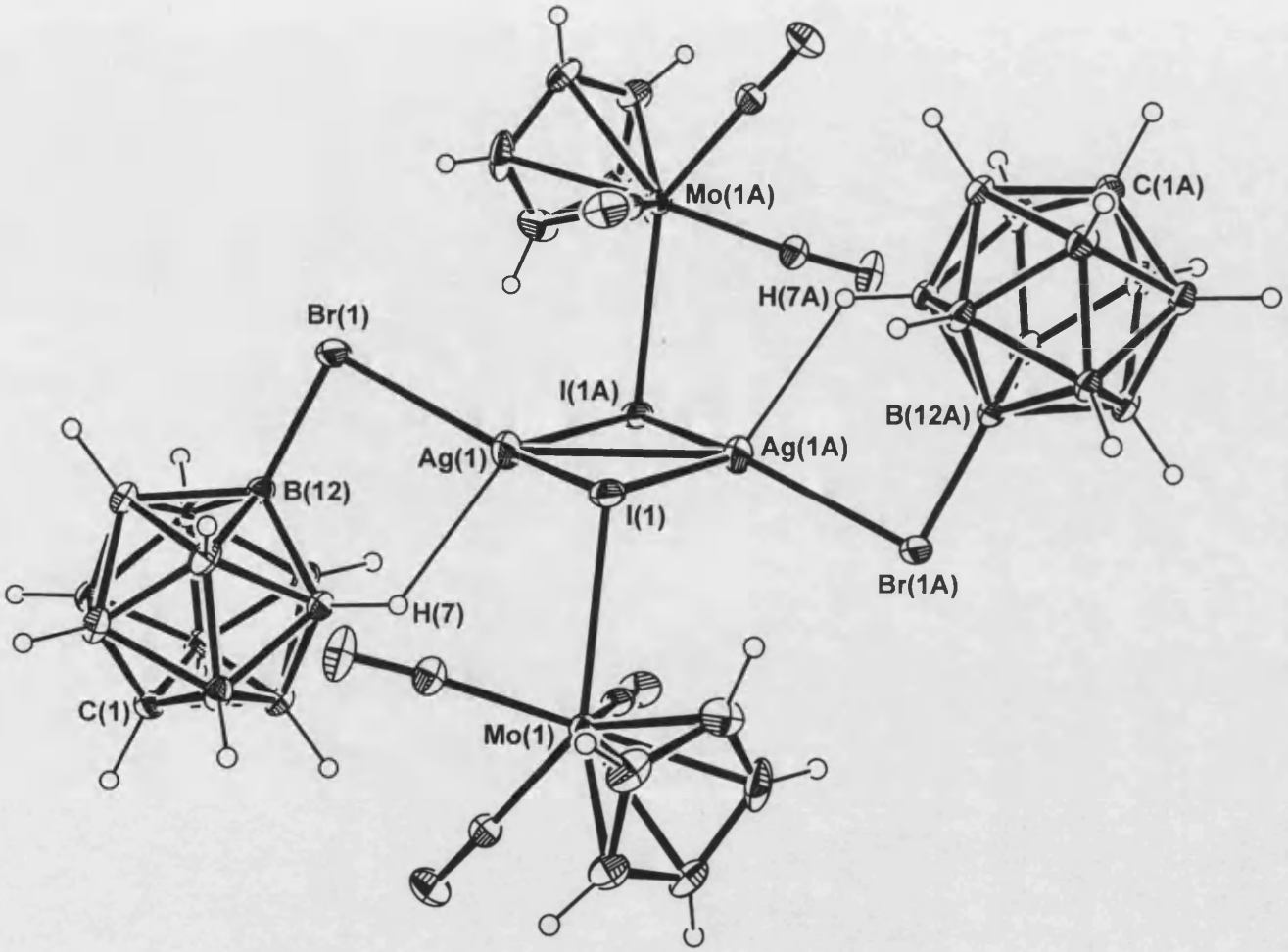

Mo(1)-I(1)	2.8792(3)Å
Ag(1)-I(1)	2.7789(3)Å
Ag(1)-I(1A)	2.9024(3)Å
Ag(1)-Ag(1A)	2.9887(3)Å
Br(1)-Ag(1)	2.6457(4)Å
B(12)···Ag(1)	3.369(3)Å
B(12)-Br(1)	2.005(3)Å
B(7)···Ag(1)	3.159(3)Å
H(7)-Ag(1)	2.43(2)Å
I(1)-Ag(1)-I(1A)	116.57(1)°
Ag(1)-I(1)-Ag(1A)	64.435(8)°
B(7)-H(7)-Ag(1)	122(3)°
B(12)-Br(1)-Ag(1)	91.76(9)°

Table 2.4: Selected bond lengths and angles for **IIIA**

Figure 2.13: Crystal structure of $[MoCp(CO)_3I{\cdot}Ag(CB_{11}H_{11}Br)]_2$, **IIIA** (Ellipsoids drawn at 30% probability level)

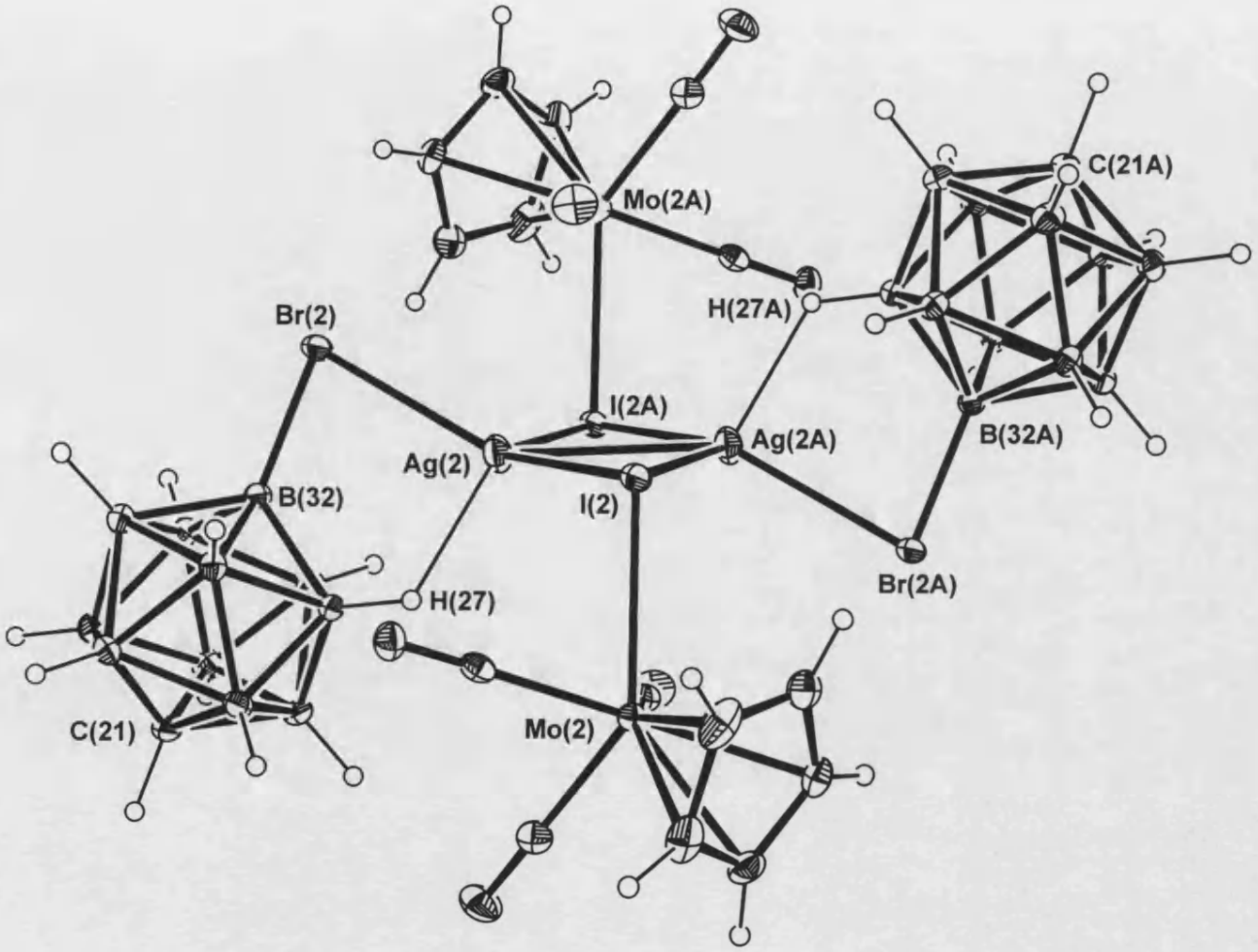

Figure 2.14: Crystal structure of $[MoCp(CO)_3I{\cdot}Ag(CB_{11}H_{11}Br)]_2$, **IIIB**
(Ellipsoids drawn at 30% probability level)

Mo(2)-I(2)	2.8735(3)Å
Ag(2)-I(2)	2.7790(3)Å
Ag(2)-I(2A)	2.8812(3)Å
Ag(2)-Ag(2A)	2.9815(3)Å
Br(2)-Ag(2)	2.7148(4)Å
B(32)···Ag(2)	3.202(3)Å
B(32)-Br(2)	2.008(3)Å
B(27)···Ag(2)	2.861(3)Å
H(27)-Ag(2)	2.13(2)Å
I(1)-Ag(1)-I(1A)	116.46(1)°
Ag(1)-I(1)-Ag(1A)	63.541(8)°
B(7)-H(7)-Ag(1)	120(2)°
B(12)-Br(1)-Ag(1)	83.95(9)°

Table 2.5: Selected bond lengths and angles for **IIIB**

situation is reversed for **IIIB** which has a shorter Ag(2)-H(27) bond length and a correspondingly longer Ag(2)-Br(2) distance. One of the most striking differences between **II** and **III** is the planar $\{Ag_2I_2\}$ core in **III**. There are a number of examples of compounds containing planar rhomboid cores similar to **III**, such as $[Ag_2I_2(m\text{-}PP)_2]$[37] [*m*-PP = 1,3-$\{Ph_2P(CH_2)\}_2$-C_6H_4], $[Ag_2X_2(PPh_3)_4]$[38] (X = Cl, Br), and the recently isolated $[AgI(R,R\text{-}DIOP)]_2$[39] [R,R-DIOP = $C_3O_2CH_2\{Ph_2P(CH_2)\}_2$] (Figure 2.15).

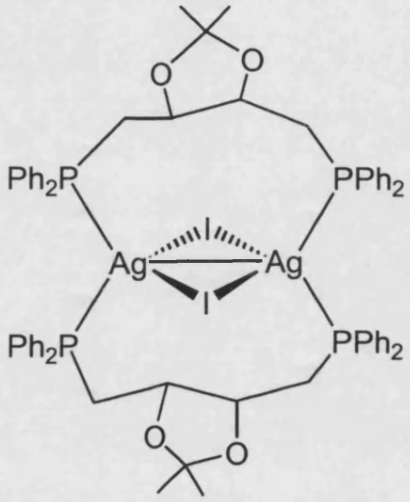

Figure 2.15: $[AgI(R,R\text{-}DIOP)]_2$

Despite the fact that two closed shell metal cations would be expected to repel one another, the bond lengths in **III** for Ag(1)-Ag(1A) [2.9887(3)Å] and Ag(2)-Ag(2A) [2.9815(3)Å] are close to that of metallic silver (2.89Å) and indicate a metal-metal interaction.[40] For complexes containing an $\{Ag_2I_2\}$ type core only $[AgI(R,R\text{-}DIOP)]_2$ has a similarly small Ag-Ag bond length [3.0650(6) Å], but no discussion of this feature is mentioned in the paper. A theoretical study has shown that metallophillic bonding does occur in the related compound $[Ag_2(PPh_2CH_2SPh)_2][ClO_4]_2$,[41] which in the solid-state has silver-silver bond distances of 2.9501(8)Å and 2.9732(9)Å that are close in value to those found for **III**. The silver bonding distance in **III** is well within

the range observed for other complexes with Ag(I)-Ag(I) interactions (2.80-3.30Å).[13, 42-46]

The solution ^{1}H NMR spectrum of **III** in CD_2Cl_2 displays a single resonance in the Cp region at δ 5.77, which is close to that found for **II** (δ 5.75). Given this, it is unsurprising to note that the CO stretches for **II** and **III** are also very similar; 2054 and 1973cm^{-1}, 2053 and 1972cm^{-1} respectively. The ^{11}B NMR spectrum of **III** shows three peaks at δ -3.4 (1B), δ -13.1 (5B) and δ -16.3 (5B). The ^{11}B-^{1}H coupling constants for the lower and upper pentagonal belts of [*closo*-$CB_{11}H_{11}Br]^-$ in **III** (139 and 157Hz respectively) are virtually the same as those seen for [$Ag(CB_{11}H_{11}Br)$] (144 and 159Hz; d_6-acetone). This indicates that in solution the lower pentagonal belt of the carborane anion is, at best, only weakly interacting with silver in **III**.

Attempts to isolate the final metathesis product, [$MoCp(CO)_3(CB_{11}H_{11}Br)$], by extended stirring of the reaction mixture, resulted in the very gradual appearance of a new species in the IR spectrum at 2070 and 1998cm^{-1}. The reaction seems to be near completion after 9 days, however a large ratio of B-H to carbonyl stretches in the IR spectrum indicates that the organometallic species has decomposed and the final metathesis product could not be isolated cleanly *via* this synthetic route. The decomposition could be due to uncharacterisable impurities in the [$Ag(CB_{11}H_{11}Br)$] starting material, or the instability of the product for extended periods of time in solution. An attempt to increase the rate of metathesis, and perhaps decrease the amount of decomposition due to solution instability, was made by using [$MoCp(CO)_3Cl$] instead of [$MoCp(CO)_3I$] which should provide a greater thermodynamic driving force towards the products of reaction. This was unsuccessful,

resulting in decomposition of the reaction mixture after just one day of stirring. Attempts to synthesise the final metathesis product via a different synthetic route will be discussed in the next chapter.

2.2.4 $[MoCp(CO)_3I{\cdot}Ag(CB_{11}H_6Br_6)]_2$

Having isolated silver salt metathesis intermediates using [*closo*-$CB_{11}H_{12}$]$^-$ and [*closo*-$CB_{11}H_{11}Br$]$^-$, attention was drawn to the next anion in this series: [*closo*-$CB_{11}H_6Br_6$]$^-$. The reaction of $[MoCp(CO)_3Cl]$ with $[Ag(CB_{11}H_6Br_6)]$ in CH_2Cl_2 resulted in no observable reaction in the IR spectrum, and after seven days stirring only unchanged starting materials were recovered from the reaction mixture (as determined by NMR spectroscopy). Moving to the analogous reaction with $[MoCp(CO)_3I]$, which was more successful with [*closo*-$CB_{11}H_{12}$]$^-$ and [*closo*-$CB_{11}H_{11}Br$]$^-$, the starting material was converted to a new species with CO stretching frequencies of 2055 and 1975cm^{-1}. These values are very similar to those seen for **II** and **III**, suggesting a similar silver halide bridged species has been formed in solution. Dark-red crystals of this species were grown by the slow evaporation of a CH_2Cl_2 solution under a flow of argon and shown to be $[MoCp(CO)_3I{\cdot}Ag(CB_{11}H_6Br_6)]_2$, complex **IV**.

The X-ray crystal structure of the dimer **IV** is displayed in Figure 2.16 with one half of the dimer symmetry generated centrosymmetrically. Relevant bond lengths and angles are shown in Table 2.6. Complex **IV** bears a planar $\{Ag_2I_2\}$ core appended

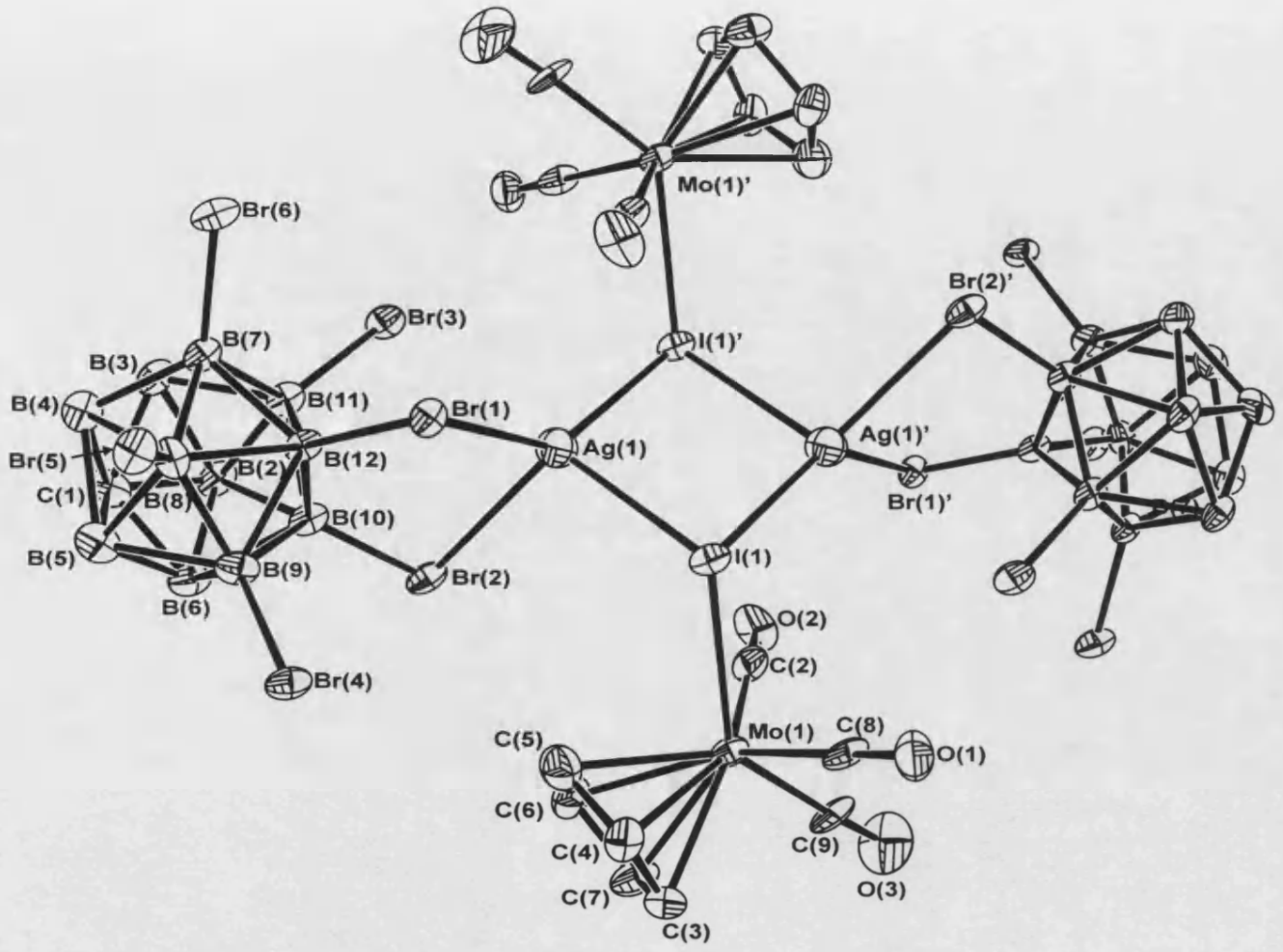

Figure 2.16: Crystal structure of $[MoCp(CO)_3I{\cdot}Ag(CB_{11}H_6Br_6)]_2$, **IV**
(Hydrogens omitted for clarity; Ellipsoids drawn at 30% probability level)

Mo(1)-I(1)	2.865(2)Å
Ag(1)-I(1)	2.778(2)Å
Ag(1)-I(1A)	2.980(2)Å
Ag(1)-Ag(1A)	3.759(3)Å
Br(1)-Ag(1)	2.803(3)Å
Br(2)-Ag(1)	2.771(3)Å
Br(3)-Ag(1)	3.249(3)Å
B(10)···Ag(1)	3.54(2)Å
B(10)-Br(2)	1.95(2)Å
B(11)···Ag(1)	3.77(2)Å
B(11)-Br(3)	1.96(2)Å
B(12)···Ag(1)	3.57(2)Å
B(12)-Br(1)	3.57(2)Å
Mo(1)-I(1)-I(1A)	118.35(6)°
I(1)-Ag(1)-I(1A)	98.59(7)°
Ag(1)-I(1)-Ag(1A)	81.41(7)°
B(10)-Br(2)-Ag(1)	95.3(7)°
B(11)-Br(3)-Ag(1)	89.2(7)°
B(12)-Br(1)-Ag(1)	96.8(6)°

Table 2. 6: Selected bond lengths and angles for **IV**

by two $\{MoCp(CO)_3\}$ fragments arranged *trans* to one another, reminiscent to that seen for compound **III**. The [*closo*-$CB_{11}H_6Br_6$]$^-$ cage is bound to silver in a bidentate fashion via Ag(1)-Br(1) [2.803(3)Å] and a slightly shorter Ag(1)-Br(2) [2.771(3)Å] bond. These bond lengths are longer than the similar Ag-Br bonds found in **III** (2.68Å average). The Ag-Br bond lengths in **IV** (2.79Å average) are slightly shorter than those found in related silver complexes of [*closo*-$CB_{11}H_6Br_6$]$^-$ such as $[Ag(CB_{11}H_6Br_6)]$[47] (Ag-Br average; 2.86Å), $[Ag(1\text{-}CH_3\text{-}CB_{11}H_5Br_6)]$[48] (Ag-Br average; 2.86Å) and $[Ag(CB_{11}H_6Br_6)_2]^-$ [49] (Ag-Br average; 2.88Å). It is pertinent to note that all of these compounds are coordination polymers and the [*closo*-$CB_{11}H_6Br_6$]$^-$ anion is η^3-coordinated to silver, as opposed to the η^2-coordination mode seen in **IV**. Further inspection of the coordination environment around Ag(1) reveals that there could be a very weak interaction from Br(3) [Ag(1)-Br(3), 3.25(3)Å] to give the more familiar η^3-coordination mode of [*closo*-$CB_{11}H_6Br_6$]$^-$. Related Ag-Br bonds that are over 3Å can be found in $[(\eta^2\text{-}C_6H_6)(\eta^1\text{-}C_6H_6)Ag_3(NO_3)(THF)][1\text{-H-}closo\text{-}CB_9Br_9]_2$ [50] that contains Ag-Br contacts of 3.007(1)Å and 3.017(1)Å in the solid state. The Ag(1)-Br(3) bond length is still significantly longer than this and whilst inside the sum of the van der Waals radii for silver and bromine (3.50Å)[51] is perhaps too long to be classed as an interaction. Rather the anion is merely orientating itself to minimise interactions with the metal ligand set. The Ag-I bond lengths [2.778(3) and 2.980(3)Å] in the $\{Ag_2I_2\}$ core are very close to those seen for **III** (average: 2.78Å and 2.89Å), but the bond angles are very different resulting in a significantly larger Ag(1)-Ag(1)' bond distance in **IV** [3.759(3)Å] compared to **III** (average: 2.99Å). This difference is highlighted Figure 2.17, which compares the space filling diagrams (van der Waal radii) of the $\{Ag_2I_2\}$ cores in compounds **III** and **IV**. The dramatic

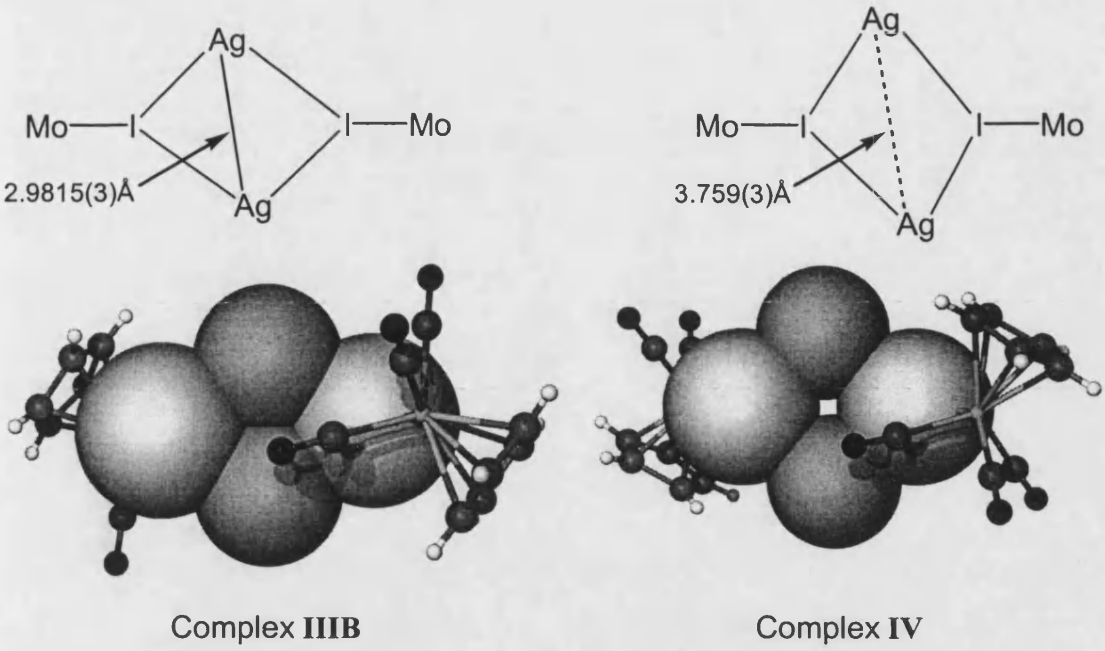

Figure 2.17: Space filling diagrams (van der Waal radii) demonstrating the difference in the $\{Ag_2I_2\}$ core geometeries of **III** and **IV**

increase in the silver-silver bond length despite similar Ag-I bond lengths is compelling evidence that there is a silver-silver attraction in **III**. Metallophilic interactions between Ag(I) atoms are generally very low in energy [52] and the difference in the solid state core geometries between **III** and **IV** is likely to be due to subtle differences in the crystal packing of these compounds.[53]

Inspection of the Cp region in the ^{1}H NMR spectrum of **IV** reveals two peaks at δ 5.84 and δ 5.73 in a ratio of 1:8, indicating the presence of two isomers in solution. The ^{109}Ag NMR spectrum also shows two peaks, in approximately the same ratio as that seen in the ^{1}H NMR spectrum, at δ 1335 (relative intensity 8) and δ 1325 (relative intensity 1). A high temperature ^{1}H NMR study of **IV** in d_8-toluene showed no change in the ratio of these peaks, demonstrating that they do not interconvert appreciably on

the NMR timescale. The two peaks in solution are tentatively assigned as *syn* and *anti* isomers of the $\{MoCp(CO)_3\}$ fragment with respect to the $\{Ag_2I_2\}$ core (Figure 2.18).

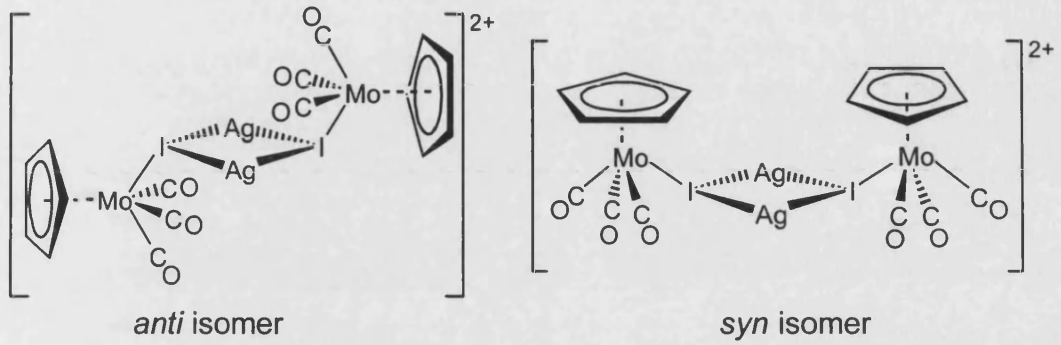

Figure 2.18: Suggested solution configurations for complex **IV**, [(*closo*-$CB_{11}H_{12}$)$^-$ cage omitted for clarity]

The Cp rings within these dimeric species are equivalent as the dimer has C_2 (*anti* isomer) or C_{2v} (*syn* isomer) symmetry, assuming facile rotation about the Mo-I bond in both. Molecular modelling calculations performed on compound **IV** by Dr. Andrew Weller show the *syn* isomer to have an energy of 442 kcal mol^{-1}, and the *anti* 440 kcal mol^{-1}. These values indicate that the predominant form in solution is likely to be the *anti* isomer, as seen in the solid state, though both are very similar in energy. The $^{11}B\{^1H\}$ NMR spectrum shows three peaks in the ratio 1:5:5 indicating the carborane has C_{5v} symmetry, unlike that seen in the solid state. This could arise from the carborane anions and the dimeric cation forming seperated ion pairs in solution, or perhaps, a very facile exchange of Br-Ag bonds that gives rise to a time averaged C_{5v} symmetric cage. The ^{109}Ag NMR shifts are very similar to those found in **II**, suggesting that it is likely that the molecule configuration of the core geometries are similar in solution with the carborane still bound to the silver. Consistent with this, the $^{11}B\{^1H\}$ NMR spectrum of $[N(^nBu)_4][CB_{11}H_6Br_6]$ in CD_2Cl_2, for which there are no metal cation-anion interactions, shows the boron atoms resonating at δ -1.8 [1B,

B(12)], δ -10.1 [5B, B(7-11)] and δ -20.4 [5B, B(2-6)]. These values are shifted downfield from the boron resonances in **IV** [ΔB(12) = δ -2.2; ΔB(7-11) = δ -2.1], consistent with the cage interacting with the silver atoms via the antipodal and lower pentagonal belt vertices in solution. Supporting this is the comparatively small downfield shift of the peak relating to the upper pentagonal belt borons [ΔB(2-6) = δ -0.8], which are not thought to interact significantly in solution. This relative shift is less pronounced than that seen upon complexation of [*closo*-$CB_{11}H_{12}$]$^-$ to form **II**, presumably a result of the bromine atoms offering a greater degree of electron shielding to the boron cage compared with hydrogen atoms.

Continued stirring of a solution of **IV** in CH_2Cl_2 for 7 days resulted in no decomposition or formation of metathesis product. The low nucleophilicity of the [*closo*-$CB_{11}H_6Br_6$]$^-$ anion has prevented the formation of AgI, effectively halting the reaction at the intermediate stage. Addition of 2 equivalents of [Ag($CB_{11}H_{12}$)] to compound **IV** in CH_2Cl_2 results in the immediate change of the IR spectrum to show **II**, followed by gradual decomposition over 7 days to yield **I** in essentially quantitative yield (Figure 2.19). The fact that the relative nucleophilicity of the anion controls the outcome of reaction indicates that its involvement in the rate determining step is important for silver salt metathesis.

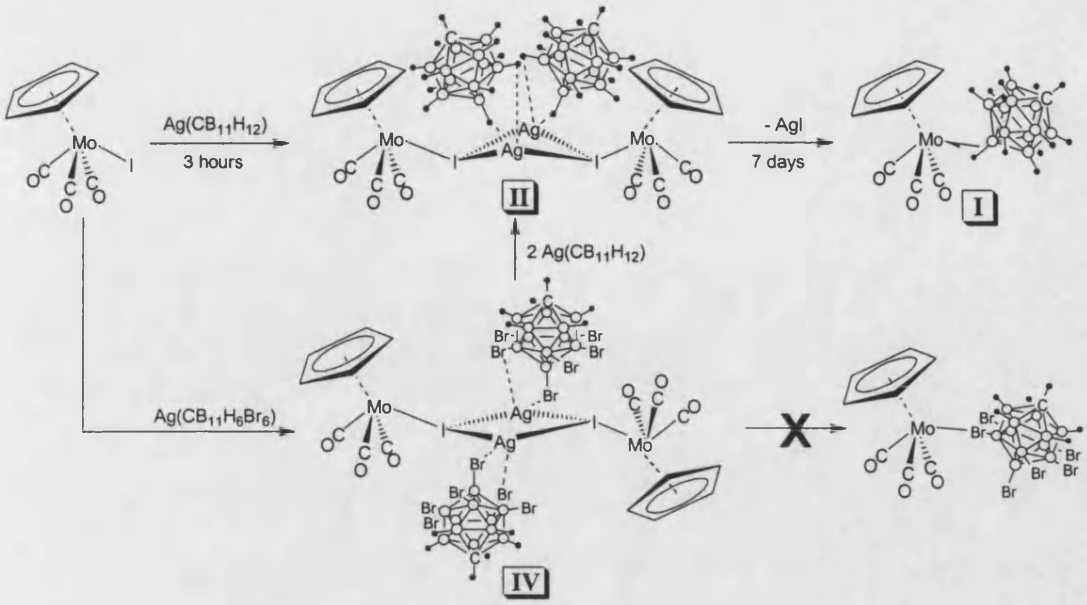

Figure 2.19: Reaction of compound **IV** to form **I**

2.3 Summary

The reaction of $[MoCp(CO)_3I]$ with silver(I) salts of $[closo\text{-}CB_{11}H_6Y_6]^-$ (Y = H, Br) anions has resulted in the isolation and, for the first time, structural characterisation of an intermediate of a silver salt metathesis reaction.[54, 55] The final metathesis product, complex **I**, is one of only a handful of examples containing $[closo\text{-}CB_{11}H_{12}]^-$ bound directly to a transition metal centre. The unanticipated stability of this complex towards H_2O and acetone compared to similar $[MoCp(CO)_3X]$ (X = weakly coordinating anion) compounds is very interesting and is likely to arise from the steric bulk and inherent inertness of $[closo\text{-}CB_{11}H_{12}]^-$ combined with the relatively strong Mo-H-B bonds it can form. This section has also shown the limits of using silver salt metathesis as a tool for introducing very weakly coordinating anions into a metal's coordination sphere. The $[closo\text{-}CB_{11}H_{11}Br]^-$ and $[closo\text{-}CB_{11}H_6Br_6]^-$ anions are too weakly nucleophilic to induce successful metathesis. When using $[closo\text{-}CB_{11}H_{11}Br]^-$

the final metathesis product decomposes in solution. The complete cessation of the reaction at the intermediate stage is observed when using the more weakly nucleophilic [*closo*-$CB_{11}H_6Br_6$]$^-$ anion. Whilst silver metathesis proceeds smoothly for [*closo*-$CB_{11}H_{12}$]$^-$, it is clear that the synthesis of highly Lewis acidic metal complexes containing very weakly coordinating anions will require the use of different synthetic strategies, and this is outlined in the next chapter.

2.4 References

1 S. H. Strauss, *Chem. Rev.* **1993**, *93*, 927.
2 C. A. Reed, *Acc. Chem. Res.* **1998**, *31*, 133.
3 A. Cutler, D. Ehntholt, W. P. Giering, P. Lennon, S. Raghu, A. Rosan, M. Rosenblum, J. Tancrede, D. Wells, *J. Am. Chem. Soc.* **1976**, *98*, 3495.
4 D. L. Reger, *Acc. Chem. Res.* **1988**, *21*, 229.
5 M. Rosenblum, D. Scheck, *Organomet.* **1982**, *1*, 397.
6 R. R. Schrock, J. A. Osborn, *J. Am. Chem. Soc.* **1971**, *93*, 2397.
7 R. H. Reimann, E. Singleton, *J. Organomet. Chem.* **1973**, *59*, C24.
8 Y. Pocker, W.-H. Wong, *J. Am. Chem. Soc.* **1975**, *97*, 7097.
9 B. M. Mattson, W. A. G. Graham, *Inorg. Chem.* **1981**, *20*, 3186.
10 D. J. Liston, Y. J. Lee, W. R. Scheidt, C. A. Reed, *J. Am. Chem. Soc.* **1989**, *111*, 6643.
11 C. A. Reed, Z. Xie, R. Bau, A. Benesi, *Science* **1993**, *262*, 402.
12 V. G. Albano, M. Di Serio, M. Monari, I. Orabona, A. Panunzi, F. Ruffo, *Inorg. Chem.* **2002**, *41*, 2672.
13 R. Uson, J. Fornies, M. Tomas, *J. Am. Chem. Soc.* **1984**, *106*, 2482.
14 D. J. Liston, C. A. Reed, C. W. Eigenbrot, W. R. Scheidt, *Inorg. Chem.* **1987**, *26*, 2739.
15 H. V. R. Dias, Z. Wang, *Inorg. Chem.* **2000**, *39*, 3890.
16 A. E. Ayers, H. V. R. Dias, *Inorg. Chem.* **2002**, *41*, 3259.
17 G. P. Gupta, G. Lang, Y. J. Lee, W. R. Scheidt, K. Shelly, C. A. Reed, *Inorg. Chem.* **1987**, *26*, 3022.
18 W. Beck, K. Z. Schloter, *Naturforsch., B* **1978**, *33b*, 1214.
19 K. Sunkel, U. Nagel, W. Beck, *J. Organomet. Chem.* **1983**, *251*, 227.
20 S. Anderson, J. C. Jeffery, Y.-H. Liao, D. F. Mullica, E. L. Sappenfield, F. G. A. Stone, *Organomet.* **1997**, *16*, 958.

21 S. A. Brew, S. J. Dossett, J. C. Jeffery, F. G. A. Stone, *J. Chem. Soc., Dalton Trans.* **1990**, 3709.
22 S. J. Dossett, I. J. Hart, M. U. Pilotti, F. G. A. Stone, *J. Chem. Soc., Dalton Trans.* **1990**, 3489.
23 M. Brookhart, M. L. H. Green, *J. Organomet. Chem.* **1983**, *250*, 395.
24 S. V. Ivanov, J. J. Rockwell, S. M. Miller, O. P. Anderson, K. A. Solntsev, S. H. Strauss, *Inorg. Chem.* **1996**, *35*, 7882.
25 D. J. Crowther, S. L. Borkowsky, D. Swenson, T. Y. Meyer, R. F. Jordan, *Organomet.* **1993**, *12*, 2897.
26 A. S. Weller, M. F. Mahon, J. W. Steed, *J. Organomet. Chem.* **2000**, *614-615*, 113.
27 Z. Xie, T. Jelinek, R. Bau, C. A. Reed, *J. Am. Chem. Soc.* **1994**, *116*, 1907.
28 W. Beck, *Inorg. Synth.* **1990**, *28*, 1.
29 D. R. E. Lide, *Handbook of Chemistry and Physics* **1997**, *77th Edition.*
30 J. Pytkowicz, S. Roland, P. Mangeney, *J. Organomet. Chem.* **2001**, *631*, 157.
31 J. T. Sampanthur, J. J. Vittal, *Crystal Engineering* **2000**, *3*, 117.
32 W. S. McNeil, D. D. DuMez, Y. Matano, S. Lovell, J. M. Mayer, *Organomet.* **1999**, *18*, 3715.
33 M. D. Curtis, N. A. Fotinos, K. R. Han, W. M. Butler, *J. Am. Chem. Soc.* **1983**, *105*, 2686.
34 J. M. Smith, N. J. Coville, L. M. Cook, J. C. A. Boeyens, *Organomet.* **2000**, *19*, 5273.
35 A. Seyam, H. Samha, H. Hodali, *Gazz. Chim. Ital.* **1990**, *120*, 527.
36 T. Jelinek, P. Baldwin, W. R. Scheidt, C. A. Reed, *Inorg. Chem.* **1993**, *32*, 1982.
37 F. Caruso, M. Camalli, H. Rimml, L. M. Venanzi, *Inorg. Chem.* **1995**, *34*, 673.
38 G. A. Bowmaker, Effendy, J. V. Hanna, P. C. Healy, B. W. Skelton, A. H. White, *J. Chem. Soc., Dalton Trans.* **1993**, 1387.
39 B. Wu, X.-T. Wu, X. Tian, W.-H. Sun, *J. Organomet. Chem.* **2001**, *640*, 57.
40 P. Pyykko, *Chem. Rev.* **1997**, *97*, 597.
41 E. J. Fernandez, J. M. Lopez-de-Luzuriaga, M. Monge, M. A. Rodriguez, O. Crespo, C. Gimeno, A. Laguna, P. G. Jones, *Inorg. Chem.* **1998**, *37*, 6002.
42 D. Perreault, M. Drouin, A. Michel, P. D. Harvey, *Inorg. Chem.* **1993**, *32*, 1903.
43 M. A. Omary, T. R. Webb, Z. Assefa, G. E. Shankle, H. H. Patterson, *Inorg. Chem.* **1998**, *37*, 1380.
44 C. Klein, E. Graf, M. W. Hosseini, A. de Cian, *New J. Chem* **2001**, *25*, 207.
45 E. Bosch, C. L. Barnes, *Inorg. Chem.* **2002**, *41*, 2543.
46 K. M. Lee, H. M. J. Wang, I. J. B. Lin, *J. Chem. Soc., Dalton Trans.* **2002**, 2852.
47 Z. Xie, B.-M. Wu, T. C. W. Mak, J. Manning, C. A. Reed, *J. Chem. Soc., Dalton Trans.* **1997**, 1213.
48 Z. Xie, C.-W. Tsang, F. Xue, T. C. W. Mak, *J. Organomet. Chem.* **1999**, *577*, 197.
49 Z. Xie, R. Bau, C. A. Reed, *Angew. Chem. Int. Ed.* **1994**, *33*, 2433.
50 C.-W. Tsang, Q. Yang, E. T.-P. Sze, T. C. W. Mak, D. T. W. Chan, Z. Xie, *Inorg. Chem.* **2000**, *39*, 3582.
51 A. Bondi, *J. Phys. Chem.* **1964**, *68*, 441.
52 L. Magnko, M. Schweizer, G. Rauhut, M. Shchutz, H. Stoll, H.-J. Werner, *Phys. Chem. Chem. Phys.* **2002**, *4*, 1006.

53 H. Schmidbaur, A. Hamel, N. W. Mitzel, A. Schier, S. Nogai, *PNAS* **2002**, *99*, 4916.
54 N. J. Patmore, A. S. Weller, J. W. Steed, *Chem. Commun.* **2000**, 1055.
55 N. J. Patmore, M. F. Mahon, J. W. Steed, A. S. Weller, *J. Chem. Soc., Dalton Trans.* **2001**, 277.

3 PROTONOLYSIS AND HYDRIDE ABSTRACTION REACTIONS

3.1 Introduction

One of the cleanest methods for the isolation of cationic organometallic Lewis acids partnered with weakly coordinating anions is the protonation of methyl complexes (Equation 3.1). This synthetic strategy has been used to generate and isolate a number

$$L_nM\text{-}CH_3 + HX \longrightarrow L_nM\text{-}X + CH_4 \quad (3.1)$$

X = weakly coordinating anion

of organometallic compounds including $[Re(CO)_5(BF_4)]$,[1] $[MCp(CO)(L)(OSO_2R)]$[2] (M = Fe, Ru; L = CO, PMe_3) and $[FeCp(CO)_2(OTeF_5)]$.[3] Protonation of molybdenum methyl complexes with the corresponding acids has been used by Beck to isolate $[MoCp(CO)_3(BF_4)]$ and $[MoCp(CO)_3(OSO_2CF_3)]$.[4] The reaction between Brookhart's acid, $[H(OEt_2)_2(BAr'_4)]$ [Ar' = 3,5-bis(trifluoromethyl)phenyl], and $[WCp(CO)_3CH_3]$ generates the etherate complex $[WCp(CO)_3(OEt_2)][BAr'_4]$[5] (Figure 3.1), demonstrating the care that is needed when dealing with extremely weakly coordinating anions such as $[BAr'_4]^-$ to avoid the introduction of competing nucleophiles.

As well as methyl complexes, other σ-alkyl and σ-allyl species can be used in protonolysis reactions. The complex $[FeCp(CO)(PPh_3)(CH_2CH_3)]$ reacts with CF_3COOH to generate $[FeCp(CO)(PPh_3)(OCOCF_3)]$.[6] Treatment of

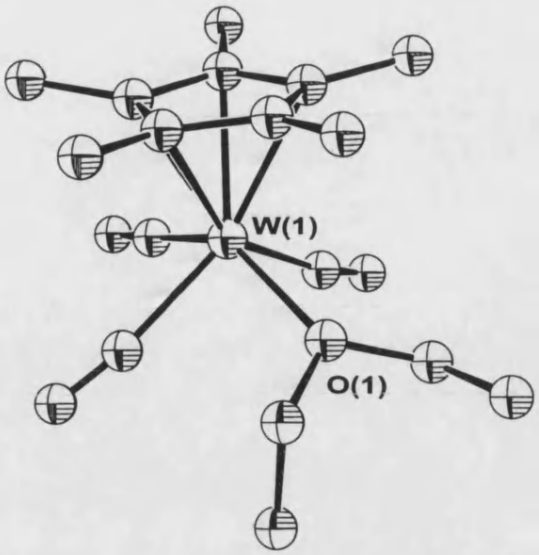

Figure 3.1: Solid state structure of the cationic portion of $[WCp(CO)_3(OEt_2)][BAr'_4]$ (reproduced from reference [5])

$[Mn(CO)_5(CH_2CH{=}CH_2)]$ with H(X) [X = $(Cl)^-$, $(NO_3)^-$, $(HSO_3)^-$, $(CF_3COO)^-$] results in the formation of a range of compounds with the general formula $[Mn(CO)_5(X)]$ and the evolution of propene gas.[7] If the acid of the more weakly coordinating $[ClO_4]^-$ anion is used instead, the product formed is $[Mn(CO)_5(CH_2{=}CHCH_3)][ClO_4]$, in which propene now coordinates to the metal. Spencer and co-workers have outlined the preparation of compounds containing ligated [*closo*-$CB_{11}H_{12}]^-$ via addition of two equivalents of $[H(OEt_2)_x][CB_{11}H_{12}]$ to $[PtR_2(L\text{-}L)]$ (R = Me, CH_2Bu^t; L-L = bis-chelating phosphine),[8] resulting in the liberation of the corresponding alkanes to generate $[Pt(L\text{-}L)(CB_{11}H_{12})][CB_{11}H_{12}]$ (Figure 3.2) that possesses a carborane bound to the platinum in an η^2-fashion.

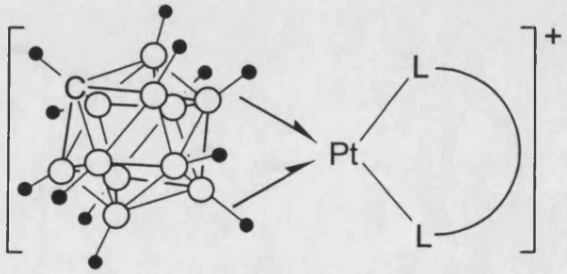

Figure 3.2: $[Pt(L\text{-}L)(CB_{11}H_{12})]^+$ cation (L-L = chelating phosphine)

A few investigations into the mechanism and kinetics of the reaction between metal alkyl complexes and strong acids have been published,[9, 10] and the reaction is generally proposed to proceed via an intermediate alkyl hydride complex. Evidence for this type of intermediate species comes from the treatment of $[RuCp^*(PMe_3)_2(CH_3)]$ with $H(BF_4)$ in diethyl ether that results in the precipitation of $[RuCp^*(PMe_3)_2(Me)(H)][BF_4]$ from solution, effectively halting the reaction at the intermediate stage.[11] If $H(SO_3CF_3)$ is used instead of $H(BF_4)$, the reaction proceeds to completion, and methane is eliminated to generate the final protonolysis product $[RuCp^*(PMe_3)_2(OEt_2)][SO_3CF_3]$. The protonolysis of a metal-alkyl complex containing both a chiral metal and a chiral alkyl ligand with HBr proceeds with retention of stereochemistry at both the carbon and metal centre to yield an organic compound with a chiral methyl group (Equation 3.2).[12] This retention of stereochemistry also implies a metal hydride intermediate is formed in the reaction.

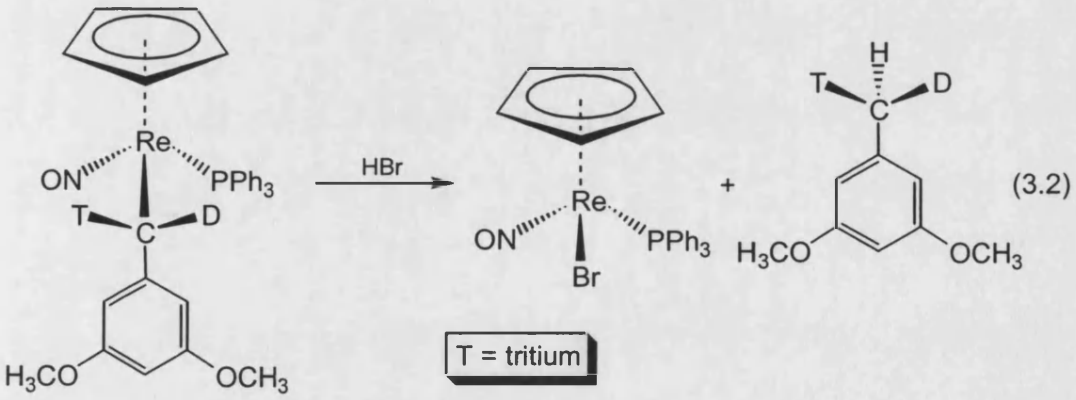

(3.2)

The elimination of hydrogen by reaction of metal hydride species with strong acids has also been studied.[13, 14] Depending on the metal the first step of this reaction can be the formation of a non-classical dihydrogen complex, supported by the isolation and characterisation of $[Fe(dppe)_2(\eta^2\text{-}H_2)(H)][HC(SO_2CF_3)_2]$[15] and $[RuCp(CO)(PR_3)(\eta^2\text{-}H_2)][BF_4]$[16] [$PR_3$ = PPh_3, PMe_3, PMe_2Ph, P(cyclohexyl)$_3$] from

the reaction of the corresponding metal hydride with $H_2C(SO_2CF_3)_2$ or $H(BF_4)$ respectively.

The treatment of $[L_nMH]$ with trityl (or more formally triphenylcarbenium) salts of weakly coordinating anions is the most commonly used technique to abstract a hydride from a transition metal complex and generate a cationic organometallic Lewis acid (Equation 3.3).

$$L_nM\text{-}H + [Ph_3C][X] \longrightarrow L_nM\text{-}X + Ph_3CH \quad (3.3)$$

X = weakly coordinating anion

Depending on the nature of the organometallic complex and the coordinating ability of the anion it is possible to isolate product species either with no anion coordination that consequently contain electron deficient metal centres, or with the metal electronically sated by coordination of a sufficiently nucleophilic solvent instead. For example, reaction of $[Ru(PPh_3)_4H_2]$ with $[Ph_3C][BF_4]$ in CH_2Cl_2 yields Ph_3CH and $[Ru(PPh_3)_4H][BF_4]$,[17, 18] a coordinatively unsaturated 16-electron metal complex with no coordination of the anion or solvent to ruthenium. In contrast, treatment of $[WCp(NO)_2H]$ with $[CPh_3][BF_4]$ in the more coordinating solvent acetonitrile yields $[WCp(NO)_2(NCCH_3)][BF_4]$,[19] a cationic complex containing bound acetonitrile.

Particularly pertinent to the work reported in this thesis is the pioneering chemistry explored by Beck and co-workers in the synthesis of $\{MoCp(CO)_3\}^+$ fragments partnered with weakly coordinating anions.[13] For example, the reaction of $[MoCp(CO)_3H]$ and $[CPh_3][BF_4]$ in CH_2Cl_2 yields Ph_3CH and $[MoCp(CO)_3(FBF_3)]$, a

complex containing coordinated $[BF_4]^-$.[20] Analogous molybdenum and tungsten compounds of coordinated $[PF_6]^-$, $[AsF_6]^-$, and $[SbF_6]^-$ have also been generated in a similar manner.[21] In the complexes $[MCp(CO)_2L(FBF_3)]$ [M = Mo, W; L = CO, PPh_3, $P(OPh)_3$], the coordinated and terminal fluorine atoms of the $[BF_4]^-$ ligand can be distinguished in low temperature (-80°C) ^{19}F NMR spectra.[22] These complexes are extremely reactive towards weak nucleophiles such as H_2O, and have to be prepared and handled at low temperatures in rigorously dried solvents under strictly anaerobic conditions to prevent decomposition.

The extremely weakly coordinating properties of $[BAr'_4]^-$ have been utilised in the synthesis of a number of complexes containing the weak solvent ligand CH_2Cl_2, using Brookhart's acid $[H(OEt_2)_2(BAr'_4)]$ or $[Ph_3C][BAr'_4]^-$ to introduce the anion.[23-25] Due to the lability of the CH_2Cl_2 ligand, these complexes are useful precursors for further reaction with appropriate σ-donors. For example, the dichloromethane ligand in *trans*-$[PtH(P^iPr_3)_2(ClCH_2Cl)][BAr'_4]$ reacts with H_2 or PhI to generate *trans*-$[PtH(P^iPr_3)_2(\eta^2\text{-}H_2)][BAr'_4]$ and *trans*-$[PtH(P^iPr_3)_2(\eta^1\text{-}IPh)][BAr'_4]$ respectively. Relevant to the systems under discussion later in this chapter is the competition between dichloromethane and $[PF_6]^-$ for metal coordination that is proposed to occur for $[MoCp(CO)_3(FPF_5)]$ dissolved in CD_2Cl_2.[22] This is evidenced by inspection of the ^{19}F NMR spectra at different temperatures. At -20°C the ^{19}F NMR spectrum displays a single doublet, consistent with the presence of uncoordinated $[PF_6]^-$ [J(PF) = 714Hz]. As the solution is allowed to warm to 15°C, three new resonances appear that correspond to coordinated $[PF_6]^-$. It is proposed that the anion is in a equilibrium with CD_2Cl_2 for metal complexation, as shown in Equation 3.4.

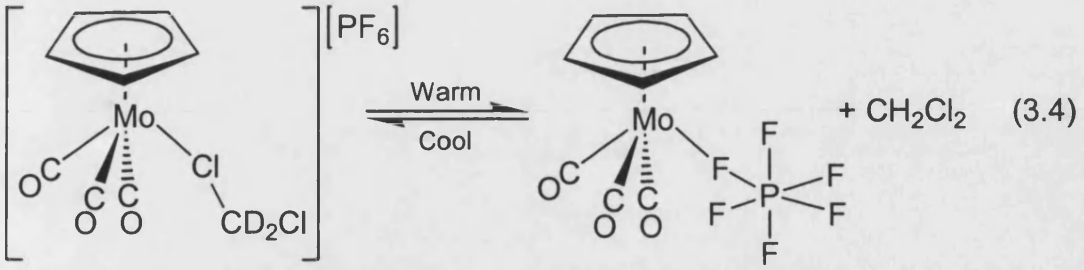

(3.4)

The synthesis and reactivity of a variety of complexes with the general formula $[MCp(CO)_2L(FBF_3)]$ (M = Mo, W; L = CO, PPh_3), and their subsequent reactions to isolate metal species with coordinated alkene, alkyne and acetone ligands is outlined by Beck and co-authors in *Inorganic Synthesis*.[26]

More recently, Bullock has used the trityl salt of $[BF_4]^-$ to measure the rates of hydride transfer from a series of neutral transition metal hydride species [MH] (M = d^6 or d^7 transition metal complex).[27, 28] Systematic changes of the metal hydride species can be made in order to examine the electronic effect of both metal and ligand on the rate of reaction. The series of substituted cyclopentadienyl tungsten hydride complexes of general formula $[WCp'(CO)_3H]$ (Cp′ = indenyl, Cp^*, C_5H_4Me, Cp, $C_5H_4CO_2Me$) have significantly different rates of reaction with $[Ph_3C][BF_4]$, with their kinetic hydricity spanning 3 orders of magnitude. The rate constants decrease as the electron density at the Cp′ ligand decreases, in the order $[W(indenyl)(CO)_3H] \approx [WCp^*(CO)_3H] > [W(C_5H_4Me)(CO)_3H] > [WCp(CO)_3H] > [W(C_5H_4CO_2Me)(CO)_3H]$. The values of the rate constants for reaction of the first, second and third row transition metal hydride complexes $[MCp^*(CO)_3H]$ (M = Cr, Mo, W) with $[CPh_3][BF_4]$ were shown to be Mo > W >> Cr. This work has been expanded very recently to encompass $[MCp^*(CO)_2H]$ (M = Fe, Ru, Os), metal hydride complexes of Group 8 metals.[29] The trend of reactivity down the group is reversed

compared to Group 6 and 7 hydrides, with $[FeCp^*(CO)_2H]$ reacting faster than $[OsCp^*(CO)_2H]$. Interestingly, each of the reactions of the three metal hydrides used with $[Ph_3C][BF_4]$ yielded different products (Equations 3.5, 3.6 and 3.7).

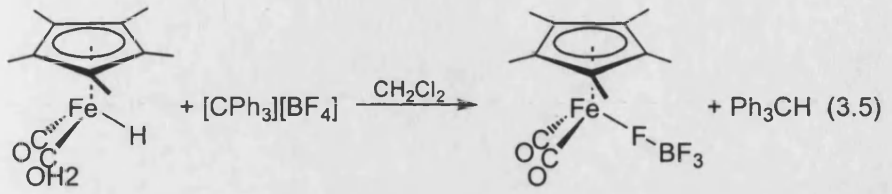

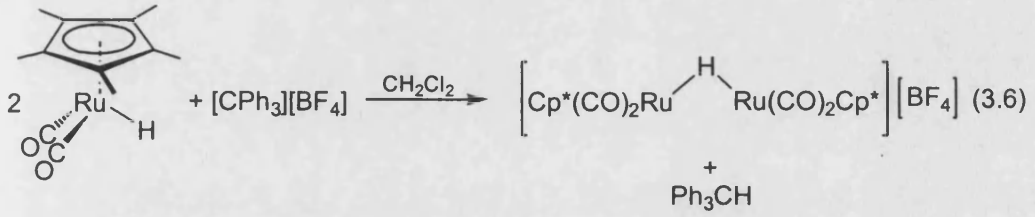

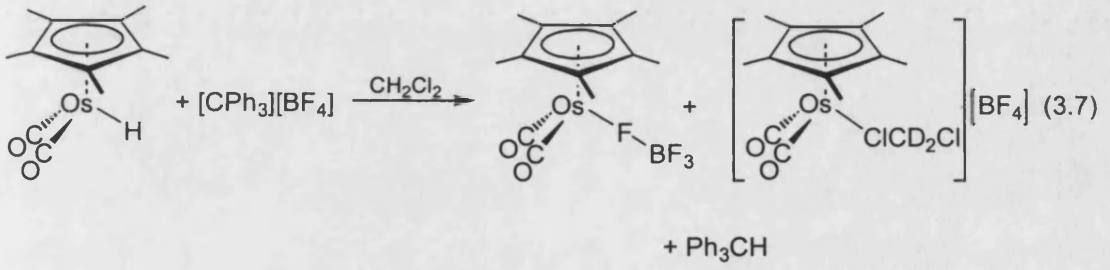

The hydride transfer from $[MoCp(CO)_2(PPh_3)H]$ to $[CPh_3][BAr'_4]$ produces a complex with an intramolecularly coordinated η^3-PPh_3 ligand, in which a C=C bond of the aryl ring is coordinated to molybdenum (Figure 3.3) highlighting the very weakly coordinating nature of $[BAr'_4]^-$.[30]

Given the volume of literature on the use of both hydride abstraction and protonolysis reactions as synthetic tools for the introduction of weakly coordinating anions into a metal's coordination sphere, it was hoped to be able to transfer these techniques for use with $[closo\text{-}CB_{11}H_{12}]^-$ and its derivatives. As outlined in the previous chapter,

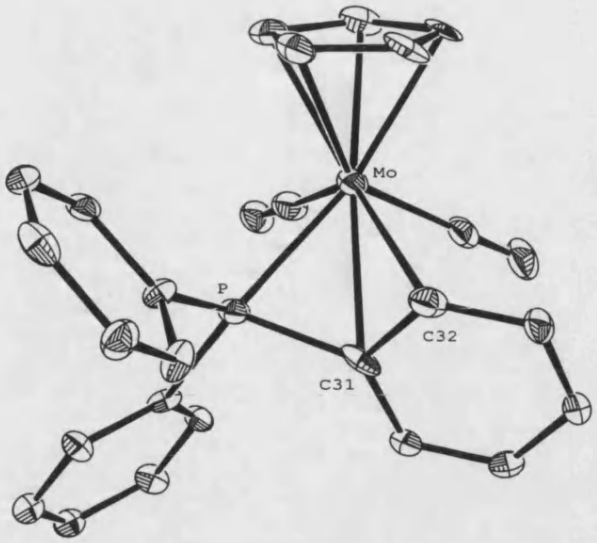

Figure 3.3: Crystal structure of the cationic component in $[MoCp(CO)_2(\eta^3\text{-}PPh_3)][BAr'_4]$ (reproduced from reference [30])
Hydrogens omitted for clarity, ellipsoids drawn at 30% probability.

silver salt metathesis has its limitations as a viable technique for the introduction of very weakly nucleophilic anions in cationic $\{MoCp(CO)_3\}^+$ organometallic fragments. For example, neither [*closo*-$CB_{11}H_{11}Br$]$^-$ or [*closo*-$CB_{11}H_6Br_6$]$^-$ analogues of compound **I** can be isolated via silver salt metathesis because of product decomposition, or cessation of the reaction at the intermediate stage. The isolation of $[MoCp(CO)_3(CB_{11}H_{11}Br)]$ and $[MoCp(CO)_3(CB_{11}H_6Br_6)]$ in addition to compound **I** would allow direct comparison of the reactivity of these carborane complexes, and facilitate the ranking of [*closo*-$CB_{11}H_{12}$]$^-$, [*closo*-$CB_{11}H_{11}Br$]$^-$, and [*closo*-$CB_{11}H_6Br_6$]$^-$ in terms of their relative nucleophilicities against other weakly coordinating anions. Another potentially interesting study would be the effect of using the more electron rich, but sterically demanding, Cp^* ligand. Given the large steric bulk of the anionic carborane ligands under study, Cp^* could reduce their ability to bind to a metal through unfavourable ligand / anion interactions.

This chapter will detail protonolysis and hydride abstraction reactions on $[MoCp(CO)_3X]$ (X = H, Me) synthons to isolate novel transition metal complexes containing ligated $[closo\text{-}CB_{11}H_{11}Br]^-$ and $[closo\text{-}CB_{11}H_6Br_6]^-$. This will allow comparison of the properties of the resulting compounds with analogous complexes containing other weakly coordinating anions such as $[BAr_F]^-$; and for the first time a chemical reactivity order for ranking these anions elucidated.

3.2 Results and Discussion

3.2.1 $[MoCp^*(CO)_3(x\text{-}\mu\text{-}H\text{-}CB_{11}H_{11})]$ (x = 7, 12)

Given the inability to isolate the Cp^* analogue of compound **I** via silver salt metathesis, as discussed in the previous chapter, other synthetic strategies needed to be investigated. One option for isolation of this analogue would be hydride abstraction, but the trityl salt of $[closo\text{-}CB_{11}H_{12}]^-$ is not accessible due to cage degradation upon synthesis.[31] The carborane acid, $[H(OEt_2)_x][CB_{11}H_{12}]$, has been synthesised previously as a volatile oil,[32] and can be isolated as a solid by crystallisation from a saturated diethyl ether solution at -80°C. Treatment of $[MoCp(CO)_3Me]$ in CH_2Cl_2 with one equivalent of $[H(OEt_2)_x][CB_{11}H_{12}]$ at -78°C resulted in a colour change of the solution from yellow to orange-red as it was allowed to warm to room temperature. The IR spectrum showed approximately 30% conversion, so a second portion of $[H(OEt_2)_x][CB_{11}H_{12}]$ was added. An IR spectrum taken 5 minutes later displayed the presence of just one compound in solution with a broad peak assigned to a bridging Mo-H-B bond observed at 2229cm^{-1} and CO

stretches at 2057 and 1986cm^{-1}, shifted to higher wavenumber than for [MoCp*(CO)$_3$Me] (2005 and 1914cm^{-1}). The solvent was removed and the resulting red solid dried *in vacuo*. The ^{1}H NMR spectrum of the crude solid showed quantitative conversion to product, but surprisingly there was no presence of any excess [H(OEt$_2$)$_x$][CB$_{11}$H$_{12}$]. An ^{11}B NMR spectrum of the contents of the Schlenk line cold-trap showed the presence of the [*closo*-CB$_{11}$H$_{12}$]$^-$ anion, indicating that [H(OEt$_2$)$_x$][CB$_{11}$H$_{12}$] is relatively volatile (10^{-3} Torr, room temperature). This also explains the need for an additional portion of [H(OEt$_2$)$_x$][CB$_{11}$H$_{12}$] to be added for the reaction to reach completion, as some would have been removed *in vacuo* when setting up the reaction using standard Schlenk line techniques. Crystals of the product were grown from a CH_2Cl_2/hexane layer at -30°C, and characterised as [MoCp*(CO)$_3$(x-μ-H-CB$_{11}$H$_{11}$)] (x = 7, 12), complex **V**, by X-ray crystallography, IR and NMR spectroscopy.

The solid state structure of the zwitterionic compound **V** is shown in Figure 3.4, with relevant bond lengths and angles in Table 3.1. The carbon atom of the cage was located by comparison of bond lengths and thermal parameters, and the bridging hydrogen H(12) was located in the electron density difference map and freely refined. All bond lengths and angles uniquely associated with the carborane cage are unremarkable. The anion is bound to molybdenum *via* the antipodal B-H vertex, forming a Mo-H-B 3 centre - 2 electron bond. The piano stool configuration adopted by molybdenum echoes the coordination environment seen for molybdenum in complex **I**. However, the steric effect of the bulky Cp* ligand is to force the cage 'down' the molecule, away from the bulky methyl groups in comparison to complex **I** in which the cage is orientated more towards the Cp ring. This change is demonstrated

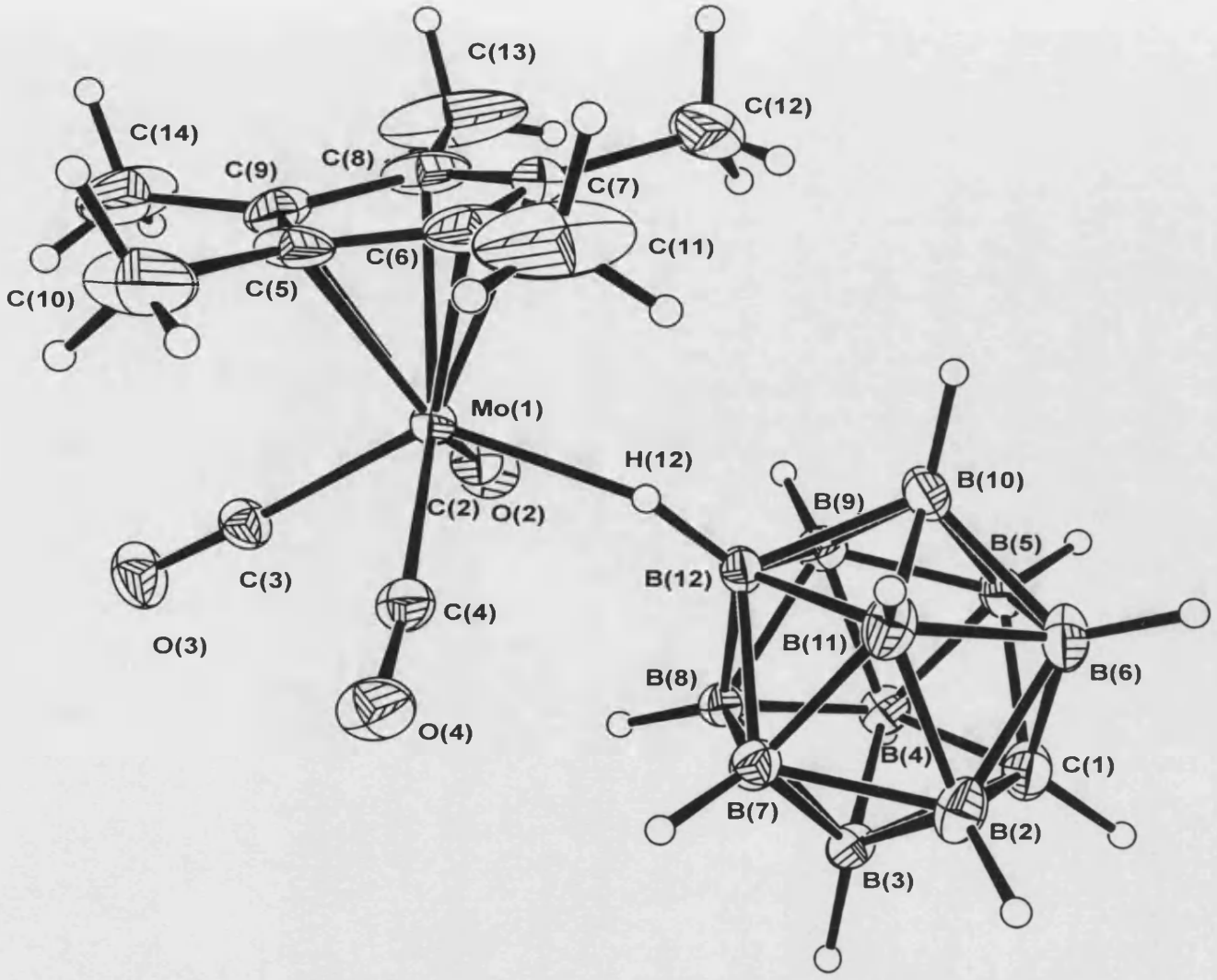

Figure 3.4: Crystal structure of $[MoCp^{*}(CO)_3(CB_{11}H_{12})]$, **V** (ellipsoids drawn at 30% probability level)

B(12)···Mo(1)	2.969(3) Å
B(12)-H(12)	1.07(5) Å
H(12)-Mo(1)	1.97(5) Å
B(12)-H(12)-Mo(1)	154(4)°
Mo(1)-B(12)-C(1)	168.4(1)°
C(1)-B(12)-H(12)	175(2)°
C(3)-Mo(1)-B(12)	122.4(1)°

Table 3.1: Selected bond lengths and angles for complex **V**

by a reduction of the C(3)-Mo(1)-B(12) bond angle in **V** [122.4(1)°] compared with that in **I** [139.8(1)°]. Within experimental error, the Mo(1)-H(12) and B(12)-H(12) bond lengths in **V** are the same as in **I**. The decrease in the CO stretching frequencies compared to complex **I** (average CO stretching frequencies: **I**, 2036cm^{-1}; **V**, 2022 cm^{-1}) indicates a more electron rich metal, due to greater electron donation from Cp*. Given this, and the increase in steric bulk of the environment around the metal it is surprising to note that the Mo(1)···B(12) bond in **V** [2.969(3)Å] is actually shorter than in **I** [3.000(3)Å], although this may just be due to the geometry forced upon the cage by the Cp* ligand. Nevertheless, the spectroscopic data and reactivity of **V**, discussed next, indicates that [*closo*-$CB_{11}H_{12}$]$^-$ is in fact bound more weakly in **V** compared to **I**. This is perhaps a consequence of the orientation of the cage, which is imposed by the Cp* ligand, preventing the efficient overlap of the B-H sigma bonding pair with the vacant metal orbital.

The ^{1}H NMR spectrum of a crystalline sample of **V** displays the bridging hydrogen as a partially collapsed quartet shifted significantly upfield from free carborane at δ -13.50, but at a slightly lower field and with a larger coupling constant [J(BH) = 98Hz] than found for the corresponding resonance in **I** [δ -15.11, J(BH) = 87Hz]. This indicates a slightly stronger B-H bond, and therefore, by inference, a weaker Mo-H bond in complex **V** compared to complex **I**. Mirroring the situation found for complex **I**, there are two Cp* resonances observed at δ 2.08 and δ 2.04, in a ratio of 1:3 respectively, indicating the presence of two isomeric forms in solution. The coalescence temperature for these two Cp* resonances in d_8-toluene is only 40°C, compared to 100°C in complex **I**, again indicating a weaker B-H-Mo bond in **V**. The ^{11}B{^{1}H} NMR spectrum also displays small peaks at δ -8.5 and δ -22.1 in addition to

the peaks of the major isomer at δ -13.9 (1B), δ -15.2 (5B) and δ -17.2 (5B). The C_{5v} symmetry of the carborane in the major isomer and large upfield shift of B(12) resonance compared to 'free' [*closo*-$CB_{11}H_{12}]^-$ (δ -8.0) once again leads to its assignment as the 12-isomer [$MoCp^*(CO)_3$(12-μ-H-$CB_{11}H_{11}$)], assuming facile rotation of the cage around the Mo-H-B bond, while assignment of the minor isomer follows as [$MoCp^*(CO)_3$(7-μ-H-$CB_{11}H_{11}$)].

Addition of acetone to a solution of **V** in CD_2Cl_2 shows no significant displacement of the carborane anion, as determined by NMR spectroscopy. If water, a stronger nucleophile, is used instead, rapid dissociation of the carborane occurs (< 15 minutes) further highlighting the weaker carborane-metal interaction in **V** compared to complex **I** (which is stable to attack from H_2O), and showing that steric effects are important when addressing the chemistry of these bulky anions.

3.2.2 [MoCp(CO)$_3$(12-μ-Br-CB$_{11}$H$_{11}$)]

As outlined in the previous chapter, the final metathesis product from the reaction of [$MoCp(CO)_3I$] and [$Ag(CB_{11}H_{11}Br)$] could not be isolated due to product decomposition so another synthetic route had to be found. To use the acid of [*closo*-$CB_{11}H_{11}Br]^-$ for methyl abstraction, similar to the synthetic route employed for **V**, was not considered practical as the acids are volatile oils at room temperature making them difficult to handle. They also contain diethyl ether solvate that could be a competing nucleophile with [*closo*-$CB_{11}H_{11}Br]^-$ for metal coordination as seen in the reaction between [$H(OEt_2)_2(BAr'_4)$] [Ar' = 3,5-bis(trifluoromethyl)phenyl] and

$[WCp(CO)_3CH_3]$.[5] The preparation of the trityl salt of $[closo\text{-}CB_{11}H_{11}Br]^-$ has not been previously reported. However, in the style of preparation used for $[CPh_3][CB_{11}H_6Br_6]$[31] the reaction of $[CPh_3Br]$ and $[Ag(CB_{11}H_{11}Br]$ in toluene/CH_3CN yields $[CPh_3][CB_{11}H_{11}Br]$, compound **VI**, in good yield (Equation 3.8). This is in contrast to $[closo\text{-}CB_{11}H_{12}]^-$, for which the trityl salt cannot be isolated

$$CPh_3Br + Ag(CB_{11}H_{11}Br) \xrightarrow[1\ hour]{CH_3CN/toluene} \underset{\textbf{(VI)}}{[CPh_3][CB_{11}H_{11}Br]} + AgBr_{(s)} \quad (3.8)$$

due to hydride abstraction from the B(12) vertex of the anion (section 1.3.2).[31] Three peaks are observed in the $^{11}B\{^1H\}$ NMR spectrum of **VI** at δ -3.0 (1B), δ -15.7 (5B) and δ -17.3 (5B). The C_{5v} symmetry observed and presence of a singlet in the ^{11}B NMR spectrum at δ -3.0 (1B) demonstrates that halogenation is exclusive to B(12). In the $^1H\{^{11}B\}$ spectrum, the cage C-H resonance is observed at δ 2.26 (s, 1H) and the upper and lower pentagonal belt B-H resonances at δ 1.90 (s, 5H) and δ 1.64 (s, 5H). The absence of an antipodal B-H resonance is in keeping with observation of a singlet in the ^{11}B NMR spectrum for B(12). The reaction of compound **VI** with $[MoCp(CO)_3H]$ to generate $[MoCp(CO)_3(CB_{11}H_{11}Br)]$ is discussed next.

$[MoCp(CO)_3H]$ was dissolved in CH_2Cl_2 and added dropwise to one equivalent of compound **VI**. After one hour stirring the IR spectrum showed the complete conversion of starting material to a new species, showing CO stretches at 2071 and 1999cm^{-1}, similar wavenumbers to complex **I** (2071 and 2001cm^{-1}). The solvent was removed *in vacuo* to yield a red powder, from which red crystals were grown in reasonable yield by redissolving in a minimum volume of CH_2Cl_2 and layering with

hexane at -30°C. The red crystals were characterised by elemental analysis, X-ray crystallography, IR and NMR spectroscopy and shown to be $[MoCp(CO)_3(CB_{11}H_{11}Br)]$, complex **VII**.

The solid state structure of complex **VII** is displayed in Figure 3.5 with relevant bond lengths and angles in Table 3.2. Again, the molybdenum centre adopts a piano stool geometry as seen in complexes **I** and **V.** The [*closo*-$CB_{11}H_{11}Br]^-$ anion is bound to the cage *via* a single dative bond from the bromine atom [Mo(1)-Br(1) 2.6759(2)Å], the length of which is in good agreement with Mo-Br distances of comparable complexes such as $[MoCp(CO)_3Br]$[33] [Mo-Br 2.651(1)Å], $[MoCp(CO)_2(PPh_3)Br]$[34] [Mo-Br 2.671(3)Å] and $[\{Cr(CO)_3(C_6H_5\text{-}C_5H_4)\}Mo(CO)_3Br]$[35] [Mo-Br 2.640(1)Å]. The assignment of the Br-Mo bond as dative rather than electrostatic in nature comes from inspection of the carborane geometry around the metal centre. The B(12)-Br(1)-Mo(1) angle is 116.43(5)° for complex **VII**. If the bromine-metal interaction was more electrostatic in action, i.e. $M^{\delta+}\cdots Br^{\delta-}$, the angle between the C(1)-B(12) axis and C(3)-Mo(1)-Br(1) plane would be closer to 180° in order to minimise any steric repulsion between the metal ligand set and cage (Figure 3.6).

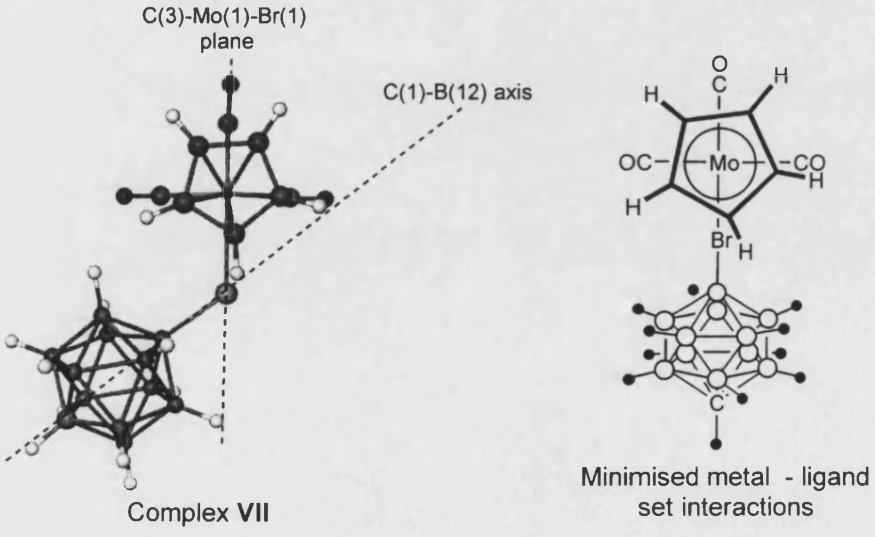

Figure 3.6: Metal ligand set - cage interactions in complex **VII**

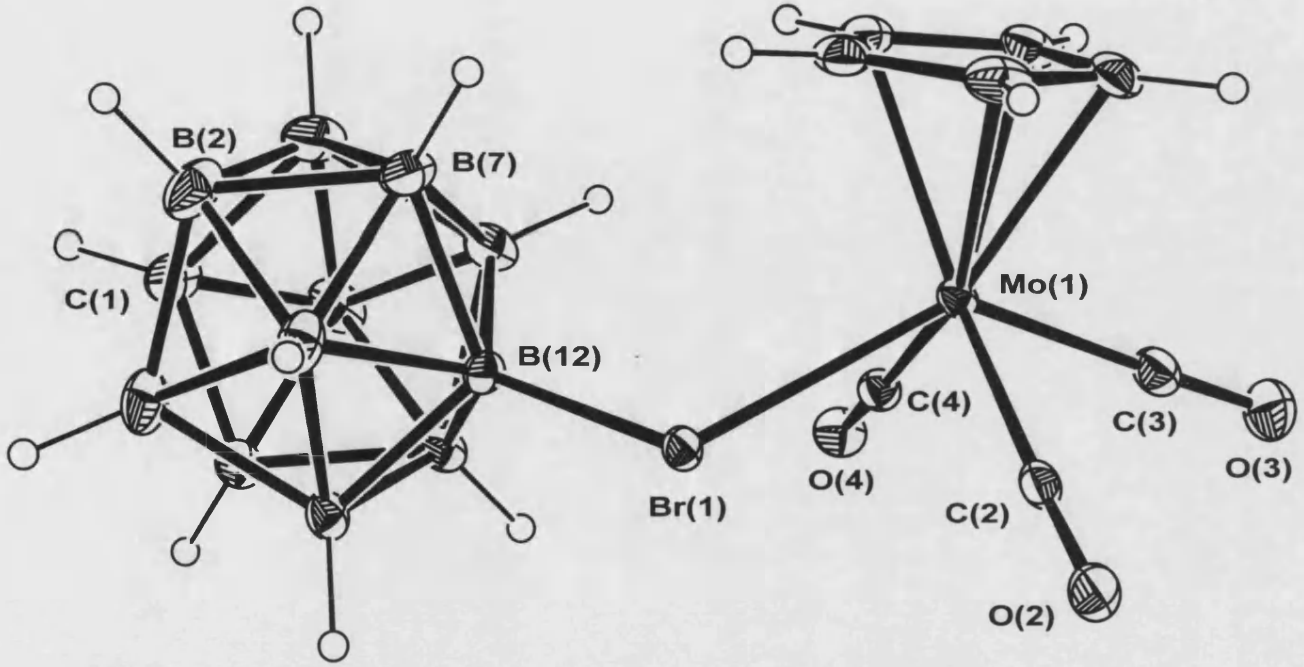

B(12)···Mo(1)	4.013(2) Å
B(12)-Br(1)	2.028(2) Å
Br(1)-Mo(1)	2.6759(2) Å
B(12)-Br(1)-Mo(1)	116.43(5)°
C(1)-B(12)-Br(1)	174.23(9)°
C(3)-Mo(1)-Br(1)	134.96(5)°

Table 3.2: Selected bond lengths and angles for complex **VII**

Figure 3.5: Crystal structure of $[MoCp(CO)_3(CB_{11}H_{11}Br)]$, **VII** (ellipsoids drawn at 30% probability level)

In support of this, E-Br-Y (E = C, B; Y = atom with suitable vacant orbital) angles are very similar for compounds containing such bonds from monodentate bromide ligands. The few examples isolated include **VII** [B-Br-Mo = 116.43(5)], $[Fe(TPP)(CB_{11}H_6Br_6)]$[36] [B-Br-Fe = 117.4(5)], $[PtH(^iPr_3P)_2(PhBr)]$ $[B\{3,5\text{-}(CF_3)_2C_6H_3\}_4]$[37] [C-Br-Pt = 116.4(7)] and $[Si(^iPr)_3(CB_{11}H_6Br_6]$[38] [B-Br-Si = 114.7(7)].

Comparison of bond lengths and angles of all the structurally characterised compounds containing [*closo*-$CB_{11}H_{11}Br]^-$ are displayed in Table 3.3. It shows a small, but significant, lengthening of the B-Br distance and a greater amount of deviation of the bromine atom from the C-$B_{antipodal}$ axis for complex **VII** (the only example of [*closo*-$CB_{11}H_{11}Br]^-$ bound to an organometallic metal centre) compared to the other compounds listed in which more electrostatic interactions are likely to occur.

Compound	Reference	B-Br Distance	C-$B_{anitpodal}$-Br Angle (θ)
$[Cs(CB_{11}H_{11}Br]$	[39]	1.995(3)Å	178.58°
$[Ag(CB_{11}H_{11}Br]$	[39]	1.998(9)Å	177.10°
IIIA	This work	2.005(3)Å	178.7(2)°
IIIB	This work	2.008(3)Å	177.4(2)°
VII	This work	2.028(2)Å	174.23(9)°

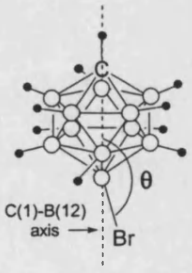

Table 3.3: Selected bond lengths and angles for all structurally characterised compounds containing [*closo*-$CB_{11}H_{11}Br]^-$ (some standard deviations unavailable)

The trends seen in the dative bonding of [*closo*-$CB_{11}H_{11}Br]^-$ to a metal are similar to those observed in the agostic bonding of [*closo*-$CB_{11}H_{12}]^-$, and whilst both are different types of interactions similar reasoning can account for these trends. The lengthening of the B-Br bond for **VII** compared to the caesium and silver salts of [*closo*-$CB_{11}H_{11}Br]^-$ is a consequence of the reduction in electron density on the

bromine atom as one of its lone pairs is donated to a suitable vacant metal orbital. In comparison the lengthening of the B-H distance in agostic interactions of [*closo*-$CB_{11}H_{12}]^-$ is a result of the σ bonding electrons of boron and hydrogen being shared with a suitable vacant metal orbital. The distortion of the C-$B_{antipodal}$-Br angle from the ideal of 180° is to allow more efficient overlap of the lone pair orbital on bromine and the vacant metal orbital, whilst minimising carborane-ligand steric interactions.

The Cp region of the $^1H\{^{11}B\}$ NMR spectrum of **VII** displays a major peak at δ 5.92, assigned to [$MoCp(CO)_3$(12-μ-Br-$CB_{11}H_{11}$)], shifted downfield (0.13 ppm) from the corresponding resonance found for the [$MoCp(CO)_3$(12-μ-H-$CB_{11}H_{11}$)] isomer of **I**. This is perhaps a consequence of the more weakly coordinating nature of [*closo*-$CB_{11}H_{11}Br]^-$ *versus* [*closo*-$CB_{11}H_{12}]^-$ being reflected in a more positive charge on the metal centre in **VII**. Closer inspection of the Cp region reveals a second peak at δ 5.96, with approximately 5% of the intensity of the main resonance, which is assigned as [$MoCp(CO)_3$(7-μ-H-$CB_{11}H_{10}Br$)], the isomeric form of **VII**. The corresponding B-H-Mo resonance of this isomer can just be observed in the ^1H NMR spectrum as a partially collapsed quartet at δ -15.08 [*J*(BH) *ca.* 89Hz], but it is an extremely weak signal due to its multiplicity and the low concentration of this isomeric form in solution. The downfield shift of the Cp resonances in [$MoCp(CO)_3$(7-μ-H-$CB_{11}H_{10}Br$)] (δ 5.96) compared to the analogous isomeric form of compound **I**, [$MoCp(CO)_3$(7-μ-H-$CB_{11}H_{11}$)] (δ 5.86), suggests a slight reduction in the basicity of the lower pentagonal belt hydrogens in [*closo*-$CB_{11}H_{11}Br]^-$ a consequence of the electron withdrawing effect that halogenation of the cage periphery has on the carborane core.[40] The ^{11}B NMR spectrum displays a singlet and two doublets at δ -1.6 (1B), δ -13.9 (5B) and δ -16.9 (5B) respectively, indicating that in solution the

cage has C_{5v} symmetry due to facile rotation of the cage around the Mo-Br bond. The peaks corresponding to the 7-isomer are not observed in the $^{11}B\{^1H\}$ NMR spectrum, although this is perhaps not surprising given its very low concentration and the predicted number of low intensity signals (in the ratio 1B:1B:1B:2B:2B:2B:2B) that are likely to be lost in spectral noise in the presence of the large broad peaks corresponding to the major isomer.

The reaction of complex **VII** with diethyl ether or H_2O does not result in the displacement of the [*closo*-$CB_{11}H_{11}Br$]$^-$ anion, as evidenced from the examination of ^1H NMR spectra taken 1 day after addition of the relevant nucleophile. Chemical inertness to water and diethyl ether is also seen for complex **I**, which suggests [*closo*-$CB_{11}H_{12}$]$^-$ and [*closo*-$CB_{11}H_{11}Br$]$^-$ complexes have similar reactivities and therefore the anions have similar coordinating abilities. However, the use of the chemical reactivity of complexes **I** and **VII** to rank the coordinating ability of [*closo*-$CB_{11}H_{12}$]$^-$ and [*closo*-$CB_{11}H_{11}Br$]$^-$ is a rough qualitative measure. In contrast, the Cp chemical shift of these compounds in the ^1H NMR spectrum provides a more quantitative measure, from which the relative coordinating abilities of these compounds can be distinguished, and [*closo*-$CB_{11}H_{11}Br$]$^-$ ranked more weakly coordinating than [*closo*-$CB_{11}H_{12}$]$^-$.

The synthesis of compounds **I** and **VII** allows direct comparison of the relative coordinating abilities of [*closo*-$CB_{11}H_{12}$]$^-$ and [*closo*-$CB_{11}H_{11}Br$]$^-$. The synthesis of the equivalent metal complex containing [*closo*-$CB_{11}H_6Br_6$]$^-$, thought to be the most weakly coordinating of these anions, will allow for the first time a direct comparison between the properties of all three of these carborane anions and is discussed in the next section.

3.2.3 $[MoCp(CO)_3(CB_{11}H_6Br_6)]$

Given the success of hydride abstraction using the trityl salt of monobromocarborane in the isolation compound **VII,** attention was focused on the reaction between $[MoCp(CO)_3H]$ and $[CPh_3][CB_{11}H_6Br_6]$ to generate the $[closo\text{-}CB_{11}H_6Br_6]^-$ analogue of complexes **I** and **VII**. This reaction is akin to those developed by Beck and co-workers to generate $[MoCp(CO)_3(X)]$ (X = weakly coordinating anion).[13]

In a typical reaction $[MoCp(CO)_3H]$ was dissolved in CH_2Cl_2 and transferred dropwise into a flask containing $[CPh_3][CB_{11}H_6Br_6]$ at -78°C, and the solution allowed to warm slowly to room temperature. The ^1H NMR spectrum of the resulting solution displayed a number of Cp resonances corresponding to reaction products which include $[MoCp(CO)_3(CB_{11}H_6Br_6)]$ and $[MoCp(CO)_3(ClCD_2Cl)][CB_{11}H_6Br_6]$, assignment of which will be discussed next.

Due to the sensitivity of the products formed to trace amounts of nucleophiles (see later discussion), *in situ* measurements were made in order to cleanly isolate the reaction products. A Young's NMR tube was charged with $[CPh_3][CB_{11}H_6Br_6]$ and a slight excess of $[MoCp(CO)_3H]$ before adding CD_2Cl_2 at -78°C. The Youngs NMR tube was then placed in a pre-cooled NMR probe and the reaction monitored by ^1H NMR spectroscopy as the solution is warmed slowly to room temperature (Figure 3.7). Even at these low temperatures the reaction is quick, with no phenyl resonances corresponding to the $[Ph_3C][CB_{11}H_6Br_6]$ starting material observed at -65°C. The Cp region of the spectrum at 16°C displays peaks at δ 5.47 and δ 5.56 corresponding to

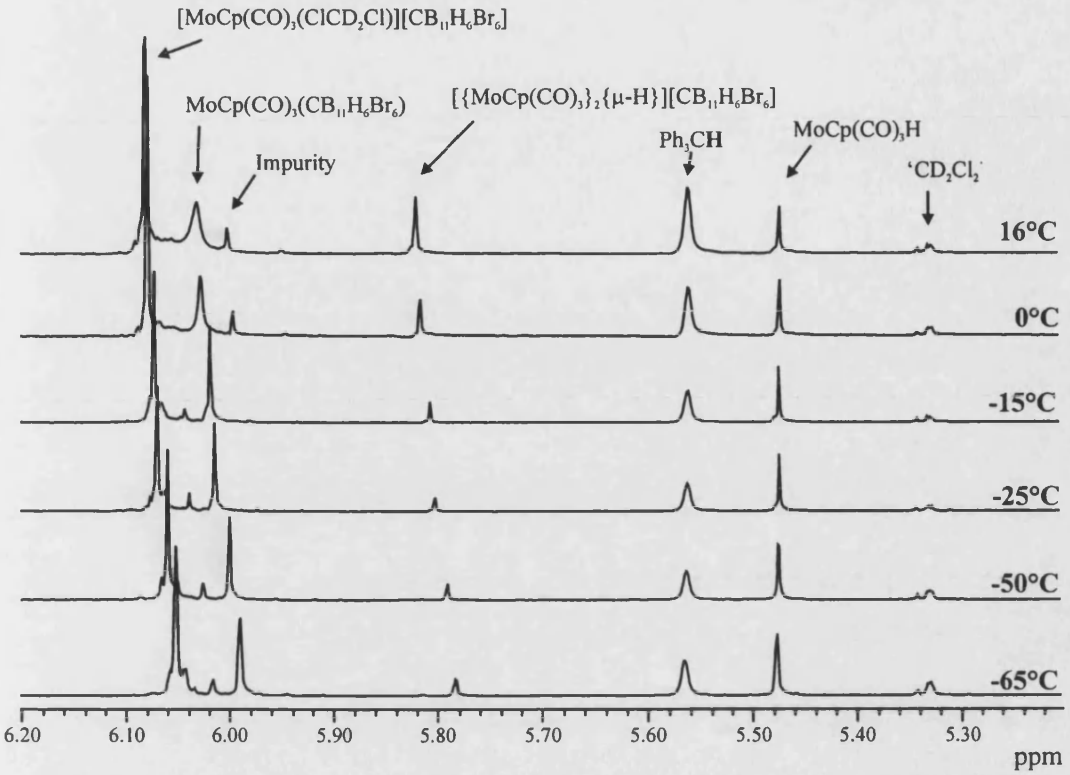

Figure 3.7: Cp region of the ^{1}H NMR spectra in the variable temperature experiments for reaction of $[MoCp(CO)_3H]$ with $[CPh_3][CB_{11}H_6Br_6]$ (see text for discussion of suggested peak assignments)

unreacted $[MoCp(CO)_3H]$ and Ph_3CH respectively, and two major product Cp resonances at δ 6.07, δ 6.02 in the ratio 4.8 : 3 respectively. The very broad nature of the peak at δ 6.02 indicates that it is perhaps a combination two isomeric species in fast exchange with one another, and appears to arise from the coalescence at 0°C of the two peaks present at δ 6.02 and δ 5.99 (relative integrals 1 : 5 respectively) in the spectrum measured at -65°C. As such, it is assigned to the isomeric compounds $[MoCp(CO)_3(7\text{-}\mu\text{-}Br\text{-}CB_{11}H_6Br_5)]$ and $[MoCp(CO)_3(12\text{-}\mu\text{-}Br\text{-}CB_{11}H_6Br_5)]$ (Figure 3.8). The presence of two isomeric forms of $[MoCp(CO)_3(CB_{11}H_6Br_6)]$ would also be in parity with that seen for complexes **I** and **VII**. Moreover, the higher coalescence temperature of the Cp resonances for the isomeric forms of complex **I** (100°C)

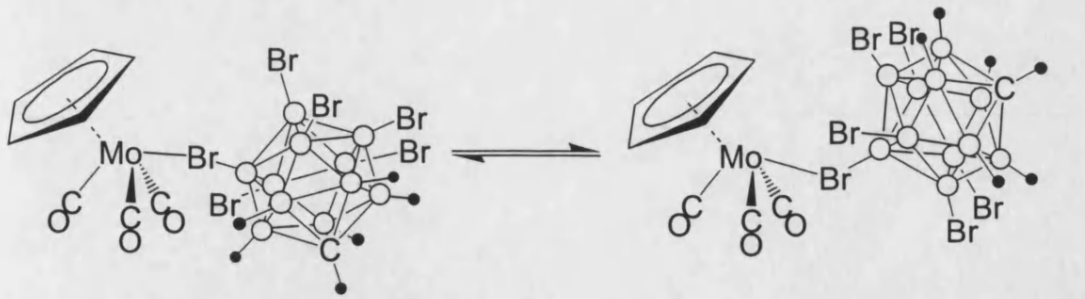

$MoCp(CO)_3(7\text{-}\mu\text{-}Br\text{-}CB_{11}H_6Br_5)$ $MoCp(CO)_3(12\text{-}\mu\text{-}Br\text{-}CB_{11}H_6Br_5)$

Figure 3.8: Isomeric forms of $[MoCp(CO)_3(CB_{11}H_6Br_6)]$

compared to $[MoCp(CO)_3(CB_{11}H_6Br_6)]$ (0°C) reflects significantly stronger coordination of $[closo\text{-}CB_{11}H_{12}]^-$ to molybdenum compared with $[closo\text{-}CB_{11}H_6Br_6]^-$, expected from previous rankings of the relative coordinating abilities of the anions.

The peak at δ 6.07 in the spectrum at 16°C (Figure 3.7) is tentatively assigned to $[MoCp(CO)_3(ClCD_2Cl)][CB_{11}H_6Br_6]$. This value is in good agreement with the chemical shift seen for the Cp resonance in $[MoCp(CO)_3(ClCD_2Cl)][PF_6]$, δ 6.06.[22] This species was shown to be in an equilibrium with $[MoCp(CO)_3(PF_6)]$ (Equation 3.4), which at higher temperatures favoured this anion coordinated species over $[MoCp(CO)_3(ClCD_2Cl)][PF_6]$. A similar situation is observed in our system, with the ratio of the Cp resonances corresponding to $[MoCp(CO)_3(CB_{11}H_6Br_6)]$ and $[MoCp(CO)_3(ClCD_2Cl)][CB_{11}H_6Br_6]$ increasing from 0.5 : 1 at -65°C to 1.1 : 1 at room temperature.

Another product Cp resonance in the ^1H NMR spectrum at 16°C, δ 5.82, is assigned as the reaction side product $[\{MoCp(CO)_3\}_2(\mu\text{-}H)][CB_{11}H_6Br_6]$ with the corresponding bridging hydride resonance observed at δ -21.09, that has a tenth of the intensity of the Cp resonance, as expected. The similar compound $[\{MoCp(CO)_3\}_2(\mu\text{-}$

H)][PF_6] [^{1}H NMR (CD_3NO_2): δ 5.93 (C_5H_5); δ -20.80 (MoHMo)] has been isolated from the reaction between 2 equivalents of [$MoCp(CO)_3H$] and one equivalent of [Ph_3C][PF_6].[20, 41] Its formation in this system arises from reaction of [$MoCp(CO)_3(CB_{11}H_6Br_6)$] (or the dichloromethane complex) with [$MoCp(CO)_3H$]. This reaction is in competition with [CPh_3][$CB_{11}H_6Br_6$] for reaction with [$MoCp(CO)_3H$], highlighted by inspection of a spectrum taken at room temperature, one hour after the one at 16°C. This is displayed in Figure 3.9 along with assignment of the peaks present. It shows the absence of any excess [$MoCp(CO)_3H$] and an increase in relative concentration of [$\{MoCp(CO)_3\}_2(\mu_2\text{-}H)$][$CB_{11}H_6Br_6$] to the expense of the combined concentrations of [$MoCp(CO)_3(ClCD_2Cl)$][$CB_{11}H_6Br_6$] and [$MoCp(CO)_3(CB_{11}H_6Br_6)$] species (relative integrals 0.2 : 1 respectively), compared with the spectrum taken 1 hour earlier at 16°C (relative integrals 0.1 : 1).

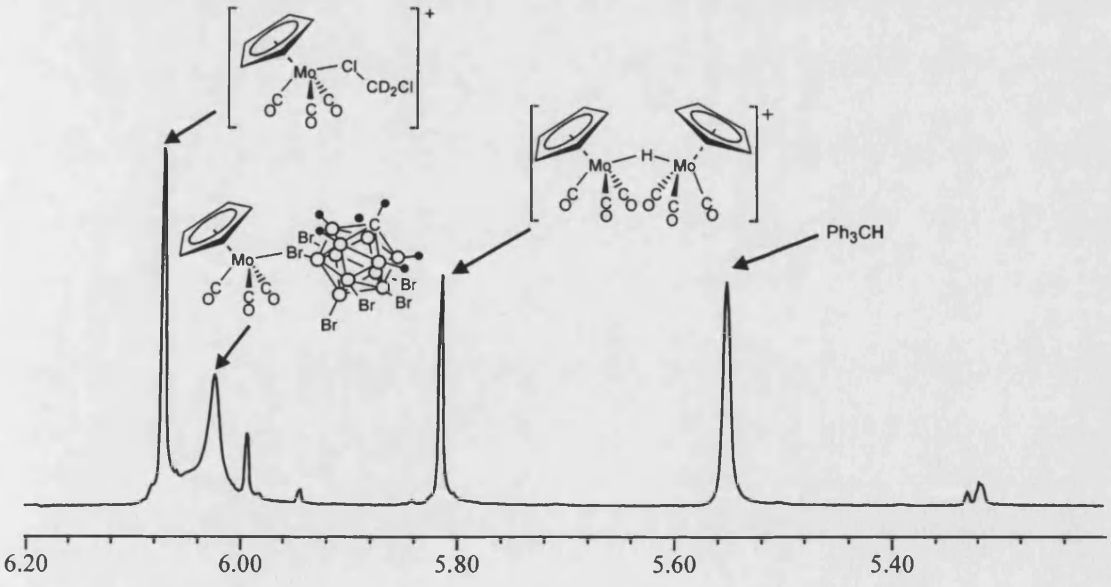

Figure 3.9: Cp region in the ^{1}H NMR spectrum of the final products at room temperature

Evidence for coordinated and uncoordinated forms of [*closo*-$CB_{11}H_6Br_6$]$^-$ also comes from inspection of the C-H_{cage} region of the ^{1}H NMR spectra. At -50°C, three broad C-H_{cage} resonances are observed (Figure 3.10), which are tentatively assigned as belonging to the two isomeric forms of [$MoCp(CO)_3(CB_{11}H_6Br_6)$] (δ 2.88, δ 2.80) and uncoordinated or 'free' [*closo*-$CB_{11}H_6Br_6$]$^-$ (δ 2.75). These assignments come, in part, from inspection of the ^{1}H NMR spectrum at the coalescence temperature (0°C) of the two isomeric species that displays just two C-H_{cage} resonances at δ 2.82 [$MoCp(CO)_3(CB_{11}H_6Br_6)$] and δ 2.76 ['free' (*closo*-$CB_{11}H_6Br_6$)$^-$]. Addition of a portion of D_2O to the mixture of products results in the exclusive formation of [$MoCp(CO)_3(OD_2)$][$CB_{11}H_6Br_6$] (see later discussion), and only one C-H_{cage} resonance is observed at δ 2.74 which corresponds to 'free' [*closo*-$CB_{11}H_6Br_6$]$^-$.

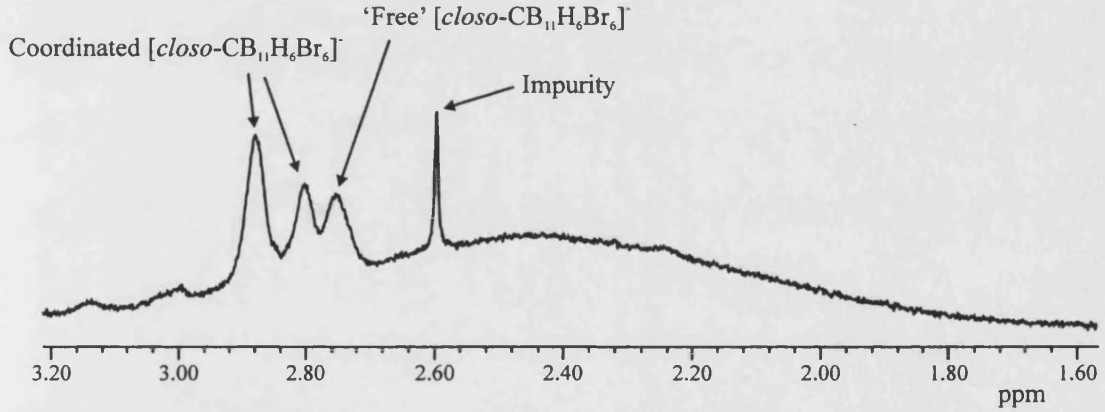

Figure 3.10: C-H_{cage} region of the ^{1}H NMR spectrum at -50°C

The $^{11}B\{^1H\}$ NMR spectrum of the reaction products displays three peaks at δ -2.0 (1B), δ -10.2 (5B) and δ -20.5 (5B). This indicates C_{5v} symmetry of the cage, and offers no clues to the anion's behaviour in solution. Kubas and co-workers have used low temperature (-80°C) ^{13}C NMR spectroscopy to characterise the coordinated dichloromethane in [*cis*-$Re(CO)_4(P^iPr_3)(ClCH_2Cl)$][$BAr_F$], which displays a weak

resonance shifted approximately 14 ppm downfield from dichloromethane solvent. Attempts to characterise $[MoCp(CO)_3(ClCD_2Cl_2)][CB_{11}H_6Br_6]$ in a similar manner were thwarted because of the low solubility of these species in dichloromethane and because, in error, the spectrum was measured in CD_2Cl_2 as opposed to CH_2Cl_2, where peak broadening due to deuterium coupling would preclude observation of this already weak signal.

A solution IR spectrum of the products of reaction between $[CPh_3][CB_{11}H_6Br_6]$ and $[MoCp(CO)_3H]$ in CD_2Cl_2 (made up in a glovebox) displayed only two ν(CO) stretches at 2073 and 1990cm^{-1} (average 2032cm^{-1}). Given the fast timescale associated with IR spectroscopy, the absence of separate stretching frequencies for $[MoCp(CO)_3(ClCD_2Cl)][CB_{11}H_6Br_6]$ and $[MoCp(CO)_3(CB_{11}H_6Br_6)]$ suggests that both species have similar CO stretching frequencies. These values are similar to the carbonyl stretching frequencies found for **VII** (2069 and 1982 cm^{-1}) and **I** (2071 and 2001 cm^{-1}) suggesting that, for this system, carbonyl stretching frequencies cannot be used to distinguish between the coordinating abilities of these carborane anions as the reactivity of the three compounds is very different, as outlined next.

For some reactions performed in CH_2Cl_2, the ^1H NMR spectrum displayed peaks correlating to coordinated diethyl ether (presumably from still-pot contamination) at δ 3.84 (q, J_{HH} = 6.8Hz) and δ 1.34 (t, J_{HH} = 6.8Hz). The related diethyl ether complex $[WCp^*(CO)_3(OEt_2)][BAr'_4]$ also displays downfield shifts for the coordinated diethyl ether ligand (δ 3.97 and δ 1.19).[5] Addition of a large excess of diethyl ether to the product mixture does not result in the exclusive formation of $[MoCp(CO)_3(OEt_2)][CB_{11}H_6Br_6]$, with peaks due to the reaction products still

observed. The coordination of OEt_2 in $[WCp^*(CO)_3(OEt_2)][BAr'_4]$ might suggest $[BAr'_4]^-$ to be a more weakly coordinating anion than $[closo\text{-}CB_{11}H_6Br_6]^-$, but the increased steric bulk around a metal when using Cp^* as opposed to Cp precludes direct contrast, as seen in the increased reactivity of **V** compared to **I** towards nucleophiles. Trace amounts of the stronger nucleophiles H_2O, MeCN or acetone were also seen in some experiments, arising from solvent contamination. Addition of 1 equivalent of these nucleophiles to the product mixture readily yields the corresponding solvent coordinated cationic metal complexes $[MoCp(CO)_3X][CB_{11}H_6Br_6]$ (X = D_2O, MeCN or acetone), with the corresponding unique Cp resonances at δ 5.92 (D_2O), δ 5.94 (MeCN), and δ 6.10 (acetone).

The products of reaction between $[MoCp(CO)_3H]$ and $[CPh_3][CB_{11}H_6Br_6]$ could not be further purified or characterised due to the high reactivity of products. Numerous attempts at recrystallisation, in order to put the products on a firm structural footing, resulted in the formation of pink-red solid or oil. In one instance, a few crystals were found present amongst the oil and were characterised by an X-ray diffraction study. They were shown to be $[MoCp(CO)_3(OH_2)][CB_{11}H_6Br_6]$ (complex **XIII**), formed by the presence of adventitious water.

The solid state structure of compound **XIII** is displayed in Figure 3.11, with salient bond lengths and angles in Table 3.4. The molybdenum adopts piano stool geometry with water and three carbonyl ligands capped by the Cp ring. The assignment of O(1) as a water ligand despite failure to locate the related hydrogens in the electron density difference map comes from examination of the Mo(1)-O(1) bond length [2.205(6) Å].

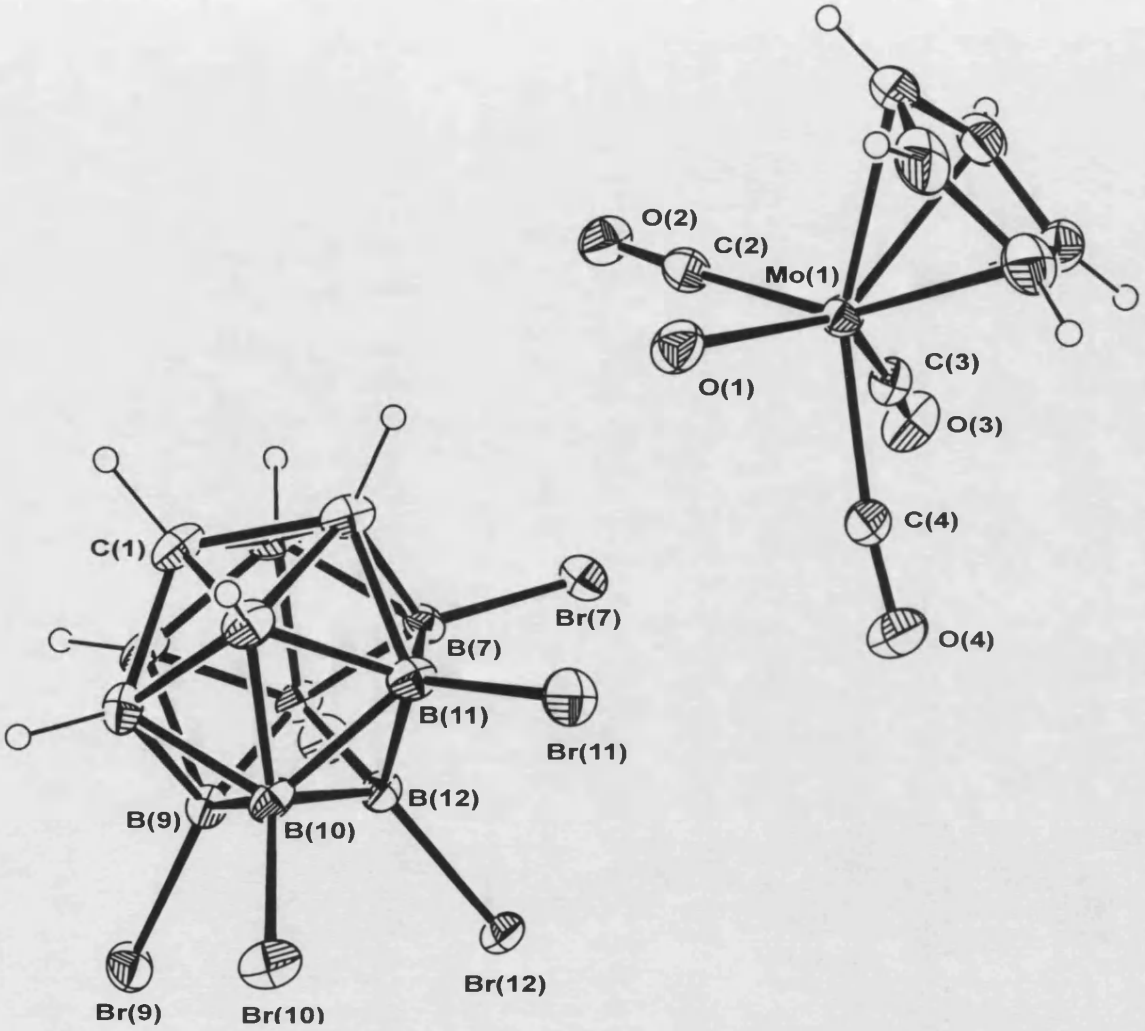

Figure 3.11: Crystal structure of $[MoCp(CO)_3(OH_2)][CB_{11}H_6Br_6]$, **XIII** (ellipsoids drawn at 30% probability level)

Mo(1)-O(1)	2.205(4) Å
Mo(1)-C(2)	2.038(7) Å
Mo(1)-C(3)	1.999(7) Å
Mo(1)-C(4)	2.044(7) Å
B(12)-Br(12)	1.959(7) Å
O(1)···Br(11)	3.469(6) Å
O(1)-Mo(1)-C(3)	138.7(3)°
C(2)-Mo(1)-C(4)	112.4(3)°
C(1)-B(12)-Br(12)	179.5(3)°

Table 3.4: Selected bond lengths and angles for complex **XIII**

This is a relatively long Mo-O bond and is significantly longer than Mo=O bonds that are typically 1.678 - 1.707 Å.[42] The longest terminal Mo-OH bond distance found in a search of the Cambridge Structural Database was 2.080(3) Å, for the Mo(III) compound $[MoCp(PMe_3)_3(OH)][BF_4]$.[43] The Mo(1)-O(1) bond distance lies within the typical range found for Mo-OH_2 bond distances, 2.112 - 2.220 Å.[44] All other bond lengths within the cation and anion are unremarkable.

Close inspection of the packing diagram reveals hydrogen bonding between Br(12)' and O(1) [Br(12)'···O(1), 3.366(6) Å]. The distance found for this interaction is comparable to similar interactions in the aqua complexes $[Co(CH_3CN)_2(H_2O)_4][Br]_2$ [3.283 - 3.315 Å][45] and $[Cu(C_6H_6N_2O)(H_2O)_2][Br]_2$ [3.31 - 3.379 Å][46]. Weaker interactions from three adjacent bromines [Br(11)···O(1), 3.469(6) Å; Br(10)'···O(1), 3.500(6) Å; Br(8)''···O(1), 3.522(6) Å] in two neighbouring asymmetric units result in each cage hydrogen bonding via four bromine atoms to the water molecule. Consequently, a 3-dimensional polymer of cations and anions is propagated in the solid state (Figure 3.12).

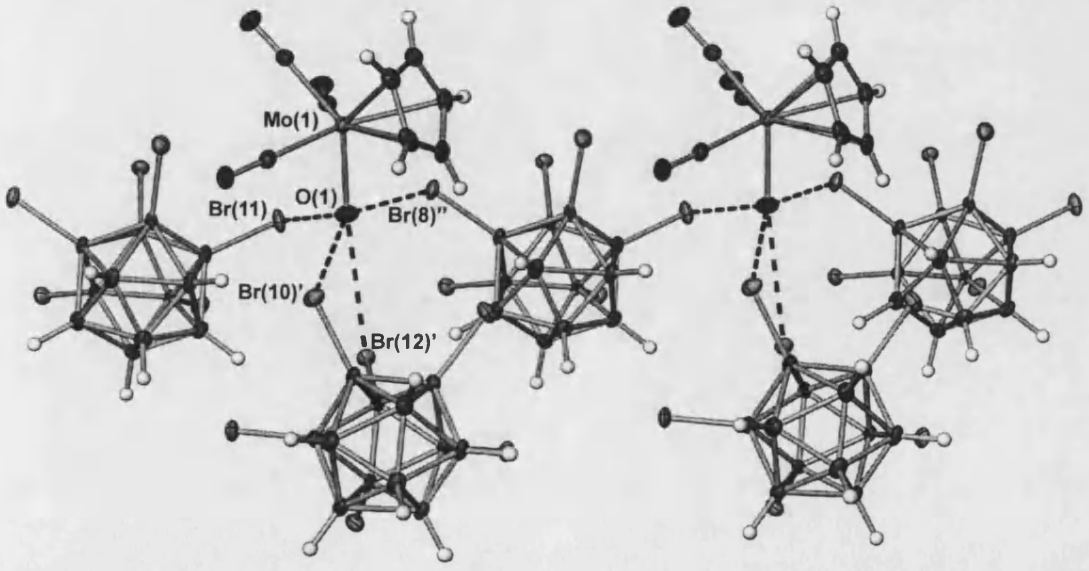

Figure 3.12: Hydrogen bonded environment of H_2O in complex **XIII**

The abstraction of a methyl group using trityl salts of weakly coordinating anions has been used to isolate $[M(CO)_5(BF_4)]$ (M = Mn, Re).[47] Attempts to mimic this reaction in order to isolate the more sterically demanding Cp^* analogue of $[MoCp(CO)_3(CB_{11}H_6Br_6)]$ was attempted by treatment of $[MoCp^*(CO)_3Me]$ with $[CPh_3][CB_{11}H_6Br_6]$ in CH_2Cl_2. The ^1H NMR spectrum of the resulting products displayed more than 5 Cp^* resonances, indicating the formation of a number of species. The products formed are very reactive and their solutions darken rapidly on exposure to air. Any attempts to further purify these mixtures in order to further characterise the products resulted in their decomposition. The formation of Ph_3CMe as a product of reaction is suggested by the presence of a large multiplet in the ^1H NMR spectrum at δ 7.10 due to phenyl resonances, with the corresponding methyl resonance lost in the myriad of Cp^* resonances [Ph_3CMe lit.[48] values ($CDCl_3$): δ 7.17 (m, 15H), δ 2.20 (s, 3H)]. This perhaps implies $[MoCp^*(CO)_3(ClCH_2Cl)][CB_{11}H_6Br_6]$ or $[MoCp^*(CO)_3(CB_{11}H_6Br_6)]$ were initially formed, but are unstable in solution. In some literature cases, using Ph_3C^+ to abstract a methyl group results in hydride transfer instead to generate a carbene complex. For example, treatment of $[ReCp(NO)PPh_3)(CH_3)]$ with $[Ph_3C][PF_6]$ affords $[ReCp(NO)(PPh_3)(=CH_2)][PF_6]$.[49] However, the absence of Ph_3CH resonances in the ^1H NMR spectrum of the products from reaction of $[MoCp^*(CO)_3Me]$ with $[CPh_3][CB_{11}H_6Br_6]$ indicates that this does not happen in this instance. Given the decomposition of the products from this reaction, it is unsurprising that the products of the analogous reaction between $[MoCp^*(CO)_3H]$ and $[CPh_3][CB_{11}H_6Br_6]$ in CH_2Cl_2 also yield a similarly large number Cp^* species in the ^1H NMR spectrum.

The product mixtures resulting from reaction of $[MoCp^*(CO)_3Me]$ or $[MoCp^*(CO)_3H]$ with $[CPh_3][CB_{11}H_6Br_6]$ can be treated with acetone to generate $[MoCp(CO)_3(C_3H_6O)][CB_{11}H_6Br_6]$ (**IX**) as the major species in solution (approximately 50% of total Cp^* integrals in ^1H NMR spectrum of products). The corresponding Cp^* peak is observed at δ 2.04 and the coordinated acetone resonance comes at δ 2.49 in the ^1H NMR spectrum of **IX**. The downfield shift of the coordinated acetone resonance compared to 'free' acetone (δ 2.17) has been observed in the related compound $[MoCp(CO)_3(O{=}CMe_2)][BF_4]$[26] (δ 2.43). This species also displays a peak a $1640cm^{-1}$ in the IR spectrum corresponding to the ν(C=O) stretching frequency of coordinated acetone. The related peak for the ν(C=O) stretching frequency in compound **IX** is displayed at $1653cm^{-1}$. Both these stretching frequencies are considerably lowered than free acetone [ν(C=O) = $1712cm^{-1}$], highlighting the weakening of the C=O bond on coordination to the metal. A CH_2Cl_2 / hexane layer of this mixture resulted in the formation of a brown oil containing orange-red crystals. An X-ray diffraction study of these crystals showed them to be $[MoCp^*(CO)_3(O{=}CMe_2)][CB_{11}H_6Br_6]$, complex **IX**.

The solid state structure for complex **IX** is displayed in Figure 3.13 with pertinent bond lengths and angles in Table 3.5. The molybdenum adopts the familiar piano stool geometry seen for its tricarbonyl cyclopentadienyl derivatives. The acetone ligand is bound to molybdenum in an η^1 manner as commonly observed for ketone complexes. The Mo(1)-O(4) distance of 2.186(7) Å is significantly shorter than other molybdenum complexes containing coordinated acetone, such as *trans*-$[Mo(=CNHPh)(O{=}CMe_2)(dppe)_2][BF_4]$[50] [2.310(3) Å] and

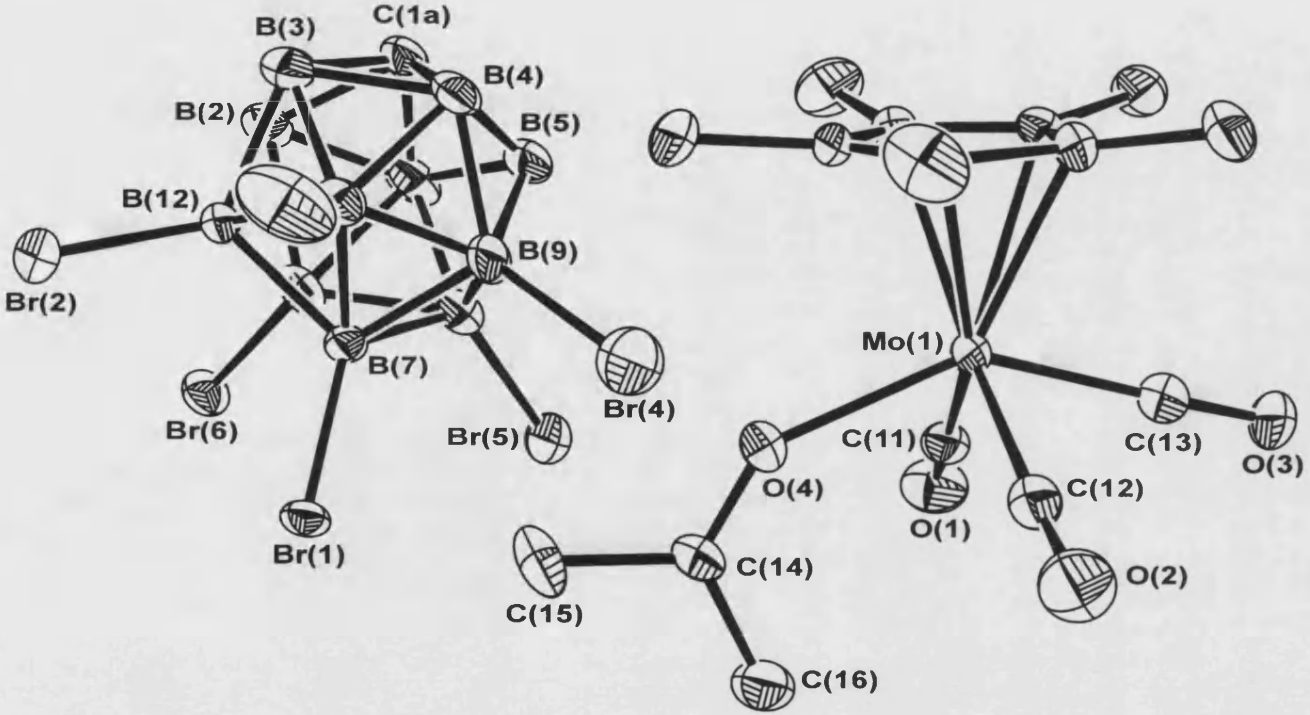

Figure 3.13: Crystal structure of $[MoCp^*(CO)_3(C_3H_6O)][CB_{11}H_6Br_6]$, **IX** (ellipsoids drawn at 30% probability level; hydrogens omitted for clarity)

Mo(1)-O(4)	2.186(7) Å
O(4)-C(14)	1.231(12) Å
C(11)-Mo(1)	2.038(12) Å
C(12)-Mo(1)	2.010(12) Å
C(13)-Mo(1)	1.987(12) Å
Mo(1)-O(4)-C(14)	141.3(7)°
C(13)-Mo(1)-O(4)	143.5(4)°
C(11)-Mo(1)-C(12)	110.6(5)°

Table 3.5: Selected bond lengths and angles for complex **IX**

$[MoO\{S_2C_2(CN)_2\}(dppe)(O{=}CMe_2)]$[51] [2.333(2) Å], implying a strong Mo-acetone interaction. However, it is not as short as that found for alkoxide complexes such as $[Mo(O^iPr)_2(bpy)_2]$[52] (Mo-O *ca.* 1.93 Å) in which significant oxygen-p-to-molybdenum-d π bonding is thought to occur. The O(4)-C(14) distance at 1.231(12) Å is typical to those in other complexes containing σ-bound acetone ligands, for example $[Mo(=CNHPh)(O{=}CMe_2)(dppe)_2][BF_4]$[50] [1.226(5) Å], $[MoO\{S_2C_2(CN)_2\}(dppe)(O{=}CMe_2)]$[51] [1.231(4) Å], and $[Ru\{C(=CHPh)OCMeO\}(O{=}CMe_2)(CO)(P^iPr_3)_2][BF_4]$[53] [1.235(10) Å].

3.2.4 Ranking Coordinating Ability: Comparisons Between [*closo*-$CB_{11}H_{12}$]$^-$, [*closo*-$CB_{11}H_{11}Br$]$^-$ and [*closo*-$CB_{11}H_6Br_6$]$^-$

The complexes $[MoCp(CO)_3(X)]$ [X = {*closo*-$CB_{11}H_{12}$}$^-$ (compound **I**), {*closo*-$CB_{11}H_{11}Br$}$^-$ (compound **VII**) and {*closo*-$CB_{11}H_6Br_6$}$^-$] have all been characterised (albeit the latter only spectroscopically), so conclusions can now be drawn as to the relative coordinating abilities of the anions. The average ν(CO) stretching frequencies for these compounds are 2036cm^{-1} (compound **I**), 2024cm^{-1} (compound **VII**) and 2032cm^{-1} $[MoCp(CO)_3(CB_{11}H_6Br_6)]$. According to the ranking scheme developed by Reed based on carbonyl stretching frequencies,[31] this value ranks the coordinating ability of these anions [$(BF_4)^-$ and $(PF_6)^-$ included for comparison] in the order $[PF_6]^-$ < [*closo*-$CB_{11}H_{12}$]$^-$ < [*closo*-$CB_{11}H_6Br_6$]$^-$ < [*closo*-$CB_{11}H_{11}Br$]$^-$ < $[BF_4]^-$. The grading of [*closo*-$CB_{11}H_{12}$]$^-$ as more weakly coordinating than [*closo*-$CB_{11}H_6Br_6$]$^-$ and [*closo*-$CB_{11}H_{11}Br$]$^-$ is counterintuitive when the reactivity of these complexes is taken into account. The supposedly most weakly coordinating anion in this ranking scheme,

[*closo*-$CB_{11}H_{12}]^-$, is not displaced by nucleophiles such as H_2O in complex **I**. In contrast, $[MoCp(CO)_3(CB_{11}H_6Br_6)]$ and the $[BF_4]^-$ congener are very reactive towards H_2O. Hence, whilst the use of carbonyl stretching frequencies to rank coordinating abilities is perhaps useful for observing general trends between anions, it is clear that it cannot be used as a definitive scale for the reactivity of these carborane complexes.

Perhaps a better system of ranking comes from analysis of the Cp resonances. The further downfield the Cp resonance is shifted, the more electron deficient the metal centre and hence more weakly nucleophilic the anion. Comparative shifts of a number of compounds with the general formula $[MoCp(CO)_3(X)]$ are displayed in Table 3.6.

X	δ (C_5H_5)[†]	Reference
SbF_6	6.04	[21]
PF_6	6.04	[21]
$CB_{11}H_6Br_6$	6.02	This work
BF_4	5.97	[4]
$CB_{11}H_{11}Br$	5.92	This work
SO_3CF_3	5.88[‡]	[4]
$CB_{11}H_{12}$	5.79	This work

[†] In CD_2Cl_2 unless otherwise noted.
[‡] In $CDCl_3$.
(Residual protio references: CH_2Cl_2 = 5.33, $CHCl_3$ = 7.25)

Table 3.6: δ (C_5H_5) for complexes of general formula $[MoCp(CO)_3(X)]$ (X = weakly coordinating anion)

The results rank the coordinating ability of the anions in the order: $[SbF_6]^- \approx [PF_6]^-$ < [*closo*-$CB_{11}H_6Br_6]^-$ < $[BF_4]^-$ < [*closo*-$CB_{11}H_{11}Br]^-$ < $[SO_3CF_3]^-$ < [*closo*-$CB_{11}H_{12}]^-$. In contrast, the carbonyl stretching frequencies of compound **I** ranks [*closo*-$CB_{11}H_{12}]^-$ just below $[BF_4]^-$ in terms of coordinating ability (Table 2.2, section 2.2.1). The

reversal of the trend from the CO stretching frequencies, by comparing the Cp resonances instead, is perhaps more realistic given the extremely sensitive nature of $[BF_4]^-$ in $[MoCp(CO)_3(BF_4)]$ towards competing nucleophiles such as H_2O and acetone.[26] This is in comparison to the air stability of complex **I** and the inertness of the $[closo\text{-}CB_{11}H_{12}]^-$ anion towards displacement by acetone or H_2O. Unfortunately, the complexes $[MoCp(CO)_3(BAr_4)]$ [Ar = 3,5-bis(trifluoromethyl)phenyl or pentafluorophenyl] could not be included in this ranking as they have not been isolated. This is presumably as they are unstable and decompose in solution, as seen in attempts to isolate the related compound $[WCp(CO)_3(BAr_4)]$.[28]

It is important to remember that these relative rankings apply to a specific system. It has been shown that increasing the steric bulk around the metal can significantly affect the coordinating ability of the large $[closo\text{-}CB_{11}H_{12}]^-$ anions, evidenced by the sensitivity of complex **V** to water and the inability to isolate $[MoCp^*(CO)_3(CB_{11}H_6Br_6)]$. The coordinating ability of smaller anions, such as $[BF_4]^-$, is likely to be affected to a lesser degree as the steric environment around a metal increases. This may perhaps result in $[closo\text{-}CB_{11}H_{12}]^-$ becoming more weakly coordinating than $[BF_4]^-$ in some instances. It is an important distinction that whilst the coordinating abilities of the anions may change according to the system in question, the relative nucleophilicities of the 'free' anions will remain the same.

The inability to rank $[closo\text{-}CB_{11}H_{12}]^-$ and its derivatives against the widely used and very weakly coordinating $[BAr_4]^-$ anions by comparison of the chemical shift for the Cp resonance in $[MoCp(CO)_3(X)]$ can be overcome by instead comparing the catalytic activities of related species, as outlined in the next section.

3.2.5 Catalytic Ionic Hydrogenation of 3-pentanone

Hydrogenation of ketones and aldehydes is an important industrial reaction, utilised in the synthesis of compounds of use in the pharmaceutical and agricultural industries. There have been numerous transition metal homogenous hydrogenation catalysts developed, based mainly on rhodium and ruthenium catalysts. Of particular note are some fantastically reactive ruthenium catalysts, developed by Noyori and co-workers for use in enantioselective hydrogenation of ketones with H_2,[54] or transfer hydrogenation reactions with isopropanol as the hydrogen source.[55]

Bullock has recently reported the use of $[MCp(CO)_2(PR_3)(\eta^1\text{-}O{=}CEt_2)][BAr'_4]$ [M = Mo, W; R = Me, Ph, cyclohexyl; Ar′ = 3,5-bis(trifluoromethyl)phenyl] complexes as catalyst precursors for the ionic hydrogenation of 3-pentanone (Equation 3.10).[56, 57]

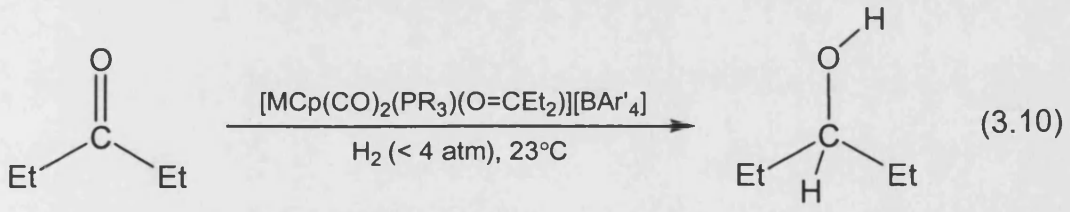

(3.10)

The catalytic precursors can be generated *in situ* from the reaction of $[MCp(CO)_2(PR_3)H]$ and $[CPh_3][BAr'_4]$ in the presence of 3-pentanone. Bullock demonstrated that the steric effects of the phosphine ligands predominated over electronic effects in influencing rate of reaction, the key step in the mechanism being the promotion of ketone dissociation from the metal (Figure 3.14) that is aided by the steric bulk of the phosphine. Although the turnover frequencies of this catalyst system are low compared to ruthenium hydrogenation catalysts,[58] it has the advantage of

utilising a cheaper metal source and molecular hydrogen as the feedstock for both the proton and hydride source.

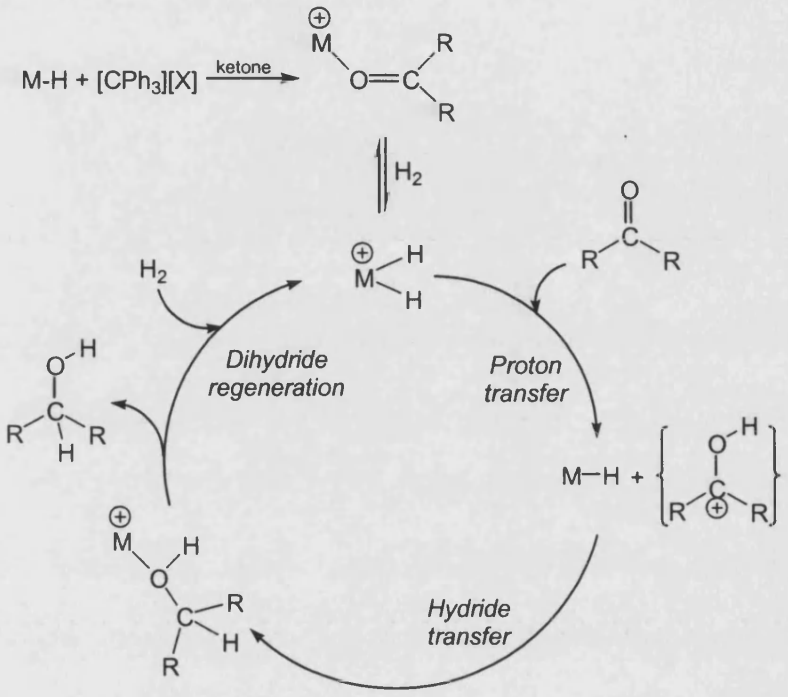

Figure 3.14: Proposed mechanism for the catalytic ionic hydrogenation of ketones with $[MCp(CO)_2(PR_3)(O{=}CEt_2)]$ (M = Mo, W) (Reproduced from reference [57])

The similarity of the catalytic species used by Bullock with complexes **I**, **VII**, and '$[MoCp(CO)_3(CB_{11}H_6Br_6)]$' prompted an investigation into whether or not these compounds containing monoanionic carborane anions would have any activity as hydrogenation catalysts. The general procedure for monitoring the hydrogenation of 3-pentanone outlined by Bullock was used,[56] along with the same catalyst and substrate ratio in order to allow realistic comparison of any observed activities to be made (see experimental section). This will allow, for the first time, direct comparison of the coordinating properties of $[BAr'_4]^-$ and monoanionic carboranes. This comparison can be made because a more coordinating anion would discourage both ketone and dihydrogen binding by coordination with the metal itself, thus reducing the rate of catalysis.

Given the stability of complex **I** in the presence of acetone, it is unsurprising that after 5 days reaction with H_2 and 10 equivalents of $Et_2C{=}O$ in CD_2Cl_2 the ^1H NMR spectrum shows unreacted starting material, and small amounts of two unidentified decomposition species (11% of total Cp concentration). A very small peak at δ 6.09 (10% of total Cp concentration) could indicate partial reaction to $[MoCp(CO)_3(O{=}CEt_2)][CB_{11}H_{12}]$, although the corresponding ethyl resonances for this compound would be swamped by the large peaks of uncoordinated 3-pentanone, and are thus not observed. The equivalent reaction with **VII** supports assignment of this lowfield Cp resonance as the ketone complex of **I**. Thus, reaction of complex **VII** with 10 equivalents of 3-pentanone under a hydrogen atmosphere for 5 days results in the Cp region of the ^1H NMR spectrum displaying a peak for unreacted **VII** at δ 5.96 (66%) and an additional peak at δ 6.11 (33%). The peak at δ 6.11 is assigned as $[MoCp(CO)_3(O{=}CEt_2)][CB_{11}H_{11}Br]$, with the corresponding ethyl resonances at δ 2.60 (q, CH_2, J_{HH} = 7.2 Hz) and δ 1.15 (t, CH_3, J_{HH} = 7.2 Hz) shifted downfield and clearly distinguishable from the large 3-pentanone peaks at δ 2.41 and δ 1.01. This slight downfield shift of coordinated compared to 'free' $O{=}CEt_2$ has previously been observed in the related $[MoCp(CO)_2(PR_3)(O{=}CEt_2)][BAr'_4]$ (R = Me and Ph) complexes.[57] The Cp resonance at δ 6.11 is the same as that found in the closely related complex $[MoCp(CO)_3(O{=}CMe_2)][BF_4]$[26] (δ 6.11). At no point was any evidence found for the presence of hydrogenation products in the ^1H NMR spectra of the reactions for both **I** and **VII**. The greater degree of ketone substitution in complex **VII** compared to complex **I** reflects a weaker metal-anion interaction for $[closo\text{-}CB_{11}H_{11}Br]^-$ *versus* $[closo\text{-}CB_{11}H_{12}]^-$.

The hydrogenation catalyst containing [*closo*-$CB_{11}H_6Br_6$]$^-$ was generated *in situ* from [$MoCp(CO)_3H$] and [CPh_3][$CB_{11}H_6Br_6$] under standard conditions. After one day of hydrogenation, the Cp region of the ^{1}H NMR spectrum displays one major peak at δ 6.14, but no hydrogenation of the ketone. The chemical shift of this major organometallic species is similar in value to the Cp resonances of the proposed ketone complex of **I** and **VII** and is correspondingly assigned as [$MoCp(CO)_3(O{=}CEt_2)$][$CB_{11}H_6Br_6$], with the resonances for the coordinated ketone clearly visible at δ 2.63 (q, CH_2, J_{HH} = 7.2 Hz) and δ 1.16 (t, CH_3, J_{HH} = 7.2 Hz). Continued reaction under a hydrogen atmosphere for a further 13 days results in the majority of this species decomposing to uncharacterised products, and no evidence of any significant hydrogenation of the ketone.

The inability of the tricarbonyl molybdenum catalysts outlined in this work to hydrogenate 3-pentanone presumably arises from their inability to promote ketone dissociation, the key step in the mechanism for this reaction (Figure 3.14). This is presumably due to insufficient steric bulk around the metal, combined with a stronger metal ketone bond for the more Lewis acidic {$MoCp(CO)_3$}$^+$ fragment in comparison to {$MoCp(CO)_2(PR_3)$}$^+$. This is further exasperated in the case of complexes **I** and **VII** because of stronger anion-metal *versus* ketone-metal interactions that inhibit the formation of the ketone complex.

Attention now turned to the [$MoCp(CO)_2(PPh_3)(O{=}CEt_2)$][$CB_{11}H_6Br_6$] catalyst precursor, analogous to Bullock's [$MoCp(CO)_2(PPh_3)(O{=}CEt_2)$][$BAr'_4$] which has been shown to be a relatively effective catalyst. The failure of the [*closo*-$CB_{11}H_{12}$]$^-$ and [*closo*-$CB_{11}H_{11}Br$]$^-$ anions in complexes **I** and **VII** to completely dissociate to

their respective ketone complexes in the tricarbonyl species precluded their inclusion in this part of the study and only [*closo*-$CB_{11}H_6Br_6$]$^-$ was used. Hydrogenation of 3-pentanone to 3-pentanol using [$MoCp(CO)_2(PPh_3)(O{=}CEt_2)$][$CB_{11}H_6Br_6$], generated *in situ* from the reaction of [$MoCp(CO)_2(PPh_3)H$] and [CPh_3][$CB_{11}H_6Br_6$] was monitored by ^1H NMR spectroscopy. Additional H_2 was added to the reaction every 6 days to maintain the hydrogen pressure that is reduced by H_2 consumption. The number of catalyst turnovers with respect to time is displayed in Figure 3.15, upon which are superimposed the results for related catalytic species as reported by Bullock.[56] These results clearly show that the catalyst containing [*closo*-$CB_{11}H_6Br_6$]$^-$ is not as active as the parallel catalyst containing [BAr'_4]$^-$, although respectable rates are still achieved.

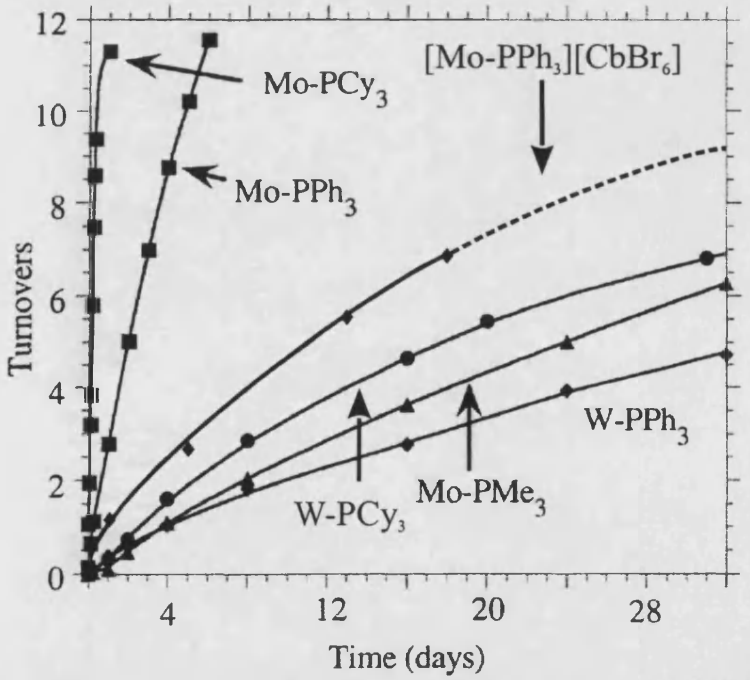

M-PR_3 = [$MoCp(CO)_2(PR_3)(O{=}CEt_2)$][$BAr'_4$] or [$WCp(CO)_2(PR_3)(O{=}CEt_2)$][$BAr'_4$]
[Mo-PPh_3][$CbBr_6$] = [$MoCp(CO)_2(PPh_3)(O{=}CEt_2)$][$CB_{11}H_6Br_6$]

Figure 3.15: Catalytic activity for the hydrogenation of $O{=}CEt_2$ with M-PR_3 (Modified diagram from reference [56])

The faster rate of reaction for [BAr'_4]$^-$ ranks it below [*closo*-$CB_{11}H_6Br_6$]$^-$ in terms of increasing coordinating ability. The [BF_4]$^-$ and [PF_6]$^-$ anions were included by

Bullock in his hydrogenation studies,[57] but the catalysts generated were not as active so only qualitative measurements were taken, thwarting direct counterion comparisons with [*closo*-$CB_{11}H_6Br_6$]$^-$ by us. However, based on the relative coordinating abilities of these anions from comparison of the shift in Cp resonances for [$MoCp(CO)_3(X)$] the rates of hydrogenation could perhaps be *predicted* to decrease in the order [BAr'_4]$^-$ > [PF_6]$^-$ > [*closo*-$CB_{11}H_6Br_6$]$^-$ > [BF_4]$^-$. Importantly, this is the first time that [BAr'_4]$^-$ and [*closo*-$CB_{11}H_6Br_6$]$^-$ have been directly compared in a catalytic reaction. In addition, Bullock notes that [OTf]$^-$ is coordinated too strongly to molybdenum to provide any significant catalysis, which is in accord with the ranking of this anion by the Cp resonance chemical shifts as similar in coordinating ability to [*closo*-$CB_{11}H_{12}$]$^-$ and [*closo*-$CB_{11}H_{11}Br$]$^-$ which are not readily displaced by ketone in **I** and **VII**.

The generation of the product alcohol in this reaction is also accompanied by the formation of smaller amounts of an ether, $(Et_2CH)_2O$, arising from the condensation of two product alcohols (Equation 3.11). The results shown in Figure 3.15 include the formation of the alcohol and its subsequent conversion to ether. After 18 days of reaction with [$MoCp(CO)_2(PPh_3)(O{=}CEt_2)$][$CB_{11}H_6Br_6$], the molar ratio of ether [$(Et_2CH)_2O$] to alcohol [Et_2CHOH] was 0.13 : 1 respectively. In contrast, when [$MoCp(CO)_2(PPh_3)(O{=}CEt_2)$][$BAr'_4$] is used as a catalyst, the molar ratio of ether to alcohol increases to 0.18 : 1 after 6 days of reaction.[57]

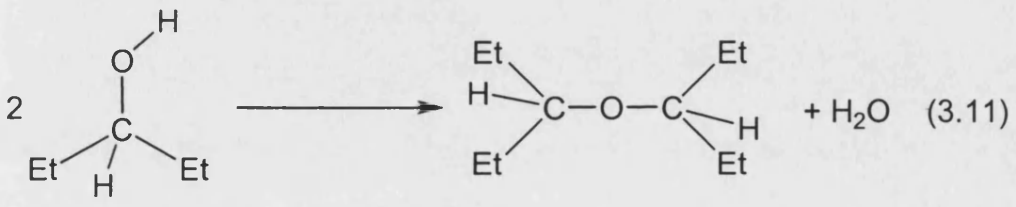

(3.11)

3.3 Summary

This chapter has explored the viability of using hydride and methyl abstraction reactions from transition metal centres in order to isolate complexes of ligated [*closo*-$CB_{11}H_{12}]^-$ and its derivatives. These reactions have allowed the isolation of novel compounds that are not accessible *via* silver salt metathesis. The [*closo*-$CB_{11}H_{12}]^-$ anion in compound **I** is not displaced by H_2O, which is in contrast to complex **V** in which the carborane can be readily substituted for H_2O. This suggests the Cp^* ligand is dictating the way in which the bulky [*closo*-$CB_{11}H_{12}]^-$ anion can bind, weakening the anion-metal bond. It demonstrates that increasing the steric environment around the metal can dramatically affect the coordinating ability of the carborane anions, highlighting the important role the large steric bulk of [*closo*-$CB_{11}H_{12}]^-$ plays in its classification as a weakly coordinating anion.

Complex **VII** is the first organometallic species isolated containing ligated [*closo*-$CB_{11}H_{11}Br]^-$, which in solution coordinates to the metal primarily *via* bromine as opposed to one of the B-H vertices.

The weakly coordinating nature of the [*closo*-$CB_{11}H_6Br_6]^-$ anion is revealed by the high reactivity of [$MoCp(CO)_3(CB_{11}H_6Br_6)$], which in CH_2Cl_2 forms an equilibrium with the solvent to yield a postulated dichloromethane complex. The inability of H_2O to displace the monobromo anion in **VII**, is in direct contrast to the high reactivity of [$MoCp(CO)_3(CB_{11}H_6Br_6)$] towards trace amounts of this nucleophile. Given that both bond through B-Br-Mo interactions, this difference in reactivity is perhaps due to the increased steric bulk of [*closo*-$CB_{11}H_6Br_6]^-$ over [*closo*-$CB_{11}H_{11}Br]^-$.

Importantly, the following ranking of anion coordinating abilities can be drawn from the chemical shift of the Cp resonances in $[MoCp(CO)_3(anion)]$: $[SbF_6]^- \equiv [PF_6]^- < [closo\text{-}CB_{11}H_6Br_6]^- < [BF_4]^- < [closo\text{-}CB_{11}H_{11}Br]^- < [SO_3CF_3]^- < [closo\text{-}CB_{11}H_{12}]^-$. However, limits to the use of the chemical shift of Cp in $[MoCp(CO)_3(anion)]$ to rank coordinating abilities is seen for $[PF_6]^-$ and $[closo\text{-}CB_{11}H_6Br_6]^-$, where dichloromethane is thought to become competitive with the anion for coordination to the metal. The increased reactivity of $[MoCp(CO)_2PPh_3(O{=}CEt_2)][BAr'_4]$ over $[MoCp(CO)_2PPh_3(O{=}CEt_2)][CB_{11}H_6Br_6]$ in the hydrogenation of 3-pentanone suggests $[BAr'_4]^-$ is a more weakly coordinating anion than $[closo\text{-}CB_{11}H_6Br_6]^-$. The relative shifts of the carbonyl stretching frequencies in the IR spectra of $[MoCp(CO)_3(anion)]$ compounds are clearly not an accurate guide to relative coordinating abilities of the anions because of the close similarity in CO stretching frequencies for **I**, **VII** and $[MoCp(CO)_3(CB_{11}H_6Br_6)]$ that is in contrast to their differing reactivities. However, the chemical shift of the Cp resonance (thermodynamic measure) is a reasonable guide to the reactivity (kinetic measure) of these complexes. This idea of comparing thermodynamic rankings (NMR, X-ray crystallography) with kinetic rankings (catalysis) is further explored in the next chapter with silver(I) phosphine compounds that are used as catalysts in a hetero-Diels-Alder reaction.

3.4 References

1 K. Raab, W. Beck, *Chem. Ber.* **1984**, *117*, 3169.
2 K. H. Griesmann, A. Stasunik, W. Angerer, W. J. Malisch, *J. Organomet. Chem.* **1986**, *303*, C29.
3 K. D. Abney, K. M. Long, O. P. Anderson, S. H. Strauss, *Inorg. Chem.* **1987**, *26*, 2638.
4 M. Appel, K. Schloter, J. Heidrich, W. Beck, *J. Organomet. Chem.* **1987**, *322*, 77.
5 C. S. Yi, D. Wodka, A. L. Rheingold, G. P. A. Yap, *Organomet.* **1996**, *15*, 2.
6 T. C. Flood, D. L. Miles, *J. Organomet. Chem.* **1977**, *127*, 33.
7 M. L. H. Green, A. G. Massey, J. T. Moelwyn-Hughes, P. L. I. Nagy, *J. Organomet. Chem.* **1966**, *8*, 511.
8 G. S. Mhinzi, S. A. Litster, A. D. Redhouse, J. L. Spencer, *J. Chem. Soc., Dalton Trans.* **1991**, 2769.
9 S. N. Anderson, C. J. Cooksey, S. G. Holton, M. D. Johnson, *J. Am. Chem. Soc.* **1980**, *102*, 2312.
10 W. N. Rogers, N. C. Baird, *J. Organomet. Chem.* **1979**, *182*, C65.
11 H. E. Bryndza, L. K. Fong, R. A. Paciello, W. Tam, J. E. Bercaw, *J. Am. Chem. Soc.* **1987**, *109*, 1444.
12 E. J. O'Connor, M. Kobayashi, H. G. Floss, J. A. Gladysz, *J. Am. Chem. Soc.* **1987**, *109*, 4837.
13 W. Beck, K. Sunkel, *Chem. Rev.* **1988**, *88*, 1405.
14 A. Davison, W. McFarlane, L. Pratt, G. J. Wilkinson, *J. Chem. Soc.* **1962**, 3653.
15 A. R. Siedle, R. A. Newmark, L. H. Pignolet, *Inorg. Chem.* **1986**, *25*, 3412.
16 M. S. Chinn, D. M. Heinekey, *J. Am. Chem. Soc.* **1987**, *109*, 5865.
17 J. R. Sanders, *J. Chem. Soc., Dalton Trans.* **1972**, 1333.
18 J. R. Sanders, *J. Chem. Soc., Dalton Trans.* **1973**, 743.
19 P. Legzdins, D. T. Martin, *Inorg. Chem.* **1979**, *18*, 1250.
20 W. Beck, K. Z. Schloter, *Naturforsch., B* **1978**, *33b*, 1214.
21 K. Sunkel, U. Nagel, W. Beck, *J. Organomet. Chem.* **1983**, *251*, 227.
22 K. Sunkel, G. Urban, W. Beck, *J. Organomet. Chem.* **1983**, *252*, 187.
23 B. A. Arndlsten, R. G. Bergman, *Science* **1995**, *270*, 1970.
24 T. S. Peng, C. H. Winter, J. A. Gladysz, *Inorg. Chem.* **1994**, *38*, 115.
25 J. Huhmann-Vincent, B. L. Scott, G. J. Kubas, *Inorg. Chem.* **1999**, *38*, 115.
26 W. Beck, *Inorg. Synth.* **1990**, *28*, 1.
27 T.-Y. Cheng, R. M. Bullock, *Organomet.* **1995**, *14*, 4031.
28 T.-Y. Cheng, B. S. Brunschwig, R. M. Bullock, *J. Am. Chem. Soc.* **1998**, *120*, 13121.
29 T.-Y. Cheng, R. M. Bullock, *Organomet.* **2002**, *21*, 2325.
30 T.-Y. Cheng, D. J. Szalda, R. M. Bullock, *Chem. Commun.* **1999**, 1629.
31 Z. Xie, T. Jelinek, R. Bau, C. A. Reed, *J. Am. Chem. Soc.* **1994**, *116*, 1907.
32 T. Jelinek, J. Plesek, S. Hermanek, B. Stibr, *Collect. Czech. Chem. Commun.* **1986**, *51*, 819.
33 T. J. Boyle, F. Takusagawa, J. A. Heppert, *Acta Cryst.* **1990**, *C46*, 892.
34 G. A. Sim, J. G. Sime, D. I. Woodhouse, *Acta Cryst.* **1979**, *B35*, 2403.
35 C. Qian, J. Guo, J. Sun, *Inorg. Chem.* **1997**, *36*, 1286.

36 D. R. Evans, C. A. Reed, *J. Am. Chem. Soc.* **2000**, *122*, 4660.
37 M. D. Butts, B. L. Scott, G. J. Kubas, *J. Am. Chem. Soc.* **1996**, *118*, 11831.
38 Z. Xie, J. Manning, R. W. Reed, R. Mathur, P. D. W. Boyd, A. Benesi, C. A. Reed, *J. Am. Chem. Soc.* **1996**, *118*, 2922.
39 T. Jelinek, P. Baldwin, W. R. Scheidt, C. A. Reed, *Inorg. Chem.* **1993**, *32*, 1982.
40 Z. Xie, C.-W. Tsang, E. T.-P. Sze, Q. Yang, D. T. W. Chan, T. C. W. Mak, *Inorg. Chem.* **1998**, *37*, 6444.
41 J. Markham, A. Cutler, *Organomet.* **1984**, *3*, 736.
42 Kluwer, Academic, Publishers, *International Tables for Crystallography* **1992**, *Volume C*, Table 9.6.3.3.
43 J. C. Fettinger, H.-B. Kraatz, R. Poli, E. A. Quadrelli, *J. Chem. Soc., Dalton Trans.* **1999**, 497.
44 P. Schollhammer, F. Y. Petillon, J. Talarmin, K. W. Muir, H. K. Fun, K. Chinnakali, *Inorg. Chem.* **2000**, *39*, 5879.
45 C. V. Depree, E. W. Ainscough, A. M. Brodie, G. J. Gainsford, C. Lensink, *Acta Cryst.* **2000**, *C56*, 17.
46 L. Sieron, M. Bukowska-Strzyzewska, *Acta Cryst.* **1997**, *C53*, 296.
47 K. Raab, B. Olgemoller, K. Schloter, W. Beck, *J. Organomet. Chem.* **1981**, *214*, 81.
48 R. E. Dixon, A. Streitwieser, *J. Org. Chem.* **1992**, *57*, 6125.
49 W. A. Kiel, G.-Y. Lin, G. S. Bodner, J. A. Gladysz, *J. Am. Chem. Soc.* **1983**, *105*, 4958.
50 H. Seino, D. Nonokawa, G. Nakamura, Y. Mizobe, M. Hidai, *Organomet.* **2000**, *19*, 2002.
51 K. M. Nicholas, M. A. Khan, *Inorg. Chem.* **1987**, *26*, 1633.
52 M. H. Chisholm, J. C. Huffman, I. P. Rothwell, P. G. Bradley, N. Kress, W. H. Woodruff, *J. Am. Chem. Soc.* **1981**, *103*, 4945.
53 M. A. Esteruelas, F. J. Lahoz, A. M. Lopez, E. Onate, L. A. Oro, *Organomet.* **1994**, *13*, 1669.
54 R. Noyori, T. Ohkuma, *Angew. Chem. Int. Ed.* **2001**, *40*, 40.
55 M. Yamakawa, H. Ito, R. Noyori, *J. Am. Chem. Soc.* **2000**, *122*, 1466.
56 R. M. Bullock, M. H. Voges, *J. Am. Chem. Soc.* **2000**, *122*, 12594.
57 M. H. Voges, R. M. Bullock, *J. Chem. Soc., Dalton Trans.* **2002**, 759.
58 T. Ohkuma, M. Koizuma, H. Doucet, T. Pham, M. Kozawa, K. Murate, E. Katayama, T. Yokozawa, T. Ikariya, R. Noyori, *J. Am. Chem. Soc.* **1998**, *120*, 13529.

4 SILVER CHEMISTRY OF ICOSAHEDRAL MONOCARBORANE ANIONS

4.1 Introduction

Silver(I) salts of icosahedral monocarborane anions have been useful in generating metal complexes containing weakly coordinating anions, such as $[FeCp(CO_3)_2(CB_{11}H_{12})]$[1], $[Fe(TPP)(CB_{11}H_{12})]$[2] and compounds **I** - **IV** as described in Chapter 2. In addition, they are of structural interest in their own right because they exhibit a number of different coordination motifs. Structures of silver(I) carborane salts often have coordinated arene molecules in the crystal lattice because of their solubility in arene solvents and the comparable donor ability of anion and solvent. Each structure has a different coordination motif that is difficult to predict, often with bridging carborane anions forming coordination polymers in the solid state. For example, $Ag(CB_{11}H_{12}).2C_6H_6$ contains a three coordinate silver with η^1 coordination of the benzene and bridging B-H bonds from B(7) and B(12) cage vertices (Figure 4.1).[3] Four coordinate silver is found in $Ag(CB_{11}H_{11}Br).C_6H_6$, again with η^1 coordination of benzene but now with B-Br and B-H bonds from bridging carboranes.[4] On changing from monobromo- to hexabromo-carborane, arene molecules are excluded from the lattice, with each carborane now bridging two silver atoms to generate a six coordinate silver atom.[5] Other examples of structurally characterised silver(I) carborane anions include $Ag(CB_{11}H_{11}F)$,[6] $Ag(1\text{-}R\text{-}CB_{11}H_6X_6)$ (R = H, Me; X = H, Cl, Br, I),[5, 7] $Ag(1\text{-}R\text{-}CB_{11}X_{11})$ (R = H, Me; X = Cl, Br),[8, 9] and $Ag(1\text{-}H\text{-}CB_{11}X_5Y_6)$ (X or Y = Cl or Br)[9] which contain 3, 4, 5, or 6 coordinate silver

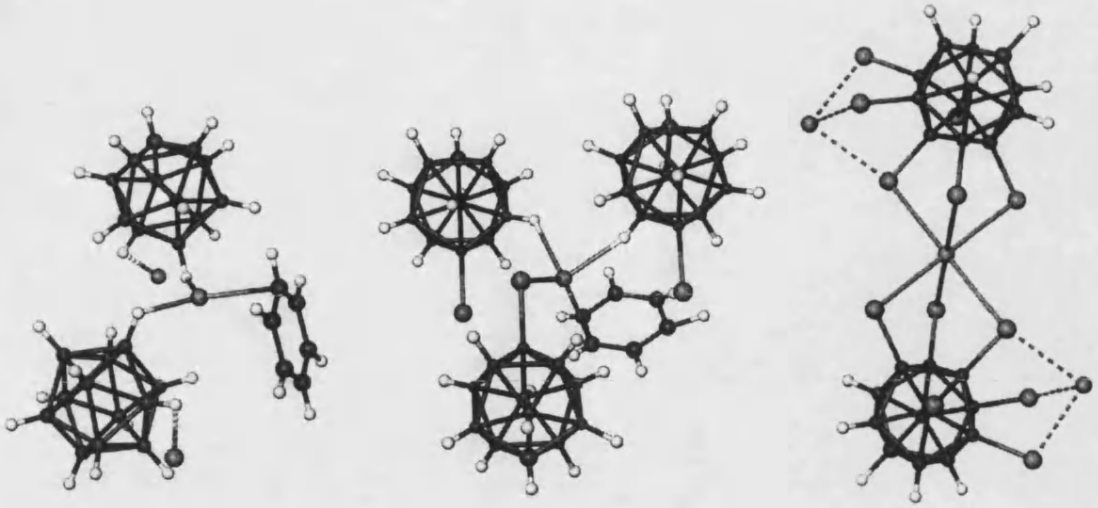

$Ag(CB_{11}H_{12})$ $Ag(CB_{11}H_{11}Br)$ $Ag(CB_{11}H_{11}Br_6)$

Figure 4.1: Coordination geometries about silver in the solid state structures of $Ag(CB_{11}H_{12})$,[3] $Ag(CB_{11}H_{11}Br)$,[4] and $Ag(CB_{11}H_6Br_6)$[5]

atoms, a variety of coordinated arene molecules and a number of different supramolecular features.

In collaboration with the group of Dr. Chris Frost (University of Bath) the investigation of the use of silver(I) carborane compounds [$Ag(CB_{11}H_{12})$ and $Ag(CB_{11}H_6Br_6)$] as catalysts for organic transformations was attempted (see later discussion). Unfortunately, they showed very little activity, thought to be a consequence of the poor solubility that these silver carboranes have in the solvent used (CH_2Cl_2). With this in mind, it was hoped to be able synthesise some more soluble versions of the simple silver(I) carboranes. The large amount of silver(I) phosphine chemistry reported in previous literature, that allows useful structural predictions to be made on the basis of spectroscopic data,[10, 11] coupled with the stability of such complexes in air encouraged us to synthesise a range silver(I) phosphine complexes containing [*closo*-$CB_{11}H_{12}$]$^-$ and its derivatives. It was hoped

that the solid-state structures of these species would show interesting supramolecular features, as seen for $Ag(CB_{11}H_{12})$ and related compounds, and that their increased solubility would improve the performance of silver(I) carboranes in homogenous catalysis. Moreover, the ability to change the anion systematically in the complexes may lead to useful structure/activity relationships being uncovered. This chapter outlines the synthesis and characterisation of silver phosphine compounds with the general formula $[Ag(PPh_3)_x(Y)]$ [x = 1, 2; Y = (*closo*-$CB_{11}H_{12})^-$, (*closo*-$CB_{11}H_{11}Br)^-$, (*closo*-$CB_{11}H_6Br_6)^-$, (*closo*-$CB_{11}H_6Cl_6)^-$], and the assessment of some of these compounds as catalysts in a hetero-Diels-Alder reaction is discussed.

4.2 Results and Discussion

4.2.1 Synthesis and Characterisation of $[Ag(PPh_3)(X)]$ [X = (*closo*-$CB_{11}H_{12})^-$, (*closo*-$CB_{11}H_{11}Br)^-$, (*closo*-$CB_{11}H_6Br_6)^-$ and (*closo*-$CB_{11}H_6Cl_6)^-$]

The silver salts of the monoanionic carborane anions having the general formula [*closo*-$CB_{11}H_6X]^-$ [X = H_6, (H_5Br), Br_6 and Cl_6] are readily prepared as air stable compounds. Dropwise addition of slightly less than one equivalent of PPh_3 (to avoid formation of the bis-phosphine derivatives, discussed later) in CH_2Cl_2 to a suspension of $[Ag(CB_{11}H_6X_6)]$ in CH_2Cl_2 results in the formation of $[Ag(PPh_3)(CB_{11}H_6X)]$ [X = H_6 (compound **X**), (H_5Br) (compound **XI**), Br_6 (compound **XII**), Cl_6 (compound **XIII**)]. Colourless crystals of all these new compounds (Figure 4.2) were isolated in good yield from the slow diffusion of hexanes into CH_2Cl_2 solutions, and fully characterised by elemental analysis, NMR spectroscopy and X-ray crystallography.

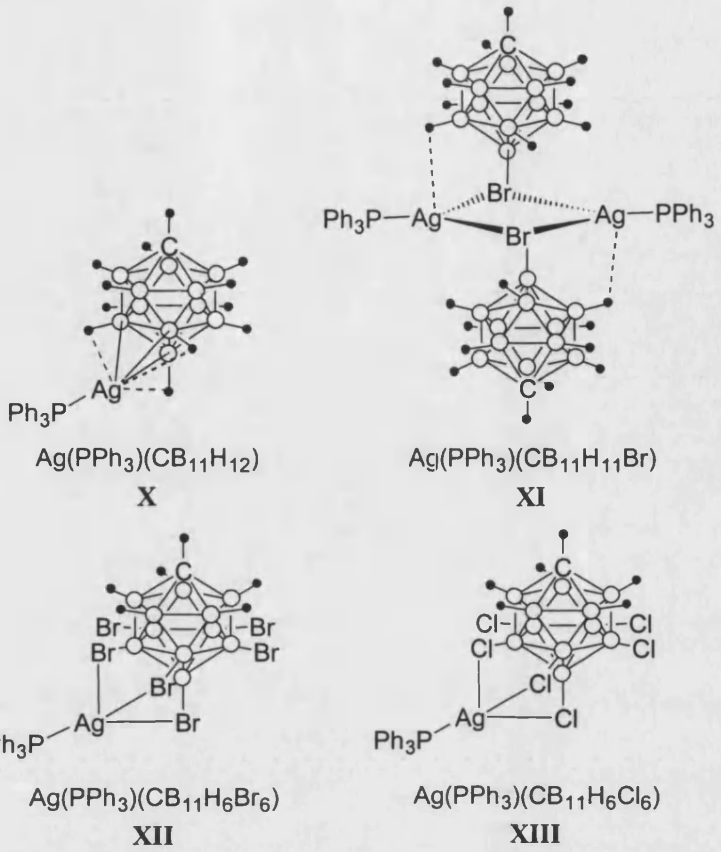

Figure 4.2: Compounds **X** – **XIII**

*[Ag(PPh$_3$)(CB$_{11}$H$_{12}$)], Compound **X***

The solid state structure of compound **X** is given in Figure 4.3, with relevant bond lengths and angles in Table 4.1. The $\{AgPPh_3\}^+$ fragment interacts with the [*closo*-$CB_{11}H_{12}]^-$ anion via three {B-H} vertexes that form the B(7)-B(8)-B(12) face of the cage. The coordination of the cage in an η^3-fashion is reminiscent to that seen previously for $[ZrCp^*(Me)_2(\eta^3\text{-}CB_{11}H_{12})]$.[12] The silver atom is located closest to B(8), not in the middle of the B(7)-B(8)-B(12) face, a feature reflected in the corresponding Ag-B bond lengths: Ag(1)-B(7), 2.619(2) Å; Ag(1)-B(8), 2.504(1) Å; Ag(1)-B(12), 2.569(3) Å. These bond lengths are in broad agreement with those seen

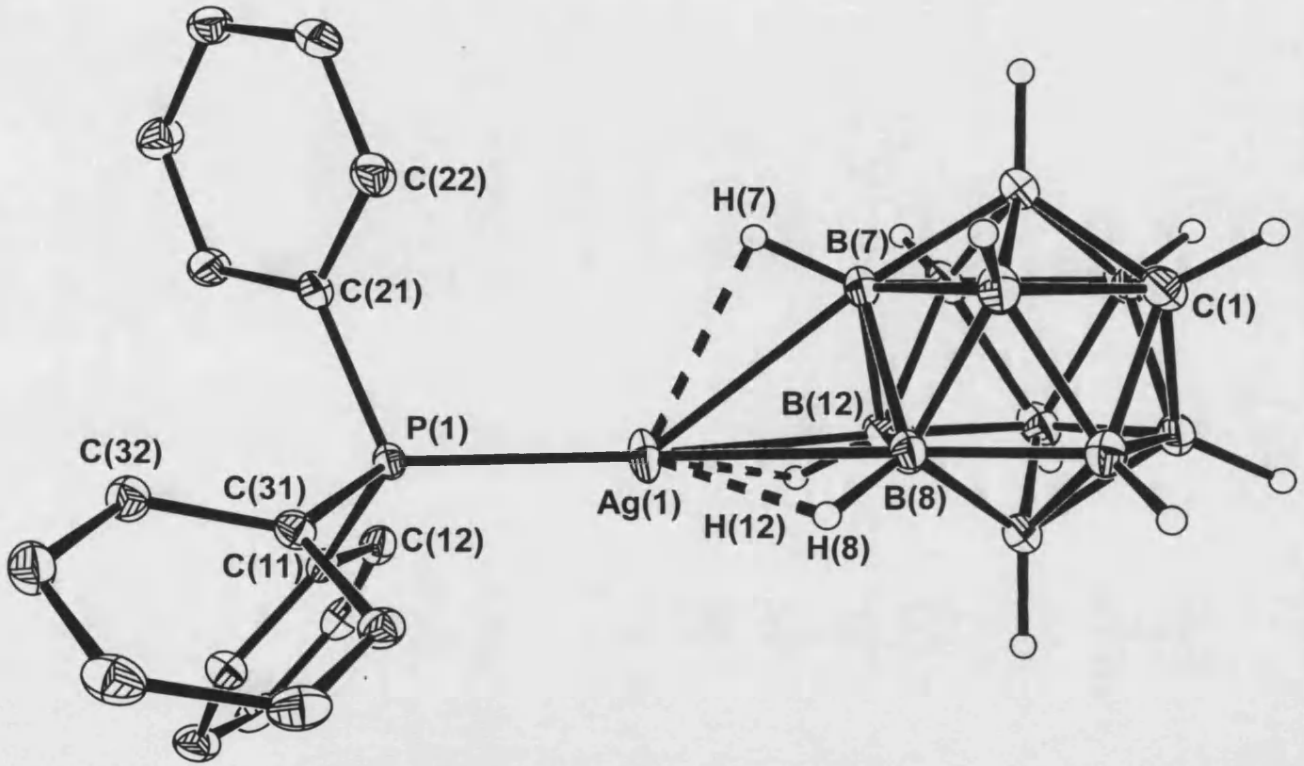

Figure 4.3: Crystal structure of $[Ag(PPh_3)(CB_{11}H_{12})]$, **X**
(phenyl hydrogen atoms omitted for clarity; ellipsoids drawn at 30% probability level)

Ag(1)-P(1)	2.3625(7) Å
Ag(1)-B(7)	2.619(3) Å
Ag(1)-B(8)	2.504(3) Å
Ag(1)-B(12)	2.569(3) Å
Ag(1)-H(7)	2.36(2) Å
Ag(1)-H(8)	2.14(2) Å
Ag(1)-H(12)	2.26(2) Å
P(1)-Ag(1)-B(7)	142.11(6)°
P(1)-Ag(1)-B(8)	158.23(6)°
P(1)-Ag(1)-B(12)	160.32(6)°
B(12)-Ag(1)-B(7)	40.37(8)°
B(12)-Ag(1)-B(8)	41.26(8)°
B(7)-Ag(1)-B(8)	40.98(8)°

Table 4.1: Selected bond lengths and angles for compound **X**

in the metallocarborane complex $[Mo(CO)_3(PPh_3)(\eta^5\text{-}7\text{-}CB_{10}H_{11})(AgPPh_3)]$ [13] synthesised by Stone and co-workers, containing a $\{AgPPh_3\}^+$ fragment exopolyhedrally bound via two B-H-Ag 3-centre-2-electron bonds [Ag-B, 2.522(4) Å and 2.589(4) Å]. The related compounds $[Re(CO)_3(\eta^5\text{-}7,8\text{-}C_2B_9H_{10})(AgPPh_3)]$[14] [Ag-B distance, 2.449(4) Å] and $[\{Re(CO)_3(\eta^5\text{-}7,8\text{-}C_2B_9H_{10})\}_2\{AgPh_2P(CH_2)_2PPh_2Ag\}]$[15] [Ag-B distance, 2.442(6) Å] contain Ag-Re bonds in addition to B-H-Ag bonds which results in shorter Ag-B bond lengths than seen in compound **X**. The silver atom sits essentially on the plane formed by P(1), B(8) and B(12) with the sum of the relevant bond angles around Ag(1) totalling 359.8° [P(1)-Ag(1)-B(8), 158.23(6)°; P(1)-Ag(1)-B(12), 160.32(6)°; B(8)-Ag(1)-B(12), 41.26(8)°]. This leaves an apparent vacant coordination site to the silver atom approximately *trans* to H(7). Inspection of the packing diagram reveals no intermolecular {B-H}···Ag interactions occupying this position. However, there is what appears to be a long intermolecular interaction from C(35)' [C(35)'-Ag(1), 3.348(3) Å], a phenyl ring carbon on a symmetry generated molecule. This Ag-C_{arene} distance is longer than that found in other structurally characterised silver carborane salts with silver-arene interactions (Ag···C_{arene} *ca.* 2.5-2.6 Å), which are in turn typical in length to those found in other silver-arene complexes.[16] Silver-arene contacts of 2.89-3.37 Å have been observed before,[17] and the long Ag-C_{arene} interaction [3.348(3) Å] in compound **X** is thought to be significant in this instance because of the orientation of the silver phosphine fragment relative to the cage. Overall, this interaction generates a dimeric motif in the solid state, shown in Figure 4.4.

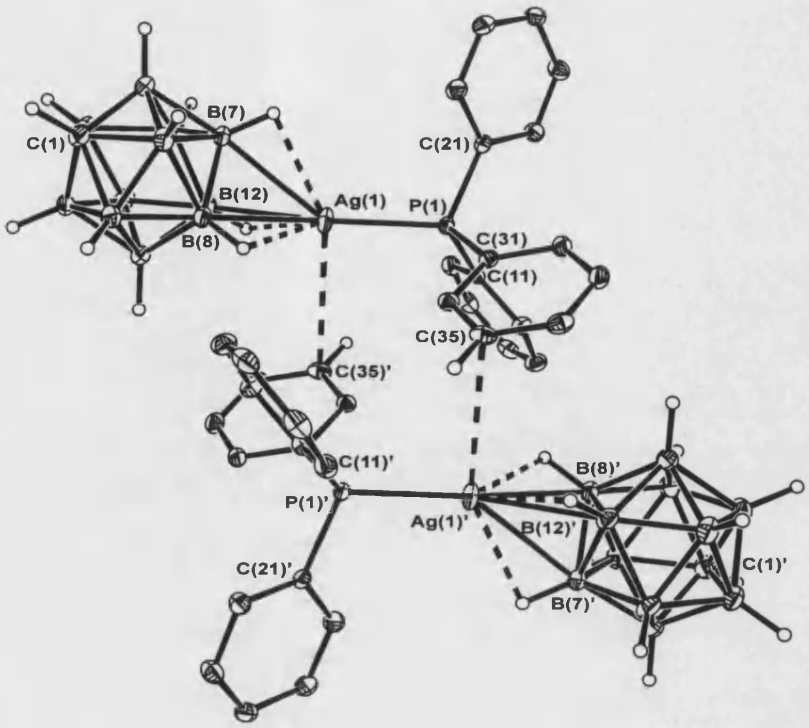

Figure 4.4: Dimeric unit formed in the extended lattice of compound **X**

The Ag(1)-P(1) distance of 2.3625(7) Å is comparable to that seen for $[Ag(PPh_3)(NO_3)]$[18] [2.369(6) Å], which places this bond at the shorter end of the range observed for silver-phosphine complexes[19] implying a strong coordination of the phosphine to silver. This is reflected in the observed value of J(AgP) in solution and the solid state, as discussed next.

In solution, the $\{Ag(PPh_3)\}^+$ fragment is fluxional over the surface of the carborane cage. The $^1H\{^{11}B\}$ NMR spectrum of compound **X** exhibits resonances for the ligated [*closo*-$CB_{11}H_{12}]^-$ anion at δ 2.55 (1H, s, C*H*), δ 2.25 (1H, s, B*H*) and δ 1.85 (10H, 5H + 5H coincidence, s, B*H*) in a 1:1 ratio of [*closo*-$CB_{11}H_{12}]^-$: triphenylphosphine. No significant changes in the spectrum are observed when the sample is cooled to -90°C, indicating the scrambling of $\{Ag(PPh_3)\}^+$ about the carborane periphery is via a low energy dynamic process that imparts time averaged C_{5v} symmetry on the cage. The

fluxional behaviour of $\{Ag(PPh_3)\}^+$ about the surface of related metallocarboranes has been noted previously.[13] The $^{11}B\{^1H\}$ NMR spectrum of **X** (CD_2Cl_2) reflects the C_{5v} symmetry seen in the $^1H\{^{11}B\}$ spectrum and displays resonances at δ -13.6 [1B, B(12)], δ -14.5 [5B, B(7-11)] and δ -15.3 [5B, B(2-6)]. The B(12) and B(7-11) resonances are shifted upfield compared with $[NBu_4][CB_{11}H_{12}]$ (CD_2Cl_2) δ -8.0 [1B, B(12)], δ -14.1 [5B, B(7-11)] and δ -16.9 [5B, B(2-6)], in which no significant cation anion interactions are likely to occur. This indicates that the $\{AgPPh_3\}^+$ fragment in compound **X** is interacting significantly with the carborane anion in solution through the B(12) and B(7-11) the faces of the cage. The upfield shift of the cage boron resonances, but the absence of any high-field peaks in the $^1H\{^{11}B\}$ NMR spectrum of **X** that are indicative of significant Ag-H bonding, perhaps implies that the carborane is binding to silver predominantly through Ag-B as opposed to Ag-H interactions. Given the strong metal-cage interactions in solution evident from the ^{11}B NMR spectrum, it is perhaps strange that no evidence of any Ag-H coupling in either the $^1H\{^{11}B\}$ or $^{11}B\{^1H\}$ NMR spectra of compound **X** is observed, a curiousity observed in related Ag-metallocarborane compounds by Stone.[13-15] This said, examples of Ag-H coupling being observed spectroscopically are rare in the literature.[20] The $^{31}P\{^1H\}$ NMR spectrum of compound **X** displays a peak due to a single species centred at δ 18.70, consisting of two doublets arising from phosphorous coupling to both ^{107}Ag [$J(^{107}AgP)$ = 691 Hz] and ^{109}Ag [$J(^{109}AgP)$ = 795 Hz] isotopes of silver. The large average coupling constant [$J(AgP)_{average}$ = 743 Hz] for this compound is consistent with the strong Ag-P bond observed in the solid state. That the gross solid state structure is maintained in solution is confirmed by inspection of the $^{31}P\{^1H\}$ CPMAS spectrum. This displays two doublets centred at δ 18.06 with an average coupling

constant of 738 Hz, closely matching that seen in the solution $^{31}P\{^{1}H\}$ NMR spectrum (Figure 4.5).

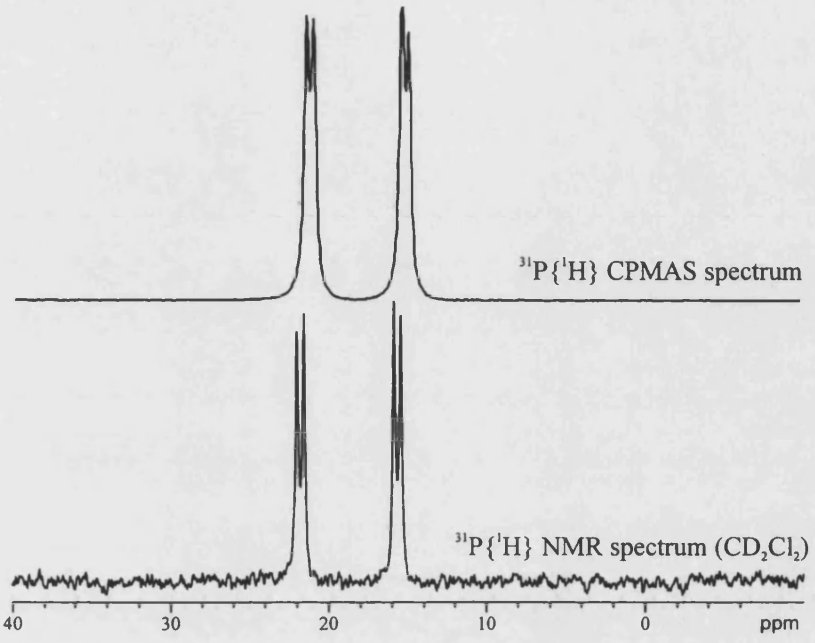

Figure 4.5: Solid state and solution $^{31}P\{^{1}H\}$ NMR spectrum of compound **X**

*[Ag(PPh$_3$)(CB$_{11}$H$_{11}$Br)], Compound **XI***

The asymmetric unit in the crystal structure of **XI** consists of one solvent molecule (CH_2Cl_2) and two chemically independent dimeric molecules of general formula [{(PPh$_3$)Ag}$_2${12-μ^2-Br-CB$_{11}$H$_{11}$}$_2$]. The dimeric species have been labelled **XIA** and **XIB** and are displayed in Figure 4.6 and Figure 4.7 respectively, alongside their corresponding tables of relevant bond lengths and angles (Tables 4.2-4.5). Each dimer displays a bromine atom from two carborane cages bridging two silver atoms via one short [Ag-Br average 2.65 Å] and one longer [Ag-Br' average = 3.09 Å] Ag-Br bond to generate a {Ag_2Br_2} core of the molecule. In addition to the halide bonds, each

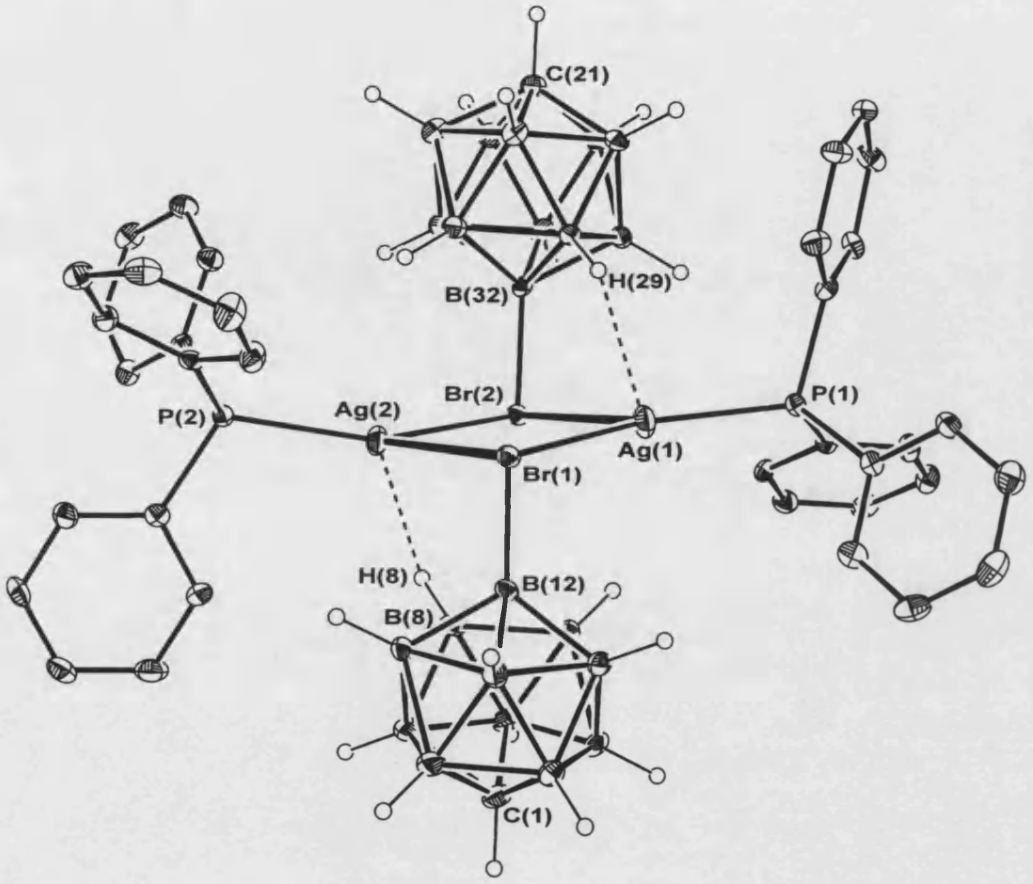

Figure 4.6: Crystal structure of $[Ag(PPh_3)(CB_{11}H_{11}Br)]$, **XIA**
(phenyl hydrogen atoms omitted for clarity; ellipsoids drawn at 30% probability level)

	(Å)
Ag(2)-Ag(1)	4.1853(6)
Ag(1)-P(1)	2.375(2)
Ag(2)-P(2)	2.394(2)
Ag(1)-Br(1)	2.6150(7)
Ag(1)-Br(2)	3.0318(8)
Ag(2)-Br(2)	2.6740(7)
Ag(2)-Br(1)	3.0852(8)
B(12)-Br(1)	2.017(6)
B(32)-Br(2)	2.021(6)
H(8)-Ag(2)	2.24
H(29)-Ag(1)	2.39
B(8)···Ag(2)	3.065(2)
B(29)···Ag(1)	3.178(5)

Table 4.2: Selected bond lengths for compound **XIA**

	(°)
P(1)-Ag(1)-Br(1)	150.54(5)
P(1)-Ag(1)-Br(2)	122.48(4)
P(2)-Ag(2)-Br(2)	148.13(4)
P(2)-Ag(2)-Br(1)	122.90(4)
Ag(1)-Br(1)-Ag(2)	94.12(2)
Ag(1)-Br(2)-Ag(2)	94.16(2)
Br(1)-Ag(1)-Br(2)	86.86(2)
Br(1)-Ag(2)-Br(2)	84.76(2)
B(12)-Br(1)-Ag(1)	95.3(2)
B(12)-Br(1)-Ag(2)	85.1(2)
B(32)-Br(2)-Ag(2)	98.0(2)
B(32)-Br(2)-Ag(1)	87.4(2)

Table 4.3: Selected bond angles for compound **XIA**

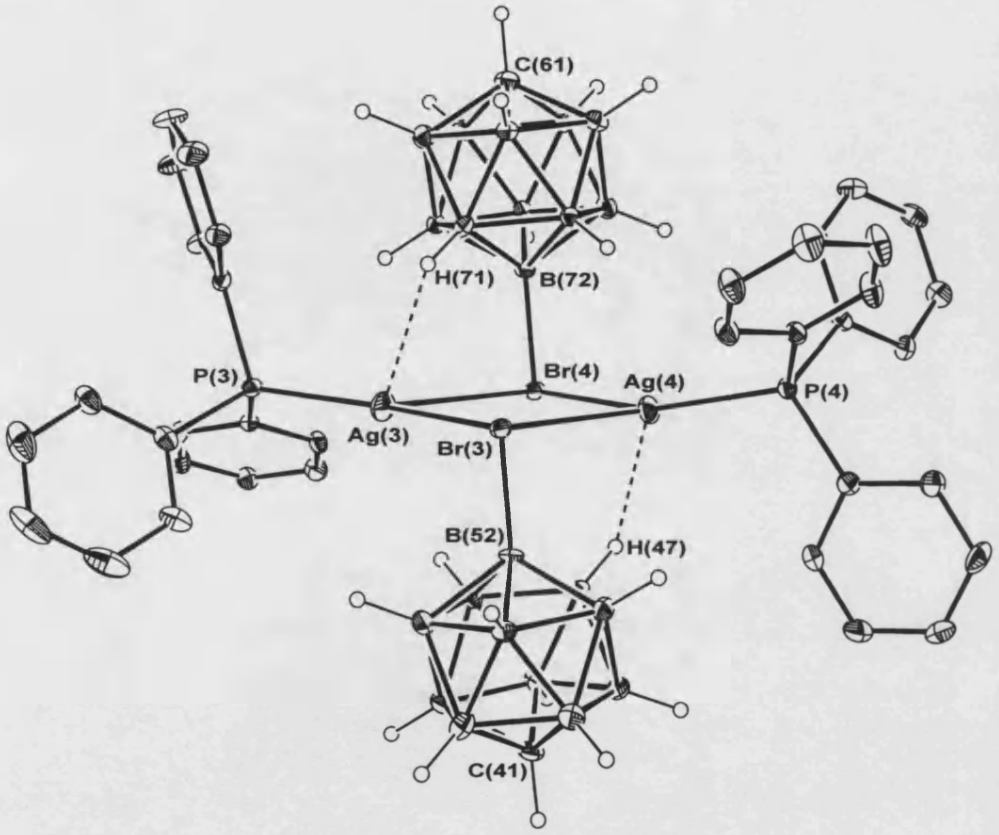

Figure 4.7: Crystal structure of $[Ag(PPh_3)(CB_{11}H_{11}Br)]$, **XIB**
(phenyl hydrogen atoms omitted for clarity; ellipsoids drawn at 30% probability level)

	(Å)
Ag(4)-Ag(3)	4.3743(6)
Ag(3)-P(3)	2.393(2)
Ag(4)-P(4)	2.401(2)
Ag(3)-Br(3)	2.6527(7)
Ag(3)-Br(4)	3.1718(8)
Ag(4)-Br(4)	2.6691(7)
Ag(4)-Br(3)	3.0568(8)
B(52)-Br(3)	2.030(6)
B(72)-Br(4)	2.029(6)
H(47)-Ag(4)	2.32
H(72)-Ag(3)	2.42
B(47)···Ag(4)	3.148(5)
B(71)···Ag(3)	3.236(5)

Table 4.4: Selected bond lengths for compound **XIB**

	(°)
P(3)-Ag(3)-Br(3)	159.30(4)
P(3)-Ag(3)-Br(4)	119.62(4)
P(4)-Ag(4)-Br(4)	151.41(4)
P(4)-Ag(4)-Br(3)	122.69(4)
Ag(3)-Br(3)-Ag(4)	99.77(2)
Ag(3)-Br(4)-Ag(4)	96.61(2)
Br(3)-Ag(3)-Br(4)	80.84(2)
Br(3)-Ag(4)-Br(4)	87.78(2)
B(52)-Br(3)-Ag(3)	95.7(2)
B(52)-Br(3)-Ag(4)	87.1(2)
B(72)-Br(4)-Ag(4)	95.8(2)
B(72)-Br(4)-Ag(3)	87.2(2)

Table 4.5: Selected bond angles for compound **XIB**

carborane interacts further with silver via a B-H-Ag interaction from a hydrogen on the B(7-11) boron belt [H-Ag' average 2.34 Å; B···Ag' average 3.16 Å], that is similar in length to B-H-Ag interactions in **IIIA** [H-Ag, 2.43 Å; B···Ag, 3.159(3) Å] but longer than those seen in compound **X** [H-Ag average 2.25 Å; B···Ag average 2.56 Å]. The silver-halide cores of **XIA** and **XIB** are *pseudo* planar, with the maximum deviation of any of these atoms from the least squares plane through them being 0.031 Å and 0.009 Å respectively. The phosphorous atoms deviate from this plane by 0.005 Å [P(1)], 0.679 Å [P(2)], 0.132 Å [P(3)] and 0.519 Å [P(4)]. The Ag···Ag distances within the $\{Ag_2Br_2\}$ cores [Ag(1)···Ag(2), 4.1853(6) Å; Ag(3)···Ag(4) 4.3746 Å] are too long to be considered Ag-Ag bonds, unlike those observed in the $\{Ag_2I_2\}$ core of **III** [Ag-Ag average, 2.99 Å]. The only other structurally characterised compounds containing a $\{Ag_2X_2\}$ (X = halide) core similar to **XI** are $[Ag\{P(C_6H_{11})_3\}Cl]_2$ and $[Ag\{P(C_6H_{11})_3\}Br]_2$.[21] The relevant bond lengths in $[Ag\{P(C_6H_{11})_3\}Br]_2$ [Ag-Br, 2.576(2) Å; Ag-Br', 2.718(2) Å; Ag···Ag, 3.493(1) Å] suggest that its $\{Ag_2Br_2\}$ core is more 'compact' than in **XI**, although the different phosphines ligands employed on the two compounds preclude accurate comparison. Whether or not the dimeric configuration of **XI** observed in the solid state persists in solution is elucidated from inspection of the NMR spectroscopy data, discussed next.

The $^1H\{^{11}B\}$ NMR spectrum of **XI** displays triphenyphosphine and $[closo\text{-}CB_{11}H_{12}]^-$ resonances with the correct ratio of intensities for a 1:1 mixture of species in solution, while no highfield resonances that might indicate strong Ag-H interactions are observed. The $^{11}B\{^1H\}$ NMR spectrum displays just three boron resonances in solution at δ -3.3 [1B, B(12)], δ -13.2 [5B, B(7-11)] and δ -16.2 [5B, B(2-6)]

indicating C_{5v} symmetry of a fluxional carborane cage. These chemical shifts are only marginally shifted when compared to $[Ag(CB_{11}H_{11}Br)]$ recorded in d_6-acetone [δ -3.1 (1B), δ -12.8 (5B), δ -17.1 (5B)] suggesting no significant Ag···{HB} interactions in solution. The real clue as to the structure of **XI** in solution comes from the Ag-P coupling constant in the $^{31}P\{^1H\}$ NMR spectrum. There are two likely configurations (Figure 4.8) that compound **XI** could adopt in solution, the obvious one being the dimeric molecule seen in the solid state. The other possibility is a monomeric species with [*closo*-$CB_{11}H_{11}Br]^-$ bound to the silver about the B(7)-B(8)-B(12) face similar to the bonding mode of [*closo*-$CB_{11}H_{12}]^-$ in complex **X**.

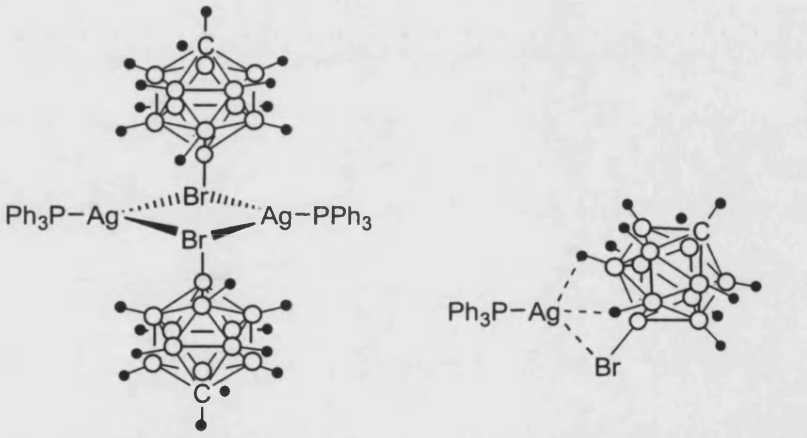

Figure 4.8: Possible configurations of compound **XI** in solution

If the monomeric species prevailed in solution an Ag-P coupling constant with a value in the region found for compound **X** (743 Hz) and [Ag(tmpp)Br][22] (tmpp = 2,4,6-trimethoxyphenylphosphine) (742 Hz) might be expected. In contrast, the dimeric species $[Ag\{P(C_6H_{11})_3\}Br]_2$ shows similar Ag-P coupling constants in both its solution (627 Hz) and solid state (612 Hz) $^{31}P\{^1H\}$ NMR spectra,[21] suggesting that the $\{Ag_2Br_2\}$ core observed in its solid state structure is likely to persist in solution. The 621 Hz average Ag-P coupling constant in the ^{31}P NMR spectrum of **XI** suggests

that the dimeric motif observed in the solid state is retained in solution. Unfortunately, no $^{31}P\{^{1}H\}$ CPMAS data is available for **XI** to directly compare solution and solid state structure.

[Ag(PPh$_3$)(CB$_{11}$H$_6$Br$_6$)], Compound XII

The solid state structure of [Ag(PPh$_3$)(CB$_{11}$H$_6$Br$_6$)] is shown in Figure 4.9, with relevant bond lengths and angles given in Table 4.6. The molecule displays [*closo*-CB$_{11}$H$_6$Br$_6$]$^-$ coordinated to a {PPh$_3$Ag}$^+$ fragment through two shorter [Ag(1)-Br(7), 2.8710(5) Å; Ag(1)-Br(8), 2.6963 (5) Å] and one longer [Ag(1)-Br(12), 3.0953(5) Å] Ag-Br bond, the lengths of which fall within the range of bond distances found for previously reported silver salts of brominated monocarboranes.[5, 7, 23, 24] On initial inspection, it is surprising that the coordination geometry about the four coordinate silver appears to be more trigonal bipyradimal, as opposed to tetrahedral, with a vacant coordination site opposite B(12). This evidenced by the bond angles that Br(7), Br(8) and P(1) make with silver totalling 360.5° [Br(7)-Ag(1)-P(1), 117.44(3)°; Br(8)-Ag(1)-P(1), 155.55(3)°; Br(7)-Ag(1)-Br(8), 87.47(1)°]. However, further examination of the packing diagram reveals a bromine [Br(11)'] from a symmetry generated cage within the lattice approaches the silver approximately *trans* to Br(12) [Br(12)-Ag(1)-Br(11)' 157.15(1)°] (Figure 4.10). The Ag(1)-Br(11)' bond distance of 3.4901(5) Å is very long (see discussion for the solid state structure of **IV**, section 2.2.4), but is within the sum of the van der Waal radii for bromine and silver (3.5 - 3.7 Å)[25] and thought to be significant in this instance because it completes a distorted trigonal bipyradimal coordination geometry around silver.

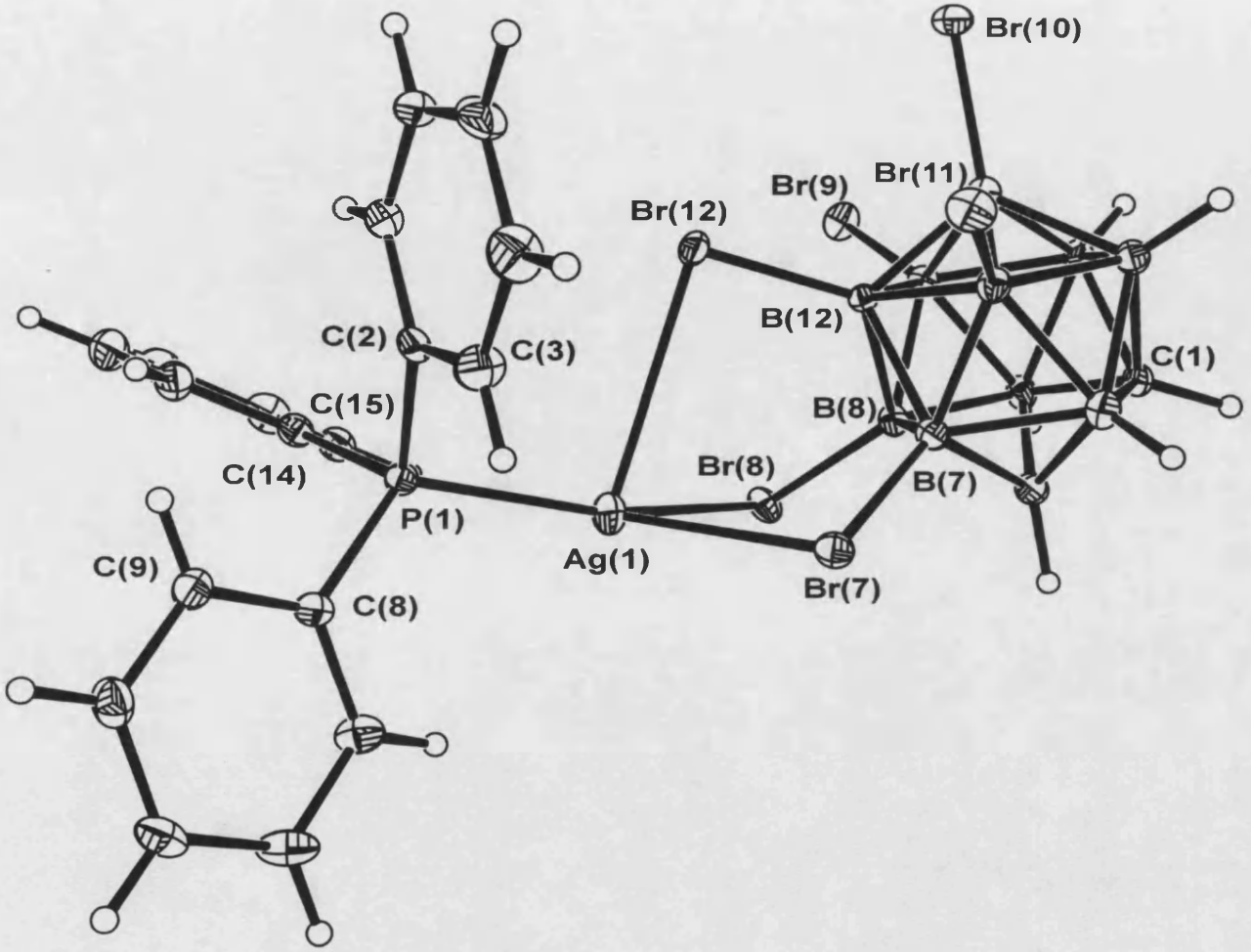

Ag(1)-P(1)	2.403(1) Å
Ag(1)-Br(7)	2.8710(5) Å
Ag(1)-Br(8)	2.6963(5) Å
Ag(1)-Br(12)	3.0953(5) Å
B(7)···Ag(1)	3.587(4) Å
B(8)···Ag(1)	3.541(4) Å
B(12)···Ag(1)	3.662(4) Å
P(1)-Ag(1)-Br(7)	117.44(3)°
P(1)-Ag(1)-Br(8)	155.55(3)°
P(1)-Ag(1)-Br(12)	93.31(3)°
Br(7)-Ag(1)-Br(8)	87.47(1)°

Table 4.6: Selected bond lengths and angles for compound **XII**

Figure 4.9: Crystal structure of $[Ag(PPh_3)(CB_{11}H_6Br_6)]$, **XII** (ellipsoids drawn at 30% probability level)

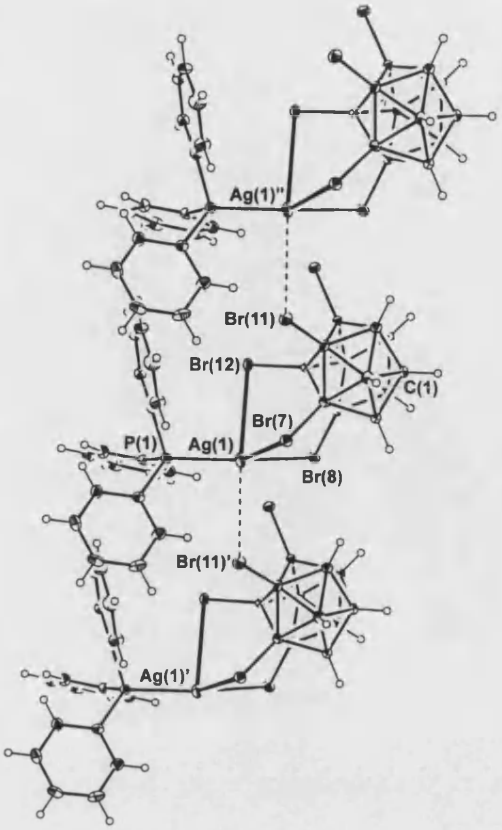

Figure 4.10: Weak axial Ag···B interactions between symmetry generated isomers of complex **XII**

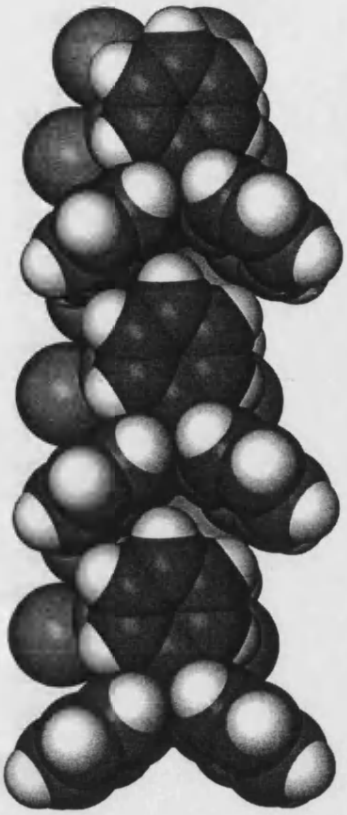

Figure 4.11: Space filling diagram (vdW radii) of complex **XII** showing orientation of phenyl groups

This interaction also results in the phenyl groups on adjacent phosphines in the lattice having a close approach in the lattice, which in combination with steric interactions from [*closo*-$CB_{11}H_6Br_6$]$^-$ leads them to be twisted from their common 'propeller' geometry to a C_s geometry (Figure 4.11), and distortion of Br(7) and Br(8) from lying equidistant to the Ag(1)-P(1) vector [P(1)-Ag(1)-Br(7), 117.44(3)°; P(1)-Ag(1)-Br(8), 155.55(3)°]. The Ag(1)-P(1) bond distance of 2.403(1) Å is longer than that found in complex **X,** but only fractionally longer than that found in **XI**.

Inspection of the phenyl and B-H resonance integrals in the $^1H\{^{11}B\}$ NMR spectrum of **XII** displays a 1:1 ratio of PPh_3 and cage ligands in solution. The $^{11}B\{^1H\}$ NMR

spectrum shows that the cage does not retain its rigid coordination to the $\{AgPPh_3\}^+$ fragment, with three peaks observed at δ -5.4 [1B, B(12)], δ -9.9 [5B, B(7-11)] and δ -20.2 [5B, B(2-6)] indicating C_{5v} symmetry of the carborane cage, a feature commonly observed for this anion in solution. In contrast to the proposed solution structure of compound **IV**, in which the bromines from both the B(12) and B(7-11) cage vertexes are thought to interacting with silver, only the B(12) boron resonance for **XII** is shifted significantly upfield (Δ = δ -4.5) in comparison to $[NBu_4][CB_{11}H_6Br_6]$. This could perhaps suggest that, in solution, [*closo*-$CB_{11}H_6Br_6]^-$ is interacting with silver predominantly through the antipodal bromine with weak, if any, interactions from the lower pentagonal belt bromines (Figure 4.12). This proposed solution configuration also perhaps minimises any phenyl ring – bromine steric interactions, that were observed in the solid state structure of **XII** (Figure X) when [*closo*-$CB_{11}H_6Br_6]^-$ was bound to $\{Ag(PPh_3)\}^+$ via a Br(7)-Br(8)-Br(12) face of the cage.

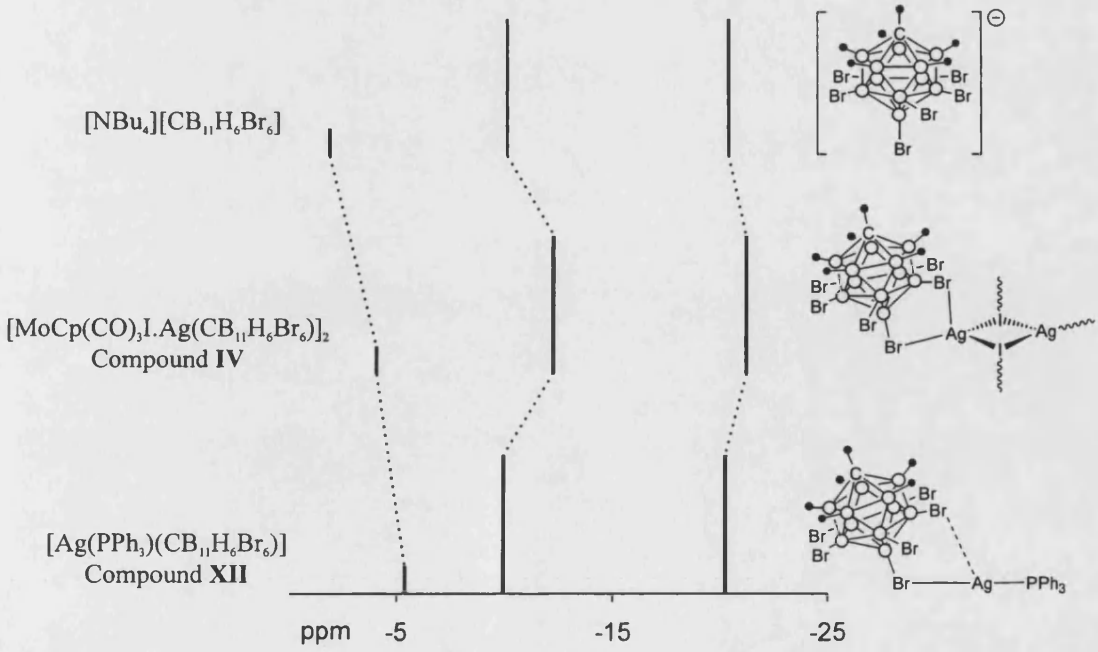

Figure 4.12: Stick diagram relating $^{11}B\{NMR\}$ chemical shifts (CD_2Cl_2) and suggested solution configurations of $[NBu_4][CB_{11}H_{12}]$, compound **IV** and compound **XII**

The $^{31}P\{^1H\}$ NMR spectrum of **XII** displays two concentric doublets in solution centred on δ 16.52 with large coupling constants, $J(AgP)_{average}$ = 715 Hz. This coupling constant is *ca.* 100 Hz larger than found for the sp^2-hybridised compounds **XI** [J(AgP) = 621 Hz] and $[Ag\{P(C_6H_{11})_3\}Br]_2$ [21] [J(AgP) = 627 Hz] but more of the order found for monomeric, sp-hybridised species like **X** [J(AgP) = 743 Hz] and [Ag(tmpp)Br][22] [J(AgP) = 742 Hz]. The extended interactions observed in the crystal lattice of **XII** (Figure 4.10) are unlikely to persist in solution, but the similarity of the solid state structure to the solution structure can be seen by comparing Ag-P coupling constants in the solid state and solution $^{31}P\{^1H\}$ NMR spectra. The $^{31}P\{^1H\}$ CPMAS spectrum for **XII** displays a broad doublet (due to the loss of resolution of the coupling to the two different silver isotopes) at δ 23.47 [$J(AgP)_{average}$ = 732 Hz], with an Ag-P coupling constant somewhat larger than observed in solution (715 Hz).

*[Ag(PPh$_3$)(CB$_{11}$H$_6$Cl$_6$)], Compound **XIII***

The solid state structure of **XIII** is grossly disordered over two sites (50:50 ratio), but can be resolved into two separate components, which themselves show disorder (Figure 4.13). For this reason bond lengths and angles are not discussed in detail for this compound.

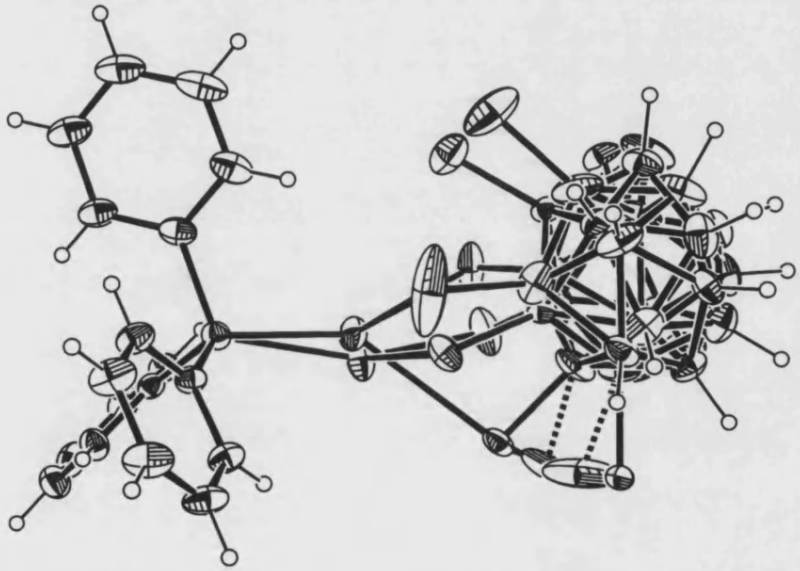

Figure 4.13: Crystal structure of **XIII** showing gross disorder of silver and [*closo*-CB$_{11}$H$_6$Cl$_6$]$^-$ over two sites in the asymmetric unit

Inspection of the packing diagram for each of the disordered components (**XIIIA** and **XIIIB**) reveals weak interactions between chlorine atoms from carborane cages in a neighbouring asymmetric unit and silver. This results in the formation of dimeric species with different orientations of the bridging carborane cages for each disordered component, displayed in Figure 4.14 (Table 4.7) for **IIIA** and Figure 4.15 (Table 4.8) for **IIIB**. In **IIIA** one of the chlorines is disordered over two sites [Cl(8a) and Cl(8b)], a situation matched for one of the chlorines in **IIIB** [Cl(18) and Cl(28)].

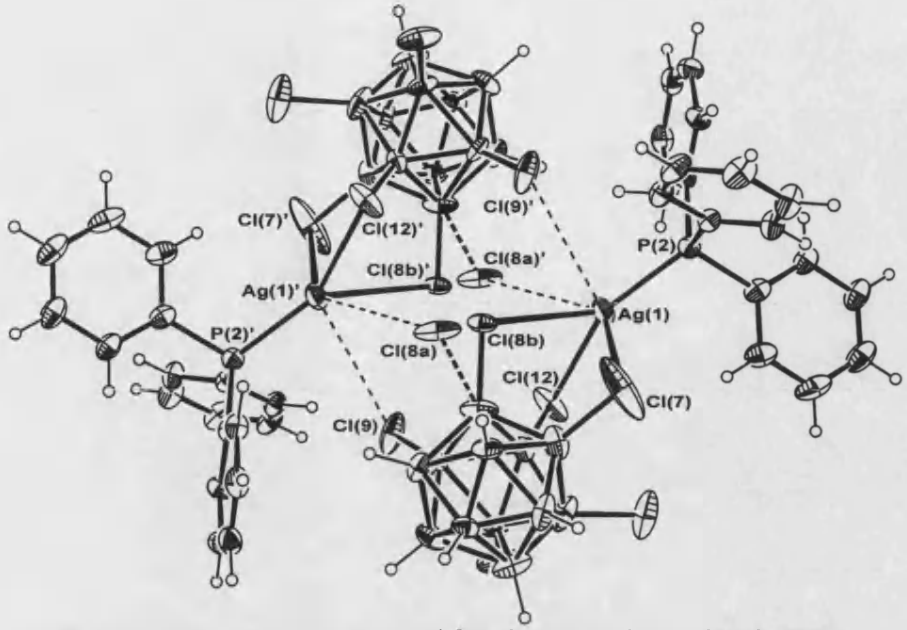

Figure 4.14: Dimeric unit generated from long range interactions in **XIIIA**

Ag(1)-P(2)	2.314(2) Å
Ag(1)-Cl(7)	2.969(4) Å
Ag(1)-Cl(8b)	3.070(4) Å
Ag(1)-Cl(12)	2.498(3) Å
Cl(8a)'-Ag(1)	3.421(7) Å
Cl(9)'-Ag(1)	3.402(3) Å
Ag(1)···Cl(8a)	3.894(7) Å
P(2)-Ag(1)-Cl(7)	97.80(9)°
P(2)-Ag(1)-Cl(8b)	131.70(9)°
P(2)-Ag(1)-Cl(12)	152.0(1)°
Cl(8b)-Ag(1)-Cl(12)	75.14(9)°

Table 4.7: Selected bond lengths and angles for **XIIIA**

Ag(2)-P(2)	2.482(2) Å
Ag(2)-Cl(27)	2.805(3) Å
Ag(2)-Cl(32)	2.421(3) Å
Cl(18)'-Ag(2)	3.137(8) Å
Cl(28)'-Ag(2)	3.455(4) Å
Cl(29)'-Ag(2)	3.505(3) Å
Ag(2)···Cl(18)	4.141(8) Å
Ag(2)···Cl(31)	3.773(3) Å
P(2)-Ag(2)-Cl(27)	100.66(9)°
P(2)-Ag(2)-Cl(32)	158.4(1)°
Cl(27)-Ag(2)-Cl(32)	87.61(1)°

Table 4.8: Selected bond lengths and angles for **XIIIB**

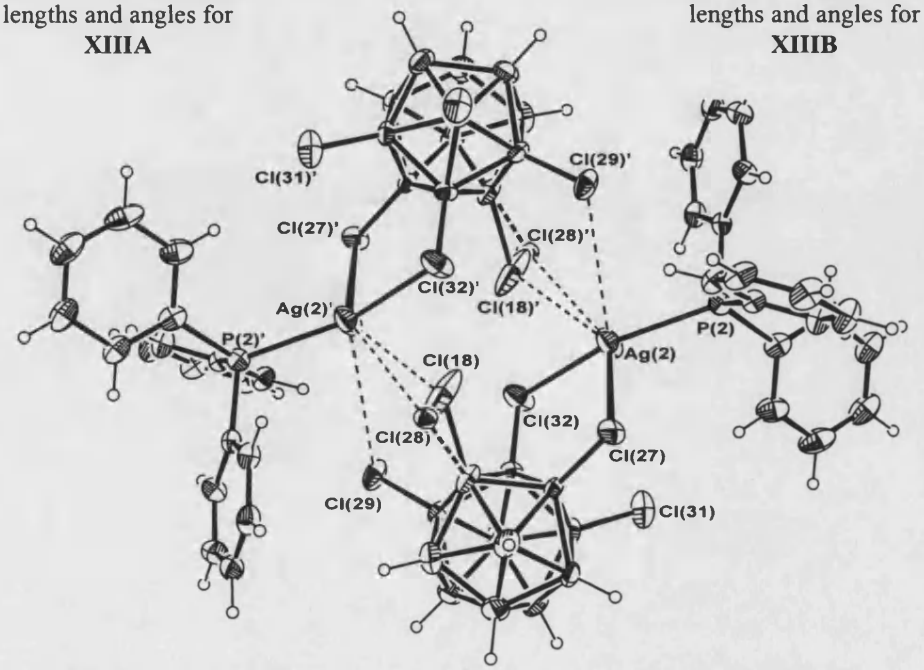

Figure 4.15: Dimeric unit generated from long range interactions in **XIIIB**

Tables 4.7 and 4.8 list relevant bond lengths and angles for **XIIIA** and **XIIIB**. Unfortunately, the heavy disorder observed in the solid state structure of **XIII** precludes any accurate correlations between the solid state and solution (NMR spectroscopy) data discussed next.

The $^{1}H\{^{11}B\}$ NMR spectrum of **XIII** displays resonances corresponding to the triphenylphosphine and carborane cage with intensities that indicate a 1:1 ratio of the ligands in solution and no highfield resonances indicative of Ag-H bonds. The $^{11}B\{^{1}H\}$ NMR spectrum displays 3 resonances at δ 0.1 [1B, B(12)], δ -6.6 [5B, B(7-11)] and δ -23.2 [5B, B(2-6)] indicating C_{5v} symmetry of the cage in solution and fluctionality of the $\{Ag(PPh_3)\}^+$ fragment around the chlorine surface of the carborane cage. The $^{11}B\{^{1}H\}$ NMR resonances of **XIII** are shifted upfield [ΔB(12) = δ -0.7, ΔB(7-11) = δ -0.5] from those of $[Ag(CB_{11}H_6Cl_6)]$ (acetone-d_6), which displays three peaks at δ 0.8 [1B, B(12)], δ -6.1 [5B, B(7-11)] and δ -23.7 [5B, B(2-6)]. This might suggest [*closo*-$CB_{11}H_6Cl_6]^-$ coordinates to $\{Ag(PPh_3)\}^+$ via an antipodal chlorine and one or two lower pentagonal belt chlorines in solution. However, the shift is very small, and indicates that [*closo*-$CB_{11}H_6Cl_6]^-$ is only interacting very weakly with $\{Ag(PPh_3)\}^+$ in solution. This observation is supported by the large Ag-P coupling constant observed in the $^{31}P\{^{1}H\}$ NMR spectrum of **XIII** [δ16.80, dd, 1P, $J(AgP)_{average}$ = 770 Hz]. This is the largest Ag-P coupling constant found for compounds **X-XIII** indicating that, in solution, **XIII** has the strongest Ag-P bond.

Comparisons between compounds X-XIII

The solid state and solution properties of compounds **X-XIII** are summarised in Table 4.9. The strength of the Ag-P bond in these compounds is an indication to the degree of Lewis acidity of the silver, and thus can be used as a guide to the relative

Compound	$^{31}P\{^{1}H\}$ NMR Spectroscopy		Ag-P bond distance
	δ	$J(AgP)_{average}$	
$Ag(PPh_3)(CB_{11}H_{12})$, **X**	18.70 (18.06)	743 (738) Hz	2.3625(7) Å
$Ag(PPh_3)(CB_{11}H_{11}Br)$, **XI**	16.85	621 Hz	2.39† Å
$Ag(PPh_3)(CB_{11}H_6Br_6)$, **XII**	16.52 (23.47)	715 (732) Hz	2.4032(3) Å
$Ag(PPh_3)(CB_{11}H_6Cl_6)$, **XIII**	16.80	770 Hz	2.314(2) Å (**XIIIA**) 2.482(2) Å (**XIIIB**)

Values in parenthesis obtained from $^{31}P\{^{1}H\}$ CPMAS; † average of values

Table 4.9: Comparative solution and solid state values for complexes **X-XIII**

coordinating ability of the carborane anions. The strength of the Ag-P bond can be measured in the solid state by Ag-P bond distances, and in solution by the magnitude of the Ag-P coupling constant in the $^{31}P\{^{1}H\}$ NMR spectrum. However, the solid state structures of **X-XIII** show a variety of intermolecular interactions that generate different extended solid state structures precluding the accurate use of the Ag-P bond lengths as a guide to the coordinating ability of the anion in these compounds. However, the majority of these intermolecular interactions are unlikely to persist in solution, where discrete monomers (apart from **XI**) are suggested by the NMR spectroscopic data. Therefore the strength of the Ag-P bond in solution can be used to measure the Lewis acidity, and hence coordinating ability of the carborane anions in this system. The silver phosphine coupling constants suggest the Lewis acidity of the complexes increases in the order **XI** < **XII** < **X** < **XIII**, implying the coordinating

ability of the anions decreases in the order [*closo*-$CB_{11}H_{11}Br]^-$ > [*closo*-$CB_{11}H_6Br_6]^-$ > [*closo*-$CB_{11}H_{12}]^-$ > [*closo*-$CB_{11}H_6Cl_6]^-$. The assignment of [*closo*-$CB_{11}H_{12}]^-$ as less coordinating than [*closo*-$CB_{11}H_6Br_6]^-$ is surprising given the previous ranking scheme developed in chapter 3 and the results of catalytic studies using these compounds, discussed later, that suggests [*closo*-$CB_{11}H_6Br_6]^-$ is more weakly coordinating than [*closo*-$CB_{11}H_{12}]^-$. In this case, the reversal from the expected is probably a consequence of the minimal steric interactions in the $\{Ag(PPh_3)\}^+$ fragment in **XII** allowing a closer approach, and hence stronger coordination of the bulky [*closo*-$CB_{11}H_6Br_6]^-$ anion compared to other systems. Evidence of the large steric bulk of [*closo*-$CB_{11}H_6Br_6]^-$ can still be seen in this system, with distortion of the phenyl ring geometry in the solid state structure of **XII**.

The comparatively low Ag-P coupling constant for **XI** is a consequence of its dimeric configuration and sp^2-hybridisation of silver in solution. By adopting this configuration the [*closo*-$CB_{11}H_{11}Br]^-$ anion is making two Br-Ag bonds, as opposed to the one Ag-Br and two B-H-Ag interactions it would make if it adopted a monomeric configuration. This suggests that an Ag-Br interaction is favoured over Ag-H-B in this instance.

4.2.2 Synthesis and Characterisation of $[Ag(PPh_3)_2(CB_{11}H_{12})]$ and $[Ag(PPh_3)_2(CB_{11}H_6Br_6)]$

In order to try and generate more silver(I) phosphine species for comparison in catalysis (discussed later) the bis-phosphine analogues of **X** and **XII** were synthesised. Addition of two equivalents of PPh_3 to $Ag(CB_{11}H_{12})$ or $Ag(CB_{11}H_6Br_6)$ in CH_2Cl_2 yields $[Ag(PPh_3)_2(CB_{11}H_{12})]$ (compound **XIV**) and $[Ag(PPh_3)_2(CB_{11}H_6Br_6)]$ (compound **XV**) as colourless solids. The compounds were characterised by elemental analysis and multinuclear NMR spectroscopy. Crystals suitable for an X-ray diffraction study were grown by slow diffusion of hexanes into saturated CH_2Cl_2 solutions of the compounds. The discussion of the data for each compound is presented next.

*$[Ag(PPh_3)_2(CB_{11}H_{12})]$, Compound **XIV***

The solid state structure of compound **XIV** is displayed in Figure 4.16 with selected bond lengths and angles given in Table 4.10. The coordination geometry about each silver atom is that of a distorted tetrahedron, with bonds to two triphenylphosphine ligands and two cage B-H vertices. Two [*closo*-$CB_{11}H_{12}]^-$ anions bridge two $\{Ag(PPh_3)_2\}^+$ fragments resulting in the formation of a dimeric, centrosymmetric $[Ag(PPh_3)_2(CB_{11}H_{12})]_2$ unit. The positions of the bridging hydrogens [H(7) and H(12)] were located in the electron difference map and freely refined. Each cage is bonded through one long [B(7)···Ag(1), 3.494(2) Å; H(7)-Ag(1), 2.51(2) Å] and one

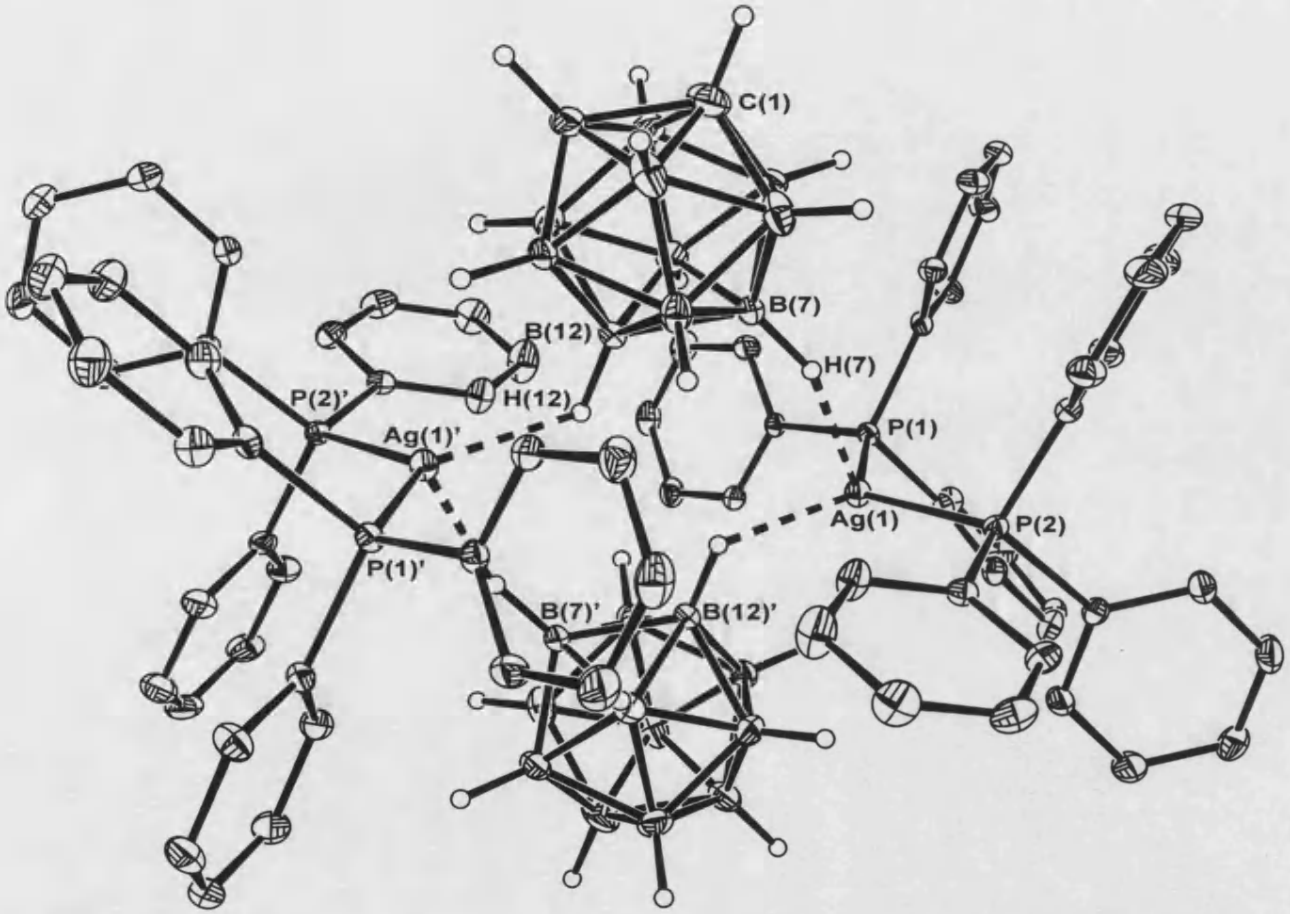

Figure 4.16: Crystal structure of $[Ag(PPh_3)_2(CB_{11}H_{12})]$, **XIV**
(phenyl hydrogens omitted for clarity; ellipsoids drawn at 30% probability level)

Ag(1)-P(1)	2.4698(3) Å
Ag(1)-P(2)	2.4741(3) Å
Ag(1)···B(7)	3.494(2) Å
Ag(1)···B(12)'	2.892(2) Å
Ag(1)-H(7)	2.51(2) Å
Ag(1)-H(12)'	2.17(2) Å
P(1)-Ag(1)-P(2)	130.90(1)°
B(7)-Ag(1)-B(12)'	72.4(6)°
B(7)-H(7)-Ag(1)	145(1)°
B(12)'-H(12)'-Ag(1)	119(1)°

Table 4.10: Selected bond lengths and angles for compound **XIV**

short [B(12)'···Ag(1), 2.892(2) Å; H(12)-Ag(1), 2.17(2) Å] interaction to silver. The bonding mode of the [*closo*-$CB_{11}H_{12}$]$^-$ anion to two different silver centres by interactions from the B(12) and B(7) vertices is similar to that seen in the extended solid state structure of [$MoCp(CO)_3I{\cdot}Ag(CB_{11}H_{12})]_2$ (compound **II**).[26, 27] The cage-silver bond lengths in **II** [B(7)···Ag(1) 2.66(1)Å; H(7)-Ag(1) 1.97Å; B(12)···Ag(1) 3.00(1)Å; H(12)-Ag(1) 1.97Å] and [$Ag(CB_{11}H_{12})$][3] (average values: B-Ag, 2.63 Å; H-Ag 1.97 Å) are considerably shorter than found for **XIV** suggesting [*closo*-$CB_{11}H_{12}$]$^-$ is interacting more weakly with silver in **XIV**. As expected on moving to two triphenylphosphine ligands the Ag-P bond distances are longer in **XIV** [Ag(1)-P(1), 2.4698(3) Å; Ag(1)-P(2), 2.4741(3) Å] compared to **X**, being similar in length to those of $[AgCl(PPh_3)_2]_2$ [2.467(2) Å and 2.472(2) Å].[28] The P(1)-Ag(1)-P(2) bond angle of 130.90(1)° is very similar to that observed in the related compound $[Ag(PPh_3)_2(HSO_4)].H_2O$ [29] [130.48(3) Å] which also contains a four coordinate silver atom.

In solution, the [*closo*-$CB_{11}H_{12}$]$^-$ anion in **XIV** only interacts very weakly with silver as shown by inspection of the $^{11}B\{^1H\}$ NMR spectrum. This displays three peaks at δ -8.4 (1B), δ -13.9 (5B) and δ -15.9 (5B) which are of a similar chemical shift to that found in the $^{11}B\{^1H\}$ NMR spectrum of [NBu_4][$CB_{11}H_{12}$] (CD_2Cl_2), which contains no anion-metal interactions. This is in sharp contrast to complex **X** for which significant silver-anion interactions are thought to persist in solution, evidenced by the large upfield shift of the boron resonances B(12) and B(7-11). This difference in ^{11}B chemical shift between bonding and non-bonding modes of [*closo*-$CB_{11}H_{12}$]$^-$ is best displayed in Figure 4.17. This data demonstrates that the cage anion in **XIV** is more like 'free' [*closo*-$CB_{11}H_{12}$]$^-$ in solution and not interacting significantly with the

$\{Ag(PPh_3)_2\}^+$ fragment, supporting the weak Ag···{HB} interactions observed in the solid state of **XIV**.

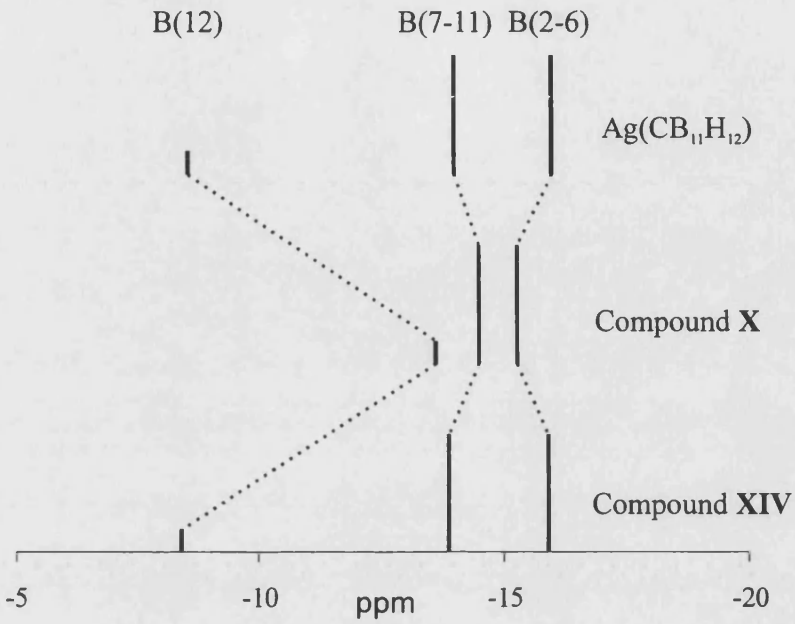

Figure 17: $^{11}B\{^1H\}$ NMR chemical shift diagram for $Ag(CB_{11}H_{12})$ (d_6-acetone), **X** (CD_2Cl_2) and **XIV** (CD_2Cl_2)

Previously, low temperature ^{31}P NMR spectroscopy has been used to demonstrate that silver-phosphine compounds of general formula $[Ag_2P_3X_2]$, $[AgP_2X]$ and $[AgP_3X]$ undergo dynamic exchange processes that result in a mixture of phosphine disproportionation products or isomeric species in solution.[30-33] The identity of these species in solution can be elucidated from the correlation between the coordination environment around silver and the magnitude of the Ag-P coupling constant.[10, 11] The $^{31}P\{^1H\}$ NMR spectrum of **XIV** at room temperature consists of a broad singlet at δ 14.8, a consequence of rapid ligand exchange that is commonly seen in the room temperature $^{31}P\{^1H\}$ NMR spectra of $[Ag(PPh_3)_2L_2]$ complexes.[33, 34] Cooling the sample to 0°C results in the formation of two broad singlets at δ 15.4 and δ 13.2. These peaks sharpen into two sets of doublets at -60°C centred at δ 13.7 [J(AgP) =

333 Hz] and δ 13.6 [$J(AgP)_{average}$ = 519 Hz] of approximately equal intensity, but coupling to ^{107}Ag-P and ^{109}Ag-P is only resolved for the latter resonance. The coupling constant of 519 Hz is of the order found for sp-hybridised $[P_2Ag][X]$ type compounds such as $[(PPh_3)_2Ag][NO_3]$[35] [J(AgP) = 500 Hz], $[(PPh_3)_2Ag][BF_4]$[19] [J(AgP) = 530 Hz] and $[\{P(mesityl)_3\}_2Ag][PF_6]$[36] [$J$(AgP) = 552 Hz]. Thus, this species is assigned as $[Ph_3P\text{-}Ag\text{-}PPh_3][CB_{11}H_{12}]$, in which the silver is sp hybridised and the phosphine ligands arranged nearly *trans* to one another (Figure 4.17). The second species observed at δ 13.7 with an Ag-P coupling constant of 333 Hz is tentatively assigned to be the dimeric species observed in the solid state structure of **XIV**. The coupling constant for this species is slightly lower than typically found for sp^3-hybridised $[P_2AgX]$ [X = bidentate monoanion, *eg*. NO_3] species *ca*. 400 Hz,[10] but is greater than the silver-phosphine coupling constant of *ca*. 280 Hz assigned for the four coordinate sp^3-hybridised configuration of $[Ag(PPh_3)_2(triazole)]$.[31] In support of this assignment, the dimerisation of $[Ag(PPh_3)_2(ClO_4)]$ in solution is thought to account for its lower than expected Ag-P coupling constant. [37]

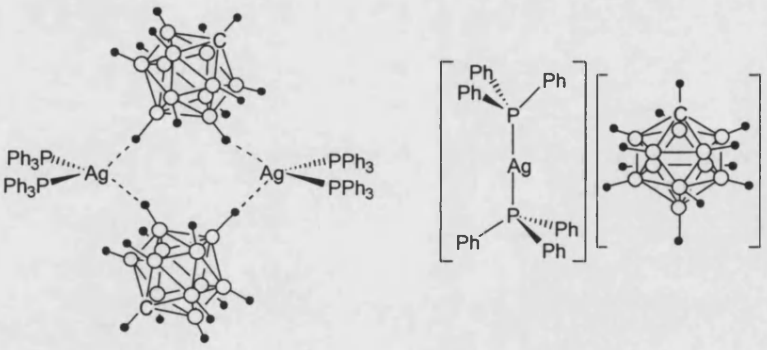

Hybridisation	sp^3		sp
$J(AgP)_{average}$	333 Hz		519 Hz
Molar ratio	1	:	1

Figure 4.17: Suggested solution configurations of **XIV** at low temperature

The $^{31}P\{^1H\}$ CPMAS spectrum of **XIV** is complicated, showing at least two species, but peaks from one of the species can be resolved. This species consists of two sets of doublet of doublets, arising from inequivalent phosphorus atoms coupling to silver (^{107}Ag and ^{109}Ag coupling unresolved) and phosphorus. The two peaks are centred on δ 16.7 [dd, ^1J(AgP) = 485 Hz, ^2J(PP) = 131 Hz] and δ 5.5 [dd, ^1J(AgP) = 456 Hz, ^2J(PP) = 129 Hz]. This is tentatively assigned as the sp-hybridised species $[Ag(PPh_3)_2][CB_{11}H_{12}]$, based upon the large Ag-P coupling constants observed. There is at least one other species present in the $^{31}P\{^1H\}$ CPMAS spectrum, although it is unresolvable under the strong signals from the inequivalent phosphorous atoms in the first species.

$[Ag(PPh_3)_2(CB_{11}H_6Br_6)]$, Compound XV

The solid state structure of $[Ag(PPh_3)_2(CB_{11}H_6Br_6)]$, **XV**, is displayed in Figure 4.18 with relevant bond lengths and angles given in Table 4.11. This shows a discrete molecule containing a four coordinate silver atom, with distorted tetrahedral geometry, bound to two PPh_3 ligands and a $[CB_{11}H_6Br_6]^-$ anion. The carborane anion is bound to silver in an η^2-fashion through two unequal bonds [Br(7)-Ag(1), 3.0477(9) Å; Br(8)-Ag(1), 2.8484(9) Å] from bromines on its lower pentagonal belt. The bonding of the cage through the bromines of the lower pentagonal belt and not the sterically least accessible antipodal bromine [Br(12)], also seen in $[Fe(TPP)(CB_{11}H_6Br_6)]$,[38] is perhaps to minimise any steric interactions between the anion and triphenylphosphine ligands. The Br-Ag bond distances are at the longer end

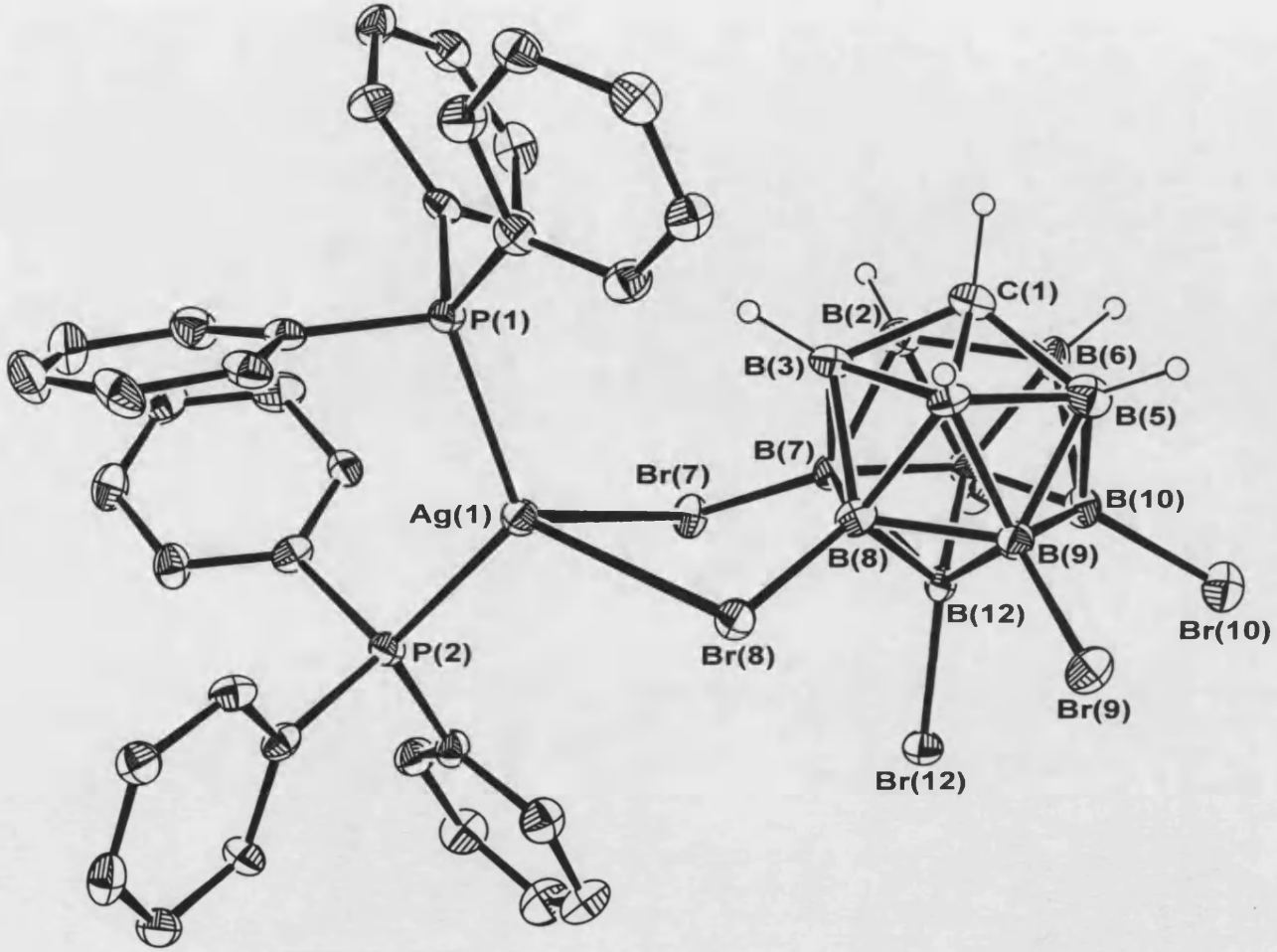

Figure 4.18: Crystal structure of $[Ag(PPh_3)_2(CB_{11}H_6Br_6)]$, **XV**
(phenyl hydrogens omitted for clartity; ellipsoids drawn at 30% probability level)

Ag(1)-P(1)	2.448(2) Å
Ag(1)-P(2)	2.451(2) Å
Ag(1)-Br(7)	3.0477(9) Å
Ag(1)-Br(8)	2.8484(9) Å
P(1)-Ag(1)-P(2)	120.43(6)°
Br(7)-Ag(1)-Br(8)	79.88(3)°
B(7)-Br(7)-Ag(1)	95.8(2)°
B(8)-Br(8)-Ag(1)	99.5(2)°
Br(7)-Ag(1)-P(1)	117.95(4)°
Br(7)-Ag(1)-P(2)	90.84(5)°
Br(8)-Ag(1)-P(1)	116.08(4)°
Br(8)-Ag(1)-P(2)	119.86(5)°

Table 4.11: Selected bond lengths and angles for compound **XV**

of the scale typically found for silver compounds of [*closo*-$CB_{11}H_6Br_6$]$^-$ [e.g. $Ag(CB_{11}H_6Br_6)$ average Ag-Br distance 2.86Å][5] implying weak coordination of the carborane anion in **XV**. The tetrahedral coordination environment for silver in both **XIV** and **XV** should allow direct comparison of the relative coordinating abilities of [*closo*-$CB_{11}H_{12}$]$^-$ and [*closo*-$CB_{11}H_6Br_6$]$^-$ by inspection of the phosphine bond lengths and angles. Previous studies on bis-phosphine silver(I) systems have shown that as the nucleophilicity of the anion decreases, the Ag-P bond distances decrease and P-Ag-P bond angle increases.[35, 39] The Ag-P distances in **XV** [Ag(1)-P(1), 2.448(2) Å; Ag(1)-P(2), 2.451(2) Å] are shorter than found in **XIV** and suggest [*closo*-$CB_{11}H_6Br_6$]$^-$ to be more weakly coordinating than [*closo*-$CB_{11}H_{12}$]$^-$. Conversely, the P(1)-Ag(1)-P(2) angle for **XV** [120.43(6)°] is less than in **XIV** [130.90(1)°] that reverses the ranking suggested by inspection of the bond lengths. However, the influence that the steric bulk of these anions must place on the metal's ligand set geometry in comparison to the smaller anions used in the previous studies [$(NO_3)^-$, $(ClO_4)^-$ and Cl^-] perhaps precludes the use of the P-Ag-P bond angles as a measure of the coordinating ability for larger anions. This is supported by consideration of the dimeric $[Ag(PPh_3)_2Br]_2.2CHCl_3$ [40] species which contains Ag-P bond lengths of 2.509(2) Å and 2.482(2) Å, that are, as expected, considerably longer than found in **XV**, but has a P-Ag-P angle of 120.15(6)° very similar to **XV**. Hence the solid state structures of **XV** and **XIV** suggest that [*closo*-$CB_{11}H_6Br_6$]$^-$ is more weakly coordinating than [*closo*-$CB_{11}H_{12}$]$^-$ to the $\{Ag(PPh_3)_2\}^+$ fragment. This is a reversal of the ranking indicated by the monophosphine silver species, likely a consequence of the increased steric bulk around silver affecting the coordinating ability of the larger [*closo*-$CB_{11}H_6Br_6$]$^-$ anion more than [*closo*-$CB_{11}H_{12}$]$^-$.

The $^{1}H\{^{11}B\}$ NMR spectrum of **XV** shows a 2:1 ratio of phosphine to cage, with no resonances observed to high field. The $^{11}B\{^{1}H\}$ NMR spectrum consists of three peaks at δ -4.6 (1B), δ -10.1 (5B) and δ -20.5 (5B) demonstrating the C_{5v} symmetry of [*closo*-$CB_{11}H_6Br_6$]$^-$ in solution. The $^{31}P\{^{1}H\}$ NMR spectrum at room temperature displays a broad singlet at δ 12.9, showing that the phosphine ligands are undergoing a rapid exchange process. As seen for compound **XIV**, this exchange process can be 'frozen' at low temperature with the $^{31}P\{^{1}H\}$ NMR spectrum at -40°C showing two species in solution with peaks centred at δ 11.9 [$J(AgP)_{average}$ = 344 Hz] and δ 11.8 [$J(AgP)_{average}$ = 505 Hz] with intensities in a ratio of 1 : 10 respectively. The coupling constant of these two species are similar to those observed for the two species present in the low temperature $^{31}P\{^{1}H\}$ NMR spectrum of **XIV** (333 and 519 Hz). They are therefore correspondingly assigned as the sp-hybridised $[Ag(PPh_3)_2][CB_{11}H_6Br_6]$ (δ 11.8) ion pair and the sp^3 hybridised $[Ag(PPh_3)_2(CB_{11}H_6Br_6)]$ (δ 11.7) (Figure 4.19) species that was observed in the solid state structure of **XV**. Unfortunately, the $^{31}P\{^{1}H\}$ CPMAS spectrum of **XV** is too broad to obtain any quantitative data because of overlapping resonances.

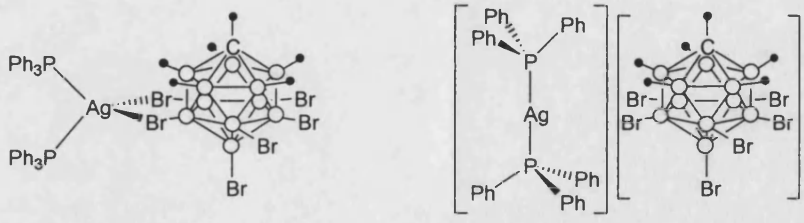

Hybridisation	sp^3		sp
$J(AgP)_{average}$	344 Hz		505 Hz
Molar ratio	1	:	10

Figure 4.19: Suggested solution configurations for **XV**

4.2.3 Evaluation of the Performance of X, XII, XIV, XV in Catalysis

Silver(I) salts, such as $Ag(BF_4)$, $Ag(ClO_4)$, $Ag(BF_4)$ and Ag(OTf), are receiving increased attention as promoters in organic transformations. They are employed as catalysts in reactions such as cycloadditions and Diels-Alder reactions, which take advantage of silver's affinity for C-C unsaturated bonds and halogen groups rather than oxygen functional groups.[41] Of particular note are silver(I) BINAP [(1,1'-binaphthalene)-2,2'-diylbis(diphenylphosphane)] compounds that have been used as asymmetric catalysts in Mukaiyama aldol reactions,[42] and hetero-Diels-Alder reactions.[43] These reactions are also accelerated by other Lewis acids (eg. Ti, B, Al, and Sn complexes), but they are typically sensitive to water, air and product inhibition, which forces high catalyst loadings to be employed. Complexes **X**, **XII**, **XIV** and **XV** show reasonable stability in air, and it was hoped that the weakly coordinating anions they contain would reveal increased activity for these compounds over more traditional counterions. Hence, the performance of these compounds in a hetero-Diels-Alder reaction of *N*-benzylideneanaline with Danishefsky's diene (Scheme 4.1) was assessed alongside analogous catalytic species containing more commonly used counterions, such as $[ClO_4]^-$, $[BF_4]^-$ and $[OTf]^-$. The results of this study are presented next.

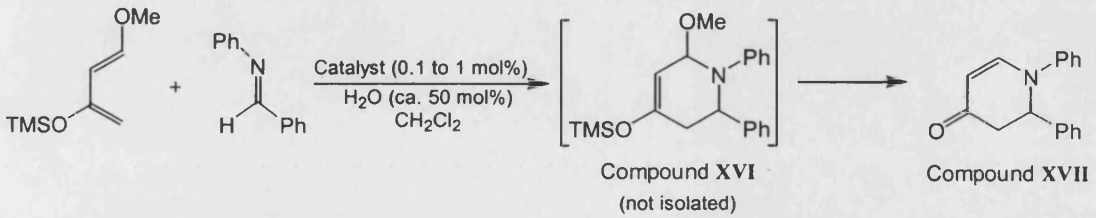

Scheme 4.1: Reaction between *N*-benzylideneaniline and Danishefsky's diene

Initial studies of the reaction were performed by Catherine Hague (Univeristy of Bath) under bench top conditions with a catalyst loading of only 1 mol%, considerably lower than the 10 mol% commonly employed for similar reactions.[44] The results (Table 4.12) showed that the catalysts efficiently converted the reactants to product (**XVII**) after 1 hour of reaction under these conditions. A counter ion effect was observed, with the activity of compounds **X** and **XII** comparable to $[Ag(PPh_3)(ClO_4)]$, but significantly more active than the $[Ag(PPh_3)(OTf)]$ and $[Ag(PPh_3)(BF_4)]$ catalysts. Importantly, a control reaction with no catalyst yielded only trace amounts (<5%) of product (**XVII**) after 24 hours of reaction.

Catalyst	Isolated Yield of XVII (%)
$[Ag(PPh_3)(BF_4)]$	35
$[Ag(PPh_3)(OTf)]$	70
$[Ag(PPh_3)(ClO_4)]$	90
$[Ag(PPh_3)(CB_{11}H_{12})]$, **X**	98
$[Ag(PPh_3)(CB_{11}H_6Br_6)]$, **XII**	99
$[Ag(PPh_3)_2(CB_{11}H_{12})]$, **XIV**	99
$[Ag(PPh_3)_2(CB_{11}H_6Br_6)]$, **XV**	85
No catalyst	<5

Table 4.12: Yields of compound **XVII** after 60 minutes reaction and workup. Catalyst (1 mol%); imine (1.1 mmol), Danishefsky's diene (1.65 mmol).

These results prompted a ^1H NMR study of the reactions in order to elucidate counterion/activity (compounds **X** and **XII**) and structure/activity (compounds **XIV** and **XV**) relationships using the silver(I) phosphine carborane compounds characterised previously in this chapter. As the reaction proceeded very quickly on the bench at 1 mol% catalyst loading (complete conversion for **X**, **XII**, and **XIV** in one hour), the catalyst loading was dropped to 0.1 mol% in the reaction monitoring experiments in the hope of better quantifying the differences between the rates of

reaction for each catalyst. Samples for study were prepared in NMR tubes by dissolving the relevant quantities of catalyst and N-benzylideneaniline in CD_2Cl_2 before charging with Danishefsky's diene and taking ^1H NMR measurements at timed intervals (see experimental section). The initial studies, using rigorously dried NMR solvents (CD_2Cl_2 distilled over CaH_2), surprisingly showed no reaction after 2 hours. It was found that addition of a substoichiometric amount of water (1μL, *ca.* 50 mol%, unoptimised) was required for the reaction to proceed.

The surprise discovery that water was needed for the reaction to proceed implies that it is needed in some way as a proton source in the reaction. This was confirmed by the following control experiments. Addition of just water and no catalyst to the imine and diene affords no product, while under the conditions used for catalysis addition of the hindered base 2,6-di-*tert*-butyl-4-methylpyridene suppressed the reaction. Overall, this suggests it is an example of a water accelerated Lewis acid catalysed reaction, examples of which are receiving increasing attention in the literature,[45] while that the rates of some Diels-Alder reactions can be significantly accelerated by addition of water has been reported previously.[46] Some recent theoretical studies have shown that the water molecules stabilise the transition state species reducing the activation energy for these reactions.[47, 48] Of particular relevance to this work is the observation of modest yield enhancements on addition of stoichiometric amounts of water to a hetero Diels-Alder reaction catalysed by lanthanide trifluoromethanesulfonylamides.[49] In the system under study here, it is likely that a polarised silver bound water molecule acts as a Lewis acid assisted Brønsted acid,[50] similar to that seen in lanthanide salt catalysed aromatic electrophilic substitutions.[51] This has been confirmed by DFT calculations performed by Dr Gus Ruggerio

(University of Bath), the results of which are displayed in Figure 4.20. The Lewis assisted Brønsted acid $\{Ag(PPh_3)(OH_2)\}^+$ catalyses the reaction by interacting with the lone pair of the imine, reducing the electron density of the C=N π-bond (Figure 4.21). This activates the imine toward reaction with the diene by lowering the energy of the lowest unoccupied molecular orbital (LUMO) on the imine, which enhances the mixing with the highest occupied molecular orbital (HOMO) of the diene, thus accelerating the rate of reaction.[47] The difference between the catalysed and uncatalysed transition state energy of 12 $kJmol^{-1}$ is thought to be significant in this instance.

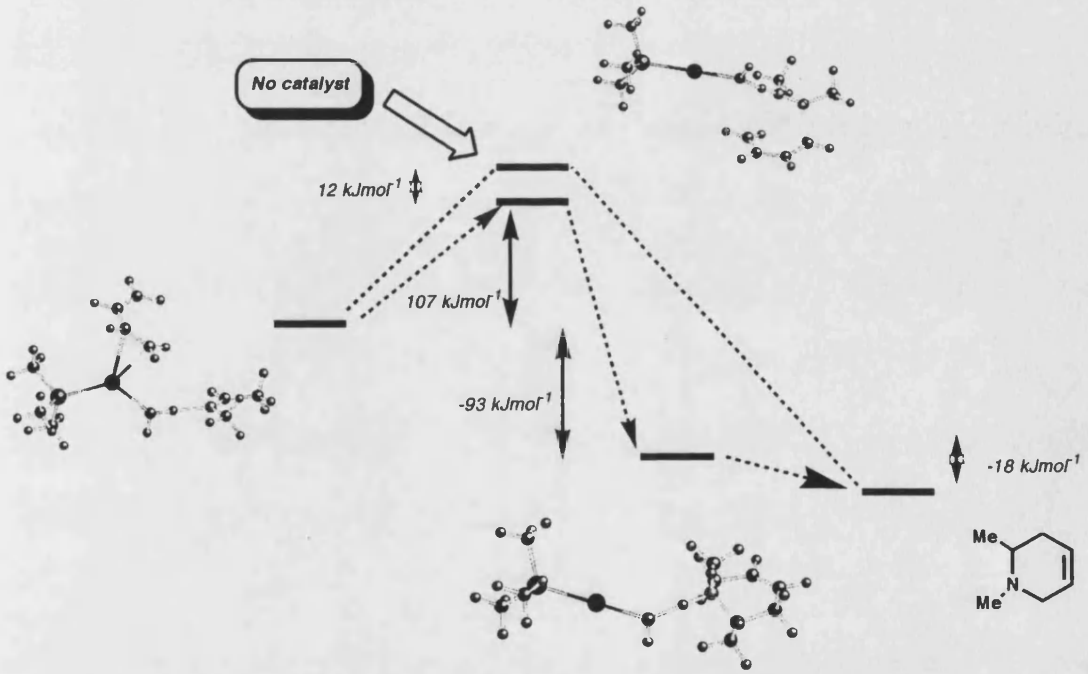

Figure 4.20: DFT calculations performed by Dr. Gus Ruggerio at the B3LYP/DZVP level

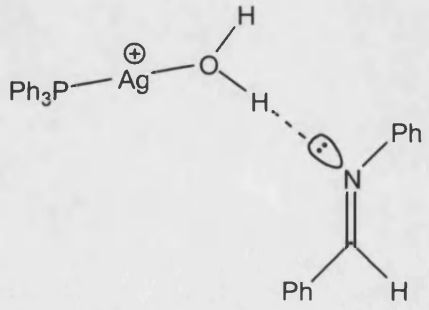

Figure 4.21: Lewis acid assisted Brønsted acid activation of *N*-benzylideneanaline

Silver monophosphine species containing $[BF_4]^-$, $[OTf]^-$ and $[ClO_4]^-$ were included in the study along with compounds **X, XII, XIV, XV** for comparison. All of the reactions monitored by ^1H NMR spectroscopy were carried out at 0.1 mol% catalyst loading with 50 mol% added water in CD_2Cl_2 solutions. The diene was added in a 1.5 molar excess to the imine as the water present in the reaction hydrolyses it in a competing reaction, although no evidence for hydrolysis of the imine to benzaldehyde was observed under the conditions used. The final products in the NMR tube were consistently intermediate (**XVI**, Scheme 1) and product (**XVII**) in an approximate ratio of 90:10 respectively. Workup of the NMR sample gives only product **XVII**, and the intermediate **XVI** was not isolated. Selected peaks due to imine, intermediate and final product were used to monitor the reaction.

The results of the ^1H NMR experiments are displayed in Figure 4.22 as the rate of product formation for catalysts **X, XI, XIV** and **XV** and related species against time. Other similar catalytic species were included in this study for counterion comparisons, the results of which are also included in Figure 4.22. The consumption of imine for each run followed the same time dependent profile (although inversed). Previous attempts at the hetero Diels-Alder synthesis of **XVII** include the use of $Yb(OTf)_3$ catalyst (10 mol% catalyst loading, 20 hours, 93% yield)[52] and the solid acid catalyst Nafion-H (10 hours, 72% yield).[53] Hence the results indicate that the majority of silver phosphine species tested are extremely efficient catalysts for this reaction, especially given the exceedingly low catalyst concentration used.

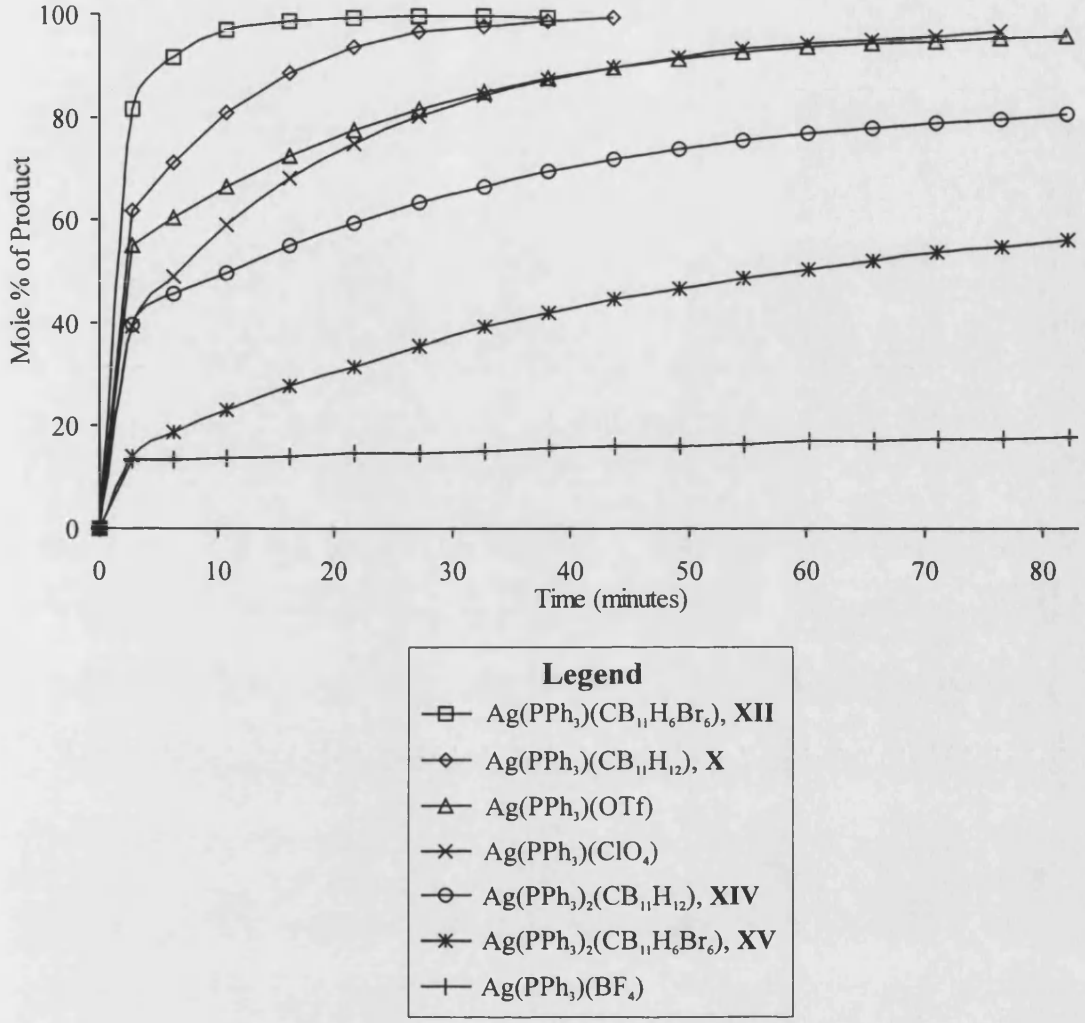

Figure 4.22: Relative rates of reaction between N-benzylideneaniline and Danishefsky's diene using 0.1 mol% loading of catalysts and 50 mol% H_2O.

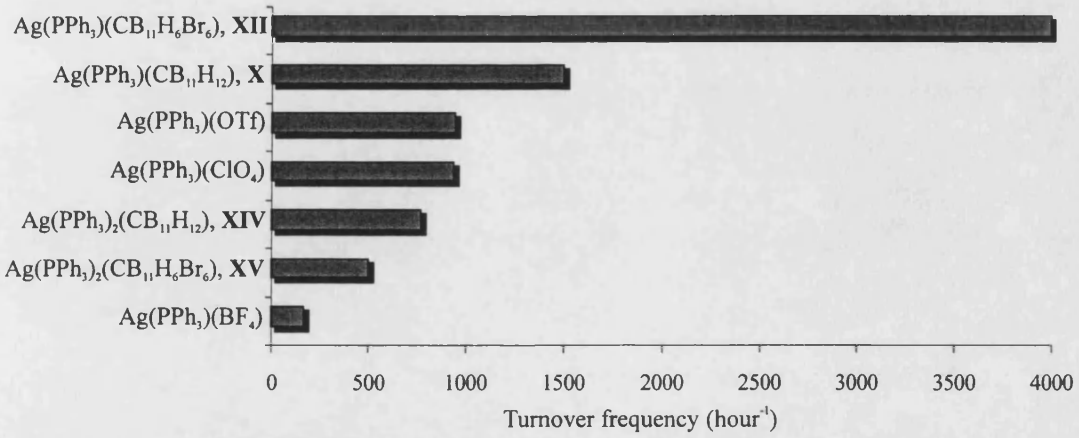

Figure 4.23: Turnover frequencies of catalysts in the reaction between N-benzylideneaniline and Danishefsky's diene

The results from monitoring the reaction by ^{1}H NMR spectroscopy can be converted to give turnover frequencies (TOF) for each catalyst (Figure 4.23). It is clear from these results that a counterion effect for the silver monophosphine $[Ag(PPh_3)(X)]$ (X = weakly coordinating anion) catalysts exists. It was encouraging to note compound **XII** gives by far the largest TOF (4000 $hour^{-1}$) followed by compound **X** (TOF = 1500 $hour^{-1}$). Catalysts $[Ag(PPh_3)(OTf)]$ and $[Ag(PPh_3)(ClO_4)]$ have similar turnover frequencies, but $[Ag(PPh_3)(BF_4)]$ has surprisingly low reactivity. Close inspection of the reaction profile for $[Ag(PPh_3)(BF_4)]$ shows it is initially active, but ceases to function after the first few minutes of reaction suggesting 'poisoning' of the catalytic species. This could be due to hydrolysis of the $[BF_4]^-$ anion under reaction conditions (0.1 mol% catalyst, 50 mol% H_2O), which has been observed previously for a number of its compounds.[54-56] Another possibility is decomposition of the catalyst in a manner similar to that previously seen for $[(P\text{-}P)Ag(BF_4)]$[39] (P-P = bis-chelating phosphine) which yields $[(P\text{-}P)Ag(\mu\text{-}F)Ag(P\text{-}P)][BF_4]$.[57] Unfortunately, the extremely low catalyst concentrations used preclude characterisation of the catalysts after they have been used in the reaction.

The higher Ag-P coupling constant of **X** (743 Hz) compared to **XII** (715 Hz) in the solution $^{31}P\{^{1}H\}$ NMR spectra of these compounds indicates that **X** is a more Lewis acidic species. It is therefore surprising to note that the most catalytically active of these two compounds is complex **XII**. One possible explanation for this observation could be that the more bulky $[closo\text{-}CB_{11}H_6Br_6]^-$ anion is less capable than $[closo\text{-}CB_{11}H_{12}]^-$ at interacting with the cationic silver atom in the reactant complex (Figure 4.21) and competing with the diene for silver coordination.

The reduced catalytic activity of the bis-phosphine compounds compared to their monophosphine analogues is perhaps expected, given the reduced Lewis activity of the silver and the increased steric bulk hindering the binding of the substrate. What is unexpected however, is the reversal of the counterion effect seen in the monophosphine catalysts where the [*closo*-$CB_{11}H_6Br_6$]$^-$ catalyst (**XII**) is more efficient than its [*closo*-$CB_{11}H_{12}$]$^-$ (**X**) analogue. That compound **XIV** [(*closo*-$CB_{11}H_{12}$)$^-$] is in fact a better catalyst than **XV** [(*closo*-$CB_{11}H_6Br_6$)$^-$] suggests that the silver is more available for substrate binding in **XIV** compared to **XV**, although there is currently insufficient data to be able to explain this observation.

Polymer supported catalysts are being increasingly studied in synthetic organic chemistry as they are easy to separate from the reaction products and are recyclable making the catalysts cleaner and more efficient.[58] However, the incorporation of catalyst onto the polymers is often a multistep synthesis. Given that polymer supported triphenylphosphine is one of the most commonly used resins, it was of interest to see if the silver phosphine catalysts used for homogenous catalysis would be effective in heterogenous catalysis. The polymer bound analogues of **X**, **XII** and [Ag(OTf)(PPh_3)] were readily prepared by stirring a suspension of a commercially available triphenylphosphine resin and [Ag(X)] [X = ($CB_{11}H_{12}$)$^-$, ($CB_{11}H_6Br_6$)$^-$ and (OTf)$^-$] in CH_2Cl_2. All three resins were tested under bench top conditions for their efficiency in the hetero-Diels-Alder reaction between *N*-benzylideneanaline and Danishefsky's diene. The reactions were run for 1 hour, with a catalyst loading of *ca.* 10 mol%, and 10 mol% of added water. All three catalysts were shown to give repeatable high yields (> 95%) over at least three runs using the same polymer bound catalyst (Figure 4.24). Moreover, low leaching levels (0.3% Ag, by AAS) were

determined and the supernatant from freshly prepared and filtered supported catalyst afforded only trace product when used in the reaction (< 5%) showing the catalysis was truly heterogenous.

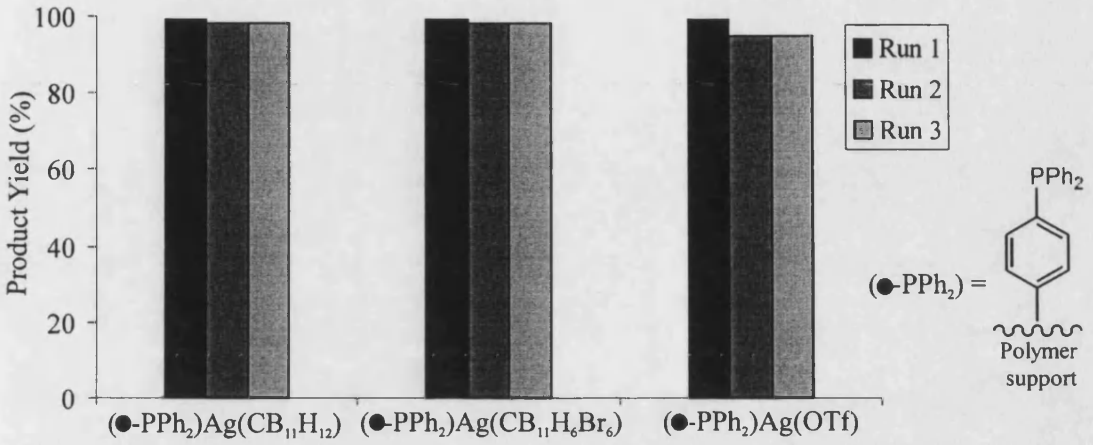

Figure 4.24: Isolated product yields for polymer supported catalysts

In agreement with the observations made in the ^{1}H NMR spectroscopy monitored reactions, the supported catalysts display a significant dependance on the presence of water. If no water is added then the polymer supported catalyst performance drops off rapidly on the second and third runs. However, the relatively high catalyst concentrations used in these experiments prevent the observation of any counter ion effects.

4.2.4 Summary for Silver(I) Phosphine Compounds

Silver monophosphine carboranes of general formula $[Ag(PPh_3)_x(Y)]$ [x = 1 or 2; Y = (*closo*-$CB_{11}H_{12}$)$^-$, (*closo*-$CB_{11}H_{11}Br$)$^-$, (*closo*-$CB_{11}H_6Br_6$)$^-$, (*closo*-$CB_{11}H_6Cl_6$)$^-$] have been synthesised and characterised both in the solid state and in solution. The crystal structures of these compounds display a number of interesting intermolecular interactions, resulting in dimerisation or formation of coordination polymers. $^{31}P\{^1H\}$ NMR spectroscopy has been used to probe solution configurations, which for the silver mono-phosphines (**X, XI, XII, XIII**) are thought to be broadly similar to the solid state. At low temperature, the silver bis-phosphine compounds (**XIV, XV**) show a number of species in solution, tentatively assigned as sp- and sp^3-hybridisation isomers.

Two ranking schemes for the coordinating ability of the carborane anions were developed using metrical data from X-ray structure determinations, and Ag-P coupling constants in solution. One of these schemes used the $\{Ag(PPh_3)\}^+$ cation, that is likely to have minimal anion - cation steric interactions, and the other a more sterically demanding bis-phosphine silver cation, $\{Ag(PPh_3)_2\}^+$. Interestingly, the relative coordinating abilities of the carborane anions are thought to be [*closo*-$CB_{11}H_{12}]^-$ < [*closo*-$CB_{11}H_6Br_6]^-$ in the mono-phosphine silver species (**X, XII**), but are reversed in the bis-phosphine silver species (**XIV, XV**) with [*closo*-$CB_{11}H_6Br_6]^-$ < [*closo*-$CB_{11}H_{12}]^-$. This is proposed to be due to greater steric interactions of [*closo*-$CB_{11}H_6Br_6]^-$ with two phosphines as opposed to one.

The silver(I) phosphine carborane species showed very high activity as Lewis acid catalysts in a hetero Diels-Alder reaction. It was pleasing to observe the catalysts containing carborane anions gave the best activities under benchtop conditions. The monitoring of the reaction by ^{1}H NMR spectroscopy allowed differences in the rates of reaction between different catalysts to be observed. The study shows the activity of Lewis acidic $\{Ag(PPh_3)\}^+$ fragment when partnered with the following counterions increases in the order $[BF_4]^-$ < $[ClO_4]^-$ ≈ $[OTf]^-$ < $[closo\text{-}CB_{11}H_{12}]^-$ < $[closo\text{-}CB_{11}H_6Br_6]^-$. This reactivity ranking apparently contradicts the suggested relative coordinating abilities of $[closo\text{-}CB_{11}H_{12}]^-$ and $[closo\text{-}CB_{11}H_6Br_6]^-$ in **X** and **XII**. What this suggests is that a ranking scale of anion coordinating ability based on thermodynamic parameters (e.g. bond lengths, coupling constants and chemical shifts) is not completely satisfactory when considering their kinetic behaviour (e.g. catalysis and transition states). In support of this, the compound $[Ag(PPh_3)(OTf)]$ has a Ag-P average coupling constant of 803 Hz ($CDCl_3$), larger than any observed for compounds **X-XIII** and suggesting it contains the most Lewis acidic silver fragment, but it is a significantly poorer catalyst than **X** or **XII** (Figures 4.22 and 4.23). Hence, the relative ranking of $[closo\text{-}CB_{11}H_{12}]^-$ and $[closo\text{-}CB_{11}H_6Br_6]^-$ using Ag-P coupling constants or bond lengths (thermodynamic) can be different to that suggested by their catalytic activity (kinetic) and a ranking scheme derived from spectroscopic data cannot necessarily be treated as the definitive reactivity scale.

4.2.5 Synthesis and Characterisation of $[Ag_2(CB_{11}H_{12})_4][Ag(IMes)_2]_2$

Having synthesised a range of silver phosphine carborane compounds it was of interest to see if this chemistry could be developed further to incorporate other neutral 2-electron donor ligands such as *N*-heterocyclic carbenes. Perhaps the most famous example of *N*-heterocyclic carbene substitution comes from the replacement of one of the phosphine ligands on Grubb's catalyst $[Ru(=CHPh)(PCy_3)_2Cl_2]$ to give $[Ru(=CHPh)(PCy_3)(IMes)Cl_2]$ (IMes = 1,3-dimesitylimidazol-2-ylidene) which has both increased thermal stability and greater reactivity than the bis-phosphine analogue.[59] Described next is the attempted synthesis of $[Ag(IMes)(CB_{11}H_{12})]$ (the carbene analogue of compound **X),** which was unsuccessful but resulted in the exclusive formation of an unanticipated, but nonetheless interesting, compound.

The treatment of $[Ag(CB_{11}H_{12}]$ with one equivalent of IMes (1,3-dimesitylimidazol-2-ylidene) dissolved in toluene results in the formation of a colourless solution, that upon cooling affords colourless crystals. These crystals were characterised by elemental analysis, NMR spectroscopy and X-ray crystallography and shown to be $[Ag(IMes)_2]_2[Ag_2(CB_{11}H_{12})_4]$, compound **XVIII** (Figure 4.25).

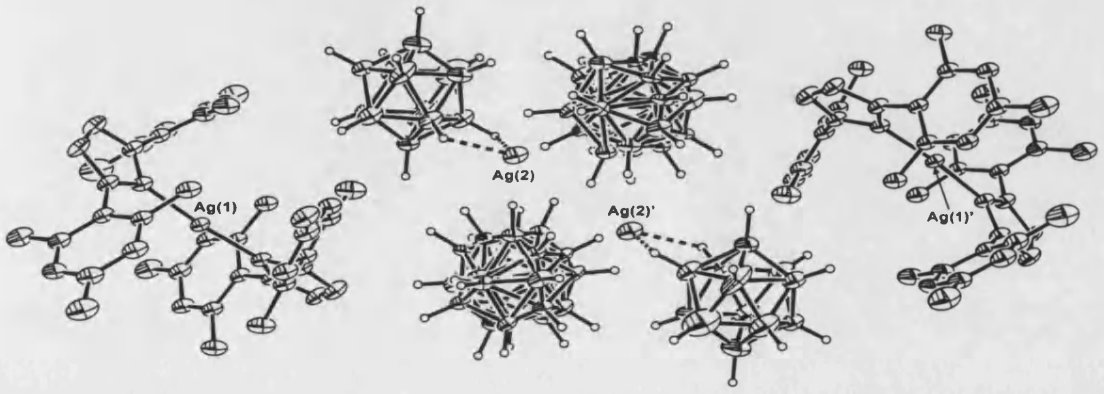

Figure 4.25: Crystal stucture of compound **XVIII** with all the disorder components included. One half of the molecule is symmetry generated from the other.

The asymmetric unit of **XVIII** consists of a cationic $[Ag(IMes)_2]^+$ fragment and an anionic $[Ag(CB_{11}H_{12})_2]^-$ fragment. The cationic $\{Ag(IMes)_2\}^+$ fragment is displayed in more detail in Figure 4.26, with relevant bond lengths and angles in Table 4.13. The silver-carbon bond lengths are crystallographically identical [Ag(1)-C(1A), 2.070(5) Å; Ag(1)-C(22), 2.069(6)Å] and equivalent in length to those seen in the related compound $[Ag(IMes)_2][CF_3SO_3]$[60] [Ag-C = 2.067(4)Å and 2.078(4) Å] which contains a compositionally identical cationic portion. The C(1A)-Ag(1)-C(22) bond angle of 174.3(2)° shows the carbene ligands are essentially bonded linear to one another around the silver atom, a feature mirrored in $[Ag(IMes)_2][CF_3SO_3]$ [C-Ag-C = 176.3(2)°]. The only major difference between the cationic portions of compound **XVIII** and $[Ag(IMes)_2][CF_3SO_3]$ is the orientation of the two imidazole rings, which are twisted from coplanarity by 59.1° and 39.7° respectively (Figure 4.27). This difference is a reflection of the different packing forces imposed by the different cations within the crystal lattice.

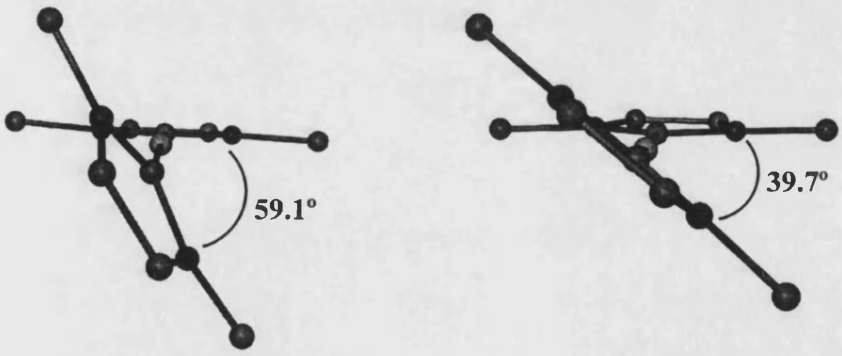

Compound **XVIII** $[Ag(IMes)_2][CF_3SO_3]$

Figure 4.27: Diagram highlighting the difference in orientation of imidazole rings for **XVIII** and $[Ag(IMes)_2][CF_3SO_3]$ in the solid state (only *ipso* carbons of mesityl groups shown for clarity)

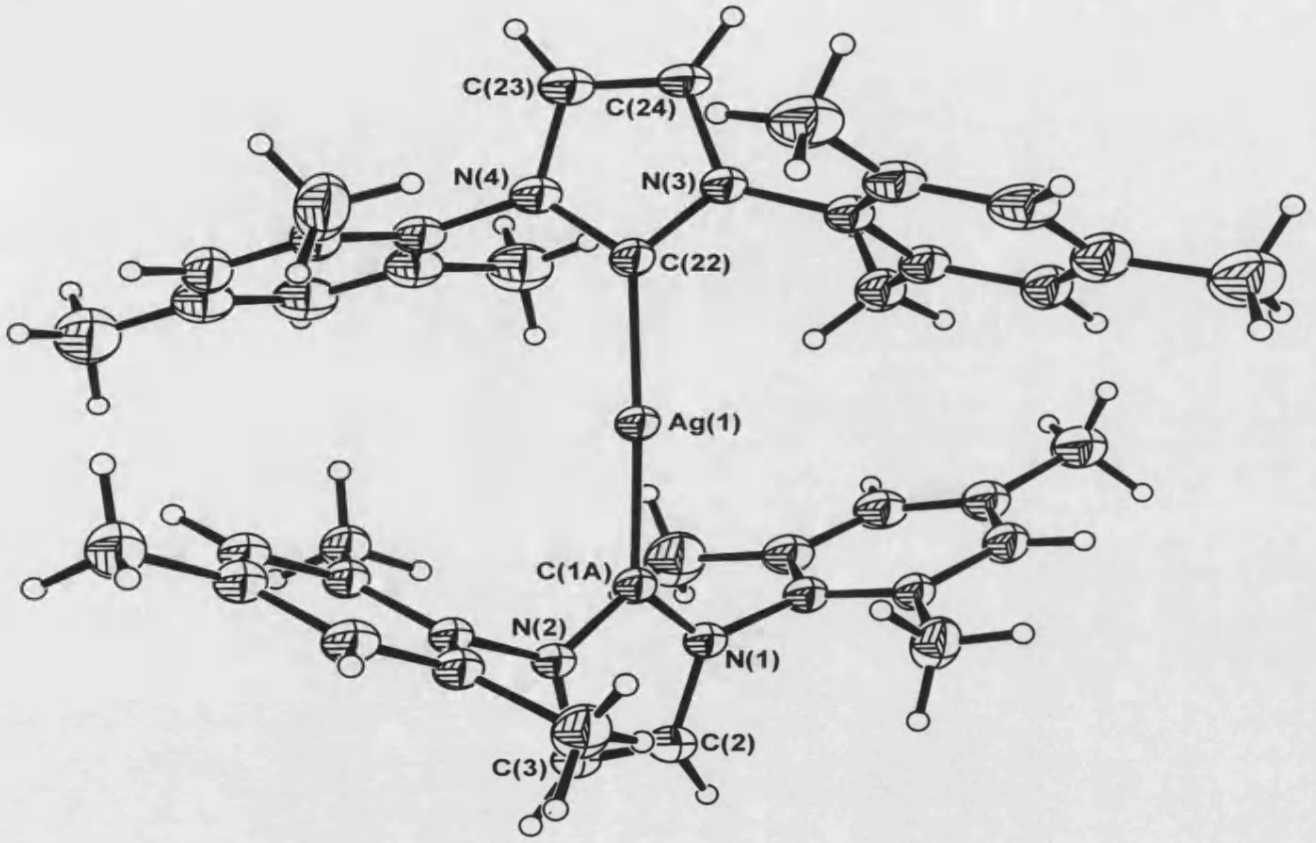

Figure 4.26: Cationic component of the asymmetric unit in Compound **XVIII** (ellipsoids drawn at 30% probability level)

Ag(1)-C(1A)	2.070(5) Å
Ag(1)-C(22)	2.069(6) Å
C(1A)-N(1)	1.366(7) Å
C(1A)-N(2)	1.355(7) Å
C(22)-N(3)	1.358(7) Å
C(22)-N(4)	1.365(7) Å
C(1A)-Ag(1)-C(22)	174.3(2)°
N(1)-C(1A)-N(2)	103.5(5)°
N(3)-C(22)-N(4)	104.1(5)°

Table 4.13: Selected bond lengths and angles for cationic portion of **XVIII**

The anionic fragment of compound **XVIII** contains another silver atom, but now interacting with two carboranes, one of which is disordered evenly (50 : 50) over two sites between positions B(21) to B(32) and B(41) to B(52). Inspection of the packing diagram reveals this anion is lying close to a centre of inversion within the crystal lattice, which symmetry generates another half to the anionic fragment and one more $[Ag(IMes)_2]^+$ fragment (Figure 4.25). Thus the anionic component of **XVIII** consists of two disordered carborane molecules bridging two silver atoms that are appended by two terminal carboranes having an empirical formula $\{Ag_2(CB_{11}H_{12})_4\}^{2-}$, displayed in Figure 4.28 with pertinent bond lengths in Table 4.14. The disorder of the bridging carborane precluded the assignment of the carbon atom within the bridging carborane cage, hence all atoms therein were refined as boron atoms. The coordination geometry around each silver atom is best described as distorted trigonal prismatic (Figure 4.29), with each disordered component within the lattice containing four longer and two shorter B-H interactions to silver.

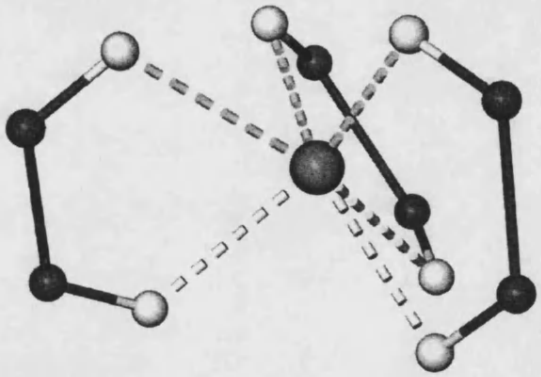

Figure 4.29: Diagram showing the coordination environment around one of the silver atoms in one disordered component of $\{Ag_2(CB_{11}H_{12})_4\}^{2-}$.

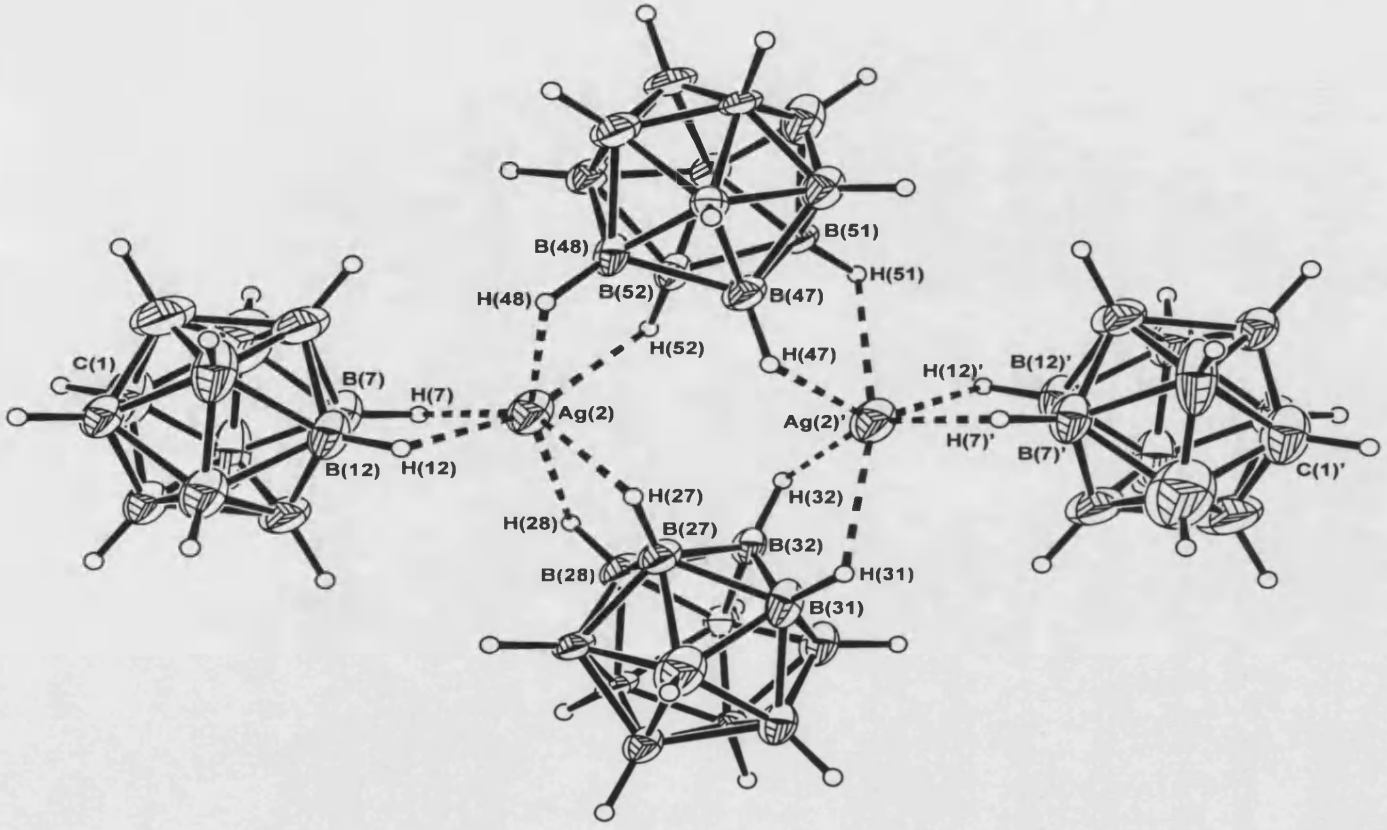

Figure 4.28: Anionic portion of compound **XVIII** showing one of the disordered components (ellipsoids drawn at 30% probability level)

Ag(2)-H(7)	2.05 Å
Ag(2)-B(7)	2.586(8) Å
Ag(2)-H(12)	2.23 Å
Ag(2)-B(12)	2.673(8) Å
Ag(2)-H(27)	2.09 Å
Ag(2)-B(27)	2.73(2) Å
Ag(2)-H(28)	2.45 Å
Ag(2)-B(28)	2.92(2) Å
Ag(2)-H(48)	2.35 Å
Ag(2)-B(48)	2.84(2) Å
Ag(2)-H(52)	2.19 Å
Ag(2)-B(52)	2.79(2) Å
Ag(2)'-H(31)	2.52 Å
Ag(2)'-B(31)	2.94(2) Å
Ag(2)'-H(32)	1.96 Å
Ag(2)'-B(32)	2.67(2) Å
Ag(2)'-H(47)	2.05 Å
Ag(2)'-B(47)	2.70(2) Å
Ag(2)'-H(51)	2.40 Å
Ag(2)'-B(51)	2.88(2) Å

Table 4.14: Selected bond lengths and angles for the anionic portion of **XVIII**

The shorter {B-H}···Ag interactions vary in distance from 1.96 to 2.23 Å (Ag-H) and 2.59 to 2.79 Å (Ag-B). The longer interactions are in the range 2.35 to 2.52 Å (Ag-H) and 2.84 to 2.94 Å (Ag-B). These Ag-B distances are shorter than those found in $[Ag(CB_{11}H_{12})].2(C_6H_6)$ [2.681(5) Å and 2.581(6) Å]. They can also be compared to those found in compounds **X** [2.504(3) to 2.619(3) Å] and **XIV** [2.892(2) to 3.494(2) Å], where strong Ag-B interactions are suggested in the former but not the latter compound. Overall, this suggests that the carborane cages are interacting significantly with the silver atoms in **XVIII**, a conclusion supported by the solution NMR spectra discussed next.

The ^{1}H and ^{13}C NMR spectra display all the correct resonances associated with the carbene ligands. However, NMR spectroscopy cannot be used to draw conclusions as to whether or not the $\{Ag_2(CB_{11}H_{12})_4\}^{2-}$ fragment observed in the solid state remains wholly intact in solution. The ^{11}B NMR spectrum, a valuable tool in elucidation of the solution structure of carborane species, does offer some clues to the extent of cage interaction with silver. The $^{11}B\{^{1}H\}$ NMR spectrum of compound **XVIII** consists of just one [*closo*-$CB_{11}H_{12}]^-$ species in solution, with two peaks observed at δ -12.4 [1B, B(12)] and δ -15.7 [5B + 5B coincidence, B(7-11) and B(2-6)] that indicates C_{5v} symmetry of carborane anions that are undergoing a fast exchange process. The resonances associated with B(12) and B(7-11) in **XVIII** are shifted significantly upfield when compared to the ^{11}B NMR spectrum of $[NBu_4][CB_{11}H_{12}]$ in CD_2Cl_2 which displays peaks at δ -8.0 [1B, B(12)], δ -14.1 [5B, B(7-11)] and δ -16.9 [5B, B(2-6)]. The chemical shifts for $[NBu_4][CB_{11}H_{12}]$ are similar to those observed in the ^{11}B NMR spectrum of $[Ag(CB_{11}H_{12})]$ recorded in d_6-acetone, a solvent in which any ion pairs are expected to be well separated (*ie.* no metal-cage interactions present).

Conversely, if the $^{11}B\{^{1}H\}$ NMR spectrum of $[Ag(CB_{11}H_{12})]$ is measured using CD_2Cl_2 (a solvent in which it is not very soluble so not often used), just two resonances are observed at δ - 11.9 [1B, B(12)] and δ -15.0 [5B + 5B coincidence, B(7-11) and B(2-6)] similar to that seen for **XVIII**, and also shifted downfield from the corresponding spectrum recorded in acetone, indicating the silver atom is interacting with the cage in this solvent. The changes in chemical shifts with compound and solvent are summarised in Figure 4.30.

The similarity between the ^{11}B NMR spectrum of $[Ag(CB_{11}H_{12})]$ measured in CD_2Cl_2 and the ^{11}B NMR spectrum of **XVIII** implies that the strong {B-H}···Ag interactions observed in the solid state structure of **XVIII** persist in solution around the antipodal and lower pentagonal belt borons of the cage. These observations have been confirmed by ab initio calculations on model complexes for **XVIII**, $[Ag(CB_{11}H_{12})]$ and $[closo\text{-}CB_{11}H_{12}]^-$.

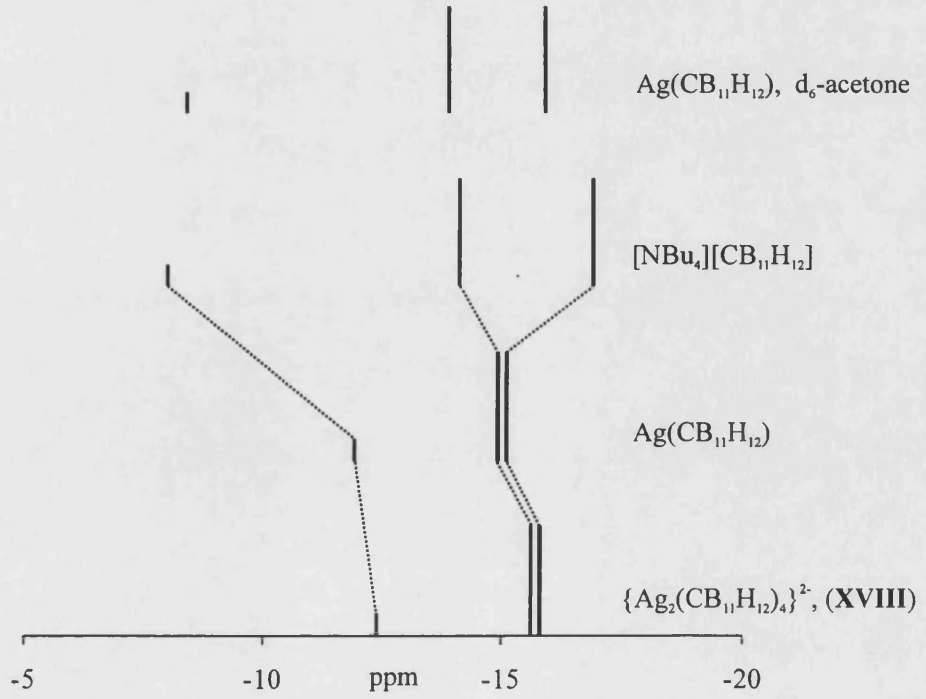

Figure 4.30: Diagrammatic representation of ^{11}B NMR spectra of selected carborane complexes. All measured in CD_2Cl_2 unless otherwise stated.

The solution structures and related ^{11}B NMR chemical shifts of compounds **A**, **B** and **C** (Figure 4.31, Table 4.15) were calculated using "ab initio/GIAO/NMR" methods by Dr. Mark Fox (University of Durham). The results of this study have been recently published[61] and will only be summarised briefly here. $[Na]^+$ was used as a model for silver, as using $[Ag]^+$ was computationally not possible at the level of theory used (MP2/6-31G*)

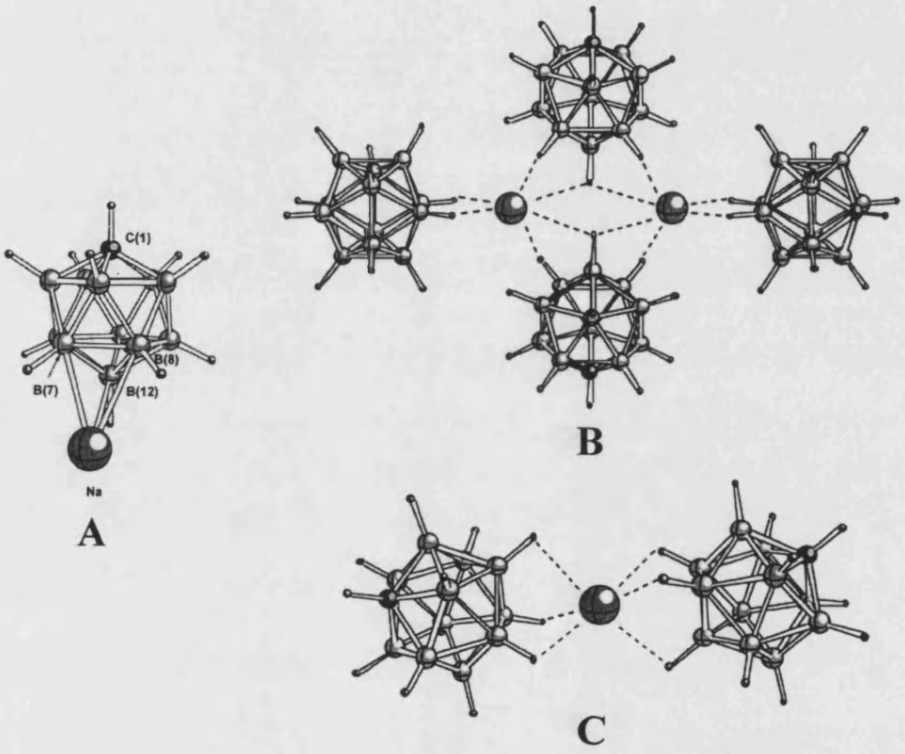

Figure 4.31: Calculated structures for $[Na(CB_{11}H_{12})]$ (**A**) (MP2/6-31G*), $\{Na_2(CB_{11}H_{12})_4\}^{2-}$ (**B**) (HF/6-31G*) and $\{Na(CB_{11}H_{12})_2\}^-$ (**C**) (MP2/6-31G*)

	Experimental[a]			Calculated[b]			
	$[NBu_4]^+$	Ag^+	**XVIII**	none	**A**	**B**[c]	**C**
B(12)	-8.0	-11.9	-12.4	-6.9	-12.5	-10.1	-10.8
B(7-11)	-14.1	-15.0	-15.7	-13.8	-15.3	-14.4	-14.9
B(2-6)	-16.9	-15.0	-15.7	-17.8	-15.4	-16.7	-16.3

[a] Measured in CD_2Cl_2. [b] Averaged values at the GIAO-B3LYP/6-311G*//MP26-31G* level. [c] Averaged values at the GIAO-B3LYP/6-311G*//HF/6-31G* level.

Table 4.15: Comparison of experimental and theoretical ^{11}B NMR shifts (δ) for various salts of $[closo\text{-}CB_{11}H_{12}]^-$

The changes in the calculated boron chemical shifts on going from optimised geometries of $[Na(CB_{11}H_{12})]$ to "free" $[closo\text{-}CB_{11}H_{12}]^-$ mirror those observed experimentally in solution for $[Ag(CB_{11}H_{12})]$ on going from a non-coordinating solvent (e.g. CD_2Cl_2) to a coordinating solvent (e.g. acetone). Structures **A**, **B** and **C** all show upfield shifts of the B(12) resonances and compression of the B(7-11) and B(2-6) signals compared to free $[closo\text{-}CB_{11}H_{12}]^-$ matching well that observed in solution for **XVIII**, and confirming the Ag···{HB} interactions in solution. However, as all the structures show the same upfield shifts, the degree of aggregation for $\{Ag(CB_{11}H_{12})_2\}^-$ in solution for **XVIII** (ie. structure **B** *versus* structure **C**) remains ambiguous. This supports the assignment made earlier of the large downfield shift in the $^{11}B\{^1H\}$ NMR spectrum of **X** being due to the strong Ag···{HB} interactions observed in its solid state structure persisting in solution.

4.3 References

1 D. J. Liston, Y. J. Lee, W. R. Scheidt, C. A. Reed, *J. Am. Chem. Soc.* **1989**, *111*, 6643.

2 K. Shelly, C. A. Reed, Y. J. Lee, W. R. Scheidt, *J. Am. Chem. Soc.* **1986**, *108*, 3117.

3 K. Shelly, D. C. Finster, Y. J. Lee, W. R. Scheidt, C. A. Reed, *J. Am. Chem. Soc.* **1985**, *107*, 5955.

4 T. Jelinek, P. Baldwin, W. R. Scheidt, C. A. Reed, *Inorg. Chem.* **1993**, *32*, 1982.

5 Z. Xie, B.-M. Wu, T. C. W. Mak, J. Manning, C. A. Reed, *J. Chem. Soc., Dalton Trans.* **1997**, 1213.

6 S. V. Ivanov, A. J. Lupinetti, S. M. Miller, O. P. Anderson, K. A. Solntsev, S. H. Strauss, *Inorg. Chem.* **1995**, *34*, 6419.

7 Z. Xie, C.-W. Tsang, F. Xue, T. C. W. Mak, *J. Organomet. Chem.* **1999**, *577*, 197.

8 Z. Xie, C.-W. Tsang, E. T.-P. Sze, Q. Yang, D. T. W. Chan, T. C. W. Mak, *Inorg. Chem.* **1998**, *37*, 6444.

9 C.-W. Tsang, Q. Yang, E. T.-P. Sze, T. C. W. Mak, D. T. W. Chan, Z. Xie, *Inorg. Chem.* **2000**, *39*, 5851.
10 E. L. Muetterties, C. W. Alegranti, *J. Am. Chem. Soc.* **1972**, *94*, 6386.
11 R. G. Goel, P. Pilon, *Inorg. Chem.* **1978**, *10*, 2876.
12 D. J. Crowther, S. L. Borkowsky, D. Swenson, T. Y. Meyer, R. F. Jordan, *Organomet.* **1993**, *12*, 2897.
13 D. D. Ellis, A. Franken, P. A. Jelliss, J. A. Kautz, F. G. A. Stone, P.-Y. Yu, *J. Chem. Soc., Dalton Trans.* **2000**, 2509.
14 D. D. Ellis, P. A. Jelliss, F. G. A. Stone, *Organomet.* **1999**, *18*, 4982.
15 D. D. Ellis, J. C. Jeffery, P. A. Jelliss, J. A. Kautz, F. G. A. Stone, *Inorg. Chem.* **2001**, *40*, 2041.
16 A. S. Batsanov, S. P. Crabtree, J. A. K. Howard, C. W. Lehmann, M. Kilner, *J. Organomet. Chem.* **1998**, *550*, 59.
17 M. Mascal, J.-L. Kerdelhue, A. J. Blake, P. A. Cooke, *Angew. Chem. Int. Ed.* **1999**, *38*, 1968.
18 R. A. Stein, C. B. Knobler, *Inorg. Chem.* **1977**, *16*, 242.
19 R. E. Bachman, D. F. Andretta, *Inorg. Chem.* **1998**, *37*, 5657.
20 H. Brunner, D. Mijolovic, B. Wrackmeyer, B. Nuber, *J. Organomet. Chem.* **1999**, *579*, 298.
21 G. A. Bowmaker, Effendy, P. J. Harvey, P. C. Healy, B. W. Skelton, A. H. White, *J. Chem. Soc., Dalton Trans.* **1996**, 2459.
22 L.-J. Baker, G. A. Bowmaker, D. Camp, Effendy, P. C. Healy, H. Schmidbaur, O. Steigelmann, A. H. White, *Inorg. Chem.* **1992**, *31*, 3656.
23 Z. Xie, R. Bau, C. A. Reed, *Angew. Chem. Int. Ed.* **1994**, *33*, 2433.
24 C.-W. Tsang, Q. Yang, E. T.-P. Sze, T. C. W. Mak, D. T. W. Chan, Z. Xie, *Inorg. Chem.* **2000**, *39*, 3582.
25 A. Bondi, *J. Phys. Chem.* **1964**, *68*, 441.
26 N. J. Patmore, A. S. Weller, J. W. Steed, *Chem. Commun.* **2000**, 1055.
27 N. J. Patmore, M. F. Mahon, J. W. Steed, A. S. Weller, *J. Chem. Soc., Dalton Trans.* **2001**, 277.
28 A. Cassel, *Acta Cryst.* **1981**, *B37*, 229.
29 G. A. Bowmaker, J. V. Hanna, C. E. F. Rickard, A. S. Lipton, *J. Chem. Soc., Dalton Trans.* **2001**, 20.
30 G. A. Ardizzoia, G. La Monica, A. Maspero, M. Moret, N. Masciocchi, *Inorg. Chem.* **1997**, *36*, 2321.
31 K. Nomiya, K. Tsuda, N. C. Kasuga, *J. Chem. Soc., Dalton Trans.* **1998**, 1653.
32 K. Nomiya, K. Tsuda, Y. Tanabe, H. Nagano, *J. Inorg. Biochem.* **1998**, *69*, 9.
33 A. Cingolani, Effendy, F. Marchetti, C. Pettinari, B. W. Skelton, A. H. White, *J. Chem. Soc., Dalton Trans.* **1999**, 4047.
34 L. Jager, C. Tretner, H. Hartung, M. Biedermann, *Eur. J. Inorg. Chem.* **1998**, 1051.
35 C. W. Liu, H. Pan, J. P. Fackler, jun., G. Wu, R. E. Wasylishen, M. Shang, *J. Chem. Soc., Dalton Trans.* **1995**, 3691.
36 E. C. Alyea, S. A. Dias, S. Stevens, *Inorg. Chimica Acta Letts.* **1980**, *44*, 203.
37 M. Camalli, F. Caruso, *Inorg. Chimica Acta* **1988**, *144*, 205.
38 D. R. Evans, C. A. Reed, *J. Am. Chem. Soc.* **2000**, *122*, 4660.
39 M. Barrow, H.-B. Burgi, M. Camalli, F. Caruso, E. Fischer, L. M. Venanzi, L. Zambonelli, *Inorg. Chem.* **1983**, *22*, 2356.
40 G. A. Bowmaker, Effendy, J. V. Hanna, P. C. Healy, B. W. Skelton, A. H. White, *J. Chem. Soc., Dalton Trans.* **1993**, 1387.

41 A. Yanagisawa in Lewis Acids in Organic Synthesis (Ed. : H. Yamamoto), Wiley-VCH, Weinheim, 2000
42 M. Ohkouchi, D. Masui, M. Yamaguchi, T. Yamagishi, *J. Mol. Catal. A* **2001**, *170*, 1.
43 S. Yao, S. Saaby, R. G. Hazell, K. A. Jorgensen, *Chem. Eur. J.* **2000**, *6*, 2435.
44 P. Buonora, J.-C. Olsen, T. Oh, *Tetrahedron* **2001**, *57*, 6099.
45 S. Ribe, P. Wipf, *Chem. Commun.* **2001**, 299.
46 R. Breslow, Z. N. Zhu, *J. Am. Chem. Soc.* **1995**, *117*, 9923.
47 J. Chandrasekhar, S. Shariffskul, W. L. Jorgensen, *J. Phys. Chem. B* **2002**, *106*, 8078.
48 L. R. Domingo, J. Andres, C. N. Alves, *Eur. J. Org. Chem* **2002**, 2257.
49 K. Mikami, O. Kotera, Y. Motoyama, H. Sakaguchi, *Synlett* **1995**, 975.
50 K. Ishihara, S. Ishida, S. Nakamura, H. Yamamoto, *Synlett* **1997**, 758.
51 A. G. M. Barrett, D. C. Braddock, J. P. Henschke, E. R. Walker, *J. Chem. Soc., Perkin Trans.* **1999**, 873.
52 S. Kobayashi, H. Ishitani, S. Nagayama, *Synthesis* **1995**, 1195.
53 R. Kumareswaran, B. G. Reddy, Y. D. Vankar, *Tet. Lett.* **2001**, *42*, 7493.
54 C. J. d. Reijer, M. Worle, P. S. Pregosin, *Organomet.* **2000**, *19*, 309.
55 L. R. Sutton, A. J. Blake, P. A. Cooke, M. Schroder, *Chem. Commun.* **2000**, 563.
56 N. G. Connelly, W. E. Geiger, *Chem. Rev.* **1996**, *96*, 877.
57 M. Camalli, F. Caruso, L. Zambonelli, *Inorg. Chimica Acta* **1982**, *61*, 195.
58 B. Clapham, T. S. Reger, K. D. Janda, *Tetrahedron* **2000**, *57*, 4637.
59 J. Louie, R. H. Grubbs, *Organomet.* **2002**, *21*, 2153.
60 A. J. Arduengo III, H. V. R. Dias, J. C. Calabrese, F. Davidson, *Organomet.* **1993**, *12*, 3405.
61 M. A. Fox, M. F. Mahon, N. J. Patmore, A. S. Weller, *Inorg. Chem.* **2002**, *41*, 4567.

5 EXPERIMENTAL

5.1 Experimental technique

5.1.1 General

All manipulations were performed under an inert atmosphere of argon, using standard Schlenk-line and glove box techniques. Glassware was dried in an oven at 130°C overnight and flamed with a blowtorch, under vacuum, three times before use. CH_2Cl_2, CH_3CN and pentane were distilled from CaH_2. Toluene, diethyl ether and hexane were distilled from sodium-benzophenone-ketyl. C_6D_6 and d_8-toluene were dried over a potassium mirror; CD_2Cl_2 was distilled under vacuum from CaH_2. Microanalyses were performed by Mr. Alan Carver (University of Bath Microanalytical Service).

5.1.2 NMR spectroscopy

^1H, $^1H\{^{11}B\}$, ^{11}B, $^{11}B\{^1H\}$, $^{13}C\{^1H\}$ and $^{31}P\{^1H\}$ NMR spectra were recorded on a Varian 400 MHz, Bruker Avance 300 MHz or Jeol 270MHz FT-NMR spectrometers. Residual protio solvent was used as reference for ^1H and $^1H\{^{11}B\}$ NMR spectra (CD_2Cl_2: $\delta = 5.33$, C_7D_8: $\delta = 2.10$, C_3D_6O: $\delta = 2.09$) and $^{13}C\{^1H\}$ NMR spectra (CD_2Cl_2: $\delta = 53.8$). ^{11}B, $^{11}B\{^1H\}$ and $^{31}P\{^1H\}$ NMR spectra were referenced against $BF_3.OEt_2$ (external) and 85% H_3PO_4 (external) respectively. ^{109}Ag NMR (19MHz) spectra were recorded by the Warwick University NMR Service. ^{31}P CPMAS spectra

were recorded by the EPSRC solid-state NMR service in Durham. Values are quoted in ppm. Coupling constants are quoted in Hz.

5.1.3 Infrared spectroscopy

Infrared spectra were recorded on a Nicolet NEXUS FT-IR spectrometer. Solid-state samples were made up using oven dried pottasium bromide. Solution spectra were recorded using a 0.1mm solution cell.

5.2 Syntheses and characterisation

5.2.1 Starting materials

The starting materials $Cs[CB_{11}H_{12}]$,[1] $Ag[CB_{11}H_{12}]$,[1] $[H(OEt_2)_x][CB_{11}H_{12}]$,[2] $Ag[CB_{11}H_{11}Br]$,[3] $Ag[CB_{11}H_6Br_6]$,[4] $Ag[CB_{11}H_6Cl_6]$,[5] $MoCp(CO)_3Cl$,[6] $MoCp(CO)_3I$,[6] $MoCp^*(CO)_3Cl$,[7] $MoCp^*(CO)_3Me$,[8] $CPh_3[CB_{11}H_6Br_6]$,[9] $MoCp(CO)_3H$,[10] and 1,3-dimesitylimidazol-2-ylidene (IMes) [11] were all prepared by published literature methods or variations thereof. All other chemicals were used as purchased from Aldrich, Acros or Fluka.

5.2.2 Synthesis

[$MoCp(CO)_3(x\text{-}\mu\text{-}H\text{-}CB_{11}H_{11})$] (x = 7, 12) (I):

From $MoCp(CO)_3Cl$: The compounds $MoCp(CO)_3Cl$ (0.134 g, 0.48 mmol) and $Ag[CB_{11}H_{12}]$ (0.120 g, 0.48 mmol) were dissolved in CH_2Cl_2 (30ml) and stirred in a foil covered Schlenk for 2 days. The suspension formed was filtered through Celite and solvent removed *in vacuo* to leave 0.158g (0.41mmol, 85% yield) of a red-brown solid. A ^1H NMR of the crude reaction mixture showed quantitative conversion to product. Crystals suitable for an X-ray diffraction study were grown by re-dissolving the solid in minimum volume of CH_2Cl_2, layering with hexane and then placing in the freezer overnight at -30°C to yield 0.082g (0.21mmol) of $MoCp(CO)_3(x\text{-}\mu\text{-}H\text{-}CB_{11}H_{11})$ (x = 7, 12) as dark red crystals.

Yield: 44%.

$\delta^1H\{^{11}B\}$ (22°C, CD_2Cl_2): 5.86 (s)*, 5.79 (5H, s, C_5H_5), 2.53 (1H, s, CH_{cage}), 1.79 (5H, s, B*H*), 1.66 (5H, s, B*H*), -15.11 (1H, s, B*H*) (Values with an asterisk next to them indicate peaks of the 7 isomer in 30% abundance).

Selected δ^1H (22°C, CD_2Cl_2): -15.11 [pcq, *J*(BH) 87Hz, B*H*Mo]

Selected $\delta^1H\{^{11}B\}$ (-90°C, CD_2Cl_2): -15.46 (s)*, -15.55 (s, B*H*Mo)

$\delta^{11}B$ (22°C, CD_2Cl_2): -8.0 [1B, d, *J*(BH) *ca.* 151Hz]*, -13.7 (1B, d, sh.), -15.0 [5B, d, *J*(BH) 151Hz], -17.2 [5B, d, *J*(BH) 151Hz], -21.9 [1B, d, *J*(BH) 68Hz]*.

IR/cm^{-1} (KBr): 2582 (m, BH), 2549 (m, BH), 2243 (br., w, BH), 2067 (s, CO), 1991 (s, CO), 1980 (s, CO).

IR/cm^{-1} (CH_2Cl_2): 2573 (m, BH), 2230 (br., w, BH), 2071 (s, CO), 2001 (br., s, CO).

Elemental Analysis: Calc. for $C_9H_{17}B_{11}MoO_3$: %C, 27.9; %H, 4.38. Found: %C, 28.0; %H, 4.39.

From $MoCp(CO)_3I$: The compounds $MoCp(CO)_3I$ (0.029 g, 0.080 mmol) and $Ag[CB_{11}H_{12}]$ (0.021 g,0.84 mmol) were dissolved in CH_2Cl_2 (20ml) and stirred in a foil covered Schlenk for 7 days. Work up identical to the previous procedure yielded 0.025 g (0.064mmol, 81% yield) of a red-brown solid. The IR and NMR spectra of product are identical to those obtained *via* the previous method of preparation.

$[MoCp(CO)_3I{\cdot}Ag(CB_{11}H_{12})]_2$ (II):

The compounds $MoCp(CO)_3I$ (0.044 g, 0.12mmol) and $Ag[CB_{11}H_{12}]$ (0.030g, 0.12 mmol) were stirred in CH_2Cl_2 (10ml) in a foil covered Schlenk for 3.5 hours. The resulting solution was filtered through Celite and solvent removed *in vacuo*, to yield 0.037g (0.095mmol) of $[MoCp(CO)_3I{\cdot}Ag(CB_{11}H_{12})]_2$ as a light sensitive red solid. Red crystals suitable for an X-ray diffraction study were grown by re-dissolving the solid in minimum CH_2Cl_2, layering with hexane, and placing in the freezer overnight at -30°C.

Yield: 79%

$\delta^1H\{^{11}B\}$ (22°C, CD_2Cl_2): 5.75 (5H, s, C_5H_5), 2.56 (1H, s, CH_{cage}), 2.12 (1H, s, B*H*), 1.86 (5H + 5H coincidence, s, B*H*).

$\delta^{11}B$ (22°C, CD_2Cl_2): -12.4 [1B, d, *J*(BH) 119Hz], -16.0 [5B + 5B coincidence, d, *J*(BH) 144Hz].

$\delta^{109}Ag$ (22°C, CD_2Cl_2): 1335 (s).

IR/cm^{-1} (KBr): 2556 (m, BH), 2531 (m, BH), 2041 (s, CO), 1971 (s, CO), 1950 (s, CO).

IR/cm^{-1} (CH_2Cl_2): 2570 (m, BH), 2054 (s, CO), 1973 (br. s, CO).

Elemental Analysis: Calc. for $C_9H_{17}O_3B_{11}MoIAg$: %C, 17.4; %H, 2.7. Found: %C, 17.8; %H, 2.8.

$[MoCp(CO)_3I{\cdot}Ag(CB_{11}H_{11}Br)]_2$ (III):

$MoCp(CO)_3I$ (51mg, 0.14mmol) and $Ag[CB_{11}H_{11}Br]$ (46mg, 0.14mmol) were stirred in CH_2Cl_2 (10ml) for one hour. This solution was cannula filtered and solvent removed *in vacuo* to yield 61mg (0.073mmol) of $[MoCp(CO)_3I{\cdot}Ag(CB_{11}H_{11}Br)]_2$ as a red solid. Red crystals suitable for an X-ray diffraction study were grown by re-dissolving the solid in minimum CH_2Cl_2, layering with hexane, and placing in the freezer overnight at -30°C.

Yield: 53%

$\delta^1H\{^{11}B\}$ (22°C, CD_2Cl_2): 5.77 (5H, s, C_5H_5), 2.45 (1H, s, CH_{cage}), 2.07 (5H, s, B*H*), 1.78 (5H, s, B*H*).

$\delta^{11}B$ (22°C, CD_2Cl_2): -3.4 (1B, s), -13.1 [5B, d, *J*(BH) 139Hz], -16.3 [5B, d, *J*(BH) 157Hz].

IR/cm^{-1} (CH_2Cl_2): 2574 (m, BH), 2053 (s, CO), 1972 (br. s, CO).

Elemental Analysis: Calc. for $C_9H_{16}O_3B_{11}BrIAgMo$: %C, 15.4; %H, 2.28. Found: %C, 14.9; %H, 2.36.

$[MoCp(CO)_3I{\cdot}Ag(CB_{11}H_6Br_6)]_2$ (IV):

$Ag[CB_{11}H_6Br_6]$ (0.060 g, 0.083mmol) and $MoCp(CO)_3I$ (0.028 g, 0.075mmol) were stirred in CH_2Cl_2 (10ml) in a foil covered Schlenk for 5 hours. The red solution formed was filtered through Celite and the solvent removed from the filtrate *in vacuo* to leave a red solid. Crystals suitable for an X-ray diffraction study were grown by

redissolving the solid product in minimum of CH_2Cl_2 and allowing slow evaporation of solvent under a flow of argon to yield 0.041g (0.021mmol) of dark red crystals.

Yield: 56%

δ^1H (22°C, CD_2Cl_2): 5.84 (s, peak from isomer, see section 2.2.4), 5.73 (5H, s, C_5H_5), 2.79 (1H, s, CH_{cage}).

δ^{11}B (22°C, CD_2Cl_2): -4.0 (1B, s), -12.2 (5B, s), -21.2 [5B, d, *J*(BH) 152Hz].

δ^{109}Ag (22°C, CD_2Cl_2): 1335 (intensity of 8, s), 1325 (intensity of 1, s)

IR/cm^{-1} (CH_2Cl_2): 2613 (m, BH), 2055 (s, CO), 1975 (br. s, CO).

Elemental Analysis: Calc. for $C_9H_{11}O_3B_{11}Br_6IAgMo$: %C, 9.86; %H, 1.00. Found: %C, 9.18; %H, 1.11.

[MoCp*(CO)$_3$(x-μ-H-$CB_{11}H_{11}$)] (x = 7, 12) (V):

MoCp*(CO)$_3$Me (0.014 g, 0.042mmol) was dissolved in CH_2Cl_2 (20ml), cooled to -78°C, and added to a Schlenk vessel containing $[H(OEt_2)_x][CB_{11}H_{12}]$ [12mg, 0.041mmol (assuming x = 2)] at -78°C. This solution was stirred and warmed to room temperature. An IR spectrum indicated the reaction had only reached 30% completion so a second portion of $[H(OEt_2)_x][CB_{11}H_{12}]$ [10mg, 0.039mmol (assuming x = 2)] was added. The IR spectrum after a further 5 minutes indicated all of the MoCp*(CO)$_3$Me starting material had been consumed. The solvent was removed *in vacuo* and the ^{1}H NMR spectrum of the red solid formed indicated no starting material or excess $[H(OEt_2)_x][CB_{11}H_{12}]$ present. $^{11}B\{^1H\}$ NMR spectrum of the contents of the Schlenk line cold-trap showed the presence of [*closo*-$CB_{11}H_{12}]^-$. The product was re-dissolved in the minimum of CH_2Cl_2, layered with hexane and stored in a freezer at -30°C to afford orange-red crystals of MoCp*(CO)$_3$(x-μ-H-$CB_{11}H_{11}$) (x = 7, 12) suitable for a X-ray diffraction study.

δ^1H (22°C, CD_2Cl_2): 2.51 (1H, br. s, C*H*$_{cage}$), 2.08 (s)*, 2.04 (15H, s, C*H*$_3$), -13.5 [1H, partially collapsed quartet, *J*(BH) = 98Hz, B*H*] (Values with an asterisk next to them indicate peaks of the 7 isomer in 40% abundance).

δ^{11}B (22°C, CD_2Cl_2): -8.5 (1B, d, *J*(BH) 128)*, -13.9 (1B, d, sh.), -15.2 [5B, d, *J*(BH) 150Hz], -17.2 [5B, d, *J*(BH) 167], -22.1 [1B, d, *J*(BH) *ca.* 65Hz]*.

IR/cm^{-1} (CH_2Cl_2): 2571 (m, BH), 2229 (br., w, MoHB), 2057 (s, CO), 1986 (br., s, CO).

$CPh_3[CB_{11}H_{11}Br]$ (VI):

$Ag[CB_{11}H_{11}Br]$ (0.337g, 1.0mmol) and CPh_3Br (0.337g, 1.0mmol) were stirred in a 1:3 toluene/CH_3CN (5:15ml) mixture for one hour, then cannula filtered. The supernatant was removed *in vacuo* and the resulting oil stirred in hexane (2 x 20ml) overnight. Hexane was removed by decantation, and the yellow/orange solid formed was dried *in vacuo* to yield 0.410g (0.88mmol) of $CPh_3[CB_{11}H_{11}Br]$.

Yield: 86%

$\delta^1H\{^{11}B\}$ (22°C, C_3D_6O): 7.32 – 7.17 (15H, m, CH_{phenyl}), 2.26 (1H, s, CH_{cage}), 1.90 (5H, s, BH), 1.64 (5H, s, BH).

δ^{11}B (22°C, C_3D_6O): -3.0 (1B, s), -15.7 [5B, d, *J*(BH) 142], -17.3 [5B, d, *J*(BH) 153].

$[MoCp(CO)_3(CB_{11}H_{11}Br)]$ (VII):

$MoCp(CO)_3H$ (30mg, 0.12mmol) was dissolved in CH_2Cl_2 (5ml) and added dropwise to a Schlenk charged with $CPh_3[CB_{11}H_{11}Br]$ (57mg, 0.12mmol). The solution was stirred for one hour, cannula filtered, and the supernatant removed *in vacuo* to leave a red solid. This was redissolved in the minimum CH_2Cl_2, layered with hexanes and

then placed in a freezer at -30°C to yield 0.031g (0.066mmol) of $MoCp(CO)_3(CB_{11}H_{11}Br)$ as dark red crystals.

Yield: 54%

$\delta^1H\{^{11}B\}$ (22°C, CD_2Cl_2): 5.92 (5H, s, C_5H_5), 2.43 (1H, br. s, CH_{cage}), 1.86 (5H, br. s, B*H*), 1.76 (5H, br. s, B*H*), .

$\delta^{11}B$ (22°C, CD_2Cl_2): -1.6 (1B, s), -13.9 [5B, d, *J*(BH) 144Hz], -16.9 [5B, d, *J*(BH) 158Hz].

IR/cm^{-1} (CH_2Cl_2): 2577 (m, BH), 2071 (s, CO), 1999 (br., s, CO).

IR/cm^{-1} (KBr): 2560 (m, BH), 2069 (s, CO), 1982 (s, CO).

Elemental Analysis: Calc. for $C_9H_{16}B_{11}O_3Mo_1Br_1$: %C, 23.2; %H, 3.43. Found: %C, 22.9; %H, 3.49.

$[MoCp(CO)_3(CB_{11}H_6Br_6)]$:

In a typical reaction: A Young's NMR tube was charged with $MoCp(CO)_3H$ (32mg, 0.13mmol) and $[CPh_3][CB_{11}H_6Br_6]$ (112mg, 0.13mmol) and CD_2Cl_2 added at -78°C. Reaction allowed to warm slowly to room temperature and NMR measurements taken immediately. Product is poorly soluble in CD_2Cl_2 and forms pink solid. Attempts to grow crystals of products via CD_2Cl_2 / hexane layers were unsuccessful. High reactivity and instability of products thwarted attempts to cleanly isolate them.

δ^1H (22°C, CD_2Cl_2): 7.31-7.11 [m, Ph_3CH], 6.07 [s, $\{MoCp(CO)_3(CH_2Cl_2)\}\{CB_{11}H_6Br_6\}$], 6.02 [s, $MoCp(CO)_3(CB_{11}H_6Br_6)$], 5.81 [s, $(\{MoCp(CO)_3\}_2\{\mu\text{-}H\})(CB_{11}H_6Br_6)$], 5.55 [s, Ph_3CH], 2.81 [br. s, CH_{cage}], 2.74 [br. s, CH_{cage}], -21.09 [s, $(\{MoCp(CO)_3\}_2\{\mu\text{-}H\})(CB_{11}H_6Br_6)$].

Selected δ^1H (-65°C, CD_2Cl_2): 6.05 [s, $\{MoCp(CO)_3(CH_2Cl_2)\}\{CB_{11}H_6Br_6\}$], 6.02 [s, $MoCp(CO)_3(CB_{11}H_6Br_6)$], 5.99 [s, $MoCp(CO)_3(CB_{11}H_6Br_6)$], 5.78 [s,

($\{MoCp(CO)_3\}_2\{\mu\text{-}H\}$)($CB_{11}H_6Br_6$)], 2.90 [br. s, C$H_{cage}$], 2.82 [br. s, C$H_{cage}$], 2.76 [br. s, C$H_{cage}$], -21.61 [s, ($\{MoCp(CO)_3\}_2\{\mu\text{-}H\}$)($CB_{11}H_6Br_6$)].

$\delta^{11}B$ (22°C, CD_2Cl_2): -2.0 (1B, s), -10.2 (5B, s), -20.5 [5B, d, *J*(BH) 164Hz].

IR/cm^{-1} (CH_2Cl_2): 2608 (m, BH), 2073 (s, CO), 1990 (br., s, CO).

[Ag(PPh_3)($CB_{11}H_{12}$)] (X):

PPh_3 (0.163 g, 0.650mmol) was dissolved in CH_2Cl_2 (10ml) and added dropwise to a Schlenk flask charged with Ag[$CB_{11}H_{12}$] (0.155 g, 0.591mmol). This solution was stirred in a foil covered Schlenk overnight and then cannula filtered. The solvent was removed *in vacuo* to leave a pale yellow solid. Colourless crystals suitable for an X-ray diffraction study were grown by redissolving the product up in minimum CH_2Cl_2, layering with hexane, then placing the sample in a freezer overnight at –30°C to yield 0.281 g (0.549mmol) of product.

Yield: 92%.

$\delta^1H\{^{11}B\}$ (22°C, CD_2Cl_2): 7.52-7.29 (15H, m, C_6H_5), 2.55 (1H, br. s, CH_{cage}), 2.25 (1H, br. s, B*H*), 1.85 (10H, 5H + 5H coincidence, B*H*).

Selected $\delta^1H\{^{11}B\}$ (-90°C, CD_2Cl_2): 2.59 (1H, br. s, CH_{cage}), 2.34 (1H, br. s, B*H*), 1.94 (5H, br. s, B*H*), 1.76 (5H, br. s, B*H*).

$\delta^{11}B\{^1H\}$ (22°C, CD_2Cl_2): -13.6 (1B, s, sh.), -14.5 (5B, s), -15.3 (5B, s).

$\delta^{11}B$ (22°C, CD_2Cl_2): -14.5 [5B + 1B coincidence, d, *J*(BH) 118Hz], -15.3 [5B, d, *J*(BH) 110Hz]

$\delta^{31}P\{^1H\}$ (22°C, CD_2Cl_2): 18.70 [dd, *J*(^{109}AgP) 795Hz, *J*(^{107}AgP) 691Hz]

IR/cm^{-1} (KBr): 2565 (vs, BH), 2517 (sh s, BH), 2372 (m, BH).

Elemental Analysis: Calc. for $C_{19}H_{27}B_{11}AgP$: %C, 44.5; %H, 5.30. Found: %C, 44.3; %H, 5.19.

[Ag(PPh$_3$)(CB$_{11}$H$_{11}$Br)] (XI):

PPh$_3$ (0.061 g, 0.232mmol) was dissolved in CH_2Cl_2 (10ml) and added dropwise to a foil covered Schlenk flask charged with Ag[CB$_{11}$H$_{11}$Br] (0.100 g, 0.303mmol), with stirring. This solution was stirred overnight and then cannula filtered. The solvent was removed *in vacuo* to leave a clear oil. Colourless crystals suitable for an X-ray diffraction study were grown by redissolving the product up in minimum CH_2Cl_2, layering with hexane, then placing the sample in a freezer overnight at –30°C to yield 0.102 g (0.172mmol) of product.

Yield: 74%

$\delta^1H\{^{11}B\}$ (22°C, CD_2Cl_2): 7.65-7.31 (15H, m, C_6H_5), 2.48 (1H, br. s, CH_{cage}), 2.19 (5H, br. s, B*H*), 1.81 (5H, br. s, B*H*).

$\delta^{11}B$ (22°C, CD_2Cl_2): -3.3 (1B, s), -13.2 [5B, d, *J*(BH) 141Hz], -16.2 [5B, d, *J*(BH) 159Hz].

$\delta^{31}P\{^1H\}$ (22°C, CD_2Cl_2): 16.85 [1P, dd, *J*(^{109}AgP) 661Hz, *J*(^{107}AgP) 581Hz]

Elemental Analysis: Calc. for $C_{19}H_{26}B_{11}AgPBr$: %C, 38.5; %H, 4.39. Found: %C, 37.8; %H, 4.39.

[Ag(PPh$_3$)(CB$_{11}$H$_6$Br$_6$)] (XII):

PPh$_3$ (0.062 g, 0.236mmol) was dissolved in CH_2Cl_2 (10ml) and added dropwise to a foil covered Schlenk charged with Ag[CB$_{11}$H$_6$Br$_6$] (0.200 g, 0.276mmol). The resulting solution was stirred overnight and filtered. The supernatant was removed *in vacuo* to leave a clear oil. Colourless crystals suitable for an X-ray diffraction study were grown by redissolving the product up in minimum CH_2Cl_2, layering with hexanes, then placing the sample in a freezer overnight at –30°C to yield 0.194 g (0.197mmol) of product [Ag(PPh$_3$)(CB$_{11}$H$_6$Br$_6$)].

Yield: 83%

$\delta^1H\{^{11}B\}$ (22°C, CD_2Cl_2): 7.52-7.22 (15H, m, C_6H_5), 2.73 (1H, br. s, CH_{cage}), 2.43 (5H, s, B*H*).

$\delta^{11}B$ (22°C, CD_2Cl_2): -5.4 (1B, s), -9.9 (5B, s), -20.2 [5B, d, *J*(BH) 157Hz].

$\delta^{31}P\{^1H\}$ (22°C, CD_2Cl_2): 16.52 [dd, $J(^{109}AgP)$ 766Hz, $J(^{107}AgP)$ 664Hz].

IR/cm^{-1} (KBr): 2608 (vs, BH), 2593 (s, BH).

Elemental Analysis: Calc. for $C_{19}H_{21}B_{11}AgPBr_6$: %C, 23.1; %H, 2.12. Found: %C, 22.6; %H, 2.17.

$[Ag(PPh_3)(CB_{11}H_6Cl_6)]$ (XIII):

PPh_3 (0.052 g, 0.198mmol) was dissolved in CH_2Cl_2 (10ml) and added dropwise to a foil covered Schlenk flask charged with $Ag[CB_{11}H_6Cl_6]$ (0.110 g, 0.240mmol), with stirring. This solution was stirred overnight and then cannula filtered. The solvent was removed *in vacuo* to leave a white solid. Colourless crystals suitable for an X-ray diffraction study were grown by redissolving the solid up in minimum CH_2Cl_2, layering with hexane, then placing the sample in a freezer overnight at –30°C to yield 0.093 g (0.129mmol) of $Ag(PPh_3)(CB_{11}H_6Cl_6)$.

Yield: 65%

$\delta^1H\{^{11}B\}$ (22°C, CD_2Cl_2): 7.64-7.34 (15H, m, C_6H_5), 2.38 (1H, br. s, CH_{cage}), 2.15 (5H, br. s, B*H*).

$\delta^{11}B$ (22°C, CD_2Cl_2): 0.1 (1B, s), -6.6 (5B, s), -23.2 [5B, d, *J*(BH) 160Hz].

$\delta^{31}P\{^1H\}$ (22°C, CD_2Cl_2): 16.80 [1P, dd, $J(^{109}AgP)$ 822Hz, $J(^{107}AgP)$ 718Hz].

Elemental Analysis: Calc. for $C_{19}H_{21}B_{11}AgPCl_6$: %C, 31.7; %H, 2.92. Found: %C, 31.2; %H, 2.99.

$[Ag(PPh_3)_2(CB_{11}H_{12})]$ (XIV):

$Ag[CB_{11}H_{12}]$ (0.075 g, 0.299mmol) and PPh_3 (0.158 g, 0.602mmol) were stirred together in CH_2Cl_2 (10ml) in a foil covered Schlenk for one hour. This solution was filtered and hexanes (20ml) added to the filtrate to induce precipitation of a colourless solid. This was isolated by decanting off the solvents and drying *in vacuo* to yield 0.204 g (0.263mmol) of $Ag(PPh_3)_2(CB_{11}H_{12})$. Redissolving a portion of the solid product in a minimum of CH_2Cl_2, layering with hexanes, and then placing in a freezer overnight at –30°C yielded crystals suitable for an X-ray diffraction study.

Yield: 88%

$\delta^1H\{^{11}B\}$ (22°C, CD_2Cl_2): 7.45-7.18 (30H, m, C_6H_5), 2.21 (1H, br. s, CH_{cage}), 1.85 (1H, br. s, $BH_{antipodal}$), 1.58 (5H + 5H coincidence, br. s, B*H*).

$\delta^{11}B\{^1H\}$ (22°C, CD_2Cl_2): -8.4 (1B, s), -13.9 (5B, s), -15.9 (5B, s).

$\delta^{11}B$ (22°C, CD_2Cl_2): -8.4 [1B, d, *J*(BH) 128Hz], -13.9 [5B, d, *J*(BH) 138Hz], -15.9 [5B, d, *J*(BH) 158Hz].

$\delta^{31}P\{^1H\}$ (22°C, CD_2Cl_2): 14.8 (br. s).

$\delta^{31}P\{^1H\}$ (-60°C, CD_2Cl_2): 13.7 [br. d, *J*(AgP) 333Hz], 13.6 [dd, $J(^{109}AgP)$ 554Hz, $J(^{107}AgP)$ 483Hz].

IR/cm^{-1} (KBr): 2544 (vs, BH), 2442 (m, BH), 2396 (m, BH).

Elemental Analysis: Calc. for. $C_{37}H_{42}B_{11}AgP_2$: %C, 57.3; %H, 5.46. Found: %C 57.2, %H 5.53.

$[Ag(PPh_3)_2(CB_{11}H_6Br_6)]$ (XV):

The compounds $Ag[CB_{11}H_6Br_6]$ (0.250 g, 0.345mmol) and PPh_3 (0.181 g, 0.690mmol) were stirred together in CH_2Cl_2 (10ml) in a foil covered Schlenk for one hour. The solution formed was filtered and solvent removed *in vacuo* to leave a white

solid. This solid was redissolved in minimum volume of CH_2Cl_2, layered with hexanes, and then placed in a freezer overnight at –30°C to yield 0.246g (0.197mmol) of $Ag(PPh_3)_2(CB_{11}H_6Br_6)$ as a colourless microcrystalline powder. Crystals suitable for an X-ray diffraction study were grown by redissolving the product up in minimum CH_2Cl_2, layering with hexanes, then placing the sample in a freezer overnight at –30°C.

Yield: 57%

$\delta^1H\{^{11}B\}$ (22°C, CD_2Cl_2): 7.45-6.87 (30H, m, C_6H_5), 2.45 (1H, br. s, CH_{cage}), 2.21 (5H, br. s, B*H*).

$\delta^{11}B$ (22°C, CD_2Cl_2): -4.6 (1B, s), -10.1 (5B, s), -20.5 [5B, d, *J*(BH) 166Hz].

$\delta^{31}P\{^1H\}$ (22°C, CD_2Cl_2): 8.1 (br. s).

$\delta^{31}P\{^1H\}$ (-80°C, CD_2Cl_2): 8.06 [dd, $J(^{109}AgP)$ 256Hz, $J(^{107}AgP)$ 223Hz].

IR/cm^{-1} (KBr): 2956 (vs, BH), 2587 (s, BH).

Elemental Analysis: Calc. for $C_{37}H_{36}B_{11}AgP_2Br_6$: %C, 35.7; %H, 2.89. Found: %C, 35.5; %H, 3.01.

$[Ag_2(IMes)_2(CB_{11}H_{12})_2]$ (XVIII):

IMes (55mg, 0.18mmol) was dissolved in toluene (5ml) and added dropwise to a foil covered Schlenk charged with $Ag[CB_{11}H_{12}]$ (47mg, 0.19mmol), with stirring. The resulting solution was stirred overnight, cannula filtered, and the supernatant removed *in vacuo*. The resulting solid was redissolved in the minimum volume of toluene and placed in a –80°C freezer for 5 days. The solvent was decanted off and product dried *in vacuo* to yield 46mg (0.041mmol) of $[Ag_2(IMes)_2(CB_{11}H_{12})_2]$ as a white crystalline solid.

Yield: 46%

$\delta^1H\{^{11}B\}$ (22°C, CD_2Cl_2): 7.00 (4H, s, NC*H*), 6.85 (8H, s, *m*-C*H*), 2.35 (12H, s, *p*-CH_3), 2.32 (2H, s, CH_{cage}), 2.25 (2H, s, B*H*), 1.69 (10H, s, B*H*), 1.65 (s, 24H, *o*-CH_3), 1.57 (s, 10H, B*H*).

$\delta^{11}B$ (22°C, CD_2Cl_2): -11.9 [1B, d, *J*(BH) 125Hz], -14.1 [5B + 5B coincidence, d, *J*(BH) 145Hz].

$^{13}C\{^1H\}$ NMR (CD_2Cl_2): 183.56 [dd, NC*N*, J(^{109}AgP) 208, J(^{107}AgP) 180], 140.21 (s, C_{phenyl}), 135.62 (s, C_{phenyl}), 135.29 (s, C_{phenyl}), 129.92 (s, C_{phenyl}), 123.63 [d, ^3J(CAg) 6.04Hz, NC*C*], 55.30 (s, CH_{cage}), 21.73 (s, CH_3), 17.75 (s, CH_3).

Elemental Analysis: Calc. for $C_{44}H_{72}Ag_2N_4B_{22}$: %C, 47.6; %H, 6.48; %N, 5.04. Found: %C, 47.7; %H, 6.55; %N, 5.04.

5.2.3 Reaction Monitoring Experiments

General procedure for the monitoring of the reaction between *N*-benzylideneaniline and Danishefsky's diene:

Solutions of catalyst were typically prepared by dissolving the compound (**X**, **XII**, **XIV** or **XV**; 1mg) in CD_2Cl_2 (1ml) using an ultrasound bath to ensure complete catalyst dissolution. The relevant quantity of this catalyst solution to give a 0.1mol% catalyst concentration (i.e. 0.00011 mmol of catalyst) was added to an NMR tube previously charged with *N*-benzylideneaniline (20mg, 0.11mmol). Danishefsky's diene (32μl, 0.17 mmol) and water (1μl) were added to the NMR tube, which was then shaken vigorously before being placed in the NMR spectrometer and measurements taken at timed intervals. The disappearance of the peak at δ = 8.51 due

to PhN=C*H*Ph was monitored, along with the growth of the peaks centred at δ = 6.64 and δ = 6.54 (3H total, intermediate **XVI**) and δ = 5.27 (1H total, final product **XVII**). A plot for each catalyst of time verses consumption of imine, and time verses total concentration of **XVI** and **XVII** showed essentially the same profile. Repeat runs for all catalysts tested showed the same time-dependant profiles.

Intermediate XVI.

^{1}H NMR (22°C, CD_2Cl_2): 7.56 [1H, d, *J*(HH) 13Hz], 7.42 – 7.40 (2H, m), 7.28 – 7.23 (1H, m), 7.10 – 7.01 (3H, m), 6.64 (1H, m), 6.54 (2H, m), 5.58 [1H, d, *J*(HH) 12Hz], 4.86 [1H, q, *J*(HH) 6Hz], 4.71 [1H, d, *J*(HH) 6Hz], 3.68 (3H, s), 2.94 [2H, dd, *J*(HH) 6Hz], 0.14 (9H, s).

^{1}H NMR reaction monitoring of the hydrogenation of 3-pentanone:

$CPh_3[CB_{11}H_6Br_6]$ (93mg, 0.11mmol), $O{=}CEt_2$ (0.11ml, 1.1mmol) and $MoCp(CO)_2(L)H$ (L = CO, 26mg, 0.10mmol; L = PPh_3, 50mg, 0.10mmol) were added to a NMR tubes equipped with a J. Young valve and dissolved in 0.35ml of CD_2Cl_2. The tube was then frozen in liquid nitrogen, opened to high vacuum and then backfilled with H_2. The pressure of H_2 in the tube after warming to room temperature should be *ca.* 4 atm. (298/77 = 3.9). The pressure was maintained by periodically refilling with H_2 as needed. In order to ensure adequate diffusion of gas into the solvent, the tubes were slowly spun using a mechanical stirring motor mounted sideways. ^{1}H NMR measurements were taken at intervals over a period of 18 days. The number of catalyst turnovers was monitored by measuring the disappearance of the $O{=}CEt_2$ peak at δ = 2.47 (q, C*H*$_2$) versus the appearance of Et_2CHOH peaks at δ = 5.54 (m, C*H*) and δ = 0.97 (t, C*H*$_3$).

For catalytic studies using $MoCp(CO)_3(CB_{11}H_{12})$ and $MoCp(CO)_3(CB_{11}H_{11}Br)$ the complexes were added directly to the NMR tube, rather than being prepared from the *in situ* reaction of the relevant hydride. Otherwise they were treated in the same manner as those described above.

5.3 Structure Determinations

Crystallographic measurements for structure **IV** were recorded on a CAD4 automatic four-circle diffractometer. Crystallographic measurements for all other structures were recorded on a Nonius KappaCCD diffractometer with $Mo_{K\alpha}$ radiation (0.71073 Å). Structure solution followed by full-matrix least-squares refinement was performed by using the SHELX suite of programs throughout. Hydrogens were included in calculated positions unless otherwise stated. Crystal data and structure refinement tables for all compounds are displayed in Appendix A. Tables of bond lengths and angles and .cif files for all structures are included in electronic format on CD, a copy of which is included at the back of this thesis.

5.4 References

1 K. Shelly, D. C. Finster, Y. J. Lee, W. R. Scheidt, C. A. Reed, *J. Am. Chem. Soc.* **1985**, *107*, 5955.

2 T. Jelinek, J. Plesek, S. Hermanek, B. Stibr, *Collect. Czech. Chem. Commun.* **1986**, *51*, 819.

3 T. Jelinek, P. Baldwin, W. R. Scheidt, C. A. Reed, *Inorg. Chem.* **1993**, *32*, 1982.

4 D. J. Liston, Y. J. Lee, W. R. Scheidt, C. A. Reed, *J. Am. Chem. Soc.* **1989**, *111*, 6643.

5 Z. Xie, J. Manning, R. W. Reed, R. Mathur, P. D. W. Boyd, A. Benesi, C. A. Reed, *J. Am. Chem. Soc.* **1996**, *118*, 2922.
6 T. S. Piper, G. Wilkinson, *J. Inorg. Nucl. Chem.* **1956**, *3*, 104.
7 A. Asdar, M.-J. Tudoret, C. Lapinte, *J. Organomet. Chem.* **1988**, *349*, 353.
8 R. B. King, M. B. Bisnette, *J. Organomet. Chem.* **1967**, *8*, 287.
9 Z. Xie, T. Jelinek, R. Bau, C. A. Reed, *J. Am. Chem. Soc.* **1994**, *116*, 1907.
10 R. B. King, F. G. A. Stone, *Inorg. Synth.* **1963**, *7*, 99.
11 A. J. Arduengo III, H. V. R. Dias, R. L. Harlow, M. Kline, *J. Am. Chem. Soc.* **1992**, *114*, 5530.

APPENDIX A

Crystal data and structure refinement tables for all compounds

Table 1: Crystal data and structure refinement for Compound **I**.

Identification code	Compound **I**
Empirical formula	$C_9 H_{17} B_{11} Mo O_3$
Formula weight	388.08
Temperature	293(2)°K
Wavelength	0.71069 Å
Crystal system	Monoclinic
Space group	$P2_1/c$
Unit cell dimensions	a = 10.1425(19)Å $\alpha = 90°$
	b = 10.4875(13)Å $\beta = 93.76(2)°$
	c = 16.515(2)Å $\gamma = 90°$
Volume	1752.9(4) $Å^3$
Z	4
Density (calculated)	1.471 Mg/m^3
Absorption coefficient	0.749 mm^{-1}
F(000)	768
Crystal size	0.30 x 0.25 x 0.25 mm
Theta range for data collection	2.01 to 26.96 °.
Index ranges	0<=h<=12; 0<=k<=13; -21<=l<=21
Reflections collected	4157
Independent reflections	3801 [R(int) = 0.0150]
Refinement method	Full-matrix least-squares on F^2
Data / restraints / parameters	3801 / 0 / 232
Goodness-of-fit on F^2	1.038
Final R indices [I>2σ(I)]	R1 = 0.0289 wR2 = 0.0780
R indices (all data)	R1 = 0.0369 wR2 = 0.0806
Largest diff. peak and hole	0.420 and -0.454 $eÅ^{-3}$
Weighting scheme	calc

Table 2: Crystal data and structure refinement for Compound **II**.

Identification code	Compound **II**
Empirical formula	$C_9 H_{17} Ag B_{11} I Mo O_3$
Formula weight	622.85
Temperature	120(2) K
Wavelength	0.71073 Å
Crystal system	Orthorhombic
Space group	Pnna
Unit cell dimensions	a = 13.8843(4) Å α= 90°.
	b = 15.7193(4) Å β= 90°.
	c = 18.1490(6) Å γ = 90°.
Volume	3961.0(2) $Å^3$
Z	8
Density (calculated)	2.089 Mg/m^3
Absorption coefficient	3.186 mm^{-1}
F(000)	2336
Crystal size	0.20 x 0.10 x 0.08 mm^3
Theta range for data collection	3.61 to 26.00°.
Index ranges	-17<=h<=17, -19<=k<=19, -22<=l<=22
Reflections collected	7282
Independent reflections	3870 [R(int) = 0.0476]
Absorption correction	Scalepack
Max. and min. transmission	0.7847 and 0.5683
Refinement method	Full-matrix least-squares on F^2
Data / restraints / parameters	3870 / 0 / 236
Goodness-of-fit on F^2	1.229
Final R indices [I>2sigma(I)]	R1 = 0.0563, wR2 = 0.1101
R indices (all data)	R1 = 0.0725, wR2 = 0.1145
Extinction coefficient	0.00059(8)
Largest diff. peak and hole	1.712 and -1.697 $e.Å^{-3}$

Table 3: Crystal data and structure refinement for Compound **III**.

Identification code	Compound **III**
Empirical formula	$C_{19}H_{34}Ag_2B_{22}Br_2Cl_2I_2Mo_2O_6$
Formula weight	1488.42
Temperature	150(2) K
Wavelength	0.71073 Å
Crystal system	Triclinic
Space group	P-1
Unit cell dimensions	a = 12.779(3)Å α = 99.47(3)°
	b = 13.530(3)Å β = 101.09(3)°
	c = 13.725(3)Å γ = 98.31(3)°
Volume	2258.6(8) $Å^3$
Z	2
Density (calculated)	2.189 Mg/m^3
Absorption coefficient	4.686 mm^{-1}
F(000)	1388
Crystal size	0.20 x 0.10 x 0.08 mm
Theta range for data collection	3.09 to 27.48 °.
Index ranges	-16<=h<=16; -17<=k<=17; -17<=l<=17
Reflections collected	36486
Independent reflections	10316 [R(int) = 0.0414]
Reflections observed (>2σ)	8863
Absorption correction	Semi-empirical from equivalents
Max. and min. transmission	1.045, 0.933
Refinement method	Full-matrix least-squares on F^2
Data / restraints / parameters	10316 / 2 / 543
Goodness-of-fit on F^2	1.051
Final R indices [I>2σ(I)]	R_1 = 0.0294 wR_2 = 0.0635
R indices (all data)	R_1 = 0.0380 wR_2 = 0.0670
Largest diff. peak and hole	1.234 and -1.518 e.$Å^{-3}$

Table 4: Crystal data and structure refinement for Compound **IV**.

Identification code	Compound **IV**
Empirical formula	$C_9 H_{11} O_3 B_{11} Br_6 Ag I Mo$
Formula weight	1096.26
Temperature	170(2) K
Wavelength	0.71070 Å
Crystal system	Triclinic
Space group	P-1
Unit cell dimensions	a = 7.7200(7)Å α = 90.871(5)°
	b = 11.8360(8)Å β = 96.678(4)°
	c = 14.7530(15)Å γ = 90.355(5)°
Volume	1338.7(2) $Å^3$
Z	2
Density (calculated)	2.720 Mg/m^3
Absorption coefficient	11.320 mm^{-1}
F(000)	992
Crystal size	0.13 x 0.08 x 0.05 mm
Theta range for data collection	3.56 to 25.17 °.
Index ranges	-9<=h<=9; -14<=k<=14; -13<=l<=17
Reflections collected	11052
Independent reflections	4679 [R(int) = 0.0967]
Reflections observed (>2σ)	3236
Max. and min. transmission	0.6014 and 0.3319
Refinement method	Full-matrix least-squares on F^2
Data / restraints / parameters	4679 / 115 / 295
Goodness-of-fit on F^2	1.011
Final R indices [I>2σ(I)]	R_1 = 0.0917 wR_2 = 0.2541
R indices (all data)	R_1 = 0.1324 wR_2 = 0.2844
Largest diff. peak and hole	2.598 and -2.947 $e.Å^{-3}$

Table 5: Crystal data and structure refinement for Compound **V**.

Identification code	Compound **V**
Empirical formula	$C_{14}\ H_{27}\ B_{11}\ Mo\ O_3$
Formula weight	458.21
Temperature	170(2) K
Wavelength	0.71069 Å
Crystal system	Orthorhombic
Space group	$P2_12_12_1$
Unit cell dimensions	a = 9.75770(10)Å $\alpha = 90^o$
	b = 14.1357(2)Å $\beta = 90^o$
	c = 16.2310(2)Å $\gamma = 90^o$
Volume	2238.77(5) $Å^3$
Z	4
Density (calculated)	1.359 Mg/m^3
Absorption coefficient	0.598 mm^{-1}
F(000)	928
Crystal size	0.30 x 0.13 x 0.13 mm
Theta range for data collection	3.56 to 27.48 °.
Index ranges	-12<=h<=12; -18<=k<=16; -21<=l<=21
Reflections collected	25921
Independent reflections	5110 [R(int) = 0.0276]
Reflections observed (>2σ)	4996
Absorption correction	Multiscan
Max. and min. transmission	0.9290 and 0.8409
Refinement method	Full-matrix least-squares on F^2
Data / restraints / parameters	5110 / 0 / 283
Goodness-of-fit on F^2	0.959
Final R indices [I>2σ(I)]	$R_1 = 0.0295$ $wR_2 = 0.0859$
R indices (all data)	$R_1 = 0.0302$ $wR_2 = 0.0870$
Absolute structure parameter	-0.03(4)
Largest diff. peak and hole	0.628 and -0.492 $e.Å^{-3}$

Table 6: Crystal data and structure refinement for Compound **VII**.

Identification code	Compound **VII**
Empirical formula	$C_9 H_{16} B_{11} Br Mo O_3$
Formula weight	466.98
Temperature	173(2) K
Wavelength	0.71073 Å
Crystal system	Triclinic
Space group	P-1
Unit cell dimensions	a = 7.64100(10)Å α = 104.8390(10)°
	b = 10.9320(2)Å β = 100.4580(10)°
	c = 11.3340(2)Å γ = 90.2010(10)°
Volume	898.72(3) $Å^3$
Z	2
Density (calculated)	1.726 Mg/m^3
Absorption coefficient	2.956 mm^{-1}
F(000)	452
Crystal size	0.50 x 0.40 x 0.20 mm
Theta range for data collection	3.59 to 30.00°
Index ranges	-10<=h<=10; -15<=k<=14; -15<=l<=15
Reflections collected	20929
Independent reflections	5224 [R(int) = 0.0523]
Reflections observed (>2σ)	4596
Data Completeness	0.996
Absorption correction	Semi-empirical from equivalents
Max. and min. transmission	0.81 and 0.66
Refinement method	Full-matrix least-squares on F^2
Data / restraints / parameters	5224 / 0 / 227
Goodness-of-fit on F^2	1.041
Final R indices [I>2σ(I)]	R_1 = 0.0278 wR_2 = 0.0670
R indices (all data)	R_1 = 0.0346 wR_2 = 0.0701
Largest diff. peak and hole	0.855 and -0.912 $eÅ^{-3}$

Table 7: Crystal data and structure refinement for Compound **VIII**.

Identification code	Compound **VIII**
Empirical formula	$C_9 H_{13} B_{11} Br_6 Mo O_4$
Formula weight	879.50
Temperature	150(2) K
Wavelength	0.71073 Å
Crystal system	Monoclinic
Space group	$P2_12_12_1$
Unit cell dimensions	a = 9.7520(2)Å α = 90°
	b = 12.8140(3)Å β = 90°
	c = 20.1420(5)Å γ = 90°
Volume	2516.99(10) $Å^3$
Z	4
Density (calculated)	2.321 Mg/m^3
Absorption coefficient	10.062 mm^{-1}
F(000)	1624
Crystal size	0.43 x 0.13 x 0.02 mm
Theta range for data collection	3.81 to 27.47°
Index ranges	-12<=h<=12; -16<=k<=16; -24<=l<=26
Reflections collected	34957
Independent reflections	5745 [R(int) = 0.0805]
Reflections observed (>2σ)	5197
Data Completeness	0.995
Absorption correction	Semi-empirical from equivalents
Max. and min. transmission	0.83 and 0.54
Refinement method	Full-matrix least-squares on F^2
Data / restraints / parameters	5745 / 0 / 286
Goodness-of-fit on F^2	1.023
Final R indices [I>2σ(I)]	R_1 = 0.0383 wR_2 = 0.0959
R indices (all data)	R_1 = 0.0449 wR_2 = 0.1009
Absolute structure parameter	0.007(10)
Largest diff. peak and hole	0.892 and -0.805 $eÅ^{-3}$

Notes: water hydrogens could not be reliably located, hence omitted from refinement

Table 8: Crystal data and structure refinement for Compound **IX**.

Identification code	Compound **IX**
Empirical formula	$C_{17}\ H_{27}\ B_{11}\ Br_6\ Mo\ O_4$
Formula weight	989.70
Temperature	170(2) K
Wavelength	0.71070 Å
Crystal system	Monoclinic
Space group	$P2_1/n$
Unit cell dimensions	a = 9.9510(2)Å $\alpha = 90^\circ$
	b = 11.7740(2)Å $\beta = 97.0060(11)^\circ$
	c = 27.9560(5)Å $\gamma = 90^\circ$
Volume	3250.95(10) $Å^3$
Z	4
Density (calculated)	2.022 Mg/m^3
Absorption coefficient	7.803 mm^{-1}
F(000)	1872
Crystal size	0.10 x 0.10 x 0.10 mm
Theta range for data collection	3.54 to 23.26 °.
Index ranges	-11<=h<=10; -13<=k<=13; -31<=l<=31
Reflections collected	29814
Independent reflections	4636 [R(int) = 0.0696]
Reflections observed (>2σ)	4094
Absorption correction	Multiscan
Max. and min. transmission	
Refinement method	Full-matrix least-squares on F^2
Data / restraints / parameters	4636 / 0 / 406
Goodness-of-fit on F^2	1.074
Final R indices [I>2σ(I)]	$R_1 = 0.0651$ $wR_2 = 0.2031$
R indices (all data)	$R_1 = 0.0724$ $wR_2 = 0.2083$
Largest diff. peak and hole	1.635 and -2.854 $e.Å^{-3}$

N.B. Xtal quality and data good. R factor held high because of negative hole approximate to Br4. Libration notes in carborane cage; thermals on boron atoms larger than for atoms around the metal core. Extreme of effects reflected in modelling Br1, Br2, Br3, Br5 and Br6 in 66:34 ratio with Br1A, Br2A, Br3A, Br5A and Br6A respectively. Br4 was best modelled at single site occupancy.

Table 9: Crystal data and structure refinement for Compound **X**.

Identification code	Compound **X**
Empirical formula	$C_{19}H_{27}AgB_{11}P$
Formula weight	513.16
Temperature	150(2) K
Wavelength	0.71073 Å
Crystal system	Triclinic
Space group	P-1
Unit cell dimensions	a = 10.282(2)Å α = 76.22(3)°
	b = 10.988(2)Å β = 75.25(3)°
	c = 11.308(2)Å γ = 75.61(3)°
Volume	1175.7(4) $Å^3$
Z	2
Density (calculated)	1.450 Mg/m^3
Absorption coefficient	0.932 mm^{-1}
F(000)	516
Crystal size	0.20 x 0.20 x 0.10 mm
Theta range for data collection	2.96 to 27.50°.
Index ranges	0<=h<=13; -13<=k<=14; -13<=l<=14
Reflections collected	20702
Independent reflections	5374 [R(int) = 0.0387]
Reflections observed (>2σ)	4538
Max. and min. transmission	0.9126 and 0.8355
Refinement method	Full-matrix least-squares on F^2
Data / restraints / parameters	5374 / 0 / 302
Goodness-of-fit on F^2	1.018
Final R indices [I>2σ(I)]	R_1 = 0.0316 wR_2 = 0.0757
R indices (all data)	R_1 = 0.0417 wR_2 = 0.0813
Largest diff. peak and hole	0.544 and -0.923 $eÅ^{-3}$

Table 10: Crystal data and structure refinement for Compound **XI**.

Identification code	Compound **XI**
Empirical formula	$C_{38.50}$ H_{53} Ag_2 B_{22} Br_2 Cl P_2
Formula weight	1226.58
Temperature	173(2) K
Wavelength	0.71073 Å
Crystal system	Triclinic
Space group	P-1
Unit cell dimensions	a = 12.87500(10)Å α = 97.4210(10)°
	b = 13.9930(2)Å β = 92.1240(10)°
	c = 32.2670(5)Å γ = 113.2810(10)°
Volume	5270.33(12) $Å^3$
Z	4
Density (calculated)	1.546 Mg/m^3
Absorption coefficient	2.401 mm^{-1}
F(000)	2420
Crystal size	0.50 x 0.40 x 0.20 mm
Theta range for data collection	2.95 to 29.94°.
Index ranges	-18<=h<=17; -19<=k<=19; -45<=l<=45
Reflections collected	63584
Independent reflections	27082 [R(int) = 0.0737]
Reflections observed (>2σ)	17472
Data Completeness	0.886
Absorption correction	Semi-empirical from equivalents
Max. and min. transmission	0.60 and 0.42
Refinement method	Full-matrix least-squares on F^2
Data / restraints / parameters	27082 / 0 / 1217
Goodness-of-fit on F^2	1.069
Final R indices [I>2σ(I)]	R_1 = 0.0639 wR_2 = 0.1276
R indices (all data)	R_1 = 0.1141 wR_2 = 0.1428
Largest diff. peak and hole	1.435 and -0.861 $eÅ^{-3}$

Table 11: Crystal data and structure refinement for Compound **XII**.

Identification code	Compound **XII**
Empirical formula	$C_{19}H_{21}AgB_{11}Br_6P$
Formula weight	986.57
Temperature	150(2) K
Wavelength	0.71073 Å
Crystal system	Monoclinic
Space group	$P2_1/c$
Unit cell dimensions	a = 8.89500(10)Å α = 90°
	b = 24.4140(4)Å β = 102.0720(10)°
	c = 14.4170(3)Å γ = 90°
Volume	3061.60(9) $Å^3$
Z	4
Density (calculated)	2.140 Mg/m^3
Absorption coefficient	8.554 mm^{-1}
F(000)	1848
Crystal size	0.10 x 0.10 x 0.05 mm
Theta range for data collection	3.71 to 27.88 °.
Index ranges	-11<=h<=11; -32<=k<=32; -17<=l<=18
Reflections collected	23164
Independent reflections	7253 [R(int) = 0.0519]
Reflections observed (>2σ)	5880
Data Completeness	0.994
Absorption correction	Semi-empirical from equivalents
Max. and min. transmission	0.66 and 0.47
Refinement method	Full-matrix least-squares on F^2
Data / restraints / parameters	7253 / 0 / 349
Goodness-of-fit on F^2	1.041
Final R indices [I>2σ(I)]	R_1 = 0.0358 wR_2 = 0.0783
R indices (all data)	R_1 = 0.0521 wR_2 = 0.0855
Largest diff. peak and hole	1.081 and -1.181 $eÅ^{-3}$

Table 12: Crystal data and structure refinement for Compound **XIII**.

Identification code	Compound **XIII**
Empirical formula	$C_{19}H_{21}AgB_{11}Cl_6P$
Formula weight	719.81
Temperature	150(2) K
Wavelength	0.71073 Å
Crystal system	Triclinic
Space group	P-1
Unit cell dimensions	a = 7.91500(10)Å α = 100.1760(10)°
	b = 13.7660(2)Å β = 102.7440(10)°
	c = 14.7500(3)Å γ = 105.6080(10)°
Volume	1461.30(4) $Å^3$
Z	2
Density (calculated)	1.636 Mg/m^3
Absorption coefficient	1.306 mm^{-1}
F(000)	708
Crystal size	0.30 x 0.25 x 0.25 mm
Theta range for data collection	3.62 to 30.09°.
Index ranges	-11<=h<=11; -19<=k<=19; -20<=l<=20
Reflections collected	28761
Independent reflections	8527 [R(int) = 0.0324]
Reflections observed (>2σ)	6554
Data Completeness	0.993
Absorption correction	Semi-empirical from equivalents
Max. and min. transmission	0.73 and 0.69
Refinement method	Full-matrix least-squares on F^2
Data / restraints / parameters	8527 / 0 / 533
Goodness-of-fit on F^2	1.066
Final R indices [I>2σ(I)]	R_1 = 0.0589 wR_2 = 0.1529
R Largest diff. peak and hole indices (all data)	R_1 = 0.0779 wR_2 = 0.1672
	1.066 and -1.085 $eÅ^{-3}$

Note: silver and carborane positions disordered over 2 sites in 50:50 ratio. Also the partial chlorines attached to B8/B28 are further split over 2 sites, which may be rationalised in terms of libration associated with the cage and the possibility of intermolecular contacts.

Table 13: Crystal data and structure refinement for Compound **XIV**.

Identification code	Compound **XIV**
Empirical formula	$C_{74}H_{84}Ag_2B_{22}P_4$
Formula weight	1550.85
Temperature	170(2) K
Wavelength	0.71069 Å
Crystal system	Triclinic
Space group	P-1
Unit cell dimensions	a = 11.6963(2)Å α = 96.8860(6)°
	b = 13.1668(2)Å β = 106.8980(7)°
	c = 14.1393(2)Å γ = 110.5370(8)°
Volume	1890.30(5) $Å^3$
Z	1
Density (calculated)	1.362 Mg/m^3
Absorption coefficient	0.646 mm^{-1}
F(000)	792
Crystal size	0.25 x 0.20 x 0.17 mm
Theta range for data collection	3.38 to 27.50°.
Index ranges	-15<=h<=15; -17<=k<=16; -18<=l<=18
Reflections collected	22570
Independent reflections	8605 [R(int) = 0.0250]
Reflections observed (>2σ)	7964
Absorption correction	Multiscan
Max. and min. transmission	1.027, 0.981
Refinement method	Full-matrix least-squares on F^2
Data / restraints / parameters	8605 / 2 / 478
Goodness-of-fit on F^2	1.050
Final R indices [I>2σ(I)]	R_1 = 0.0289 wR_2 = 0.0738
R indices (all data)	R_1 = 0.0323 wR_2 = 0.0763
Largest diff. peak and hole	1.727 and -0.584 e.$Å^{-3}$

Notes: H7 and H12 positionally refined at a distance of 1.12 Å from B7 and B12 respectively

Table 14: Crystal data and structure refinement for Compound **XV**.

Identification code	Compound **XV**
Empirical formula	C_{39} H_{40} Ag B_{11} Br_6 Cl_4 P_2
Formula weight	1418.69
Temperature	150(2) K
Wavelength	0.71073 Å
Crystal system	Orthorhombic
Space group	$P2_12_12_1$
Unit cell dimensions	a = 12.9130(2)Å $\alpha = 90^\circ$
	b = 17.6430(3)Å $\beta = 90^\circ$
	c = 22.5880(5)Å $\gamma = 90^\circ$
Volume	5146.09(16) $Å^3$
Z	4
Density (calculated)	1.831 Mg/m^3
Absorption coefficient	5.351 mm^{-1}
F(000)	2736
Crystal size	0.20 x 0.25 x 0.05 mm
Theta range for data collection	3.58 to 27.49°
Index ranges	-15<=h<=16; -19<=k<=22; -29<=l<=29
Reflections collected	32411
Independent reflections	11621 [R(int) = 0.0789]
Reflections observed (>2σ)	7750
Data Completeness	0.994
Absorption correction	Semi-empirical from equivalents
Max. and min. transmission	0.64 and 0.48
Refinement method	Full-matrix least-squares on F^2
Data / restraints / parameters	11621 / 0 / 569
Goodness-of-fit on F^2	0.972
Final R indices [I>2σ(I)]	$R_1 = 0.0506$ $wR_2 = 0.1009$
R indices (all data)	$R_1 = 0.0989$ $wR_2 = 0.1162$
Absolute structure parameter	0.013(9)
Largest diff. peak and hole	0.731 and -1.324 $eÅ^{-3}$

Table 15: Crystal data and structure refinement for Compound **XVIII**.

Identification code	Compound **XVIII**
Empirical formula	C_{22} H_{36} Ag B_{11} N_2
Formula weight	555.31
Temperature	150(2) K
Wavelength	0.71073 Å
Crystal system	Monoclinic
Space group	$P2_1/n$
Unit cell dimensions	a = 15.4570(2)Å $\alpha = 90^\circ$
	b = 20.1150(3)Å $\beta = 108.558(1)^\circ$
	c = 19.2130(3)Å $\gamma = 90^\circ$
Volume	5663.04(14) $Å^3$
Z	8
Density (calculated)	1.303 Mg/m^3
Absorption coefficient	0.727 mm^{-1}
F(000)	2272
Crystal size	0.13 x 0.13 x 0.15 mm
Theta range for data collection	3.66 to 24.71°
Index ranges	-18<=h<=18; -23<=k<=20; -22<=l<=22
Reflections collected	85847
Independent reflections	9621 [R(int) = 0.1469]
Reflections observed (>2σ)	5969
Data Completeness	0.996
Absorption correction	Semi-empirical from equivalents
Max. and min. transmission	0.97 and 0.87
Refinement method	Full-matrix least-squares on F^2
Data / restraints / parameters	9621 / 0 / 749
Goodness-of-fit on F^2	1.043
Final R indices [I>2σ(I)]	$R_1 = 0.0543$ $wR_2 = 0.1160$
R indices (all data)	$R_1 = 0.1055$ $wR_2 = 0.1419$
Largest diff. peak and hole	0.489 and -0.623 $eÅ^{-3}$

APPENDIX B

Publications

Transition metal complexes of the weakly coordinating carborane anion $[CB_{11}H_{12}]^-$: the first isolation and structural characterisation of an intermediate in a silver salt metathesis reaction.
N. J. Patmore, J. W. Steed, A. S. Weller, *Chem. Commun.*, **2000**, 1055

Synthesis and characterisation of $\{Mo(\eta\text{-}L)(CO)_3\}^+$ (η-L = C_5H_5 or C_5Me_5) fragments ligated with $[CB_{11}H_{12}]^-$ and derivatives. Isolation and structural characterisation of an intermediate in a silver salt metathesis reaction.
N. J. Patmore, M. F. Mahon, J. W. Steed, A. S. Weller, *J. Chem. Soc., Dalton Trans.*, **2001**, 277

Chelating Monoborane Phosphines: Rational and High-Yield Synthesis of $[(COD)Rh\{(\eta^2\text{-}BH_3)Ph_2PCH_2PPh_2\}][PF_6]$ (COD = 1,5-cyclooctadiene).
M. Ingleson, N. J. Patmore, G. D. Ruggeriero, C. G. Frost, M. F. Mahon, M. C. Willis, A. S. Weller, *Organomet.*, **2001**, *20*, 4434

$[(PPh_3)Ag(CB_{11}H_6Y_6)]$ (Y = H, Br): highly active, selective and recyclable Lewis acids for a hetero-Diels-Alder reaction.
C. Hague, N. J. Patmore, C. G. Frost, M. F. Mahon, A. S. Weller, *Chem. Commun.*, **2001**, 2286

Silver Phosphanes Partnered with Carborane Monoanions: Synthesis, Structures and Use as Highly Active Lewis Acid Catalysts in a Hetero-Diels-Alder Reaction.
N. J. Patmore, C. Hague, J. H. Cotgreave, M. F. Mahon, C. G. Frost, A. S. Weller, *Chem. Eur. J.*, **2002**, *8*, 2088

Rhodium Phosphines Partnered with the Carborane Monoanions $[CB_{11}H_6Y_6]^-$ (Y = H, Br). Synthesis and Evaluation as Alkene Hydrogenation Catalysts.
A. Rifat, N. J. Patmore, M. F. Mahon, A. S. Weller, *Organomet.*, **2002**, *21*, 2856

Solution and Solid-State Structure of the Anion $[Ag_2\{closo\text{-}CB_{11}H_{12}\}_4]^{2-}$.
M. A. Fox, M. F. Mahon, N. J. Patmore, A. S. Weller, *Inorg. Chem.*, **2002**, *41*, 4567

$[(PPh_3)Ag(HCB_{11}Me_{11})]$: A Complex with Intermolecular Ag···H_3C Interactions.
M. J. Ingleson, M. F. Mahon, N. J. Patmore, G. D. Ruggiero, A. S. Weller, *Angew. Chem. Int. Ed.*, **2002**, *41*, 3694

Aspects of this work have also been presented in poster form at the following international conferences:

Boron Americas VIII, Death Valley, USA, January 2-5, 2002

XXth International Conference On Organometallic Chemistry, Corfu, Greece, July 7-12, 2002

ChemComm

Transition metal complexes of the weakly coordinating carborane anion $[CB_{11}H_{12}]^-$: the first isolation and structural characterisation of an intermediate in a silver salt metathesis reaction

Nathan J. Patmore,[a] Jonathan W. Steed[b] and Andrew S. Weller*[a]

[a] *Department of Chemistry, University of Bath, Bath, UK BA2 7AY. E-mail: a.s.weller@bath.ac.uk*
[b] *Department of Chemistry, Kings College London, The Strand, London, UK WC2R 2LS*

Received (in Cambridge, UK) 31st March 2000, Accepted 8th May 2000

Reaction between $CpMo(CO)_3I$ and $Ag[CB_{11}H_{12}]$ eventually affords $CpMo(CO)_3(\eta^1\text{-}CB_{11}H_{12})$, *via* the dimeric compound $[CpMo(CO)_3I{\cdot}Ag\{CB_{11}H_{12}\}]_2$ which represents the first structurally characterised intermediate in a silver salt metathesis reaction.

The ubiquitous silver halide metathesis reaction, used to generate vacant sites on a metal fragment, finds application in many transition metal-mediated reactions, especially *in situ* catalyst generation.[1] Typically, the counter ion paired in such transformations is triflate, $[OTf]^-$, $[BF_4]^-$ or $[PF_6]^-$, and halide metathesis is considered to be rapid. Over ten years ago, Reed and coworkers reported[2] that very weakly coordinating anions, such as the monocarborane $[closo\text{-}CB_{11}H_{12}]^-$,[3] could dramatically slow the rate of metathesis when paired with Ag^+, suggesting that the exceptionally low nucleophilicity of the anion was a limiting factor in these reactions. Reaction between $CpFe(CO)_2I$ ($Cp = \eta^5\text{-}C_5H_5$) and $Ag[CB_{11}H_{12}]$ was proposed (by ^1H NMR and IR data) to proceed through an intermediate adduct, $CpFe(CO)_2I{\cdot}Ag[CB_{11}H_{12}]$, similar to Mattson and Graham's[4] proposed intermediate adduct, formed between $CpFe(CO)_2I$ and $Ag[BF_4]$. However, neither of these transient species (or other related[5] compounds) have been placed on a firm structural footing. Given the widespread use of the silver salt metathesis reaction, the identity of the intermediates in these reactions is of significant interest.

We have a current interest in the transition metal chemistry associated with carboranes such as $[CB_{11}H_{12}]^-$, and as part of this investigation have been studying the reactions of $CpMo(CO)_3X$ ($X = Cl, I$) with $Ag[CB_{11}H_{12}]$ and derivatives, with the anticipation of forming complexes *via* extrusion of AgX. We report here, the isolation and full characterisation, including the X-ray crystal structure, of the intermediate formed in this silver salt metathesis reaction.

Reaction between $CpMo(CO)_3Cl$ and $Ag[CB_{11}H_{12}]$ in CH_2Cl_2 over 2 days resulted in the precipitation of AgCl and the isolation, in essentially quantitative yield, of $CpMo(CO)_3(\eta^1\text{-}CB_{11}H_{12})$ **2** (Scheme 1). Compound **2** has been fully characterised by multinuclear NMR spectroscopy† and by an X-ray diffraction study[6] and shows the expected[2] 3c–2e Mo–H–B agostic bonding. Compound **2** displays two CO stretching modes in its IR spectrum, at 2071 and 2001 cm^{-1}. Monitoring the reaction by IR spectroscopy showed that the reaction proceeded through an intermediate species [as found for $CpFe(CO)_2I$[2]], but at no time was there a single component observed in the reaction mixture. Moving to $CpMo(CO)_3I$ resulted in a slowing down of the reaction, so that formation of **2** now took 7 days, while after *ca.* 3 h of stirring there was only one component in the reaction mixture, which displayed IR stretches at 2054 and 1973 cm^{-1}, intermediate between the starting material and product. Monitoring this reaction by IR and ^1H NMR spectroscopies showed that this was indeed an intermediate species, continued stirring for 7 days resulting in the clean formation of **2**. Careful recrystallisation of this intermediate overnight at −30 °C afforded small red crystals in reasonable isolated yield (50%), which were pure by IR, microanalysis and NMR spectroscopy,‡ and shown by X-ray diffraction§ to be $[CpMo(CO)_3I{\cdot}Ag\{CB_{11}H_{12}\}]_2$ **1**: the first structurally characterised intermediate in a silver salt metathesis reaction.

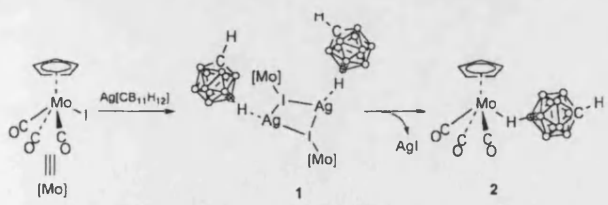

Scheme 1

The solid state structure of **1** is shown in Fig. 1. It is apparent that it adopts a centrosymmetric dimeric structure, with an I–Ag–I–Ag central core hinged around the Mo(1)–I(1)–I(1A)–Mo(1A) vector by 123.2°. The two Ag–I lengths are significantly different, Ag(1)–I(1) 2.9748(10) Å and Ag(1)–I(1A) 2.7599(9) Å. While similar central cores to **1** are known,[7,8] the presence of two additional [M]–I–Ag bridges appended to such a motif is unprecedented. However, there are silver adduct species of transition metal halides that show similar features,[9] such as the recently reported complex $[\{TpRe(NC_6H_4Me\text{-}p)(Ph)I\}_2Ag][PF_6]$[10] [Tp = tris(pyrazolyl)borate] in which silver bridges two {[Re]–I} fragments. The carborane anion is intimately connected with silver, showing a short (1.96 Å) Ag–H–B interaction [Ag(1)–B(12) 2.659(10) Å]. The cages are orientated *syn* to one another with respect to the Mo–I–I–Mo vector, leaving the silver atoms with an apparent vacant coordination site. Inspection of the packing diagram for **1** reveals that this site is occupied by another short (1.96 Å) Ag–H–B interaction arising from an adjacent carborane cage in the lattice, meaning that each cage bridges two silver centres [through H(12) and H(7)]. This results in a chain-like structure

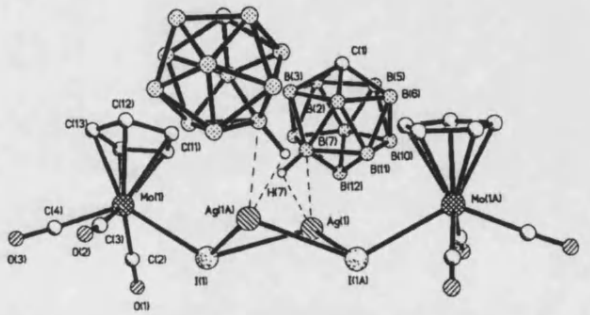

Fig. 1 Structure of the dimeric unit in complex **1**. Atom labels suffixed 'A' are generated crystallographically. Hydrogen atoms [except H(7)] are omitted for clarity. Selected bond lengths (Å) and angles (°): Mo(1)–I(1) 2.8599(8), Ag(1)–I(1) 2.9748(10), Ag(1A)–I(1) 2.7599(9), Ag(1)–B(7) 2.659(10), Ag(1)–H(7) 1.96; Ag(1)–I(1)–Ag(1A) 71.19(3), I(1)–Ag(1)–I(1A) 97.10(3).

DOI: 10.1039/b002585m

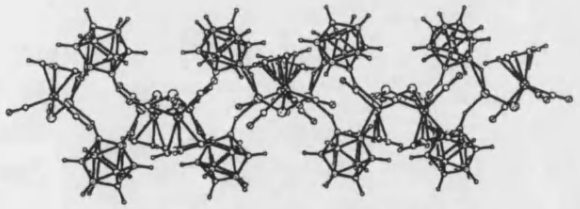

Fig. 2 Extended solid state structure of **1** viewed along the crystallographic '*a*' axis.

along the '*a*' axis in the crystal (Fig. 2). A similar bridging motif has been observed in the simple salt $Ag[CB_{11}H_{12}]\cdot 2C_6H_6$,[2] while dimeric structures formed from single Ag–H–B interactions have also been reported.[11,12]

Although it is unlikely that this polymeric structure persists on dissolution in CH_2Cl_2, evidence for coordination of the carborane cage to Ag in solution comes from inspection of the ^{11}B NMR spectra. The room temperature $^{11}B\{^1H\}$ NMR spectrum (128 MHz) shows two peaks at $\delta -11.1$ and -14.6 in the ratio 1 : 10 (latter peak a 5 + 5 coincidence), significantly different from the free anion (*vide infra*), the unique boron resonance being shifted upfield by *ca.* 5.5 ppm with respect to $Ag[CB_{11}H_{12}]$ [$\delta_{^{11}B}$ −5.4 (1B), −10.6 (5B) and −12.3 (5B) in d_6-acetone]. This chemical shift difference suggests sustained Ag–H–B interaction(s) in solution and is consistent with the observed Ag–H–B contacts in the solid state. In the room-temperature $^1H\{^{11}B\}$ NMR spectrum the unique BH is observed at δ 2.12 and shifts slightly to δ 1.92 on cooling to −90 °C, showing no Ag–H coupling, although such interactions are rarely observed. The ^{109}Ag NMR spectrum displayed a single sharp line at δ 1335, shifted significantly downfield from the normal range ($\delta_{^{109}Ag}$ *ca.* 500) expected for Ag(I) centres.[13]

Overall metathesis can be dramatically suppressed in this system by moving to the less nucleophilic and sterically bulkier carborane anion $Ag[CB_{11}H_6Br_6]$. Stirring for 1 h results in the clean formation of the analogous intermediate complex to **1**,[14] but, surprisingly, no subsequent metathesis was observed, even after extended stirring for 7 days. This result is in accord with the previous observation that the relative nucleophilicity of the conjugate anion in these reactions is rate determining.[2] Nevertheless, the cessation of this reaction at the intermediate stage is, to our knowledge, without precedent. It should be noted, however, that metathesis does not proceed to completion when Vaska's complex and $Ag[CB_{11}H_{12}]$ are combined, but in this system a strong Ag–Ir bond is formed instead,[15] very different from the structure of **1**.

In summary, we have presented here the first fully characterised (NMR, X-ray diffraction) intermediate in a silver salt metathesis reaction, and found it to have a dimeric {[Mo]–I}–Ag–{[Mo]–I}–Ag core in the solid state. This result leads us to speculate upon the motifs accessible using combinations of other $CpML_nX_y$ fragments and monocarborane anions, and we are currently actively pursuing this. Moreover, the lack of metathesis consummation with $Ag[CB_{11}H_6Br_6]$ demonstrates that there is a significant degree of kinetic control in a reaction that is normally considered very facile. This has potential implications for the synthesis of transition metal complexes bearing very weakly coordinating anions *via* silver salt metathesis.

We thank the EPSRC and King's College London for the provision of the X-ray diffractometer and the Nuffield Foundation for the provision of computing equipment (J. W. S.). The Royal Society (A. S. W.) and the University of Bath (N. J. P.) are thanked for financial support. Dr Mary Mahon is thanked for useful discussions and Dr J. P. Rourke is thanked for his assistance in obtaining the ^{109}Ag spectrum of **1**.

Notes and references

† *Spectroscopic data* for **2**: $\delta_{H\{^{11}B\}}$(400 MHz, CD_2Cl_2) 5.86*, 5.79 (5H, s), 2.53 (1H, s, $C_{cage}H$), 1.79 (5H, s, BH), 1.66 (5H, s, BH), −15.11 (1H, s, Mo–H–B). Selected δ_H: −15.11 [1H, partially collapsed quartet, J(BH) 90]. $\delta_{^{11}B}$ (128 MHz, CD_2Cl_2) −4.7*, −10.4 (1B, d sh), −11.7 [5B, d, J(HB) 151 Hz], −13.9 [5B, d, J(HB) 151 Hz], −18.6* (* indicates peaks relating to a minor isomer[6]). Found: C, 28.0; H, 4.4. Calc. for $C_9H_{17}O_3B_{11}Mo$: C, 27.9; H, 4.4%. IR (KBr, cm^{-1}): 2582m, 2549m, 2243w br, 2067s, 1991s, 1980s. (CH_2Cl_2): 2573m, 2230w, vbr, 2071s 2001s br.

‡ *Spectroscopic data* for **1**: 273 K: $\delta_{H\{^{11}B\}}$(CD_2Cl_2) 5.75 (5H, s), 2.56 (1H, s, $C_{cage}H$), 2.12 (1H, s, BH) and 1.86 (10H, s, BH). $\delta_{^{11}B}$(CD_2Cl_2) −11.1 [1B, d, J(HB) 119 Hz], −14.6 [5B + 5B, app. d, J(HB) *ca.* 144 Hz]. 183 K: $\delta_{H\{^{11}B\}}$(CD_2Cl_2) 5.76 (5H, s), 2.56 (1H, s, $C_{cage}H$), 1.92 (1H, s, BH), 1.73 (5H, s, BH) and 1.68 (5H, s, BH). $\delta_{^{11}B}$(CD_2Cl_2) −10.1 (1B, br), −14.0 (10B, br). $\delta_{^{109}Ag}$(18 MHz, CD_2Cl_2) 1335 (s). Found: C, 17.8; H, 2.8. Calc. for $C_9H_{17}AgB_{11}IMoO_3$: C, 17.4; H, 2.7%. IR (KBr, cm^{-1}) 2556m, 2531m, 2041s, 1971s, 1950s, (CH_2Cl_2): 2570m, 2054s, 1973s br.

§ *Crystal data* for **1**: $C_9H_{17}AgB_{11}IMoO_3$, M = 622.85, λ = 0.71073 Å, orthorhombic, space group *Pnna*, a = 13.8843(4), b = 15.7193(4), c = 18.1490(6) Å, U = 3961.0(2) Å^3, Z = 8, T = 120(2) K, D_c = 2.089 g cm^{-3}, μ = 3.186 mm^{-1}, F(000) = 2336, crystal 0.20 × 0.10 × 0.08 mm, 3870 unique reflections (R_{int} = 0.0476), R_1 = 0.0563, wR_2 = 0.1101 [$I > 2\sigma(I)$].

CCDC 182/1630. See http://www.rsc.org/suppdata/cc/b0/b002585m/ for crystallographic files in .cif format.

1 *Catalytic Asymmetric Synthesis*, ed. I. Ojima, Wiley-VCH, Weinheim, 1993.
2 D. J. Liston, Y. J. Lee, W. R. Scheidt and C. A. Reed, *J. Am. Chem. Soc.*, 1989, **111**, 6643.
3 C. A. Reed, *Acc. Chem. Res.*, 1998, **31**, 133.
4 B. M. Mattson and W. A. G. Graham, *Inorg. Chem.*, 1981, **20**, 3186.
5 D. J. Crowther, S. L. Borkowsky, D. Swenson, T. Y. Meyer and R. F. Jordan, *Organometallics*, 1993, **12**, 2897.
6 N. J. Patmore, M. F. Mahon and A. S. Weller, unpublished results.
7 G. A. Bowmaker, Effendy, P. J. Harvey, P. C. Healy, B. W. Skelton and A. H. White, *J. Chem. Soc., Dalton Trans.*, 1996, 2459 and references therein.
8 B.-K. Teo and J. C. Calabrese, *J. Chem. Soc., Chem. Commun.*, 1976, 185.
9 T. N. Sal'nikova, V. G. Andrianov and Y. T. Struchkov, *Koord. Kkim.*, 1976, **2**, 707.
10 W. S. McNeil, D. D. DuMez, Y. Matano, S. Lovell and J. M. Mayer, *Organometallics*, 1999, **18**, 3715.
11 Y. W. Park, J. Kim and Y. Do, *Inorg. Chem.*, 1994, **33**, 1.
12 H. M. Colquhoun, T. J. Greenhough and M. G. H. Wallbridge, *J. Chem. Soc., Chem. Commun.*, 1980, 192.
13 R. Eujen, B. Hoge and D. J. Brauer, *Inorg. Chem.*, 1997, **36**, 1464.
14 IR ν(CO) cm^{-1}: 2054 and 1975 cm^{-1}. Found: C, 9.28; H, 1.11. Calc.: C, 9.86; H, 1.00%.
15 D. J. Liston, C. A. Reed, C. W. Eigenbrot and W. R. Scheidt, *Inorg. Chem.*, 1987, **26**, 2739.

DALTON
FULL PAPER

Synthesis and characterisation of $\{Mo(\eta\text{-}L)(CO)_3\}^+$ (η-L = C_5H_5 or C_5Me_5) fragments ligated with $[CB_{11}H_{12}]^-$ and derivatives. Isolation and structural characterisation of an intermediate in a silver salt metathesis reaction

Nathan J. Patmore,[a] Mary F. Mahon,[a] Jonathan W. Steed[b] and Andrew S. Weller[a]*

[a] *Department of Chemistry, University of Bath, Bath, UK BA2 7AY*
[b] *Department of Chemistry, Kings College London, The Strand, London, UK WC2R 2LS*

Received 12th October 2000, Accepted 22nd November 2000
First published as an Advance Article on the web 11th January 2001

The synthesis of $\{Mo(\eta\text{-}L)(CO)_3\}^+$ (η-L = C_5H_5 or C_5Me_5) fragments, ligated to the mono-anionic, weakly co-ordinating, carboranes [*closo*-1-$CB_{11}H_{12}]^-$ and [*closo*-$CB_{11}Br_6H_6]^-$, has been investigated. Treatment of $[MoCp(CO)_3X]$ (X = Cl or I) with $Ag[CB_{11}H_{12}]$ eventually affords the zwitterionic complex $[MoCp(CO)_3$-(x-μ-H-1-$CB_{11}H_{12}$)] (x = 12 or 7), *via* an intermediate dimeric species $[MoCp(CO)_3X{\cdot}Ag(CB_{11}H_{12})]_2$. For X = I this intermediate has been characterised by ^1H, ^{11}B NMR spectroscopy and X-ray crystallography and represents the first structurally characterised intermediate in a silver salt metathesis reaction. When the less nucleophilic carborane $[CB_{11}Br_6H_6]^-$ (as its silver salt) is used metathesis is halted at the intermediate stage, affording the complex $[MoCp(CO)_3I{\cdot}Ag(CB_{11}Br_6H_6)]_2$. Silver salt metathesis does not proceed using the sterically more demanding $[Mo(Cp^*)(CO)_3I]$, with only intractable products isolated. The carborane anion can be introduced into the co-ordination sphere of this complex by reaction of $[H(OEt_2)_x][CB_{11}H_{12}]$ with $[Mo(Cp^*)(CO)_3Me]$ affording $[Mo(Cp^*)(CO)_3$(x-μ-H-1-$CB_{11}H_{12}$)] (x = 12 or 7). All new compounds have been characterised by multinuclear NMR spectroscopy and X-ray crystallography.

Introduction

The use of mono-anionic icosahedral carboranes as candidates for the 'least co-ordinating' anions has been championed by work from the groups of Reed[1] and Strauss.[2] Elegant demonstrations of the high chemical inertness and low nucleophilicity of these anions has recently been demonstrated by the isolation of protonated benzene as a weighable, room temperature stable, crystalline solid[3] and the use of perfluorinated $[1\text{-Et-}CB_{11}F_{11}]^-$ to isolate normally inaccessible organometallic compounds.[4] However, to date, there have been few studies associated with the co-ordination chemistry of $[CB_{11}H_{12}]^-$, and its derivatives, with transition metal fragments. This is perhaps surprising as many academically and commercially relevant processes rely on the generation, and subsequent stabilisation, of Lewis acidic fragments. Studies of the chemistry of $[CB_{11}H_{12}]^-$ associated with Group 4,[5] 8[6] and 10[7] cations have appeared, while related chemistry utilising mono- and di-anionic rhenacarboranes has recently been reported by Stone and co-workers with respect to reactivity with transition metal fragments.[8] Compared to the other major, now ubiquitous, least co-ordinating anion $[BAr_f]^-$,[9] and derivatives thereof [BAr_f = $B(C_6F_5)_4$ or $B\{C_6H_3(CF_3)_2\}_4$], the transition metal chemistry associated with $[CB_{11}H_{12}]^-$ is underdeveloped. With this in mind we are interested in using carborane anions as weakly co-ordinating anionic ligands, stabilising reactive Lewis-acidic metal fragments by offering a 'virtual co-ordination site'.[10]

In this investigation we have initially chosen $[Mo(\eta\text{-}L)(CO)_3X]$ as one of the systems to study. The ability systematically to vary the ancillary π ligands (*e.g.* η-L = Cp or Cp*) and the nature of X (*e.g.* Cl, Br, I, H or Me) in this species, coupled with the spectroscopic handle afforded by the carbonyl groups, made this an attractive system. In addition, work by Beck,[11,12] on a series of $[Mo]$–FBF_3 compounds {[Mo] = $Mo(Cp)(CO)_2L$, L = 2 electron ligand} and the recent report of hydride transfer reactions in $[Mo(\eta\text{-}L)(CO)_3H]$ and related compounds to afford reactive 16 electron cationic complexes of the type $[Mo(\eta\text{-}L)(CO)_3]^+$[13] present a firm base with which to compare and contrast the systems under investigation. Aspects of this work have been reported previously as a communication.[14]

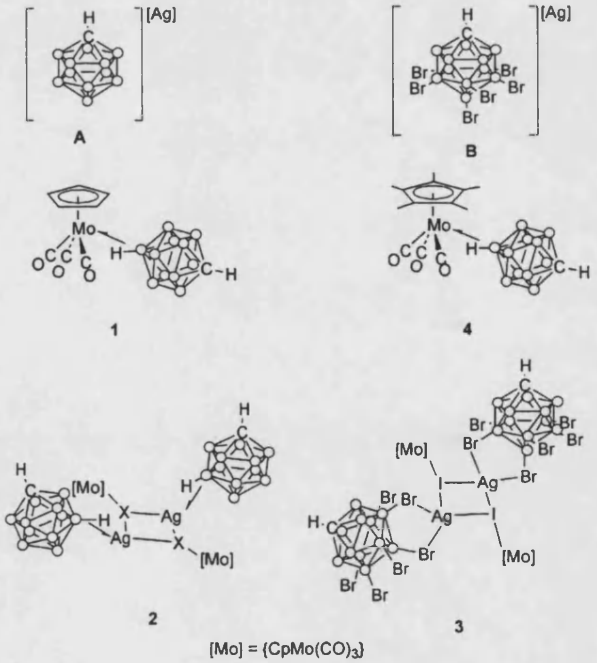

Scheme 1

DOI: 10.1039/b008222h

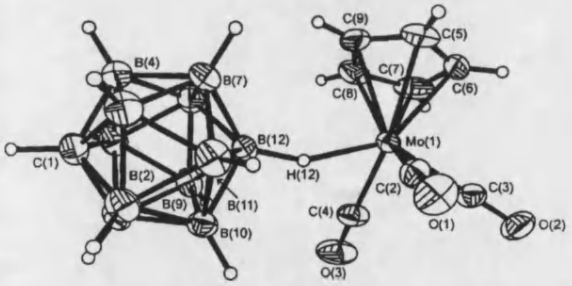

Fig. 1 Solid state structure of complex **1** showing the atom labelling scheme used. Thermal ellipsoids are shown at the 30% probability level.

Results and discussion

Treatment of $[MoCp(CO)_3Cl]$ ($Cp = \eta\text{-}C_5H_5$) with one equivalent of $Ag[CB_{11}H_{12}]$, **A** (see Scheme 1), in CH_2Cl_2 while monitoring the CO stretching region of the IR spectrum over a period of 30 minutes initially shows the replacement of the two stretching bands associated with the starting material (2056 and 1977 cm^{-1}) with two stretching bands at higher frequency (2064 and 1980 cm^{-1}). Continued stirring for 2 days results in these latter peaks being replaced by ones at even higher wavenumber (2071 and 2001 cm^{-1}) and the concomitant formation of AgCl precipitate. This final product was identified as the zwitterionic compound $[MoCp(CO)_3(x\text{-}\mu\text{-}H\text{-}1\text{-}CB_{11}H_{11})]$, **1** (see Scheme 1, $x = 7$ or 12), formed in good yield as the only organometallic product. Compound **1** has been characterised by multinuclear NMR spectroscopy and X-ray crystallography.

The solid state structure of compound **1** is shown in Fig. 1, and salient bond lengths and angles are given in Table 1. The molecule adopts a four-legged piano-stool geometry, with the carborane anion bonded to Mo by a single 3-centre 2-electron (3c–2e) B–H–Mo bond, affording the metal centre an overall 18 EAN count. The hydrogen atom associated with the antipodal boron atom [H(12)] was located in the difference map and freely refined. Bond lengths and angles in the cage anion are unremarkable. The cage interacts with the Mo centre *via* the antipodal B–H linkage, B(12)–H(12) [Mo(1)···B(12) 3.003(3) Å], in accordance with this being the most basic region in the cage, that is it is the vertex most susceptible to electrophilic attack.[15] Although the C atom was unambiguously located in the solid state structure, caution should be exercised when translating this to the solution state structure. This is demonstrated when the NMR spectroscopic data for complex **1** are taken into account (see below) which show the presence of two isomers in solution. Such potential ambiguity between solution and solid state structural assignment has previously been noted in related systems.[16] The antipodal cage B–H bond [H(12)] is canted off the B(12)–C(1) vector by 18(1)°, allowing efficient overlap between the bonding σ electron pair with a suitable orbital on the molybdenum centre in addition to minimising the steric interactions between the cage and the metal–ligand set. The Mo–H–B angle, at 152(2)°, also reflects this scenario. Other structures which have similar monodentate Mo–H–B linkages where cage hydrogen atoms have also been refined, show similar M–H–B angles, *viz.* $[Fe(Cp)(CO)_2(CB_{11}H_{12})]$ 141(2)° and $[Fe(TPP)(CB_{11}H_{12})]$ (TPP = tetraphenylphorphyrinate) 151(2)°.[6]

The solution spectroscopic data for compound **1** are in broad agreement with the solid state structure. The IR spectrum shows the expected two CO stretching bands (A_1 + E), at 2071 and 2001 cm^{-1} (average 2036 cm^{-1}) shifted to higher frequency than those from $[MoCp(CO)_3Cl]$. The bridging Mo–*H*(12)–B(12) atom is observed as a very broad stretch centred around 2240 cm^{-1} (2243 cm^{-1} in the solid state, see Experimental section). These ν_{CO} values can be compared with those found for $[MoCp(CO)_3(FBF_3)]$ at 2067 and 1975 cm^{-1} (average 2021 cm^{-1}) and $[MoCp(CO)_3(FSbF_5)]$ at 2079 and 2001 cm^{-1} (average 2040 cm^{-1}).[11] Both of these latter complexes contain weakly co-ordinated anions, and on a ranking ionicity scale of the $[M]^+\cdots[Y]^-$ interaction using CO stretching frequencies as a guide $CB_{11}H_{12}$ fits in between SbF_6 and BF_4 in this system. This order matches that found previously in $FeCp(CO)_2Y$ (Y = non-co-ordinating anion).[17] The $^1H\text{-}\{^{11}B\}$ NMR spectrum of **1** displays two peaks in the Cp region, in an approximate 1:2.5 ratio; signals are also observed due to cage C–H and B–H groups and a single, slightly broad, peak at δ −15.11 is assigned to Mo–*H*–B. This latter signal is observed as a partially collapsed quartet in the ^1H NMR spectrum with a reduced B–H coupling constant [*J*(BH) 87 Hz], as expected for a B–H–M bond. This peak is at unusually high field relative to that expected for B–H–M linkages (δ −5 to −11), similar to that which has been noted previously in related systems.[8c] On cooling to −90 °C the ratio of Cp resonances does not change but, due to thermal decoupling at lower temperatures, the high field resonance now is observed as two sharper peaks in the $^1H\text{-}\{^{11}B\}$ NMR spectrum (Fig. 2) in the same ratio as the two Cp resonances. We assign these two sets of peaks to positional isomers in which the $CB_{11}H_{12}$ cage is either bonded to the metal *via* the antipodal B(12)–H(12) bond or *via* a B–H linkage on the lower pentagonal belt. The observation of isomers in $[FeCp(CO)_2(CB_{11}H_{12})]$ and $[FeCp(CO)_2(CB_9H_{10})]$ has previously been noted by Strauss and co-workers.[16] For the latter, the two species are assigned as isomers in which the carborane bonds to the metal centre through an antipodal and a single lower pentagonal belt hydrogen atom respectively. Confirmation of the isomeric pair in **1** comes from inspection of the $^{11}B\text{-}\{^1H\}$ NMR spectrum. The major peaks observed are due to a C_5 symmetric carborane (assigned to the 12 isomer, assuming free rotation around the Mo–H–B vector) at δ −10.4 (1 B) −11.7 (5 B) and −13.9 (5 B) as well as less intense peaks, at δ −4.7 and −18.6, which we tentatively assign to the 7 isomer. The other signals for this isomer are presumably masked under the resonances for the major isomer. Coupling constants and chemical shifts are in accord with this formulation. For the 12 isomer the unique antipodal B–H appears to have a reduced coupling constant [*J*(HB) *ca.* 90 Hz], although as this peak appears as a shoulder to a larger high field peak this value should be treated with caution. This antipodal B–H coupling may be better gleaned from the ^1H NMR spectra (see above). Reduced *J*(HB) coupling constants have ample precedent as being diagnostic of M–H–B co-ordination,[18] while this signal is also shifted some 6 ppm upfield from $Ag[CB_{11}H_{12}]$, also indicative of {B–H} co-ordination. This upfield shift on *exo* co-ordination of an anionic borane has been observed previously.[19,20] For the 7

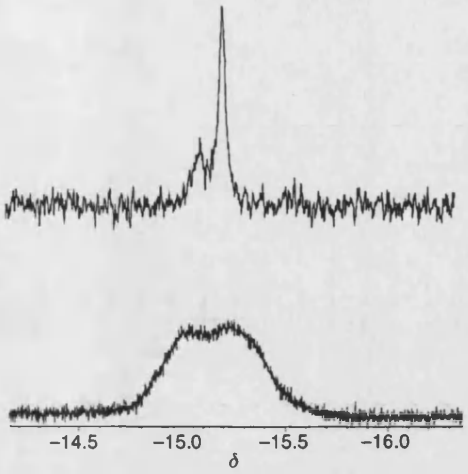

Fig. 2 High field region of the −90 °C (top) $^1H\text{-}\{^{11}B\}$ and room temperature ^1H (bottom) NMR spectra of compound **1** (CD_2Cl_2).

isomer, the antipodal B atom resonates at δ −4.7, similar to that found for $CsCB_{11}H_{12}$, while a peak integrating to 1 B at δ −18.6 is assigned to *B*(7)–H(7)–Mo which also exhibits a correspondingly smaller coupling constant [*J*(HB) 68 Hz].

Warming a sample of compound **1** in d_8-toluene to 80 °C resulted in coalescence of the two Cp peaks, demonstrating chemical exchange of the isomers, while the high field resonance at δ *ca.* −15 did not shift appreciably. Further confirmation of this exchange process comes from a ^{1}H EXSY experiment (EXchange SpectroscopY), which shows clear exchange cross peaks between the two Cp resonances. Thus the 12 and 7 isomers in complex **1** are in slow exchange with one another in solution.

It is interesting to compare the chemical robustness of **1** with the complexes previously prepared by Beck, such as $[MoCp(CO)_3(FBF_3)]$, which are extremely moisture sensitive and must routinely be handled at low temperature.[12] By contrast, **1** is stable at room temperature and can withstand handling in air for appreciable amounts of time. However, both compounds show similar frequencies for their CO stretching bands, suggesting that both $[BF_4]^-$ and $[CB_{11}H_{12}]^-$ possess similar weakly co-ordinating properties. This difference in chemical behaviour may arise either because the cage affords some kinetic stabilisation by virtue of its steric bulk or is intrinsically more strongly bound to the metal centre than $[BF_4]^-$. In support of this hypothesis, the cage anion in **1** is only replaced by strong nucleophiles such as chloride, weaker nucleophiles such as acetone or water leaving **1** unchanged after 30 minutes (according to NMR spectroscopy), while a strong Mo–H–B interaction is evidenced by the high field chemical shift and small value of *J*(BH) associated with H(12). Although spectroscopic measurements can provide a valuable comparative guide to the weakly co-ordinating properties of this class of anion, it is apparent that, in this system at least, this may not necessarily be a unique guide to the chemical properties of the system.

Having established the identity of the final product in this metathesis reaction our attention now turned to the intermediate species observed. Although intermediates have been observed in silver salt metathesis before, notably by Mattson and Graham,[21] it was the work of Reed and co-workers[6] that first highlighted the role of the counter ion in such reactions, observing by IR spectroscopy the formation of an intermediate adduct species, postulated as $[FeCp(CO)_2I{\cdot}AgCB_{11}H_{12}]$. It was suggested that the low nucleophilicity of the carborane counter ion resulted in the relatively long lifetime of this intermediate species. The corollary of this theory is that the anion is intimately involved in the rate-determining step in metathesis. However, to our knowledge, such intermediates have never been put on a firm spectroscopic or structural footing. Given the observation of an intermediate species in the reaction of $[MoCp(CO)_3Cl]$ with $Ag[CB_{11}H_{12}]$ to afford **1**, we sought further to characterise this product. For the chloride species, IR spectroscopy revealed that the intermediate was never the sole component in solution. Moving to $[MoCp(CO)_3I]$ resulted in a slowing down of this reaction (presumably a consequence of the reduced thermodynamic driving force of AgI formation over AgCl), so that complete metathesis took 7 days, and that after 30 minutes the only component of the reaction mixture was the intermediate species. Cessation of the reaction at this point, by cooling, followed by recrystallisation at low temperature afforded the intermediate species $[MoCp(CO)_3I{\cdot}Ag\{CB_{11}H_{12}\}]_2$, **2**, in *ca.* 50% isolated yield as a red crystalline solid. Compound **2** was fully characterised by X-ray crystallography, multinuclear NMR spectroscopy, IR and microanalysis.

The solid state structure of compound **2** is shown in Fig. 3, with relevant bond lengths and angles in Table 1. The molecule adopts a crystallographically imposed C_2 dimeric structure, with each of the silver atoms bonded to an iodine from each of the $\{CpMo(CO)_3I\}$ fragments. The central core is hinged

Table 1 Selected bond lengths (Å) and angles (°) for compounds **1** to **4**

Compound **1**			
Mo(1)–C(2)	2.011(3)	Mo(1)–C(3)	2.007(3)
Mo(1)–C(4)	2.017(3)	C(2)–O(1)	1.127(3)
C(3)–O(2)	1.123(3)	C(4)–O(3)	1.125(3)
Mo(1)–H(12)	1.90(3)	B(12)–H(12)	1.18(3)
Mo(1)···B(12)	3.003(3)		
Mo(1)–B(12)–C(1)	176.4(1)	Mo(1)–H(12)–B(12)	152(2)
Compound **2**			
Mo(1)–C(2)	1.997(10)	Mo(1)–C(3)	2.000(10)
Mo(1)–C(4)	2.027(9)	Mo(1)–I(1)	2.8599(8)
C(2)–O(2)	1.159(12)	O(3)–C(3)	1.22(11)
C(4)–O(4)	1.134(11)	Ag(1)–H(7)	1.96
I(1)–Ag(1)	2.9748(10)	Ag(1)–I(1A)	2.7599(9)
Ag(1)–B(7)	2.659(10)		
Ag(1A)–I(1)–Ag(1)	71.19(3)	I(1)–Ag(1)–I(1A)	97.10(3)
Compound **3**			
Mo(1)–C(2)	2.08(3)	Mo(1)–C(8)	1.99(2)
Mo(1)–C(9)	2.03(3)	C(2)–O(2)	1.09(3)
C(8)–O(1)	1.13(3)	C(9)–O(3)	1.05(3)
Mo(1)–I(1)	2.865(2)	Ag(1)–I(1)′	2.980(3)
Ag(1)–I(1)	2.778(3)	Ag(1)–Br(1)	2.803(3)
Ag(1)–Br(2)	2.771(3)		
Ag(1)–I(1)–Ag(1)′	81.41(8)	I(1)–Ag(1)–I(1)′	98.59(8)
Br(1)–Ag(1)–Br(2)	87.24(8)	Ag(1)–I(1)–Mo(1)	107.87(7)
Ag(1)′–I(1)–Mo(1)	114.20(7)		
Compound **4**			
Mo(1)–C(2)	1.988(3)	Mo(1)–C(3)	2.034(3)
Mo(1)–C(4)	2.049(3)	C(2)–O(1)	1.146(3)
C(3)–O(2)	1.128(4)	C(4)–O(3)	1.124(3)
Mo(1)–H(12)	1.97(5)	B(12)–H(12)	1.07(5)
Mo(1)–B(12)	2.969(3)		
Mo(1)–B(12)–C(1)	168.4(1)	Mo(1)–H(12)–B(12)	154(4)

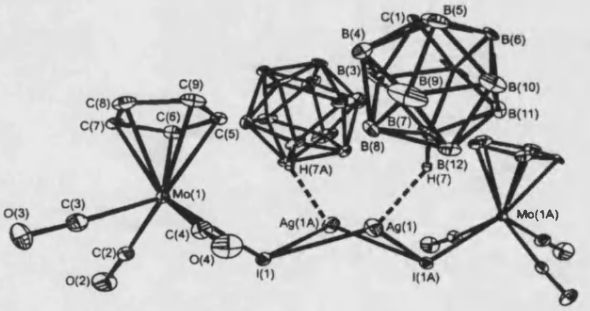

Fig. 3 Solid state structure of complex **2**. H atoms, apart from H(7), are omitted for clarity. Equivalent atoms generated by the operation $-x + \frac{1}{2}, -y, z$. Other details as in Fig. 1.

around the Mo(1A)–I(1A)–I(1)–Mo(1) vector by 123.3°, and has significantly different Ag–I bond lengths, Ag(1)–I(1) 2.9748(10) and Ag(1)–I(1A) 2.7599(9) Å. This difference in Ag–X distances in $\{Ag_2X_2\}$ fragments has been observed previously,[22] while the Ag–I bond lengths are a little longer and shorter respectively than found in similar {I–Ag–I} fragments.[23] There are silver adduct species of transition metal halides that show similar features as to those of **2**, such as the recently reported, ion pair separated, $[\{ReTp(NC_6H_4Me\text{-}p)(Ph)I\}_2Ag][PF_6]$[24] [Tp = tris(pyrazolyl) borate] in which a single silver bridges two {[Re]–I} fragments. However, to our knowledge, **2** is the first example of a $\{Ag_2X_2\}$ motif with appended metal fragments. The Mo–I bond distance in **2** lies within the expected range.[25] In the dimeric unit in **2** each silver has a close contact with a carb-

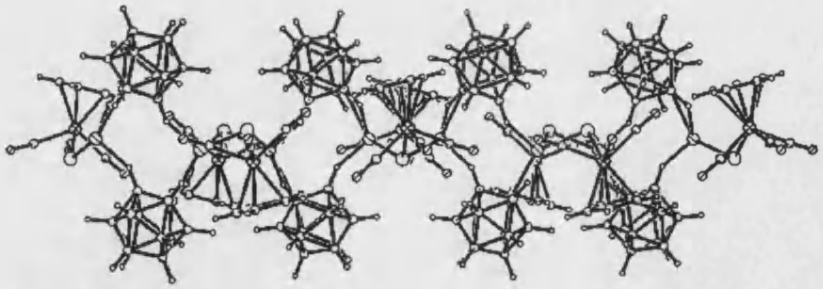

Fig. 4 The crystallographic packing diagram for complex **2** viewed along the *a* axis, showing the extended cation–anion interactions in the solid state.

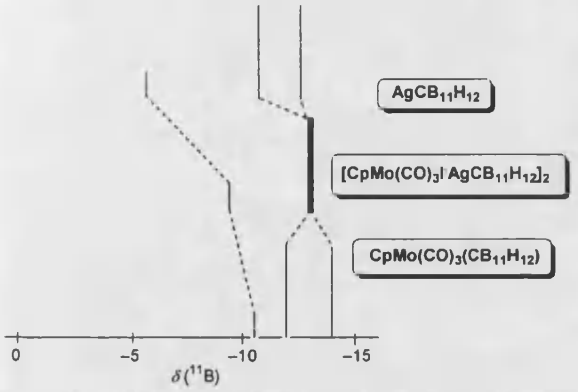

Fig. 5 Comparative ^{11}B NMR 'stick' diagram of complexes **1**, **2** and $Ag[CB_{11}H_{12}]$.

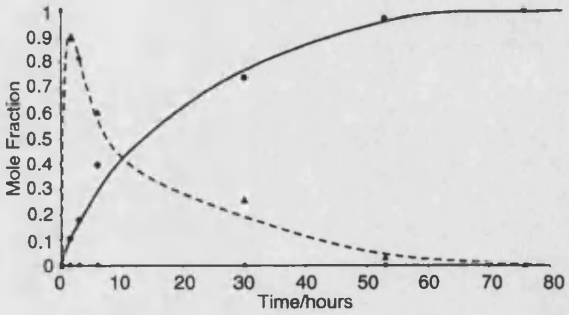

Fig. 6 Graph of the relative concentration of species **1**, **2** and $[MoCp(CO)_3I]$ against time in CD_2Cl_2 at room temperature. ▲ $[MoCp(CO)_3I{\cdot}Ag(CB_{11}H_{12})]_2$, ◆ $[MoCp(CO)_3I]$ and ● $[MoCp(CO)_3(CB_{11}H_{12})]$; relative concentrations measured as the integral values of the respective Cp resonances of each complex.

orane anion *via* a B–H–Ag 3c–2e interaction, B(7)–H(7)–Ag(1) 1.96 Å [Ag(1)–B(7) 2.659(10) Å]. This distance is slighter longer than that observed in the recently reported complex [2,2,2-$(CO)_3$-2-PPh_3-7,12-$(\mu\text{-}H)_2$-7,12-{$Ag(PPh_3)$}-*closo*-2,1-$MoCB_{10}H_9$], in which the $\{Ag(PPh_3)\}^+$ fragment is ligated in a dihapto manner on the surface of the cage.[26] The apparently vacant site around each silver atom in compound **2** is filled by an intramolecular Ag–H–B interaction. In particular, H(12) interacts with an adjacent silver [H(12)–Ag(1′) 1.96 Å] to form a ribbon of alternating cation and bridging anions (Fig. 4). This bridging mode has been observed previously in the simple silver salt of $[CB_{11}H_{12}]^-$, $Ag[CB_{11}H_{12}]{\cdot}2C_6H_6$.[27] The Ag–H and Ag–B bond distances therein are similar to those found in complex **2**.

Although it is unlikely that the polymeric structure in complex **2** persists in solution (CH_2Cl_2), evidence for interaction between the cage and silver comes from inspection of the NMR spectroscopic data. The ^1H-{^{11}B} NMR spectrum shows only one Cp resonance, at δ 5.75, with the expected peaks due to C–H and B–H groups observed in the range δ 2.56 to 1.86. No high field resonances were observed, even on cooling of the sample to −80 °C. The room temperature ^{11}B NMR spectrum shows two peaks at δ −9.11 and −12.65 in the ratio 1 : 10 (the latter peak representing a 5 + 5 coincidence), indicating C_5 symmetry in solution, and thus rapid site exchange of Ag–H–B interactions. These resonances are significantly shifted relative to those of 'free' $Ag[CB_{11}H_{12}]$. This change is better seen in a stick diagram (Fig. 5), which shows the relationship between the ^{11}B resonances of **1**, **2** and $Ag[CB_{11}H_{12}]$. The boron atoms that are involved in bonding to the metal centre (either Ag or Mo) are shifted upfield. Thus in **1** (only the 12 isomer is shown) only the unique boron atom resonance is shifted appreciably. Evidence for B–H interactions in **2** is demonstrated by both the upfield shift of B(12) from that found for $Ag[CB_{11}H_{12}]$ ($\Delta\delta_{11B}$ *ca.* 4 ppm) and the boron atoms associated with the lower pentagonal belt ($\Delta\delta_{11B}$ *ca.* 2 ppm). In agreement with this observation, the B–H coupling constant in **2** for the unique boron atom is slightly smaller than that found in $Ag[CB_{11}H_{12}]$ (119 *vs.* 125 Hz respectively). These chemical shifts suggest that in solution both the antipodal and lower pentagonal belt B–H groups interact with Ag, similar to the η^2-bidentate co-ordination found in $[Rh(COD)(CB_{11}H_{12})]$ in which the $\{Rh(COD)\}^+$ fragment is fluxional over the surface of the cage.[28] Further evidence for this unusual central core in solution comes from the ^{109}Ag resonance for **2**, δ 1335, which is significantly shifted from that normally found for silver(I)[29] complexes [*ca.* δ 500].

In order conclusively to prove that complex **2** is an intermediate on the pathway to **1** the reaction between $[MoCp(CO)_3I]$ and $Ag[CB_{11}H_{12}]$ in CD_2Cl_2 was monitored by ^1H NMR spectroscopy. The time dependent concentration profile of this reaction is shown in Fig. 6. This clearly shows the rapid formation of **2** and its gradual disappearance with concomitant growth of complex **1**. The mass balance of the system remains constant showing that **2** converts smoothly into **1**.

Having prepared complex **1**, *via* the intermediate species **2**, we were interested in investigating the silver salt metathesis reaction of $[MoCp(CO)_3X]$ with the even more non-nucleophilic, more weakly co-ordinating anion $[CB_{11}Br_6H_6]^-$, **B**. Reaction of $[MoCp(CO)_3Cl]$ with $Ag[CB_{11}H_{12}]$ did not result in any observable reaction by IR, only unchanged starting materials returned after 7 days stirring at room temperature. The parallel reaction using $[MoCp(CO)_3I]$, with the softer iodide atom, resulted in a gradual shift to higher wavenumber of the CO stretching bands over *ca.* 1 hour, moving to 2055 and 1975 cm^{-1} which are very similar, but slightly higher, than those found for **2**. ^1H, ^{11}B NMR spectroscopy and X-ray crystallography characterised this new species as $[MoCp(CO)_3I{\cdot}Ag(CB_{11}Br_6H_6)]_2$, **3**.

The solid state structure of complex **3**, shown in Fig. 7, bears close similarities with that found in **2**, with a centrosymmetric central $\{Ag_2I_2\}$ core appended with two $\{CpMo(CO)_3I\}$ fragments and two bidentate $CB_{11}Br_6H_6$ cages. The two metal fragments are orientated *trans* with respect to one another and

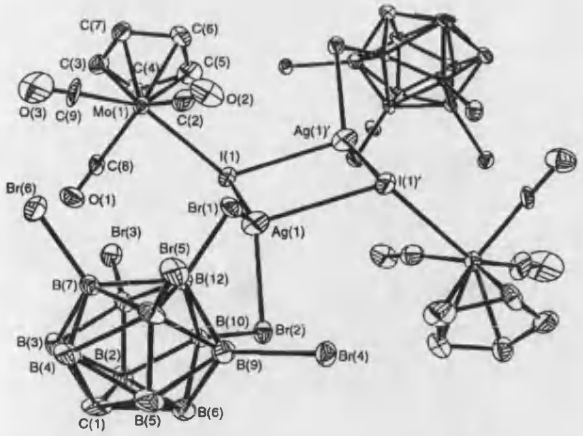

Fig. 7 Solid state structure of complex **3**. H atoms are omitted for clarity. Equivalent atoms generated by the operation $-x, -y, -z$. Other details as in Fig. 1.

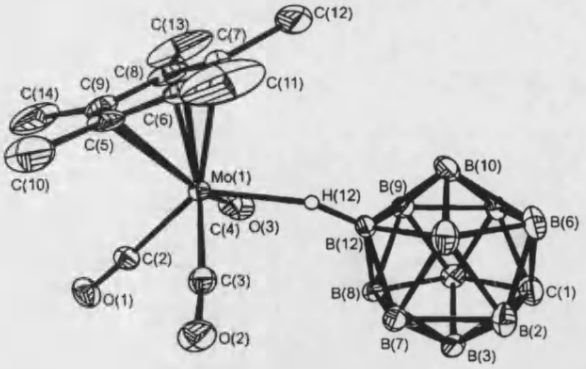

Fig. 8 Solid state structure of complex **4**. H atoms, apart from H(12), are omitted for clarity. Other details as in Fig. 1.

the central $\{Ag_2I_2\}$ core. This central core in **3** is planar, unlike that in **2**. In fact the $\{Ag_2I_2\}$ rhomboid is similar to that found in $[Ag_2X_2(PPh_3)_4]$[22] (X = Cl or Br) which also contains four-co-ordinate silver. The hexabromocarborane co-ordinates to the silver atoms in a bidentate manner reminiscent of that found in the simple silver salts $Ag[CB_{11}H_6Cl_6]\cdot C_6H_6$,[30] $Ag[1\text{-}CH_3\text{-}CB_{11}Br_{10}H]\cdot C_6H_4Me_2\text{-}p$.[31] The Ag–Br bonds lengths in **3** [Ag(1)–Br(1) 2.803(3), Ag(1)–Br(2) 2.771(3) Å] are slightly shorter than generally found for both $Ag[CB_{11}Br_6H_6]$ and related complexes[31,32] and dibromoalkane complexes of silver.[10]

The ^{1}H NMR spectrum of complex **3** shows two Cp resonances, in the approximate ratio 1:8, at δ 5.84 and 5.73 respectively, with a broad peak having a high field shoulder centred at δ 2.79 assigned to the cage C–H resonances. The ^{109}Ag NMR spectrum also shows two peaks, in the same approximate ratio as found in the ^{1}H NMR spectrum, at δ 1335 (relative intensity 8) and 1325 (1). We assign these pairs of peaks to two isomers in solution, one in which the Cp groups are *trans* and the other in which the Cp groups are *cis* to one another, with respect to the central $\{Ag_2I_2\}$ core. Both of these isomers retain equivalent Cp groups in solution (local C_2 and C_{2v} symmetry respectively), assuming facile libration around the Mo(1)–I(1) bond, consistent with the NMR data. The ^{11}B NMR spectrum displays three resonances in the ratio 1:5:5, suggesting either dissociation of the carborane in solution or rapid site exchange of Ag–Br–B interactions. Support of the latter comes from the observation of very similar ^{109}Ag NMR chemical shifts for **3** and **2** implying similar structures in solution. Dissolution of crystalline **3** generates an identical spectrum, with the same ratio of isomers observed.

Complex **3** remains unchanged when in CH_2Cl_2 solution for 7 days, with no metathesis product or decomposition observed (by ^{1}H NMR and IR spectroscopy). This is consonant with the low nucleophilicity of $[CB_{11}Br_6H_6]^-$ and the involvement of the anion in the rate-determining step in silver halide metathesis, by effectively halting metathesis at the intermediate stage in **3**. Addition of two equivalents of $Ag[CB_{11}H_{12}]$ to a CH_2Cl_2 solution of **3** results in immediate change in the IR spectrum to afford **2** which then gradually (7 days) changes to yield **1** in essentially quantitative yield. This result suggests that kinetic factors (*i.e.* the relative nucleophilicities of the anions) control the outcome of reaction in this system. Although there has been a recent brief report of arrested silver salt metathesis in R_3SiI systems,[1] to our knowledge this is the first fully characterised example involving a transition metal halide species in such a reaction that is clearly dependent only on the anion.

Reaction of $Ag[CB_{11}H_{12}]$ with the sterically more demanding $[MoCp^*(CO)_3Cl]$ [$Cp^* = \eta^5\text{-}C_5Me_5$] in CH_2Cl_2 resulted in a move to higher wavenumbers of the carbonyl stretches in the IR spectrum, but the ^{1}H NMR spectrum showed at least 5 Cp* peaks for the reaction mixture. Failing to cleanly abstract halide from $[MoCp^*(CO)_3Cl]$, an alternative method of introducing the carborane anion in to the co-ordination sphere was needed. Spencer and co-workers have demonstrated that reaction of $[H(OEt_2)_2][CB_{11}H_{12}]$ with $[PtR_2(L\text{–}L)]$ (R = Me or CH_2Bu^t, L–L = bidentate phosphine) affords complexes in which the carborane is η^2 ligated through two B–H–Pt bonds, *via* elimination of two equivalents of the corresponding alkane.[7] In this spirit, reaction of $[H(OEt_2)_x][CB_{11}H_{12}]$ with $[MoCp^*(CO)_3Me]$ at −78 °C afforded, on warming to room temperature, the new complex $[MoCp^*(CO)_3(x\text{-}\mu\text{-}H\text{-}1\text{-}CB_{11}H_{11})]$ **4** (x = 7 or 12) in essentially quantitative yield. The IR spectrum of this solution shows two CO stretching bands at 2057 and 1986 cm^{-1}, with a broad weak peak at 2229 cm^{-1} assigned to the Mo–H–B stretch. The isolation of **4** indicates that the failure of the silver salt metathesis is not due to steric hindrance in the final complex, and is perhaps due to steric interactions in a condensed intermediate species similar to **2**. The solid state structure of **4** is shown in Fig. 8, and selected bond lengths and angles are given in Table 1. The carborane anion in complex **4** is bound *via* the antipodal boron atom in the expected B–H–M 3c–2e bond, with the bridging hydrogen atom located and freely refined. Given the increased bulk of the Cp* ligand it is perhaps somewhat surprising that the Mo(1)–B(12) distance [2.969(3) Å] is slightly shorter than in **1**. The only gross structural difference between **1** and **4** is that the carborane ligand in the latter is tilted further away from the Cp* ring, in contrast to **1** where the carborane anion is closer to the Cp ring. This does not significantly effect the Mo–H(12)–B(12) angle which at 154(4)° is broadly similar.

The ^{1}H and ^{11}B NMR spectra demonstrate the presence of an isomeric pair in solution, as found for complex **1**, which is assigned to $[Mo(Cp^*)(CO)_3(x\text{-}\mu\text{-}H\text{-}1\text{-}CB_{11}H_{11})]$ (x = 12 or 7). Thus, two Cp* peaks are observed at δ 2.08 and 2.04 in the ratio 1:3, a situation that is mirrored in the ^{11}B NMR spectrum with two sets of peaks also seen. As found for **1** it is the 12 isomer that is the major component in solution. Although the structural metrics in **4** are similar to those in **1**, the increased steric bulk in **4** is manifested by the lower coalescence temperature for the fast exchange limit of the two isomers. Heating the sample to 40 °C (compared with 80 °C for **1**) afforded a single sharp line in the Cp* region of the ^{1}H NMR spectrum. The bridging hydrogen is observed in complex **4** as a partially collapsed quartet, centred at δ −13.5, slightly to lower field than that found for **1** indicating a weaker (*i.e.* less hydridic) Mo–H–B bond. This signal also has a larger coupling constant [J(HB) 98 Hz], as expected for a weaker Mo–H–B interaction. Reflecting this less intimate Mo–H–B bond compared with that in **1**, addition of water rapidly (<5 minutes) displaces the cage anion from the co-ordination sphere of the metal fragment.

Table 2 Crystallographic data for the new complexes **1** to **4**

	1	2	3	4
Empirical formula	$C_9H_{17}B_{11}MoO_3$	$C_9H_{17}AgB_{11}IMoO_3$	$C_9H_{11}AgB_{11}Br_6IMoO_3$	$C_{14}H_{27}B_{11}MoO_3$
Formula weight	388.08	622.85	1096.26	458.21
T/K	293(2)	120(2)	170(2)	170(2) K
Crystal system	Monoclinic	Orthorhombic	Triclinic	Orthorhombic
Space group	$P2_1/c$	*Pnna*	$P\bar{1}$ (no. 2)	$P2_12_12_1$
a/Å	10.1425(19)	13.8843(4)	7.7200(7)	9.75770(10)
b/Å	10.4875(13)	15.7193(4)	11.8360(8)	14.1357(2)
c/Å	16.515(2)	18.1490(6)	14.7530(15)	16.2310(2)
α/°			90.871(5)	
β/°	93.76		96.678(4)	
γ/°			90.355(5)	
U/Å^3	1752.9(4)	3961.0(2)	1338.7(2)	2238.77(5)
Z	4	8	2	4
μ/mm^{-1}	0.749	3.186	11.320	0.598
Reflections collected	4157	7282	11052	25921
Independent reflections	3801 [R_{int} = 0.0150]	3870 [R_{int} = 0.0476]	4679 [R_{int} = 0.0967]	5110 [R_{int} = 0.0276]
Final $R1$, $wR2$ indices [$I > 2\sigma(I)$]	0.0289, 0.0780	0.0563, 0.1101	0.0917, 0.2541	0.0295, 0.0859
(all data)	0.0369, 0.0806	0.0725, 0.1145	0.1324, 0.2844	0.0302, 0.0870

Experimental

General

All manipulations were carried out under an argon atmosphere using standard Schlenk line or dry-box techniques. CH_2Cl_2 was distilled from CaH_2, hexane from sodium.[33] NMR spectra were measured on a Varian-400 or JEOL-270 FT-NMR spectrometer in CD_2Cl_2 solutions. Residual protio solvent was used as reference (CD_2Cl_2, δ 5.33) in ^{1}H NMR, $BF_3{\cdot}OEt_2$ (external) in ^{11}B NMR spectra. Infrared spectra were measured on a Perkin-Elmer 1600 FT spectrometer. Elemental analysis was performed in-house in the Department of Chemistry, University of Bath. The complexes [$MoCp(CO)_3X$] (X = Cl or I),[34] [$MoCp^*(CO)_3Me$],[35] $Ag[CB_{11}H_{12}]$,[27] $Ag[CB_{11}Br_6H_6]$[6] and $[H(OEt_2)_x][CB_{11}H_{12}]$[36] were prepared by the published literature routes or variations thereof.

Preparations

$[MoCp(CO)_3(CB_{11}H_{12})]$ 1. *From [$MoCp(CO)_3Cl$].* The compounds [$MoCp(CO)_3Cl$] (0.134 g, 0.48 mmol) and $Ag[CB_{11}H_{12}]$ (0.120 g, 0.48 mmol) were stirred in 30 ml of CH_2Cl_2 in the dark for 2 days. The solution was filtered through Celite and solvent removed *in vacuo* to leave 0.158 g (0.41 mmol, 85% yield) of a red-brown solid. Crystals suitable for an X-ray diffraction study were grown by dissolving the solid up in the minimum of CH_2Cl_2, layering with hexane and then placing in a freezer overnight at −30 °C to yield 0.82 g (0.21 mmol) of dark red crystals: yield 44%. $\delta_{H\{^{11}B\}}$(400 MHz, CD_2Cl_2, 22 °C) 5.86*, 5.79 (5H, s), 2.53 (1H, s), 1.79 (5H, s), 1.66 (5H, s) and −15.11 [1H, partially collapsed quartet, J(BH) 87 Hz]. $\delta_{^{11}B}$(128 MHz, CD_2Cl_2) −4.72* [1B, d, J(HB) *ca.* 151], −10.41 [1B, d, sh, J(HB) *ca.* 90], −11.72 [5B, d, J(HB) 151], −13.85 [5B, d, J(HB) 151] and −18.56* [1B, d, J(HB) 68 Hz]. Values with an asterisk indicate peaks of the 7 isomer. Found: C, 28.0; H, 4.4. Calc. for $C_9H_{17}B_{11}MoO_3$: C, 27.9; H, 4.4%. IR (cm^{-1}): (KBr) 2582m, 2549m, 2243w (broad), 2067s, 1991s and 1980s; (CH_2Cl_2) 2573m, 2230w, br, 2071s and 2001s, br.

From [$MoCp(CO)_3I$]. The compounds [$MoCp(CO)_3I$] (0.029 g, 0.080 mmol) and $Ag[CB_{11}H_{12}]$ (0.021 g, 0.84 mmol) were stirred in 20 ml of CH_2Cl_2 in the dark for 7 days. Work up was identical to that above and 0.025 g (0.064 mmol) of a red-brown solid was obtained in 81% yield. IR and NMR spectroscopic data identical to those from the previous method.

$[MoCp(CO)_3I{\cdot}Ag(CB_{11}H_{12})]_2$ 2. The compounds [$MoCp(CO)_3I$] (0.044 g, 0.12 mmol) and $Ag[CB_{11}H_{12}]$ (0.030 g, 0.12 mmol) were stirred in 30 ml of CH_2Cl_2 in the dark. After 3.5 hours the solution was filtered through Celite and solvent removed *in vacuo* in the dark, to leave 0.037 g (0.095 mmol, 79% yield) of a light sensitive red solid. Crystals suitable for an X-ray diffraction study were grown by dissolving the solid in the minimum of CH_2Cl_2, layering with hexane, and placing in a freezer overnight at −30 °C. $\delta_{H\{^{11}B\}}$(400 MHz, CD_2Cl_2) 5.75 (5H, s), 2.56 (1H, s, $C_{cage}H$), 2.12 (1H, s, BH) and 1.86 (10H, 5+ 5 coincidence, s, BH). $\delta_{^{11}B}$(128 MHz, CD_2Cl_2) −9.11 [1B, d, J(BH) 119] and −12.65 [10B, d, 5+ 5 coincidence, J(BH) 144 Hz]. $\delta_{^{109}Ag}$(19MHz, CD_2Cl_2) 1335 (s). Found: C, 17.8; H, 2.8. Calc. for $C_9H_{17}AgB_{11}IMoO_3$: C, 17.4; H, 2.7%. IR (cm^{-1}): (KBr) 2556m, 2531m, 2041s, 1971s and 1950s; (CH_2Cl_2) 2570m, 2054s and 1973s br.

$[MoCp(CO)_3I{\cdot}Ag(CB_{11}Br_6H_6)]_2$ 3. $Ag[CB_{11}Br_6H_6]$ (0.060 g, 0.083 mmol) and [$MoCp(CO)_3I$] (0.028 g, 0.075 mmol) were stirred in 20 ml of CH_2Cl_2 in the dark for 5 hours. The red solution formed was filtered through Celite and the solvent removed from the filtrate *in vacuo* to leave a red solid. Crystals suitable for an X-ray diffraction study were grown by redissolving the solid product in the minimum of CH_2Cl_2 and allowing slow evaporation of solvent under a flow of argon to yield 0.041 g (0.021 mmol, yield 56%) of dark red crystals. δ_H(400 MHz, CD_2Cl_2) 5.84 (s, peak from isomer), 5.73 (5H, s) and 2.79 (1H, s). $\delta_{^{11}B}$ (128 MHz, CD_2Cl_2) −0.7 (1B, s), −7.86 (5B, s) and −17.94 [d, 5B, J(BH) 152 Hz]. $\delta_{^{109}Ag}$(19 MHz, CD_2Cl_2) 1335 (s, relative intensity 8) and 1325 (s, 1). Found: C, 9.18; H, 1.11. Calc. for $C_9H_{11}AgB_{11}Br_6IMoO_3$: C, 9.86; H, 1.00%. IR (CH_2Cl_2, cm^{-1}): 2613w, 2055s and 1975s br.

$[MoCp^*(CO)_3(CB_{11}H_{12})]$ 4. The compound $[H(OEt_2)_x][CB_{11}H_{12}]$ (0.007 g, 0.039 mmol (assuming $x = 2$)) was measured into a pre-weighed Schlenk vessel at −78 °C. To this was added a solution of [$MoCp^*(CO)_3Me$] (0.014 g, 0.042 mmol) in 20 ml of CH_2Cl_2 with stirring at −78 °C. A change from yellow to orange-red was observed as the reactant mixture was allowed to warm slowly to room temperature. The IR spectrum indicated the reaction had only reached approximately 30% completion. A second 10 mg portion of $[H(OEt_2)_x][CB_{11}H_{12}]$ was added and another IR spectrum taken 5 minutes later indicated all of the [$MoCp^*(CO)_3Me$] starting material had been consumed. The solvent was removed *in vacuo* and the ^{1}H NMR spectrum of the red solid formed indicated no starting material or excess of $[H(OEt_2)_x][CB_{11}H_{12}]$ present. A ^{11}B NMR spectrum of the contents of the cold trap of the Schlenk line showed the presence of $[H(OEt_2)_x][CB_{11}H_{12}]$. The product was re-dissolved in the minimum of CH_2Cl_2, layered with hexane and stored in a freezer at −30 °C to afford orange-red crystals suitable for an X-ray diffraction study. δ_{1H}(400 MHz, CD_2Cl_2) 2.51 (1H, s, br),

2.08*, 2.04 (15H, s) and −13.5 [1H, partially collapsed quartet, J(BH) 98 Hz]. δ_{11B}(128 MHz, CD_2Cl_2) −5.15 [1B, d, J(HB) 128]*, −10.62 [1B, d, sh], −11.91 [5B, d, J(HB) 150], −13.94 [5B, d, J(HB) 167] and −18.79 [1 B, d br, J(HB) *ca.* 65 Hz]* (values with an asterisk indicate peaks relating to the 7 isomer of the product). IR (CH_2Cl_2, cm^{-1}): 2571m, 2229w br, 2057s and 1986s br.

X-Ray crystallography

The crystal structure data for compound **1** were collected on an Enraf-Nonius CAD4 diffractometer, those for **2**, **3** and **4** on a Nonius KappaCCD. Structure solution followed by full-matrix least squares refinement was performed using the SHELX suite of programs throughout.[37] Hydrogens were included at calculated positions in all cases except for H12 in **1** and **4**. In these instances the hydrogen atom was readily located in the penultimate difference Fourier electron density map and allowed to refine freely. The crystal data presented for **3** arose from the fourth data set collected on a crystal from the batch, in an effort to improve the quality of the refinement. Although the mosaicity of the final crystal selected (0.874°) was not excessive, it does not adequately reflect the poor peak profiles observed during data frames. However, the data quality *is* reflected in the errors on the unit cell parameters, the R values and in the large peak and hole that are manifest in the final difference Fourier map despite the small sample size and application of an absorption correction. A brief perusal of the thermal displacement parameters of complex **4** suggests that there might be some libration in the pentamethylcyclopentadienyl ring. Unfortunately, stringent efforts to model this disorder failed consistently. Crystal data are summarised in Table 2.

CCDC reference number 186/2282.

See http://www.rsc.org/suppdata/dt/b0/b008222h/ for crystallographic files in .cif format.

Acknowledgements

The Royal Society (A. S. W.) and the University of Bath (N. J. P.) are thanked for financial support. The JREI/EPSRC and The University of Bath are thanked for providing funds to purchase an X-ray diffractometer at Bath. The EPSRC and King's College London are thanked for provision of the X-ray diffractometer and the Nuffield Foundation for computing equipment (J. W. S.). Dr Jonathon Rourke is thanked for his assistance in obtaining the ^{109}Ag NMR spectra, Dr Georgina M. Rosair is thanked for initial structural investigations on complex **1**.

References

1 C. A. Reed, *Acc. Chem. Res.*, 1998, **31**, 133.
2 S. H. Strauss, *Chem. Rev.*, 1993, **93**, 927.
3 C. A. Reed, N. L. P. Fackler, K.-C. Kim, D. Stasko, D. R. Evans, P. D. W. Boyd and C. E. F. Rickard, *J. Am. Chem. Soc.*, 1999, **121**, 6314.
4 A. J. Lupinetti, M. D. Havighurst, S. M. Miller, O. R. Anderson and S. H. Strauss, *J. Am. Chem. Soc.*, 1999, **121**, 1190.
5 D. J. Crowther, S. L. Borkowsky, D. Swenson, T. Y. Meyer and R. F. Jordan, *Organometallics*, 1993, **12**, 2897.
6 D. J. Liston, Y. J. Lee, W. R. Scheidt and C. A. Reed, *J. Am. Chem. Soc.*, 1989, **111**, 6643; K. Shelly, C. A. Reed, Y. J. Lee and W. R. Scheidt, *J. Am. Chem. Soc.*, 1986, **108**, 3117.
7 G. S. Mhinzi, S. A. Litster, A. D. Redhouse and J. L. Spencer, *J. Chem. Soc., Dalton Trans.*, 1991, 2769.
8 (*a*) D. D. Ellis, A. Franken, P. A. Jelliss, J. A. Kautz, F. G. A. Stone and P.-Y. Yu, *J. Chem. Soc., Dalton Trans.*, 2000, 2509; (*b*) J. C. Jeffery, P. A. Jelliss, L. H. Rees and F. G. A. Stone, *Organometallics*, 1998, **17**, 2258; (*c*) D. D. Ellis, P. A. Jelliss and F. G. A. Stone, *Organometallics*, 1999, **18**, 4982.
9 E. Y.-X. Chen and T. J. Marks, *Chem. Rev.*, 2000, **100**, 1391.
10 D. M. Van Seggen, P. K. Hurlburt, O. P. Anderson and S. H. Strauss, *Inorg. Chem.*, 1995, **34**, 3453.
11 W. Beck and K. Sünkel, *Chem. Rev.*, 1988, **88**, 1405.
12 W. Beck, *Inorg. Synth.*, 1990, **28**, 1.
13 T.-Y. Cheng, B. S. Brunschwig and R. M. Bullock, *J. Am. Chem. Soc.*, 1998, **120**, 13121.
14 N. J. Patmore, J. W. Steed and A. S. Weller, *Chem. Commun.*, 2000, 1055.
15 T. Jelinek, P. Baldwin, W. R. Scheidt and C. A. Reed, *Inorg. Chem.*, 1993, **32**, 1982.
16 S. V. Ivanov, J. J. Rockwell, S. M. Miller, O. P. Anderson, K. A. Solntsev and S. H. Strauss, *Inorg. Chem.*, 1996, **35**, 7882.
17 Z. Xie, T. Jelinek, R. Bau and C. A. Reed, *J. Am. Chem. Soc.*, 1994, **116**, 1907.
18 S. A. Brew and F. G. A. Stone, *Adv. Organomet. Chem.*, 1993, **35**, 135.
19 M. Elrington, N. N. Greenwood, J. D. Kennedy and M. Thornton-Pett, *J. Chem. Soc., Dalton Trans.*, 1987, 451.
20 Interestingly, *metallocarboranes* with *exo* co-ordinated metal fragments and a metal–metal bond show downfield shifts of the involved boron atoms,[18] opposite to that found for $CB_{11}H_{12}$ and other *closo* carboranes and boranes, while the addition of bridging hydrogen atoms across M–B bonds in M_yB_x species normally shifts ^{11}B resonances upfield (N. P. Rath and T. P. Fehlner, *J. Am. Chem. Soc.*, 1987, **109**, 5273).
21 B. M. Mattson and W. A. G. Graham, *Inorg. Chem.*, 1981, **20**, 3186.
22 G. A. Bowmaker, Effendy, J. V. Hanna, P. C. Healy, B. W. Skelton and A. H. White, *J. Chem. Soc., Dalton Trans.*, 1993, 1387.
23 T. N. Sal'nikova, V. G. Andrianov and Yu. T. Struchkov, *Koord. Khim.*, 1976, 707.
24 W. S. McNeil, D. D. DuMez, Y. Matano, S. Lovell and J. M. Mayer, *Organometallics*, 1999, **18**, 3715.
25 See for example M. A. Bush, A. D. U. Hardy, L. Manojlovic-Muir and G. A. Sim, *J. Chem. Soc. A*, 1971, 1003.
26 D. D. Ellis, A. Franken, P. A. Jelliss, J. A. Kautz, F. G. A. Stone and P.-Y. Yu, *J. Chem. Soc., Dalton Trans.*, 2000, 2509.
27 K. Shelly, D. C. Finster, Y. J. Lee, W. R. Scheidt and C. A. Reed, *J. Am. Chem. Soc.*, 1985, 107, 5955.
28 A. S. Weller, M. F. Mahon and J. W. Steed, *J. Organomet. Chem.*, 2001, **614–615**, 113.
29 R. Eujen, B. Hoge and D. J. Brauer, *Inorg. Chem.*, 1997, **36**, 1464.
30 Z. Xie, B.-M. Wu, T. C. W. Mak, J. Manning and C. A. Reed, *J. Chem. Soc., Dalton Trans.*, 1997, 1213.
31 Z. Xie, C.-W. Tsang, E. T.-P. Sze, Q. Yang, D. T. W. Chan and T. C. W. Mak, *Inorg. Chem.*, 1998, **37**, 6444.
32 Z. Xie, R. Bau and C. A. Reed, *Angew. Chem., Int. Ed. Engl.*, 1994, **33**, 2433.
33 D. F. Shriver and M. A. Drezdon, *The Manipulation of Air-Sensitive Compounds*, 2nd edn., Wiley-Interscience, New York, 1986.
34 T. S. Piper and G. Wilkinson, *J. Inorg. Nucl. Chem.*, 1956, **3**, 104.
35 R. B. King and M. B. Bisnette, *J. Organomet. Chem.*, 1967, **8**, 287.
36 T. Jelinek, J. Plesek, S. Hermanek and B. Stibr, *Collect. Czech. Chem. Commun.*, 1986, **51**, 819.
37 G. M. Sheldrick, SHELX 97, A computer program for refinement of crystal structures, University of Göttingen, 1997.

Notes

Chelating Monoborane Phosphines: Rational and High-Yield Synthesis of $[(COD)Rh\{(\eta^2\text{-}BH_3)Ph_2PCH_2PPh_2\}][PF_6]$ (COD = 1,5-cyclooctadiene)

Michael Ingleson, Nathan J. Patmore, Giuseppe D. Ruggiero, Christopher G. Frost, Mary F. Mahon, Michael C. Willis, and Andrew S. Weller*

Department of Chemistry, University of Bath, Bath, U.K. BA2 7AY

Received May 8, 2001

*Summary: The rational and high-yield synthesis of [(COD)Rh{(η²-BH₃)Ph₂PCH₂PPh₂}][PF₆] (**1**), which bears a chelating monoborane phosphine, is reported; the solid-state structure shows that the borane coordinates to the metal via two 2e−3c B−H−Rh bonds, which in solution at room temperature are fluxional between all three B−H bonds. Complex **1** is isolated as an air-stable crystalline salt, and its applicability as a catalyst in organic synthesis has been demonstrated in the coupling of boronic acids with enones.*

Introduction

The coordination chemistry of phosphine boranes of the type $R_3P{\cdot}BH_3$ and $(R_3P)_2{\cdot}B_2H_4$ has recently been explored by Shimoi, as exemplified by the synthesis of complexes such as $(CO)_5Cr(\eta^1\text{-}R_3P{\cdot}BH_3)$ and $(CO)_4Cr(\eta^1{:}\eta^1\text{-}(R_3P)_2{\cdot}B_2H_4)$.[1] However, the related compounds in which the borane moiety is complexed with a chelating phosphine have only been mentioned twice in the literature. One of these, recently reported by Barton et al., has a dppm (diphenylphosphinomethane) ligand with an appended BH_3 unit that is chelated to a polyhedral rhodathiaborane (**A**).[2] The other contains a formally anionic $[PR_3{\cdot}BH_2]^-$ ligand chelated to a cobaltacarbonyl: $(CO)_2(\eta^1\text{-dppm})Co(\mu\text{-dppm})BH_2$ (**B**).[3] Both complexes are formed by addition of a monoborane reagent to a suitable metal−phosphine precursor by an undetermined mechanism. It struck us that both of these chelating ligands contain dppm functionalized with monoborane and that such a situation results in the formation of a favored five-membered chelate ring. Consequently we have pursued the synthesis of transition metal coordination complexes with *preformed* $Ph_2PCH_2PPh_2{\cdot}BH_3$,[4] seeking a high-yield, rational route toward complexes that contain this interesting hybrid[5] ligand. This report outlines the synthesis, structural and preliminary catalytic studies of one such complex: $[(COD)Rh\{(\eta^2\text{-}BH_3)Ph_2PCH_2PPh_2\}][PF_6]$ (**1**) (COD = cycloocta-1,5-diene).

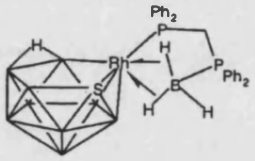

(A)

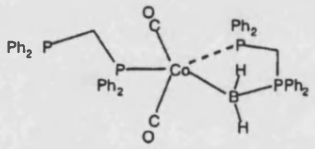

(B)

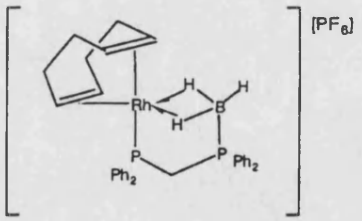

(1)

Results and Discussion

Addition of $Ph_2PCH_2PPh_2{\cdot}BH_3$ to $[(COD)RhCl]_2$, followed by halide abstraction using $TlPF_6$, affords complex **1**, $[(COD)Rh\{(\eta^2\text{-}BH_3)Ph_2PCH_2PPh_2\}][PF_6]$, in excellent yield (85% isolated) as an air-stable microcrystalline solid after workup. Full spectroscopic analysis was performed on this salt, but repeated attempts to produce crystals suitable for X-ray diffraction failed. Anion metathesis replacing $[PF_6]^-$ with the bulky $[BPh_4]$ anion

* Corresponding author. E-mail: a.s.weller@bath.ac.uk. Fax: +44 (1225) 826231.

(1) Shimoi, M.; Nagai, S.-I.; Ichikawa, M.; Kawano, Y.; Katoh, K.; Uruichi M.; Ogino, H. *J. Am. Chem. Soc.* **1999**, *121*, 11704.
(2) Macías, R.; Rath, N. P.; Barton, L. *Angew. Chem., Int. Ed.* **1999**, *38*, 162.
(3) Elliot, D. J.; Levy, C. J.; Puddephatt, R. J.; Holah, D. G.; Hughes, A. N.; Magnuson, V. R.; Moser, I. M. *Inorg. Chem.* **1990**, *29*, 5014.
(4) Martin, D. R.; Merkel, C. M.; Ruiz, J. P. *Inorg. Chim. Acta* **1986**, *115*, L29.
(5) Braunstein, P.; Naud, F. *Angew. Chem., Int. Ed.* **2001**, *40*, 680.

10.1021/om0103759 CCC: $20.00
Publication on Web 10/08/2001

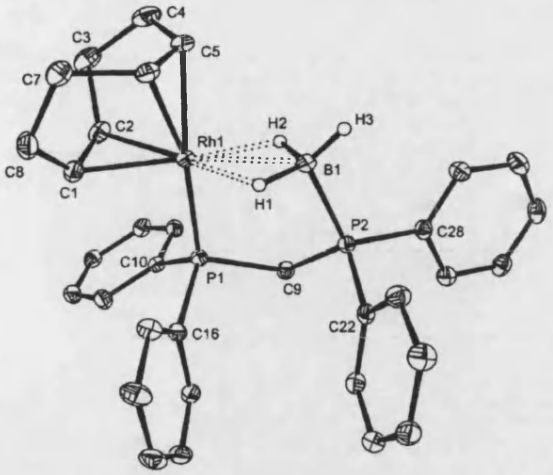

Figure 1. Cation in $[(COD)Rh\{(\eta^2\text{-}BH_3)Ph_2PCH_2PPh_2\}][BPh_4]\cdot C_7H_8$, **1**. Ellipsoids are shown at the 30% probability level.

Table 1. Selected Bond Lengths (Å) and Angles (deg) for Complex 1

B(1)−H(1)	1.16(3)	Rh(1)−H(1)	1.82(4)
B(1)−H(2)	1.16(3)	Rh(1)−H(2)	1.91(3)
B(1)−H(3)	1.09(3)	Rh(1)−B(1)	2.313(3)
Rh(1)−C(1)	2.126(3)	Rh(1)−C(2)	2.124(3)
Rh(1)−C(5)	2.249(3)	Rh(1)−C(6)	2.271(3)
Rh(1)−P(1)	2.2743(7)	Rh(1)−B(1)	2.313(3)
P(1)−C(9)	1.849(3)	P(1)−B(1)	1.923(3)
P(1)−B(1)−H(1)	102(3)	P(1)−B(1)−H(2)	102(1)
P(1)−B(1)−H(3)	114(1)	P(2)−C(9)−P(1)	109.74(13)
P(1)−Rh(1)−B(1)	87.26(8)	C(9)−P(1)−Rh(1)	110.93(9)
Rh(1)−B(1)−P(2)	113.07(15)		

afforded suitable crystals for a X-ray study. The solid-state structure of the cation in **1** is presented in Figure 1. This shows that the rhodium is bracketed by a coordinated COD ligand and the chelating phosphine borane. The phosphine ligates to the metal via both the terminal phosphine and BH_3 moiety, the latter through *two* B−H−Rh three-center two-electron bonds. This η^2-coordination motif of the borane was initially unexpected, as the formally d^8 Rh(I) metal center requires only one B−H−Rh interaction to attain a 16-electron count. However, similar pentacoordination has been observed previously in $Rh(7\text{-}PPh_2\text{-}8\text{-}Me\text{-}7,8\text{-}C_2B_9H_{10})(COD)$.[6] All hydrogen atoms on the borane were located and freely refined in the crystal structure. Inspection of the bond lengths and angles surrounding B(1) (Table 1) shows that the two bridging hydrogens [H(1) and H(2)] exhibit similar distances from Rh(1). Notwithstanding that all B−H distances are similar within the bounds of experimental error, there also appears to be a trend suggesting that the B−H bond distances to H(1) and H(2) are slightly longer than found for the terminal hydride, H(3), as expected. The BH_3 unit is not tetrahedral, the two bridging hydrogens having compressed P(1)−B(1)−H angles to facilitate efficient bonding with the metal center. The Rh−B distance [2.313(3) Å] is similar to that found in **A** [2.323(2) Å] which also contains a bidentate $\{PBH_2\}$ ligand, this bond length also comparable to those found in $\{RhL_2\}$ fragments *exo*

(6) Viñas, C.; Núñez, R.; Teixidor, F.; Kivekäs, R.; Sillanpää, R. *Organometallics* **1998**, *17*, 2376.

Table 2. Crystallographic Data for Complex 1

empirical formula	$C_{64}H_{65}B_2P_2Rh$
fw	1020.63
temperature (K)	150(2)
cryst syst	monoclinic
space group	$P2_1/n$
a (Å)	15.2130(2)
b (Å)	17.1060(3),
c (Å)	21.2800(3)
α (deg)	90
β (deg)	106.2960(9),
γ (deg)	90
U (Å^3)	5315.29(14)
Z	4
μ (mm^{-1})	0.421
no. of reflns collected	61 419
no. of ind reflns	12 152 [R_{int} = 0.0887]
final R1, wR2 indices [$I > 2\sigma(I)$]	0.0430, 0.0905
R1, wR2 indices (all data)	0.0765, 0.1037
largest diff peak and hole	0.805 and −0.677 e Å^{-3}

coordinated to polyboranes.[7] The P(1)−Rh(1)−B(1) bite angle at 87.26(8)° is also similar to that in **A** [88.36(6)°]. Comparison of the $Rh-C_{COD}$ bond lengths demonstrates the differing *trans* influences operating in the chelating ligand in **1**. In particular, the alkene carbon−Rh bonds *trans* to the weakly bound $\{BH_2\}$ fragment are significantly shorter than those *trans* to the phosphine [2.125 Å average for Rh−C(1), Rh−C(2) versus 2.259 Å average for Rh−C(5), Rh−C(6)].

The η^2-BH_3 binding motif observed in the solid state is not maintained in solution at room temperature, where the NMR spectrum reveals that all of the borane hydrogen atoms are equivalent, with one integral 3H resonance observed at δ −0.25 ppm. This demonstrates that rapid exchange of the three BH bonds in bonding to the Rh center occurs, facilitated through rotation around the P−B bond (as has been observed previously in compound **A**[2]). Cooling to −50 °C resulted in replacement of this single resonance by two peaks in the $^1H\{^{11}B\}$ NMR spectrum, at 2.25 ppm (1 H) and −1.48 ppm (2 H), associated with terminal B−H and bridging Rh−H−B bonds, respectively. This low-temperature NMR spectrum is fully consistent with the solid-state structure. Further cooling to −90 °C did not affect the observed spectrum. The remaining observed ^1H, ^{31}P, and ^{11}B NMR resonances are entirely consistent with the proposed structure. DFT calculations on complex **1** are in agreement with the observed solid-state and low-temperature solution structures, η^2-coordination of the borane favored over η^1-binding on optimization at the B3PW39/6-31G** level.

We have tested the applicability of complex **1** in C−C bond-forming reactions via 1,4-addition of boronic acids to α,β-unsaturated ketones.[8] Preliminary investigations have shown that **1** is an effective precatalyst (1 mol % catalyst loading) for the addition of phenylboronic acid to cyclohexenone to afford 3-phenylcyclohexanone in 82% isolated yield. We have not investigated the structure of the active catalyst in this reaction, but it is likely that the COD ligand dissociates to afford a species such as $[Rh\{(\eta^2\text{-}BH_3)Ph_2PCH_2PPh_2\}(solvent)][PF_6]$ (solvent = dimethoxyethane).[9]

(7) Weller, A. S.; Mahon, M. F.; Steed, J. W. *J. Organomet. Chem.* **2000**, *614–615*, 113.

(8) Sakai, M.; Hayashi, H.; Miyaura, N. *Organometallics* **1997**, *16*, 4229.

(9) Miyaura, N. *Contemporary Boron Chemistry*; Davidson, M. G., et al., Eds.; Royal Society of Chemistry, 2000; p 399.

The η^2-coordination mode of the borane to Rh in **1** is similar to that observed in early transition metal complexes of organohydroborates.[10,11] It is further reminiscent of the way that alkanes are suggested to bind with highly electrophilic late transition metal centers.[12–15] The unexpected η^2-binding mode, air stability, and the preliminary catalytic studies reported here prompt us to suggest that complex **1** and its derivatives should display interesting and accessible chemistry associated with the Rh–H–B linkage in this chelating ligand system, and we are currently actively pursing this.

Experimental Section

General Procedures. All manipulations were carried out under an argon atmosphere using standard Schlenk line or drybox techniques. CH_2Cl_2 was distilled from CaH_2, and hexane and toluene were distilled from sodium. NMR spectra were measured on Brüker Advance 300 MHz and Varian Mercury 400 MHz FT-NMR spectrometers in CD_2Cl_2 solutions. Residual protio solvent was used as reference (δ, ppm: CD_2Cl_2 5.33) in ^1H NMR. ^{11}B NMR spectra were referenced to $BF_3{\cdot}OEt_2$ (external), and ^{31}P NMR spectra were referenced to H_3PO_4 (external). Coupling constants are given in hertz. Elemental analysis was performed in-house in the Department of Chemistry, University of Bath.

Compound 1. $[(COD)RhCl]_2$ (0.105 g, 0.213 mmol) and $Ph_2PCH_2PPh_2{\cdot}BH_3$ (0.170 g, 0.426 mmol) were dissolved in CH_2Cl_2 (15 cm^3) and the reaction stirred for 10 min. $TlPF_6$ (0.15 g, 0.43 mmol) was added, and stirring was continued overnight. Filtration away from insoluble TlCl and recrystallization by addition of hexanes afforded pale yellow microcrystals of $[(COD)Rh\{(\eta^2\text{-}BH_3)Ph_2PCH_2PPh_2\}][PF_6]$ (0.273 g, 85% yield). Crystals suitable for an X-ray diffraction study were obtained by methathesis of a CH_2Cl_2 solution of **1** with excess $NaBPh_4$, filtration, and recrystallization from CH_2Cl_2/toluene.

Spectroscopic Data for 1. ^1H (400 MHz) (298 K, CD_2Cl_2): 7.61–7.38 (m, 20 H, Ph), 5.82 (s, 2 H, cod), 3.32 (s, 2 H, cod), 2.17 [virtual t, 2 H, CH_2, J(PH) 8], 2.49 (m, 4 H, cod), 2.30 (m, 4 H, cod), −0.25 [partially collapsed quartet, 3 H, BH_3, J(BH) 82]. $^{31}P\{^1H\}$ (121 MHz) (298 K, CD_2Cl_2): 47.1 [dd, 1 P, J(PP) 61, J(RhP) 145 Hz], 20.3 (br, 1 P), −142.8 [septet, 1 P, PF_6, J(FP) 701], $^{11}B\{^1H\}$ (96 MHz) (298 K, CD_2Cl_2): −24.1 [d br, J(PB) 96]. Selected $^1H\{^{11}B\}$ (400 MHz, 223 K, CD_2Cl_2): 2.25 (1 H, BH), −1.48 (2 H, B–H–Rh). Anal. Calcd for $C_{33}H_{37}BP_3F_6Rh$: C 52.5; H 4.91. Found: C 51.5; H 4.76.

Catalysis. Rhodium complex **1** (1 mol %) and phenylboronic acid (1.5 mmol) were added to a flask containing a magnetic stirring bar. The flask was flushed with nitrogen and then charged with DME (3 mL) and cyclohexanone (1.0 mmol). The mixture was then stirred at 65 °C for 16 h. The product was extracted with ethyl acetate, washed with brine, and dried over $MgSO_4$. Chromatography over silica gel (hexane–ethyl acetate, 10:1) afforded 3-phenylcyclohexenone in 82% yield. The identity of this known compound was confirmed by comparison of its ^1H NMR spectrum with an authentic sample.

DFT Calculations. Calculations on the system were performed using the G98 package.[16] All geometries were optimized using the density functional theory with Becke's three-parameter hybrid exchanged[17] and the Perdue–Wang correlation function (B3PW91).[18] The starting point of the geometry optimizations was derived from the X-ray structure, with the four phenyl groups substituted for methyls. For Rh the Stuttgart-Dresden[19] basis set with corresponding effective core potentials was applied (replacing 28 core electrons for Rh), and the 6-31G** basis set was used for the rest of the atoms.

X-ray Crystallography. The crystal structure data for compound **1** were collected on a Nonius KappaCCD. Structure solution followed by full-matrix least-squares refinement was performed using the SHELX suite of programs throughout.[20]

Acknowledgment. The Royal Society is thanked for financial support (A.S.W.). Professor Ian Williams and Dr. Michael Whittlesey are thanked for stimulating discussions.

Supporting Information Available: Tables giving details of data collection, structure solution and refinement, atomic coordinates, thermal parameters, and bond lengths and angles for $1{\cdot}[BPh_4]{\cdot}C_6H_7$. This material is available free of charge via the Internet at http://pubs.acs.org.

OM0103759

(10) Liu, F.-C.; Du, B.; Liu, J.; Meyers, E. A.; Shore, S. G. *Inorg. Chem.* **1999**, *38*, 3228.
(11) Chase, P. A.; Piers, W. E.; Parvez, M. *Organometallics* **2000**, *19*, 2040.
(12) Geftakis, S.; Ball, G. E. *J. Am. Chem. Soc.* **1998**, *120*, 9953.
(13) Heiberg, H.; Johansson, L.; Gropen, O.; Ryan, O. B.; Swang O.; Tilset, M. *J. Am. Chem. Soc.* **2000**, *122*, 10831.
(14) Schneider, J. J. *Angew. Chem., Int. Ed. Engl.* **1996**, *35*, 1068.
(15) Hall, C.; Perutz, R. N. *Chem. Rev.* **1996**, *96*, 3125.
(16) Frisch, M. J.; Trucks, G. W.; Schlegel, H. B.; Scuseria, G. E.; Robb, M. A.; Cheeseman, J. R.; Zakrzewski, V. G.; Montgomery, J. A., Jr.; Stratmann, R. E.; Burant, J. C.; Dapprich, S.; Millam, J. M.; Daniels, A. D.; Kudin, K. N.; Strain, M. C.; Farkas, O.; Tomasi, J.; Barone, V.; Cossi, M.; Cammi, R.; Mennucci, B.; Pomelli, C.; Adamo, C.; Clifford, S.; Ochterski, J.; Petersson, G. A.; Ayala, P. Y.; Cui, Q.; Morokuma, K.; Malick, D. K.; Rabuck, A. D.; Raghavachari, K.; Foresman, J. B.; Cioslowski, J.; Ortiz, J. V.; Stefanov, B. B.; Liu, G.; Liashenko, A.; Piskorz, P.; Komaromi, I.; Gomperts, R.; Martin, R. L.; Fox, D. J.; Keith, T.; Al-Laham, M. A.; Peng, C. Y.; Nanayakkara, A.; Gonzalez, C.; Challacombe, M.; Gill, B. Johnson, P. M. W.; Chen, W.; Wong, M. W.; Andres, J. L.; Gonzalez, C.; Head-Gordon, M.; Replogle, E. S.; Pople, J. A. *Gaussian 98*, Revision A.6; Gaussian, Inc.: Pittsburgh, PA, 1998.
(17) (a) Becke, A. D. *Phys. Rev. A* **1988**, *38*, 3089. (b) Becke, A. D. *J. Chem. Phys.* **1993**, 5648.
(18) Perdue, J. P.; Wang, Y. *Phys. Rev. B* **1991**, *45*, 13244.
(19) Andrae, D.; Haussermann, U.; Dolg, M.; Stoll, H.; Preuss, H. *Theor. Chim. Acta* **1990**, *77*, 123
(20) Sheldrick, G. M. *SHELX-97*, A computer program for refinement of crystal structures; University of Gottingen. 1997.

CHEMCOMM Communication
www.rsc.org/chemcomm

[(PPh$_3$)Ag(CB$_{11}$H$_6$Y$_6$)] (Y = H, Br): highly active, selective and recyclable Lewis acids for a hetero-Diels–Alder reaction†

Catherine Hague, Nathan J. Patmore, Christopher G. Frost,* Mary F. Mahon and Andrew S. Weller*

Department of Chemistry, University of Bath, Bath, UK BA2 7AY. E-mail: c.g.frost@bath.ac.uk; a.s.weller@bath.ac.uk

Received (in Cambridge, UK) 25th July 2001, Accepted 1st October 2001
First published as an Advance Article on the web 17th October 2001

The complex [(PPh$_3$)Ag(CB$_{11}$H$_6$Br$_6$)] 1 is an effective and selective catalyst (0.1 mol% loading) for a hetero-Diels–Alder reaction, which shows a marked dependence on the presence of trace amounts of water, while addition of Ag[Y] [Y = CB$_{11}$H$_{12}$, CB$_{11}$H$_6$Br$_6$, O$_3$SCF$_3$] to a phosphine functionalised support gives an efficient and recyclable Lewis acid catalyst for this transformation.

Cationic silver(I)–phosphine complexes have been used as effective promoters for a wide-range of organic transformations including allylation, aldol, ene and glycosylation reactions, asymmetric aldol reactions, Mukaiyama aldol reactions, asymmetric allylations and hetero-Diels–Alder reactions.[1] It is well established that these reactions are accelerated by other Lewis acids (for example; Ti, B, Al and Sn complexes). However, many of these established catalysts are sensitive to air, water and product inhibition and consequently are used in a low substrate/catalyst ratio. The use of silver(I)–phosphine complexes can provide a practical solution to this problem, as many complexes are stable in air and retain activity in the presence of reaction product. Nevertheless, the best examples from the literature routinely employ high catalytic loadings (5–10 mol%) to achieve competitive rates and product yields. We are interested in developing silver(I) Lewis acids partnered with the carborane anion [1-*closo*-CB$_{11}$H$_{12}$]$^-$ and derivatives,[2] in the anticipation that the weakly coordinating nature of these anions will reveal enhanced activity for these systems. As the hetero-Diels–Alder reaction is one of the most useful methods for the synthesis of bioactive heterocycles we chose to test the new complexes in this challenging reaction.

We report here the synthesis of two new silver(I)–phosphine complexes containing [CB$_{11}$H$_{12}$]$^-$ and [CB$_{11}$H$_6$Br$_6$]$^-$ respectively and their use as efficient catalysts at low loadings for a hetero-Diels–Alder reaction. Additionally, we report that this methodology may be transferred to a solid support with good activity, low leaching and promising recycleability.

Addition of 1 equivalent of PPh$_3$ to a CH$_2$Cl$_2$ solution of Ag[CB$_{11}$H$_6$Br$_6$] or Ag[CB$_{11}$H$_{12}$] affords the new complexes (PPh$_3$)Ag(CB$_{11}$H$_6$Br$_6$) **1** and (PPh$_3$)Ag(CB$_{11}$H$_{12}$) **2**, respectively, in good yields after recrystallisation from CH$_2$Cl$_2$–hexanes. Both complexes have been fully characterised‡ by multinuclear NMR spectroscopy, microanalysis and X-ray crystallography. In solution the complexes display C_{5v} symmetry in both the ^{11}B and ^{1}H{^{11}B} NMR spectra, showing that the {AgPPh$_3$}$^+$ fragment is fluxional over the cage surface, as has been observed previously for other *exo* polyhedrally bound {Ag(PPh$_3$)} fragments.[3] The ^{31}P{^{1}H} NMR spectra show a pair of concentric doublets for both **1** and **2**: J(AgP$_{average}$) 715 Hz and J(AgP$_{average}$) 743 Hz, respectively. The solid state structure of complex **1** is shown in Fig. 1.§ In the asymmetric unit, the silver is ligated by one phosphine and the three bromine atoms

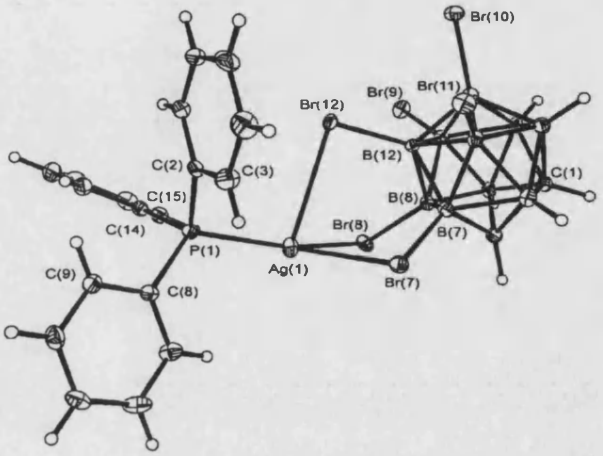

Fig. 1 Solid state structure of complex **1**. Ellipsoids are shown at the 50% probability level. Selected bond lengths (Å) and angles (°): Ag(1)–Br(7) 2.8710(5), Ag(1)–Br(8) 2.6963(5), Ag(1)–Br(12) 3.0953(5), Ag(1)–P(1) 2.4032(10); P(1)–Ag(1)–Br(7) 117.44(3), P(1)–Ag(1)–Br(8) 155.55(3), Br(8)–Ag(1)–Br(7) 87.471(14).

that radiate from the B(7)–B(8)–B(12) triangular face of the cage. Bond lengths and angles are unremarkable, aside from the fact that the silver centre appears to have a vacant site lying roughly opposite to B(12). Examination of the supramolecular structure revealed that this site is filled by a long Ag(1)–Br interaction [Ag(1)–Br(11)′ 3.4901(5) Å], affording a ribbon-like structure in the lattice (ESI†). The asymmetric unit found for **2** is grossly similar to **1**, the {AgPPh$_3$} fragment interacting with the cage through three 3-centre–2-electron Ag–H–B, interactions.

We have investigated the reaction between *N*-benzylidene aniline **I** and Danishefsky's diene **II** (Scheme 1) using as catalysts the silver complexes **1**, **2** and, for comparison, (PPh$_3$)Ag(OTf) (OTf = O$_3$SCF$_3$). In the absence of any catalyst there was only a trace (< 5%) of product after 24 h at room temperature. On the bench (2 h, room temperature, 1 mol% catalyst, CH$_2$Cl$_2$) both complexes **1** and **2** afforded essentially quantitative (> 99%) yields of **III** on workup, while (PPh$_3$)Ag(OTf) gave **III** in 70% yield. However, it was only when catalyst loadings were reduced to 0.1 mol% and the reactions were monitored by NMR spectroscopy that the efficiency of complex **1**, in particular, for this transformation was revealed.

Fig. 2 shows a plot of time *vs.* reaction course for complexes **1**, **2** and (PPh$_3$)Ag(OTf). [(PPh$_3$)Ag(ClO$_4$)] was also tested, not

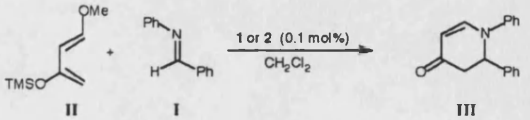

Scheme 1

† Electronic supplementary information (ESI) available: Fig. S1: extended solid state structure apparent in **1**. Figs. S2 and S3: bar charts showing isolated yield of product **III** using supported catalysts **3**–**5** in the absence and presence of water. See http:www/rsc.org/suppdata/cc/b1/b106719b/

 DOI: 10.1039/b106719b

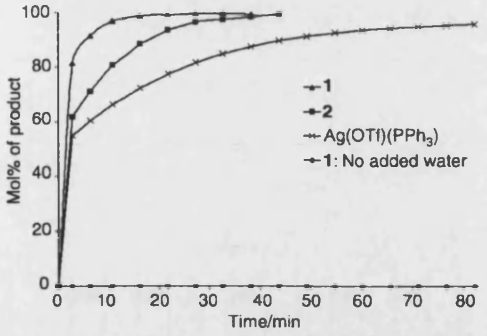

Fig. 2 Relative rates of reaction CD_2Cl_2 solutions, 0.1 mol% **1**, **2** and $(PPh_3)Ag(OTf)$, 50 mol% added H_2O. Also shown: **1** with no added water.

shown here, and showed a very similar time dependent profile to $(PPh_3)Ag(OTf)$.] It is clear that complex **1** gives the fastest rate of catalysis, the reaction being complete in ~15 min, yielding a turnover frequency (TOF) of *ca.* 4000 h^{-1}. Complex **2** is slower than **1**, with complete reaction effected after 50 min, while $(PPh_3)Ag(OTf)$ does not attain 100% conversion, even after 80 min. Although these results reflect the previously enunciated relative weakly coordinating properties of carborane anions,[2] especially the halogenated examples,[4] it is pleasing to see that these ideas can be applied to a synthetically useful transformation, using well defined catalysts.

Importantly, and somewhat surprisingly, we have found that water plays an important role in this reaction. When these NMR experiments are performed in rigorously dry solvent (CD_2Cl_2, vacuum distilled from CaH_2), no catalysis occurs (Fig. 2). Addition of a substoichiometric (1 μl, 50 mol%, unoptimised) amount of H_2O to the sample immediately initiates catalysis. While water-accelerated catalysis is becoming appreciated more widely,[5] we currently can only speculate as to its rôle in this system. These results, however, implicate a polarised, silver-bound water molecule in the catalytic process, with the resulting Lewis-assisted Brønsted-acid similar to that previously reported in lanthanide catalysed aromatic electrophilic substitutions[6] and the catalytic role of coordinated water in certain zeolites.[7] Consonant with this idea, when the reaction was repeated in the presence of the hindered base 2,6-di-*tert*-butyl-4-methylpyridine no product was formed, while a control experiment taking **I** and **II** with just 50 mol% water also resulted in no product formation. On the bench, it is probably adventitious water that is made available to the reaction.

Catalyst **1** is also selective for imines over aldehydes in this reaction. A competition experiment demonstrated preferential activation of imine **I** in the presence of an equimolar amount of benzaldehyde. Thus, after 15 min at room temperature the product arising from reaction with the imine was isolated in 70% yield whilst the aldehyde adduct was produced in only 5% yield.

Polymer supported Lewis acids have been recently attracting significant attention as they represent one method of generating clean, efficient and re-usable catalysts.[8] However, the incorporation of the Lewis acidic sites onto the polymer often requires a multistep synthesis. Given that one of the most popular supports is polymer bound triphenylphosphine,[9] we were interested to see if the high activity and efficiency shown by complexes **1** and **2** could be transferred to this support. Stirring a CH_2Cl_2 solution of Ag[Y][Y = $CB_{11}H_{12}$ **3**, $CB_{11}H_6Br_6$ **4**, OTf **5**] with commercially available resin (Fluka) afforded a material that was an efficient catalyst in all three cases for the hetero-Diels–Alder reaction under investigation.¶ Moreover, all the resins were shown to be re-usable over at least three catalyst runs (>95% isolated yield, *vide infra*). In concert with this, low leaching levels (0.3% Ag, by AAS) where also determined, while the supernatant from freshly prepared and filtered supported catalyst afforded only trace product (<5%) when used in the reaction. These supported catalysts also show a significant dependence on the presence of water. If no water is added then catalyst performance drops off rapidly on the second and third runs, however with 10 mol% water high yields of >95% are afforded over three consecutive cycles (ESI†). At the relatively high catalyst loadings (10 mol%) used in these preliminary experiments the counter ion effects observed in the homogeneous system are not observed.

In conclusion, we have demonstrated that silver(I)–phosphine complexes partnered by carborane anions based on $[CB_{11}H_{12}]$ are effective and active catalysts in a hetero-Diels–Alder transformation, and that water dramatically effects the observed rate of reaction. These catalysts may also be supported on commercially available resin to give active and recyclable Lewis acid catalysts. Full details of the synthesis, solution and solid state structures of **1** and **2** along with comparisons of the catalytic performance when other common anions are partnered with silver(I)–phosphines will be reported in due course.[10]

A. S. W. thanks the Royal Society for a University Research Fellowship. The EPSRC and JERI are thanked for providing funds for the purchase of a diffractometer. The referees are thanked for useful comments.

Notes and references

‡ NMR data (CD_2Cl_2 solutions, 22 °C, 300 MHz). Complex **1**: $^1H\{^{11}B\}$, δ 7.52–7.22 (15H, m, C_6H_5), 2.73 (1H, s br, CH_{cage}), 2.43 (5H, BH). $^{11}B\{^1H\}$, δ −2.09 (1B), −6.59 (5B), −16.88 (5B). $^{31}P\{^1H\}$, δ 16.52 [1P, d d, $J(Ag^{109}P)$ 766, $J(Ag^{107}P)$ 664 Hz]. IR/cm^{-1} (KBr): 2608vs (BH), 2593s (BH). Calc. for $C_{19}H_{21}B_{11}AgPBr_6$: C, 23.1; H, 2.12. Found: C, 22.6; H 2.17%. Complex **2**: $H\{^{11}B\}$, δ 7.52–7.29 (15H, m, C_6H_5), 2.55 (1H, s br, CH_{cage}), 2.25 (1H, s br, BH), 1.85 (10H, 5 + 5 coincidence, BH): $^{11}B\{^1H\}$. δ −10.27 (1B, s br), −11.18 (5 B), −12.02 (5 B). $^{31}P\{^1H\}$, δ 18.70 [1P, dd, $J(Ag^{109}P)$ 795, $J(Ag^{107}P)$ 691 Hz]. IR/cm^{-1} (KBr): 2565vs (BH), 2517s (sh) (BH), 2372m (BH). Calc. for $C_{19}H_{27}B_{11}AgP$: C, 44.5; H, 5.30. Found: C, 44.3; H, 5.19%.

§ *Crystallographic data*: for **1**: $C_{19}H_{21}AgB_{11}Br_6P$, M = 986.57, λ = 0.71073 Å, monoclinic, space group $P2_1/c$, a = 8.8950(10), b = 24.4140(4), c = 14.4170(3) Å, β = 102.0720(10)°, U = 3061.60(9) $Å^3$, Z = 4, T = 150(2) K, D_c = 2.140 g cm^{-3}, μ = 8.554 mm^{-1}, $F(000)$ = 1848, crystal: 0.10 × 0.10 × 0.05 mm, 7253 unique reflections (R_{int} = 0.0519), R_1 = 0.0358, wR_2 = 0.0783 [$I > 2\sigma(I)$]. For **2**: $C_{19}H_{27}AgB_{11}P$, M = 513.16, λ = 0.71073 Å, triclinic, space group $P\bar{1}$, a = 10.282(2), b = 10.988(2), c = 11.308(2) Å, α = 76.22(3), β = 75.25(3), γ = 75.61(3)°, U = 1175.7(4) $Å^3$, Z = 2, T = 150(2) K, D_c = 1.450 g cm^{-3}, μ = 0.932 mm^{-1}, $F(000)$ = 516, crystal 0.20 × 0.20 × 0.10 mm, 5374 unique reflections (R_{int} = 0.0387), R_1 = 0.0316, wR_2 = 0.0757 [$I > 2\sigma(I)$].

CCDC reference numbers 171721 and 168828. See http://www.rsc.org/suppdata/cc/b1/b106719b/ for crystallographic data in CIF or other electronic format.

¶ *General procedure*: ~3 mmol g^{-1} polymer-bound PPh_3 (Fluka, 200–300 mesh) with a slight excess of Ag[Y] in CH_2Cl_2 was used to generate the polymer bound catalyst. After washing with CH_2Cl_2 and drying *in vacuo*, catalytic runs were performed using *ca.* 10 mol% catalyst and 10 mol% H_2O in CH_2Cl_2 (5 ml) (1 h, room temp.). The support was recycled by cannula filtration of the supernatent under argon and drying *in vacuo*.

1 *Lewis Acids in Organic Synthesis*, ed. H. Yamamoto, Wiley-VCH, Weinheim, 2000; P. Buonora, J. C. Olsen and T. Oh, *Tetrahedron*, 2001, **57**, 6099.
2 C. A. Reed, *Acc. Chem. Rev.*, 1998, **31**, 133.
3 D. D. Ellis, A. Franken, P. A. Jellis, J. A. Kautz and F. G. A. Stone, *J. Chem. Soc., Dalton Trans.*, 2000, 2509; D. D. Ellis, J. C. Jeffery, P. A. Jellis, J. A. Kautz and F. G. A. Stone, *Inorg. Chem.*, 2001, **40**, 2041.
4 C. A. Reed, K. C. Kim, R. D. Bolskar and L. J. Mueller, *Science*, 2000, **289**, 101.
5 S. Ribe and P. Wipf, *Chem. Commun.*, 2001, 299.
6 A. G. M. Barrett, D. C. Braddock, J. P. Henschke and E. R. Walker, *J. Chem. Soc., Perkin Trans. 1*, 1999, 873.
7 H.-M. Kao, C. P. Grey, K. Pitchumani, P. H. Lakshminarasimhan and V. Ramamurthy, *J. Phys. Chem. A.*, 1998, **102**, 5627.
8 S. V. Ley, A. R. Baxendale, R. N. Bream, P. S. Jackson, A. G. Leach, D. A. Longbottom, M. Nesi, J. S. Scott, R. I. Storer and S. J. Taylor, *J. Chem. Soc., Perkin Trans. 1*, 2000, 3815; S. Itsuno, in *Lewis Acids in Organic Synthesis*, ed. H. Yamamoto, Wiley-VCH, Weinheim, 2000.
9 A. C. Comely, S. E. Gibson and N. J. Hales, *Chem. Commun.*, 2000, 305.
10 C. Hague, N. J. Patmore, J. H. Cotgreave, M. F. Mahon, C. G. Frost and A. S. Weller, manuscript in preparation.

Silver Phosphanes Partnered with Carborane Monoanions: Synthesis, Structures and Use as Highly Active Lewis Acid Catalysts in a Hetero-Diels–Alder Reaction

Nathan J. Patmore, Catherine Hague, Jamie H. Cotgreave, Mary F. Mahon, Christopher G. Frost,* and Andrew S. Weller*[a]

Abstract: Four Lewis acidic silver phosphane complexes partnered with $[1\text{-}closo\text{-}CB_{11}H_{12}]^-$ and $[1\text{-}closo\text{-}CB_{11}H_6Br_6]^-$ have been synthesised and studied by solution NMR and solid-state X-ray diffraction techniques. In the complex $[Ag(PPh_3)(CB_{11}H_{12})]$ (**1**), the silver is coordinated with the carborane by two stronger 3c–2e B–H–Ag bonds, one weaker B–H–Ag interaction and a very weak Ag···C_{arene} contact in the solid state. In solution, the carborane remains closely connected with the $\{Ag(PPh_3)\}^+$ fragment, as evidenced by ^{11}B chemical shifts. Complex **2** $[Ag(PPh_3)_2(CB_{11}H_{12})]_2$ adopts a dimeric motif in the solid state, each carborane bridging two Ag centres. In solution at low temperature, two distinct complexes are observed that are suggested to be monomeric $[Ag(PPh_3)_2][CB_{11}H_{12}]$ and dimeric $[Ag(PPh_3)_2(CB_{11}H_{12})]_2$. With the more weakly coordinating anion $[CB_{11}H_6Br_6]^-$ and one phosphane, complex **3** $[Ag(PPh_3)(CB_{11}H_6Br_6)]$ is isolated. Complex **4**, $[Ag(PPh_3)_2(CB_{11}H_6Br_6)]$, has been characterised spectroscopically. All of the complexes have been assessed as Lewis acids in the hetero-Diels–Alder reaction of *N*-benzylideneaniline with Danishefsky's diene. Exceptionally low catalyst loadings for this Lewis acid catalysed reaction are required (0.1 mol %) coupled with turnover frequencies of 4000 h^{-1} (quantitative conversion to product after 15 minutes using **3** at room temperature). Moreover, the reaction does not occur in rigorously dry solvent as addition of a substoichiometric amount of water (50 mol %) is necessary for turnover of the catalyst. It is suggested that a Lewis assisted Brønsted acid is formed between the water and the silver. The effect of changing the counterion to $[BF_4]^-$, $[OTf]^-$ and $[ClO_4]^-$ has also been studied. Significant decreases in reaction rate and final product yield are observed on changing the anion from $[CB_{11}H_6Br_6]^-$, thus demonstrating the utility of weakly coordinating carborane anions in organic synthesis.

Keywords: carboranes · cluster compounds · cycloaddition · homogeneous catalysis · silver

Introduction

Monoanionic carborane anions based around $[closo\text{-}1\text{-}CB_{11}H_{12}]^-$ (**A**, see Scheme 1) are among the most inert and least coordinating anions currently known.[1, 2] The high chemical stability and low nucleophilicity of these ions means that they have been used to stabilise exotic cationic species, which are not isolatable with other, more coordinating, anions.[3–6] Such anions also have the potential to act as partners with cationic Lewis acidic transition metal complexes that take part in various catalytic processes. Somewhat surprisingly, given the almost ubiquitous use of $[B(C_6F_5)_4]^-$ and derivatives in such applications, there are only a few reports of anions such as **A** or related compounds utilised in catalytic processes,[7–10] despite their potential advantages over perfluorinated borates.[11, 12]

The coordination chemistry of cationic silver(I) phosphane complexes (combined with a range of anions) has been studied in some detail,[13–16] to the point that useful structural predications may be made on the basis of spectroscopic data.[17] Silver phosphanes *exo*-coordinated to polyhedral boranes are rarer,[18] but recent work, particularly from Stone et al.[19–21] has established this area. Related complexes in which *exo*-coordinated silver is bound to ligands other than phosphane,[22–25] or arene solvent molecules[26–29] or where the silver is partnered with halogeno-substituted carboranes[27, 30–33] are also known.

One of us has a current interest in the synthesis, structures and reactivity of Lewis acidic transition metal complexes partnered with anion **A** and derivatives.[24, 25] Concurrently, there is also interest in Lewis acid catalysis using silver(I) salts as effective promoters of a wide-range of organic transformations including allylation, aldol, ene and glycosylation

[a] Dr. C. G. Frost, Dr. A. S. Weller, N. J. Patmore, C. Hague
J. H. Cotgreave, Dr. M. F. Mahon
Department of Chemistry, University of Bath
Bath, BA27AY (UK)
Fax: (+44) 1225-826231
E-mail: c.g.frost@bath.ac.uk, a.s.weller@bath.ac.uk

0947-6539/02/0809-2088 $ 20.00+.50/0 *Chem. Eur. J.* **2002**, *8*, No. 9

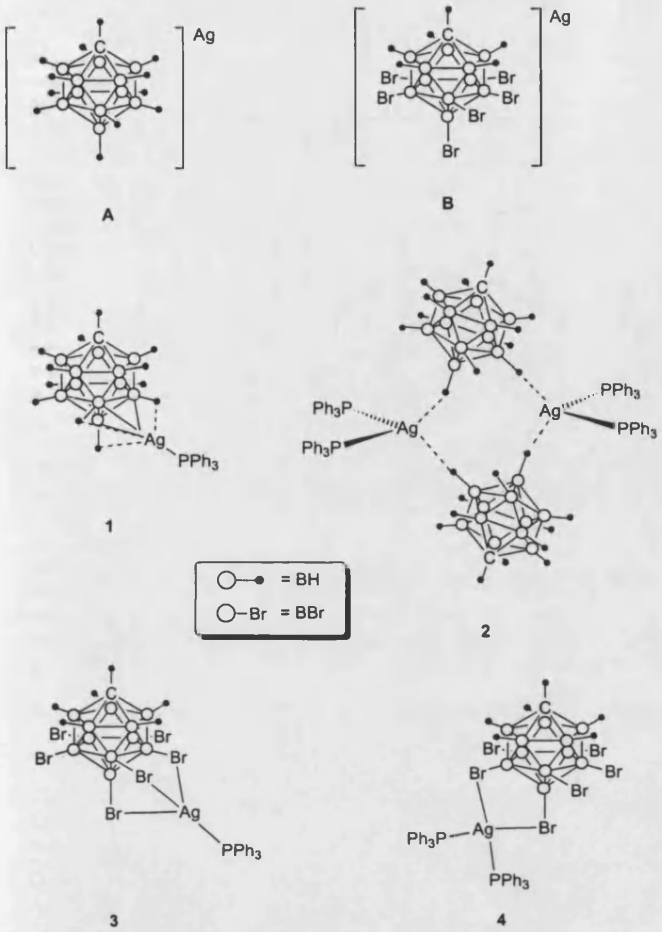

Scheme 1. Structures **A** and **B** and **1**–**4**.

reactions.[34] Of particular note is the use of silver(I) BINAP ([1,1′-binaphthalene]-2,2′-diylbis(diphenylphosphane)) complexes in asymmetric aldol reactions,[35–38] Mukaiyama aldol reactions,[39] asymmetric allylations[40] and hetero-Diels–Alder reactions.[41] It is well established that these reactions are accelerated by other Lewis acids (for example: Ti, B, Al, Sn complexes). However, many of these established catalysts are sensitive to air, water and product inhibition and consequently are used at a low substrate/catalyst ratio. The use of silver(I) phosphane complexes can provide a practical solution, with many precatalysts being stable in air and retaining activity in the presence of reaction product. Nevertheless, the best examples from the literature routinely employ high catalytic loadings (5–10 mol%) to achieve competitive rates and product yields. We are thus interested in developing silver(I) Lewis acids complexed with carborane anions in anticipation that the weakly coordinating nature of the anions will reveal enhanced activity for these systems. The hetero-Diels–Alder reaction is one of the most useful methods for the synthesis of bioactive heterocycles. Hence we chose to test our new complexes in this challenging reaction with the intention of identifying structure–activity relationships when the coordination sphere of the silver (number of phosphanes, anion) is systematically changed.

We report here the synthesis and solution and solid-state structural investigations for complexes of the formula $[Ag(PPh_3)_n(CB_{11}H_6Y_6)]$ ($n = 1, 2$; Y = H, Br) and their use as active catalysts in the hetero-Diels–Alder reactions of *N*-benzylideneaniline with Danishefsky's diene. Aspects of this work have been communicated previously.[42]

Results and Discussion

Synthesis and structures: Silver(I) salts of monoanionic carborane anions are readily prepared and are air stable and useful synthons for subsequent reactions. For example, they can be used in silver salt metathesis reactions to introduce a carborane anion into a metal's coordination sphere[23, 25, 29, 43, 44] or to generate synthetically useful salts.[28] In addition they often have significant solubility in aromatic solvents compared with other cations, facilitating more complete characterisation of the cation/anion pair. In principle, they also provide a useful starting point for the investigation of silver(I) complexes of the general formula $[Ag(L)_n(CB_{11}H_6Y_6)]$ (L = two electron donor; Y = H, halogen) as simple addition of the required ligand (L) results in complex formation.

Addition of slightly less than one equivalent (to avoid formation of **2**, vide infra) of PPh_3 to a suspension of $Ag[CB_{11}H_{12}]$ in CH_2Cl_2 results in the formation of $[Ag(PPh_3)(CB_{11}H_{12})]$, **1**, as an analytically pure solid in good isolated yield after recrystallisation (Tables 1 and 2). The solid-state structure of **1** is presented in Figure 1. The $\{AgPPh_3\}^+$ fragment interacts with the carborane anion through the three {BH} units that form the B(12)–B(7)–B(8) polyhedral face, a coordination motif seen previously in $[(Cp^*)ZrMe_2\text{-}\eta^3\text{-}(CB_{11}H_{12})]$.[10] The silver phosphane fragment does not sit over the centre of this face but is more localised towards B(8) and the corresponding Ag–B bond lengths reflect this: Ag(1)–B(8) 2.504(1) Å, Ag(1)–B(12) 2.569(3) Å, Ag(1)–B(7) 2.619(2) Å. These bond lengths are broadly similar to those previously reported for the related complex $[2,2,2\text{-}(CO)_3\text{-}2\text{-}PPh_3\text{-}7,12\text{-}\{Ag(PPh_3)\}\text{-}closo\text{-}2,1\text{-}MoCB_{10}H_9]$[20, 21] (2.552(4) Å and 2.589(4) Å), in which the Ag centre is bound dihapto by the cage and is the only other *closo*-polyhedral borane structure reported with an *exo*-$\{AgPR_3\}$ fragment, although there are others reported with ligands other than phosphane,[22] with Ag–metal bonds[21] and with *endo* coordination of a silver fragment.[18] The location of the silver phosphane fragment in relation to the B(8)–B(12) bond is such that the silver atom adopts a planar coordination motif with respect to P(1), B(8) and B(12) with the sum of relevant angles around Ag(1) 359.7°. P(1) essentially lies on the same plane formed by Ag(1), B(8) and B(12) (max deviation from plane 0.083 Å for P(1)), resulting in an apparent vacant coordination site *transoid* to H(7). Inspection of the extended lattice packing diagram shows that there are no Ag···H–B intermolecular interactions directed towards this vacant site.[18, 20] However, there is a long intermolecular interaction (3.348 Å) between Ag(1) and C(35)′ of a phenyl ring in a symmetry related molecule (Figure 2), and the arene carbon approaches the silver from the reverse of the trigonal

  0947-6539/02/0809-2089 $ 20.00+.50/0

Table 1. Crystal data and structure refinement for **1**, **2** and **3**.

	1	**2**	**3**
empirical formula	$C_{19}H_{27}AgB_{11}P$	$C_{74}H_{84}Ag_2B_{22}P_4$	$C_{19}H_{21}AgB_{11}Br_6P$
M_r	513.16	1550.85	986.57
T [K]	150(2)	170(2)	150(2)
λ [Å]	0.71073	0.71069	0.71073
crystal system	triclinic	triclinic	monoclinic
space group	$P\bar{1}$	$P\bar{1}$	$P2_1/c$
a [Å]	10.282(2)	11.6963(2)	8.89500(10)
b [Å]	10.988(2)	13.1668(2)	24.4140(4)
c [Å]	11.308(2)	14.1393(2)	14.4170(3)
α [°]	76.22(3)	96.8860(6)	90
β [°]	75.25(3)	106.8980(7)	102.0720(10)
γ [°]	75.61(3)	110.5370(8)	90
V [Å^3]	1175.7(4)	1890.30(5)	3061.60(9)
Z	2	1	4
ρ_{calcd} [mg m^{-3}]	1.450	1.362	2.140
μ [mm^{-1}]	0.932	0.646	8.554
F(000)	516	792	1848
crystal size [mm]	0.20 × 0.20 × 0.10	0.25 × 0.20 × 0.17	0.10 × 0.10 × 0.05
θ range [°]	2.96 to 27.50	3.38 to 27.50	3.71 to 27.88
reflections collected	20702	22570	23164
independent reflections	5374 [R(int) = 0.0387]	8605 [R(int) = 0.0250]	7253 [R(int) = 0.0519]
reflections observed ($>2\sigma$)	4538	7964	5880
max and min transmission	0.9126 and 0.8355	1.027, 0.981	0.66 and 0.47
data/restraints/parameters	5374/0/302	8605/2/478	7253/0/349
goodness of fit on F^2	1.018	1.050	1.041
final R indices [$I > 2\sigma$(I)]	$R_1 = 0.0316$ $wR_2 = 0.0757$	$R_1 = 0.0289$ $wR_2 = 0.0738$	$R_1 = 0.0358$ $wR_2 = 0.0783$
R indices (all data)	$R_1 = 0.0417$ $wR_2 = 0.0813$	$R_1 = 0.0323$ $wR_2 = 0.0763$	$R_1 = 0.0521$ $wR_2 = 0.0855$
largest diff. peak and hole [e Å^{-3}]	0.544 and −0.923	1.727 and −0.584	1.081 and −1.181

Table 2. Selected bond lengths [Å] and angles [°] for the new compounds **1**–**3**.

Compound **1**			
Ag(1)–P(1)	2.3625(7)	P(1)–Ag(1)–B(7)	142.11(6)
Ag(1)–B(7)	2.619(3)	P(1)–Ag(1)–B(8)	158.23(6)
Ag(1)–B(8)	2.504(3)	P(1)–Ag(1)–B(12)	160.32(6)
Ag(1)–B(12)	2.569(3)	B(12)–Ag(1)–B(8)	41.26(8)
Ag(1)–H(7)	2.36(2)	B(12)–Ag(1)–B(7)	40.37(8)
Ag(1)–H(8)	2.14(2)	B(7)–Ag(1)–B(8)	40.98(8)
Ag(1)–H(12)	2.26(2)		
Compound **2**			
Ag(1)–P(1)	2.4698(3)	Ag(1)–H(12)′	2.17(2)
Ag(1)–P(2)	2.4741(3)	Ag(1)–H(7)	2.51(2)
Ag(1)–B(7)	3.494(2)	P(1)–Ag(1)–P(2)	130.90(1)
Ag(1)–B(12)′	2.892(2)	B(7)–Ag(1)–B(12)′	72.4(6)
Compound **3**			
Ag(1)–P(1)	2.4032(10)	P(1)–Ag(1)–Br(7)	117.44(3)
Ag(1)–Br(7)	2.8710(5)	P(1)–Ag(1)–Br(8)	155.55(3)
Ag(1)–Br(8)	2.6963(5)	P(1)–Ag(1)–Br(12)	93.31(3)
Ag(1)–Br(12)	3.0953(5)	P(1)–Ag(1)–Br(11)′	157.15(1)
Ag(1)–Br(11)′	3.4901(5)	Br(7)–Ag(1)–Br(8)	87.471(14)

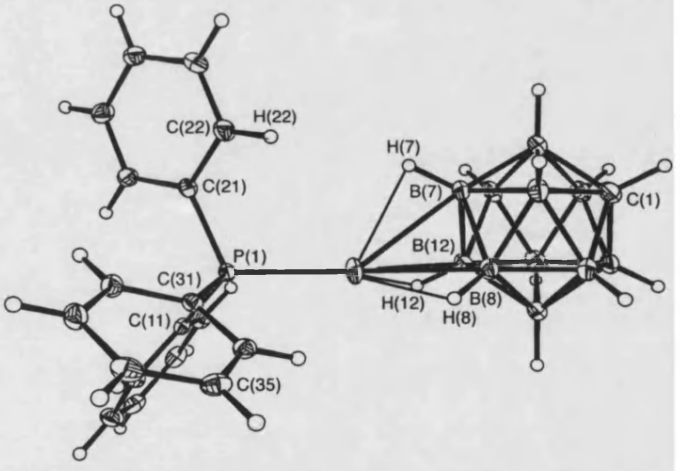

Figure 1. Molecular structure of complex **1**, showing the atom-numbering scheme. Thermal ellipsoids are drawn at the 50% probability level.

plane formed by B(8), B(12), Ag(1) and P(1). Although this distance is very long compared with other reported silver–arene bond lengths found in the solid-state structure of Ag carboranes (ca. 2.5–2.6 Å), we suggest that it may be significant, given the observed orientation of the silver phosphane fragment with respect to the cage. Indeed, gas-phase DFT calculations on **1** show that the silver adopts the expected tetrahedral geometry when there are no intermolecular interactions,[45] while comparable weak silver–arene contacts have been previously identified.[46, 47] The Ag(1)–P(1) distance, at 2.3625(7) Å, is at the shorter end of the range reported for [Ag(PPh$_3$)L] or [Ag(PPh$_3$)]X (X = counterion or two-electron ligand (L)) molecules[14, 16] suggesting a relatively strong AgP bond.

In solution, the ^{1}H{^{11}B} NMR spectrum of **1** shows a 1:1 ratio of phosphane to carborane anion. Resonances due to {BH} groups are observed at $\delta = 2.25$ and $\delta = 1.85$ in the ratio 1:10 (the latter is a 5+5 coincidence), with no high-field resonances potentially indicative of M–H–B interactions observed.[48] That only two {BH} resonances are observed suggests that the {AgPPh$_3$} fragment is fluxional over the surface of the cage and affords time-averaged C_{5v} symmetry in solution. This facile process is evidenced by no significant change observed in the spectrum when recorded at −90 °C.

0947-6539/02/0809-2090 $ 20.00+.50/0 *Chem. Eur. J.* **2002**, *8*, No. 9

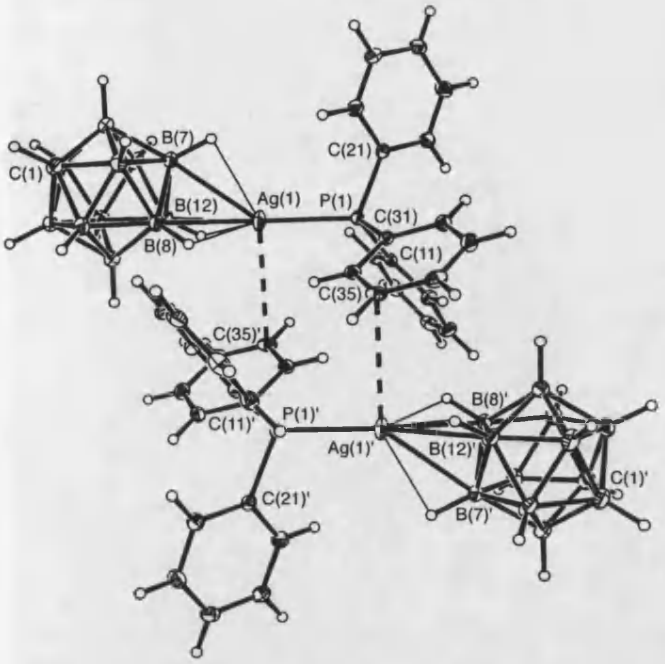

Figure 2. Dimeric unit formed in the extended lattice by Ag···C_{arene} contacts (Ag–C(35)′ 3.348 Å). Atom labelling and other details as in Figure 1.

Related metallaboranes with *exo*-coordinated {$AgPPh_3$} fragments are also highly fluxional in solution.[20, 21] We were initially surprised to observe that the $^{11}B\{^1H\}$ NMR spectrum shows that both the antipodal [B(12)] and lower pentagonal belt [B(7)–(11)] borons undergo a significant upfield shift on complexation with the {$AgPPh_3$} fragment when compared with $Ag[CB_{11}H_{12}]$ (Figure 3), while there is no significant shift in the {BH} resonances observed in the $^1H\{^{11}B\}$ NMR spectrum. This was unexpected as coordination of an *exo*-metal fragment results in significant upfield shifts of the *exo*-metal coordinated {BH} units in *both* the ^1H and ^{11}B NMR spectra in other systems.[25, 44] Specifically, in the $^{11}B\{^1H\}$ NMR spectrum, resonances are observed at $\delta = -10.3$, $\delta = -11.2$ and $\delta = -12.0$ in the ratio 1:5:5. This dichotomy between ^1H and ^{11}B chemical shifts may be indicative of the cage-silver bonding predominantly originating from Ag–B interactions,[49] with a reduced contribution (or perhaps a more electrostatic interaction) from the cage hydrogens. It is noteworthy that AgH interactions can be observed by ^1H NMR spectroscopy in certain cases and show both significant chemical shifts and AgH coupling constants,[50] neither of which are observed for complex **1**, or previously in related Ag cage compounds.[19–21]

Given that only the antipodal [B(12)] and lower pentagonal belt [B(7)–B(11)] boron atoms appear significantly perturbed in the ^{11}B NMR spectrum on coordination of the {$AgPPh_3$} fragment, we suggest a mechanism to explain the observed fluxionality that incorporates the metal phosphane precessing around the five triangular faces formed between B(7)–B(11) and B(12). This mechanism is similar to that previously observed for the movement of $\{Rh(cod)\}^+$[44] or $\{Pt(tBu_2P(CH_2)_3PtBu_2)\}^+$[51] over the surface of [*closo*-$CB_{11}H_{12}]^-$. In the $^{31}P\{^1H\}$ NMR spectrum of **1**, a peak centred at $\delta = 18.70$ is observed as a pair of concentric doublets, due to ^{109}AgP and ^{107}AgP coupling, having an average value for $J(AgP)_{average}$ of 743 Hz. This large value is consistent with the strong AgP bond seen in the solid state and is also indicative of a low-coordinate silver phosphane species;[13] this suggests the observed solution and solid-state structures of **1** are similar.

Addition of two equivalents of PPh_3 to $Ag[CB_{11}H_{12}]$ gives complex **2**, having the empirical formula $[Ag(PPh_3)_2(CB_{11}H_{12})]$, which has been characterised by solution NMR spectroscopy and in the solid state by X-ray diffraction. The extra PPh_3 ligand has the effect of disturbing the silver-cage bonding from **1**, so that a dimeric, centrosymmteric, $[Ag(PPh_3)_2(CB_{11}H_{12})]_2$ unit is now observed (Figure 4), in which each carborane unit bridges two silver centres. Each cage interacts with the two silver centres through one shorter (Ag(1)–H(12)′ 2.17(2) Å, Ag(1)–B(12)′ 2.892(2) Å) and one longer (Ag(1)–H(7) 2.51(2) Å, Ag(1)–B(7) 3.494(2) Å) Ag···H–B interaction. This bonding mode to the two silver centres by the antipodal [B(12)] and a single lower pentagonal belt [B(7)] vertex is similar to that observed in the extended solid-state structure of $[Mo(Cp)(CO)_3I \cdot Ag(CB_{11}H_{12})]_2$.[24] Dimeric and tetrameric silver carborane complexes with cages other than $[CB_{11}H_{12}]^-$ have also been previously reported.[18, 20–22] As expected on moving to a higher coordination number in going from **1** to **2**, the Ag–P bond lengths are relatively longer in the latter complex (Ag(1)–P(1) 2.4698(3) Å, Ag(1)–P(2) 2.4741(3) Å). The P(1)–Ag(1)–P(2) angle of 130.90(1)° is similar to that observed in the three-coordinate complex $[Ag(PPh_3)_2(NCMe)][BF_4]$ (129.37(2)°).[14]

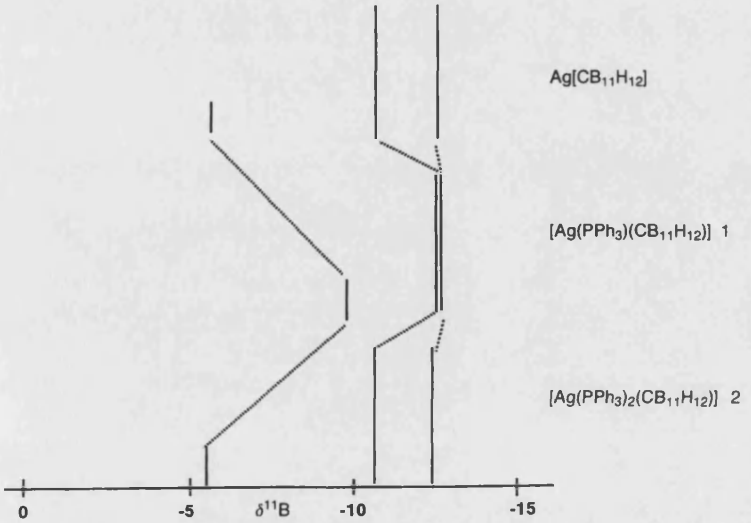

Figure 3. ^{11}B NMR chemical shift "stick" diagram comparing complexes **1** and **2** (solutions in CD_2Cl_2) with $Ag[CB_{11}H_{12}]$ (solution in [D_6]acetone).

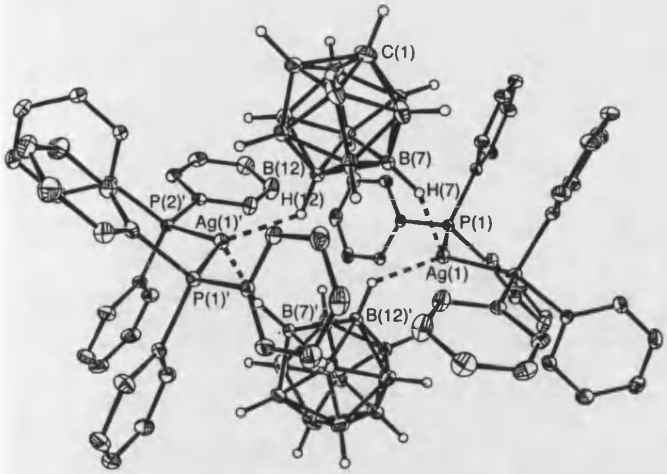

Figure 4. Molecular structure of complex **2**, showing the atom-numbering scheme. Phenyl hydrogen atoms are omitted for clarity. Thermal ellipsoids are drawn at the 50% probability level.

In solution at room temperature in **2**, the carborane does not interact significantly with the metal centre. This is evidenced in the ^{11}B NMR spectrum, which does not show any appreciable perturbation from that found for $Ag[CB_{11}H_{12}]$, with three resonances observed at $\delta = -5.1$, -10.6 and -12.6 in the ratio 1:5:5 (Figure 3). These data reflect the significantly weaker Ag···H–B interactions apparent in **2**, relative to **1**, in the solid state. In the room-temperature $^{31}P\{^1H\}$ NMR spectrum of **2**, a single broad resonance centred at $\delta = 14.8$ is observed, suggesting that the phosphane ligands are undergoing an exchange process. Progressive cooling affords two broad singlets at $\delta = 15.4$ and $\delta = 13.2$ at 0 °C, which gradually sharpen into two sets of doublets at -60 °C, of approximately equal proportions, centred at $\delta = 13.7$ ($J(AgP) = 333$ Hz) and $\delta = 13.6$. The latter resonance is further observed as a pair of concentric doublets, showing coupling to both ^{109}Ag and ^{107}Ag ($J(AgP)_{average} = 519$ Hz). These changes in the NMR spectrum on cooling are consonant with the presence of two different complexes in solution at low temperature, which interconvert at ambient temperature. The species that reveals the larger AgP coupling constant has a value very similar to that reported for two-coordinate $[Ag(PPh_3)_2][BF_4]$ ($J(AgP) = 530$ Hz),[14] while the alternative species has a coupling constant intermediate between the three-coordinate $[Ag(PPh_3)_2Br]$ ($J(AgP) = 385$ Hz)[15] and four-coordinate $[Ag(PPh_3)_4][PF_6]$ ($J(^{107}AgP) = 224$ Hz)[13] silver phosphane complexes. On the basis of these observations, we tentatively suggest that, at low temperature an approximate 1:1 mixture consisting of the two-coordinate, ion-pair separated, species $[Ag(PPh_3)_2][CB_{11}H_{12}]$ and the dimeric $[Ag(PPh_3)_2(CB_{11}H_{12})]_2$ is formed. No evidence for the disproportionation of **2** to form $[Ag(PPh_3)][CB_{11}H_{12}]$ and $[Ag(PPh_3)_3][CB_{11}H_{12}]$ was seen in the low-temperature $^{31}P\{^1H\}$ NMR spectrum.[13] The low-temperature $^{11}B\{^1H\}$ NMR spectrum exhibits two broad peaks at $\delta = -5.8$ (1B) and $\delta = -11.6$(10B), essentially unshifted from room-temperature values.

The coordination chemistry of the anion [*closo*-$CB_{11}H_{12}]^-$ can be usefully compared with that of [*closo*-$CB_{11}H_6Br_6]^-$, in which the six lower hydrogen atoms in the cage are replaced with bromines, and it is considered to be significantly more weakly coordinating than $[CB_{11}H_{12}]^-$. While there are now a significant number of solid-state structural investigations on the silver salts of perhalogenated anions,[27, 30–33] there are few studies in which both the solution and solid-state structures of their transition metal complexes have been investigated. Addition of one equivalent of PPh_3 to a suspension of $Ag[CB_{11}H_6Br_6]$ in CH_2Cl_2 affords the new complex $[Ag(PPh_3)(CB_{11}H_6Br_6)]$ (**3**). The solid-state structure of **3** is presented in Figure 5. On first inspection, the silver(I) centre is coordinated with the carborane anion through two shorter (2.6963(5) Å and 2.8710(5) Å) Ag–Br interactions and one longer one (3.0953(5) Å), all of which fall comfortably within the sum of the van der Waals radii for silver and bromine. These bond lengths are of similar values to those previously reported for silver complexes of $[CB_{11}H_6Br_6]^-$[31] and dibromoalkane complexes of silver.[52] The silver phosphane bond length (2.4032(10) Å) is slightly longer than that found in **1**. The phosphane phenyl groups adopt a relatively uncommon C_{2v} arrangement, a result of one phenyl group (C(2)–C(7)) twisting to minimise interactions with Br(12). Given that the silver is formally 4-connected in the asymmetric unit, the fact that it appears to adopt a *pseudo*trigonal planar, as opposed to a tetrahedral coordination motif (sum of relevant angles around Ag(1) is 360.5°) was on first inspection puzzling to us. However, similar to **1**, the packing diagram (Figure 6) reveals a long interaction (3.4901(5) Å) between Ag(1) and Br(11)′ on a symmetry related cage in the lattice; this bromine atom approaches Ag(1) approximately *trans* to Br(12) (Br(12)–Ag(1)–Br(11)′ 157.15(1)°). Although this distance is long, the coordination motif around the silver suggests that it is significant in the solid state. This interaction completes the coordination sphere at the silver centre. It also results in phenyl groups on symmetry related phosphanes having a close approach in the lattice (Figure 6), and the Ag(1)–P(1) vector being canted from lying equidistant between Br(7)

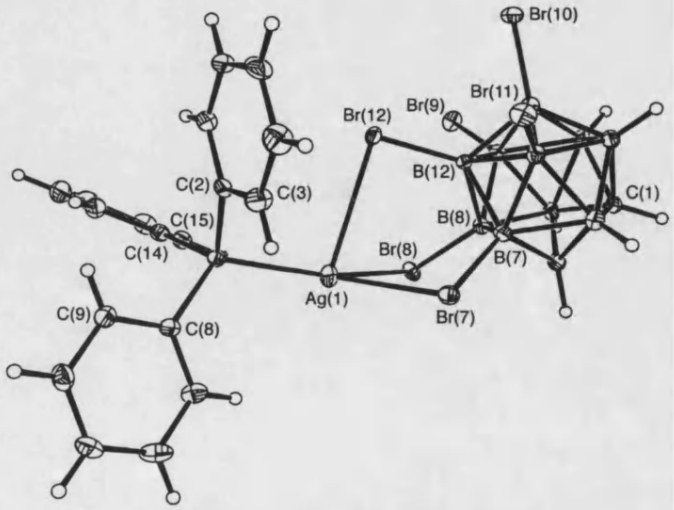

Figure 5. Molecular structure of complex **3**, showing the atom-numbering scheme. Thermal ellipsoids are drawn at the 50% probability level.

0947-6539/02/0809-2092 $ 20.00+.50/0 *Chem. Eur. J.* **2002**, *8*, No. 9

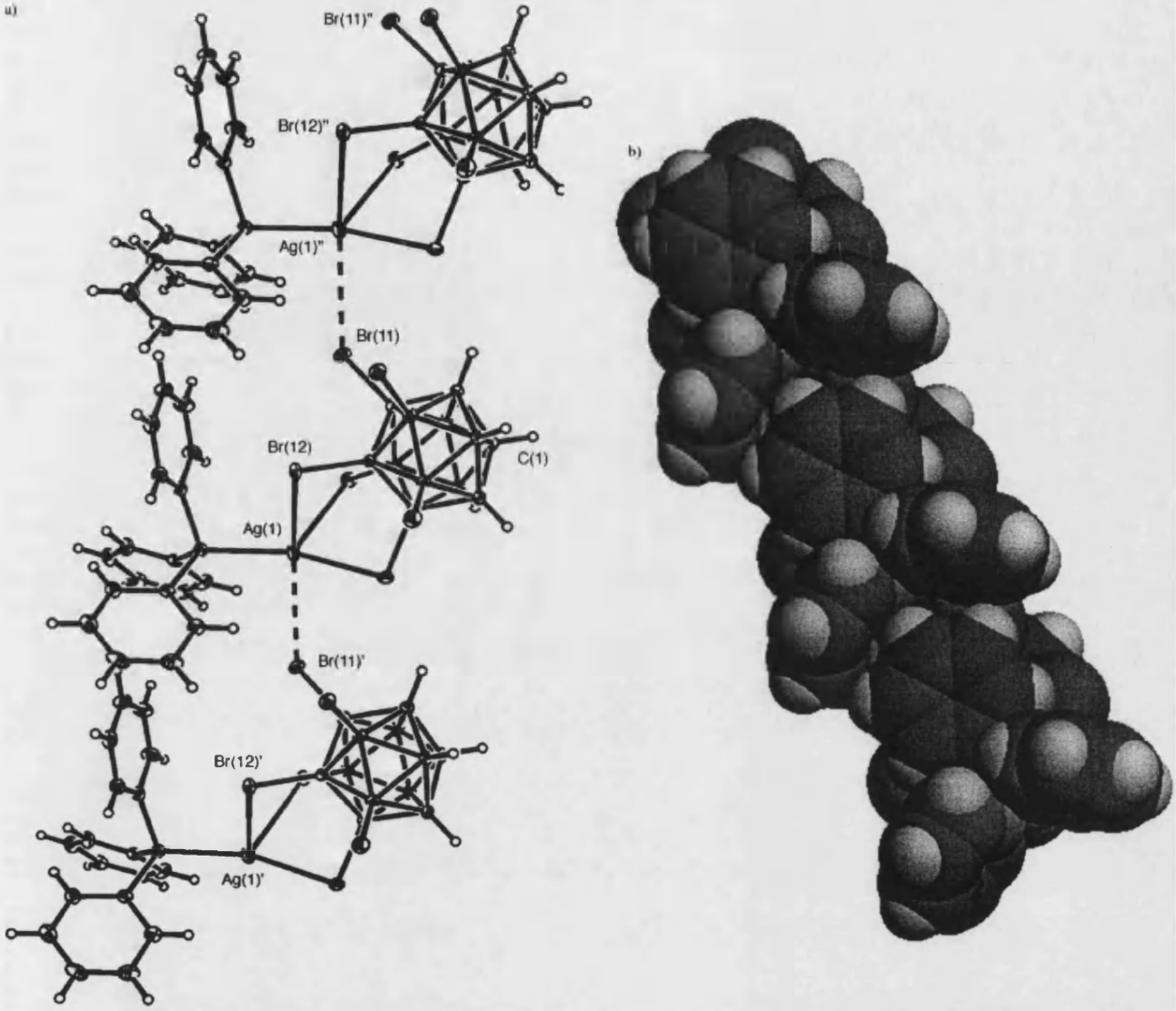

Figure 6. Extended solid-state structure apparent in complex **3**: a) showing weak axial Ag···Br interactions; b) space-filling diagram showing orientation of phenyl groups in the solid state.

and Br(8) (P(1)–Ag(1)–Br(8) 155.55(3)°, P(1)–Ag(1)–Br(7) 117.44(3)°).

In solution, C_{5v} symmetry is observed for the cage anion in the ^{11}B NMR spectrum, which shows that the $\{AgPPh_3\}^+$ fragment does not retain a rigid coordination motif with respect to the cage. The $^{31}P\{^1H\}$ NMR spectrum of **3** is similar to that of **1** with a resonance centred at $\delta = 16.52$ is observed as a concentric pair of doublets, $J(AgP)_{average} = 715$ Hz, suggesting that similar structures are adopted in solution for both complexes. This value is slightly smaller than that observed for **1**, in line with the slightly longer Ag–P bond observed in the solid state for **3** compared with complex **1**.[17]

Addition of two equivalents of PPh_3 to $Ag[CB_{11}H_6Br_6]$ results in the isolation of a white solid having the empirical formula $[Ag(PPh_3)_2(CB_{11}H_6Br_6)]$ (**4**). Despite repeated attempts, crystals suitable for X-ray diffraction could not be obtained, so characterisation of complex **4** was limited to NMR spectroscopy and microanalysis. In solution at room temperature, the $^{31}P\{^1H\}$ NMR spectrum of **4** has a broad singlet at $\delta = 12.9$, showing that the phosphane ligands are undergoing exchange under ambient conditions. The corresponding $^1H\{^{11}B\}$ NMR spectrum shows a 2:1 ratio of phosphane to cage, with no signals observed at high field. The low-temperature (−80 °C) $^{31}P\{^1H\}$ NMR spectrum shows that one species is present at this temperature, due to two concentric doublets centred around $\delta = 8.1$. The magnitude of the AgP coupling constant ($J(AgP)_{average} = 240$ Hz) is very small and of the same order of that associated with $[Ag(PPh_3)_4]^+$.[13] To account for this, a low-temperature limiting structure that has a sp^3 hybridised silver(I) centre is suggested, in which the hexabromo carborane anion is coordinated to the silver by two of the bromines on the cage. That there is a more intimate contact between the halogenated cage and silver in **4** compared with the silver-cage contact

  0947-6539/02/0809-2093 $ 20.00+.50/0

in **2** is further reflected in the relative catalytic activities of these two compounds, which will be presented later. While we have taken measures to use pure samples (recrystallised material used exclusively for NMR and catalysis experiments), we cannot completely rule out the presence of small amounts of free PPh_3 in **2** and **4**, which would lead to rapid phosphane exchange at room temperature.[13]

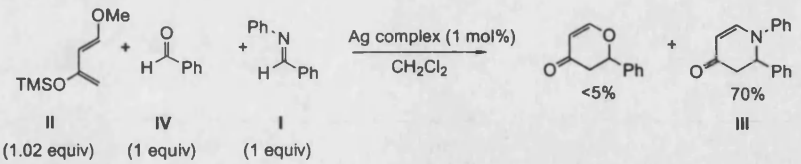

Scheme 3. Activation of imines in the presence of aldehydes by silver complex **3**.

Catalysis: We have investigated the reaction between *N*-benzylideneaniline (**I**) and Danishefsky's diene (**II**) (Scheme 2) with the silver complexes **1** to **4**. Importantly, in the absence of any catalyst there was only a trace (less than 5%) of product after 24 hours at room temperature. Initial experiments using freshly distilled reagent grade solvents revealed that the addition of 1 mol% of silver complex promoted the efficient formation of the product (**III**) in less than one hour at room temperature (Table 3). On the bench under these conditions, complexes **1** to **4** were significantly more active than $[Ag(PPh_3)(OTf)]$ and $[Ag(PPh_3)(BF_4)]$ whilst $[Ag(PPh_3)(ClO_4)]$ was of comparable activity. Remarkably, the catalyst loading could be lowered to 0.1 mol% of complex **3** and the reaction was still complete in less than thirty minutes to afford an isolated yield of 99% product (>2000 turnovers $hour^{-1}$).

Table 3. Yields of compound **III**. Catalyst (1 mol%); imine **I** (1.1 mmol); Danishefsky's diene (**II**) (1.65 mmol). Yields reported are after reaction for 60 minutes at room temperature and workup (see Experimental Section for full details).

	Complex	Isolated yield of **III** [%]
1	$[Ag(PPh_3)(BF_4)]$	35
2	$[Ag(PPh_3)(OTf)]$	70
3	$[Ag(PPh_3)(ClO_4)]$	90
4	$[Ag(PPh_3)(CB_{11}H_{12})]$ (**1**)	98
5	$[Ag(PPh_3)_2(CB_{11}H_{12})]$ (**2**)	99
6	$[Ag(PPh_3)(CB_{11}H_6Br_6)]$ (**3**)	99
7	$[Ag(PPh_3)_2(CB_{11}H_6Br_6)]$ (**4**)	85

A competition experiment illustrated that silver complex **3** could preferentially activate imines in the presence of aldehydes (Scheme 3). When Danishefsky's diene (**II**) was added to a 1:1 mixture of benzaldehyde (**IV**) and imine (**I**) in the presence of 1 mol% of **3**, the product arising from the reaction, after 15 minutes at room temperature, was isolated in 70% yield whilst the aldehyde adduct was produced in only 5% yield. According to the classification system suggested by Kobayashi et al.,[53] the silver catalyst is thus an A-2 Lewis acid (active, imine selective).

Prompted by these results we decided to follow the reactions by ^1H NMR spectroscopy, using catalyst loadings of 0.1 mol%, in the anticipation of uncovering structure–activity relationships involving counterion and/or phosphane ligands. This initially resulted in the unexpected observation that the reaction between diene **II** and imine **I** did not proceed (no reaction after ca. two hours at room temperature) when in the NMR tube, using rigorously dried solvent (CD_2Cl_2 vacuum distilled from CaH_2). However, addition of a substoichiometric amount of water (ca. 50 mol%, 1 μL, unoptimised) to these solutions resulted in rapid initiation of the reaction. This is an example of a water-accelerated Lewis acid catalysed reaction; such reactions, in which water is an important partner, are being increasingly appreciated.[54] Pertinent to this observation, modest yield enhancements on addition of stoichiometric amounts of water to a hetero-Diels–Alder reaction catalysed by lanthanide trifluoromethanesulfonylamides[55] have been reported previously. Currently, we are unsure about the exact role of the water in the reaction. It is likely, however, that a polarised, silver-bound, water molecule acts as a Lewis assisted Brønsted acid, similar to that in lanthanide salt catalysed aromatic electrophilic substitutions.[56] It is also similar to the role metal-coordinated water is suggested to play in certain catalytic processes.[57] In support of this, preliminary DFT calculations on the model system $[Ag(Me_3P)(OH_2)(MeNH{=}CHMe)]^+$ indicate that a coordinated water molecule plays an important function in the silver promoted [2+4] addition of imine to diene. A putative intermediate in this process is shown in Scheme 4, in which the water molecule forms a hydrogen bond with the nitrogen atom.[45] This proposed intermediate accounts for both the observed dependence on trace amounts of water in this reaction and the strong counterion effect observed (vide infra), with both the Lewis assisted Brønsted acidity (OH···N hydrogen bond) and the need for a vacant site (alkene coordination) playing important roles. Experimentally, what is clear is that trace

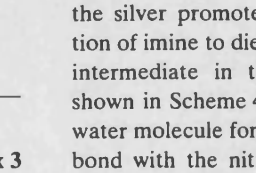

Scheme 4. Proposed intermediate structure.

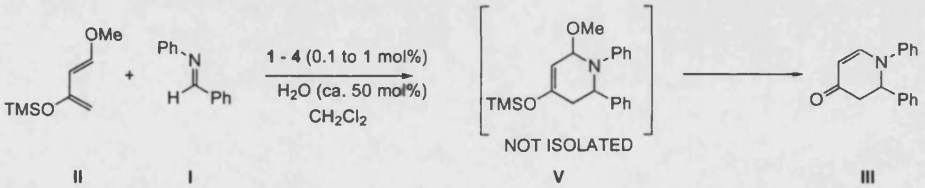

Scheme 2. Reaction between *N*-benzylideneaniline (**I**) and Danishefsky's diene (**II**) with the silver complexes **1**–**4**.

0947-6539/02/0809-2094 $ 20.00+.50/0 *Chem. Eur. J.* **2002**, *8*, No. 9

amounts of water are needed for this reaction to proceed, which is probably made available to the reaction, when at the bench, by adventitious water.

That a silver-bound water molecule is strongly implicated as a catalytic proton source in these reactions is demonstrated by the following control experiments. Addition of just water to a mixture of **I** and **II** affords no product, while under the standard conditions used for catalysis addition of the hindered base 2,6-di-*tert*-butyl-4-methylpyridine suppressed the reaction completely.[56] Moreover, water need not be the unique proton source. The reaction is easily repeated replacing an alcohol (methanol, 20 mol%) for water, resulting in essentially identical product yields and reaction times.

The results of these NMR experiments, in which water is added, are shown in Figure 7 for the new complexes **1** through **4** and for comparison the complexes $[Ag(PPh_3)(BF_4)]$, $[Ag(PPh_3)(ClO_4)]$[58] and $[Ag(PPh_3)(OTf)]$.[16] All of these experiments were carried out at 0.1 mol% catalyst loading with 50 mol% added water in solutions in CD_2Cl_2, with the diene in 1.5 molar excess. The final products in the NMR tube are a consistent mixture of intermediate **V** and final product **III** (ca. 90:10 ratio), which on workup gives only the final product. The reactions were monitored by selected peaks due to intermediate **V** and the final product (see Experimental Section). No hydrolysis of the imine to benzaldehyde was observed under the conditions used, while the consumption of imine **I** in each run followed the same time-dependent profile (although inversed) as the increase in **V** and **III**.

It is clear from Figure 7 that complex **3** gives the fastest rate of catalysis, complete conversion being apparent after 15 minutes. This equates to a turnover frequency (TOF) of 4000 $hour^{-1}$, which is excellent for a Lewis acid catalysed reaction of this type. Complex **1**, although a slower catalyst than **3**, also yields complete conversion of the imine after ≈40 minutes. Not unsurprisingly the monophosphane complexes, $[Ag(PPh_3)(ClO_4)]$ and $[Ag(PPh_3)(OTf)]$, which contain more nucleophilic counterions, are less active than **1** and **3**. The addition of an extra PPh_3 ligand would be expected to both reduce the Lewis acidity of the metal centre while also adding more steric bulk and blocking a potential vacant site. It is not unexpected then, that complexes **2** and **4** are significantly poorer catalysts than any of the monophosphane complexes. Interestingly the relative reaction rates for the bisphosphane complexes **2** and **4** are reversed from those seen for the monophosphane/carborane complexes. Complex **2**, which incorporates the $[CB_{11}H_{12}]$ anion, catalyses the reaction significantly faster than **4**. Although this is perhaps counter-intuitive given the relative coordinating abilities of these two anions, when the solution structures at −60 °C are compared (vide supra), complex **4** shows a considerably smaller value for $J(AgP)$, suggesting a silver centre that has a higher formal coordination number in **4** than in **2**. This implies that the $[CB_{11}H_6Br_6]^-$ anion interacts significantly with the metal centre at this temperature in **4**. Although we do not have the solid-state structure of **4** to hand,[59] this correlation between the magnitude of $J(AgP)$ at low temperature and the relative rates of **2** and **4** is compelling. This difference in rate is also reflected in the relative product yields on the bench after one hour (entries 5 and 7 in Table 3).

The catalyst $[Ag(PPh_3)(BF_4)]$ ceases to function after only a few minutes of activity, giving only modest yields of cycloaddition product in both the NMR and the bench-top experiments (Figure 7 and Table 3, entry 1). We suggest that under the conditions used for catalysis (0.1 mol% catalyst, 50 mol% water), rapid (<2 minutes) silver(I) mediated hydrolysis of the $[BF_4]^-$ anion occurs to afford an oxyborate anion that binds strongly with the metal centre, shutting down the catalytic cycle dramatically. In support of this, hydrolysis of $[BF_4]^-$ to afford coordinated oxyborates has been reported previously.[60, 61]

Conclusion

The preparation of the four silver(I) phosphane complexes partnered with the carborane anions [*closo*-$CB_{11}H_{12}$] and

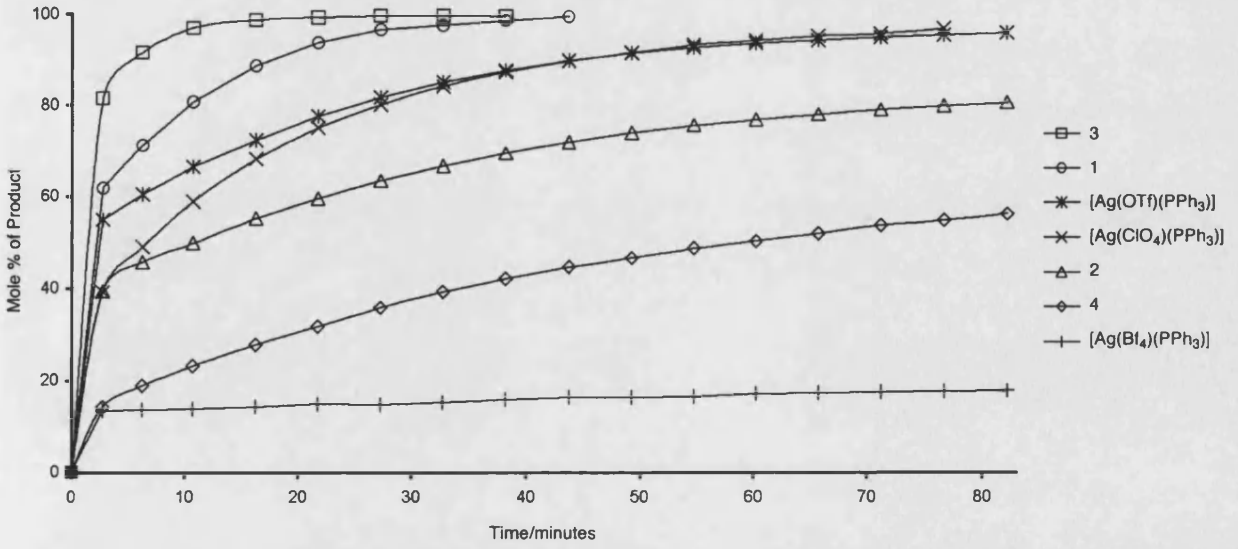

Figure 7. Chart showing relative rates of reaction between **I** and **II** by using 0.1 mol% of catalysts **1**–**4** and $[Ag(PPh_3)(Y)]$ [Y = OTf, BF_4, ClO_4] and 50 mol% added H_2O at room temperature in CD_2Cl_2. See text for other details.

  0947-6539/02/0809-2095 $ 20.00+.50/0

[*closo*-$CB_{11}H_6Br_6$] has allowed a study to be made of the relationship between solid and solution structures and performance as partners to cationic Lewis acids of these anions in an organic transformation. Not unsurprisingly, given the now well-documented[4, 5] inertness coupled with the low nucleophilicity of the hexahalageno anions and the precedent for pronounced counterion effects in Lewis acid catalysed cycloadditions,[62–64] the monophosphane complex **3** is a significantly better catalyst than both **1** and all of the other systems examined. In addition, compound **3** (and presumably the others, although not tested) is selective for imines and can be used at significantly lower catalyst loadings than previously reported for Lewis acid catalysed hetero-Diels–Alder reactions.

To us, the surprising result is that the relative ordering in rate of catalysis between $[CB_{11}H_{12}]$ and $[CB_{11}H_6Br_6]$ is reversed when two phosphanes are coordinated to the silver centre. Although this was unexpected, it is pleasing that a gross correlation exists between observable NMR properties in solution (magnitude of J(AgP)) and the catalytic activity. Thus, complexes **1** and **3**, which have large AgP coupling constants, are better catalysts than **2** and **4**, with the latter complex exhibiting the poorest performance and the lowest coupling constant by far (albeit measured at low temperature). Overall this suggests that when considering catalyst performance in these, and related systems, the influence of counterion and ligands are not independent and need to be considered together. It is however encouraging that useful catalyst performance indicators may be gleaned from simple NMR experiments, which could help in the identification of promising catalytic systems. To this end, we are currently investigating the applicability of complexes such as **3** in other Lewis acid catalysed reactions and will report on these in due course.

Experimental Section

General: All manipulations were carried out under an argon atmosphere by using standard Schlenk line or dry box techniques. CH_2Cl_2 was distilled from CaH_2 and hexane was distilled from sodium. Solution NMR spectra were measured on Varian 400 MHz and Bruker Advance 300 MHz FT-NMR spectrometers in solutions in CD_2Cl_2. Residual protio solvent was used as a reference (CD_2Cl_2, $\delta = 5.33$) in ^{1}H NMR, $BF_3 \cdot OEt_2$ (external) in ^{11}B NMR and 85% H_3PO_4 (external) for ^{31}P NMR spectra. Coupling constants are given in Hz. Elemental analyses were performed in-house at the Department of Chemistry. The complexes $Ag[CB_{11}H_{12}]$[26] and $Ag[CB_{11}H_6Br_6]$[13] were prepared by the published literature routes or variations thereof. All other chemicals were used as purchased from Aldrich.

Preparations

$[Ag(PPh_3)(CB_{11}H_{12})]$ (***1***): PPh_3 (0.163 g, 0.650 mmol) was dissolved in CH_2Cl_2 (10 mL) and added dropwise to a Schlenk flask charged with $Ag[CB_{11}H_{12}]$ (0.155 g, 0.591 mmol), in the dark and with stirring. This solution was stirred overnight and then cannula filtered. The solvent was removed in vacuo to leave a pale yellow solid. Colourless crystals suitable for an X-ray diffraction study were grown by redissolving the product up in minimum CH_2Cl_2, layering with hexane, then placing the sample in a freezer overnight at −30 °C (0.281 g, 92% yield).

^{1}H{^{11}B} (22 °C): $\delta = 7.52-7.29$ (m, 15H; C_6H_5), 2.55 (brs, 1H; CH_{cage}), 2.25 (brs, 1H; BH), 1.85 (10H; 5+5 coincidence, BH); selected ^{1}H{^{11}B} (−90 °C): $\delta = 2.59$ (brs, 1H; CH_{cage}), 2.34 (brs, 1H; BH), 1.94 (5H; BH), 1.76 (5H; BH); ^{11}B{^{1}H} (22 °C): $\delta = -10.3$ (shbr, 1B), −11.2 (br, 5B), −12.0 (5B); ^{11}B $\delta = -10.3$ (d, 5+1 coincidence, J(HB) = 118 Hz), −12.0 (d, J(HB) = 110 Hz, 5B); ^{31}P{^{1}H} (22 °C): $\delta = 18.70$ (dd, $J(Ag^{109}P) = 795$, $J(Ag^{107}P) = 691$ Hz, 1P); IR (KBr): $\tilde{\nu} = 2565$ (vs, BH), 2517 (shs, BH), 2372 cm^{-1} (m, BH); elemental analysis calcd (%) for $C_{19}H_{27}B_{11}AgP$: C 44.5, H 5.30; found: C 44.3, H 5.19.

$[Ag(PPh_3)_2(CB_{11}H_{12})]$ (***2***): $Ag[CB_{11}H_{12}]$ (0.075 g, 0.299 mmol) and PPh_3 (0.158 g, 0.602 mmol) were stirred together in CH_2Cl_2 (15 mL) in the dark for 1 hour. This solution was filtered and hexane (20 mL) added to the filtrate to induce crystallisation. The colourless product was isolated by decanting off the solvent and drying in vacuo (0.204 g, 88% yield). Crystals suitable for an X-ray diffraction study were grown by redissolving a portion of the solid product in a minimum of CH_2Cl_2, layering with hexanes and then placing in a freezer overnight at −30 °C to yield white crystals.

^{1}H{^{11}B} (22 °C): $\delta = 7.45-7.18$ (m, 30H; C_6H_5), 2.21 (brs, 1H; CH_{cage}), 1.85 (brs, 1H; BH_a), 1.58 (brs, 10H; 5+5 coincidence, BH); ^{11}B{^{1}H} (CD_2Cl_2, 22 °C): $\delta = -5.1$ (brs, 1B), −10.6 (brs, 5B), −12.6 (brs, 5B); ^{11}B (22 °C): $\delta = -5.1$ (d, J(HB) = 128 Hz, 1B), −10.6 (d, J (HB) = 138 Hz, 5B), −12.6 (d, J(HB) = 158 Hz, 5B); ^{31}P{^{1}H} (CD_2Cl_2, 22 °C): $\delta = 14.8$ (s, br); ^{31}P{^{1}H} (−60 °C): $\delta = 13.7$ (brd, J(AgP) = 333 Hz), 13.6 (dd, $J(Ag^{109}P) = 554$, $J(Ag^{107}P) = 483$ Hz); IR (KBr): 2544 (vs, BH), 2442 (m, BH), 2396 cm^{-1} (m, BH); elemental analysis calcd (%) for $C_{37}H_{42}B_{11}AgP_2$: C 57.3, H 5.46; found: C 57.2, H 5.53.

$[Ag(PPh_3)(CB_{11}H_6Br_6)]$ (***3***): PPh_3 (0.062 g, 0.236 mmol) was dissolved in CH_2Cl_2 (10 mL) and added dropwise to a Schlenk flask charged with $Ag[CB_{11}H_6Br_6]$ (0.200 g, 0.276 mmol) in the dark and with stirring. The resulting solution was stirred overnight and filtered. The supernatent solvent was removed in vacuo to leave a clear oil. Crystals suitable for an X-ray diffraction study were grown by redissolving the product up in minimum CH_2Cl_2, layering with hexane, then placing the sample in a freezer overnight at −30 °C (0.194 g, 83% yield).

^{1}H{^{11}B}: $\delta = 7.52-7.22$ (m, 15H; C_6H_5), 2.73 (brs, 1H; CH_{cage}), 2.43 (5H; BH); ^{11}B: $\delta = -2.1$ (brs, 1B, B), −6.6 (brs, 5B, BBr), −16.9 (d, J(HB) = 157 Hz, 5B, BH); ^{31}P{^{1}H}: $\delta = 16.52$ (d of d, $J(Ag^{109}P) = 766$, $J(Ag^{107}P) = 664$ Hz, 1P); IR (KBr): 2608 (vs, BH), 2593 cm^{-1} (s, BH); elemental analysis calcd (%) for $C_{19}H_{21}B_{11}AgPBr_6$: C 23.1, H 2.12; found: C 22.6, H 2.17.

$[Ag(PPh_3)_2(CB_{11}H_6Br_6)]$ (***4***): The compounds $Ag[CB_{11}H_6Br_6]$ (0.250 g, 0.345 mmol) and PPh_3 (0.181 g, 0.690 mmol) were stirred together in CH_2Cl_2 (20 mL) in the dark for 1 hour. The solution formed was filtered and solvent removed in vacuo to leave a white solid. This solid was redissolved in minimum CH_2Cl_2, layered with hexane and placed in a freezer overnight at −30 °C to afford a colourless microcrystalline powder (0.246 g, 57%).

^{1}H{^{11}B}: $\delta = 7.45-6.87$ (m, 30H; C_6H_5), 2.45 (brs, 1H; CH_{cage}), 2.21 (brs, 5H); ^{11}B: $\delta = 1.3$ (brs, 1B, B), −6.8 (s, 5B), −17.2 (d, J(HB) = 166 Hz, 5B); ^{31}P{^{1}H} (22 °C): $\delta = 8.1$ (brs); ^{31}P{^{1}H} (−80 °C): $\delta = 8.06$ (dd, $J(^{109}AgP) = 256$, ^{107}J(AgP) = 223 Hz); IR (KBr): 2956 (vs, BH), 2587 cm^{-1} (s, BH); elemental analysis calcd (%) for $C_{37}H_{36}B_{11}AgP_2Br_6$: C 35.7, H 2.89; found: C 35.5, H 3.01.

General experimental procedure for catalytic studies: The imine **I** (0.200 g, 1.1 mmol) in dichloromethane (1.5 mL) at room temperature was added to a stirring solution of freshly recrystallised catalyst (1 mol%) in dichloromethane (3.5 mL). The reaction mixture was allowed to stir for 5 minutes then Danishefsky's diene (**II**) (320 μL, 1.65 mmol) was added dropwise. After 60 minutes, the reaction was quenched with aqueous sodium hydrogen carbonate and extracted with ethyl acetate. The crude product was purified by chromatography on silica gel (hexane/ethyl acetate 4:1) to afford the product **III**.

^{1}H NMR: $\delta = 7.67$ (dd, J(HH) = 1, 7 Hz, 1H), 7.35–6.99 (m, 10H), 5.27 (dd, J(HH) = 1, 7 Hz, 2H), 3.29 (dd, J(HH) = 7, 16 Hz, 1H), 2.77 (ddd, J(HH) = 1, 3, 16 Hz, 1H).

General procedure for NMR tube reactions: Solutions of catalyst were typically prepared by dissolving the compound (1 mg) in CD_2Cl_2 (1 mL) with the use of an ultrasound bath to ensure complete catalyst dissolution, although, by eye, the solids seemed to have dissolved completely. The relevant quantity of catalyst solution to give a 0.1 mol% catalyst concentration (i.e. 0.00011 mmol of catalyst) was taken from this standard solution and placed in an NMR tube previously charged with *N*-benzylideneaniline (20 mg, 0.11 mmol). Danishefsky's diene (32 μL, 0.17 mmol) and water (1 μL, 0.056 mmol) were added to the NMR tube, which was then shaken

0947-6539/02/0809-2096 $ 20.00+.50/0 *Chem. Eur. J.* **2002**, *8*, No. 9

vigorously before being placed in the NMR spectrometer and measurements were taken at timed intervals. The disappearance of the peak at $\delta = 8.51$ due to PhN=C*H*Ph was monitored, along with the growth of the peaks centred at $\delta = 6.64$ and $\delta = 6.54$ [3H total, intermediate **V**] and $\delta = 5.27$ [1H total, final product **III**]. A plot for each catalyst, of time verses consumption of **I** and time verses total concentrations of **V** and **III** showed essentially the same profile. Repeat runs for all the catalysts tested showed the same time-dependent profiles.

Intermediate **V**: ^{1}H NMR: $\delta = 7.56$ (d, J(HH) = 13 Hz, 1H), 7.42–7.40 (m, 2H), 7.28–7.23 (m, 1H), 7.10–7.01 (m, 3H), 6.64 (m, 1H), 6.54 (m, 2H), 5.58 (d, J(HH) = 12 Hz, 1H), 4.86 (q, J(HH) = 6 Hz, 1H), 4.71 (d, J(HH) = 6 Hz, 1H), 3.68 (s, 3H), 2.94 (dd, J(HH) = 6 Hz, 22H), 0.144 (s, 9H).

X-ray crystallography: The crystal structure data for compounds **1**–**3** were collected on a Nonius KappaCCD. Structure solution followed by full-matrix least-squares refinement was performed by using the SHELX suite of programs throughout.[65] Hydrogens were included at calculated positions throughout, with the exception of H7 and H12 in compound **2**. These latter hydrogens were readily located in the penultimate difference Fourier map and refined at a fixed distance 1.12 Å from parent atoms B(7) and B(12), respectively. Plots were produced by using ORTEX.[66]

CCDC-171721 (**1**), 171769 (**2**) and 168828 (**3**) contain the supplementary crystallographic data for this paper. These data can be obtained free of charge via www.ccdc.cam.ac.uk/conts/retrieving.html (or from the Cambridge Crystallographic Data Centre, 12 Union Road, Cambridge CB21EZ, UK; fax: (+44) 1223-336-033; or e-mail: deposit@ccdc.cam.ac.uk).

Acknowledgements

A.S.W. thanks the Royal Society for a University Research Fellowship and equipment grant. The University of Bath is also thanked for financial support (studentships to N.J.P. and C.H.). C.G.F. thanks Astra-Zeneca for generous support from their strategic research fund. The use of the Cambridge Structural Database at Daresbury service is acknowledged. The EPSRC/JERI are acknowledged for funding for the diffractometer.

[1] C. A. Reed, *Acc. Chem. Res.* **1998**, *31*, 133.
[2] S. H. Strauss, *Chem. Rev.* **1993**, *93*, 927.
[3] I. Zharov, B. T. King, Z. Havlast, A. Pardi, J. Michl, *J. Am. Chem. Soc.* **2000**, *122*, 10253.
[4] C. A. Reed, N. L. P. Fackler, K. C. Kim, D. Stasko, D. R. Evans, P. D. W. Boyd, C. E. F. Rickard, *J. Am. Chem. Soc.* **1999**, *121*, 6314.
[5] C. A. Reed, K. C. Kim, R. D. Bolskar, L. J. Mueller, *Science* **2000**, *289*, 101.
[6] A. J. Lupinetti, M. D. Havighurst, S. M. Miller, O. P. Anderson, S. H. Strauss, *J. Am. Chem. Soc.* **1999**, *121*, 11920.
[7] H. W. Turner, European Patent Application 277003, **1988**; [*Chem. Abstr.* **1988**, *110*, 58291].
[8] G. G. Hlatky, R. R. Eckman, H. W. Turner, *Organometallics* **1992**, *11*, 1413.
[9] G. G. Hlatky, H. W. Turner, R. R. Eckman, *J. Am. Chem. Soc.* **1989**, *111*, 2728.
[10] D. J. Crowther, S. L. Borkowsky, D. Swenson, T. Y. Meyer, R. F. Jordan, *Organometallics* **1993**, *12*, 2897.
[11] W. V. Konze, B. L. Scott, G. J. Kubas, *Chem. Commun.* **1999**, 1807.
[12] J. Powell, A. Lough, T. Saeed, *J. Chem. Soc. Dalton Trans.* **1997**, 4137.
[13] E. L. Muetterties, C. W. Alegranti, *J. Am. Chem. Soc.* **1972**, *94*, 6386.
[14] R. E. Bachmann, D. F. Andretta, *Inorg. Chem.* **1998**, *37*, 5657.
[15] G. A. Bowmaker, Effendy J. V. Hanna, P. C. Healy, B. W. Skelton, A. H. White, *J. Chem. Soc. Dalton Trans.* **1993**, 1387.
[16] M. Bardají, O. Crespo, A. Laguna, A. K. Fischer, *Inorg. Chim. Acta.* **2000**, *304*, 7.
[17] G. A. Bowmaker, J. V. Hanna, C. E. F. Rickard, A. S. Lipton, *Dalton Trans.* **2001**, 20.
[18] H. M. Colquohoun, T. J. Greenhough, M. G. H. Wallbridge, *J. Chem. Soc. Chem. Commun.* **1980**, 192.
[19] D. D. Ellis, P. A. Jellis, F. G. A. Stone, *Organometallics* **1999**, *18*, 4982.
[20] D. D. Ellis, A. Franken, P. A. Jellis, J. A. Kautz, F. G. A. Stone, *Dalton Trans.* **2000**, 2509.
[21] D. D. Ellis, J. C. Jeffery, P. A. Jelliss, J. A. Kautz, F. G. A. Stone, *Inorg. Chem.* **2001**, *40*, 2041.
[22] Y.-W. Park, J. Kim, Y. Do, *Inorg. Chem.* **1994**, *33*, 1.
[23] D. J. Liston, C. A. Reed, C. W. Eigenbrot, W. R. Scheidt, *Inorg. Chem.* **1987**, *26*, 2739.
[24] N. J. Patmore, J. W. Steed, A. S. Weller, *Chem. Commun.* **2000**, 1055.
[25] N. J. Patmore, M. F. Mahon, J. W. Steed, A. S. Weller, *Dalton Trans.* **2001**, 277.
[26] K. Shelly, D. C. Finster, Y. J. Lee, W. R. Scheidt, C. A. Reed, *J. Am. Chem. Soc.* **1985**, *107*, 5955.
[27] S. V. Ivanov, A. J. Lupinetti, S. M. Miller, O. P. Anderson, K. A. Solnstev, S. H. Strauss, *Inorg. Chem.* **1995**, *34*, 6419.
[28] Z. W. Xie, T. Jelinek, R. Bau, C. A. Reed, *J. Am. Chem. Soc.* **1994**, *116*, 1907.
[29] S. V. Ivanov, J. J. Rockwell, S. M. Miller, O. P. Anderson, K. A. Solntsev, S. H. Strauss, *Inorg. Chem.* **1996**, *35*, 7882.
[30] C.-W. Tsang, Q. Yang, E. T.-P. Sze, T. C. W. Mak, D. T. W. Chan, Z. Xie, *Inorg. Chem.* **2000**, *39*, 5851.
[31] Z. Xie, B.-M. Wu, T. C. W. Mak, J. Manning, C. A. Reed, *J. Chem. Soc. Dalton Trans.* **1997**, 1213.
[32] Z. Xie, R. Bau, C. A. Reed, *Angew. Chem.* **1994**, *106*, 2566; *Angew. Chem. Int. Ed. Engl.* **1994**, *33*, 2433.
[33] T. Jelinek, P. Baldwin, W. R. Scheidt, C. A. Reed, *Inorg. Chem.* **1993**, *32*, 1982.
[34] A. Yanagisawa in *Lewis Acids in Organic Synthesis* (Ed.: H. Yamamoto), Wiley-VCH, Weinheim, **2000**.
[35] T. Hayashi, M. Sawamura, Y. Ito, *Tetrahedron* **1999**, *48*, 1992.
[36] A. Togni, S. D. Pastor, *J. Org. Chem.* **1990**, *55*, 1649.
[37] A. Yanagisawa, H. Nakashima, A. Ishiba, H. Yamamoto, *J. Am. Chem. Soc.* **1996**, *118*, 4723.
[38] A. Yanagisawa, Y. Nakatuska, K. Asakawa, H. Kageyama, H. Yamamoto, *Synlett* **2001**, 69.
[39] M. Ohkouchi, D. Masui, M. Yamaguchi, T. Yamagishi, *J. Mol. Catal. A* **2001**, *170*, 1.
[40] A. Yanagisawa, Y. Matsumoto, H. Nakashima, K. Asakawa, H. Yamamoto, *J. Am. Chem. Soc.* **1997**, *119*, 9319.
[41] S. Yoo, S. Saaby, R. G. Hazell, K. A. Jørgensen, *Chem. Eur. J.* **2000**, *6*, 2435.
[42] C. Hague, N. J. Patmore, C. G. Frost, M. F. Mahon, A. S. Weller, *Chem. Commun.* **2001**, 2286.
[43] D. J. Liston, Y. J. Lee, W. R. Scheidt, C. A. Reed, *J. Am. Chem. Soc.* **1989**, *111*, 6643.
[44] A. S. Weller, M. F. Mahon, J. W. Steed, *J. Organomet. Chem.* **2000**, *614–615*, 113.
[45] G. D. Ruggiero, A. S. Weller, I. H. Williams, unpublished results.
[46] H.-P. Wu, C. Janiak, G. Rheinwald, H. Lang, *J. Chem. Soc. Dalton Trans.* **1999**, 183.
[47] C. Kleina, E. Graf, M. W. Hosseini, A. D. Cian, J. Fischer, *Chem. Commun.* **2000**, 239.
[48] S. A. Brew, F. G. A. Stone, *Adv. Organomet. Chem.* **1993**, *35*, 135.
[49] A. S. Weller, T. P. Fehlner, *Organometallics* **1999**, *18*, 447.
[50] H. Brunner, D. Mijolovic, B. Wrackmeyer, B. Nuber, *J. Organomet. Chem.* **1999**, *579*, 298.
[51] G. S. Mhinzi, S. A. Litster, A. D. Redhouse, J. L. Spencer, *J. Chem. Soc. Dalton Trans.* **1991**, 2769.
[52] D. M. V. Seggen, P. K. Hurlburt, O. P. Anderson, S. H. Strauss, *Inorg. Chem.* **1995**, *34*, 3453.
[53] H. Kobayashi, T. Busujima, S. Nagayama, *Chem. Eur. J.* **2000**, *6*, 3491.
[54] S. Ribe, P. Wipf, *Chem. Commun.* **2001**, 299.
[55] K. Mikami, O. Kotera, Y. Motoyama, H. Sakaguchi, *Synlett* **1995**, 975.
[56] A. G. M. Barrett, D. C. Braddock, J. P. Henschke, E. R. Walker, *Perkin Trans. 1* **1999**, 873.
[57] N.-M. Kao, C. P. Grey, K. Pitchumai, P. H. Lakshminarasimhan, V. Ramamurthy, *J. Phys. Chem.* **1998**, *102*, 5627.
[58] T. G. M. H. Dikkhoff, R. G. Goel, E. L. Muetterties, C. W. Alegranti, *Inorg. Chim. Acta* **1980**, *44*, L72.
[59] Note added in proof: After the manuscript was submitted the solid-state structure of compound **4** was determined and it shows a monomeric $[Ag(PPh_3)_2]^+$ fragment bound to one $[CB_{11}H_6Br_6]$ cage

by two lower pentagonal belt bromine atoms, consistent with the structure proposed from the low-temperature $^{31}P\{^1H\}$ NMR spectrum.
[60] C. J. d. Reijer, M. Wörle, P. S. Pregosin, *Organometallics* **2000**, *19*, 309.
[61] G. Brauers, F. J. Feher, M. Green, J. K. Hogg, A. G. Orpen, *J. Chem. Soc. Dalton Trans.* **1996**, 3387.
[62] A. Lightfoot, O. Schinder, A. Pfaltz, *Angew. Chem.* **1998**, *110*, 3047; *Angew. Chem. Int. Ed.* **1998**, *37*, 2897.
[63] E. P. Kündig, C. M. Saudan, G. Bernardinelli, *Angew. Chem.* **1999**, *111*, 1298; *Angew. Chem. Int. Ed.* **1999**, *38*, 1220.
[64] D. A. Evans, J. A. Murry, P. v. Matt, R. D. Norcross, S. J. Miller, *Angew. Chem.* **1995**, *107*, 864; *Angew. Chem. Int. Ed. Engl.* **1995**, *34*, 798.
[65] G. M. Sheldrick, SHELX-97. Program for Refinement of Crystal Structures, University of Göttingen, Göttingen (Germany), **1997**.
[66] P. McArdle, *J. Appl. Crystallogr.* **1995**, *28*, 65.

Received: October 15, 2001 [F3613]

  0947-6539/02/0809-2098 $ 20.00+.50/0

Organometallics **2002**, *21*, 2856–2865

Rhodium Phosphines Partnered with the Carborane Monoanions $[CB_{11}H_6Y_6]^-$ (Y = H, Br). Synthesis and Evaluation as Alkene Hydrogenation Catalysts

Adem Rifat, Nathan J. Patmore, Mary F. Mahon, and Andrew S. Weller*

Department of Chemistry, University of Bath, Bath BA2 7AY, U.K.

Received January 31, 2002

Addition of Ag[*closo*-$CB_{11}H_{12}$] to $[(PPh_3)_2RhCl]_2$ affords the new *exo*polyhedrally coordinated complex $[(PPh_3)_2Rh(closo\text{-}CB_{11}H_{12})]$ (**1**), which has been characterized by multinuclear NMR spectroscopy and X-ray crystallography. Using the less nucleophilic [*closo*-$CB_{11}H_6Br_6]^-$ anion afforded the arene-bridged dimer $[(PPh_3)(PPh_2\text{-}\eta^6\text{-}C_6H_5)Rh]_2[closo\text{-}CB_{11}H_6Br_6]_2$ (**2**) with poor compositional purity. However, with the new precursor complexes $[(PPh_3)_2Rh(nbd)][Y]$ (Y = *closo*-$CB_{11}H_{12}$ (**3**), *closo*-$CB_{11}H_6Br_6$ (**4**); nbd = norbornadiene) as starting materials, treatment with H_2 affords **1** and **2** in good yield and compositional purity. Complex **2** has been characterized by multinuclear NMR spectroscopy and X-ray diffraction. The new complexes **3** and **4** have been evaluated as internal alkene hydrogenation catalysts using the substrates cyclohexene, 1-methylcyclohexene, and 2,3-dimethylbut-2-ene under the attractive conditions of room temperature and pressure. These new catalysts have also been compared with $[(PPh_3)_2Rh(nbd)][BF_4]$ and Crabtree's catalyst, $[(py)(PCy_3)Ir(cod)][PF_6]$ (cod = 1,5-cyclooctadiene). A clear counterion effect is observed. For the hydrogenation of cyclohexene the $[BF_4]^-$ and [*closo*-$CB_{11}H_{12}]^-$ salts are broadly similar, but the [*closo*-$CB_{11}H_6Br_6]^-$ salt is significantly better, matching Crabtree's catalyst in hydrogenation efficiency. This pattern is mirrored in the hydrogenation of 1-methylcyclohexene and the sterically hindered 2,3-dimethylbut-2-ene, although with the latter substrate Crabtree's catalyst does outperform **4**. Nevertheless, these results are excellent for a rhodium complex, which have traditionally been considered as ineffectual catalysts for the hydrogenation of internal alkenes at room temperature and pressure. The deactivation product in the catalytic cycle, $[(PPh_3)_2HRh(\mu\text{-}Cl)_2(\mu\text{-}H)RhH(PPh_3)_2][CB_{11}H_{12}]$ (**5**), has been characterized by multinuclear NMR spectroscopy and X-ray crystallography.

Introduction

The use of rhodium-based catalysts of the general types $RhCl(PR_3)_3$ and $[(PR_3)_2Rh(nbd)]^+$ (nbd = norbornadiene) for the hydrogenation of olefins has been a topic of significant academic and commercial interest over the last 30 years.[1−4] However, one limitation of these systems is that they are relatively slow for the hydrogenation of internal double bonds under ambient laboratory conditions.[5,6] This methodological gap is, in part, filled by iridium-based catalysts, such as [(cod)Ir(pyridine)PCy_3][PF_6] (cod = 1,5-cyclooctadiene)[5,7,8] or related compounds,[9] which are significantly better at the room-temperature and -pressure hydrogenation of sterically demanding internal alkenes than their rhodium counterparts $[(PPh_3)_2Rh(nbd)][PF_6]$ and $RhCl(PPh_3)_3$. Since the catalysts of choice for hydrogenation of an alkene are often based around cationic metal fragments, such as $\{(L)_2Rh(diene)\}^+$ and $\{(L)_2Ir(diene)\}^+$ (L = phosphine), it is always necessary to pair these with an anionic counterion such as $[BF_4]^-$ or $[PF_6]^-$. The role of the counterion in metal-mediated catalysis in general is becoming increasingly appreciated,[10−12] and as far as hydrogenation reactions are concerned, notable examples exist of increases in both overall efficiency and enantioselectvity on changing the counterion.[13−16] Central to the work reported here is the use of *least*

* To whom correspondence should be addressed. Tel: (01225) 323394. Fax: (01225) 826231. E-mail: a.s.weller@bath.ac.uk.

(1) Brunner, H. Hydrogenation. In *Applied Homogeneous Catalysis with Organometallic Compounds*; Cornils, B., Hermann, W. A., Eds.; Wiley-VCH: Weinheim, Germany, 2000; p 201.
(2) Schrock, R. R.; Osborn, J. A. *J. Am. Chem. Soc.* **1976**, *98*, 2134.
(3) Noyori, R. *Asymmetric Catalysis in Organic Synthesis*; Wiley: New York, 1994.
(4) Gridnev, I. D.; Yasutake, M.; Higashi, N.; Imamoto, T. *J. Am. Chem. Soc.* **2001**, *123*, 5268.
(5) Crabtree, R.; Gautier, A.; Giordano, G.; Khan, T. *J. Organomet. Chem.* **1977**, *141*, 113.
(6) Parshall, G. W.; Ittel, S. D. *Homogeneous Catalysis*, 2nd ed.; Wiley: New York, 1992.
(7) Crabtree, R. *Acc. Chem. Res.* **1979**, *12*, 331.
(8) Crabtree, R.; Demou, P. C.; Eden, D.; Mihelcic, J. M.; Parnell, C. A.; Quirk, J. M.; Morries, G. E. *J. Am. Chem. Soc.* **1982**, *104*, 6994.
(9) Lee, H. M.; Jiang, T.; Stevens, E. D.; Nolan, S. P. *Organometallics* **2001**, *20*, 1255.
(10) Evans, D. A.; Lectka, T.; Matt, P. V.; Miller, S. J. *J. Am. Chem. Soc.* **1999**, *121*, 7559.
(11) Kündig, E. P.; Saudan, C. M.; Bernardinelli, G. *Angew. Chem., Int. Ed.* **1999**, *38*, 1220.
(12) Chen, E. Y. X.; Marks, T. J. *Chem. Rev.* **2000**, *100*, 1391.
(13) Ohta, T.; Ikegami, H.; Miyake, T.; Takaya, H. *J. Organomet. Chem.* **1995**, *502*, 169.
(14) Buriak, J. M.; Osborn, J. A. *Organometallics* **1996**, *15*, 3161.
(15) (a) Lightfoot, A.; Schinder, O.; Pfaltz, A. *Angew. Chem., Int. Ed.* **1998**, *37*, 2897. (b) Blackmond, D. G.; Lightfoot, A.; Pflatz, A.; Rosner, T.; Schnider, P.; Zimmermann, N. *Chirality* **2000**, *12*, 442.
(16) Buriak, J. M.; Klein, J. C.; Herrington, D. G.; Osborn, J. A. *Chem. Eur. J.* **2000**, *6*, 139.

10.1021/om020077r CCC: $22.00
Publication on Web 06/04/2002

coordinating anions[17] to increase reaction rates and yields of product in catalytic processes that implicate a cationic, unsaturated metal center. We have a current interest in the use of weakly coordinating carborane monoanions[18] partnered with Lewis acidic metal/ligand fragments,[19-21] and have recently demonstrated that significant gains in rate enhancement and catalyst stability can be brought about by using anions derived from [*closo*-$CB_{11}H_{12}]^-$ in a silver(I) phosphine catalyzed hetero Diels–Alder reaction.[22] In particular, the use of the hexabromo-substituted carborane [*closo*-$CB_{11}H_6Br_6]^-$ affords a catalyst that shows significant increases in observed rate for this reaction over [*closo*-$CB_{11}H_{12}]^-$ and other, more conventional counterions such as perchlorate and tetrafluoroborate.

Metallacarboranes, and especially rhodacarboranes, have been shown to be active homogeneous catalysts for alkene hydrogenation. This was first demonstrated by Hawthorne,[23-28] who also elucidated the mechanistic aspects of these catalysts,[29] showing that an *exo-nido*-$\{Rh(PR_3)_2\}^+$ fragment plays an important part in the catalytic cycle. More recently, Teixidor and co-workers have extended this idea by using tethered *exo-nido*-monophosphinorhodacarboranes and -monothiorhodacarboranes,[30-33] while other workers have also contributed to the area, especially in enantioselective catalysis using rhodacarboranes.[34,35] In general, all these catalysts show good activities for the hydrogenation of terminal olefins such as 1-hexene[23,25,30] at room temperature and pressure, while to effect the efficient hydrogenation of internal alkenes, such as cyclohexene, elevated pressures are required (ca. 20 atm).[33]

Given the stated methodological gap in the ability of rhodium phosphines to hydrogenate internal alkenes efficiently, an obvious synthetic target is a rhodium complex that might compete with iridium catalysts in the hydrogenation of relatively hindered internal alkenes under the attractive conditions of room temperature and pressure. The question we were interested in asking was whether this could be realized by changing the counterion from $[BF_4]^-$ or $[PF_6]^-$ to one derived from [*closo*-$CB_{11}H_{12}]^-$, on the basis that the technological advances in performance made with rhodium-based systems (i.e. chiral ligands, precatalyst design, mechanistic elucidation) could be incorporated directly into new, potentially more efficient catalysts. In this contribution we report the synthesis and characterization of new rhodium catalyst precursors based around the anions [*closo*-$CB_{11}H_{12}]^-$ (**I**) and [*closo*-$CB_{11}H_6Br_6]^-$ (**II**) (Chart 1), and their subsequent evaluation as olefin hydrogenation catalysts. We demonstrate that this methodology affords complexes that are broadly competitive with Crabtree's catalyst in the room-temperature and -pressure hydrogenation of the internal alkenes cyclohexene, 1-methylcyclohexene, and 2,3-dimethyl-2-butene.

Results

Our initial synthetic goal was to prepare representative examples of rhodium phosphine complexes partnered with anions **I** and **II**, affording complexes that are active precatalysts for olefin hydrogenation. In such complexes, the weakly coordinating carborane anion could, in principle, easily move to one side to allow olefin and dihydrogen to coordinate to the rhodium, while remaining available in order to stabilize any unsaturated metal center in a catalytic cycle by B–H–M or B–Br–M interactions. Given the established ability for carborane monoanions, especially the perhalogeno derivatives, to stabilize reactive cationic species[18,36-39] and reveal faster rates in Lewis acid catalyzed reactions,[22,40] we have synthesized precatalysts based on the Schrock–Osborn cationic system, of the general formula $\{[(PPh_3)_2Rh][Y]\}_n$ (L = PPh_3; Y = [*closo*-$CB_{11}H_{12}]$, $n = 1$; Y = [*closo*-$CB_{11}H_6Br_6]$, $n = 2$). These have been synthesized by two routes: silver salt metathesis and hydrogenation of a precursor norbornadiene complex.

Silver Salt Metathesis. Reaction of 1 equiv of $[(PPh_3)_2RhCl]_2$ with Ag[*closo*-$CB_{11}H_{12}]$ affords a red solution from which the new complex [$(PPh_3)_2$Rh(*closo*-$CB_{11}H_{12}$)] (**1**) can be isolated in good yield as crystalline material. The solid-state structure of complex **1** is shown in Figure 1, with salient bond lengths and angles given in Table 2.

An X-ray diffraction study demonstrates that the $\{Rh(PPh_3)_2\}^+$ fragment is bound to the periphery of the cage by two B–H–Rh three-center–two-electron bonds. Exopolyhedrally coordinated $\{Rh\text{-}L_2\}^+$ (L = two-electron donor) fragments with carborane anions have been reported previously. For example, we have recently

(17) Strauss, S. H. *Chem. Rev.* **1993**, *93*, 927.
(18) Reed, C. A. *Acc. Chem. Res.* **1998**, *31*, 133.
(19) Patmore, N. J.; Steed, J. W.; Weller, A. S. *Chem. Commun.* **2000**, 1055.
(20) Patmore, N. J.; Mahon, M. F.; Steed, J. W.; Weller, A. S. *J. Chem. Soc., Dalton Trans.* **2001**, 277.
(21) Weller, A. S.; Mahon, M. F.; Steed, J. W. *J. Organomet. Chem.* **2000**, *614–615*, 113.
(22) Hague, C.; Patmore, N. J.; Frost, C. G.; Mahon, M. F.; Weller, A. S. *Chem. Commun.* **2001**, 2286.
(23) Delaney, M. S.; Knobler, C. B.; Hawthorne, M. F. *Chem. Commun.* **1980**, 849.
(24) Baker, R. T.; Delaney, M. S.; King, R. E., III; Knobler, C. B.; Long, J. A.; Marder, T. B.; Paxson, T. E.; Teller, R. G.; Hawthorne, M. F. *J. Am. Chem. Soc.* **1984**, *106*, 2965.
(25) Behnken, P. E.; Belmont, J. A.; Busby, D. C.; Delaney, M. S.; King, R. E., III; Kreimendahl, C. W.; Marder, T. B.; Wilczynski, J. J.; Hawthorne, M. F. *J. Am. Chem. Soc.* **1984**, *106*, 3011.
(26) Knobler, C. B.; Marder, T. B.; Mizusawa, E. A.; Teller, R. G.; Long, J. A.; Behnken, P. E.; Hawthorne, M. F. *J. Am. Chem. Soc.* **1984**, *106*, 2990.
(27) Long, J. A.; Marder, T. B.; Behnken, P. E.; Hawthorne, M. F. *J. Am. Chem. Soc.* **1984**, *106*, 2979.
(28) Long, J. A.; Marder, T. B.; Hawthorne, M. F. *J. Am. Chem. Soc.* **1984**, *106*, 3004.
(29) Belmont, J. A.; Soto, J.; King, R. E., III; Donaldson, A. J.; Hewes, J. D.; Hawthorne, M. F. *J. Am. Chem. Soc.* **1989**, *111*, 7475.
(30) Teixidor, F.; Flores, M. A.; Viñas, C.; Kivekäs, R.; Sillanpää, R. *Angew. Chem., Int. Ed. Engl.* **1996**, *35*, 2251.
(31) Teixidor, F.; Flores, M. A.; Viñas, C.; Kivekäs, R.; Sillanpää, R. *Organometallics* **1998**, *17*, 4675.
(32) Viñas, C.; Flores, M. A.; Núñez, R.; Teixidor, F.; Kivekäs, R.; Sillanpää, R. *Organometallics* **1998**, *17*, 2278.
(33) Teixidor, F.; Flores, M. A.; Viñas, C.; Sillanpää, R.; Kivekäs, R. *J. Am. Chem. Soc.* **2000**, *122*, 1963.
(34) Pirotte, B.; Felekidis, A.; Fontaine, M.; Demonceau, A.; Noels, A. F.; Delarge, J.; Chizhevesky, I. T.; Zinevich, T. V.; Pisareve, I. V.; Bregadze, V. I. *Tetrahedron Lett.* **1993**, *34*, 1471.
(35) Brunner, H.; Apfelbacher, A.; Zabel, M. *Eur. J. Inorg. Chem.* **2001**, 917.
(36) Xie, Z. W.; Manning, J.; Reed, R. W.; Mathur, R.; Boyd, P. D. W.; Benesi, A.; Reed, C. A. *J. Am. Chem. Soc.* **1996**, *118*, 2922.
(37) Reed, C. A.; Fackler, N. L. P.; Kim, K. C.; Stasko, D.; Evans, D. R.; Boyd, P. D. W.; Rickard, C. E. F. *J. Am. Chem. Soc.* **1999**, *121*, 6314.
(38) Reed, C. A.; Kim, K. C.; Bolskar, R. D.; Mueller, L. J. *Science* **2000**, *289*, 101.
(39) Lupinetti, A. J.; Havighurst, M. D.; Miller, S. M.; Anderson, O. P.; Strauss, S. H. *J. Am. Chem. Soc.* **1999**, *121*, 11920.
(40) Dubay, W. J.; Grieco, P. A.; Todd, L. J. *J. Org. Chem.* **1994**, *59*, 6898.

Chart 1

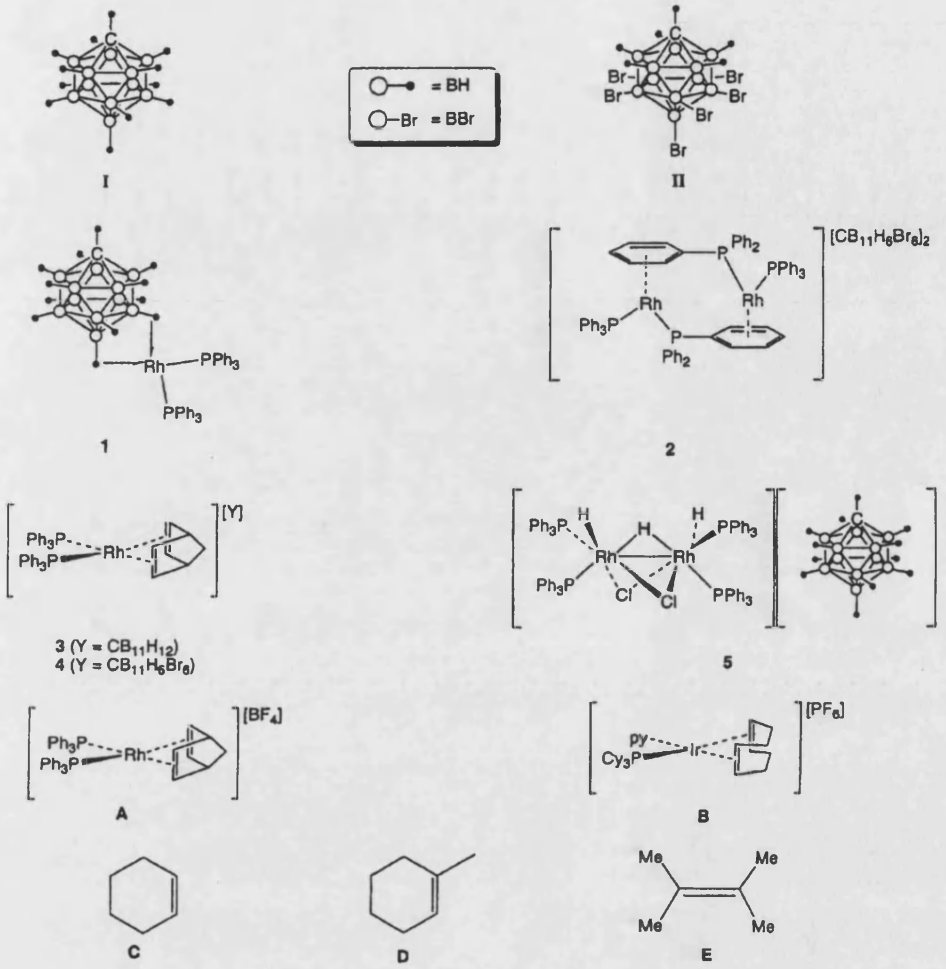

reported the synthesis and solid-state structure of [(cod)Rh(*closo*-$CB_{11}H_{12}$)],[21] while structures incorporating *nido*-{C_2B_9} cages, such as [*exo-nido*-{$Rh(PPh_3)_2$}-7-Me-8-Ph-7,8-$C_2B_9H_{10}$],[26] [Rh(7-SR-8-R′-7,8-$C_2B_9H_{10}$)(cod)],[33] and [10-*endo*-{$Au(PPh_3)$}-5,10-(μ-H)$_2$-*exo*-{$Rh(PPh_3)_2$}-7,8-Me_2-*nido*-$C_2B_9H_7$],[41] are well-established. The spectroscopic characterization of the related complex [$Re(CO)_3$-*exo*-{$Rh(PPh_3)_2$}-7,8-Me_2-*nido*-7,8-$C_2B_9H_9$] has also been reported.[42] The {$Rh(PPh_3)_2$}$^+$ fragment in **1** is coordinated with the cage via two three-center−two-electron bonds through {BH(12)} and {BH(7)}, giving the molecule approximate C_s symmetry, similar to that observed for [(cod)Rh(*closo*-$CB_{11}H_{12}$)], and is as expected on the basis of charge distribution in the cage.[43] Although the location of the {CH} vertex in carboranes can sometimes be problematic, C(1) was located unambiguously by inspection of its thermal parameters and bond lengths to neighboring atoms. The two Rh−B distances are similar, Rh(1)−B(7) = 2.359(3) Å and Rh(1)−B(12) = 2.407(3) Å. These bond lengths are comparable to those observed in [(cod)Rh(*closo*-$CB_{11}H_{12}$)]: viz., 2.391(3) and 2.385(3) Å. The rhodium center in **1** is pseudo square planar coordinated, as reflected in the P(1)−P(2)−B(12)−B(7) dihedral angle of 7.35°. All other bond lengths and angles in **1** are within the ranges expected and are unremarkable.

In solution, the solid-state structure of **1** is not retained. The {$Rh(PPh_3)_2$}$^+$ fragment is fluxional over the lower surface of the cage on the NMR time scale, which is evidenced by local C_{5v} symmetry for the cage being observed in both the $^{11}B\{^1H\}$ and $^1H\{^{11}B\}$ NMR spectra. Thus, three environments are seen in the $^{11}B\{^1H\}$ NMR spectrum, at δ −9.9, −13.5, and −14.1, in the ratio 1:5:5. This pattern is also mirrored in the B−H region of the $^1H\{^{11}B\}$ NMR spectrum. Coordination of a metal fragment to [*closo*-$CB_{11}H_{12}$]$^-$ generally results in a diagnostic upfield shift of those {BH} vertexes involved in bonding,[19,21] and the room-temperature $^{11}B\{^1H\}$ and $^1H\{^{11}B\}$ NMR spectra of complex **1** reflect this by a shift of the signals assigned to the {BH(12)} vertex and the lower pentagonal belt {BH} vertexes, B(7) to B(11), compared with Ag[$CB_{11}H_{12}$].[20] In particular, the unique antipodal {BH} unit is observed at δ −1.97 in the $^1H\{^{11}B\}$ NMR spectrum, which becomes a well-resolved quartet with a reduced value for the BH coupling constant (J(BH) = 119 Hz) in the ^1H NMR spectrum. This is consistent with coordination of a metal fragment and reduction of the B−H bond

(41) Jeffery, J. C.; Jelliss, P. A.; Stone, F. G. A. *J. Chem. Soc., Dalton Trans.* **1993**, 1073.
(42) Ellis, D. D.; Jellis, P. A.; Stone, F. G. A. *Organometallics* **1999**, *18*, 4982.
(43) Hoffmann, R.; Lipscomb, W. N. *J. Chem. Phys.* **1962**, *36*, 3489.

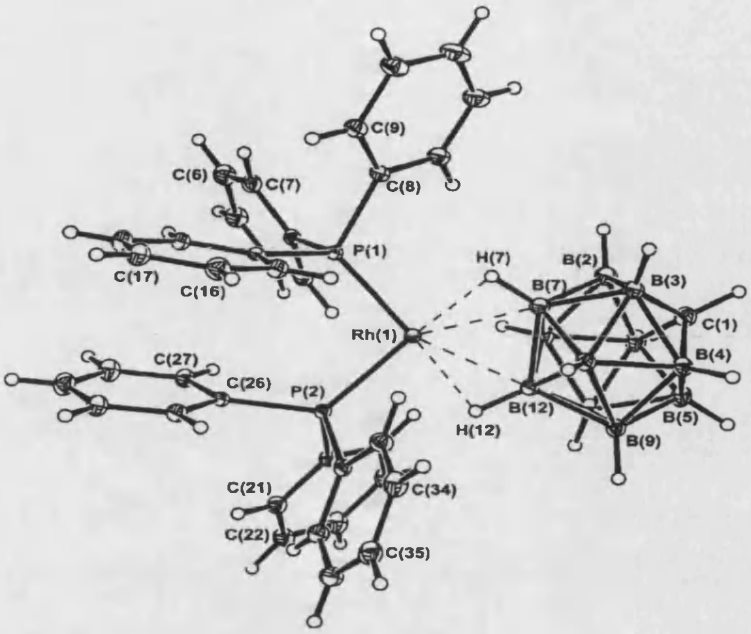

Figure 1. ORTEX drawing of complex **1**. Thermal ellipsoids are drawn at the 30% probability level.

Table 1. Crystal Data and Structure Refinement for Complexes 1, 2, and 5

	1	2	5
empirical formula	$C_{37}H_{42}B_{11}P_2Rh$	$C_{74}H_{72}B_{22}Br_{12}P_4Rh_2 \cdot 2.78CH_2Cl_2$	$C_{74}H_{77}B_{11}Cl_4P_4Rh_2$
fw	770.47	2723.85	1556.77
T/K	293(2)	150(2)	150(2)
cryst syst	monoclinic	monoclinic	monoclinic
space group	$P2_1/c$	$C2/c$	$P2_1/n$
a/Å	9.22630(10)	26.9570(6)	20.5720(7)
b/Å	14.5292(2)	15.0290(4)	16.3620(5)
c/Å	28.4345(3)	27.8970(7)	21.5570(8)
α/deg	90	90	90
β/deg	93.3510(6)	113.284(2)	90.699(2)
γ/deg	90	90	90
U/Å^3	3805.15(8)	10381.6(4)	7255.5(4)
Z	4	4	4
μ/mm^{-1}	0.561	5.181	0.733
no. of rflns collected	57 907	72 519	53 162
no. of indep rflns	8703 (R_{int} = 0.0468)	9133 (R_{int} = 0.1239)	12 705 (R_{int} = 0.2739)
final R1, wR2 indices			
$I > 2\sigma(I)$	0.0309, 0.0850	0.0699, 0.1261	0.0827, 0.1358
all data	0.0447, 0.1048	0.1247, 0.1471	0.1886, 0.1742

strength.[44] The lower pentagonal belt hydrogen atoms are observed as a broader quartet shifted upfield to δ 0.1; while the upper belt hydrogens, which are not involved with metal binding, are essentially unshifted. The fluxional process also renders the phosphine ligands equivalent on the NMR time scale, with one environment being observed at δ 49.0 (J(RhP) = 194 Hz). These observations are consistent with the mechanism previously proposed for the dynamic process occurring with other {L_2M} fragments coordinated to [*closo*-$CB_{11}H_{12}]^-$,[21,45] [*nido*-$C_2B_9H_{11}]^-$,[26] or its derivatives.[42]

Reaction of $[(PPh_3)_2RhCl]_2$ with 1 equiv of Ag[*closo*-$CB_{11}H_6Br_6$] affords a red solution which, after filtration, contains only one compound, spectroscopically identified as $[(PPh_3)_2Rh(\eta^6\text{-}C_6H_5Me)][CB_{11}H_6Br_6]$ by a doublet at δ 45.1 (J(RhP) = 206 Hz) in the $^{31}P\{^1H\}$ NMR spectrum and characteristic signals due to coordinated arene in the ^1H NMR spectrum. These chemical shifts and coupling constants are similar to those reported for $[(dppe)Rh(\eta^6\text{-}C_6H_6)][BF_4]$,[46] and we presume that the coordinated toluene arises from residual solvent left over from the preparation of $[(PPh_3)_2RhCl]_2$. In our hands, repeated washing of the starting material did not completely remove toluene and the arene-coordinated cation persisted. Employing $[(PPh_3)_2RhCl]_2$ prepared using methyl ethyl ketone as solvent[47] gave a mixture of products, although the toluene-coordinated complex was absent. We have not actively pursued the complete identification of all the components of this mixture, but we could assign the major species as being the arene-bridged dimer complex $[(Ph_3P)\{PPh_2(\eta^6\text{-}C_6H_5)\}Rh]_2$-

(44) Crowther, D. J.; Borkowsky, S. L.; Swenson, D.; Meyer, T. Y.; Jordan, R. F. *Organometallics* **1993**, *12*, 2897.
(45) Mhinzi, G. S.; Litster, S. A.; Redhouse, A. D.; Spencer, J. L. *J. Chem. Soc., Dalton Trans.* **1991**, 2769.
(46) Singewald, E. T.; Slone, C. S.; Stern, C. L.; Mirkin, C. A.; Yap, G. P. A.; Liable-Sands, L. M.; Rheingold, A. L. *J. Am. Chem. Soc.* **1997**, *119*, 3048.
(47) Osborn, J. A.; Jardine, F. H.; Young, J. F.; Wilkinson, G. *J. Chem. Soc. A* **1966**, 1711.

Scheme 1

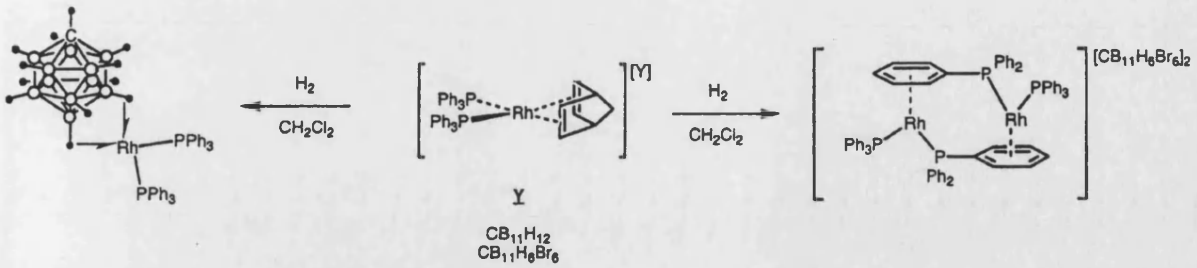

Table 2. Selected Interatomic Distances (Å) and Angles (deg) for Compounds 1, 2, and 5

Compound 1			
Rh(1)–P(1)	2.2192(6)	Rh(1)–P(2)	2.2391(6)
Rh(1)–B(7)	2.359(3)	Rh(1)–B(12)	2.407(3)
P(1)–Rh(1)–P(2)	95.73(2)	P(1)–Rh(1)–B(7)	113.88(7)
P(2)–Rh(1)–B(7)	150.39(7)	P(1)–Rh(1)–B(12)	155.46(6)
P(2)–Rh(1)–B(12)	107.98(6)	B(7)–Rh(1)–B(12)	42.57(9)
Compound 2			
Rh(1)–P(1)	2.248(2)	Rh(1)–P(2)	2.262(3)
Rh(1)–C(2)	2.399(8)	Rh(1)–C(3)	2.365(8)
Rh(1)–C(4)	2.269(8)	Rh(1)–C(5)	2.333(9)
Rh(1)–C(6)	2.316(9)	Rh(1)–C(7)	2.254(8)
Rh(1)–P(1)	2.247(2)	Rh(1)–P(2)	2.262(2)
Rh(1)–Br(7)	5.848(1)		
Rh(1)–P(1)–C(2)	108.9(3)	P(1)–Rh(1)–P(2)	95.96(8)
Compound 5			
Rh(1)–Rh(2)	2.776(1)	Rh(1)–H(1)	1.59(7)
Rh(2)–H(2)	1.60(9)	Rh(1)–H(3)	1.82(6)
Rh(2)–H(3)	1.82(6)	Rh(1)–P(1)	2.257(3)
Rh(1)–P(2)	2.313(3)	Rh(2)–P(3)	2.257(3)
Rh(2)–P(4)	2.301(3)	Rh(1)–Cl(1)	2.416(3)
Rh(1)–Cl(2)	2.553(2)	Rh(2)–Cl(1)	2.538(3)
Rh(2)–Cl(2)	2.394(2)		
Rh(1)–Cl(1)–Rh(2)	68.11(7)	Rh(1)–Cl(2)–Rh(2)	68.19(7)
Rh(1)–H(3)–Rh(2)	99(3)	P(1)–Rh(1)–P(2)	99.01(9)
P(3)–Rh(1)–P(4)	102.3(1)		
H(1)–Rh(1)–Cl(2)	163(3)	H(2)–Rh(2)–Cl(1)	168(4)

[*closo*-$CB_{11}H_6Br_6$]$_2$, which can be prepared quantitatively using an alternative method (vide infra). Given that the silver salt metathesis route using Ag[*closo*-$CB_{11}H_6Br_6$] did not give a clean reaction, an alternative method was used to generate precatalyst partnered with this weakly coordinating anion.

Norbornadiene Precursor Complexes. An attractive aspect of cationic Schrock–Osborn rhodium catalysts is that air-stable precatalysts such as [$(L)_2$Rh(nbd)][PF_6] (L = phosphine) can be readily prepared. In coordinating solvents the active hydrogenation catalyst [$(L)_2RhH_2(solvent)_2$][PF_6] is straightforwardly produced by treating a solution of these olefin complexes with 1 atm of hydrogen.[2] In noncoordinating solvents, such as dichloromethane, treatment of [(L_2)Rh(nbd)][BF_4] (L_2 = chelating diphosphine) affords dimeric species with bridging arene groups.[48,49] With relatively more coordinating anions than $[BF_4]^-$ or $[PF_6]^-$, such as perchlorate or sulfonates, monomeric species are suggested to occur.[14,49] When the counterion also contains phenyl groups, arene-bound zwitterions such as (η^6-$PhBPh_3$)Rh(dppb) (dppb = diphenylphosphinobutane) can be formed.[50] The kinetic aspects of the hydrogenation of alkenes and alkynes by [$(PPh_3)_2$Rh(nbd)][BF_4] in noncoordinating solvents such as CH_2Cl_2 has also been discussed.[51,52]

Treatment of a dichloromethane solution of the new complex [$(PPh_3)_2$Rh(nbd)][*closo*-$CB_{11}H_{12}$] (**3**) with H_2 (1 atm) for 10 min resulted in a color change from orange to red. After removal of volatiles in vacuo, NMR spectroscopy (^1H, $^{31}P\{^1H\}$, and $^{11}B\{^1H\}$) showed that compound **1** is formed essentially quantitatively (Scheme 1). This puts [*closo*-$CB_{11}H_{12}]^-$ in the same league as anions such as sulfonates and perchlorate with regard to coordinating ability, as all of these anions can form complexes with $\{L_2Rh\}^+$ fragments. In contrast, exposure of [$(PPh_3)_2$Rh(nbd)][*closo*-$CB_{11}H_6Br_6$] (**4**) to H_2 in dichloromethane affords a claret-colored solution from which the dimeric species [$(PPh_3)(PPh_2$-η^6-$C_6H_5)Rh]_2$-[*closo*-$CB_{11}H_6Br_6]_2$ (**2**) can be isolated as an air-sensitive crystalline solid. Compound **2** was characterized by solution NMR spectroscopy and a single-crystal X-ray diffraction study and shown to have a structure in which an arene ring from one of the phosphines on each rhodium bridges to the second metal center in the cation. The isolation of the dimeric species with [*closo*-$CB_{11}H_6Br_6]^-$ is in agreement with the relative weakly coordinating abilities of this anion compared with [*closo*-$CB_{11}H_{12}]^-$ [18] and other anions.[20,53] Conversion of **4** to **2** is essentially quantitative (by NMR).

Comparison of the ^1H and $^{13}P\{^1H\}$ NMR spectra of **2** with those of other reported complexes that contain η^6-arene-bridged structures shows close similarities.[49,54] Specifically, the observation of diagnostic peaks between δ 5.32 and 7.43 in the ^1H NMR spectrum is strongly indicative of the proposed arene-bridged structure. In the $^{31}P\{^1H\}$ NMR spectrum two environments are observed at δ 44.6 and 47.5, which show coupling to ^{31}P and ^{103}Rh in a second-order AA′BB′XX′ system, again consistent with previously reported arene-bridged complexes containing chelating phosphine ligands.[54] The $^{31}P\{^1H\}$ NMR spectrum of complex **2** may be simulated satisfactorily using the program gNMR[55] (see Supporting Information). Inspection of the $^1H\{^{11}B\}$ NMR spectrum confirmed the ratio of phosphines to cage as 2:1. Although such bridged arene structures have been

(48) Halpern, J.; Riley, D. P.; Chan, A. S. C.; Pluth, J. J. *J. Am. Chem. Soc.* **1977**, *99*, 8055.
(49) Fairlie, D. P.; Bosnich, B. *Organometallics* **1988**, *7*, 936.
(50) Zhou, Z.; Facey, G.; James, B. R.; Alper, H. *Organometallics* **1996**, *15*, 2496.
(51) Esteruelas, M. A.; González, I.; Herrero, J.; Oro, L. A. *J. Organomet. Chem.* **1998**, *551*, 49.
(52) Esteruelas, M. A.; Herrero, J.; Martín, M.; Oro, L. A.; Real, V. M. *J. Organomet. Chem.* **2000**, *599*, 178.
(53) Evans, D. R.; Reed, C. A. *J. Am. Chem. Soc.* **2000**, *122*, 4660.
(54) Allen, D. G.; Wild, S. B.; Wood, D. L. *Organometallics* **1986**, *5*, 1009.
(55) Budzelaar, P. gNMR; Cherwell Scientific Publishing, Oxford, U.K., 1997.

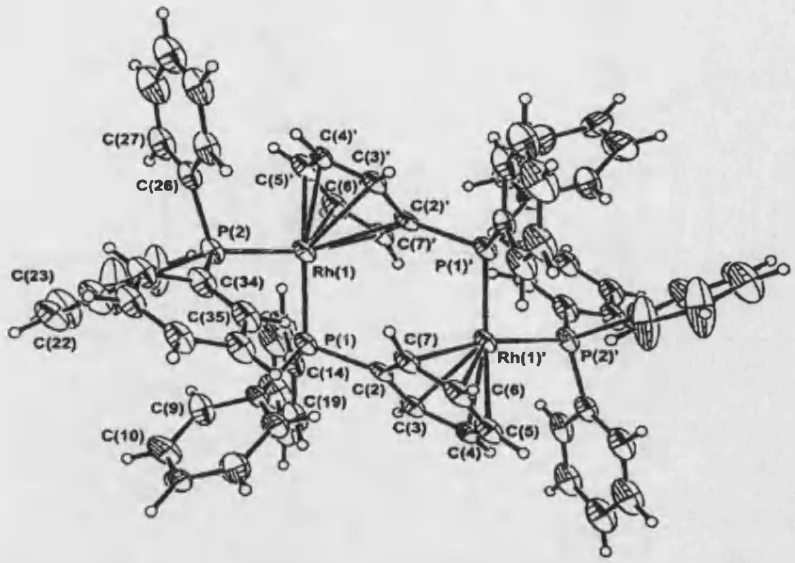

Figure 2. ORTEX drawing of the dicationic portion of complex **2**. Thermal ellipsoids are drawn at the 30% probability level. The disorder present in phenyl ring C(32)−C(37) and its symmetry equivalent is not shown, with only the major component (65% occupancy) drawn.

Table 3. Catalytic Hydrogenation of Selected Alkenes Using Complexes 3, 4, I, and II[a]

entry	catalyst	substrate	time, h	yield,[b] %	TOF, h^{-1}
1	$[(PPh_3)_2Rh(nbd)][CB_{11}H_{12}]$ **(3)**	cyclohexene	2	43	22
2	$[(PPh_3)_2Rh(nbd)][CB_{11}H_6Br_6]$ **(4)**	cyclohexene	<0.5	100	>200
3	$[(PPh_3)_2Rh(nbd)][BF_4]$ **(A)**	cyclohexene	2	29	15
4	$[(PPh_3)_2Rh(nbd)][CB_{11}H_{12}]$ **(3)**	1-methyl-1-cyclohexene	6	4	0.7
5	$[(PPh_3)_2Rh(nbd)][CB_{11}H_6Br_6]$ **(4)**	1-methyl-1-cyclohexene	5	95	19
6	$[(py)(PCy_3)Ir(cod)][PF_6]$ **(B)**	1-methyl-1-cyclohexene	5	100	20
7	$[(PPh_3)_2Rh(nbd)][CB_{11}H_6Br_6]$ **(4)**	2,3-dimethylbut-2-ene	24	68	3
8	$[(py)(PCy_3)Ir(cod)][PF_6]$ **(B)**	2,3-dimethylbut-2-ene	16	95	6

[a] Conditions: catalyst, 1 mol %; CH_2Cl_2 5 cm^3; H_2, 10 psi; temperature, 20 °C. [b] Yields quoted are the average of two runs and were determined by GC.

established in the literature for some time, to our knowledge compound **2** is the first example isolated using a monodentate phosphine. A single-crystal X-ray diffraction study was therefore undertaken to confirm the structure, for which an ORTEX[56] representation is given in Figure 2. Despite repeated attempts, only very small, poorly shaped crystals of **2** could be grown, and consequently the final refinement is not as good as we would traditionally expect from data collected on our diffractometers. Nevertheless, the gross structural features of the molecule can be seen, even if discussion of individual bond lengths and angles is not appropriate.

The solid-state structure of **2** supports the solution NMR data, in that each rhodium center is bound to two PPh_3 ligands, one of which bridges to another rhodium center via an η^6 interaction, resulting in a formal 18-electron count at each metal center. The molecule crystallizes with a crystallographically imposed inversion center. The two carborane anions do not interact with the metal centers, the shortest Rh···Br distance being 5.85 Å. It is of note that the room-temperature ^1H NMR spectrum shows a particularly high-field-shifted resonance of one of the bridging arene protons, at δ 5.32, and we assign this to the hydrogen atom H(4) and its symmetry equivalent in the solid-state structure which lies approximately over the center of the phenyl ring C(26)−C(31).

(56) McArdle, P. *J. Appl. Crystallogr.* **1995**, *28*, 65.

Catalytic Hydrogenations. The precatalysts **3** and **4** have been tested for their efficiency in the hydrogenation of the internal alkenes: cyclohexane (**C**), 1-methylcyclohex-1-ene (**D**), and 2,3-dimethylbut-2-ene (**E**), which are progressively more sterically hindered and have historically not been suitable substrates for cationic $[(R_3P)_2Rh(nbd)]^+$-based catalysts under ambient laboratory conditions. Hydrogenation reactions were performed at room temperature under 10 psi of hydrogen pressure in Schlenk tubes fitted with septa, using 1 mol % of catalyst in ca. 5 cm^3 of CH_2Cl_2. The catalytic activity of $[(PPh_3)_2Rh(nbd)][BF_4]$ (**A**) and Crabtree's catalyst $[(py)(PCy_3)Ir(cod)][PF_6]$ (**B**) under the conditions used by us for the evaluation of the new catalyst here have been included for comparison. Table 3 summarizes selected results from this investigation.

The data presented in Table 3 show that changing the counterion from $[closo\text{-}CB_{11}H_{12}]^-$ to $[closo\text{-}CB_{11}H_6Br_6]^-$ results in a dramatic effect on both the overall yield of hydrogenated product and the turnover frequency (TOF). While precatalyst **3** (and thus complex **1** on initial hydrogenation) gives modest yields of saturated product for cyclohexene after 2 h (entry 1), precatalyst **4** (giving complex **2** on initial hydrogenation) affords complete hydrogenation of cyclohexene to cyclohexane in under 30 min (entry 2), with an concomitant order of magnitude difference in TOF compared with **3** on changing the counterion from $[closo\text{-}CB_{11}H_{12}]^-$ to

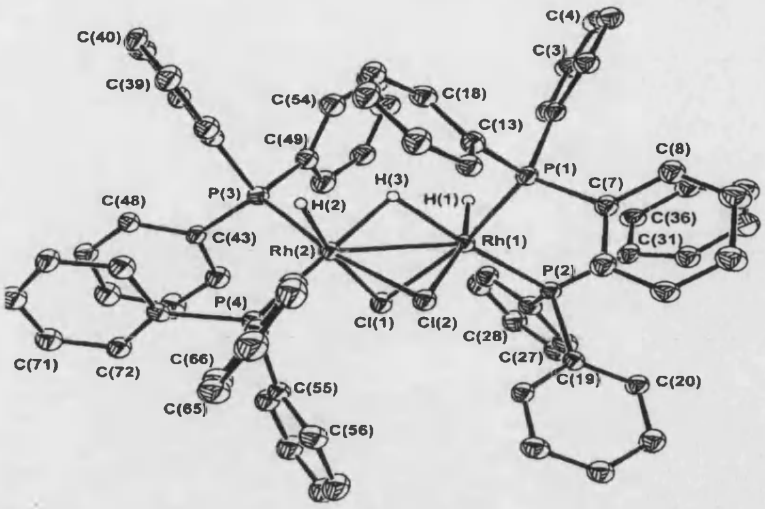

Figure 3. ORTEX drawing of the cationic portion of complex **5**. Thermal ellipsoids are drawn at the 30% probability level. Hydrogen atoms, apart from those associated with the rhodium metal centers, are omitted for clarity.

[*closo*-$CB_{11}H_6Br_6$]$^-$. When $[BF_4]^-$ is used as the counterion (entry 3), the yield of hydrogenated product is comparable to that of **3** but significantly smaller than that of **4**. Moving to the more sterically hindered olefin 1-methyl-1-cyclohexene, the effect of anion is even more pronounced (entries 4 and 5). After 5 h almost complete conversion (95%) is observed with **4**, while complex **3** barely effects hydrogenation. For comparison we have tested Crabtree's catalyst under these conditions and find that complete hydrogenation of **D** is effected after 5 h (entry 6). Even with the sterically very hindered alkene 2,3-dimethylbut-2-ene, complex **4** effects 68% conversion to the alkane (entry 7). Although this is not as good as we find for Crabtree's catalyst (entry 8), as far as we are aware this is excellent for a rhodium catalyst under the benign conditions of room temperature and pressure. Comparable activities have recently been reported for neutral β-diimine rhodium complexes, hydrogenation in this case being performed in neat olefin.[57]

Deactivation Product. The fact that the reduction of the hindered alkene 2,3-dimethyl-but-2-ene did not go to completion suggested that a catalytically inactive complex is formed during hydrogenation, similar to the dimeric and trimeric hydride-bridged iridium cations, such as $[Ir_2H_5(PPh_3)_4]^+$ and $[Ir_3H_7(PCy_3)_3(py)_3]^+$, that are the deactivation products with Crabtree's catalyst and related complexes[7] or the catalytically inactive dimeric rhodium complexes formed on hydrogenation of Schrock–Osborn type systems.[16] A ^{1}H NMR spectrum of the residue from the hydrogenation of 2,3-dimethyl-but-2-ene with preacatalyst **4** shows that there is one major organometallic product (ca. 95%). Initially we partially characterized this as the cationic hydride- and halide-bridged dimer $[(PPh_3)_2HRh(\mu\text{-}Cl)_2(\mu\text{-}H)RhH(PPh_3)_2]$[*closo*-$CB_{11}H_6Br_6$] (**(5)**[$CB_{11}H_6Br_6$]) by multinuclear NMR spectroscopy. The structure was only ultimately resolved by a single-crystal X-ray analysis of the [*closo*-$CB_{11}H_{12}$]$^-$ salt, which was formed by treatment of a CH_2Cl_2 solution of **3** with H_2 over 4 days to afford **(5)**[*closo*-$CB_{11}H_{12}$] as the major product. Although we have isolated single crystals of the [*closo*-$CB_{11}H_{12}$]$^-$ salt, NMR data are identical for both anions, disregarding the resonances associated with the cage hydrogen atoms, demonstrating that they adopt the same structural motif. An ORTEX representation of **(5)**[$CB_{11}H_{12}$] is shown in Figure 3.

The complex **(5)**[$CB_{11}H_{12}$] is a cationic 34-CVE dimer, with a Rh–Rh distance that suggests a significant metal–metal interaction (2.776(1) Å). Each rhodium is spanned by two chloride atoms and one hydride ligand, while one terminal hydride is found on each metal center along with two PPh_3 ligands. The hydrides were located in the difference map and their positions confirmed by NMR data. The terminal hydride ligands are orientated in an anti configuration with respect to the Rh–Rh vector, giving the molecule approximate, noncrystallographic C_2 symmetry. One carborane anion is located in the unit cell, giving the metal complex an overall positive charge. This makes each metal center formally Rh^{3+}, consistent with the observed diamagnetism. The Rh–Rh distance is in the range associated with dinuclear rhodium complexes with a metal–metal bond.[58–60] The two chloride ligands do not span the Rh–Rh vector symmetrically, one Rh–Cl distance in each Rh–Cl–Rh unit being significantly longer than the other: viz., Rh(2)–Cl(1) = 2.538(3) Å and Rh(1)–Cl(1) = 2.416(3) Å. This difference can be traced back to the approximate trans orientation of the terminal hydrides with respect to the chloride ligands (H(2)–Rh(2)-Cl(1) = 168(4)° and H(1)–Rh(1)–Cl(2) = 163(3)°), meaning that each bridging chloride is approximately trans to both a phosphine and a hydride, with a resulting differential in the observed Rh–Cl bond lengths. Similarly, the phosphine trans to the bridging hydride on each rhodium has a slightly longer Rh–P bond length: Rh(1)–P(1) = 2.257(3) Å and Rh(1)–P(2) = 2.313(3) Å. The complex **(5)**[$CB_{11}H_{12}$] is closely related to the

(57) Budzelaar, P.; Moonen, N. N. P.; De Gelder, R.; Smits, J. M. M.; Gal, A. W. *Eur. J. Inorg. Chem.* **2000**, 753.

(58) Herrmann, W. A. *Adv. Organomet. Chem.* **1982**, *20*, 159.

(59) Isoke, K.; Vázquez De Miguel, A.; Bailey, P. M.; Okeya, S.; Maitlis, P. M. *J. Chem. Soc., Dalton Trans.* **1983**, 1441.

(60) Koizumi, T.; Osakada, K.; Yamamoto, T. *Organometallics* **1998**, *17*, 5721.

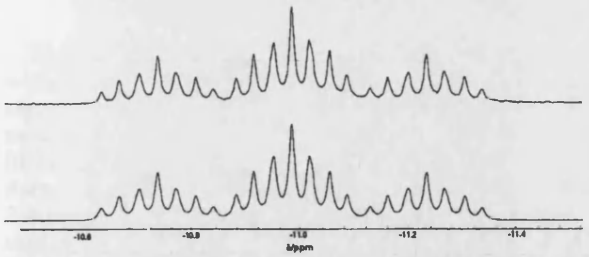

Figure 4. Experimental (top) and simulated (bottom) ^1H NMR spectra for the bridging hydride region in the cation $[(PPh_3)_2RhH(\mu\text{-}H)(\mu\text{-}Cl)_2HRh(PPh_3)_2]^+$.

structurally characterized $[Ir_2H_5(PPh_3)_4]^+$,[7] apart from the replacement of two bridging hydrides in the iridium complex by chlorides, which must originate from the dichloromethane solvent used in the hydrogenation reactions. In addition, the cation **[5]**$^+$ is the rhodium congener of $[Ir_2(H(PPh_3)_2)_2(\mu\text{-}H)(\mu\text{-}Cl)_2]^+$ formed from addition of HCl to $[Ir(H(PPh_3)_2)(\mu\text{-}H)_3]^+$.[61,62] Attempts to avoid dimer formation by hydrogenation in THF rather than dichloromethane led only to low activities (ca. 10% for cyclohexene, [*closo*-$CB_{11}H_6Br_6$] counterion) in this coordinating solvent. In addition to dimeric rhodium hydride compounds previously observed as deactivation products in Schrock–Osborn type systems, dimeric complexes formed on hydrogenation of rhodacarboranes have been reported previously,[23] while, in contrast, certain exo-substituted rhodacarboranes have been shown to be recoverable after catalytic hydrogenation in toluene or THF.[32]

With the identity of the cation **[5]**$^+$ in hand, the ^1H and ^{31}P NMR spectra can be confidently interpreted as being fully consistent with the solid-state structure. The $^{31}P\{^1H\}$ NMR spectrum displays two strongly second-order coupled resonances at δ 36.0 and δ 51.5, corresponding to the two phosphine environments in **[5]**$^+$. The spectrum has been successfully simulated as an AA′BB′XX′ spin system (see the Supporting Information). In the hydride region of the ^1H NMR spectrum two resonances are observed in the ratio 1:2 at δ −11.0 and −16.5, assigned to the bridging and terminal hydrides, respectively. The latter resonance is observed as an apparent quartet (doublet of doublet of doublets), showing coupling to one ^{103}Rh center and two ^{31}P nuclei, which simplifies to a doublet in the $^1H\{^{31}P\}$ NMR spectrum. The fact that no $^1H-^1H$ coupling is observed (or it is very close to 0 Hz) was confirmed by a selected homonuclear decoupling experiment that showed no change in peak pattern or intensity for either of the hydride peaks on irradiation of the other. The bridging hydride at δ −11.0 is observed as a complicated multiplet that resembles a triplet of septets, which simplifies to a binomial triplet in the $^1H\{^{31}P\}$ NMR spectrum, thus confirming the Rh–H–Rh motif. The coupling pattern has been successfully simulated as a AA′BB′MXX′ spin system (Figure 4) (full details of the resolved coupling constants are given in the Supporting Information). The large triplet coupling arises (J(PH) = 75 Hz) from trans coupling of the bridging hydride with the two chemically equivalent phosphorus atoms P(2) and P(4). Similarly large PH coupling constants in related, spectroscopically characterized, binuclear rhodium phosphines with bridging hydrides have been observed previously.[16,63,64] All other ^1H and $^{31}P\{^1H\}$ spectral features are fully consistent with the solid-state structure.

Discussion

Clearly, from these results there is a large effect associated with changing the counterion from $[BF_4]^-$ to [*closo*-$CB_{11}H_{12}]^-$ or [*closo*-$CB_{11}H_6Br_6]^-$, the perhalogeno anion giving precatalysts that are significantly more active in alkene hydrogenation, which is on first inspection consistent with the coordinating ability of these anions.[17,38,65] The large difference observed between **4** (*closo*-$CB_{11}H_6Br_6$) and **A** (BF_4) is interesting, as on hydrogenation in CH_2Cl_2 both form complexes in which the anion does not interact with the metal[70] (i.e. complex **2**), unlike with **3**, where there exists a more intimate bond between metal center and carborane on initial hydrogenation (complex **1**). Whether these results suggest that the notionally least coordinating [*closo*-$CB_{11}H_6Br_6]^-$ counterion plays a significant role in the catalytic cycle, perhaps by stabilizing a reactive intermediate better than $[BF_4]^-$ does; or that, in contrast, the carborane simply does not interact with the metal center significantly compared with $[BF_4]^-$, resulting in faster turnover of the catalytic cycle, is not clear. The role of the counterion in olefin hydrogenation by cationic rhodium phosphine fragments partnered with sulfonate anions has recently been discussed, and it is suggested that the anion remains coordinated with the metal center throughout the catalytic cycle.[16] The proposed "low-pressure route" discussed in this particular system (ca. 1 atm of H_2) involves coordination of alkene first followed by oxidative addition of dihydrogen, with the sulfonate anion changing its denticity accordingly through the catalytic cycle. Significant counterion effects have also been reported in cationic iridium phosphanodihydrooxazole-based hydrogenation systems: moving from $[PF_6]^-$ to $[BAr_f]^-$ type counterions has a positive effect on conversion, enantiomeric excess, and catalyst stability in the high-pressure (50 bar) hydrogenation of sterically very-hindered stilbene derivatives, although the exact role of the counterion in the catalytic cycle remains unresolved.[15,66] In comparison, catalyst **4** effects essentially no conversion at room temperature and pressure of trans-α-methylstilbene to the corresponding alkane (<2% by GC after 6 h). This is probably due to the $\{(PPh_3)_2Rh\}^+$ fragment forming a catalytically inactive (at room temperature and pressure) η^6-arene complex with the stilbene precursor. In agreement with this observation, the toluene complex $[(PPh_3)_2Rh(\eta^6\text{-}C_6H_5Me)]$[*closo*-$CB_{11}H_6Br_6$] is a significantly poorer catalyst than **4** for the hydrogenation of cyclohexene, with only 10% conversion observed after 6 h under ambient conditions.

(61) Crabtree, R.; Parnell, C. A.; Uriate, R. J. *Organometallics* **1987**, *6*, 696.
(62) Crabtree, R.; Felkin, H.; Morris, G. E. *J. Organomet. Chem.* **1977**, *141*, 205.
(63) Butler, I. R.; Cullen, W. R.; Mann, B. E.; Nurse, C. R. *J. Organomet. Chem.* **1985**, *280*, C47.
(64) Morran, P. D.; Duckett, S. B.; Howe, P. R.; McGrady, J. E.; Colebrooke, S. A.; Eisenberg, R.; Partridge, M. G.; Lohman, J. A. B. *J. Chem. Soc., Dalton Trans.* **1999**, 3949.
(65) Patmore, N. J.; Hague, C.; Cotgreave, J.; Mahon, M. F.; Frost, C. G.; Weller, A. S. *Chem. Eur. J.* **2002**, *8*, 2088.
(66) Hou, D.-R.; Reibenspies, J.; Colacot, T.; Burgess, K. *Chem. Eur. J.* **2001**, *7*, 5391.

Conclusion

We have demonstrated that changing the counterion within the domain of *closo*-monocarboranes can have a significant effect on the efficiency of hydrogenation by cationic rhodium phosphine catalysts, to the extent that $[(PPh_3)_2Rh(nbd)][closo\text{-}CB_{11}H_6Br_6]$ will hydrogenate hindered alkenes, in reasonable yield, such as 2,3-dimethyl-2-butene, while $[(PPh_3)_2Rh(nbd)][closo\text{-}CB_{11}H_{12}]$ is essentially ineffectual, struggling to hydrogenate the less hindered methylcyclohexene. While this is not necessarily completely surprising, given the relative coordinating properties of these two carborane anions, it is satisfying to see that the system can be enhanced to significant effect by simply changing the carborane counterion. What is interesting is that $[BF_4]^-$ salts are significantly poorer than $[closo\text{-}CB_{11}H_6Br_6]^-$ salts for the hydrogenation of alkenes, especially when one considers that both anions do not interact significantly with the metal center on initial hydrogenation of the norbornadiene precursor. This perhaps implicates one of the following: (i) putative intermediate(s) in the catalytic cycle involve coordination of the counterion (which has precedent with other anions[13,16]), (ii) the $[BF_4]^-$ anion is somehow degraded in the catalytic cycle to form inactive metal fluorides or oxyborates, possibly activated toward this by coordination with the metal center, or (iii) a different mechanism operates with each of the two anions.

Overall this suggests that in Schrock–Osborn hydrogenation systems, as found with other systems where the cation/anion interaction is important such as metallocene olefin polymerization catalysts,[12] the match between anion and cation is a finely balanced one. The nature of the interaction between cation and anion is therefore of significant interest with regard to selecting the best combination and, thus, optimal performance. With regard to this we are currently considering the role of the carborane counterion in the catalytic cycle and anticipate reporting on this at a future date.

Experimental Section

All manipulations were carried out under an atmosphere of argon using standard Schlenk line techniques. Solvents were dried according to standard procedures and distilled under nitrogen. NMR solvents were dried over CaH_2 for at least 24 h, vacuum distilled, and freeze–pump–thawed prior to use. Cyclohexene, 1-methylcyclohexene, and 2,3-dimethyl-2-butene were passed through a column of activated alumina and freeze–pump–thawed prior to use. Gas chromatography was performed on a Perkin-Elmer Autosystem XL. NMR spectra were recorded on either a Bruker 300 MHz or a Varian 400 MHz spectrometer. ^1H NMR spectra were referenced using residual protio solvents, and ^{31}P NMR and ^{11}B NMR spectra were referenced to an external H_3PO_4 or $BF_3{\cdot}OEt_2$ reference, respectively. All NMR spectra were recorded at room temperature. Coupling constants are quoted in Hz. $[(PPh_3)_2RhCl]_2$,[47] $[(PPh_3)_2Rh(nbd)][BF_4]$,[49] $Ag[closo\text{-}CB_{11}H_{12}]$,[67] and $Ag[closo\text{-}CB_{11}H_6Br_6]$[68] were prepared by the reported literature routes. $[(py)(PCy_3)Ir(cod)][PF_6]$ was purchased from Aldrich and used as received.

$[(Ph_3P)_2Rh(closo\text{-}CB_{11}H_{12})]$ (1). $[(Ph_3P)_2RhCl]_2$ (0.212 g, 15.8 mmol) and $Ag[closo\text{-}CB_{11}H_{12}]$ (79 mg, 31.7 mmol) were dissolved in 5 mL of CH_2Cl_2, and the mixture was stirred for 3 h. The solution was filtered, and the CH_2Cl_2 solution was layered with hexane to afford **1** as red crystalline blocks (0.114 g, 47% yield). Anal. Calcd for for $C_{37}H_{42}B_{11}P_2Rh$: C, 57.68; H, 5.49. Found: C, 57.3; H, 5.25. ^1H NMR ($CDCl_3$): δ −1.97 (br q, J(BH) = 119, 1H, B*H*), −0.6–0.8 (broad q, J(BH) = 80.0, 5H, B*H*), 1.1–2.4 (br q, 5H B*H*), δ 2.6 (s, 1H CH_{cage}), 7.1–7.6 (m, 30H, C_6H_6). $^1H\{^{11}B\}$ NMR ($CDCl_3$): δ −1.97 (s, 1H, B$H_{antipodal}$), 0.1 (s, 5H, B*H*), δ 1.7 (s, 5H, B*H*), δ 2.6 (s, CH_{cage}), δ 7.1–7.6 (m, 30H, C_6H_6). $^{31}P\{^1H\}$ NMR: δ 49.0 (d, J(RhP) = 194 Hz). $^{11}B\{^1H\}$ NMR: δ −9.9 (1B), −13.5 (5B), −14.1 (5B).

$[(Ph_3P)(PPh_2\text{-}\eta^6\text{-}C_6H_5)Rh]_2[closo\text{-}CB_{11}H_6Br_6]_2$ (2). $[(Ph_3P)_2Rh(C_7H_8)][closo\text{-}CB_{11}H_{12}]$ (**4**; 25 mg, 0.0187 mmol) in 10 mL of CH_2Cl_2 was placed in a 100 mL Schlenk tube fitted with a new rubber septum. Via a needle, H_2 was bubbled through the solution for 10 min. The solution changed color from a golden orange to a claret red. The solvent was removed in vacuo. Crystals suitable for a single-crystal X-ray analysis were grown by slow diffusion of hexane into a CH_2Cl_2 solution of **2**. Yield: 0.021 g (90%). Anal. Calcd for $C_{74}H_{72}B_{22}Br_{12}P_4Rh_2{\cdot}1.4CH_2Cl_2$: C, 33.8; H, 2.9. Found: C, 34.1; H, 2.98. $^1H\{^{11}B\}$ NMR (CD_2Cl_2): δ 2.32 (s, 5H, B*H*), δ 2.54 (s, 1H, CH_{cage}), 5.32 (t, J(HH) = 6.6, 1H, C_6H_5), 6.58 (t, J(HH) = 6.6, 2H, C_6H_5), 6.97 (t, J(HH) = 6.6, 2H, C_6H_5), 7.0–7.25 (m, 20H, C_cH_5), 7.30 (t, J(HH) = 5.7, 4H, C_6H_5), 7.43 (t, J(HH) = 7.5, 4H, C_6H_5). ^1H NMR (CD_2Cl_2): δ 2.5–2.0 (br q, 5H, B*H*), 2.54 (s, 1H, CH_{cage}), 5.32 (t, J(HH) = 6.6, 1H, C_6H_5), 6.58 (t, J(HH) = 6.6, 2H, C_6H_5), 6.97 (t, J(HH) = 6.6, 2H, C_6H_5), 7.0–7.25 (m, 20H, C_cH_5), 7.30 (t, J(HH) = 5.7, 4H, C_6H_5), 7.43 (t, J(HH) = 7.5, 4H, C_6H_5). $^{31}P\{^1H\}$ (CD_2Cl_2): AA′BB′XX′ system, δ 47.5 (complex multiplet, J(RhP) = 216.6, J(RhP) = −0.2, J(PP) = 8.6), 44.6 (complex multiplet, J(RhP) = −1.0, J(Rh′P) = −199.3, J(PP) = 37.8, J(PP) = 1.32).

$[(Ph_3P)_2Rh(C_7H_8)][closo\text{-}CB_{11}H_{12}]$ (3). $(Ph_3P)_3RhCl$ (100 mg, 0.11 mmol), 2,5-norbornadiene (13 μL, 14 mmol), and $[Cs][closo\text{-}CB_{11}H_{12}]$ (30 mg, 0.11 mmol) were stirred in a 1:3 mixture of acetone and CH_2Cl_2 for 2 h. The resulting orange solution was filtered and concentrated in vacuo. The compound was crystallized by addition of ethanol. The solid was collected and washed with three portions of ethyl alcohol and dried in vacuo. Yield: 0.107 g (57%). Anal. Calcd for $C_{44}H_{50}B_{11}P_2Rh$: C, 61.26; H, 5.84. Found: C, 61.5; H, 5.85. ^1H NMR (CD_2Cl_2): δ 7.4–7.0 (m, 30H, C_6H_6), 4.5 (s, 4H, C_7H_8), 4.0 (s, 2H, C_7H_8), 2.7–1.0 (br q, 11H, B*H*), 2.35 (s br, 1H, CH_{cage}), 1.5 (s, 2H, C_7H_8). $^{31}P\{^1H\}$ NMR (CD_2Cl_2): δ 30.5 (d, J(RhP) = 154.5). $^{11}B\{^1H\}$ NMR (CD_2Cl_2): δ −4.0 (s, 1B), −10.3 (s, 5B), −13.1 (s, 5B).

$[(Ph_3P)_2Rh(C_7H_8)][closo\text{-}CB_{11}H_6Br_6]$ (4). $(Ph_3P)_3RhCl$ (100 mg, 0.11 mmol), 2,5-norbornadiene (13 μL, 14 mmol), and $[Cs][closo\text{-}CB_{11}H_6Br_6]$ (81 mg, 0.11 mmol) were stirred in a 1:3 mixture of acetone and CH_2Cl_2 for 2 h. The compound was isolated in the same manner as described for compound **3**. Yield: 0.162 g (60%). Anal. Calcd for $C_{46}H_{45}B_{11}Br_6P_2Rh$: C, 40.59; H, 3.33. Found: C, 40.4; H, 3.38. $^1H\{^{11}B\}$ NMR ($CDCl_3$): δ 7.4–7.0 (m, 30H, C_6H_6), 4.5 (s, 4H, C_7H_8), 4.0 (s, 2H, C_7H_8), 2.5 (s, 1H, CH_{cage}), 2.25 (s, 5H, B*H*), 1.5 (s, 2H, C_7H_8). $^{11}B\{^1H\}$ NMR ($CDCl_3$): δ 1.7 (s, 1B), −6.6 (s, 5B), −17.1 (s, 5B). $^{31}P\{^1H\}$ NMR ($CDCl_3$): δ 30.6 (J(RhP) = 155).

$[(Ph_3P)_2HRh(\mu\text{-}H)(\mu\text{-}Cl)_2RhH(PPh_3)_2][closo\text{-}CB_{11}H_{12}]$ (5). $[(Ph_3P)_2Rh(nbd)][closo\text{-}CB_{11}H_{12}]$ (25 mg, 0.03 mmol) in 10 mL of CH_2Cl_2 in a 100 mL Schlenk tube fitted with a rubber septum was pressurized with 20 psi of H_2 for 3 days. The solvent was concentrated in vacuo, and hexane (1 equal volume) was added via cannula. After refrigeration for 4–5 days the compound precipitated as yellow crystalline filaments suitable for a single-crystal X-ray analysis. This crystalline material contained ca. 5% of an unidentified product, which, in our hands, could not be removed by repeated recrystallization. Hence, accurate mass spectrometry on a bulk sample was used as an alternative to microanalysis. $^1H\{^{11}B\}$ NMR ($CDCl_3$): δ 7.3 (m, 60H, C_6H_6), 2.54 (s, 1H, CH_{cage}), 2.32 (s,

(67) Shelly, K.; Finster, D. C.; Lee, Y. J.; Scheidt, W. R.; Reed, C. A. *J. Am. Chem. Soc.* **1985**, *107*, 5955.
(68) Liston, D. J.; Lee, Y. J.; Scheidt, W. R.; Reed, C. A. *J. Am. Chem. Soc.* **1989**, *111*, 6643.

5H, B*H*), −11.0 (complex multiplet, 1H, part of a AA′BB′MXX′ system, Rh(*μ*-*H*), *J*(RhH) = 10, *J*(PH) = 21, 75), −16.5 (virtual quartet, 2H, *J*(RhP) = 15, *J*(PP) = 15, 15). $^{31}P\{^1H\}$ NMR ($CDCl_3$): *δ* 51.5 (complex m, AA′BB′XX′ system), 36.0 (complex m, AA′BB′XX′ system). Accurate mass spectrometry (ES+): calcd 1327.1367, found 1327.1353. Identical NMR spectra in the phosphine and hydride regions are obtained using $[CB_{11}H_6Br_6]$ as the counterion (i.e., starting from complex **4**).

General Procedure for Catalysis. In a Schlenk tube fitted with a new septum, the appropriate amount of catalyst was dissolved in CH_2Cl_2 (5 cm^3) to give a catalyst-to-substrate ratio of 1:100. The appropriate amount of alkene was added, and H_2 was bubbled (pressure 10 psi), via a needle, through the solution using an outlet needle for 10 min. The H_2 and outlet needles were then removed, and the reaction mixture was stirred for the appropriate amount of time, as indicated in Table 3. At this time a sample was prepared for gas chromatography by passing a portion (ca. 1 cm^3) of the solution through a short silica plug, washing the silica with CH_2Cl_2 (ca. 1 cm^3), and combining these two fractions.

X-ray Crystallography. The crystal structure data for compounds **1**, **2**, and **5** were collected on a Nonius KappaCCD, with pertinent details given in Table 1. Structure solution followed by full-matrix least-squares refinement was performed using the SHELX suite of programs throughout.[69,70] Plots were produced using ORTEX.[56]

Compound 2. Despite copious recrystallization efforts it did not prove possible to grow crystals of complex **2** with substantial dimensions for an X-ray structure determination. Thus, the crystal selected, while being the largest available from several batches, was extremely thin and of mediocre quality (mosaicity 1.56°). The smallest crystal dimension of 0.03 mm is reflected in the substantially larger than desirable *R*(int) and *R*(*σ*) values (coupled with a not entirely satisfactory weighting scheme) than we normally obtain for data from our diffractometers. The electron density map of the asymmetric unit (half of a dimer molecule, proximate to a crystallographic inversion center) in this structure was also seen to contain two areas pertaining to solvent. The first of these was modeled as one whole molecule of dichloromethane with the two chlorines therein refined over four positions, each at half-occupancy. The second solvent area was more diffuse, and several models were tried. The best convergence was achieved by refining this area as 0.39 of a dichloromethane molecule with the two associated chlorines equally disordered over three sites. Hydrogen atoms were omitted from the refinement in the solvent areas due to the disorder. One of the phenyl rings in the rhodium dimer also exhibited disorder, which was successfully modeled at 65:35 occupancy for C(32)−C(37) and C(32)′−C(37)′, respectively. Trial runs of applying an absorption correction to the data for this structure afforded no improvement in convergence, and hence, this correction type was omitted.

Compound 5. As with **2**, numerous efforts at recrystallization proved unsuccessful in growing crystals with substantial dimensions for an X-ray structure determination for complex **5**. The crystal selected, while being the best available, was extremely thin and of very poor quality. As with **2**, the smallest crystal dimension (0.05 mm) is reflected in the larger than desirable *R*(int) and *R*(*σ*) values and poorer *R* factors than we would normally obtain from our diffractometers. Nevertheless, the structure converged well and, surprisingly, the reliable location of the hydrogens attached to the rhodium centers was possible. These particular hydrogens were positionally refined subject to constraints in the final least-squares analysis. The asymmetric unit in this structure was also seen to contain one molecule of dichloromethane, disordered over 2 sites in a 50:50 ratio. Trial runs of applying an absorption correction to the data for this structure afforded no improvement in convergence and, hence, were abandoned in the final least-squares cycles.

Acknowledgment. A.S.W. thanks the Royal Society for a University Research Fellowship and equipment grant (GC). The EPSRC and the University of Bath are also thanked for financial support (studentships to A.R. and N.J.P., respectively). The use of the Cambridge Structural Database at Daresbury service is acknowledged. The EPSRC/JREI is acknowledged for funding for a Nonius Kappa-CCD diffractometer, while use of the EPSRC mass spectrometry service at the University of Swansea is also acknowledged. Johnson Matthey PLC is thanked for the loan of platinum group metal salts.

Supporting Information Available: Tables giving crystallographic data and structure refinement details, positional and thermal parameters, and bond distances and angles for complexes **1**, **2**, and **(5)**$[CB_{11}H_{12}]$ (these data are also available as CIF files) and figures giving calculated and experimental $^{31}P\{^1H\}$ NMR spectra for complexes **2** and $[\mathbf{5}]^+$. This material is available free of charge via the Internet at http://pubs.acs.org.

OM020077R

(69) Sheldrick, G. M. SHELX-97: A Computer Program for Refinement of Crystal Structures; University of Göttingen, Göttingen, Germany.

(70) A CH_2Cl_2 solution $[(PPh_3)_2Rh(nbd)][BF_4]$ was treated with H_2 for 10 min, the volatiles were removed in vacuo, and the residue was taken up in CD_2Cl_2. ^1H NMR and $^{31}P\{^1H\}$ NMR spectroscopy indicated the formation of an arene-briged dimer complex, similar to **2**.

Inorg. Chem. **2002**, *41*, 4567–4573

Solution and Solid-State Structure of the Anion $[Ag_2\{closo\text{-}CB_{11}H_{12}\}_4]^{2-}$

Mark A. Fox,[†] Mary F. Mahon,*[‡] Nathan J. Patmore,[‡] and Andrew S. Weller*[‡]

Department of Chemistry, University of Bath, Bath BA2 7AY, U.K., and Department of Chemistry, University Science Laboratories, South Road, Durham DH1 3LE, U.K.

Received May 20, 2002

Addition of the carbene 1,3-dimesitylimidazol-2-ylidene (IMes) to a toluene solution of Ag[*closo*-$CB_{11}H_{12}$] results in the formation of the complex $[(IMes)_2Ag]_2[Ag_2\{closo\text{-}CB_{11}H_{12}\}_4]$, the anionic component of which contains two silver(I) centers bridged by two carboranes in addition to one terminally bound carborane on each metal, in the solid-state. Comparison of the observed $^{11}B\{^1H\}$ NMR chemical shifts of $[(IMes)_2Ag]_2[Ag_2\{closo\text{-}CB_{11}H_{12}\}_4]$ or Ag[*closo*-$CB_{11}H_{12}$] with $[NBu_4]$[*closo*-$CB_{11}H_{12}$] in CD_2Cl_2 demonstrates that the silver ion interacts significantly with the cage in solution. Theoretical investigations using the ab initio/GIAO/NMR method of [*closo*-$CB_{11}H_{12}]^-$ and Na[*closo*-$CB_{11}H_{12}$] as model geometries for the silver salts support experimental evidence for these Ag···{BH} interactions in solution.

Introduction

Structurally characterized examples of the simple silver(I)-salts of the carborane mono anion [*closo*-$CB_{11}H_{12}]^-$ and its derivatives are well documented, as these complexes frequently provide crystalline materials suitable for X-ray diffraction studies of this important class of least coordinating anion.[1] In the solid-state, there are three general structural types observed: (i) coordination polymers, often with the carborane being complemented by a bound arene molecule at the silver center;[2−6] (ii) discrete molecules in which both arene and carborane interactions occur;[4,7] (iii) discrete molecules in which only silver and carborane interactions are present, although only two examples have been reported, namely [Fe(tpp)][Ag(*closo*-$CB_{11}H_6Br_6)_2$][8] [tpp = tetraphenylporphyrinatoiron(III)] and the recently reported tetrameric complex $[ReAg\{\mu\text{-}5,6,10\text{-}(H)_3\text{-}\eta^5\text{-}7,8\text{-}C_2B_9H_8\}(CO)_3]_4$.[9] Although many of these structures show close Ag···{HB} interactions in the solid-state, these interactions are rarely observed in solution.[5,6,10] This is no doubt a result of the fact that the NMR spectra of these complexes are routinely recorded in coordinating solvents, such as acetone, that encourage well separated ion-pairs.

We have recently reported the coordination chemistry of silver phosphine fragments partnered with [*closo*-$CB_{11}H_{12}]^-$ and its derivatives, such as (PPh_3)Ag(*closo*-$CB_{11}H_{12}$), and have shown that these complexes are highly active catalysts for hetero Diels−Alder reactions.[10,11] As part of this ongoing research, we were interested in substituting the phosphine ligand by a alternative, neutral, 2-electron donor. *N*-Heterocyclic carbenes such as 1,3-dimesitylimidazol-2-ylidene (IMes) have been successfully used to substitute phosphine ligands in a number of catalytically relevant systems, perhaps the best example being their use in Grubbs'-type catalysts to afford significantly more active complexes.[12] We describe here that attempts to substitute PPh_3 by IMes did not afford

* To whom correspondence should be addressed. E-mail: a.s.weller@bath.ac.uk (A.S.W.). Fax: +44 (0)1225 386231 (A.S.W.).
† University Science Laboratories.
‡ University of Bath.

(1) Reed, C. A. *Acc. Chem. Res.* **1998**, *31*, 133.
(2) Shelly, K.; Finster, D. C.; Lee, Y. J.; Scheidt, W. R.; Reed, C. A. *J. Am. Chem. Soc.* **1985**, *107*, 5955.
(3) Tsang, C. W.; Yang, Q. C.; Sze, E. T. P.; Mak, T. C. W.; Chan, D. T. W.; Xie, Z. W. *Inorg. Chem.* **2000**, *39*, 3582. Xie, Z.; Tsang, C.-W.; Sze, E. T.-P.; Yang, Q.; Chan, D. T. W.; Mak, T. C. W. *Inorg. Chem.* **1998**, *37*, 6444. Xie, Z. W.; Wu, B. M.; Mak, T. C. W.; Manning, J.; Reed, C. A. *J. Chem. Soc., Dalton Trans.* **1997**, 1213. Jelinek, T.; Baldwin, P.; Scheidt, W. R.; Reed, C. A. *Inorg. Chem.* **1993**, *32*, 1982.
(4) Tsang, C.-W.; Yang, Q.; Sze, E. T.-P.; Mak, T. C. W.; Chan, D. T. W.; Xie, Z. *Inorg. Chem.* **2000**, *39*, 5851.
(5) Patmore, N. J.; Mahon, M. F.; Steed, J. W.; Weller, A. S. *J. Chem. Soc., Dalton Trans.* **2001**, 277.
(6) Xie, Z. W.; Jelinek, T.; Bau, R.; Reed, C. A. *J. Am. Chem. Soc.* **1994**, *116*, 1907.
(7) Ivanov, S. V.; Rockwell, J. J.; Miller, S. M.; Anderson, O. P.; Solntsev, K. A.; Strauss, S. H. *Inorg. Chem.* **1996**, *35*, 7882. Ivanov, S. V.; Lupinetti, A. J.; Miller, S. M.; Anderson, O. P.; Solntsev, K. A.; Strauss, S. H. *Inorg. Chem.* **1995**, *34*, 6419.
(8) Xie, Z.; Bau, R.; Reed, C. A. *Angew. Chem., Int. Ed. Engl.* **1994**, *33*, 2433.
(9) Ellis, D. D.; Jeffery, J. C.; Jelliss, P. A.; Kautz, J. A.; Stone, F. G. A. *Inorg. Chem.* **2001**, *40*, 2041.
(10) Patmore, N. J.; Hague, C.; Cotgreave, J. H.; Mahon, M. F.; Frost, C. G.; Weller, A. S. *Chem.—Eur. J.* **2002**, *8*, 2088.
(11) Hague, C.; Patmore, N. J.; Frost, C. G.; Mahon, M. F.; Weller, A. S. *Chem. Commun.* **2001**, 2286.

10.1021/ic025730h CCC: $22.00
Published on Web 07/27/2002

the initially anticipated complex, (IMes)Ag(*closo*-$CB_{11}H_{12}$), but instead, the bis-carbene cation $[(IMes)_2Ag]^+$ results with the concomitant formation of the novel silver−carborane dianion $[Ag_2\{closo\text{-}CB_{11}H_{12}\}_4]^{2-}$: a novel coordination motif for the discrete silver salts of the carborane anions. Aided by ab initio/GIAO/NMR calculations, we also report on the solution-state structures of the simple salts of [*closo*-$CB_{11}H_{12}]^-$ and show that in a noncoordinating solvent (CH_2Cl_2) there are significant interactions between metal ion and carborane anion, analogous to those observed in the solid-state.

Results and Discussion

Addition of a toluene solution of the free carbene IMes (IMes = 1,3-dimesitylimidazol-2-ylidene) to a stirred solution of Ag[*closo*-$CB_{11}H_{12}$] results in a colorless solution that affords colorless crystals of a compound of empirical formula $[Ag(IMes)_2][Ag\{closo\text{-}CB_{11}H_{12}\}_2]$ (**1**) on cooling. Compound **1** has been characterized by elemental analyses, single-crystal X-ray diffraction (Table 1), and multinuclear NMR spectroscopy.

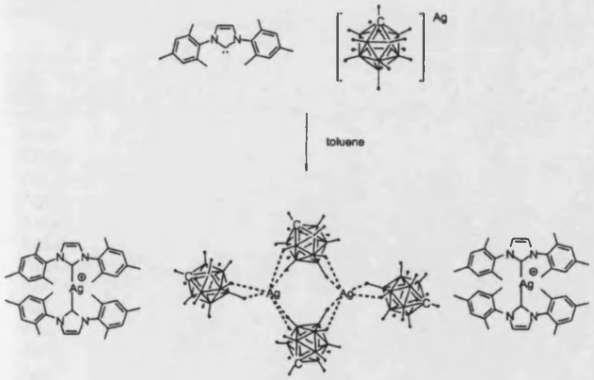

X-ray Crystallography. The asymmetric unit in **1** consists of one cationic $[(IMes)_2Ag]^+$ moiety and one anionic fragment based on a silver atom and two [*closo*-$CB_{11}H_{12}]^-$ cages. The silver−carbene fragment (Figure 1) is compositionally identical to that previously reported for $[(IMes)_2Ag][O_3SCF_3]$ (**A**).[13] The metal−$C_{(carbene)}$ distances of the cationic fragment in **1** are indistinguishable [Ag(1)−C(22) 2.069(6) Å, Ag(1)−C(1A) 2.070(5) Å] and are also identical to those found in **A** [2.067(4) and 2.078(4) Å]. The C(22)−Ag(1)−C(1A) angle at the metal center is nonlinear [C(22)−Ag(1)−C(1A) 174.3(2)°], similar to that found in **A** [176.3(2)°]. The only significant structural difference between the cation in **1** and **A** is the angle between the least-squares planes of the five-membered imidazole rings, which is 59.1° in **1** and 39.7° in **A**. This is no doubt due to differences in the crystal packing imposed by the anions in the two complexes.

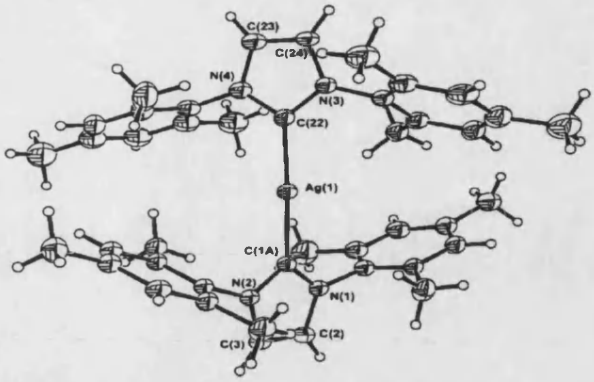

Figure 1. Cationic component of the asymmetric unit in complex **1**. Thermal ellipsoids are given at the 30% probability level.

Table 1. Crystal Data and Structure Refinement for **1**, $[(IMes)_2Ag][Ag\{Closo\text{-}CB_{11}H_{12}\}_2]$

empirical formula	$C_{22}H_{36}AgB_{11}N_2$
fw	555.31
T	150(2) K
wavelength	0.71073 Å
cryst syst	monoclinic
space group	$P2_1/n$
unit cell dimensions	a = 15.4570(2) Å
	b = 20.1150(3) Å; β = 108.558(1)°
	c = 19.2130(3) Å
V	5663.04(14) Å^3
Z	8
D_{calcd}	1.303 Mg/m^3
abs coeff	0.727 mm^{-1}
F(000)	2272
cryst size	0.13 × 0.13 × 0.15 mm^3
θ range for data collection	3.66 to 24.71°
reflns collected	85847
independent reflns	9621 [R(int) = 0.1469]
reflns obsd (> 2σ)	5969
data completeness	0.996
abs correction	semiempirical from equivalents
max and min transmission	0.97 and 0.87
refinement method	full-matrix least-squares on F^2
data/restraints/params	9621/0/749
GOF on F^2	1.043
final R indices [I > 2σ(I)]	R1 = 0.0543; wR2 = 0.1160
R indices (all data)	R1 = 0.1055; wR2 = 0.1419
largest diff peak and hole	0.489 and −0.623 eÅ^{-3}

The anionic fragment containing the second silver atom and carborane anions is proximate to a crystallographic inversion center in the asymmetric unit, which generates a [*closo*-$CB_{11}H_{12}]^-$ bridged dimer where the symmetry related silver atoms are also terminally coordinated to the second cage (Figure 2). The bridging carborane anions are disordered in a 1:1 ratio between positions B(21) to B(32) and B(41) to B(52), respectively. This disorder can be readily resolved into the dimeric motif that contains two different orientations of the bridging carborane cages. The two disorder components are chemically and structurally identical. The presence of this disorder precluded accurate assignment of the cage carbon in the bridging carborane, and hence all atoms therein were refined as boron atoms. However, assignment of the cage carbon in the terminally bound cage [C(1)−B(12)] was unambiguous. The resulting $Ag_2[closo\text{-}CB_{11}H_{12}]_4$ anion has an overall dinegative charge and is thus associated with two $[(IMes)_2Ag]^+$ cations (see Supporting Information). The coordination geometry around each silver atom is ap-

(12) Huang, J. K.; Stevens, E. D.; Nolan, S. P.; Petersen, J. L. *J. Am. Chem. Soc.* **1999**, *121*, 2674. Weskamp, T.; Schattenmann, W. C.; Spiegler, M.; Herrmann, W. A. *Angew. Chem., Int. Ed.* **1998**, *37*, 2490. Scholl, M.; Trnka, T. M.; Morgan, J. P.; Grubbs, R. H. *Tetrahedron Lett.* **1999**, *40*, 2247.

(13) Arduengo, A. J., III; Dias, H. V. R.; Calabrese, J. C.; Davidson, F. *Organometallics* **1993**, *12*, 3405.

Structure of $[Ag\{closo\text{-}CB_{11}H_{12}\}_4]^{2-}$

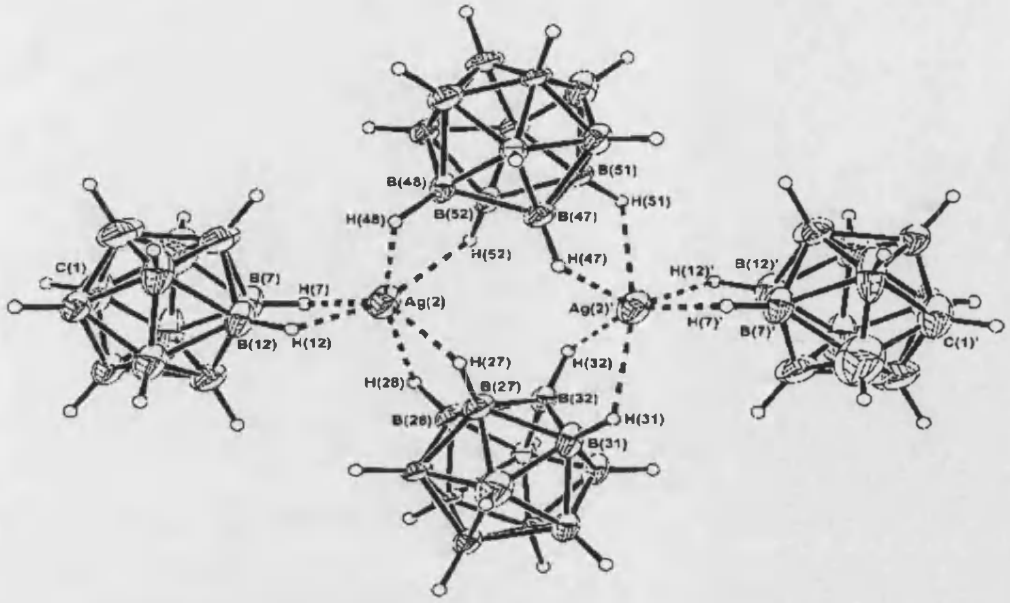

Figure 2. Anionic portion of complex **1** showing one of the disordered components. Atoms with primed labels are related to those in the asymmetric unit by the operation $-x + 1, -y, -z$. Disorder in the bridging carborane anions is omitted for clarity. Thermal ellipsoids are given at the 30% probability level.

Table 2. Bond Lengths (Å) and Angles (deg) Associated with Ag(1), Ag(2) and Ag(2)′ in Complex **1** for One of the Disordered Components in the Lattice

Ag(1)−C(22)	2.069(6)	Ag(1)−C(1A)	2.070(5)
C(22)−Ag1−C(1A)	174.3(2)		
Ag(2)−H(7)	2.05	Ag(2)−B(7)	2.586(8)
Ag(2)−H(12)	2.23	Ag(2)−B(12)	2.673(8)
Ag(2)−H(27)	2.09	Ag(2)−B(27)	2.73(2)
Ag(2)−H(28)	2.45	Ag(2)−B(28)	2.92(2)
Ag(2)−H(48)	2.35	Ag(2)−B(48)	2.84(2)
Ag(2)−H(52)	2.19	Ag(2)−B(52)	2.79(2)
Ag(2)′−H(31)	2.52	Ag(2)−B(31)′	2.94(2)
Ag(2)′−H(32)	1.96	Ag(2)−B(32)′	2.67(2)
Ag(2)′−H(47)	2.05	Ag(2)′−B(47)	2.70(2)
Ag(2)′−H(51)	2.40	Ag(2)′−B(51)	2.88(2)

proximately trigonal prismatic, with each metal center surrounded by four shorter and two longer {BH} interactions. Salient metrical data for Ag(2) and Ag(2)′ are given in Table 2. The shorter Ag···{HB} interactions vary in distance ranging from 1.96 to 2.23 Å (Ag−H) and 2.586(7) to 2.79(2) Å (Ag−B). The longer interactions are in the range 2.84(2)−2.94(2) Å (Ag−B). These Ag−B distances can be compared with those found in the silver(I)−phosphine complexes $(PPh_3)Ag(closo\text{-}CB_{11}H_{12})$ [2.504(3)−2.619(3) Å] and $(PPh_3)_2Ag(closo\text{-}CB_{11}H_{12})$ [2.892(2)−3.494(2) Å], where significant Ag−B interactions are suggested to exist in solution in the former but not the latter complex, on the basis of observed ^{11}B chemical shifts.[10] The shorter Ag···{HB} distances are also comparable with those found in the benzene solvate of $Ag[closo\text{-}CB_{11}H_{12}]$ [2.581(6) and 2.681(5) Å][2] but are shorter than those found in the tetrameric complex $[ReAg\{\mu\text{-}5,6,10\text{-}(H)_3\text{-}\eta^5\text{-}7,8\text{-}C_2B_9H_8\}(CO)_3]_4$ [2.978(7), 2.905(6) Å] in which the Ag−{HB} interactions are suggested to lie between regular covalent agostic and longer range electrostatic.[9] Overall, these comparisons suggest that the Ag···{HB} interactions in **1** are significant, with this interpretation strengthened by the solution ^{11}B NMR data and ab initio/GIAO/NMR calculations.

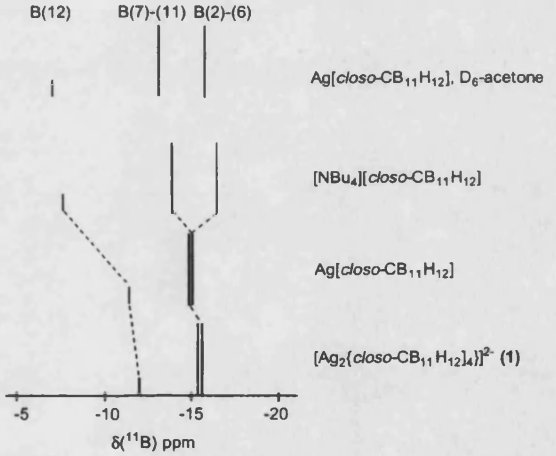

Figure 3. Diagrammatic stick diagram of ^{11}B chemical shifts observed for **1**, $[NBu_4][closo\text{-}CB_{11}H_{12}]$, and $Ag[closo\text{-}CB_{11}H_{12}]$, all measured as CD_2Cl_2 solutions, and $Ag[closo\text{-}CB_{11}H_{12}]$ measured in d_6-acetone.

^{11}B NMR Spectroscopy. Although NMR spectroscopy alone does not allow us to determine whether the $\{Ag_2(closo\text{-}CB_{11}H_{12})_4\}$ motif remains wholly intact in solution, the presence of significant Ag···{HB} interactions is indicated by the solution $^{11}B\{^1H\}$ NMR spectrum of **1** in CD_2Cl_2. This shows resonances due to one $\{closo\text{-}CB_{11}H_{12}\}$ cage species with C_{5v} symmetry that displays a marked upfield shift for the cage boron atoms B(7)−B(11) and B(12) when compared with that found for $[closo\text{-}CB_{11}H_{12}]^-$ partnered with the non-Lewis-acidic counterion $[NBu_4]^+$ (Figure 3). Thus, in the $^{11}B\{^1H\}$ NMR spectrum of **1**, signals are observed at δ −12.4 (1B) and −15.7 (5B + 5B coincidence), compared with δ −8.0 (1B), −14.1 (5B), −16.9 (5B) found for $[NBu_4][closo\text{-}CB_{11}H_{12}]$. Values found for $Ag[closo\text{-}CB_{11}H_{12}]$ and **1** in acetone, a solvent in which any ion-pairs would be expected to be well separated, are similar to those found for $[Cs]^+$ or

$[NBu_4][closo\text{-}CB_{11}H_{12}]$,[14,15] cations with which the carborane periphery is not expected to interact significantly in solution.

The $^{11}B\{^1H\}$ NMR spectrum of $Ag[closo\text{-}CB_{11}H_{12}]$ in CD_2Cl_2 (in which it is poorly soluble and hence not usually used as a solvent) is very similar to that of **1**, with signals observed at δ −11.9 (1B) and −15.0 (5 + 5 coincidence) (Figure 3). Although in **1** the ratio $Ag/[closo\text{-}CB_{11}H_{12}]$ is 1:2, while for $Ag[closo\text{-}CB_{11}H_{12}]$ it is 1:1, this similarity suggests that comparable Ag···{HB} interactions are present in solution in these two species, and perhaps that $Ag[closo\text{-}CB_{11}H_{12}]$ exists in CD_2Cl_2 solution as weakly associated oligomeric units, similar to **1**. The very low solubility of $Ag[closo\text{-}CB_{11}H_{12}]$ in CD_2Cl_2 is perhaps indicative of this extended structure. Reed and co-workers have observed similar chemical shift changes for $Ag[closo\text{-}CB_9H_{10}]$ when measured in toluene and acetone or acetonitrile.[6] Similar interactions (and relative ^{11}B NMR chemical shift differences) have been previously proposed by us as being present in solution for the silver-salt metathesis intermediate complex $[CpMo(CO)_3I\cdot Ag\{closo\text{-}CB_{11}H_{12}\}]_2$ (Cp = η^5-C_5H_5).[5] We have also previously shown that significant upfield shifts occur in the ^{11}B NMR spectra of $[closo\text{-}CB_{11}H_{12}]^-$ when coordinated to $[(\eta^5\text{-}C_5R_5)Mo(CO)_3]^+$ (R = H, Me),[5] $[(cod)Rh]^+$ (cod = 1,5-cyclooctadiene),[16] and $[Ag(PPh_3)]^+$ [10] fragments. The data in hand here suggest that the Ag cation in **1** interacts significantly with the carborane periphery in CD_2Cl_2 solution and, in particular, with the boron atoms B(12) and B(7)−B(11). This is confirmed by the results of ab initio calculations on model complexes for **1**, $Ag[closo\text{-}CB_{11}H_{12}]$, and "free" $[closo\text{-}CB_{11}H_{12}]^-$, which follow.

Calculations. In the past decade, the reliable "ab initio/GIAO/NMR" method has been used to determine the molecular structures of carboranes in solution.[17−20] However, there are only two reports of the method being used to determine the likely geometries of metal salts of carborane anions in solution.[21] Given the marked differences observed between the ^{11}B NMR spectra of $Ag[closo\text{-}CB_{11}H_{12}]$ when measured in CD_2Cl_2 versus acetone, we sought to use the ab initio/GIAO/NMR method to elucidate the structures of the species present in these two solvents, in addition to the structure of complex **1** in solution. However, the silver cation $[Ag]^+$ is at present not computationally feasible at the MP2/6-31G* level of theory required for the accurate determination of chemical shifts.[18] Copper would be an obvious replacement, but it is computationally inhibitive at the MP2/6-31G* level for the compounds under discussion. We have thus chosen to replace $[Ag]^+$ by $[Na]^+$ in ab initio computations described here. Although $[Na]^+$ and $[Ag]^+$ are hard and soft Lewis acids, respectively, and thus may be expected to interact somewhat differently with the cage (electrostatic and covalent respectively), our approach is validated by that fact that they have similar ionic radii[22] and that calculations (MP2 level optimized geometries) on the model complexes $Na(BH_4)$ and $Ag(BH_4)$ show that both complexes adopt very similar structures (tridentate, C_{3v}).[23] Moreover, the chemical shifts calculated for $Na[closo\text{-}CB_{11}H_{12}]$ (vide infra) are very close to those experimentally observed for $Ag[closo\text{-}CB_{11}H_{12}]$, further supporting this approach.

Initially, we focused on modeling the structure of $Ag[closo\text{-}CB_{11}H_{12}]$ in a noncoordinating solvent, such as CD_2Cl_2, where ^{11}B NMR spectroscopy shows that tight ion pairs are likely to be present. A geometry optimization of $Na[closo\text{-}CB_{11}H_{12}]$ at the MP2/6-31G* level of theory gave the lowest energy minimum **I** with the sodium metal capping the triangular face defined by B(7), B(8), and B(12) (Figure 4). This structure is similar to that which we have observed for $(PPh_3)Ag(closo\text{-}CB_{11}H_{12})$[10] and also that calculated for protonated $[closo\text{-}CB_{11}H_{12}]^-$,[24] in agreement with $[Na]^+$ and

(14) Hermanek, S. *Chem. Rev.* **1992**, *92*, 325.
(15) During the course of this work, we found that the ^{11}B chemical shift literature values for $Ag[closo\text{-}CB_{11}H_{12}]$ in acetone differed from those one of us (A.S.W.) had previously reported by δ −3.3. Examination of authentic carborane samples recorded at Bath and Durham with literature values confirmed this discrepancy. Although in this paper, and all subsequent contributions from Bath, ^{11}B chemical shifts are correctly referenced to $BF_3\cdot OEt_2$, previous papers from us do not take this into account. However, in all discussions, as it is the relative positions of the resonances which are important, this small change in chemical shift does not alter any conclusions made on the basis of ^{11}B NMR spectroscopy.
(16) Weller, A. S.; Mahon, M. F.; Steed, J. W. *J. Organomet. Chem.* **2000**, *614−615*, 113.
(17) Bühl, M.; Gauss, J.; Hofmann, M.; Schleyer, P. v. R. *J. Am. Chem. Soc.* **1993**, *115*, 12385. Schleyer, P. v. R.; Gauss, J.; Bühl, M.; Greatrex, R.; Fox, M. A. *Chem. Commun.* **1993**, 1766.
(18) Bühl, M.; Schleyer, P. v. R. *J. Am. Chem. Soc.* **1992**, *114*, 477.
(19) Bausch, J. W.; Matoka, D. J.; Carroll, P. J.; Sneddon, L. G. *J. Am. Chem. Soc.* **1996**, *118*, 11423. Bausch, J. W.; Rizzo, R. C.; Sneddon, L. G.; Wille, A. E.; Williams, R. E. *Inorg. Chem.* **1996**, *35*, 131. Fox, M. A.; Greatrex, R.; Hofmann, M.; Schleyer, P. v. R. *Angew. Chem., Int. Ed. Engl.* **1994**, *33*, 2298. Fox, M. A.; Greatrex, R.; Hofmann, M.; Schleyer, P. V. R.; Williams, R. E. *Angew. Chem., Int. Ed. Engl.* **1997**, *36*, 1498. Fox, M. A.; Greatrex, R.; Nikrahi, A.; Brain, P. T.; Picton, M. J.; Rankin, D. W. H.; Robertson, H. E.; Bühl, M.; Li, L.; Beaudet, R. A. *Inorg. Chem.* **1998**, *37*, 2166. Fox, M. A.; Greatrex, R.; Hofmann, M.; Schleyer, P. v. R. *J. Organomet. Chem.* **2000**, *614−615*, 262. Fox, M. A.; Goeta, A. E.; Howard, J. A. K.; Hughes, A. K.; Johnson, A. L.; Keen, D. A.; Wade, K.; Wilson, C. C. *Inorg. Chem.* **2001**, *40*, 173. Gangnus, B.; Stock, H.; Siebert, W.; Hofmann, M.; Schleyer, P. v. R. *Angew. Chem., Int. Ed. Engl.* **1994**, *33*, 2296. Hnyk, D.; Rankin, D. W. H.; Robertson, H. E.; Hofmann, M.; Schleyer, P. V. R.; Bühl, M. *Inorg. Chem.* **1994**, *33*, 4781. Hofmann, M.; Fox, M. A.; Greatrex, R.; Schleyer, P. v. R.; Bausch, J. W.; Williams, R. E. *Inorg. Chem.* **1996**, *35*, 6170. Hofmann, M.; Fox, M. A.; Greatrex, R.; Williams, R. E.; Schleyer, P. v. R. *J. Organomet. Chem.* **1998**, *550*, 331. Tebben, A. J.; Ji, G.; Williams, R. E.; Bausch, J. W. *Inorg. Chem.* **1998**, *37*, 2189. Wrackmeyer, B.; Schanz, H. J.; Hofmann, M.; Schleyer, P. v. R. *Angew. Chem., Int. Ed. Engl.* **1998**, *37*, 1245. Wrackmeyer, B.; Schanz, H. J.; Hofmann, M.; Schleyer, P. v. R. *Eur. J. Inorg. Chem.* **1998**, *5*, 633.
(20) Gruner, B.; Jelinek, T.; Plzak, Z.; Kennedy, J. D.; Ormsby, D. L.; Greatrex, R.; Stibr, B. *Angew. Chem., Int. Ed.* **1999**, *38*, 1806. Jaballas, J.; Onak, T. *J. Organomet. Chem.* **1998**, *550*, 101. Jelinek, T.; Stíbr, B.; Holub, J.; Bakardjiev, M.; Hnyk, D.; Ormsby, D. L.; Kilner, C. A.; Thornton-Pett, M.; Schanz, H.-J.; Wrackmeyer, B.; Kennedy, J. D. *Chem. Commun.* **2001**, 1756. Lee, H.; Onak, T.; Jaballas, J.; Tran, U.; Truong, T. U.; To, H. T. *Inorg. Chim. Acta* **1999**, *289*, 11. Onak, T.; Jaballas, J.; Barfield, M. *J. Am. Chem. Soc.* **1999**, *121*, 2850. Shedlow, A.; Sneddon, L. G. *Organometallics* **1995**, *14*, 4046. Shedlow, A.; Sneddon, L. G. *Collect. Czech. Chem. Commun.* **1999**, *64*, 865. Wille, A. E.; Plesek, J.; Holub, J.; Stíbr, B.; Carroll, P. J.; Sneddon, L. G. *Inorg. Chem.* **1996**, *35*, 5342.
(21) Ezhova, M. B.; Zhang, H. M.; Maguire, J. A.; Hosmane, N. S. *J. Organomet. Chem.* **1998**, *550*, 409. Fox, M. A.; Hughes, A. K.; Johnson, A. L.; Paterson, M. A. J. *J. Chem. Soc., Dalton Trans.* **2002**, 2009.
(22) Huheey, J. E.; Keiter, E. A.; Keiter, R. L. *Inorganic Chemistry: Principles of Structure and Reactivity*; New York: Harper Collins, 1993.
(23) Francisco, J. S.; Williams, I. H. *J. Phys. Chem.* **1992**, *96*, 7567. Musaev, D. G.; Morokuma, K. *Organometallics* **1995**, *14*, 3327.
(24) Koppel, I. A.; Burk, P.; Koppel, I.; Leito, I.; Sonoda, T.; Mishima, M. *J. Am. Chem. Soc.* **2000**, *122*, 5114.

Structure of [Ag{closo-$CB_{11}H_{12}$}$_4$]$^{2-}$

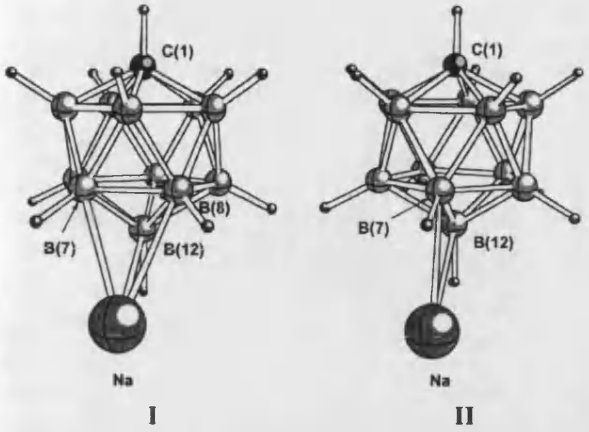

Figure 4. Ball and stick representation of the MP2/6-31G* calculated structures for Na[*closo*-$CB_{11}H_{12}$] showing the μ^3 (**I**) and μ^2 (**II**) bridging modes of the Na ion, respectively.

Table 3. Comparison of Experimental and Theoretical ^{11}B NMR Shifts (δ) for Various Salts of [*closo*-$CB_{11}H_{12}$]$^-$

	experiment[a]			calculated[b]			
	$[NBu_4]^+$	$[Ag]^+$	**1**	none	**I**	**III**[c]	**IV**
B(12)	−8.0	−11.9	−12.4	−6.9	−12.5	−10.1	−10.8
B(7)−B(11)	−14.1	−15.0	−15.7	−13.8	−15.3	−14.4	−14.9
B(2)−B(6)	−16.9	−15.0	−15.7	−17.8	−15.4	−16.7	−16.3

[a] Measured in CD_2Cl_2. [b] Averaged values at the GIAO-B3LYP/6-311G*//MP2/6-31G* level. [c] Averaged values at the GIAO-B3LYP/6-311G*//HF/6-31G* level.

$\{(PPh_3)Ag\}^+$ being nominally isolobal with a proton.[25] Because observed NMR data for Ag[*closo*-$CB_{11}H_{12}$] show 5-fold symmetry with the greatest perturbation from $[NBu_4]$[*closo*-$CB_{11}H_{12}$] observed for B(7)−B(12) (Figure 3), the metal ion must be fluxional over all triangular faces involving the B(12) vertex. In agreement with this, the symmetry-constrained minimum **II** with the sodium atom bridging between B(7) and B(12) is only ca. 3.0 kcal mol^{-1} higher in energy than **I**. This small energy difference supports the metal ion being fluxional over the five triangular faces of the cage in solution, moving from face to face via bridging a B−B vertex. This low calculated energy barrier is also reflected experimentally by the fact that $\{Ag(PPh_3)\}$,[10] {Rh(cod)},[16] and $\{Rh(PPh_3)_2\}$[26] fragments are highly fluxional over the lower surfaces of [*closo*-$CB_{11}H_{12}$]. Values obtained by averaging the calculated ^{11}B NMR shifts (at B3LYP/6-311G*) generated from the optimized geometry of Na[*closo*-$CB_{11}H_{12}$] **I** are in very good agreement with observed ^{11}B chemical shifts for Ag[*closo*-$CB_{11}H_{12}$] and **1** in CD_2Cl_2 (Table 3). Importantly, the computed ^{11}B shifts generated from the MP2/6-31G* geometry[27] for "free" [*closo*-$CB_{11}H_{12}$]$^-$ are also in good agreement with observed shifts for Ag[$CB_{11}H_{12}$] in acetone and $[NBu_4][CB_{11}H_{12}]$ in CD_2Cl_2 (Table 3).

These changes in the calculated boron chemical shifts on going from optimized geometries of Na[*closo*-$CB_{11}H_{12}$] to "free" [*closo*-$CB_{11}H_{12}$]$^-$ mirror those observed experimentally in solution for Ag[*closo*-$CB_{11}H_{12}$] on going from a noncoordinating solvent (e.g., CD_2Cl_2) to a coordinating solvent (e.g., acetone). Particularly noteworthy is that all the chemical shift changes observed experimentally are accurately reflected in the calculations, with both the upfield shifts for B(12) and B(7)−B(11) along with the more subtle downfield shift of B(2)−B(6) being reproduced. It is clear from these computations that metal−carborane interactions exist in noncoordinating solvents for Ag[*closo*-$CB_{11}H_{12}$] and thus, by implication, also for **1**, confirming our experimental observations. The geometry optimization of the dianion $\{Na_2$(*closo*-$CB_{11}H_{12})_4\}^{2-}$ (**III**), as a model geometry for the dianion in **1**, further demonstrates that replacement of $[Na]^+$ for $[Ag]^+$ is valid, showing a similar structural motif at the HF/6-31G* level of theory as that found in the X-ray structure of **1** (Figure 5), with only the small twist of the bridging carborane cages not being reproduced. However, these calculations do not determine the molecular structures of either **1** or Ag[*closo*-$CB_{11}H_{12}$] in a noncoordinating solvent, that is, whether the structural motif of the dianion in **1** is retained in solution and whether Ag[$CB_{11}H_{12}$] is a discrete monomer, dimer, or oligomer in solution. In an attempt to address this, we have performed the same ab initio/GIAO/NMR calculations on $\{Na$[*closo*-$CB_{11}H_{12}]_2\}^-$, **IV**, and for $\{Na_2$(*closo*-$CB_{11}H_{12})_4\}^{2-}$, **III**, although for this latter compound the computationally less intensive HF/6-31G* basis set was used because of the relatively large number of atoms in the molecule. The calculated geometries of **III** and **IV** are presented in Figure 5, which shows that for **IV** the sodium ion is η^3-sandwiched between two carborane anions.

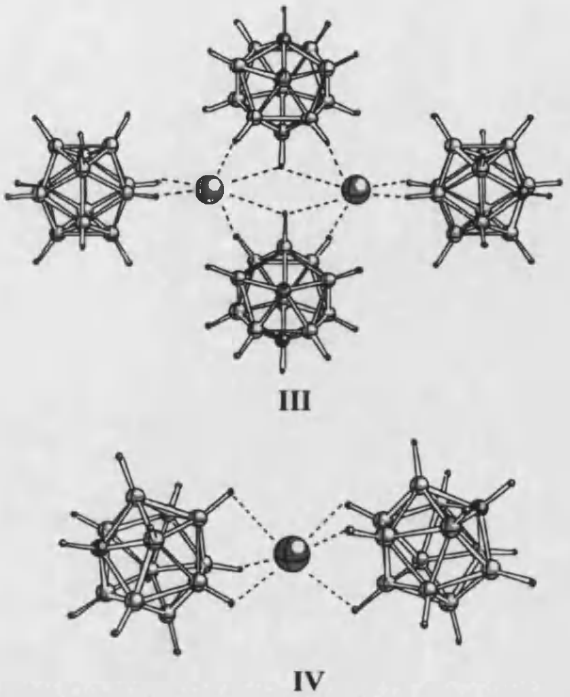

Figure 5. Ball and stick representations of the calculated structures for $\{Na_2$[*closo*-$CB_{11}H_{12}]_4\}^{2-}$ (**III**) (HF/6-31G*) and $\{Na$[*closo*-$CB_{11}H_{12}]_2\}^-$ (**IV**) (MP2/6-31G*).

(25) Kickelbick, G.; Schubert, U. *Inorg. Chim. Acta* **1997**, *262*, 61.
(26) Rifat, A.; Patmore, N. J.; Mahon, M. F.; Weller, A. S. *Organometallics* **2002**, *21*, 2842.
(27) Schleyer, P. V. R.; Najafian, K. *Inorg. Chem.* **1998**, *37*, 3454.

The averages of the calculated ^{11}B NMR shifts (at B3LYP/6-311G*) generated from these optimized geometries are given in Table 3 and show a close similarity to both those calculated for **I** and observed for **1** and Ag[*closo*-$CB_{11}H_{12}$] in CD_2Cl_2, even though model compound **III** was geometry optimized at a lower level of theory (HF/6-31G*) and silver has been substituted for sodium. The match is nevertheless a good one, with the difference between experiment and theory when **1** and **III** are compared ranging between 2.3 and 1.0 ppm. Moreover, the calculated shifts for **III** and **IV** show the upfield shift of the B(12) vertex and a compression of the two integral 5-B signals, as is observed experimentally for **1**. The close similarity of all these data (compound **1**, model compounds **I**, **III**, and **IV**) suggests that the actual solution structure, as determined by ^{11}B NMR spectroscopy, is ambiguous with regard to the degree of aggregation, although it is clear that significant Ag···{HB} interactions do occur in noncoordinating solvent. However, it is more than likely that a species such as [Ag(IMes)$_2$][Ag(*closo*-$CB_{11}H_{12}$)$_2$] (model compound **IV**) exists as the predominant species in solution, similar to that observed for [Ag(*closo*-$CB_{11}H_6Br_6$)$_2$]$^-$.[8]

Conclusions

Addition of IMes to Ag[*closo*-$CB_{11}H_{12}$] results in the formation of the novel complex [(IMes)$_2$Ag][Ag$_2${*closo*-$CB_{11}H_{12}$}$_4$] in the solid-state, an anion in which each silver is surrounded by three carborane units. In CD_2Cl_2 solution, the Ag−carborane interactions are still present, as evidenced by significant downfield shifts being observed in the ^{11}B NMR spectrum. That these shifts are due to Ag···{HB} interactions is confirmed by the following: (i) The ^{11}B chemical shifts of Ag[*closo*-$CB_{11}H_{12}$] in coordinating solvent (acetone) and [NMe_4][*closo*-$CB_{11}H_{12}$] in CD_2Cl_2 are similar and closely match the computed ^{11}B shifts for "naked" [*closo*-$CB_{11}H_{12}$]$^-$. (ii) Calculated ^{11}B chemical shifts for Na[*closo*-$CB_{11}H_{12}$], {Na[*closo*-$CB_{11}H_{12}$]$_2$}$^-$, and {Na$_2$[*closo*-$CB_{11}H_{12}$]$_4$}$^{2-}$ which all have metal cation−anion interactions agree well with experimental ^{11}B data measured for **1** and Ag[*closo*-$CB_{11}H_{12}$] in CD_2Cl_2, suggesting that both silver complexes form significant ion-pairs in solution with similar structural features. This close match between calculated and experimentally determined chemical shifts initially surprised us given the disparity in the relative hardness of the two cations $[Na]^+$ and $[Ag]^+$. However, this perhaps suggests that the $[Ag]^+$ interactions with the cage periphery in [*closo*-$CB_{11}H_{12}$] are in fact more electrostatic than covalent (agostic) in nature than previously assumed, as we have suggested previously.[10] We have also shown that the previously proposed model for the interactions of metal fragments across the lower surface of [*closo*-$CB_{11}H_{12}$]$^-$ in solution may be confirmed by the calculations reported here.

Overall, these results show that metal cation−carborane anion interactions significantly affect the ^{11}B NMR shifts of the simple salts of carborane anions and that the solvent and the conjugate cation both need to be taken into account when comparing the ^{11}B chemical shifts of different salts.

Experimental

All manipulations were carried out under an argon atmosphere using standard Schlenk line or drybox techniques. Hexane and toluene were distilled from sodium. NMR spectra were measured on Brüker Advance 300 MHz and Varian Mercury 400 MHz FT-NMR spectrometers in CD_2Cl_2 solutions. Residual protio solvent was used as reference (δ, ppm: CD_2Cl_2 5.33) in ^1H NMR spectra. ^{11}B NMR spectra were referenced to $BF_3{\cdot}OEt_2$ (external). Coupling constants are given in hertz. Spectra were recorded at room temperature in CD_2Cl_2 solutions. Elemental analysis was performed in-house in the Department of Chemistry, University of Bath. The compounds Ag[*closo*-$CB_{11}H_{12}$][2] and IMes[28] were prepared by published procedures or slight variations thereof. [NBu_4][*closo*-$CB_{11}H_{12}$] was prepared by metathesis of Cs[*closo*-$CB_{11}H_{12}$] with [NBu_4]Cl in CH_2Cl_2, filtration, and crystallization from CH_2Cl_2/hexanes.

[(IMes)$_2$Ag][Ag$_2${*closo*-$CB_{11}H_{12}$}$_4$] (1). IMes (55 mg, 0.18 mmol) was dissolved in toluene (5 mL) and added dropwise to a Schlenk tube charged with Ag[*closo*-$CB_{11}H_{12}$] (47 mg, 0.19 mmol) dissolved in toluene, and then the mixture stirred for 16 h. This solution was cannula filtered and the toluene removed in vacuo. The resulting solid was dissolved in the minimum volume of toluene and crystals of product grown at −80 °C for 5 days. The solvent was decanted and the resulting product dried under high vacuum to yield 46 mg (46%) of white crystalline solid.

$^1H\{^{11}B\}$: 1.57 (s, 10H, BH), 1.65 (s, 12H, o-CH_3), 1.69 (s, 10H, BH), 2.25 (s, 2H, BH), 2.32 (s, 2H, CH_{cage}), 2.35 (s, 6H, p-CH_3), 6.85 (s, 8H, m-CH), 7.00 (s, 4H, NCH). ^{11}B: −12.4 [d, 2B, J(BH) 125], −15.7 [d, 10B + 10B coincidence, J(BH) 145]. $^{13}C\{^1H\}$: 17.8 (s, CH_3), 21.7 (s, CH_3), 55.3 (s br, CH_{cage}), 123.6 (s, NCCN), 129.9 (s, C_{phenyl}), 135.3 (s, C_{phenyl}), 135.6 (s, C_{phenyl}), 140.2 (s, C_{phenyl}), 183.6 [dd, NCN, J(^{109}AgC) 208, J(^{107}AgC) 180]. Calcd: %C, 47.6; %H, 6.48; %N, 5.04. Found: 47.7%, 6.55%, 4.93%.

X-ray Crystallography. The crystal structure data for compound **1** were collected on a Nonius Kappa-CCD diffractometer at 150 K. The asymmetric unit in **1** consists of one biscarbene silver moiety and of a fragment based on a silver atom and two carborane anions. The second fragment in the asymmetric unit is proximate to a crystallographic inversion center, which serves to generate a carborane bridged dimer where each of the symmetry related silver atoms are terminally coordinated to a second carborane cage. It is noteworthy that the bridging carborane is disordered in a 1:1 ratio between positions B(21) to B(32) and B(41) to B(52), respectively. The presence of disorder precluded accurate assignment of the cage carbon in the bridging carborane, and hence, all atoms therein were refined as borons. Assignment of the cage carbon in the terminally bound cage was unambiguous. Structure solution followed by full-matrix least squares refinement was performed using the SHELX suite of programs throughout.[29] All non-hydrogen atoms were treated anisotropically, and hydrogen atoms were included at calculated positions throughout. Diagrams were produced using ORTEX.[30]

Computational. All ab initio computations were carried out with the Gaussian 98 package.[31] The geometries discussed here were first optimized at the HF/6-31G* level with no symmetry constraints for **I**, **III**, and **IV** and C_s symmetry constraints for **II**. Frequency calculations were computed on these optimized geometries at the

(28) Arduengo, A. J., III; Dias, H. V. R.; Harlow, R. L.; Kline, M. *J. Am. Chem. Soc.* **1992**, *114*, 5530.
(29) Sheldrick, G. M. *SHELX-97. A computer program for refinement of crystal structures*; University of Göttingen: Göttingen, Germany, 1997.
(30) Mcardle, P. *J. Appl. Crystallogr.* **1995**, *28*, 65.

HF/6-31G* level for imaginary frequencies. None were found for **I**, **III**, and **IV**, and one imaginary frequency was found for geometry **II**. Optimization of geometries **I**, **II**, and **IV** were then carried out at the computationally intensive MP2/6-31G* level. NMR shifts were calculated on these MP2-optimized geometries at the GIAO-B3LYP/6-311G* level. Theoretical ^{11}B chemical shifts at the GIAO-B3LYP/6-311G*//MP2/6-31G* level listed in the table have been referenced to B_2H_6 (16.6 ppm[32]) and converted to the usual BF_3·OEt_2 scale: $\delta(^{11}B) = 102.83 - \sigma(^{11}B)$. For ^{11}B shifts at the GIAO-B3LYP/6-311G*//HF/6-31G* level, the equation $\delta(^{11}B) = 102.49 - \delta(^{11}B)$ was used. Relative energies were computed at the MP2/6-31G* level with ZPE (calculated at HF/6-31G*) corrections scaled by 0.89.

(31) Frisch, M. J.; Trucks, G. W.; Schlegel, H. B.; Scuseria, G. E.; Robb, M. A.; Cheeseman, J. R.; Zakrzewski, V. G.; Montgomery, J. A., Jr.; Stratmann, R. E.; Burant, J. C.; Dapprich, S.; Millam, J. M.; Daniels, A. D.; Kudin, K. N.; Strain, M. C.; Farkas, O.; Tomasi, J.; Barone, V.; Cossi, M.; Cammi, R.; Mennucci, B.; Pomelli, C.; Adamo, C.; Clifford, S.; Ochterski, J.; Petersson, G. A.; Ayala, P. Y.; Cui, Q.; Morokuma, K.; Malick, D. K.; Rabuck, A. D.; Raghavachari, K.; Foresman, J. B.; Cioslowski, J.; Ortiz, J. V.; Stefanov, B. B.; Liu, G.; Liashenko, A.; Piskorz, P.; Komaromi, I.; Gomperts, R.; Martin, R. L.; Fox, D. J.; Keith, T.; Al-Laham, M. A.; Peng, C. Y.; Nanayakkara, A.; Gonzalez, C.; Challacombe, M.; Gill, P. M. W.; Johnson, B. G.; Chen, W.; Wong, M. W.; Andres, J. L.; Head-Gordon, M.; Replogle, E. S.; Pople, J. A. *Gaussian 98*; Gaussian, Inc.: Pittsburgh, PA, 1998.
(32) Onak, T. P.; Landesman, H. L.; Williams, R. E. *J. Phys. Chem.* **1959**, *63*, 1533.

Acknowledgment. EPSRC and Royal Society are acknowledged for research fellowships (M.A.F. and A.S.W., respectively). The University of Bath is also thanked (N.J.P.). EPSRC/JREI are acknowledged for funding for a Nonius Kappa-CCD diffractometer (Bath) and for a high performance computer (Durham). The referees of this paper are thanked for useful comments.

Supporting Information Available: Tables giving crystallographic data and structure refinement details, positional and thermal parameters, and bond distances and angles for complex **1**, and computational details for structures **I** to **IV**. This material is available free of charge via the Internet at http://pubs.acs.org.

IC025730H

amines in excellent yields and enantioselectivities. Further optimizations and applications of this methodology as well as a detailed mechanistic study are in progress.

Received: June 4, 2002 [Z19442]

[1] For examples, see a) M. J. Bishop, R. W. McNutt, *Bioorg. Med. Chem. Lett.* **1995**, *5*, 1311; b) C. M. Spencer, D. Foulds, D. H. Peters, *Drugs* **1993**, *46*, 1055; c) S. Sakurai, N. Ogawa, T. Suzuki, K. Kato, T. Ohashi, S. Yasuda, H. Kato, Y. Ito, *Chem. Pharm. Bull.* **1996**, *44*, 765.

[2] M. Gillard, C. van der Perren, N. Moguilevsky, R. Massingham, P. Chatelain, *Mol. Pharmacol.* **2002**, *61*, 391.

[3] For reviews on auxiliary controlled additions to C=N, see a) D. Enders, U. Reinhold, *Tetrahedron: Asymmetry* **1997**, *8*, 1895; b) R. Bloch, *Chem. Rev.* **1998**, *98*, 1407; c) G. Alvaro, D. Savoia, *Synlett* **2002**, 651; for reviews on corresponding catalytic processes, see d) S. Kobayashi, H. Ishitani, *Chem. Rev.* **1999**, *99*, 1069; e) S. E. Denmark, O. J.-C. Nicaise in *Comprehensive Asymmetric Catalysis* (Eds.: E. N. Jacobsen, A. Pfaltz, H. Yamamoto), Springer, Berlin, **1999**, p. 924.

[4] a) C. J. Opalka, T. E. D'Ambra, J. J. Faccone, G. Bodson, E. Cossement, *Synthesis* **1995**, 766; b) E. Cossement, G. Motte, G. Bodson, J. Gobert, UK Patent Appl. 2225321 **1990** [*Chem. Abstr.* **1990**, 113, 191396]; c) for a large-scale preparative HPLC (on a chiral stationary phase) approach, see D. A. Pflum, H. S. Wilkinson, G. J. Tanoury, D. W. Kessler, H. B. Kraus, C. H. Senanayake, S. A. Wald, *Org. Process Res. Dev.* **2001**, *5*, 110.

[5] E. J. Corey, C. J. Helal, *Tetrahedron Lett.* **1996**, *37*, 4837.

[6] a) D. A. Pflum, D. Krishnamurthy, Z. Han, S. A Wald, C. H. Senanayake, *Tetrahedron Lett.* **2002**, *43*, 923; b) N. Plobeck, D. Powell, *Tetrahedron: Asymmetry* **2002**, *13*, 303.

[7] T. Hayashi, M. Ishigedani, *J. Am. Chem. Soc.* **2000**, *122*, 976. This method gives rise to diarylmethylamines in very high enantioselectivities but requires the use of five equivalents of the stannane to obtain the products in high yields.

[8] a) C. Bolm, N. Hermanns, J. P. Hildebrand, K. Muñiz, *Angew. Chem.* **2000**, *112*, 3607; *Angew. Chem. Int. Ed.* **2000**, *39*, 3465; b) C. Bolm, M. Kesselgruber, N. Hermanns, J. P. Hildebrand, G. Raabe, *Angew. Chem.* **2001**, *113*, 1536; *Angew. Chem. Int. Ed.* **2001**, *40*, 1488; c) C. Bolm, N. Hermanns, M. Kesselgruber, J. P. Hildebrand, *J. Organomet. Chem.* **2001**, *624*, 157; d) C. Bolm, M. Kesselgruber, A. Grenz, N. Hermanns, J. P. Hildebrand, *New J. Chem.* **2001**, *25*, 13; e) for a recent review on catalyzed asymmetric arylations, see C. Bolm, J. P. Hildebrand, K. Muñiz, N. Hermanns, *Angew. Chem.* **2001**, *113*, 3382; *Angew. Chem. Int. Ed.* **2001**, *40*, 3284.

[9] S. Dahmen, S. Bräse, *J. Am. Chem. Soc.* **2002**, *124*, 5940.

[10] For other recent examples for the enantioselective addition of diethylzinc to imines, see a) H. Fujihara, K. Nagai, K. Tomioka, *J. Am. Chem. Soc.* **2000**, *122*, 12055; b) J. R. Porter, J. F. Traverse, A. H. Hoveyda, M. L. Snapper, *J. Am. Chem. Soc.* **2001**, *123*, 984; c) J. R. Porter, J. F. Traverse, A. H. Hoveyda, M. L. Snapper, *J. Am. Chem. Soc.* **2001**, *123*, 10409.

[11] J. Sisko, M. Mellinger, P. W. Sheldrake, N. H. Baine, *Tetrahedron Lett.* **1996**, *37*, 8113.

[12] For reports on mixed alkyl- and alkenylzinc species, see a) H. Nehl, W. R. Scheidt, *J. Organomet. Chem.* **1985**, *289*, 1; b) W. Oppolzer, R. N. Radinov, *Helv. Chim. Acta* **1992**, *75*, 170; c) S. Berger, F. Langer, C. Lutz, P. Knochel, T. A. Mobley, C. K. Reddy, *Angew. Chem.* **1997**, *109*, 1603; *Angew. Chem. Int. Ed.* **1997**, *36*, 1454; d) C. Lutz, P. Knochel, *J. Org. Chem.* **1997**, *62*, 7895.

[13] The [2.2]paracyclophane-based N,O-ligands have previously been employed in the dialkylzinc and the alkenylzinc addition to aldehydes: a) S. Dahmen, S. Bräse, *Chem. Commun.* **2002**, 26; b) S. Dahmen, S. Bräse, *Org. Lett.* **2001**, *3*, 4119; c) for the synthesis of compounds **4** and **6**, see V. Rozenberg, T. Danilova, E. Sergeeva, E. Vorontsov, Z. Starikova, K. Lysenko, Y. Belokon, *Eur. J. Org. Chem.* **2000**, 3295.

[14] For (*S*)-**10b**: $[\alpha]_D^{20} = +10.8$ ($c = 2.18$, ethanol), see G. R. Clemo, C. Gardner, R. Raper, *J. Chem. Soc.* **1939**, 1958.

[15] The absolute configurations of all other products should be *R* as well if an analogous stereochemical reaction pathway is assumed.

[16] Attempts to determine the enantiomeric excess of amine **10b** itself by means of HPLC on a chiral stationary phase were unsuccessful.

[(PPh$_3$)Ag(HCB$_{11}$Me$_{11}$)]: A Complex with Intermolecular Ag···H$_3$C Interactions**

Michael J. Ingleson, Mary F. Mahon, Nathan J. Patmore, Giuseppe D. Ruggiero, and Andrew S. Weller*

Dedicated to Professor Thomas P. Fehlner on the occasion of his 65th birthday

The "least-coordinating" peralkylated monoanionic carboranes based around [1-*closo*-CB$_{11}$R$_{12}$]$^-$ (R = alkyl)[1,2] are of significant technological interest. They can form stable, lipophilic, free radicals that are also strong oxidants,[3] novel electrolytes,[2] act as partners with lithium ions as catalysts for pericyclic rearrangements,[4] or can be used to isolate reactive cations such as [*n*Bu$_3$Sn]$^+$[5] or Me$^+$.[6] They constitute some of weakest nucleophiles within the family of icosahedral monocarborane anions,[7] and also have the attractive properties of being relatively chemically robust[8] and available in gram quantities. Given that much of the interest in least-coordinating anions, such as the perfluorinated tetraaryl borates, is based around the generation of cationic Lewis acidic metal centers that show enhanced catalytic properties,[9] analogous complexes partnered with peralkylated carborane anions are of significant interest. The fact that peralkylated anions such as **1** can be considered as being negatively charged "alkane balls" is of particular relevance as there is considerable interest in the isolation and structure of metal–alkane complexes.[10] The structures of simple alkali-metal salts of [1-*closo*-CB$_{11}$Me$_{12}$]$^-$ have been reported,[11] while the main-group-metal complex [*n*Bu$_3$Sn][1-*closo*-CB$_{11}$Me$_{12}$] is a closely associated ion-pair in the solid state, a structure that is thought to be retained in solution.[5] However, no analogous transition-metal complexes have been described. We have a current interest in the chemistry of metal–ligand complexes partnered with monoanionic carborane anions[12] and report here the first example of a d-block-metal complex containing

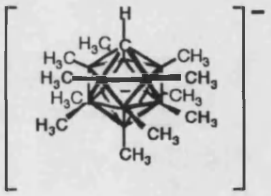

1

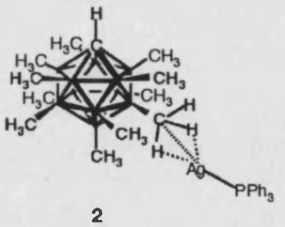

2

[*] Dr. A. S. Weller, M. J. Ingleson, Dr. M. F. Mahon, N. J. Patmore, Dr. G. D. Ruggiero
Department of Chemistry
University of Bath
Bath, BA2 7AY (UK)
Fax: (+44) 1225-386-231
E-mail: a.s.weller@bath.ac.uk

[**] This work was supported by the Royal Society (A.S.W.), the EPSRC (GR/R36824), and the University of Bath. Dr. M. A. Fox (University of Durham) is thanked for his help and useful discussions.

Supporting information for this article is available on the WWW under http://www.angewandte.org or from the author.

  0044-8249/02/4119-3694 $ 20.00+.50/0

a peralkylated carborane, $[PPh_3Ag][1\text{-}closo\text{-}HCB_{11}Me_{11}]$ (**2**), that displays unprecedented intermolecular Ag···H_3C interactions between the silver center and the carborane periphery in both the solid and solution state.

The addition of a solution of triphenylphosphane in CH_2Cl_2 to $Ag[1\text{-}closo\text{-}HCB_{11}Me_{11}]$ ($[Ag]\mathbf{1}$)[13] affords a colorless solution from which crystalline $[PPh_3Ag][1\text{-}closo\text{-}HCB_{11}Me_{11}]$ (**2**) can be isolated in good yield. The solid-state structure of **2** is shown in Figure 1.

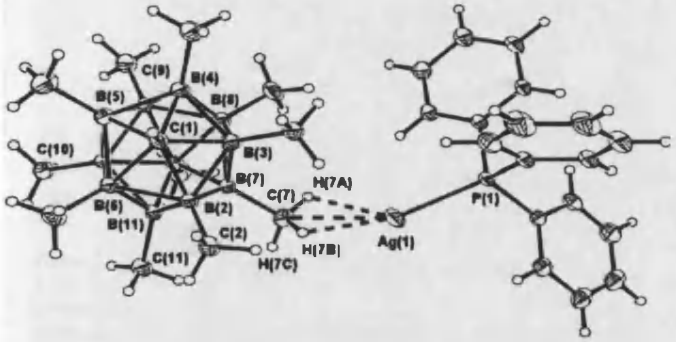

Figure 1. ORTEX diagram[27] of complex **2** showing thermal ellipsoids at the 30% probability level. Selected bond lengths [Å] and angles [°]: Ag(1)-H(7A) 2.19(3), Ag(1)-H(7B) 2.20(3), Ag(1)-H(7C) 3.033, C(7)-H(7A) 0.93(3), C(7)-H(7B) 0.93(3), C(7)-H(7C) 0.93(4), Ag(1)-C(7) 2.544(2), Ag(1)-P(1) 2.3871(5); C(7)-Ag(1)-P(1) 152.21(4), H(7A)-C(7)-B(7) 109(1), H(7B)-C(7)-B(7) 109(1), H(7C)-C(7)-B(7) 112(2).

In the solid state, the asymmetric unit shows that the silver–phosphane fragment is in close contact to one of the methyl groups (C(7)) on the lower pentagonal belt of the cage. The interactions between the $\{Ag(PPh_3)\}^+$ fragment and the C(7) methyl group are significant, as judged by the Ag(1)···C(7) separation (2.544(2) Å) being longer than that found for a Ag–C single bond (for example, 2.144(5) Å in $[(PPh_3)AgCH_2C_6F_5)]$)[14] but much shorter than the sum (3.29 Å) of the van der Waals radius of a methyl group (2.00 Å) and the ionic radius of an Ag^I ion (1.29 Å).[15] Moreover, the Ag(1)···C(7) separation is only slightly longer than those found in silver–arene complexes (2.47 Å) in which significant silver–carbon interactions are suggested to occur.[16] The hydrogen atoms on C(7) were located in the penultimate Fourier difference map and refined freely. There are two close H···Ag contacts (Ag(1)···H(7A) 2.19(3) and Ag(1)···H(7B) 2.20(3) Å) in the asymmetric unit; the separation from the third methyl hydrogen atom (Ag(1)···H(7C) 3.033 Å) is significantly longer resulting in a B(7)-C(7)-Ag(1) angle of 138.9(2)°. While acknowledging the limitations of X-ray diffraction in the accurate location of hydrogen atoms, it is reasonable to say that there is no lengthening of the C–H bonds for the hydrogen atoms in close proximity to Ag(1) in **2**. The structural motif in **2** is similar on first inspection to that reported for the zwitterionic complexes $[\{1,3\text{-}(SiMe_3)_2C_5H_3\}_2ZrMe(\mu\text{-}Me)B(C_6F_5)_3]$ (**A**)[17] and $[(1,2\text{-}Me_2Cp)_2ZrCH_3(\mu\text{-}Me)B(C_6F_5)_3]$ (**B**)[18] in which Zr···H_3C agostic interactions are suggested to be present. In the extended lattice (Figure 2) there are two further, significantly longer, Ag···C contacts from permethylated cages proximate

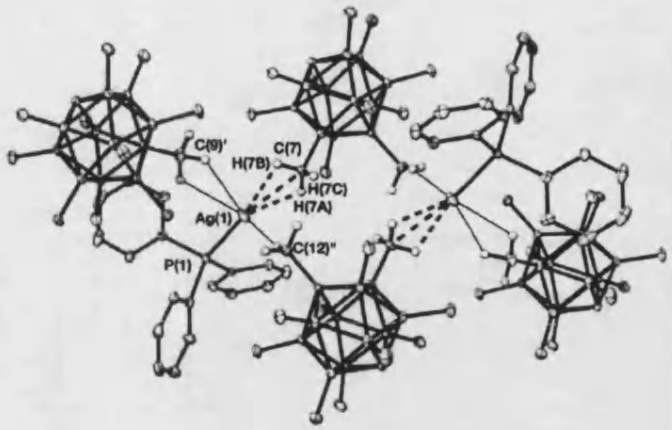

Figure 2. Packing diagram for **2** showing the extended $\{BCH_3\}$···$\{Ag\}$ interactions in the solid state. Only the hydrogen atoms on C(7), C(9)′, and C(12)″ are shown for clarity. Selected bond lengths [Å]: Ag(1)-C(9)′ 3.154(2), Ag(1)-C(12)″ 3.336(2).

in the lattice: Ag(1)···C(9)′ 3.154(2), Ag(1)···C(12)″ 3.336(2) Å. The associated hydrogen atoms were located and refined; one methyl group (C(9)′) is bidentate with respect to the Ag···H interactions, while the other (C(12)″) is monodentate. The overall structural motif is reminiscent of that found for $Li[B(CH_3)_4]$, in which extended tridentate and bidentate CH_3···Li interactions are observed in the solid state.[19]

Energy minimization at the B3LYP/DZVP level for $[\mathbf{1}]^-$ and the three possible isomers of **2** shows that there is a small energy difference between the isomers (Table 1), with the metal fragment favoring interaction with the (7)–(11) vertices as observed experimentally, very closely followed by vertex (12). This observation is consistent with the distribution of charge on the three chemically different $\{B(CH_3)\}$ moieties in the free anion, $[\mathbf{1}]^-$ (Table 1) and is similar to that previously reported for $[n\text{Bu}_3\text{Sn}][1\text{-}closo\text{-}CB_{11}Me_{12}]$.[5]

Table 1. Comparison of the charges (from natural bond orbital (NBO) analysis) on $[1\text{-H-}closo\text{-}1\text{-}CB_{11}Me_{11}]^-$, ($[\mathbf{1}]^-$), and the relative energies of the isomers of $[1\text{-H-}closo\text{-}1\text{-}CB_{11}Me_{11}][AgPPh_3]$ (**2**), all calculated at the B3LYP/DZVP level.

	$[HCB_{11}Me_{11}]^-$		$[HCB_{11}Me_{11}][AgPPh_3]$
Vertex/isomer	CH_3	$B(CH_3)$	energy [kJ mol^{-1}]
(12)	−0.28	−0.09	+6
(7)–(11)	−0.28	−0.13	0
(2)–(6)	−0.29	+0.07	+24

In solution the Ag···H_3C interactions are still present and significant, as shown by NMR spectroscopy. The $^1H\{^{11}B\}$ NMR spectrum of **2** shows a 5:1:5 pattern for the cage methyl groups. These signals are considerably broadened compared with those of $[Me_4N][1\text{-}closo\text{-}HCB_{11}Me_{11}]$ ($[Me_4N]\mathbf{1}$) (Figure 3), which is indicative of interaction with $\{Ag(PPh_3)\}$, while other peaks in the spectrum were sharp and well-resolved. $^1H\{^{11}B\text{-selective}\}$ NMR experiments were used to assign the methyl resonances, and demonstrate that the signal for the unique C(12) methyl carbon atom is shifted by

  0044-8249/02/4119-3695 $ 20.00+.50/0

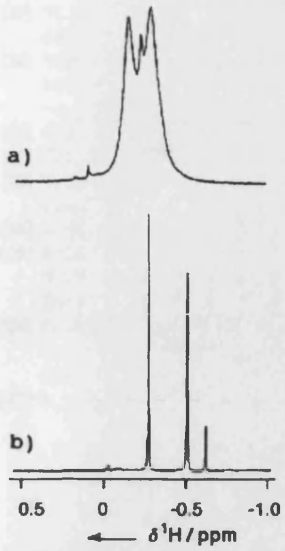

Figure 3. $^1H\{^{11}B\}$ NMR spectra of **2** (a) and **1**[NMe_4][13] (b). Peak assignments (downfield to upfield) for **2**: C(7)–C(11), C(12), C(2)–C(6) and for **1**[NMe_4]: C(2)–C(6), C(7)–C(11), C(12).

0.41 ppm downfield relative to that of **1**[NMe_4].[13,20] There is also a comparable downfield shift observed for the methyl groups on the lower pentagonal belt (0.37 ppm), while C(2)–C(6) are not shifted significantly. These results are consistent with the metal fragment interacting mostly with the C(7)–C(12) unit in solution. Similar downfield shifts have been reported for the $BeCH_3$ protons in [$(\eta^5$-$C_5Me_5)_2Yb(\mu$-Me)Be-$(\eta^5$-$C_5Me_5)$] (**C**) in which the Yb···{H_3CBe} interaction may be considered more electrostatic.[21] In contrast, in related complexes such as **A** and **B**, where agostic Zr···{H_3CB} interactions are proposed,[9] upfield shifts of the BCH_3 group are observed.[22] The $^{11}B\{^1H\}$ NMR spectrum of **2** confirms C_{5v} symmetry for the cage in solution (1:5:5 pattern), while in the $^{31}P\{^1H\}$ NMR spectrum a single phosphorus environment reveals coupling to both ^{109}Ag and ^{107}Ag nuclides ($J(Ag_{av}P)$ 824 Hz). No significant change was observed in either the ^1H or the $^{31}P\{^1H\}$ NMR spectra on cooling the solution to −60 °C. Progressive heating of the sample ($C_2D_2Cl_4$, 20–70 °C) resulted in gradual decomposition to unidentified species.

The Ag···{H_3CB} interactions in **2** may be switched off by addition of one equivalent of [NBu_4][1-*closo*-$CB_{11}H_6Br_6$][23] to a solution of **2** in CD_2Cl_2, which results in rapid exchange of the permethylated carborane for the hexabromocarborane anion at the silver(I) center. The ^1H NMR spectrum of the resulting solution shows sharpening of the methyl signals, and chemical shifts identical to pure [NMe_4]**1**, while the $^{31}P\{^1H\}$ NMR spectrum shows evidence for the clean formation of [(PPh_3)Ag(1-*closo*-$CB_{11}H_6Br_6$)].[12] [1-*closo*-$HCB_{11}Me_{11}$] can thus be considered to be less nucleophilic than [1-*closo*-$CB_{11}H_6Br_6$], which itself is one of the least-coordinating anions known.[7]

Metal–alkane complexes are of considerable current interest,[10,24] but complexes isolated under standard laboratory conditions are rare.[25] Complexes such as **A**–**C**, which possess methyl groups that coordinate in an intermolecular fashion, are models for alkane complexes of the early transition metals. However, to our knowledge, no later d-block-metal complexes showing analogous interactions are known. Complex **2** represents the first example of a silver metal center interacting with an alkyl (CH_3) group in either an intra- or intermolecular fashion, and is thus a model for an interaction between a d^{10} metal center and an alkane.[24] The fact that these interactions are readily observed by ^1H NMR spectroscopy suggests that they will provide a useful spectroscopic marker in the development of the transition-metal chemistry of peralkylated carborane anions.

Experimental Section

2: Triphenylphosphane (60 mg, 0.23 mmol) was dissolved in CH_2Cl_2 (5 mL) and added dropwise to a Schlenk flask charged with [Ag{$CB_{11}Me_{11}H$}][13] (92 mg, 0.23 mmol). The resulting solution was stirred in the dark for 16 h, cannula filtered, and the solvent removed in vacuo. The resultant white solid was redissolved in the minimum volume of CH_2Cl_2, layered with hexanes, then placed in a freezer overnight at −30 °C to afford colorless crystals (122 mg, 81 %).

$^1H\{^{11}B\}$ NMR (300 MHz, CD_2Cl_2, 22 °C , assignments from $^1H\{^{11}B$-selective} experiments): $\delta = 7.66$–7.36 (15 H, m, Ph), 1.26 (1 H, s, C_{cage}-H), −0.14 (15 H, brs, BCH_3, B(7)CH_3–B(11)CH_3), −0.22 (3 H, brs B(12)CH_3), −0.28 ppm (15 H, brs, BCH_3, B(2)CH_3–B(6)CH_3). ^{11}B NMR (96 MHz, CD_2Cl_2, 22 °C, assignments from ^{11}B-^{11}B COSY): $\delta = -1.3$ (1 B, s, B(12)), −9.0 (5 B, s, B(7)–B(11)), −11.9 ppm (5 B, s, B(2)-B(6)). $^{13}C\{^1H\}$ NMR (75 MHz, CD_2Cl_2, 22 °C): $\delta = 133.9$ (s, C_{phenyl}), 132.3 (s, C_{phenyl}), 130.0 (s, C_{phenyl}), 128.2 (d, C_{phenyl}, $J(CP) = 37$ Hz), 61.3 (s, C_{cage}), −0.7–−6.0 ppm (br, CH_3). $^{31}P\{^1H\}$ (122 MHz, CD_2Cl_2, 22 °C): $\delta = 17.5$ ppm (dd, $J(Ag^{109}P)$ 853 Hz, $J(Ag^{107}P)$ 794 Hz). IR (KBr): $\tilde{\nu} = 2921$, 2895, 2829, 2736 cm^{-1} (CH_3); elemental analysis calcd for $C_{30}H_{49}Ag_1B_{11}P_1$: C 54.0, H 7.35 %; found: C 53.4, H 7.30 %.

Crystal data for **2**: triclinic, space group $P\bar{1}$, a = 9.18400(10), b = 13.6170(2), c = 15.1520(3) Å, $\alpha = 111.6370(10)$, $\beta = 95.0050(10)$, $\gamma = 100.3360(10)°$, $V = 1708.23(5)$ Å^3, $Z = 2$, $\rho_{calcd} = 1.298$ Mg m^{-3}. Data were collected at 173(2) K on a Nonius kappaCCD diffractomter, $Mo_{K\alpha}$ radiation (0.71073 Å), 9965 measured reflections to $2\theta_{max} = 60.12°$, giving 7255 unique reflections ($R_{int} = 0.0417$). The structure was solved by direct methods, and refined against F^2 using all data.[26] The final discrepancy indices were $R_1 = 0.0378$, $wR_2 = 0.0941$. CCDC-187180 contains the supplementary crystallographic data for this paper. These data can be obtained free of charge via www.ccdc.cam.ac.uk/conts/retrieving.html (or from the Cambridge Crystallographic Data Centre, 12, Union Road, Cambridge CB2 1EZ, UK; fax: (+44) 1223-336-033; or deposit@ccdc.cam.ac.uk).

Received: June 21, 2002
Revised: July 25, 2002 [Z19582]

[1] a) B. T. King, Z. Janousek, B. Gruner, M. Trammell, B. C. Noll, J. Michl, *J. Am. Chem. Soc.* **1996**, *118*, 3313; b) C. W. Tsang, Z. W. Xie, *Chem. Commun.* **2000**, 1839.
[2] B. T. King, I. Zharov, J. Michl, *Chem. Innovation* **2001**, 23.
[3] B. T. King, B. C. Noll, A. J. McKinley, J. Michl, *J. Am. Chem. Soc.* **1996**, *118*, 10902.
[4] S. Moss, B. T. King, A. de Meijere, S. I. Kozhushkov, P. E. Eaton, J. Michl, *Org. Lett.* **2001**, *3*, 2375.
[5] I. Zharov, B. T. King, Z. Havlas, A. Pardi, J. Michl, *J. Am. Chem. Soc.* **2000**, *122*, 10253.
[6] D. Stasko, C. A. Reed, *J. Am. Chem. Soc.* **2002**, *124*, 1148.
[7] C. A. Reed, *Acc. Chem. Res.* **1998**, *31*, 133.
[8] B. T. King, J. Michl, *J. Am. Chem. Soc.* **2000**, *122*, 10255.
[9] E. Y. X. Chen, T. J. Marks, *Chem. Rev.* **2000**, *100*, 1391.
[10] C. Hall, R. N. Perutz, *Chem. Rev.* **1996**, *96*, 3125.
[11] B. T. King, B. Noll, J. Michl, *Collect. Czech. Chem. Commun.* **1999**, *64*, 1001.
[12] N. J. Patmore, C. Hague, J. H. Cotgreave, M. F. Mahon, C. G. Frost, A. S. Weller, *Chem. Eur. J.* **2002**, *8*, 2088.
[13] Prepared by an adaptation of the method given in ref [1a]; J. Michl, **2002**, personal communication.
[14] R. Uson, A. Laguna, A. Uson, P. G. Jones, K. Meyer-Base, *J. Chem. Soc. Dalton Trans.* **1988**, 341.
[15] J. E. Huheey, E. A. Keiter, R. L. Keiter, *Inorganic Chemistry: Principles of Structure and Reactivity*, Harper Collins, New York, **1993**.
[16] E. A. H. Griffith, E. L. Amma, *J. Am. Chem. Soc.* **1974**, *96*, 743.
[17] M. Bochmann, S. J. Lancaster, M. B. Hursthouse, K. M. A. Malik, *Organometallics* **1994**, *13*, 2235.
[18] X. M. Yang, C. L. Stern, T. J. Marks, *J. Am. Chem. Soc.* **1994**, *116*, 10015.

  0044-8249/02/4119-3696 $ 20.00+.50/0

[19] W. E. Rhine, G. Stucky, S. W. Peterson, *J. Am. Chem. Soc.* **1975**, *97*, 6401.
[20] $^1H\{^{11}B\}$ NMR data for [1]NMe_4 (300 MHz, CD_2Cl_2): $\delta = 3.19$ (12H, s, NMe_4), 1.09 (1H, brs, C_{cage}-H), −0.26 (15H, s, B(2)CH_3–B(6)CH_3, −0.51 (15H, s, B(7)CH_3–B(11)CH_3), −0.63 ppm (3H, s, B_{12}-CH_3).
[21] C. J. Burns, R. A. Andersen, *J. Am. Chem. Soc.* **1987**, *109*, 5853.
[22] C. L. Beswick, T. J. Marks, *Organometallics* **1999**, *18*, 2410.
[23] T. Jelinek, J. Plesek, S. Hermanek, B. Stibr, *Collect. Czech. Chem. Commun.* **1986**, *51*, 819.
[24] A. E. Shilov, G. B. Shul'pin, *Chem. Rev.* **1997**, *97*, 2879.
[25] S. Geftakis, G. E. Ball, *J. Am. Chem. Soc.* **1998**, *120*, 9953; D. R. Evans, T. Drovetskaya, R. Bau, C. A. Reed, P. D. W. Boyd, *J. Am. Chem. Soc.* **1997**, *119*, 3633.
[26] G. M. Sheldrick, SHELX-97, A computer program for refinement of crystal structures, University of Göttingen, Göttingen (Germany), **1997**.
[27] P. McArdle, *J. Appl. Crystallogr.* **1995**, *28*, 65.

A Simple, Reliable, Catalytic Asymmetric Allylation of Ketones**

Karen M. Waltz, Jason Gavenonis, and Patrick J. Walsh*

The asymmetric allylation of carbonyl groups to furnish homoallylic alcohols is a fundamental transformation in synthetic organic chemistry.[1–3] Several catalysts will promote the asymmetric allylation of aldehydes to give secondary homoallylic alcohols with excellent enantioselectivities.[4–15] The catalytic asymmetric allylation of ketones, however, has proven to be a more challenging transformation owing to the significant difference in reactivity between aldehydes and ketones. Thus, with one exception,[16] catalysts that promote the enantioselective allylation of aldehydes fail to catalyze the analogous reaction with ketones. In general, the enantioselective formation of quaternary stereocenters, as generated in the asymmetric allylation of ketones, is of considerable difficulty.[17,18]

To compensate for the reduced reactivity of ketones, a more reactive allylating agent was needed. Baba and co-workers found that tetraallylstannane added to ketones in the presence of methanol and 200 mol% binol to give the homoallylic alcohol in up to 60% *ee*.[19] An important discovery in the asymmetric allylation of ketones was recently reported by Casolari, D'Addario, and Tagliavini.[20] Their catalyst preparation involved the reaction of $[Cl_2Ti(OiPr)_2]$ and binol with allyltributylstannane. After mixing for one hour, tetraallylstannane and the substrate ketone were added. They observed the formation of the ketone allylation product with up to 65% *ee* at 20 mol% binol (80% *ee* with 40 mol% binol).

Based on the results of the Italian team,[20] Maruoka and co-workers[16] recently reported a system for the catalytic asymmetric allylation of aldehydes with a catalyst that is based on titanium, binol, and an achiral diamine spacer (2:2:1 ratio). This catalyst (60 mol% titanium and binol) was examined in the asymmetric allylation of only two ketones, acetophenone and methyl 2-naphthyl ketone, which underwent allylation with 90 and 92% *ee*, respectively.[16] More recently, Cunningham and Woodward[21] demonstrated that monothiobinaphthol will promote the allylation of acetophenone derivatives with a mixture of $[RSn(allyl)_3]/[Sn(allyl)_4]$ (R = Et, Bu) with *ee* values as high as 92% (51% yield).

The ketone allylation reaction of Casolari, D'Addario, and Tagliavini[20] attracted our attention because of our interest in the mechanisms of titanium-based asymmetric Lewis acid catalysts[22–24] and the need for a more versatile and enantioselective catalyst for this important process. While investigating the catalyst structure of the Tagliavini system, we made several key observations that allowed us to develop the most general and enantioselective catalyst for the asymmetric allylation of ketones to date.

We repeated the catalyst preparation of Tagliavini[20] described above in $CDCl_3$ to probe the nature of the (binolate)Ti species by NMR spectroscopy. Like Tagliavini and co-workers,[20] we observed the production of tributyltin chloride. However, we were surprised to find that the major titanium-containing product was [(binolate)$Ti(OiPr)_2$], which is dimeric in solution and trimeric in the solid state.[25,26] We prepared this compound on a gram scale simply by mixing titanium tetraisopropoxide and binol followed by removal of the solvent and liberated 2-propanol.[26] Using the isolated [(binolate)$Ti(OiPr)_2$], we found that the enantioselectivities in the allylation reaction were about the same as those reported by Tagliavini and co-workers.[20] An important breakthrough was made when the catalyst was prepared directly from titanium tetraisopropoxide and binol (1:1, 20 or 30 mol%) *without removal of the liberated 2-propanol*. When we employed this catalyst preparation, the *ee* of the product formed from 3-methylacetophenone rose from 51% to 73%. These results suggested that the liberated 2-propanol had a beneficial impact on the enantioselectivity of the catalyst. We therefore prepared the catalyst with additional 2-propanol and observed a significant increase in the catalyst enantioselectivity [Eq. (1)].

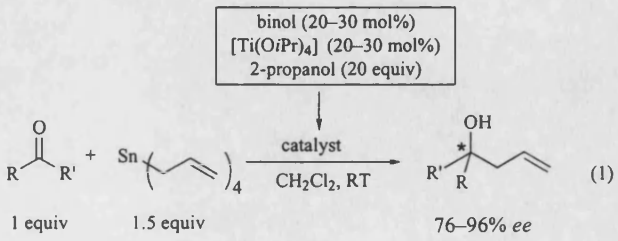

(1)

The advantageous effect of the 2-propanol on the enantioselectivity of the catalyst reached a maximum when 20 equiv

[*] Prof. P. J. Walsh, Dr. K. M. Waltz, J. Gavenonis
P. Roy and Diane T. Vagelos Laboratories
Department of Chemistry, University of Pennsylvania
231 South 34th Street, Philadelphia, PA 19104-6323 (USA)
Fax: (+1) 215-571-6743
E-mail: pwalsh@sas.upenn.edu

[**] Financial Support for this research is from the National Science Foundation in the form of a Career Award to PJW (CHE-9733274) and the National Institutes of Health (GM58101).

Supporting information for this article is available on the WWW under http://www.angewandte.org or from the author.

  0044-8249/02/4119-3697 $ 20.00+.50/0